

POLY(ETHYLENE GLYCOL) TAILORED POLYMERS: NANOMICELLES WITH
TUNABLE LOWER CRITICAL SOLUTION TEMPERATURE BEHAVIOR

By

Yu-Ling Lien

A DISSERTATION

Submitted to
Michigan State University
in partial fulfillment of the requirements
for the degree of

Chemistry – Doctor of Philosophy

2018

ABSTRACT

POLY(ETHYLENE GLYCOL) TAILORED POLYMERS: NANOMICELLES WITH TUNABLE LOWER CRITICAL SOLUTION TEMPERATURE BEHAVIOR

By

Yu-Ling Lien

Propargyl and 1,1-dimethyl propargyl substituted poly(ethyleneoxides) (propargyl substituted = poly(**PGE**), 1,1'-dimethyl propargyl substituted = poly(**MGE**)) have been prepared by ring-opening polymerization of epoxides, which were synthesized from epichlorohydrin and propargyl or 1,1-dimethyl propargyl alcohol via Williamson ether synthesis. The resulting polymers were modified by Cu-catalyzed azide alkyne cycloaddition (CuAAC) of the polymer propargyl groups and organic azides. When these reactions were carried out with mixtures of azides, the ratios of azides incorporated in the polymer side chains were equal to the molar ratios of the organic azides reactants ($\pm 2\%$).

Mixtures of hydrophobic (**decyl azide**) and hydrophilic (**mDEG azide**) azides result in amphiphilic polymers that exhibited a lower critical solution temperature (LCST) behavior. The polymer LCSTs scaled from 48 to 97 ± 2 °C (poly(**PGE**) derived amphiphiles) and 4 to 46 ± 1 °C (poly(**MGE**) derived amphiphiles) in a roughly linear fashion with the mole fraction of hydrophilic side chains in the polymer. When charged azides, **COOH azide** and **aminium azide**, were used, the physical property as well as the LCST behavior of the polymers were changed. The LCSTs of polymers incorporating charged azides were increased and the LCSTs were decreased by adding salts in the solutions. The hydrodynamic radii (R_H) obtained from DLS measurements indicate that polymers form unimolecular micelles in water ($M_n = 52,000$ g/mol, PDI = 1.19, $R_H = 6 \pm 2$ nm), and TEM data showed monodisperse domains (20 ± 4 nm, for $M_n = 52,000$) when

water was evaporated at room temperature from solutions cast on TEM grids. This length scale is consistent with domains that consist of single polymer chains. When the TEM grid was heated during evaporation, the domain size increased to 74 ± 45 nm.

In solution, the unimolecular micelles can solubilize hydrophobic small molecules, such as *trans*-azobenzene (*trans*-PhN=NPh) in water. DLS data suggested that polymer encapsulating *trans*-PhN=NPh (*trans*-PhN=NPh@poly(**PGE**) or poly(**MGE**)) derived amphiphiles) showed signs of aggregation in one case ($R_H = 12 \pm 8$ nm) and no signs of aggregation in another case ($R_H = 5 \pm 2$ nm). When the resulting solutions were raised above the polymer LCST the polymer and small molecule precipitated. When the mixture was cooled below the LCST, the polymer and hydrophobic small molecule re-dissolved. The unimolecular micelles were used to encapsulate a hydrophilic macromolecule, Subtilisin Carlsberg (SC), in aqueous solution and organic media. Poly(**PGE**) or poly(**MGE**) derived amphiphiles with COOH pendant group slowed down SC aggregation in aqueous environment. Also, the activity of SC@poly(**MGE**) derived amphiphiles with COOH pendant group was assayed and the half-life of SC was increased to 10 h from 2 h at 50 °C. Initial studies of SC@poly(**PGE**) or poly(**MGE**) derived amphiphiles in organic media showed enzymatic activity in toluene after 16 h at 37 °C.

For those who believed in me

ACKNOWLEDGMENTS

I would like to thank my advisor, Dr. Mitch Smith, for the guidance during my graduate study. I appreciate the freedom I had to explore my ideas for the project. I'm also grateful for the critics and questions from him so I can build the project on a sound scientific foundation. I would also like to thank my guidance committee, Dr. Xuefei Huang, Dr. James Geiger, and Dr. Rémi Beaulac, for their suggestions and help.

Thanks to Dr. Kathy Severin, Dr. Dan Holmes, and Dr. Ardeshir Azadnia for teaching me various characterization techniques. Also, I would like to thank the previous and current group member, Budda, Dmitry, Sean, Behnaz, Kristin, Don, Tim, Olivia, Gina, Greg, Zhe, Salinda, Jack, Meisam, Zahra, Po-Jen, Reza, Mona, Ryan, Alex, Seokjoo, Jack, Chris, Aalyah, Suzi. Thank you for your support throughout my graduate study. Special thanks to the talented undergraduate students I worked with, Jack and Chris. Your work made great impacts on the project.

I would like to thank all my friends from MSU, Tim, Kristin, Kristen, Travis, Tanner, Michelle, Pengchao, Corey, Matt, Tyler, Ruwi, Cho-Ying, Feng-Kuo, Yen-Yao, Zhong-En, Tung-Wu, Yung-Hsiu, Jing-Ru, Lenore, Dana. You brought so much joys to my life in East Lansing. Jay, thank you for your support and encouragement! Finally, I would like to thank my family for their support.

TABLE OF CONTENTS

LIST OF TABLES	viii
LIST OF FIGURES	ix
LIST OF SCHEMES.....	xxii
KEY TO ABBREVIATIONS	xxiv
Chapter 1. Introduction	1
1.1. Overview of Polyether Synthesis	1
1.2. Overview of Post-Polymerization Modification	6
1.3. Overview of Lower Critical Solution Temperature (LCST).....	10
1.4. Overview of the Formation of Unimolecular Micelles (Unimicelles)	12
1.5. Overview of Nanocarriers.....	15
1.6. Overview of the Synthesis of Biocatalysts	18
1.7. Protein Folding and Molecular Chaperones.....	21
1.8. Artificial Chaperones.....	25
Chapter 2. Synthesis, Characterization, and Post-Polymerization Modification of Propargyl-Substituted Poly(ethylene oxide)s	32
2.1. Introduction.....	32
2.2. Synthesis and Characterization of Monomers.....	33
2.3. Living Anionic Ring-opening Polymerization.....	37
2.4. Post-polymerization Modification (PPM) via “Click” Chemistry	44
2.5. Summary	58
Chapter 3. Lower Critical Solution Temperature (LCST) Behavior and Formation of Unimolecular Micelles.....	59
3.1. Lower Critical Solution Temperature (LCST) Behavior	59
3.2. Formations of Unimolecular Micelles	75
3.3. Summary	78
Chapter 4. Unimicelles as Nanocarriers for Hydrophobic and Hydrophilic Guest Molecules	79
4.1. Encapsulation of Hydrophobic Guest Molecules.....	79
4.2. Encapsulation of Hydrophilic Guest Biomacromolecules	84
4.3. Summary	97
Chapter 5. Experimental Section.....	99
5.1. Materials	99
5.2. Characterization.....	99
5.3. Procedures.....	101

<i>Synthesis of propargyl glycidyl ether (PGE)</i> ²²²	101
<i>Synthesis of 1,1'-dimethyl propargyl glycidyl ether (MGE)</i>	101
<i>General Procedure for Polymerization</i>	102
<i>Synthesis of poly(propargyl glycidyl ether) (poly(PGE))</i>	103
<i>Synthesis of poly(1,1'-dimethyl propargyl glycidyl ether) (poly(MGE))</i>	104
<i>General Procedure for "Click" Functionalization</i> ^{49,95}	105
<i>Synthesis of poly(PGE_{0.50})</i>	105
<i>Synthesis of poly(MGE_{0.50})</i>	106
<i>Safety Information for Synthesizing, Purifying, and Handling Organic Azides</i> ²⁷⁰	107
<i>Synthesis of 1-azidodecane (decylazide)</i> ^{95,225,226}	108
<i>Synthesis of 1-(2-azidoethoxy)-2-(2-methoxyethoxy)ethane (mDEG azide)</i> ⁹⁵	108
<i>Synthesis of 1-azido poly(ethylene glycol) monomethyl ether, 550 (mPEG550 azide)</i> ^{229,230}	110
<i>Synthesis of 1-azido poly(ethylene glycol) monomethyl ether, 750 (mPEG750 azide)</i> ^{229,230}	111
<i>Synthesis of 1-azido poly(ethylene glycol) monomethyl ether, 2000 (mPEG2000 azide)</i> ^{229,230}	112
<i>Synthesis of 6-azidohexanoic acid (COOH azide)</i> ²³¹	113
<i>Synthesis of 3-azido-N,N,N-trimethylpropan-1-aminium iodide (aminium azide)</i> ^{232,233}	114
<i>General Procedure for Azobenzene (transPhN=NPh) Encapsulation</i>	115
<i>General Procedure for Subtilisin Carlsberg (SC) Encapsulation in Aqueous Media</i>	115
<i>General Procedure for Subtilisin Carlsberg (SC) Encapsulation in Organic Media</i>	115
<i>General Procedure for N-succinyl-Ala-Ala-Pro-Phe-p-nitroanilide (Suc-AAPF-pNA) Assay</i>	116
APPENDIX	117
REFERENCES	266

LIST OF TABLES

Table 1. Examples for cross-linking chemistry for the formation of SCNPs. ¹¹⁵	14
Table 2. Results of polymerization of PGE and MGE	40
Table 3. GPC results of poly(PGE _{0.x}).	50
Table 4. GPC results of poly(MGE _{0.x}).	51
Table 5. Selective polymers and their LCSTs. ^{92,93,234–238}	65
Table 6. Selective examples from literatures showing LCSTs at various concentrations. ^{239,241–244}	71
Table 7. Effects of SC concentration and temperatures on SC stability.	91
Table 8. Results of $t_{1/2}$ in the presence of various polymers.	94

LIST OF FIGURES

Figure 1. Examples of functionalized epoxides.	1
Figure 2. Models for intermolecular cross-linking of a polymer chain. ¹¹⁵	13
Figure 3. Historical timeline of clinical-stage nanoparticle technologies. Reprinted from ref. 143. Copyright 2011 American Chemical Society. ¹⁴³	16
Figure 4. Structure of poly(lactic- <i>co</i> -glycolic acid) (PLGA). ¹⁵⁷	17
Figure 5. Schematic illustration of the formation of polymeric micelles and unimicelles.	18
Figure 6. Timeline of nanotechnology-based biocatalysts. Reprinted from ref. 165. Copyright 2012 Springer Science+Business Media New York. ¹⁶⁵	19
Figure 7. Energy landscape scheme of protein folding and aggregation. Reprinted from ref. 182. Copyright 2009 Nature America, Inc. ¹⁸²	22
Figure 8. Protein fates in the proteostasis network. Reprinted from ref. 196. Copyright 2011 Macmillan Publishers Limited. ¹⁹⁶	23
Figure 9. Schematic representation mechanism of GroEL/GroES chaperone-mediated protein folding. Reprinted from ref. 187. Copyright 2013 Garland Science, Taylor & Francis Group, LLC. ¹⁸⁷	25
Figure 10. Artificial chaperone-assisted protein refolding (uppermost path) vs. dilution additive-assisted protein refolding (lowermost path) reported by Gellman and co-workers. ²⁰⁴	26
Figure 11. Schematic illustration of the C ₁₂ ESG nanogel-mediated one-step protein refolding system. Reprinted from ref 213. Copyright 2013 The Royal Society of Chemistry. ²¹³	27
Figure 12. Schematic representation mechanism of MSPMs-assisted protein refolding. Reprinted from ref 214. Copyright 2013 Wiley-VCH Verlag GmbH & Co. KGaA, Weinheim. ²¹⁴	29
Figure 13. 500 MHz ¹ H NMR spectra of a) PGE b) poly(propargyl glycidyl ether) (poly(PGE)) in CDCl ₃	34
Figure 14. 125 MHz ¹³ C NMR spectra of a) PGE b) poly(propargyl glycidyl ether) (poly(PGE)) in CDCl ₃	35

Figure 15. 500 MHz ^1H NMR spectra of a) MGE b) poly(1,1'-dimethyl propargyl glycidyl ether) (poly(MGE)) in CDCl_3	36
Figure 16. 125 MHz ^{13}C NMR spectra of a) MGE b) poly(1,1'-dimethyl propargyl glycidyl ether) (poly(MGE)) in CDCl_3	37
Figure 17. Measurements of refractive index increment, dn/dc , of poly(PGE). Trial 1 (blue diamond), trial 2 (red square), and trial 3 (green triangle).	41
Figure 18. Measurements of refractive index increment, dn/dc , of poly(MGE). Trial 1 (blue diamond), trial 2 (red square), and trial 3 (green triangle).	42
Figure 19. Variation of the number-average molar mass (black square) and PDI (red square) with MGE conversion ($[\text{M}]: [\text{Al}]: [\text{I}] = 200: 2: 1$).	43
Figure 20. Conversion vs. time of the polymerization of MGE ($[\text{M}]: [\text{Al}]: [\text{I}] = 200: 2: 1$).	44
Figure 21. 500 MHz ^1H NMR spectra of a) poly(PGE) b) poly(PGE ₀) c) poly(PGE _{1.0}) d) poly(PGE _{0.50}) in CDCl_3	47
Figure 22. 500 MHz ^1H NMR spectra of a) poly(MGE) b) poly(MGE ₀) c) poly(MGE _{1.0}) d) poly(MGE _{0.50}) in CDCl_3	48
Figure 23. GPC traces of poly(MGE) ($M_n = 21000$, PDI = 1.20; black line) and poly(MGE ₀) ($M_n = 49000$, PDI = 1.20; red line). The polymers were analyzed in THF at 35 °C, at 1 mL/min flow rate.	50
Figure 24. 500 MHz ^1H NMR spectra of poly(PGE _{0.60}) (red line), poly(PGE _{0.57} - Pos _{0.05}) (green line), and poly(PGE _{0.57} - Neg _{0.05}) (blue line) in CDCl_3 in aromatic region.	54
Figure 25. 500 MHz ^1H NMR spectra of poly(MGE _{0.75}) (red line), poly(MGE _{0.71} - Pos _{0.05}) (green line), and poly(MGE _{0.71} - Neg _{0.05}) (blue line) in CDCl_3 in aromatic region.	56
Figure 26. 500 MHz ^1H NMR spectra of poly(MGE _{0.71} - Neg _{0.05}) (red line) and poly(MGE _{0.68} - Neg _{0.10}) (green line) in CDCl_3 in aromatic region.	57
Figure 27. Photographs showing the lower critical solution temperature behavior of polymers p-MGE _{0.65} and <i>trans</i> -PhN=NPh@poly(MGE _{0.65}) in Milli-Q water. a) poly(MGE _{0.65}) (right) and <i>trans</i> -PhN=NPh@poly(MGE _{0.65}) (left) below LCST (taken at 25 °C) b) poly(MGE _{0.65}) (right) and <i>trans</i> -PhN=NPh@poly(MGE _{0.65}) (left) above LCST (taken at 33 °C).	61
Figure 28. LCST determination via UV-vis spectrometer for poly(MGE _{0.70}) ($M_n = 54,000$, PDI = 1.21) in Milli-Q water (5 mg/mL) under various temperatures at 1 °C/3 min.....	62

- Figure 29.** Plots of LCSTs vs. the mole fraction of mDEG chains in poly(**PGE_{0.x}**) and poly(**MGE_{0.x}**) obtained by UV-Vis spectrometer under various temperatures at 1 °C/3 min except poly(**MGE_{0.50}**) (at 1 °C/60 min). 64
- Figure 30.** Plots of LCSTs vs. the mole fraction of mDEG chains in poly(**PGE_{0.x}**) and poly(**MGE_{0.x}**), and poly(**PGL_{0.x}**) obtained by UV-Vis spectrometer..... 66
- Figure 31.** LCST determination via UV-vis spectrometer at 450 nm for poly(**MGE_{0.50}**) ($M_n = 54,000$, PDI = 1.19) in Milli-Q water (10 mg/mL) under various temperatures at 1 °C/3 min (blue diamond) and 1 °C/60 min (red diamond)..... 67
- Figure 32.** LCST determination via UV-vis spectrometer at 450 nm for poly(**MGE_{0.70}**) ($M_n = 54,000$, PDI = 1.21) in Milli-Q water (5 mg/mL) under various temperatures at 1 °C/3 min..... 68
- Figure 33.** LCST determination via DLS for poly(**MGE_{0.70}**) ($M_n = 54,000$, PDI = 1.21) in Milli-Q water (5 mg/mL) under various temperatures at 1 °C/3 min. 69
- Figure 34.** Plots of LCSTs vs. the mole fraction of mDEG chains in poly(**PGE_{0.x}**) by UV-Vis spectrometer (black circle) and by DLS (red triangle) and poly(**MGE_{0.x}**) by UV-Vis spectrometer (black diamond) and by DLS (red square). 70
- Figure 35.** LCSTs as a function of concentration of poly(**MGE_{0.65}**) (blue circles) and polyphosphazene reported by Bi and co-workers (red circles)..... 73
- Figure 36.** LCST values of poly(**MGE_{0.75}**) (red square) measured in sodium bicarbonate solutions at concentrations from 0 to 0.3 M, poly(**MGE_{0.71}-Neg_{0.05}**) (blue circle) measured in sodium bicarbonate solutions at concentrations from 0 to 0.4 M, and poly(**MGE_{0.71}-Neg_{0.05}**) (orange circle) measured in sodium chloride solutions at concentrations from 0 to 0.3 M. 75
- Figure 37.** DLS results for poly(**MGE_{0.65}**) ($M_n = 52,000$ g/mol, PDI = 1.19, $R_H = 6 \pm 2$ nm) in Milli-Q water at different concentrations. 76
- Figure 38.** TEM images of poly(**MGE_{0.65}**) ($M_n = 52,000$ g/mol, PDI = 1.19) a) below (taken at 100,000x, scale bar = 100 nm, 20 ± 4 nm) and b) above (taken at 40,000x, scale bar = 200 nm, 74 ± 45 nm) its LCST. 77
- Figure 39.** UV-vis spectra of *trans*-PhN=NPh, poly(**PGE_{0.60}**) ($M_n = 44,000$ g/mol, PDI = 1.33), and *trans*-PhN=NPh@poly(**PGE_{0.60}**) in Milli-Q water at room temperature. 80
- Figure 40.** a) DLS results for poly(**MGE_{0.65}**) (blue curve, $M_n = 52,000$ g/mol, PDI = 1.19, $R_H = 7 \pm 2$ nm) and *trans*-PhN=NPh@poly(**MGE_{0.65}**) (red curve) in Milli-Q. b) DLS results for poly(**MGE_{0.75}**) (blue curve, $M_n = 52,000$ g/mol, PDI = 1.22, $R_H = 6 \pm 2$ nm) and *trans*-PhN=NPh@poly(**MGE_{0.75}**) (red curve) in Milli-Q..... 82
- Figure 41.** a) DLS results for poly(**MGE_{0.65}**) (blue curve, $M_n = 52,000$ g/mol, PDI = 1.19, $R_H = 7 \pm 2$ nm), *trans*-PhN=NPh@poly(**MGE_{0.65}**) (orange curve, 50 mg/mL; green

curve, dilute to 10 mg/mL from 50 mg/mL; red curve, 10 mg/mL) in Milli-Q. b) DLS results for poly(**MGE**_{0.75}) (blue curve, $M_n = 52,000$ g/mol, PDI = 1.22, $R_H = 6 \pm 2$ nm) and *trans*-PhN=NPh@poly(**MGE**_{0.75}) (orange curve, 50 mg/mL; green curve, dilute to 10 mg/mL from 50 mg/mL; red curve, 10 mg/mL) in Milli-Q 83

Figure 42. DLS results of SC (blue line), poly(**MGE**_{0.71}-**mPEG2000-Pos**_{0.05}) (orange line) and SC with 5 μ L of poly(**MGE**_{0.71}-**mPEG2000-Pos**_{0.05}) added (green line) in Milli-Q water. 85

Figure 43. DLS results of SC (blue line), poly(**MGE**_{0.71}-**mPEG2000-Pos**_{0.05}) (orange line) and SC with 50 μ L of poly(**MGE**_{0.71}-**mPEG2000-Pos**_{0.05}) added (green line) in Milli-Q water. 85

Figure 44. DLS results of SC (blue line), poly(**MGE**_{0.71}-**mPEG2000-Pos**_{0.05}) (orange line) and SC with poly(**MGE**_{0.71}-**mPEG2000-Pos**_{0.05}) added (green line) in Milli-Q water. 86

Figure 45. DLS results of SC (dotted line) and SC@poly(**MGE**_{0.71}-**mPEG2000-Pos**_{0.05}) (solid line) in Milli-Q water over 48 h. 88

Figure 46. DLS results of SC (dotted line) and SC@poly(**MGE**_{0.71}-**mPEG2000-Neg**_{0.05}) (solid line) in Milli-Q water over 48 h. 88

Figure 47. UV-Vis spectra of the catalytic conversion of Suc-AAPF-*p*NA to *p*-nitroaniline overtime. 90

Figure 48. UV-Vis spectra of the conversion of Suc-AAPF-*p*NA (blue solid line) to *p*-nitroaniline (yellow solid line) by aliquots of SC (1 h, orange dotted line; 4 h green dotted line) or SC@poly(**MGE**_{0.71}-**mPEG750-Neg**_{0.05}) (1 h, purple solid line; 4 h, red solid line) taken at 1 or 4 h after heated at 50 °C. 93

Figure 49. DLS results of SC (dotted line) and SC@poly(**MGE**_{0.71}-**mPEG750-Neg**_{0.05}) (solid line) in Tris-HCl buffer at 50 °C for 4 h. 95

Figure 50. UV-Vis spectra of SC suspension in toluene (blue line), poly(**MGE**_{0.65}) in toluene (green line), and SC@ poly(**MGE**_{0.65}) in toluene (red line). 97

Figure A1. 500 MHz ¹H NMR spectrum of **PGE** in CDCl₃. 118

Figure A2. 500 MHz ¹H NMR spectrum of **PGE** in CDCl₃ between 2.0-4.5 ppm. 119

Figure A3. 125 MHz ¹³C NMR spectrum of **PGE** in CDCl₃. 120

Figure A4. 2D HSQC NMR spectrum of **PGE** in CDCl₃. 121

Figure A5. 2D HSQC NMR spectrum of **PGE** in CDCl₃. 122

Figure A6. 500 MHz ¹H NMR spectrum of **MGE** in CDCl₃. 123

Figure A7. 500 MHz ^1H NMR spectrum of MGE in CDCl_3 between 1.0-4.0 ppm.....	124
Figure A8. 125 MHz ^{13}C NMR spectrum of MGE in CDCl_3	125
Figure A9. 2D HSQC NMR spectrum of MGE in CDCl_3 . Methyl region was omitted for clarity.....	126
Figure A10. 500 MHz ^1H NMR spectrum of poly(PGE) in CDCl_3	127
Figure A11. 125 MHz ^{13}C NMR spectrum of poly(PGE) in CDCl_3	128
Figure A12. 125 MHz ^{13}C NMR spectrum of poly(PGE) in CDCl_3 between 25.0-35.0 ppm.....	129
Figure A13. 500 MHz ^1H NMR spectrum of poly(MGE) in CDCl_3	130
Figure A14. 125 MHz ^{13}C NMR spectrum of poly(MGE) in CDCl_3	131
Figure A15. Mass spectrum of poly(PGE) ($M_n = 2800$, PDI = 1.14) via positive electrospray ionization.	132
Figure A16. Mass spectrum of poly(MGE) ($M_n = 3900$, PDI = 1.16) via positive electrospray ionization.	133
Figure A17. Variation of the number-average molar mass (black square) and PDI (red square) with PGE conversion ($[\text{M}]: [\text{Al}]: [\text{I}] = 200: 2: 1$).	134
Figure A18. Conversion vs. time of the polymerization of PGE ($[\text{M}]: [\text{Al}]: [\text{I}] = 200: 2: 1$).	134
Figure A19. GPC traces of poly(PGE). The polymers were analyzed in THF at 35 °C, at 1 mL/min flow rate.....	135
Figure A20. GPC traces of poly(MGE). The polymers were analyzed in THF at 35 °C, at 1 mL/min flow rate.....	135
Figure A21. GPC traces of poly(PGE _{0.x}). The polymers were analyzed in THF at 35 °C, at 1 mL/min flow rate.	136
Figure A22. GPC traces of poly(MGE _{0.x}). The polymers were analyzed in THF at 35 °C, at 1 mL/min flow rate.	136
Figure A23. 500 MHz ^1H NMR spectrum of poly(PGE ₀) in CDCl_3	137
Figure A24. 125 MHz ^{13}C NMR spectrum of poly(PGE ₀) in CDCl_3	138
Figure A25. 500 MHz ^1H NMR spectrum of poly(PGE _{0.20}) in CDCl_3	139
Figure A26. 125 MHz ^{13}C NMR spectrum of poly(PGE _{0.20}) in CDCl_3	140

Figure A27. 500 MHz ^1H NMR spectrum of poly(PGE _{0.40}) in CDCl_3	141
Figure A28. 125 MHz ^{13}C NMR spectrum of poly(PGE _{0.40}) in CDCl_3	142
Figure A29. 500 MHz ^1H NMR spectrum of poly(PGE _{0.50}) in CDCl_3	143
Figure A30. 125 MHz ^{13}C NMR spectrum of poly(PGE _{0.50}) in CDCl_3	144
Figure A31. 500 MHz ^1H NMR spectrum of poly(PGE _{0.55}) in CDCl_3	145
Figure A32. 125 MHz ^{13}C NMR spectrum of poly(PGE _{0.55}) in CDCl_3	146
Figure A33. 500 MHz ^1H NMR spectrum of poly(PGE _{0.60}) in CDCl_3	147
Figure A34. 125 MHz ^{13}C NMR spectrum of poly(PGE _{0.60}) in CDCl_3	148
Figure A35. 500 MHz ^1H NMR spectrum of poly(PGE _{0.65}) in CDCl_3	149
Figure A36. 125 MHz ^{13}C NMR spectrum of poly(PGE _{0.65}) in CDCl_3	150
Figure A37. 500 MHz ^1H NMR spectrum of poly(PGE _{0.70}) in CDCl_3	151
Figure A38. 125 MHz ^{13}C NMR spectrum of poly(PGE _{0.70}) in CDCl_3	152
Figure A39. 500 MHz ^1H NMR spectrum of poly(PGE _{0.75}) in CDCl_3	153
Figure A40. 125 MHz ^{13}C NMR spectrum of poly(PGE _{0.75}) in CDCl_3	154
Figure A41. 500 MHz ^1H NMR spectrum of poly(PGE _{0.80}) in CDCl_3	155
Figure A42. 125 MHz ^{13}C NMR spectrum of poly(PGE _{0.80}) in CDCl_3	156
Figure A43. 500 MHz ^1H NMR spectrum of poly(PGE _{0.85}) in CDCl_3	157
Figure A44. 125 MHz ^{13}C NMR spectrum of poly(PGE _{0.85}) in CDCl_3	158
Figure A45. 500 MHz ^1H NMR spectrum of poly(PGE _{0.90}) in CDCl_3	159
Figure A46. 125 MHz ^{13}C NMR spectrum of poly(PGE _{0.90}) in CDCl_3	160
Figure A47. 500 MHz ^1H NMR spectrum of poly(PGE _{0.95}) in CDCl_3	161
Figure A48. 125 MHz ^{13}C NMR spectrum of poly(PGE _{0.95}) in CDCl_3	162
Figure A49. 500 MHz ^1H NMR spectrum of poly(PGE _{1.0}) in CDCl_3	163
Figure A50. 125 MHz ^{13}C NMR spectrum of poly(PGE _{1.0}) in CDCl_3	164
Figure A51. 500 MHz ^1H NMR spectrum of poly(MGE ₀) in CDCl_3	165

Figure A52. 125 MHz ^{13}C NMR spectrum of poly(MGE ₀) in CDCl_3	166
Figure A53. 500 MHz ^1H NMR spectrum of poly(MGE _{0.20}) in CDCl_3	167
Figure A54. 125 MHz ^{13}C NMR spectrum of poly(MGE _{0.20}) in CDCl_3	168
Figure A55. 500 MHz ^1H NMR spectrum of poly(MGE _{0.40}) in CDCl_3	169
Figure A56. 125 MHz ^{13}C NMR spectrum of poly(MGE _{0.40}) in CDCl_3	170
Figure A57. 500 MHz ^1H NMR spectrum of poly(MGE _{0.50}) in CDCl_3	171
Figure A58. 125 MHz ^{13}C NMR spectrum of poly(MGE _{0.50}). in CDCl_3	172
Figure A59. 500 MHz ^1H NMR spectrum of poly(MGE _{0.55}) in CDCl_3	173
Figure A60. 125 MHz ^{13}C NMR spectrum of poly(MGE _{0.55}) in CDCl_3	174
Figure A61. 500 MHz ^1H NMR spectrum of poly(MGE _{0.60}) in CDCl_3	175
Figure A62. 125 MHz ^{13}C NMR spectrum of poly(MGE _{0.60}) in CDCl_3	176
Figure A63. 500 MHz ^1H NMR spectrum of poly(MGE _{0.65}) in CDCl_3	177
Figure A64. 125 MHz ^{13}C NMR spectrum of poly(MGE _{0.65}) in CDCl_3	178
Figure A65. 500 MHz ^1H NMR spectrum of poly(MGE _{0.70}) in CDCl_3	179
Figure A66. 125 MHz ^{13}C NMR spectrum of poly(MGE _{0.70}) in CDCl_3	180
Figure A67. 500 MHz ^1H NMR spectrum of poly(MGE _{0.75}) in CDCl_3	181
Figure A68. 125 MHz ^{13}C NMR spectrum of poly(MGE _{0.75}) in CDCl_3	182
Figure A69. 500 MHz ^1H NMR spectrum of poly(MGE _{0.80}) in CDCl_3	183
Figure A70. 125 MHz ^{13}C NMR spectrum of poly(MGE _{0.80}) in CDCl_3	184
Figure A71. 500 MHz ^1H NMR spectrum of poly(MGE _{0.85}) in CDCl_3	185
Figure A72. 125 MHz ^{13}C NMR spectrum of poly(MGE _{0.85}) in CDCl_3	186
Figure A73. 500 MHz ^1H NMR spectrum of poly(MGE _{0.90}) in CDCl_3	187
Figure A74. 125 MHz ^{13}C NMR spectrum of poly(MGE _{0.90}) in CDCl_3	188
Figure A75. 500 MHz ^1H NMR spectrum of poly(MGE _{0.95}) in CDCl_3	189
Figure A76. 125 MHz ^{13}C NMR spectrum of poly(MGE _{0.95}) in CDCl_3	190

Figure A77. 500 MHz ^1H NMR spectrum of poly(MGE _{1.0}) in CDCl_3	191
Figure A78. 125 MHz ^{13}C NMR spectrum of poly(MGE _{1.0}) in CDCl_3	192
Figure A79. 500 MHz ^1H NMR spectrum of poly(PGE _{0.57} - Pos _{0.05}) in CDCl_3	193
Figure A80. 125 MHz ^{13}C NMR spectrum of poly(PGE _{0.57} - Pos _{0.05}) in CDCl_3	194
Figure A81. 500 MHz ^1H NMR spectrum of poly(PGE _{0.57} - mPEG550-Pos _{0.05}) in CDCl_3	195
Figure A82. 500 MHz ^1H NMR spectrum of poly(PGE _{0.57} - mPEG750-Pos _{0.05}) in CDCl_3	196
Figure A83. 500 MHz ^1H NMR spectrum of poly(PGE _{0.57} - mPEG2000-Pos _{0.05}) in CDCl_3	197
Figure A84. 500 MHz ^1H NMR spectrum of poly(PGE _{0.57} - mPEG2000-Pos _{0.05}) in CDCl_3 . Peak height was increased for clarity.	198
Figure A85. 500 MHz ^1H NMR spectrum of poly(PGE _{0.57} - Neg _{0.05}) in CDCl_3	199
Figure A86. 125 MHz ^{13}C NMR spectrum of poly(PGE _{0.57} - Neg _{0.05}) in CDCl_3	200
Figure A87. 500 MHz ^1H NMR spectrum of poly(PGE _{0.57} - mPEG550-Neg _{0.05}) in CDCl_3	201
Figure A88. 500 MHz ^1H NMR spectrum of poly(PGE _{0.57} - mPEG750-Neg _{0.05}) in CDCl_3	202
Figure A89. 500 MHz ^1H NMR spectrum of poly(PGE _{0.57} - mPEG2000-Neg _{0.05}) in CDCl_3	203
Figure A90. 500 MHz ^1H NMR spectrum of poly(PGE _{0.57} - mPEG2000-Neg _{0.05}) in CDCl_3 . Peak height was increased for clarity.	204
Figure A91. 500 MHz ^1H NMR spectrum of poly(PGE _{0.57} - Neg _{0.025} - Pos _{0.025}) in CDCl_3	205
Figure A92. 500 MHz ^1H NMR spectrum of poly(MGE _{0.71} - Pos _{0.05}) in CDCl_3	206
Figure A93. 125 MHz ^{13}C NMR spectrum of poly(MGE _{0.71} - Pos _{0.05}) in CDCl_3	207
Figure A94. 500 MHz ^1H NMR spectrum of poly(MGE _{0.71} - mPEG550-Pos _{0.05}) in CDCl_3	208
Figure A95. 500 MHz ^1H NMR spectrum of poly(MGE _{0.71} - mPEG750-Pos _{0.05}). in CDCl_3	209

Figure A96. 500 MHz ^1H NMR spectrum of poly(MGE_{0.71}-mPEG2000-Pos_{0.05}) in CDCl_3	210
Figure A97. 500 MHz ^1H NMR spectrum of poly(MGE_{0.71}-mPEG2000-Pos_{0.05}) in CDCl_3 . Peak height was increased for clarity.	211
Figure A98. 500 MHz ^1H NMR spectrum of poly(MGE_{0.71}-Neg_{0.05}) in CDCl_3	212
Figure A99. 125 MHz ^{13}C NMR spectrum of poly(MGE_{0.71}-Neg_{0.05}) in CDCl_3	213
Figure A100. 500 MHz ^1H NMR spectrum of poly(MGE_{0.71}-mPEG550-Neg_{0.05}) in CDCl_3	214
Figure A101. 500 MHz ^1H NMR spectrum of poly(MGE_{0.71}-mPEG750-Neg_{0.05}) in CDCl_3	215
Figure A102. 500 MHz ^1H NMR spectrum of poly(MGE_{0.71}-mPEG2000-Neg_{0.05}) in CDCl_3	216
Figure A103. 500 MHz ^1H NMR spectrum of poly(MGE_{0.71}-mPEG2000-Neg_{0.05}) in CDCl_3 . Peak height was increased for clarity.	217
Figure A104. 500 MHz ^1H NMR spectrum of poly(MGE_{0.71}-Neg_{0.025}-Pos_{0.025}) in CDCl_3	218
Figure A105. 500 MHz ^1H NMR spectrum of poly(MGE_{0.68}-Neg_{0.10}) in CDCl_3	219
Figure A106. 500 MHz ^1H NMR spectra of poly(PGE_{0.60}) (red), poly(PGE_{0.57}-Pos_{0.05}) (green), and poly(PGE_{0.57}-Neg_{0.05}) (blue) in CDCl_3	220
Figure A107. 500 MHz ^1H NMR spectra of poly(PGE_{0.60}) (red), poly(PGE_{0.57}-Pos_{0.05}) (green), and poly(PGE_{0.57}-Neg_{0.05}) (blue) in CDCl_3 in aliphatic region.	221
Figure A108. 500 MHz ^1H NMR spectra of poly(MGE_{0.75}) (red), poly(MGE_{0.71}-Pos_{0.05}) (green), and poly(MGE_{0.71}-Neg_{0.05}) (blue) in CDCl_3	222
Figure A109. 500 MHz ^1H NMR spectra of poly(MGE_{0.75}) (red), poly(MGE_{0.71}-Pos_{0.05}) (green), and poly(MGE_{0.71}-Neg_{0.05}) (blue) in CDCl_3 in aliphatic region.	223
Figure A110. 500 MHz ^1H NMR spectrum of mDEG azide in CDCl_3	224
Figure A111. 500 MHz ^1H NMR spectrum of decyl azide in CDCl_3	225
Figure A112. 500 MHz ^1H NMR spectrum of mPEG550 OTs in CDCl_3	226
Figure A113. 125 MHz ^{13}C NMR spectrum of mPEG550 OTs in CDCl_3	227
Figure A114. 500 MHz ^1H NMR spectrum of mPEG550 azide in CDCl_3	228

Figure A115. 125 MHz ^{13}C NMR spectrum of mPEG550 azide in CDCl_3	229
Figure A116. 500 MHz ^1H NMR spectrum of mPEG750 OTs in CDCl_3	230
Figure A117. 500 MHz ^1H NMR spectrum of mPEG750 azide in CDCl_3	231
Figure A118. 125 MHz ^{13}C NMR spectrum of mPEG750 azide in CDCl_3	232
Figure A119. 500 MHz ^1H NMR spectrum mPEG2000 OTs in CDCl_3	233
Figure A120. 500 MHz ^1H NMR spectrum of mPEG2000 azide in CDCl_3	234
Figure A121. 125 MHz ^{13}C NMR spectrum of mPEG2000 azide in CDCl_3	235
Figure A122. 500 MHz ^1H NMR spectrum of COOH azide in CDCl_3	236
Figure A123. 125 MHz ^{13}C NMR spectrum of COOH azide in CDCl_3	237
Figure A124. 500 MHz ^1H NMR spectrum of aminium azide in D_2O	238
Figure A125. 125 MHz ^{13}C NMR spectrum of aminium azide in D_2O	239
Figure A126. Study of LCST behavior of poly(PGE_{0.65}) via UV-vis.	240
Figure A127. Study of LCST behavior of poly(PGE_{0.70}) via UV-vis.	240
Figure A128. Study of LCST behavior of poly(PGE_{0.75}) via UV-vis.	241
Figure A129. Study of LCST behavior of poly(PGE_{0.80}) via UV-vis.	241
Figure A130. Study of LCST behavior of poly(PGE_{0.85}) via UV-vis.	242
Figure A131. Study of LCST behavior of poly(PGE_{0.90}) via UV-vis.	242
Figure A132. Study of LCST behavior of poly(PGE_{0.95}) via UV-vis.	243
Figure A133. Study of LCST behavior of poly(PGE_{1.0}) via UV-vis.	243
Figure A134. Study of LCST behavior of poly(MGE_{0.55}) via UV-vis.	244
Figure A135. Study of LCST behavior of poly(MGE_{0.50}) via UV-vis.	244
Figure A136. Study of LCST behavior of poly(MGE_{0.65}) via UV-vis.	245
Figure A137. Study of LCST behavior of poly(MGE_{0.75}) via UV-vis.	245
Figure A138. Study of LCST behavior of poly(MGE_{0.80}) via UV-vis.	246
Figure A139. Study of LCST behavior of poly(MGE_{0.85}) via UV-vis.	246

Figure A140. Study of LCST behavior of poly(MGE_{0.90}) via UV-vis.	247
Figure A141. Study of LCST behavior of poly(MGE_{0.95}) via UV-vis.	247
Figure A142. Hydrodynamic diameter of poly(PGE_{0.55}) determined by DLS.....	248
Figure A143. Hydrodynamic diameter of poly(MGE_{0.60}) determined by DLS.	248
Figure A144. Study of LCST behavior of poly(PGE_{0.60}) via DLS.....	249
Figure A145. Study of LCST behavior of poly(PGE_{0.65}) via DLS.....	249
Figure A146. Study of LCST behavior of poly(PGE_{0.70}) via DLS.....	250
Figure A147. Study of LCST behavior of poly(PGE_{0.75}) via DLS.....	250
Figure A148. Study of LCST behavior of poly(PGE_{0.80}) via DLS.....	251
Figure A149. Study of LCST behavior of poly(PGE_{0.85}) via DLS.....	251
Figure A150. Study of LCST behavior of poly(PGE_{0.90}) via DLS.....	252
Figure A151. Study of LCST behavior of poly(PGE_{0.95}) via DLS.....	252
Figure A152. Study of LCST behavior of poly(MGE_{0.60}) via DLS.	253
Figure A153. Study of LCST behavior of poly(MGE_{0.65}) via DLS.	253
Figure A154. Study of LCST behavior of poly(MGE_{0.70}) via DLS.	254
Figure A155. Study of LCST behavior of poly(MGE_{0.75}) via DLS.	254
Figure A156. Study of LCST behavior of poly(MGE_{0.80}) via DLS.	255
Figure A157. Study of LCST behavior of poly(MGE_{0.85}) via DLS.	255
Figure A158. Study of LCST behavior of poly(MGE_{0.90}) via DLS.	256
Figure A159. Study of LCST behavior of poly(MGE_{0.95}) via DLS.	256
Figure A160. Study of LCST behavior of poly(MGE_{1.0}) via DLS.....	257
Figure A161. DLS results of SC (blue line), poly(PGE_{0.57}-mPEG2000-Pos_{0.05}) (orange line) and SC with 5 μ L of poly(PGE_{0.57}-mPEG2000-Pos_{0.05}) added (green line) in Milli-Q water.	257
Figure A162. DLS results of SC (blue line), poly(PGE_{0.57}-mPEG2000-Pos_{0.05}) (orange line) and SC with 50 μ L of poly(PGE_{0.57}-mPEG2000-Pos_{0.05}) added (green line) in Milli-Q water.	258

Figure A163. DLS results of SC (blue line), poly(PGE _{0.57} -mPEG2000-Pos _{0.05}) (orange line) and SC with poly(PGE _{0.57} -mPEG2000-Pos _{0.05}) added (green line) in Milli-Q water.	258
Figure A164. DLS results of SC (blue line), poly(PGE _{0.57} -mPEG2000-Pos _{0.05}) (orange line) and SC with 5 μ L of poly(PGE _{0.57} -mPEG2000-Pos _{0.05}) added (green line) in PBS.	259
Figure A165. DLS results of SC (blue line), poly(PGE _{0.57} -mPEG2000-Pos _{0.05}) (orange line) and SC with 50 μ L of poly(PGE _{0.57} -mPEG2000-Pos _{0.05}) added (green line) in PBS.	259
Figure A166. DLS results of SC (blue line), poly(PGE _{0.57} -mPEG2000-Pos _{0.05}) (orange line) and SC with poly(PGE _{0.57} -mPEG2000-Pos _{0.05}) added (green line) in PBS.....	260
Figure A167. DLS results of SC (blue line), poly(MGE _{0.71} -mPEG2000-Pos _{0.05}) (orange line) and SC with 5 μ L of poly(MGE _{0.71} -mPEG2000-Pos _{0.05}) added (green line) in PBS.	260
Figure A168. DLS results of SC (blue line), poly(MGE _{0.71} -mPEG2000-Pos _{0.05}) (orange line) and SC with 50 μ L of poly(MGE _{0.71} -mPEG2000-Pos _{0.05}) added (green line) in PBS.....	261
Figure A169. DLS results of SC (blue line), poly(MGE _{0.71} -mPEG2000-Pos _{0.05}) (orange line) and SC with poly(MGE _{0.71} -mPEG2000-Pos _{0.05}) added (green line) in PBS.	261
Figure A170. DLS results of control experiments for SC (dotted line) and SC@poly(MGE _{0.71} -mPEG2000-Pos _{0.05}) (solid line) in Milli-Q water over 48 h.	262
Figure A171. DLS results of control experiments for SC (dotted line) and SC@poly(MGE _{0.71} -mPEG2000-Neg _{0.05}) (solid line) in Milli-Q water over 48 h.....	262
Figure A172. Concentrations of <i>p</i> -nitroaniline converted by SC (blue diamond, 0.04 mg/mL; red square, 0.1 mg/mL; orange triangle, 1.0 mg/mL) over time at room temperature.	263
Figure A173. Concentrations of <i>p</i> -nitroaniline converted by SC (blue diamond, 0.04 mg/mL; red square, 0.1 mg/mL; orange triangle, 1.0 mg/mL) over time at 40 °C.....	263
Figure A174. Concentrations of <i>p</i> -nitroaniline converted by SC (blue diamond, 0.04 mg/mL; red square, 0.1 mg/mL) over time at 50 °C.	264
Figure A175. Concentrations of <i>p</i> -nitroaniline converted by SC (1 mg/mL) over time at 50 °C.....	264
Figure A176. DLS results of SC (dotted line) and SC@poly(MGE _{0.71} -mPEG750-Neg _{0.05}) (solid line) in Tris-HCl buffer at 50 °C for 4 h.....	265

LIST OF SCHEMES

Scheme 1. Anionic ring-opening polymerization (AROP) of epoxides initiated by alkali metal alkoxides. ⁴	2
Scheme 2. Chain transfer reaction in AROP. ⁵	3
Scheme 3. The “activated monomer” reaction mechanism for epoxide ROP, exemplified for the polymerization of propylene oxide (PO). ¹	4
Scheme 4. Epoxide polymerization with bimetallic cobalt catalyst and [PPN][OAc]. ¹² ...	5
Scheme 5. Post-polymerization modification of polymers	6
Scheme 6. Schematic representations of “click” reactions used as PPM.	8
Scheme 7. Proposed mechanism of copper(I)-catalyzed 1,3-dipolar cycloaddition via dinuclear copper intermediate. ⁵³	9
Scheme 8. Synthesis and PPM of poly(PGL) and poly(PGL _{0,x}).	10
Scheme 9. Schematic representation of LCST behavior.	11
Scheme 10. Schematic representation of the properties of poly(PGL _{0,x}) and poly(PGL _{0,x}) as nanocarriers for hydrophobic and the hydrophilic guest molecules.	30
Scheme 11. Synthesis and post-polymerization modification poly(PGL) and poly(PGL _{0,x}). ⁴⁹	32
Scheme 12. Synthesis and polymerization of propargyl glycidyl ether (PGE) and 1,1'-dimethyl propargyl glycidyl ether (MGE).	33
Scheme 13. Proposed mechanism of ring-opening polymerization of functionalized epoxides using triisobutylaluminum (<i>i</i> -Bu ₃ Al) and tetraoctylammonium bromide (Oct ₄ NBr). ⁸	38
Scheme 14. Post-polymerization modification (PPM) of poly(PGE) and poly(MGE) with mDEG azide and decyl azide	44
Scheme 15. PPM of poly(PGE) and poly(MGE) with mDEG azide , decyl azide , mPEG550 azide , mPEG750 azide , mPEG2000 azide , COOH azide , and aminium azide	51
Scheme 16. Synthesis of mPEG550 azide , mPEG750 azide , and mPEG2000 azide . ..	52
Scheme 17. Synthesis of COOH azide	52

Scheme 18. Synthesis of aminium azide	53
Scheme 19. Schematic representation of LCST behavior.....	59
Scheme 20. Schematic representative of azobenzene encapsulation.....	79
Scheme 21. Schematic representation of Subtilisin Carlsberg (SC) encapsulation.	87
Scheme 22. Catalytic hydrolysis of Suc-AAPF- <i>p</i> NA to <i>p</i> -nitroaniline by SC or SC@polymer.....	90
Scheme 23. Schematic representation of SC encapsulation in toluene.	95

KEY TO ABBREVIATIONS

AGE	Allyl glycidyl ether
AROP	Anionic ring-opening polymerization
ATRP	Atom transfer radical polymerization
b.p.	Boiling point
CAB	Carbonic anhydrase B
CuAAC	Copper-catalyzed alkyne-azide cycloaddition
β -CD	β -Cyclodextrin
CHP	Cholesteryl group-bearing pullulan
cmc	Critical micelle concentration
CTAB	Cetyltrimethylammonium bromide
d	Doublet
δ	Chemical shift
Da	Dalton
dd	Doublet of doublets
DLS	Dynamic light scattering
DMF	<i>N,N</i> -Dimethylformamide
ECH	Epichlorohydrin
EEGA	Ethoxy ethyl glycidyl ether
ESG	Enzymatically synthesized glycogen
FG	Functional group
GMA	Glycidyl methacrylate

GPC	Gel permeation chromatography
h	Hour
HSQC	Heteronuclear single quantum coherence
Hz	Hertz
IR	Infrared spectroscopy
<i>J</i>	Coupling constant
LC	Liquid chromatography
LCST	Lower critical solution temperature
m	Multiplet
M	Molar
m/z	Mass of ion (atomic units)/its charge number
MALS	Multiangle light scattering detector
mDEG	Triethylene glycol monomethyl ether
mg	Milligram
MGE	1,1'-Dimethyl propargyl glycidyl ether
MHz	MegaHertz
min	Minute
mL	Milliliter
M_n	Number-average molecular weight
mPGE	Poly(ethylene glycol) monomethyl ether
MS	Mass spectrometry
MSPM	Mixed-shell polymeric micelles
M_w	Weight-average molecular weight

MWCO	Molecular weight cutoff
NMR	Nuclear magnetic resonance
PBS	Phosphate buffered saline
PCL	Poly(ϵ -caprolactone)
PDI	Polydispersity index
PEG	Poly(ethylene glycol)
PEO	Poly(ethylene oxide)
PGE	Propargyl glycidyl ether
Poly(MGE)	Poly(1,1'-dimethyl propargyl glycidyl ether)
PMMA	Poly(methyl methacrylate)
PNIPAM	Poly(<i>N</i> -isopropylacrylamide)
PO	Propylene oxide
Poly(PGE)	Poly(propargyl glycidyl ether)
Poly(PGL)	Poly(propargyl glycolide)
ppm	Part per million
PPM	Post-polymerization modification
PPO	Poly(propylene oxide)
PTFE	Poly(tetrafluoroethylene)
RAFT	Reversible-addition fragmentation chain transfer
<i>rac</i>	Racemic
R_H	Hydrodynamic radius
ROP	Ring-opening polymerization
rt	Room temperature

s	Singlet
SC	Subtilisin Carlsberg
SCNPs	Single-chain nanoparticles
SEC	Size exclusion chromatography
Suc-AAPF- <i>p</i> NA	<i>N</i> -Succinyl-Ala-Ala-Pro-Phe- <i>p</i> -nitroanilide
t	Triplet
TEM	Transmission electron microscopy
<i>tert</i>	Tertiary
T_g	Glass transition temperature
THF	Tetrahydrofuran
TOF	Turnover frequency
Tris-HCl	Tris(hydroxymethyl)aminomethane hydrochloride
UV-Vis	Ultraviolet-visible

Chapter 1. Introduction

1.1. Overview of Polyether Synthesis

Polyethers represent an important class of polymers whose unique properties, in particular the high flexibility, low glass transition temperatures (T_g), and hydrophilicity, arise from their C–O–C backbones. Polyethers are typically synthesized via the ring-opening polymerization (ROP) of epoxide monomers.¹ Among the polyethers, poly(ethylene oxide) (PEO, molecular weight > 30,000 g/mol)/poly(ethylene glycol) (PEG, molecular weight < 30,000 g/mol) is widely used in pharmaceutical, cosmetic, and medical applications as a result of its biocompatibility, non-toxicity and non-immunogenic nature.^{1,2} More recent research has explored syntheses and applications of polyethers where the polyether backbone has pendant chemical functionality. These materials are most often prepared from epoxides bearing functional groups, like those in Figure 1.^{1,3,4}

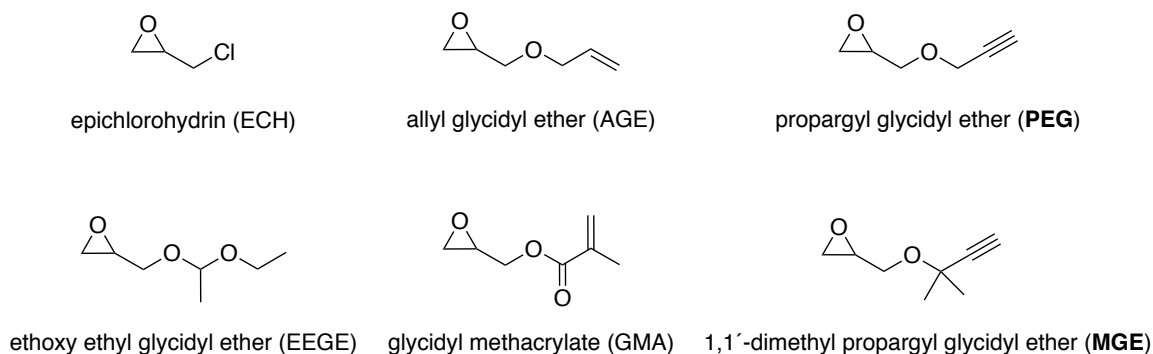
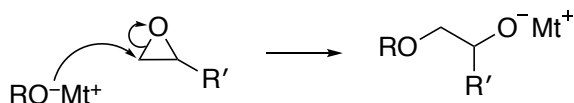


Figure 1. Examples of functionalized epoxides.

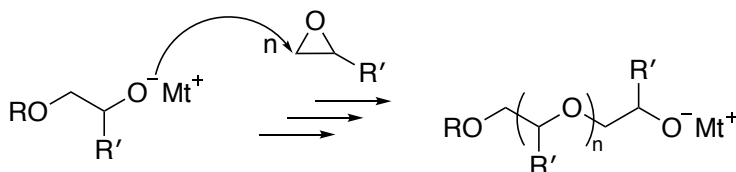
Scheme 1. Anionic ring-opening polymerization (AROP) of epoxides initiated by alkali metal alkoxides.⁴

Initiation Step

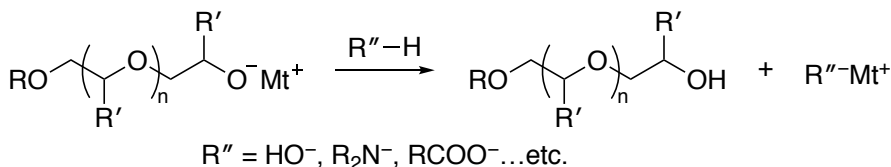


Mt = Na, K, Cs
R = H, alkyl, polymer...etc.

Propagation Step

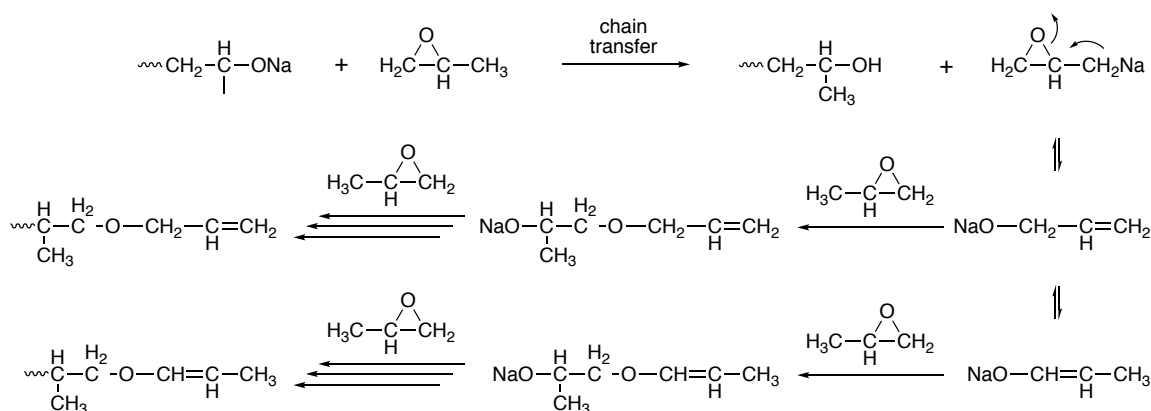


Termination Step



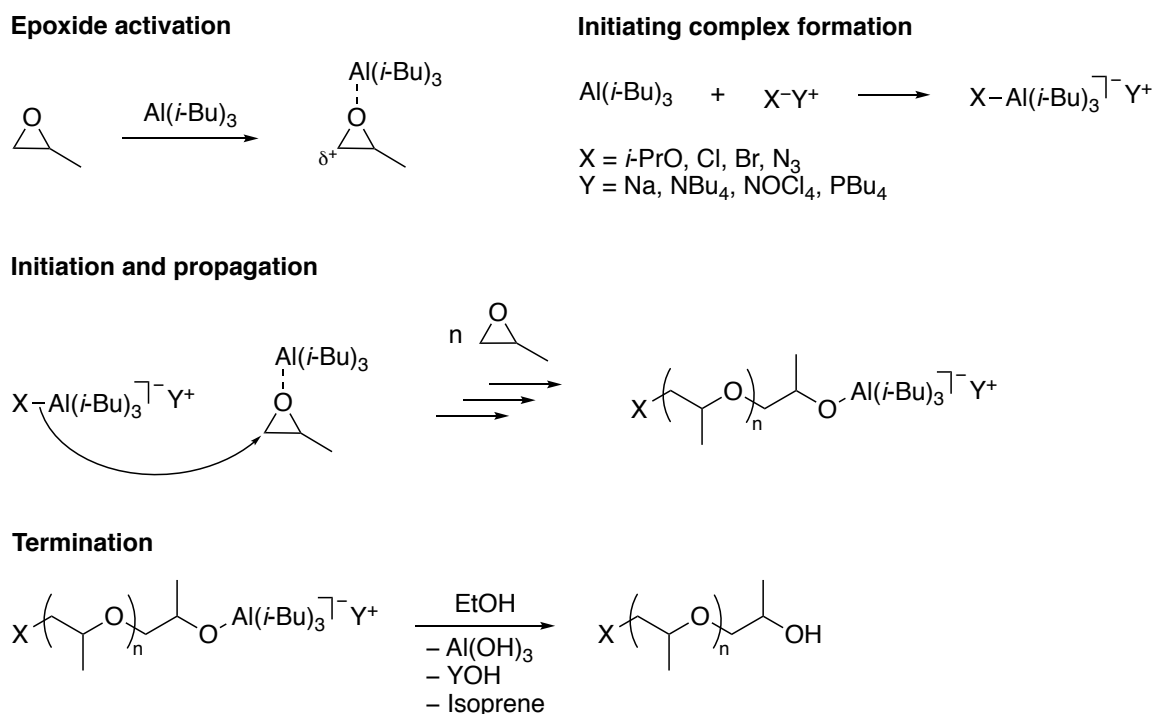
PEO/PEG is often obtained by the anionic ring-opening polymerization (AROP) of ethylene oxide in the presence of metal hydroxide or alkoxide initiator (Scheme 1).^{1,4-6} Alkali metal derivatives (hydrides, alkyls, aryls, amides, and alkoxides) are commonly used initiators and the polymerizations are carried out in polar aprotic solvents when high molecular weights are desired. In AROP, the epoxide monomer undergoes nucleophilic attack by the anionic initiator to generate a new alkoxide species. Subsequent attack by this species on the monomer propagates the chain in an iterative fashion. The addition of alcohols or water terminates AROP. AROP is an efficient method for synthesizing PEO/PEG from ethylene oxide, but AROP of mono-substituted epoxides is hampered by chain transfer side reactions (Scheme 2),⁵ which broaden molecular weight distributions

for the polyethers. Also, the resulting polyethers synthesized from mono-substituted epoxides by AROP are atactic in nature; therefore, the physical properties are different from their stereoregular counterparts. The efforts to overcome the shortcomings have resulted in two main approaches: the activation of the monomers and the formation of stereospecific reactive molecules.



dichloromethane. To date, this method, using specifically triisobutylaluminum (*i*-Bu₃Al) as the catalyst and tetraoctylammonium bromide (Oct₄NBr) as the initiator, has been applied to the synthesis of various mono-functionalized epoxides including the work will be presented in the following chapter.^{4,8}

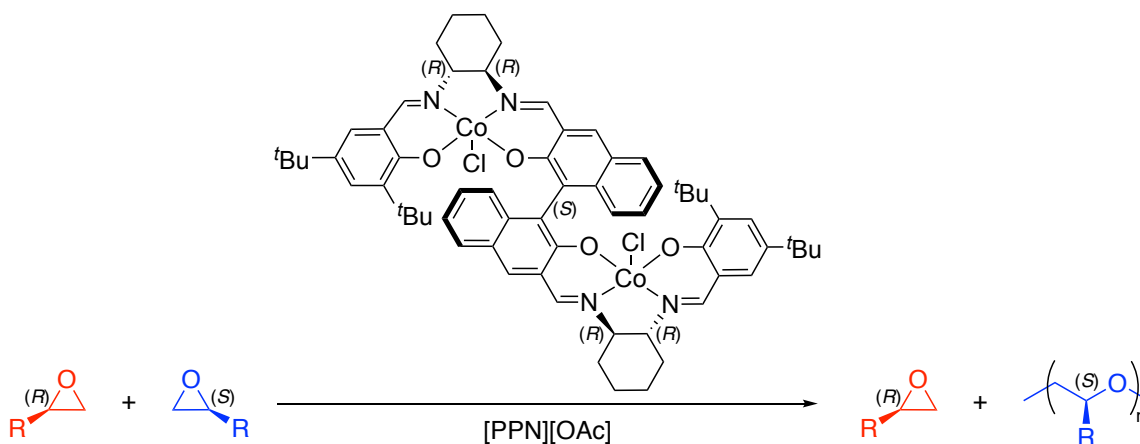
Scheme 3. The “activated monomer” reaction mechanism for epoxide ROP, exemplified for the polymerization of propylene oxide (PO).¹



The polymer stereochemistry, known as tacticity, greatly influences the physical property of the polymers.^{9,10} For instance, PPO synthesized by traditional AROP is a flexible material with a low *T_g* due to its atactic (random stereochemical) backbone. However, isotactic PPO, where all methyl substituents are located on the same side of the zigzag plane of the extended polyether backbone, is semicrystalline. Although the discovery of isotactic PPO was reported in 1949, further advance in the synthesis of

stereoregular PPO was not made until recent years.¹⁰ Among the various catalysts, a cobalt-based system developed by Coates and co-workers is especially attractive.^{11,12} In 2005, Coates and co-workers published the first catalyst to generate regioregular *rac*-isotactic PPO from *rac*-PO.¹¹ As shown in Scheme 4, in 2008, a homogeneous bimetallic catalyst, which is activated by an ionic cocatalyst salt, bis(triphenylphosphine)iminium acetate ([PPN][OAc]), was used for the polymerization of a variety of mono-substituted epoxides.¹² This bimetallic catalyst and cocatalyst system is capable of kinetically resolving racemic epoxides into valuable enantiopure epoxides and isotactic polyethers with high turnover frequencies (TOFs) up to 30,000 h⁻¹.¹²⁻¹⁴ This bimetallic cobalt catalyst system remains one of the most efficient system for synthesizing isotactic PPO but the synthesis of the ligand for the catalyst is non-trivial with low total yield. In 2018, Coates and co-workers reported a new bimetallic chromium system to overcome the high polydispersity indices (PDIs) of the isotactic PPOs obtained by the cobalt system.¹⁵

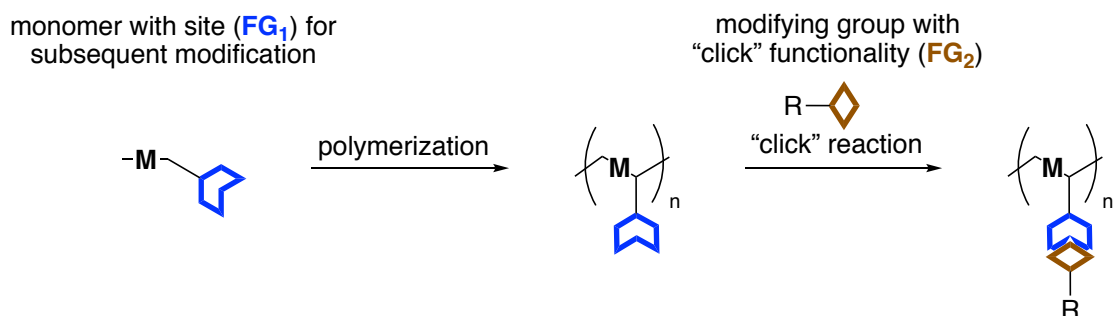
Scheme 4. Epoxide polymerization with bimetallic cobalt catalyst and [PPN][OAc].¹²



1.2. Overview of Post-Polymerization Modification

Post-polymerization modification (PPM) of polymers is a valuable approach for synthesizing a range of polymers with diverse properties from a single polymer synthon.^{16–23} PPM not only overcomes the limited functional group tolerance of many common polymerization techniques, but it also reduces the number of synthetic steps when new polymers are synthesized. Scheme 5 illustrates the PPM concept. Monomers bearing certain functional groups (FG₁), which are inert toward polymerization conditions, are polymerized. Subsequent reactions with modifying groups (FG₂) allows to transform the polymer synthon into a variety of different polymers.

Scheme 5. Post-polymerization modification of polymers

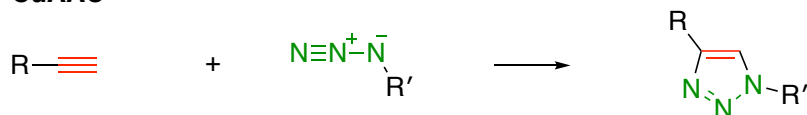


For PPM to be effective, the polymer synthon must possess a functional group that reacts with molecular or macromolecular entities with high fidelity and broad compatibility with other functionalities. In the most synthetically-flexible examples, reactions can be carried out in a wide range of solvents. It is possible in this way to prepare polymers that are otherwise difficult—even impossible—to prepare by direct polymerization of functional co-monomers. Among the various synthetic strategies for PPM, “click” chemistry is a powerful and an effective way for fabricating polymer architectures.^{24–27}

The term “click” chemistry was first introduced by Sharpless and co-workers in 2001.²⁸ It refers to reactions that are “*modular, wide in scope, high yields, generating only inoffensive byproducts that can be removed by nonchromatographic methods, and stereospecific.*” Copper(I)-catalyzed 1,3-dipolar cycloaddition of azides and alkynes (CuAAC), developed simultaneously by Fokin, Sharpless and co-workers²⁹ and Meldal and co-workers^{30,31} is one of the most used “click” reactions. Several other types of reaction have also been identified to fulfill these criteria such as thiol-ene addition,^{32–38} thiol-yne addition,^{39–41} Diels-Alder cycloaddition,^{42,43} and Michael addition (Scheme 6).^{38,44} CuAAC^{24,45–51} for PPM will be discussed further since it is the “click” reaction used for PPM in this thesis.

Scheme 6. Schematic representations of “click” reactions used as PPM.

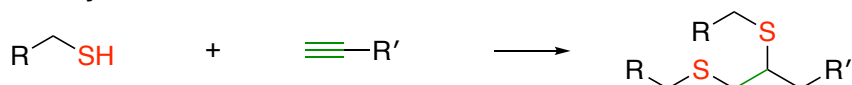
CuAAC



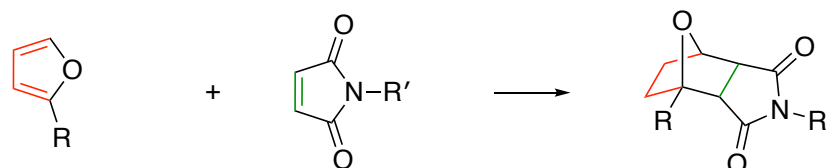
Thiol-ene



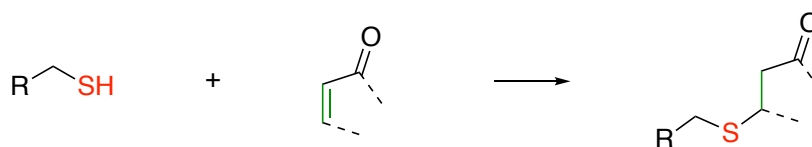
Thiol-yne



Diels-Alder



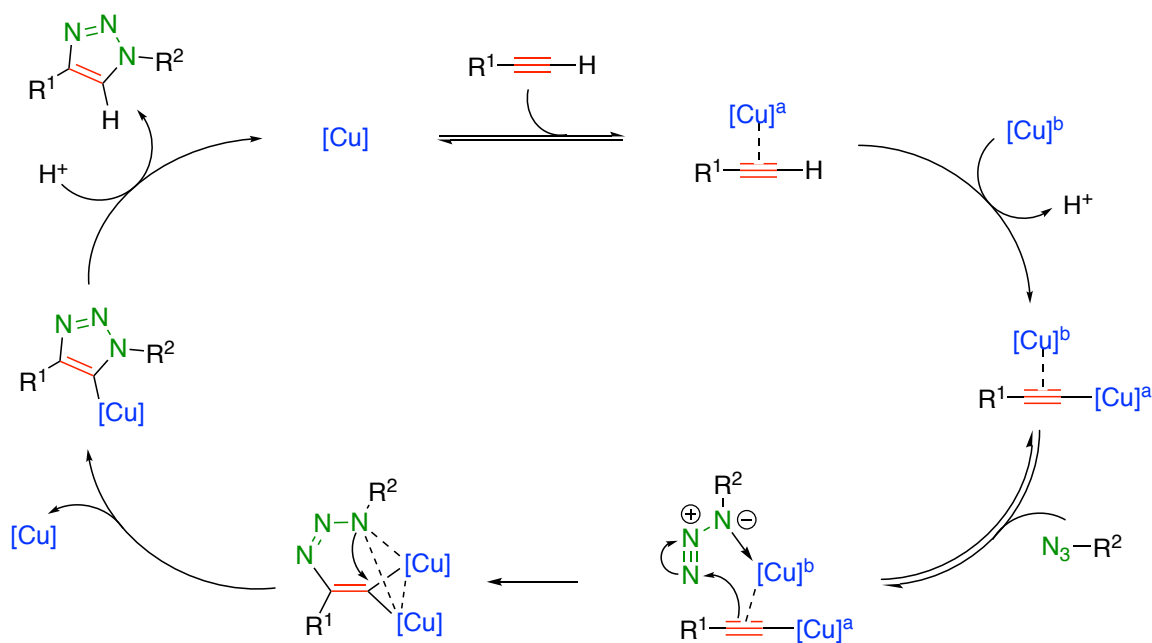
Michael addition



The classic thermal Huisgen 1,3-dipolar cycloaddition of azides and alkynes often yields a mixture of regioisomers hence it fails to meet the criteria of “click” chemistry.⁵² However, CuAAC affords the 1,4-disubstituted regioisomer with high fidelity and has broad functional group tolerance under a wide range of reaction conditions. Additionally, the products can usually be purified by nonchromatographic methods. This makes it a great fit as a “click” reaction. Fokin and co-workers conducted extensive research on the mechanism of CuAAC and found direct evidence for a dinuclear copper intermediate in CuAAC.⁵³ Scheme 7 shows the proposed mechanisms of CuAAC from Fokin and co-

workers. The reaction begins with the π -complexation of the acetylene to the first copper ($[\text{Cu}]^a$). Then coordination of the second copper ($[\text{Cu}]^b$), is accompanied by proton loss and migration of $[\text{Cu}]^a$ to generate a σ -bound acetylide. Then, the reversible coordination of the organic azide to the active complex results in the formation of the dinuclear copper intermediate. After the generation of C-N bond and the removal of one copper, a triazolyl-copper derivative is formed. Protonation of Cu-C bond releases the triazole product and reforms the initial copper catalyst.

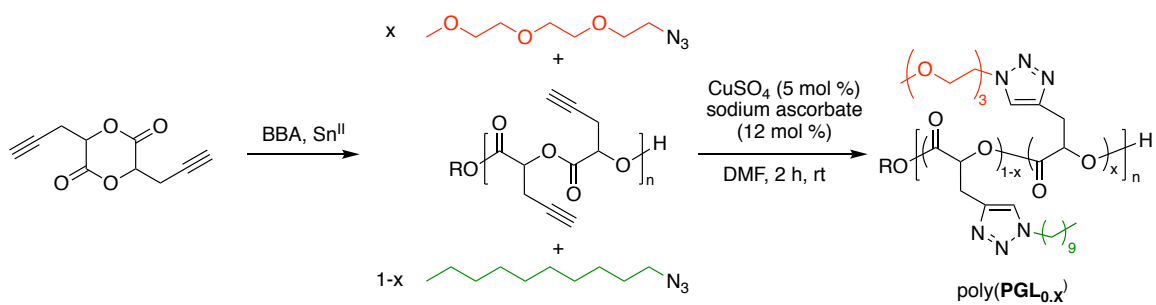
Scheme 7. Proposed mechanism of copper(I)-catalyzed 1,3-dipolar cycloaddition via dinuclear copper intermediate.⁵³



In previous research done in our group, “clickable” polyglycolides, poly(propargyl glycolide) (poly(**PGL**)) were synthesized and applied CuAAC as PPM to modify the properties of poly(PGL)s (Scheme 8).⁴⁹ Hydrophilic azide, 1-(2-azidoethoxy)-2-(2-methoxyethoxy)-ethane (**mDGE azide**), and hydrophobic azide (**decyl azide**), 1-

azidodecane, were used to synthesize the amphiphilic polymers, poly(**PGL**_{0,x}), where X = the mole fraction of hydrophilic azide incorporated in the polymer. poly(**PGL**_{0,x}) presented several properties that will be reviewed in the following sections.

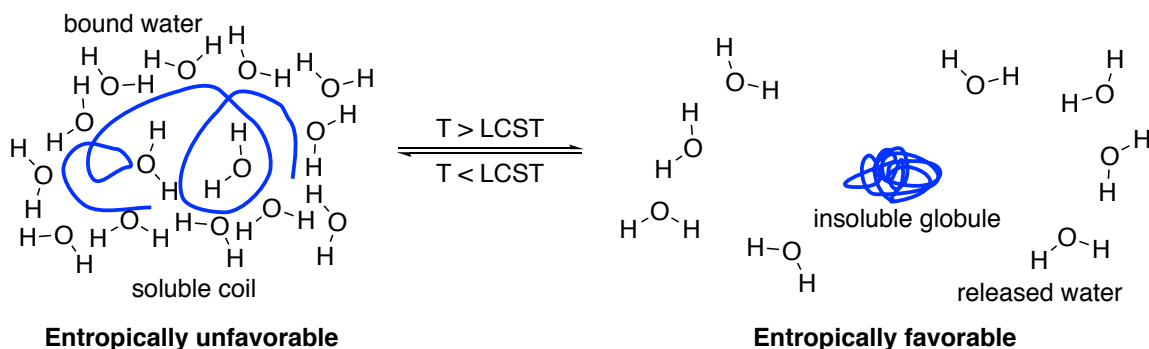
Scheme 8. Synthesis and PPM of poly(**PGL**) and poly(**PGL**_{0,x}).



1.3. Overview of Lower Critical Solution Temperature (LCST)

PPM is also a convenient tool for designing stimuli-responsive polymers.^{54–57} Stimuli-responsive polymers, which are capable of chemical or conformational changes in response to external stimuli, have attracted attention in diverse applications such as biomedical and drug delivery,^{58–63} sensing,^{64–67} smart surfaces,⁶⁸ and biological interfaces.⁶⁹ Temperature,^{20,70–76} pH,^{77,78} and light,^{79–81} are a few examples of stimuli that can induce a change in polymer properties. Thermoresponsive polymers are an interesting class of stimuli-responsive materials. A common temperature response is a change in polymer solubility. Certain polymers precipitate from solution, typically aqueous, when the temperature is *increased*. This phenomenon is referred to as lower solution temperature (LCST) behavior (Scheme 9).^{71,75,82–85}

Scheme 9. Schematic representation of LCST behavior.



An early challenge in polymer chemistry was understanding the deviation of phase behaviors of polymer solutions from the law for ideal solutions of ions and small molecules. Independently, Flory^{86,87} and Huggins^{88,89} proposed theories for these phase behaviors of polymer solutions, but explaining phase separation of polymer solutions at temperatures above the LCST remained a great challenge. Although LCST was known to exist in other systems, the first experimental results of LCST phenomenon in non-polar polymer solutions was observed in 1960 by Freeman and Rowlinson.⁹⁰ In many polymer systems, the critical temperature was close to the boiling point of the solvent. Hence, the difficulty for observations was the result of the increasing system pressures at critical temperatures.⁹¹

LCST behavior of polymer solutions can be understood in terms of the entropy of solvation, ΔS_{solv} . For some water-soluble polymers, the water molecules in the solvation sphere are highly ordered and $\Delta S_{\text{solv}} < 0$. As the temperature is increased, the polymer precipitates when $|T\Delta S_{\text{solv}}| > |\Delta H_{\text{solv}}|$ (i.e., $\Delta G_{\text{solv}} > 0$). One of the most studied polymers exhibiting LCST behavior in water are poly(N-isopropylacrylamide) (PNIPAM) and its copolymers for their potential in biomedical applications.^{60,65,66,75,92–94} Previous research done in our group on amphiphilic degradable mDEG/alkyl-grafted poly(propargyl

glycolide) polymers, p-PGL_{0,X}, where **X** is the mole fraction of mDEG side chains, showed tunable LCST behavior by adjusting the ratio between hydrophilic and hydrophobic side chains.^{49,95}

1.4. Overview of the Formation of Unimolecular Micelles (Unimicelles)

The term unimolecular micelles, first described by Newkome and co-workers,^{96,97} was used to refer to depicting spherical single molecular polymers that are capable of molecule inclusion. These cascade polymers, now known as dendrimers, are one of the earliest examples of unimicelles.^{97,98} Since then, dendrimers have been attractive materials for various applications.^{99–106} Two major strategies have been developed for dendrimer synthesis, the so-called divergent and convergent synthesis.^{100,101,103,107} The divergent method, also known as “inside-out” strategy, is the growth of a dendron from the core of the dendrimer to the molecular surface. The convergent method, also known as “outside-in” strategy, starts the synthesis from the molecular surface inward to the focal point at the core. Dendrimers are important examples of unimicelles, but their syntheses require multiple steps and the number of branches from the core limits their size, which seldom exceeds 10 nm diameter.

In the past two decades, interest in the formation of the single-chain polymeric nanoparticles by chain-collapse has increased.^{108–115} These single-chain nanoparticles (SCNPs) also exhibit properties associated with unimicelles. Three models of chain-collapsing were proposed for the construction of SCNPs: homofunctional, heterofunctional, and cross-linker mediated collapse (Figure 2).¹¹⁵ Homofunctional collapse is where the polymer chain is functionalized with one type of reactive pendent groups that react

intramolecularly through covalent bonding or non-covalent interactions. In the heterofunctional collapse model, the polymer chain carries two functional side chains, which undergo intramolecular reaction to form SCNPs. The cross-linker mediated collapse involves the reaction between a monofunctional polymer and bifunctional cross-linkers.

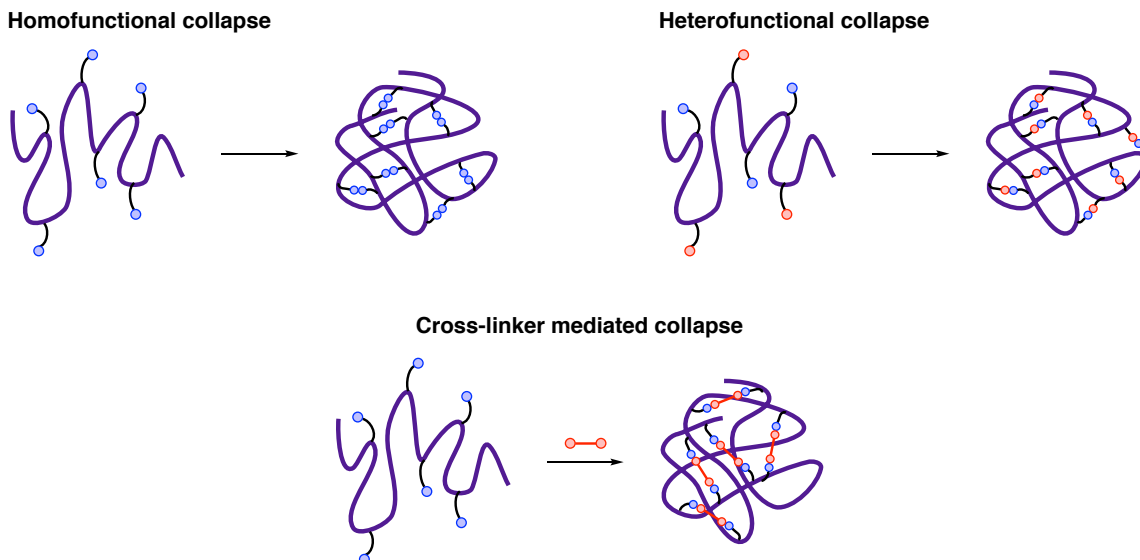
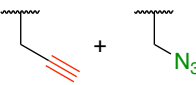
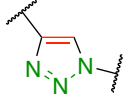
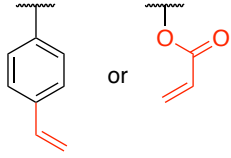
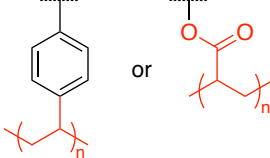
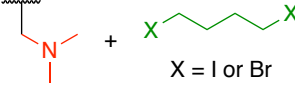
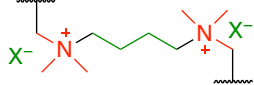

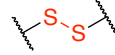
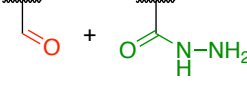
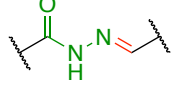
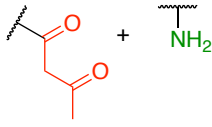
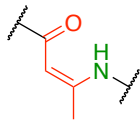
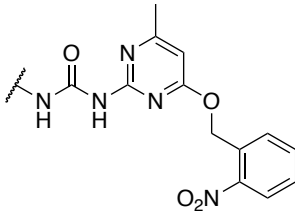
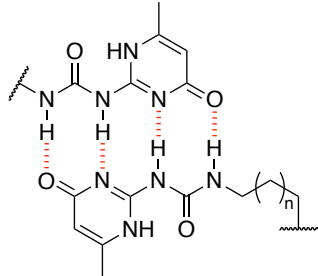


Figure 2. Models for intermolecular cross-linking of a polymer chain.¹¹⁵

Three synthetic approaches for intramolecular cross-linking have been employed to the formation of SCNPs: irreversible covalent, reversible covalent (dynamic), and noncovalent cross-linking (Table 1).¹¹⁵ “Click” reactions,¹¹² free radical coupling of alkenes,¹¹⁶ and amine quaternization¹¹⁷ are few of the examples that have been used for irreversible covalent cross-linking. Dynamic covalent cross-linking is achievable by disulfide,¹¹⁸ hydrazone,¹¹⁹ and enamine chemistry.¹²⁰ Hydrogen bonding,¹²¹ hydrophobic interaction,¹²² and metal complexation¹²³ are often applied in noncovalent cross-linking. The synthesis of SCNPs allows for precise size control and tailored functionality. The

increasing interest in SCNPs also prompted further research on their potential applications.^{19,113,124–126} Although much progress has been made, challenges remain.¹¹⁴

Table 1. Examples for cross-linking chemistry for the formation of SCNPs.¹¹⁵

Cross-linking chemistry (Model)	FG precursors	Cross-linked structure
CuAAC “click” chemistry (Hetero)		
Free radical coupling (Homo)		
Amine quaternization (Cross-linker)		
Disulfide chemistry (Homo)		
Hydrazone chemistry (Hetero)		
Enamine chemistry (Hetero)		
Upy dimerization (Homo)		

1.5. Overview of Nanocarriers

Nanoparticles, which can be prepared from metals, ceramics, polymeric materials, and composite materials, are defined as particles with at least one dimension sized between 1 to 100 nm. With unique size-dependent properties different from the bulk materials, extensive research has invested in exploring applications in electronics,¹²⁷ energy,^{128,129} and medical fields.^{130–139} The development of functional nanoparticles is a relatively new avenue toward advancement in biological and medical fields for applications such as imaging, sensing, and delivery.^{63,130,132,134,140,141} It has been shown that engineered functional nanoparticles can improve the solubility of poorly water soluble drugs, enhance drug half-life by reducing immunogenicity, and achieve controlled releasing and targeted delivery.^{130,131,139,142–144} To date, some therapeutic nanoparticle platforms have been approved and commercialized, and many others have entered clinical trials (Figure 3).¹⁴³ In the following, nanocarriers will be used to describe these therapeutic nanoparticle platforms.

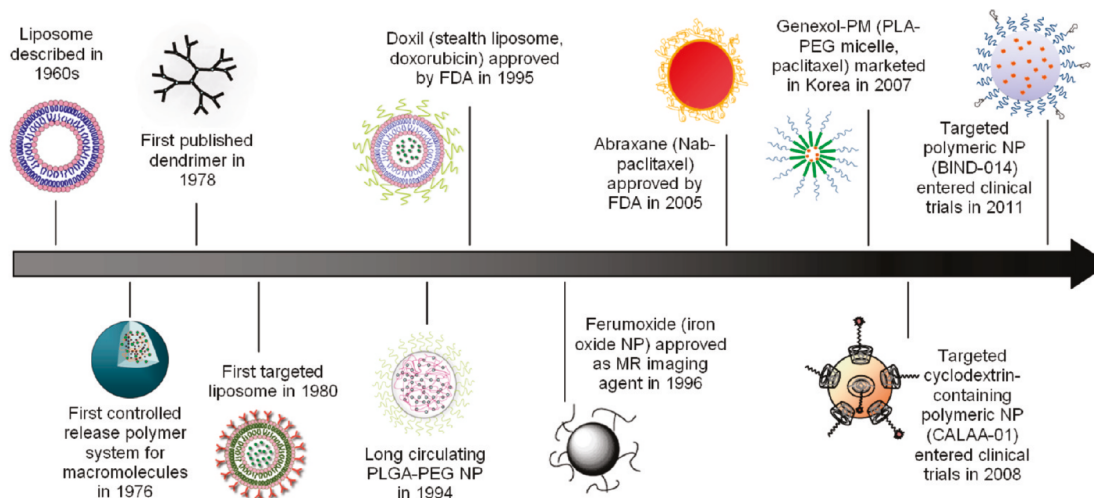


Figure 3. Historical timeline of clinical-stage nanoparticle technologies. Reprinted from ref. 143. Copyright 2011 American Chemical Society.¹⁴³

Liposomes, first reported in 1960s,^{145,146} are spherical vesicles formed by one or more phospholipid bilayers with size between 50 to 100 nm.¹³⁴ Liposomes are attractive nanocarriers because they are biocompatible, biodegradable, non-toxic, and non-immunogenic. In addition, liposomes can encapsulate both hydrophobic and hydrophilic guest molecules.^{131,134,139,141} The similarity between liposomes and cellular membranes assists in delivering the guest molecules into the cell. In 1995, liposomes became the first nanocarrier to reach commercialization with the FDA approval of DOXIL (doxorubicin-liposome).¹⁴³ Since then, liposomal formulations have been widely utilized for *in vivo* delivery.¹⁴⁷ Despite their significant impact as nanocarriers, liposomes have limitations. For example, the common synthesis of liposomes first generates multilamellar vesicles, which have several bilayers, and the single vesicles that are obtained via sonication often have broad size distributions.¹⁴⁸ Further processing is required for reducing their

polydispersity. Moreover, burst release of guest molecules from liposomes is common and often undesirable.^{131,137,149}

Polymeric micelles, generated by self-assembly of amphiphilic block copolymers in aqueous solutions, have also been used as nanocarriers.^{130,131,139,141,144,150–153} Polymeric micelles consist of hydrophobic core and hydrophilic corona, and are thus similar to micelles constructed from conventional detergents, but are usually more stable owing to low critical micelle concentrations (cmc).¹³³ One advantage of polymeric nanocarriers is that they can be prepared in a simple and reproducible manner with precise control over morphology and architecture.^{133,154–156} The tunability of the designs makes it possible to produce stimuli-responsive or targeted delivery vehicles. Moreover, polymeric nanocarriers are often made with biocompatible and biodegradable materials, which are important criteria for biomedical applications.

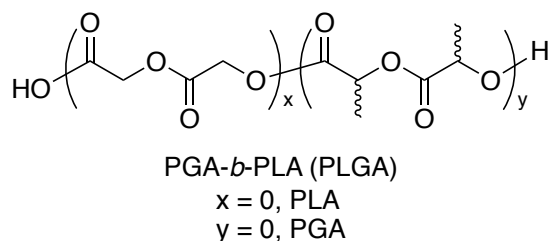


Figure 4. Structure of poly(lactic-*co*-glycolic acid) (PLGA).¹⁵⁷

Aliphatic polyesters derived from lactide, glycolide, and ϵ -caprolactone are especially attractive materials for delivery application.¹⁵⁸ Delivery devices composed by US Food and Drug Administration(FDA)-approved poly(lactic-*co*-glycolic acid) (PLGA) polymers have been an important component in some commercialized drugs such as Lupron Depot and Decapeptyl (Figure 4).¹⁵⁷ PEG/PEO is one of the most studied non-

degradable biocompatible polyethers and is widely used in composing nanocarriers. PEG is often used with PLA in block copolymers because PLA is water insoluble. PEG's hydrophilicity makes PLA-*b*-PEG polymers water soluble.^{159,160} Although there have been many successes, micelle formation is still concentration-dependent, which can pose challenges for these polymeric nanocarriers (Figure 5).^{131,161,162} As mentioned in previous section, SCNPs, which can function as unimicelles in solution, have unique features as nanocarriers for delivery applications.^{19,113,124–126}

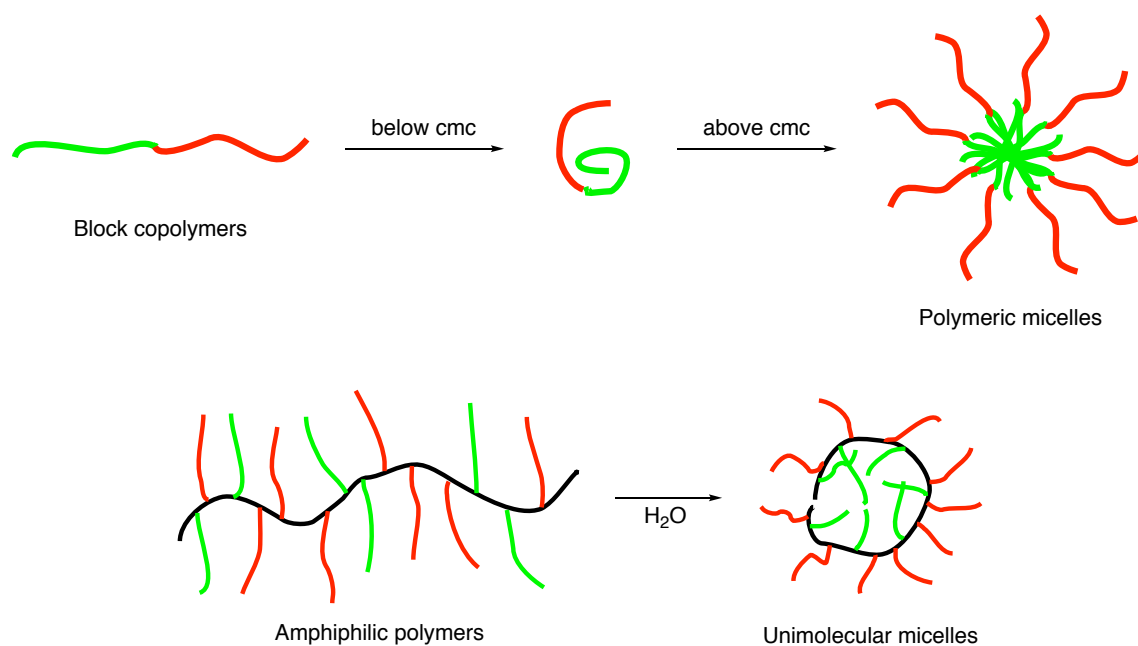


Figure 5. Schematic illustration of the formation of polymeric micelles and unimicelles.

1.6. Overview of the Synthesis of Biocatalysts

As interest in nanocarriers as delivery vehicles has grown, research on coupling nanomaterials and biology, dubbed bionanotechnology, has also blossomed.^{163,164} One particular area drawing significant attention is advancing biocatalysis by conjugating

proteins with synthetic polymers.¹⁶⁵ As shown in Figure 6, the first polymer-protein conjugates, specifically, PEG-enzyme conjugates, were approved by FDA in 1990s, but the concept of PEG-protein conjugation, now known as PEGylation, was first envisioned and pioneered by Davis and co-workers.^{166–168} PEGylation is now a well-established method that is used to enhance the solubility and stability of enzymes and to decrease the immunogenicity. Since then, many researches have been focused on developing various types of biocatalysts to expand applications of enzyme on different fronts.^{165,168–171}

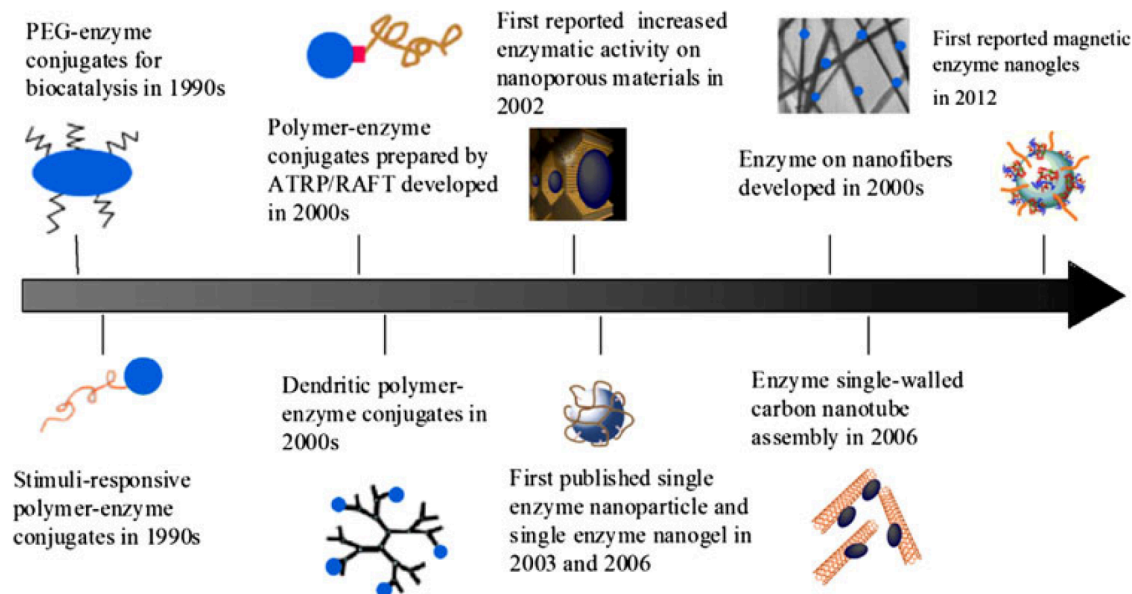


Figure 6. Timeline of nanotechnology-based biocatalysts. Reprinted from ref. 165. Copyright 2012 Springer Science+Business Media New York.¹⁶⁵

Enzyme immobilization can be an effective method and is used routinely in industry.^{172–176} Enzyme immobilization facilitates their handling, reusing, and isolation ...etc., therefore minimizing the protein contamination to other products during the process. It was also shown that immobilized enzymes have increased stability and/or

improved activity or selectivity.^{174,176} Enzyme immobilization is categorized into three types: support binding, entrapment, and cross-linking. Support binding can be accomplished by hydrophobic or van der Waals interactions, electrostatic interactions, or covalent binding. Depending on the strength of the interactions, leaching or reusability are potential issues. Entrapment can be used to confine enzymes in a polymer matrix, but extra treatment may be needed to prevent enzyme leaching. Cross-linking of enzymes is a support-free approach that uses bifunctional reagents to make intermolecular connections between enzymes. Reaction rates can increase significantly because the concentration of active sites is higher than when enzymes are attached to an inert support.

Polymer-enzyme conjugates offer the potential of merging the advantages from both worlds.^{165,168–170,177,178} The implement of polymers renders the conjugates soluble in aqueous or organic environments, which is beneficial for substrates with poor water solubility. By using stimuli-responsive polymers, recyclable polymer-enzyme conjugates can be designed that preserve the benefits of immobilization. In addition, the properties of polymer-enzyme conjugates can be modified by changing the polymer architecture and composition. Polymer-enzyme conjugates can be synthesized by two methods: “grafting to” or “grafting from”. “Grafting to” starts with presynthesized, end-functionalized polymers whose functionality reacts with accessible amino acid side chains or end termini on the enzymes. A wide variety of monomers and polymers that can be used in the “grafting to” method, but excess polymer reactants is often required to fully convert the native enzyme to the conjugate form. The separation of unreacted polymer from the conjugates can be difficult. In the “grafting from” method, the polymerization is initiated directly from the surface of enzymes via controlled radical polymerization. Atom transfer radical

polymerization (ATRP) and reversible-addition fragmentation chain transfer (RAFT) are often employed since both polymerizations can be performed under biological relevant conditions. Separation of unreacted monomer is easier in “grafting from” method and obtaining high polymer density conjugates is achievable.

1.7. Protein Folding and Molecular Chaperones

Protein folding converts newly synthesized polypeptide chains into their native three-dimensional structures.^{179–184} In the early 1960s, Anfinsen and co-workers conducted groundbreaking protein folding experiments with ribonuclease A (RNase A), which catalyzes the cleavage of RNA into ribonucleotides.^{185–188} By adding and removing a denaturant and a reducing agent, the catalytic activity of RNase A was suppressed and restored, respectively. Assuming the catalytic activity of RNase A only exists when it folds into its proper three-dimensional structure, Anfinsen and co-workers concluded that RNase A was unfolded and refolded reversibly *in vitro*. They also demonstrated that the structural information of RNase A is encrypted in its amino acid sequence.^{185–188} These conclusions provided the foundation for the thermodynamic hypothesis for protein folding. The thermodynamic hypothesis states that the native structure of a protein is determined solely by the intrinsic properties of its amino acid sequence and is not the result of an external template.

Thermodynamics is considered to be the governing factor for protein folding.^{187–189} In the free-energy landscape of protein folding, shown in Figure 7, the native state of the protein resides at a local energy minimum and unfolded conformations occupy at higher energies, where each of the conformations folds along a unique pathway. The folding

energy landscape allows proteins to fold into their native structure within a reasonable amount of time. However, the unfolded conformation can also follow a reaction coordinate to undesired minima like amorphous aggregates and amyloid fibrils.

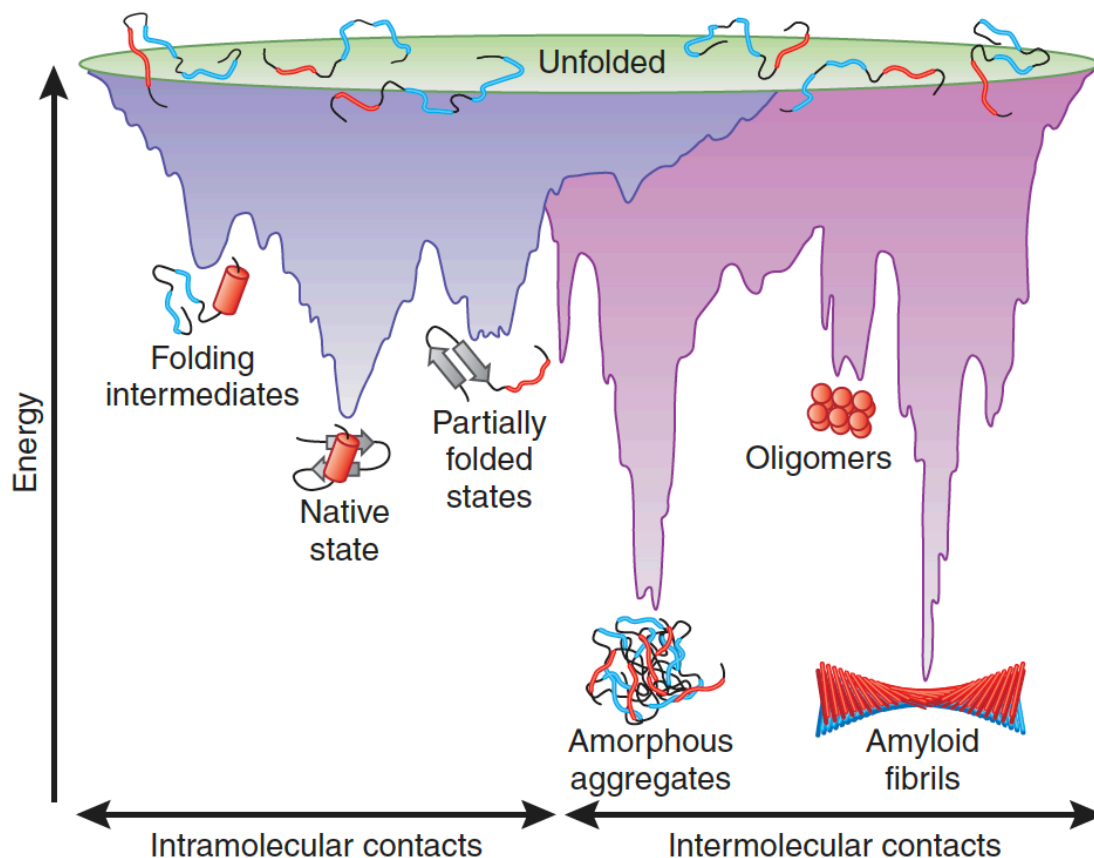


Figure 7. Energy landscape scheme of protein folding and aggregation. Reprinted from ref. 182. Copyright 2009 Nature America, Inc.¹⁸²

Hydrophobic interactions between hydrophobic protein residues, driven by the entropic gains as water molecules are expelled from the solvation sphere, is the main driving force for protein folding.^{184,190–192} In addition, noncovalent interactions such as hydrogen bonding,¹⁸⁴ salt-bridge interaction,¹⁹³ and aromatic-aromatic interaction¹⁹⁴ can

further stabilize the native structure. Hydrophobic interactions are not only the key driving force for protein folding but also the cause of protein aggregation at high concentration of unfolded or partially folded proteins. When high concentration of unfolded or partially folded proteins are present in solution, the intermolecular hydrophobic interaction between the exposed hydrophobic residues can lead to amorphous aggregates or amyloid fibrils at or near the global minimum of reaction coordinate. Amyloid fibrils, the irreversibly ordered fibrils, are related to neurodegenerative diseases, such as Alzheimer's disease, Parkinson's disease and spongiform neuro encephalopathies.^{187,195} Although the formation of amorphous aggregates or amyloid fibrils can be thermodynamically favored, cells have developed strategies to avoid or reduce the formation of aggregates in the early stage (Figure 8).

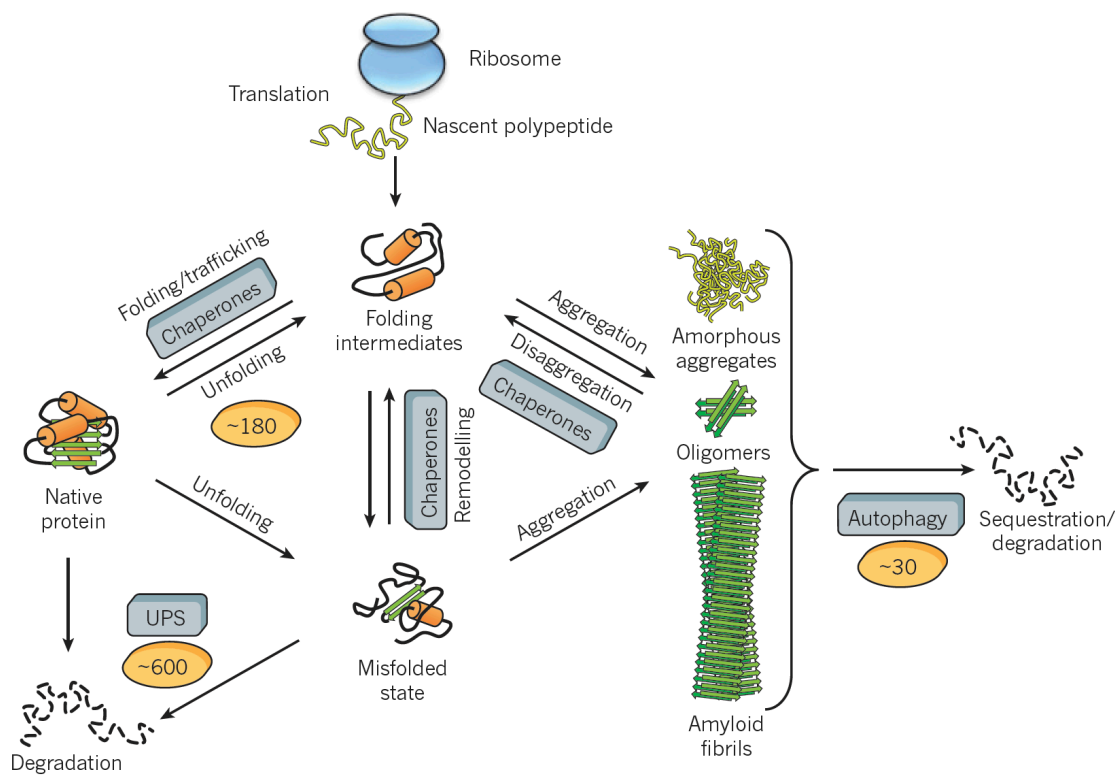


Figure 8. Protein fates in the proteostasis network. Reprinted from ref. 196. Copyright 2011 Macmillan Publishers Limited.¹⁹⁶

Molecular chaperones, whose functions include preventing protein aggregation, assisting proper protein folding and assembly, and disassembling aggregates or misfolded proteins, are functionally related families of proteins.^{181,182,187,196–201} Molecular chaperones often convert between two states, driven by adenosine triphosphate (ATP) binding and hydrolysis. In one state, chaperones have the ability to bind unfolded or partially folded polypeptides via hydrophobic interactions to prevent aggregation. In the other state, the binding affinity decreases to release the protein. Molecular chaperones bind to the unfolded or partially folded polypeptides to impede protein aggregation. They can also induce conformational changes in misfolded proteins to assist correct protein folding.

One of the most studied molecular chaperone families is a bacterial chaperonin system, known as GroEL and GroES.^{182,187,197–199,202} The term “GroE” is from the name of a bacterial gene that was discovered and the “L” and “S” in GroEL and GroES indicates the larger and the smaller of the two subunits. Three structural domains can be found in GroEL, the apical domain containing binding sites for unfolded proteins, intermediate, and equatorial domain containing the ATP-binding site. The internal structure of GroEL is a hollow cylinder divided by the equatorial domain to form two cage-like chambers, known as Anfinsen cages. The co-chaperone GroES is a dome-like structure acts as a cap while binding to GroEL. GroES and ATP are bound to GroEL after the unfolded polypeptide chain enters GroEL. This isolated environment allows polypeptide to fold into the native state without aggregation, with the hydrolysis of ATP functioning as a timer to open the chambers and to release the folded protein (Figure 9).¹⁸⁷

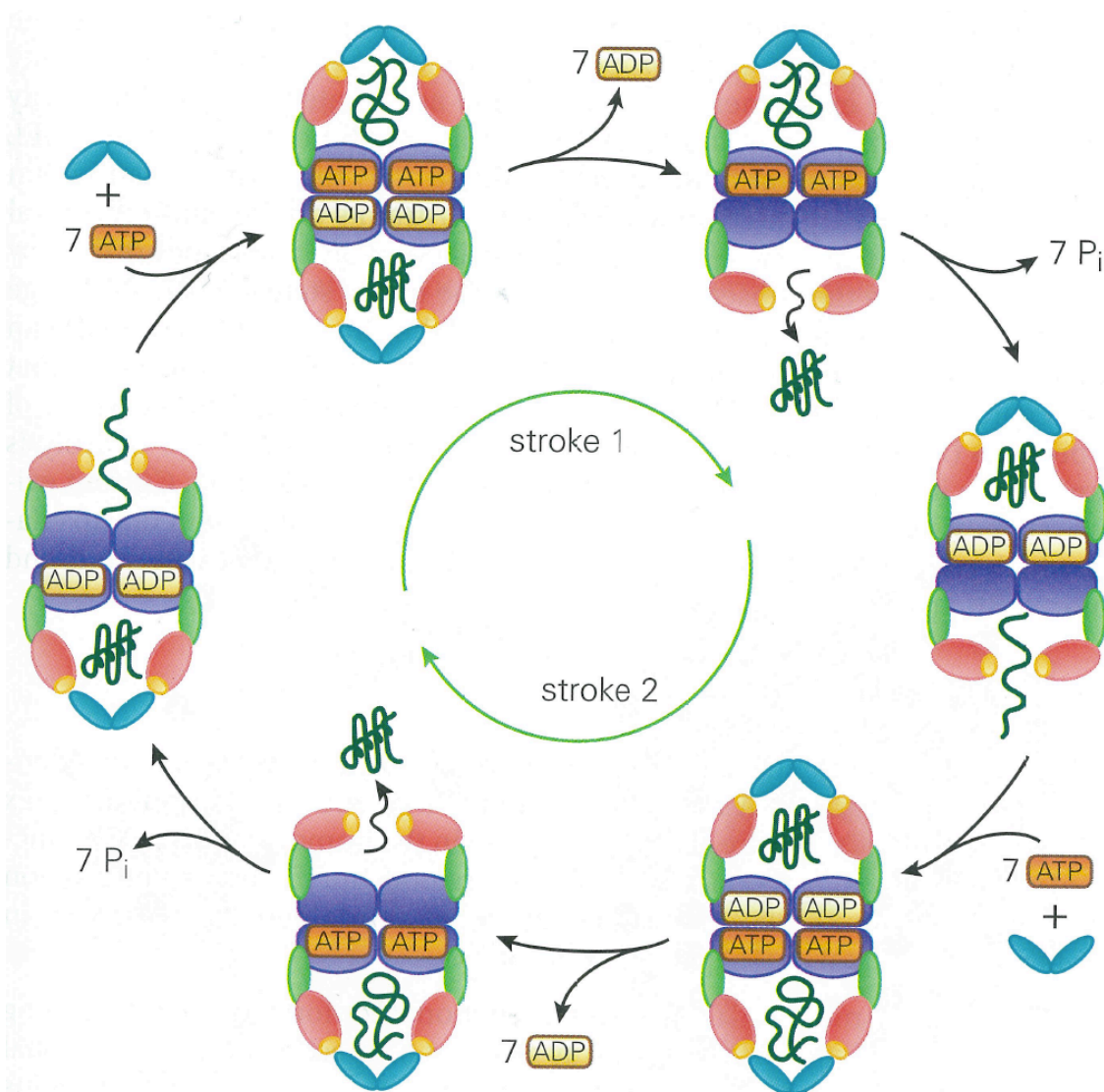


Figure 9. Schematic representation mechanism of GroEL/GroES chaperone-mediated protein folding. Reprinted from ref. 187. Copyright 2013 Garland Science, Taylor & Francis Group, LLC.¹⁸⁷

1.8. Artificial Chaperones

Aggregation during protein folding can be eliminated in the presence of molecular chaperones. However, in the absence of molecular chaperones, protein aggregation is a common occurrence *in vitro*. The idea of artificial chaperons was first reported by Gellman and co-workers in 1995.²⁰³ Inspired by molecular chaperones, they used small molecules,

detergents or cyclodextrins, to discourage the aggregation and to guide the folding process.^{203–205} Similar to molecular chaperones, this artificial chaperone system consists of two consecutive steps. In the first step, a cationic detergent (cetyltrimethylammonium bromide, CTAB) was added to the denatured protein solution to create protein-detergent complexes and to prevent denatured proteins from aggregation. In the second step, β -cyclodextrin (β -CD) was introduced to the solution and to interact with the detergents and to allow proper refolding of the proteins. Figure 10 shows the schematic view of artificial chaperone-assisted protein refolding vs. additive-assisted protein refolding reported by Gellman and co-workers.²⁰⁴

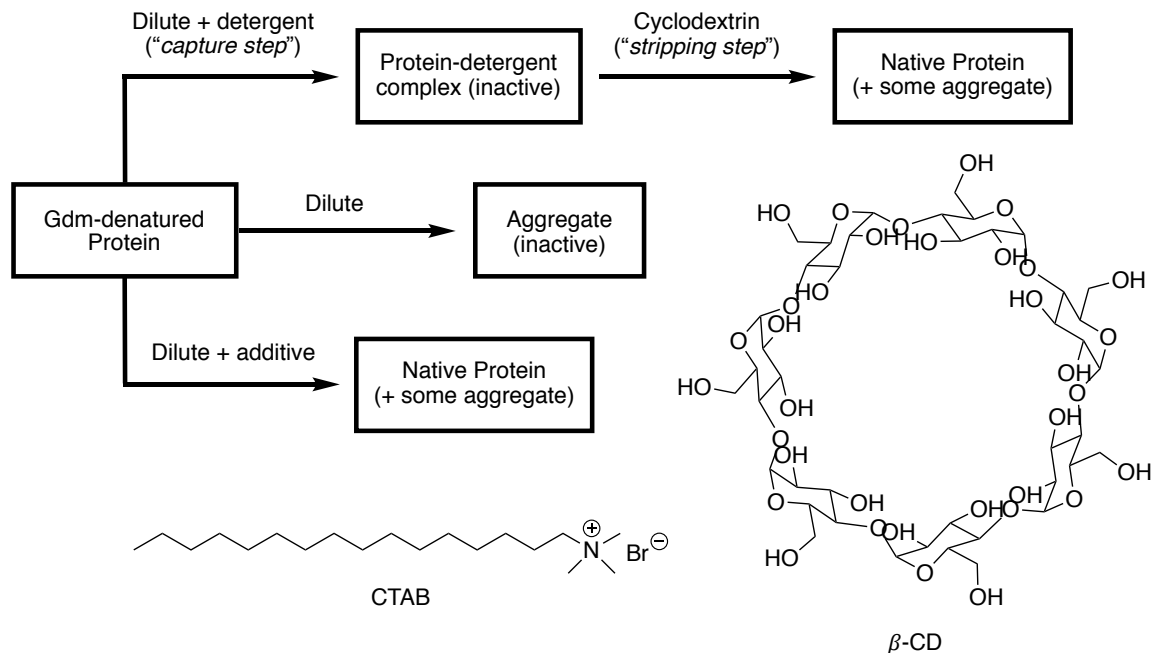


Figure 10. Artificial chaperone-assisted protein refolding (uppermost path) vs. dilution additive-assisted protein refolding (lowermost path) reported by Gellman and co-workers.²⁰⁴

Since 2003, Akiyoshi and co-workers developed series of polysaccharide-based self-assembled nanogels, cholesteryl group-bearing pullulan (CHP)^{206–212} and dodecyl group-bearing enzymatically synthesized glycogen (C₁₂ESG),²¹³ as artificial chaperones. Similar to the work by Gellman,^{203–205} CHPs showed the ability to complex with denatured proteins and to prevent the aggregation. Upon the addition of cyclodextrin to disassemble CHPs, the refolded proteins were recovered retaining their activity. C₁₂ESGs also demonstrated the ability to capture denatured proteins. The release of the refolded proteins relied on the fine balance of hydrophobic interaction between the nanogels and the proteins; therefore, the addition of cyclodextrin was no longer required (Figure 11).

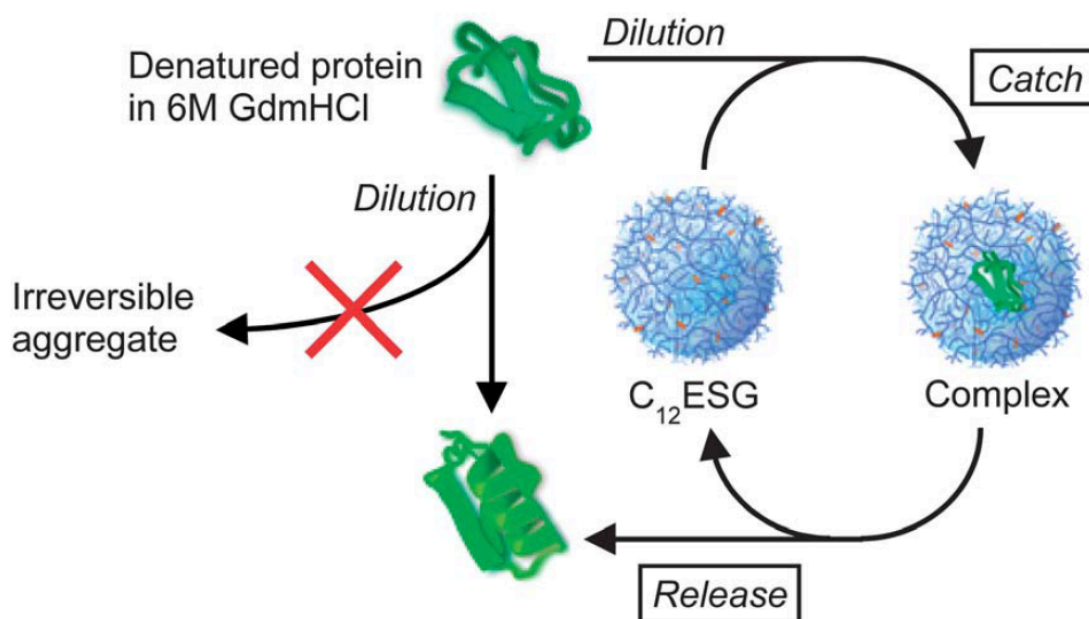


Figure 11. Schematic illustration of the C₁₂ESG nanogel-mediated one-step protein refolding system. Reprinted from ref 213. Copyright 2013 The Royal Society of Chemistry.²¹³

Shi and co-workers designed temperature-responsive mixed-shell polymeric micelles (MSPMs) as a one-step artificial chaperone system that mimics the GroEL/GroES molecular chaperones.²¹⁴⁻²¹⁹ The MSPMs usually consisted of two types of block copolymers. One is composed by a mixture of hydrophobic segment, poly(lactide) (PLA) or poly(ϵ -caprolactone) (PCL), and hydrophilic segment, PEG. The other one is constructed with the same hydrophobic portion and a temperature-responsive portion, usually PNIPAM. Poly(2-(2-methoxyethoxy) ethyl methacrylate) was also used as the temperature-responsive section with a LCST around 26 °C. After self-assembly of the polymeric micelles, the MSPMs evolved into core-shell-corona micelles above the LCST of the temperature-responsive polymer. The collapse of the temperature-responsive polymer in the mixed shell left behind cavities surrounded by PEG inner walls. The denatured proteins enter these cavities and refold. Figure 12 shows the first MSPMs-assisted protein refolding published by Shi and co-workers. In this case, MSPMs were generated by PLA₁₀₀-*b*-PEG₄₅ and PLA₁₂₅-*b*-PNIPAM₁₈₀ and it effectively prevented the aggregation and assist the refolding of denatured carbonic anhydrase B (CAB). In more recent reports, Shi and co-workers studied the effects of surface charges or surface hydrophobic/hydrophilic ratio on the properties of MSPMs for designing more efficient artificial chaperones.^{217,218}

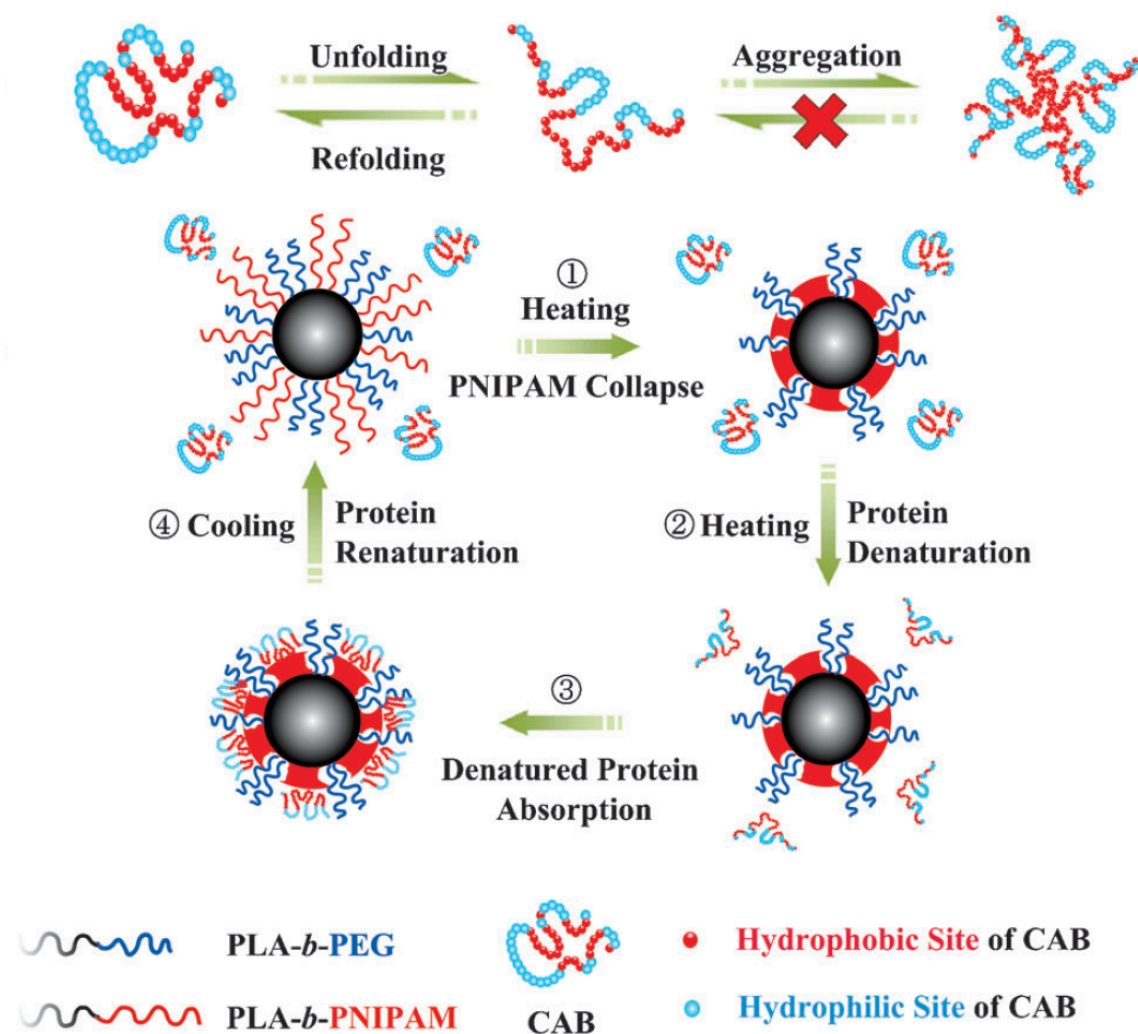
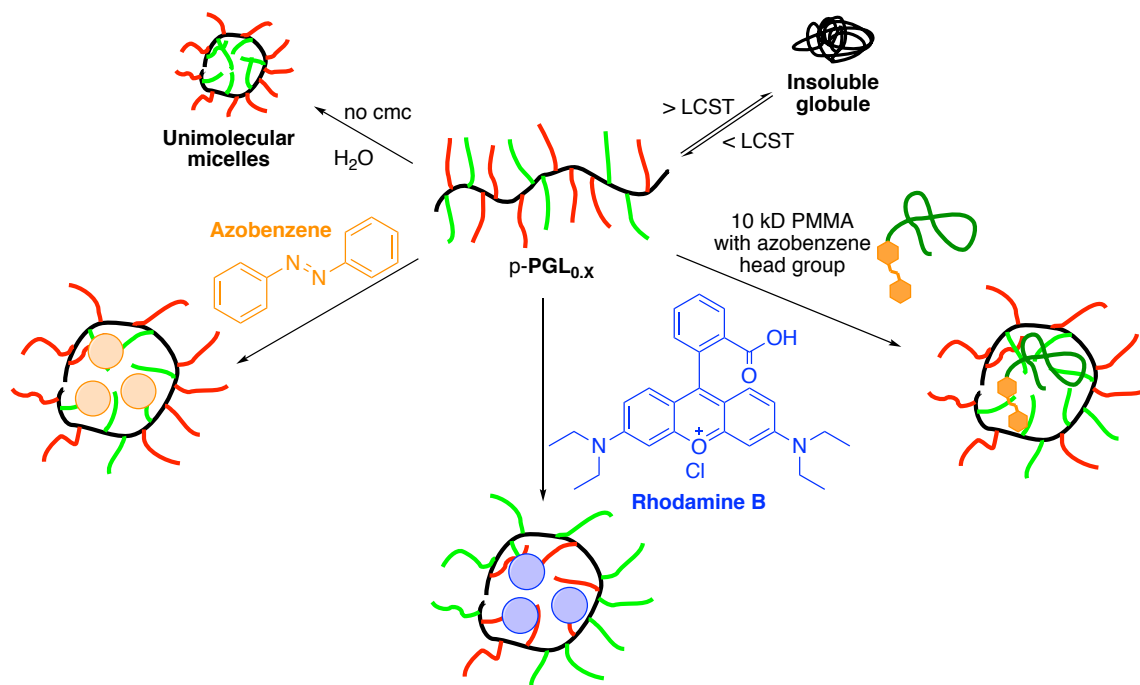


Figure 12. Schematic representation mechanism of MSPMs-assisted protein refolding. Reprinted from ref 214. Copyright 2013 Wiley-VCH Verlag GmbH & Co. KGaA, Weinheim.²¹⁴

As mentioned earlier, the formation of polymeric micelles is limited by their cmc. Hence, we explored the possibility of using SCNPs as artificial chaperones. In previous research, our group examined the properties of poly(PGL_{0.x}) and observed that poly(PGL_{0.x}) formed unimicelles and exhibited tunable LCSTs.^{49,95,220} To survey the potential of using poly(PGL_{0.x}) as nanocarriers, the encapsulation of hydrophobic and hydrophilic small guess molecules was investigated. Furthermore, poly(PGL_{0.x}) was used

to encapsulated 10 kDa azobenzene-initiated poly(methyl methacrylate) (azobenzene-PMMA) (Scheme 10).⁹⁵ The success of macromolecule encapsulation opens up the possibility of utilizing poly(**PGL**_{0,x}) in biomacromolecule-related study such as nanocarriers for protein delivery and artificial chaperones for assisting protein refolding. The biocompatibility and biodegradability poly(**PGL**_{0,x}) is desirable for some applications, degradability can pose challenges in synthesizing unimicelles and studying their properties.

Scheme 10. Schematic representation of the properties of poly(**PGL**_{0,x}) and poly(**PGL**_{0,x}) as nanocarriers for hydrophobic and the hydrophilic guest molecules.



In order to evaluate the effect of the degradability, we have designed non-degradable “clickable” polyether analogs of poly(**PGL**), poly(propargyl glycidyl ether) (poly(**PGE**)) and poly(1,1'-dimethyl propargyl glycidyl ether) (poly(**MGE**)), which were prepared via ROP of alkyne-functionalized epoxides. The ROP method developed by

Carlotti, Deffieux, and co-workers was employed considering the catalyst and the initiator are commercially available and controlled polymerization can be achieved. By applying PPM via “click” chemistry, we were able to adjust the properties of the “clickable” polyethers and the resulting amphiphilic polymers formed SCNPs as nanocarriers. Further modifications enabled us to install charge pendant groups on the polymer backbone and to increase the interaction between polymers and biomacromolecules. The results will be presented in the following chapters.

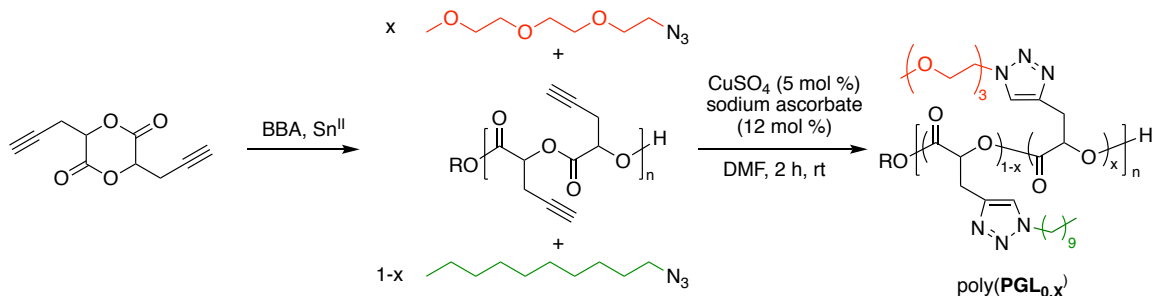
Chapter 2. Synthesis, Characterization, and Post-Polymerization

Modification of Propargyl-Substituted Poly(ethylene oxide)s

2.1. Introduction

In previous research, our group synthesized a “clickable” polyglycolides and applied PPM to generate degradable mDEG/alkyl-grafted poly(propargyl glycolide) polymers, poly(**PGL**_{0.X}), where **X** is the mole fraction of mDEG side chains (Scheme 11).⁴⁹ It was showed that LCSTs are between 25 °C to 65 °C for poly(**PGL**_{0.X}) and it could be tuned by modifying ratios between hydrophilic and hydrophobic pendant groups. It was also demonstrated that poly(**PGL**_{0.X}) forms unimolecular micelles with 31 nm hydrodynamic radius in Milli-Q water.⁹⁵ These unimicelles were further used to encapsulate hydrophobic and hydrophilic guest molecules as a proof of concept for delivery vehicles.⁹⁵

Scheme 11. Synthesis and post-polymerization modification poly(**PGL**) and poly(**PGL**_{0.X}).⁴⁹



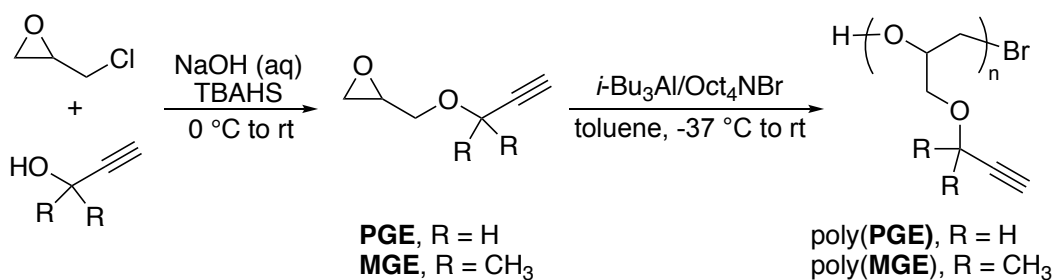
To further extend this concept and assess the effects of degradability, we designed and synthesized “clickable” poly(ethylene glycol)s (PEGs) polymers as non-degradable analogs of poly(propargyl glycolide). We envisioned the synthesis of these materials using

the ring-opening polymerization scheme developed by Carlotti, Deffieux, and co-workers^{8,221} to polymerize propargyl glycidyl ether (**PGE**) and 1,1'-dimethyl propargyl glycidyl ether (**MGE**). The resulting polymers could then be modified via CuAAC reactions of the polymers with azides. The polymer side chains significantly impact the LCST behavior. In addition, experiments show that these polymers function as unimolecular micelles in aqueous solution and do not aggregate when films are cast on surfaces below the LCST.

2.2. Synthesis and Characterization of Monomers

The preparation of **PGE** and **MGE** is outlined in Scheme 12. The synthesis of **PGE** was modified from a literature report from the reaction of (\pm)-epichlorohydrin and propargyl alcohol in a Williamson ether synthesis using tetrabutylammonium hydrogensulfate (TBAHS) as a phase transfer reagent.²²² Pure, colorless **PGE** was isolated as liquid in 76% yield upon distillation of the reaction mixture. The dimethyl analog, **MGE**, was synthesized in similar fashion from the reaction of (\pm)-epichlorohydrin and 2-methyl-3-butyne-2-ol as a colorless oil in 50% yield.

Scheme 12. Synthesis and polymerization of propargyl glycidyl ether (**PGE**) and 1,1'-dimethyl propargyl glycidyl ether (**MGE**).



The ^1H NMR spectrum of **PGE** is shown in Figure 13a. The acetylene proton (H_e) appears as a triplet centered at 2.44 ppm. This splitting pattern arises from $^4J_{\text{HH}}$ coupling with the diastereotopic propargyl methylene protons, H_d and $\text{H}_{d'}$. The two doublets centered at 4.19 ppm and 4.20 ppm correspond to H_d and $\text{H}_{d'}$. The two doublets of doublets centered at 3.46 ppm and 3.81 ppm correspond to the diastereotopic methylene protons H_c , $\text{H}_{c'}$ that are alpha to the epoxide ring. Resonances for H_a , $\text{H}_{a'}$, and H_b are assigned based on data from related structures and 2D HSQC.²²² The $^{13}\text{C}\{^1\text{H}\}$ NMR spectrum of **PGE** is shown in Figure 14a, which shows six distinct signals. The epoxide carbons, C_1 and C_2 , appear at 44.18 and 50.40 ppm, respectively, and the acetylene carbons (C_5 and C_6) are observed at 79.18 and 74.78 ppm, respectively.

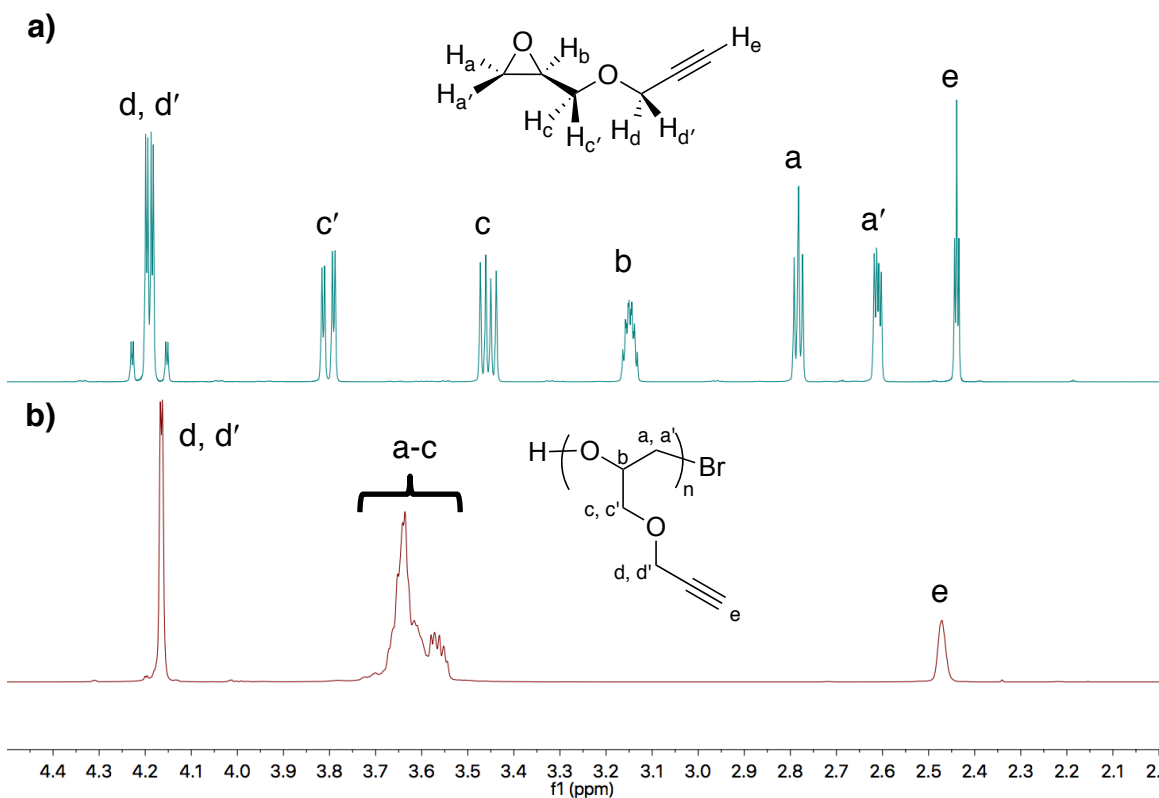


Figure 13. 500 MHz ^1H NMR spectra of a) **PGE** b) poly(propargyl glycidyl ether) (poly(**PGE**)) in CDCl_3 .

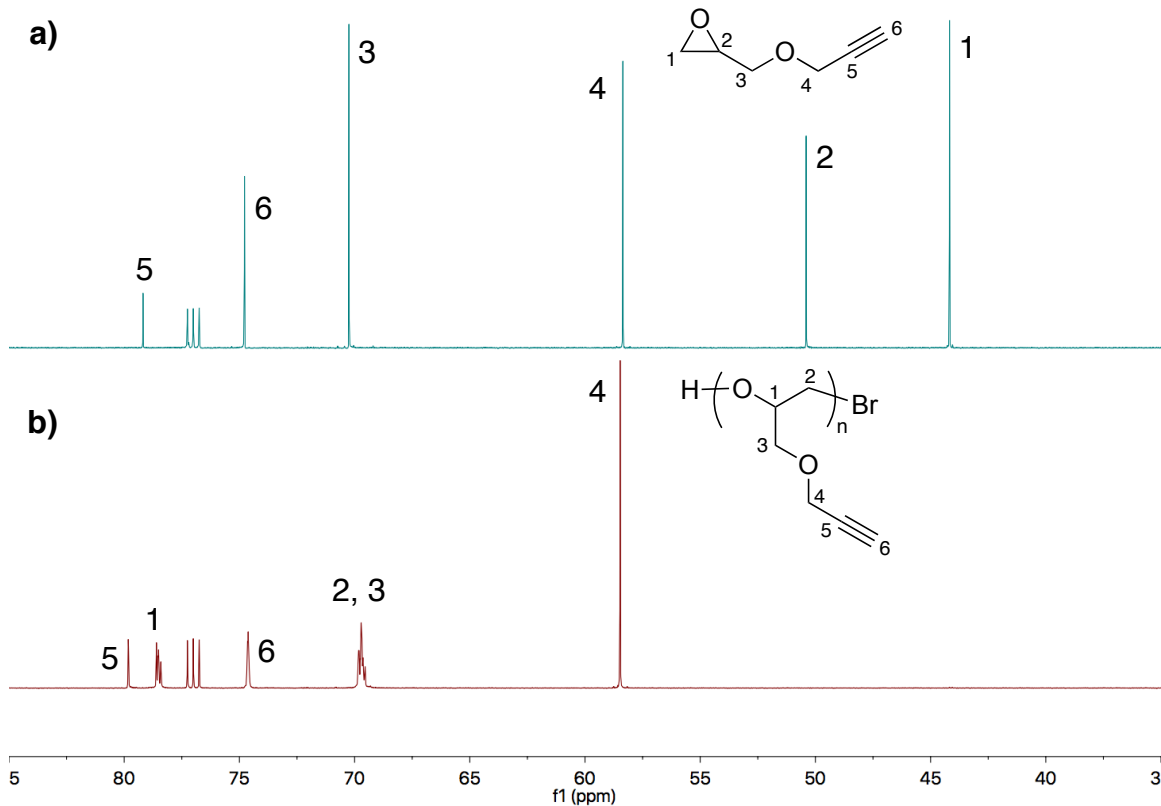


Figure 14. 125 MHz ^{13}C NMR spectra of a) **PGE** b) poly(propargyl glycidyl ether) (poly(**PGE**)) in CDCl_3 .

Figure 15a shows the ^1H NMR spectrum of **MGE**. The acetylene proton, H_e , appears as a singlet at 2.42 ppm and protons for the diastereotopic methyl groups, H_d and $\text{H}_{d'}$, appear as resolved singlets at 1.45 ppm and 1.46 ppm. The diastereotopic methylene protons H_c and $\text{H}_{c'}$ appear as doublets of doublets centered at 3.55 ppm and 3.75 ppm. The epoxide protons are assigned as above. The $^{13}\text{C}\{^1\text{H}\}$ NMR spectrum of **MGE** is shown in Figure 16a. Carbons for the diastereotopic methyl groups (C_7 and $\text{C}_{7'}$) are observed at 28.41 and 28.66 ppm, respectively. Two peaks represent epoxide carbons, C_1 and C_2 , appear at 44.84 and 50.86 ppm, similar to the ones seen in **PGE**. The acetylene carbons, C_5 and C_6 , are shown at 85.52 and 72.35 ppm, respectively.

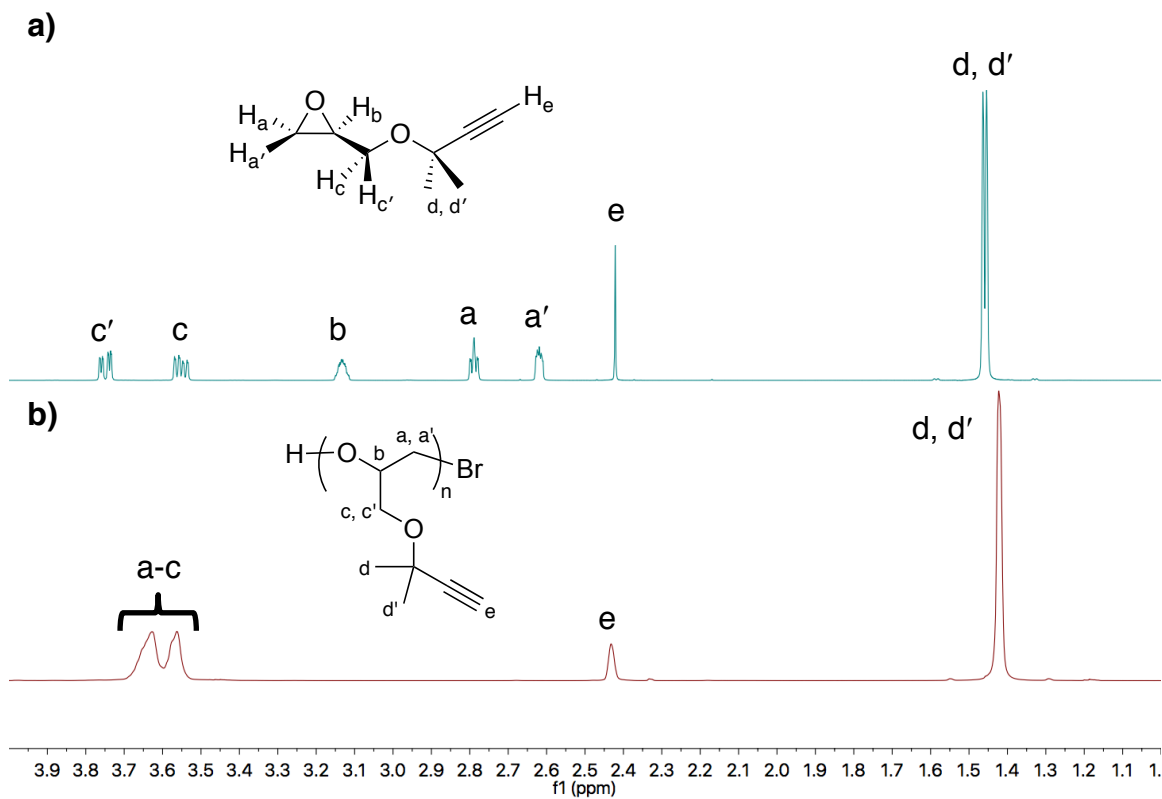


Figure 15. 500 MHz ^1H NMR spectra of a) **MGE** b) poly(1,1'-dimethyl propargyl glycidyl ether) (poly(**MGE**)) in CDCl_3 .

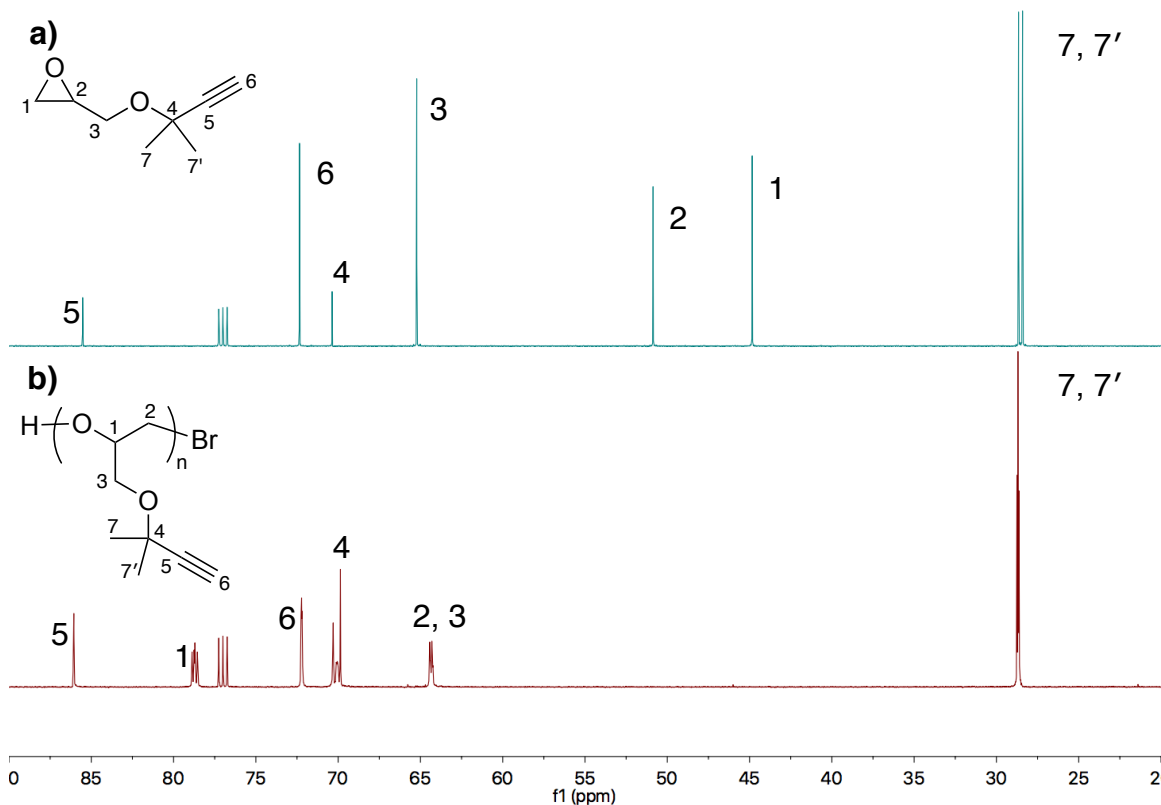


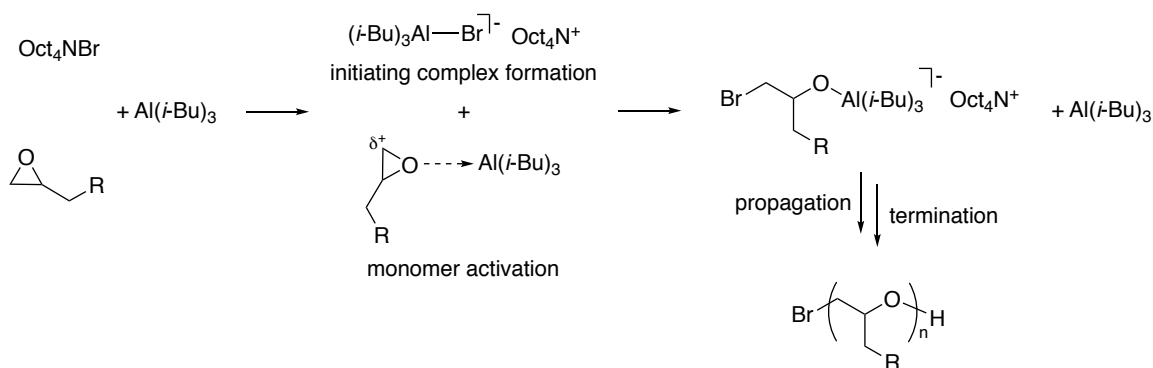
Figure 16. 125 MHz ^{13}C NMR spectra of a) **MGE** b) poly(1,1'-dimethyl propargyl glycidyl ether) (poly(**MGE**)) in CDCl_3

2.3. Living Anionic Ring-opening Polymerization

Anionic ring-opening polymerization of epoxides is one of the most studied and important methods for epoxide polymerization. In 2008, Carlotti, Deffieux and co-workers reported a new living/controlled polymerization of functionalized epoxides, which operates via an anionic coordination mechanism.^{8,221} In the reports, triisobutylaluminum ($i\text{-Bu}_3\text{Al}$) was used as the catalyst and tetraoctylammonium bromide (Oct_4NBr) was used as the initiator, which resulted in controlled molecular weight polymers under moderate conditions. Scheme 13 shows the proposed mechanism of the ring-opening polymerization of functionalized epoxides. Two events were proposed including the formation of initiating complex and the activation of the monomer in the initiation step. When the catalyst and

initiator ratio is greater than one, the initiating complex will be formed, and the excess catalyst will activate the corresponding monomer by coordinating with the oxygen atom on the epoxide. Nonetheless, to the best of our knowledge, there is no spectroscopic evidence for the bromide end group in these polymers.

Scheme 13. Proposed mechanism of ring-opening polymerization of functionalized epoxides using triisobutylaluminum ($i\text{-Bu}_3\text{Al}$) and tetraoctylammonium bromide (Oct_4NBr).⁸



Polymerizations of **PGE** and **MGE** were performed in toluene using $i\text{-Bu}_3\text{Al}$ as the catalyst and Oct_4NBr as the initiator. The reagents were combined at -37°C and the stirred reaction mixtures were allowed to warm to room temperature, after which stirring was continued from 2.5 to 24 h. Poly(propargyl glycidyl ether) (poly(**PGE**)) and poly(1,1'-dimethyl propargyl glycidyl ether) (poly(**MGE**)) were obtained in good yields (Table 2). As shown in Table 2, the $[i\text{-Bu}_3\text{Al}]/[\text{Oct}_4\text{NBr}]$ ratio was 2:1 for all polymerizations of **PGE**. Polymerization conversions were calculated by comparing the ^1H NMR integrations of the monomer epoxide peaks at 2.66 ppm with those on the polymer backbone at 3.52-3.63 ppm (Figure 13b). Resonances from the pendant propargyl groups of poly(**PGE**) were observed in ^1H NMR spectra at 2.46 ppm (H_e) and the alkyne carbon (C_5 and C_6) resonances appear

in ^{13}C NMR spectra at 79.82 and 74.56 ppm (Figure 14b), respectively, similar to the resonances observed in **PGE** (79.18 and 74.78 ppm). It is worth noting that carbons on the polymer backbone (C_1 , C_2 , and C_3) showed multiple peaks compared to **PGE**. This can be attributed to variations in the poly(**PGE**) backbone stereochemistry and/or the regioselectivity of ROP for the epoxide.

The **MGE** monomer was polymerized in analogous fashion except for entry 10 of Table 2, where the $[\textit{i}\text{-Bu}_3\text{Al}]/[\text{Oct}_4\text{NBr}]$ ratio was increased to 3:1 from 2:1. Polymerization conversions were determined from ^1H NMR spectra as described above for **PGE** by comparing the ^1H NMR integration of the residual epoxide peak at 2.64 ppm with those on polymer backbone at 3.56-3.63 ppm (Figure 15b). The pendant alkyne group was confirmed by ^1H NMR spectrum at 2.43 ppm and ^{13}C NMR spectrum at 72.2 and 86.1 ppm (Figure 15b and Figure 16b). The acetylene proton (H_e) is observed at 2.43 ppm and the alkyne carbons appear as multiple peaks at 72.17-72.27 ppm (C_6) and 86.06 and 86.08 ppm (C_5). More resonances were also observed that the tertiary carbon (C_4) and carbons on polymer backbone (C_1 , C_2 , and C_3) compared to poly(**PGE**). It is proposed that the dimethyl groups impede the rotation of the side chains and cause the differences in chemical environment.

It is worth mentioning that, in ^{13}C NMR spectrum of poly(**PGE**), a peak at 29.6 ppm is observed, which could be assigned to the carbon attached to the bromine end group. In the MS spectra of low molecular weight poly(**PGE**) ($M_n = 2800$, PDI = 1.14) and poly(**MGE**) ($M_n = 3900$, PDI = 1.16) (Figure A15 and Figure A16, Appendix), the distinct isotope peaks for bromine are also detected.

Table 2. Results of polymerization of **PGE** and **MGE**.

Entry	Monomer	[M]: [Al]: [I]	Time (h)	Conversion (%) ^a	M_n^{theory} (g mol ⁻¹) ^b	M_n^{exp} (g mol ⁻¹) ^c	PDI
1	PGE	25: 2: 1	2.5	> 99	2800	2800	1.14
2	PGE	50: 2: 1	2.5	98	5500	5500	1.30
3	PGE	100: 2: 1	2.5	> 99	11000	10000	1.19
4	PGE	200: 2: 1	2.5	97	22000	19000	1.26
5	MGE	25: 2: 1	2.5	> 99	3500	3900	1.16
6	MGE	50: 2: 1	2.5	> 99	7000	7000	1.15
7	MGE	100: 2: 1	2.5	> 99	14000	12000	1.17
8	MGE	200: 2: 1	2.5	> 99	28000	24000	1.24
9	MGE	500: 2: 1	24	48	34000	22000	1.10
10	MGE	500: 3: 1	24	73	51000	31000	1.33

^aDetermined by ¹H NMR. ^b Calculated from the monomer to initiator ratio and corrected for conversion. ^c Measured by GPC in THF via light scattering.

Typical results for the polymerization of **PGE** and **MGE** are listed in Table 2. The molecular weights of poly(**PGE**) and poly(**MEG**), measured by GPC in THF via light scattering, were in close agreement with the theoretical values with narrow to moderate polydispersities. The refractive index increment (dn/dc) is the change in refractive index of a solution at a given increment in concentration. The dn/dc values for poly(**PGE**) (0.0939 mL/g, Figure 17) and poly(**MGE**) (0.0750 mL/g, Figure 18) were measured and applied during data processing. Weight-average molecular weight (M_w) and dn/dc are connected through Zimm equation. A simplified version of the Zimm equation is shown below^{223,224}

$$\frac{Kc}{R_\theta} = \left(\frac{1}{M_w} + 2A_2c \right) \frac{1}{P_\theta}$$

where R_θ is the Rayleigh ratio, c is the sample concentration, θ is the measurement angle, A_2 is the second Virial coefficient, and K is defined as

$$K = \frac{4\pi^2}{\lambda_0^4 N_A} \left(n_0 \frac{dn}{dc} \right)^2$$

where λ_0 is the laser wavelength in a vacuum, N_A is Avogadro's number, and n_0 is the refractive index of the solvent.

P_θ is the single chain form factor, whose reciprocal is given by

$$\frac{1}{P_\theta} = 1 + \frac{16\pi^2 n_0^2 R_g^2}{3\lambda_0^2} \sin^2\left(\frac{\theta}{2}\right)$$

where R_g is the molecule's radius of gyration.

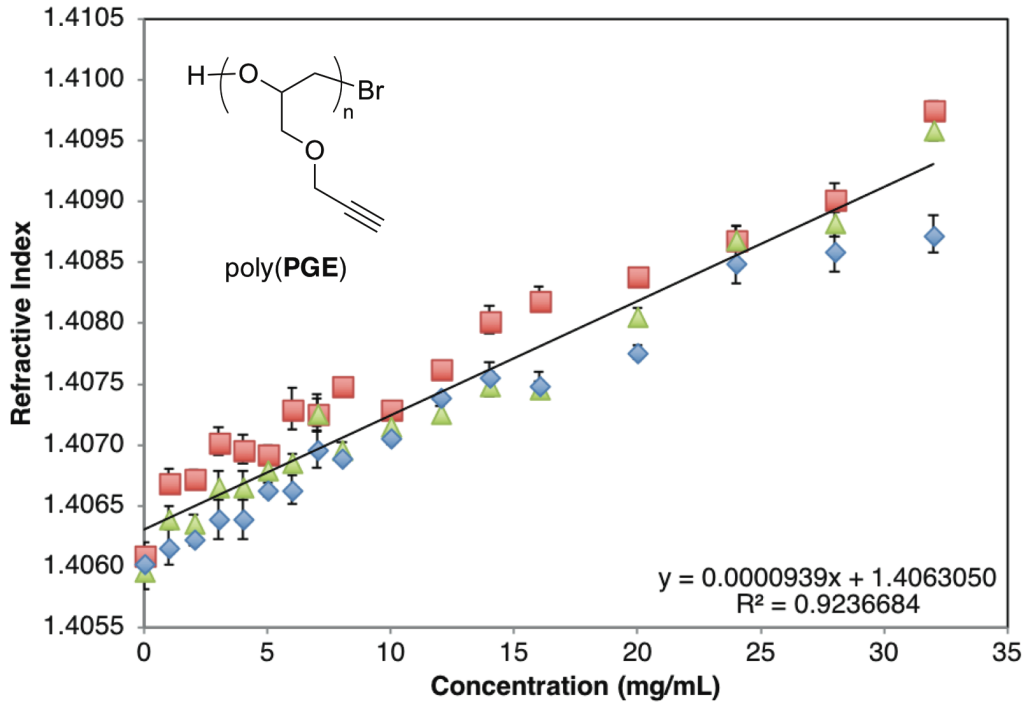


Figure 17. Measurements of refractive index increment, dn/dc , of poly(PGE). Trial 1 (blue diamond), trial 2 (red square), and trial 3 (green triangle).

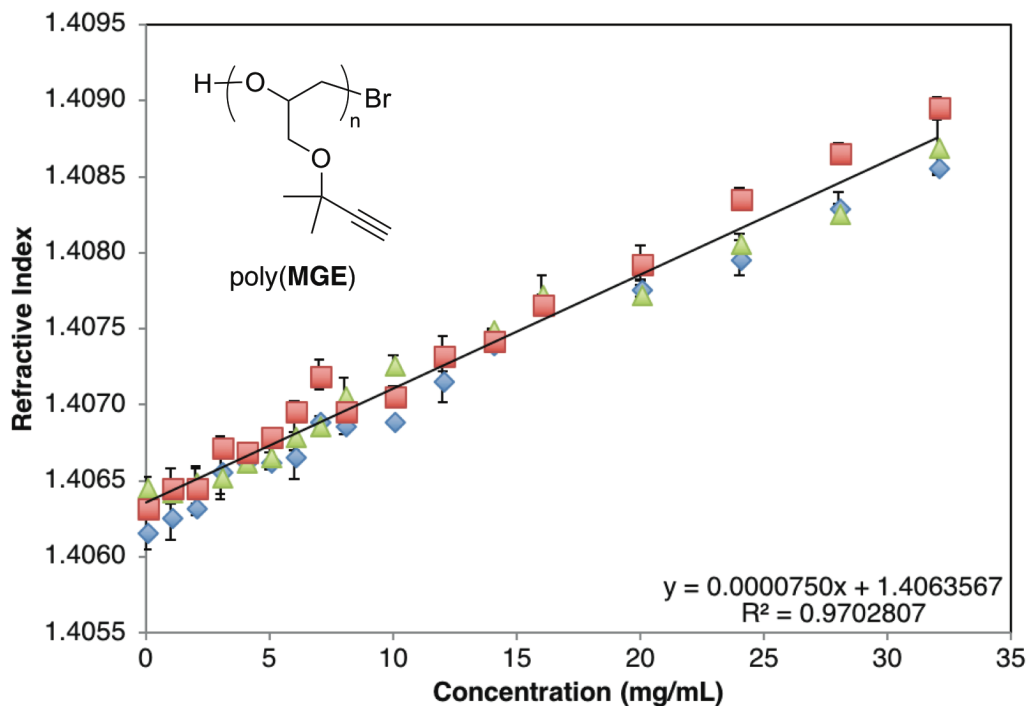


Figure 18. Measurements of refractive index increment, dn/dc , of poly(MGE). Trial 1 (blue diamond), trial 2 (red square), and trial 3 (green triangle).

In the attempts to synthesize polymers with higher molecular weights in entries 9 and 10, a higher $[i\text{-Bu}_3\text{Al}]/[\text{Oct}_4\text{NBr}]$ ratio was necessary to increase the conversion and molecular weight. However, full conversion was not achieved with 3:1 $[i\text{-Bu}_3\text{Al}]/[\text{Oct}_4\text{NBr}]$ ratio. A higher ratio may be needed to complete the polymerization.

The progression of poly(MGE) number-average molecular weight (M_n) with monomer conversion is shown in Figure 19. A linear increase of the M_n with percent conversion is observed. The linear relationship between M_n and percent conversion and low PDIs indicate a controlled polymerization mechanism without any noticeable undesired reactions. A kinetic study of poly(MGE) consumption with time at room temperature, following initiation at $-37\text{ }^\circ\text{C}$, was also performed (Figure 20). It revealed two

distinct polymerization regimes. The polymerization is rapid up to ~85% conversion, after which the polymerization slows down. These results are consistent with the previous reports by Carlotti and co-workers.^{8,221}

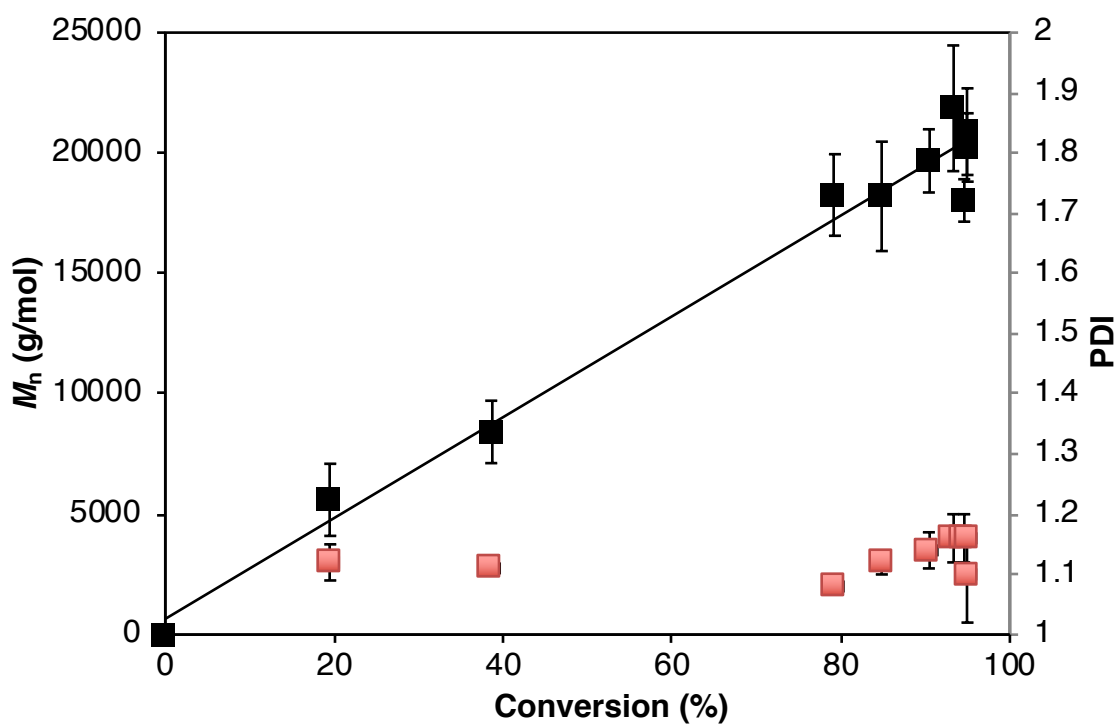


Figure 19. Variation of the number-average molar mass (black square) and PDI (red square) with **MGE** conversion ($[M]: [Al]: [I] = 200: 2: 1$).

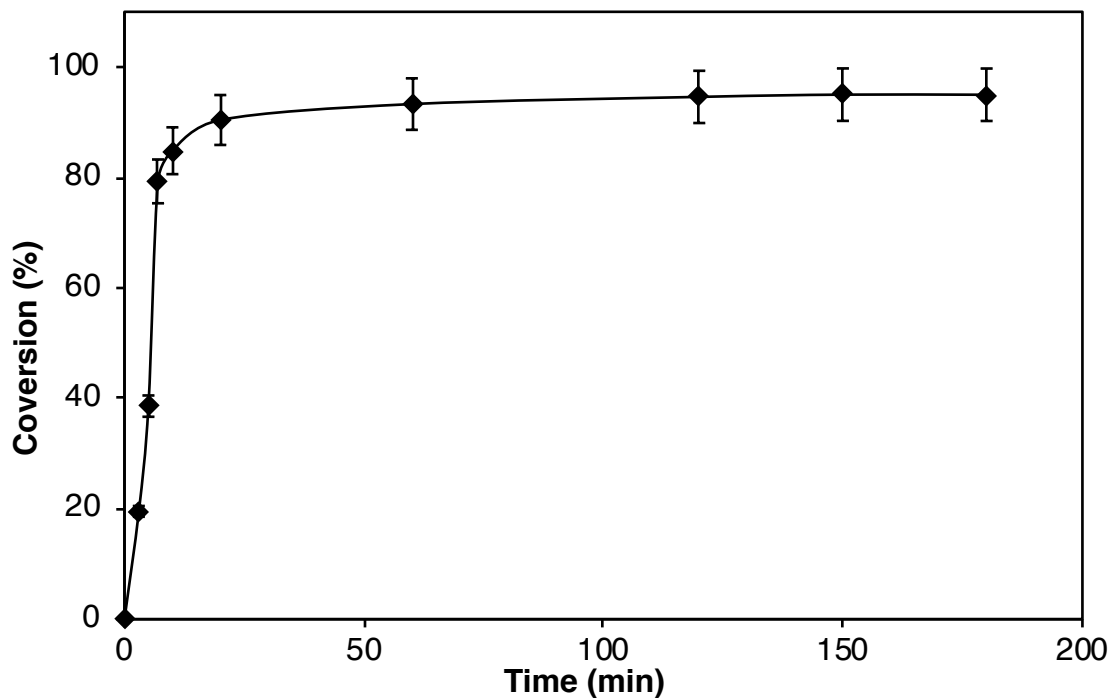
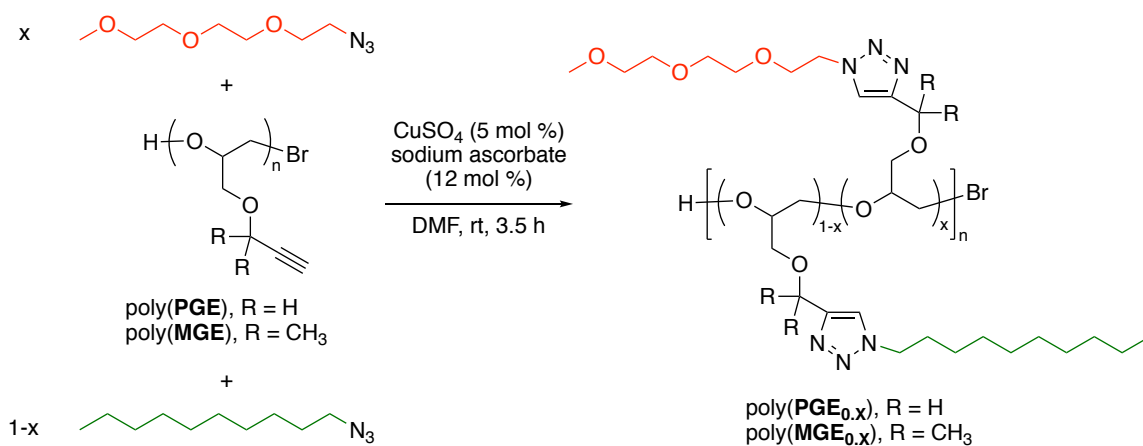


Figure 20. Conversion vs. time of the polymerization of **MGE** ([M]: [Al]: [I] = 200: 2: 1).

2.4. Post-polymerization Modification (PPM) via “Click” Chemistry

Scheme 14. Post-polymerization modification (PPM) of poly(**PGE**) and poly(**MGE**) with **mDEG azide** and **decyl azide**.



To further extend the scope of the polymer properties, “click” chemistry, specifically copper(I)-catalyzed 1,3-dipolar cycloaddition of azides and alkynes (CuAAC), was used for PPM. The synthesis of “click” modified polymers is illustrated in Scheme 14. The “click” reaction was performed in the presence of $\text{CuSO}_4 \cdot 5\text{H}_2\text{O}$ and sodium ascorbate in DMF at room temperature. 1-(2-Azidoethoxy)-2-(2-methoxyethoxy)ethane (**mDEG azide**) was synthesized from triethylene glycol monomethyl ether and sodium azide.⁹⁵ Also, 1-azidodecane (**decyl azide**) was synthesized from 1-bromodecane and sodium azide.^{95,225,226} To synthesize polymer poly(**PGE_{0,x}**) the desired amount of **mDEG azide** and/or **decyl azide**, and 12 mol % sodium ascorbate were dissolved in DMF (all equivalents and mole percentages are with respect to acetylene units in poly(**PGE**) ($M_n = 18000$, PDI = 1.35 or $M_n = 19000$, PDI = 1.26). Then, 5 mol % of $\text{CuSO}_4 \cdot 5\text{H}_2\text{O}$ in DMF was added via syringe. After the desired reaction time, the residual copper was removed by stirring the polymer solution with ion exchange resin beads (Amberlite® IRC-748 ion exchange resin) for 16-24 hours. The polymers were purified by dialysis (molecular weight cutoff (MWCO) = 6-8 kDa).^{49,95} Similar procedures were followed to synthesize poly(**MGE_{0,x}**) from poly(**MGE**) ($M_n = 22000$, PDI = 1.13, $M_n = 21000$, PDI = 1.20). By varying the ratio of **mDEG azide** and **decyl azide**, a series of polymers poly(**PGE_{0,x}**) and poly(**MGE_{0,x}**) (X is mole percent of **mDEG azide**) were obtained.

In ^1H NMR spectra, the absence of acetylene protons at 2.44 ppm poly(**PGE**) (Figure 21) and 2.43 ppm poly(**MGE**) (Figure 22) confirmed that the reactions were complete after 3.5 hours. As shown in Figure 21b, c, and d, triazole proton resonances at 7.66 ppm and/or 7.76 ppm are observed for poly(**PGE_{0,x}**). The spectrum of poly(**PGE₀**) shows that the triazole proton for alkyl side chain is the upfield resonance, 7.66 ppm, and

in the spectrum of poly(**PGE**_{1.0}), the triazole proton for mDEG side chain is the down field resonance, 7.76 ppm. Likewise, new peak(s) for the proton on the triazole ring appear(s) at 7.59 ppm and/or 7.66 ppm for poly(**MGE**_{0.x}) (Figure 22b, c, and d), where the proton for the triazole for alkyl side chain is upfield and for alkyl side chain is downfield. The ratio of the incorporated **mDEG azide** and **decyl azide** in polymer side chain was calculated by the integration of the triazole protons and it was within 2% error of the molar ratio used in the reaction.

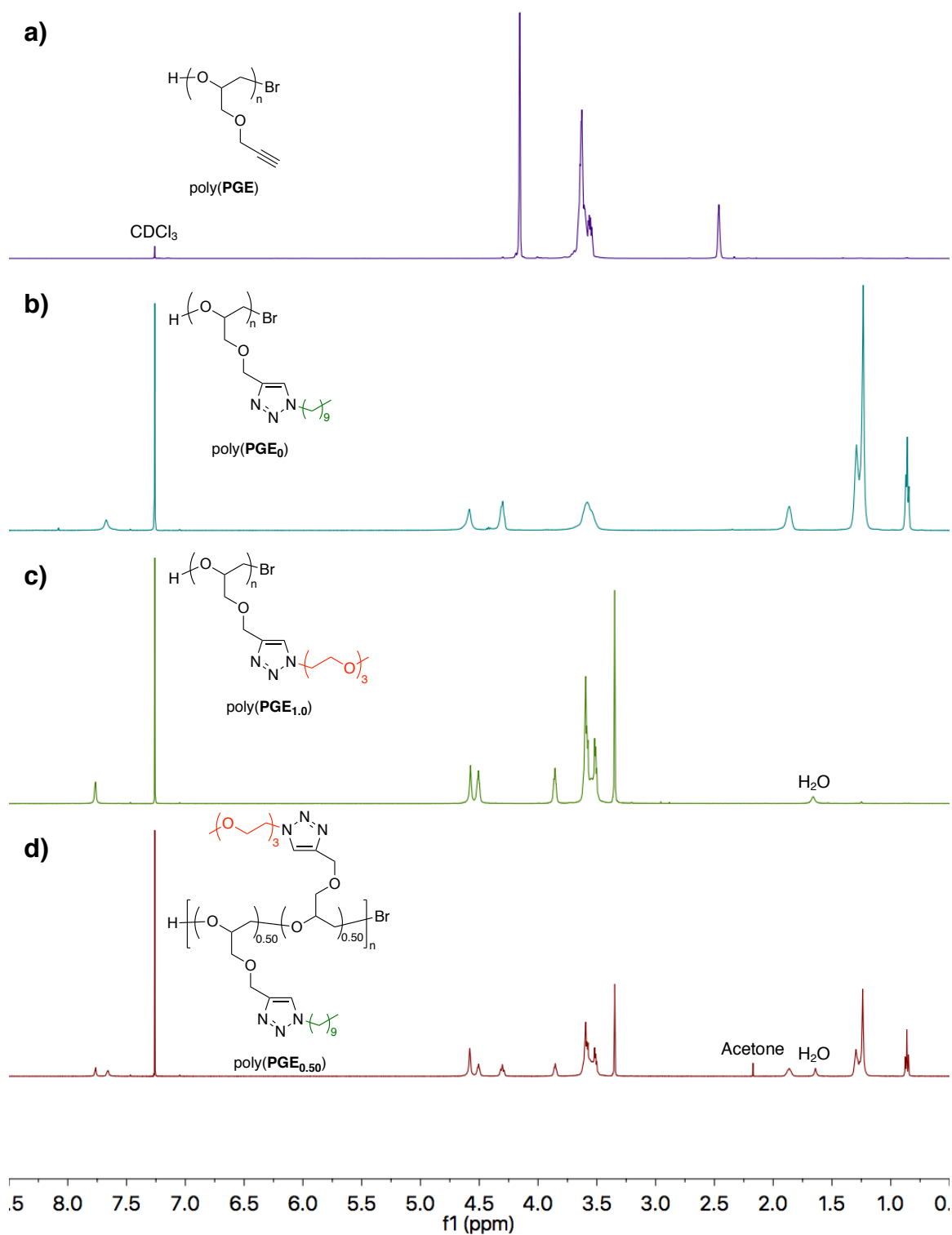


Figure 21. 500 MHz ¹H NMR spectra of a) poly(PGE) b) poly(PGE₀) c) poly(PGE_{1.0}) d) poly(PGE_{0.50}) in CDCl₃.

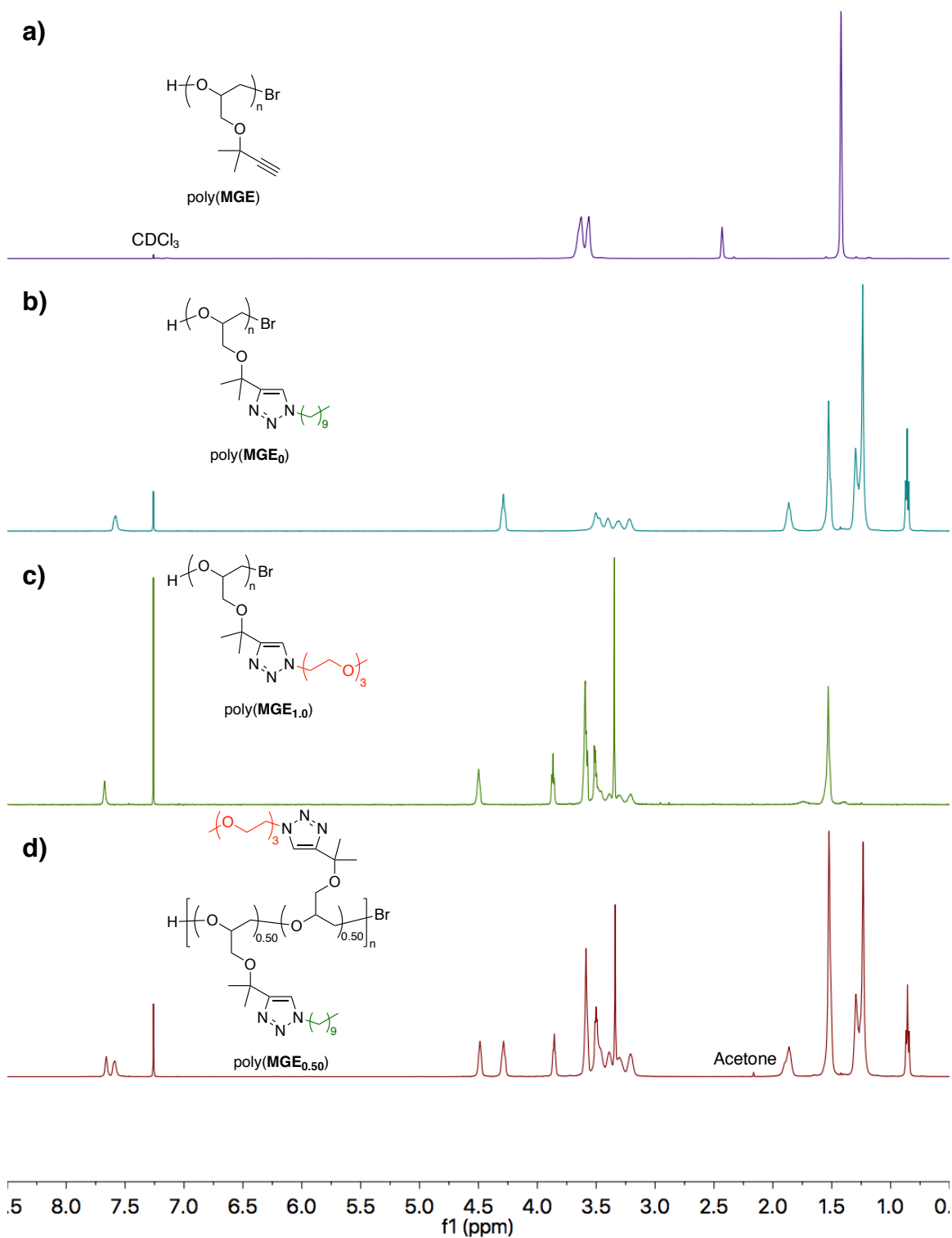


Figure 22. 500 MHz ¹H NMR spectra of a) poly(MGE) b) poly(MGE₀) c) poly(MGE_{1.0}) d) poly(MGE_{0.50}) in CDCl₃.

The increase in the molecular weight of the resulting polymer poly(**PGE_{0.x}**) and poly(**MGE_{0.x}**) was confirmed by size exclusion chromatography coupled with a multiangle light scattering detector (SEC-MALS) (Table 3 and Table 4). The experimental values of poly(**PGE_{0.x}**) and poly(**MGE_{0.x}**) are in good agreement of calculated values with slight to no change in polydispersity, which is consistent with high fidelity in the “click” reaction. In Figure 5, the GPC traces for poly(**MGE**) ($M_n = 21000$, PDI = 1.20) and the product from its “click” reaction with decyl azide, poly(**MGE₀**) ($M_n^{\text{calc.}} = 50000$, $M_n^{\text{expt.}} = 49000$, PDI = 1.20), have similar retention times with no noticeable change in peak shape and polydispersity. The small difference in retention times despite a 2.3-fold increase in M_n is likely due to similar hydrodynamic volumes for poly(**MGE**) and highly branched poly(**MGE₀**), as has been observed for other branched polymers.^{227,228}

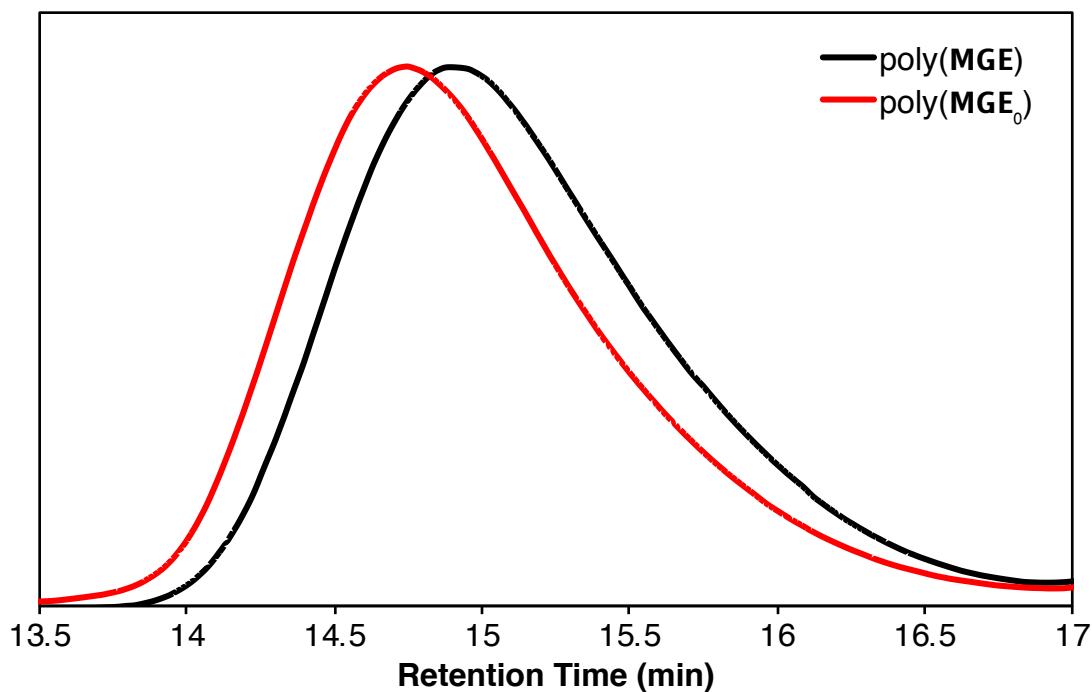


Figure 23. GPC traces of poly(MGE) ($M_n = 21000$, PDI = 1.20; black line) and poly(MGE₀) ($M_n = 49000$, PDI = 1.20; red line). The polymers were analyzed in THF at 35 °C, at 1 mL/min flow rate.

Table 3. GPC results of poly(PGE_{0,x}).

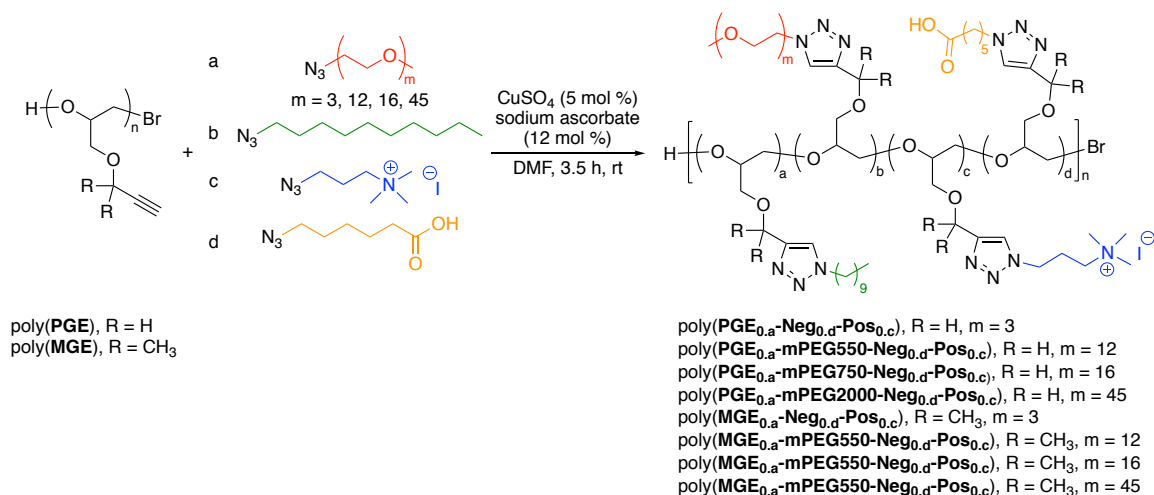
Polymer	M_n^{orig} (g mol ⁻¹) ^a	mol % mDEG	M_n^{theory} (g mol ⁻¹)	M_n^{exp} (g mol ⁻¹) ^a	M_w^{exp} (g mol ⁻¹) ^a	PDI
poly(PGE ₀)	18000	0	49000	27000	35000	1.30
poly(PGE _{0.20})	18000	20.3	49000	35000	45000	1.29
poly(PGE _{0.40})	20000	40.7	49000	41000	48000	1.17
poly(PGE _{0.50})	18000	48.2	49000	46000	54000	1.17
poly(PGE _{0.55})	20000	54.4	49000	44000	51000	1.16
poly(PGE _{0.60})	18000	60.0	49000	44000	59000	1.34
poly(PGE _{0.65})	20000	62.9	49000	45000	54000	1.20
poly(PGE _{0.70})	20000	71.9	49000	50000	58000	1.16
poly(PGE _{0.75})	20000	72.5	49000	53000	60000	1.13
poly(PGE _{0.80})	18000	78.1	49000	47000	53000	1.13
poly(PGE _{0.85})	20000	82.4	49000	51000	57000	1.12
poly(PGE _{0.90})	20000	90.3	50000	55000	61000	1.11
poly(PGE _{0.95})	20000	95.4	50000	52000	59000	1.13
poly(PGE _{1.0})	18000	100	50000	53000	58000	1.09

^aMeasured by GPC in THF via light scattering.

Table 4. GPC results of poly(MGE_{0.x}).

Polymer	M_n^{orig} (g mol ⁻¹) ^a	mol % mDEG	M_n^{theory} (g mol ⁻¹)	M_n^{exp} (g mol ⁻¹) ^a	M_w^{exp} (g mol ⁻¹) ^a	PDI
poly(MGE ₀)	22000	0	49000	49000	60000	1.22
poly(MGE _{0.20})	22000	20.5	50000	55000	63000	1.15
poly(MGE _{0.40})	21000	39.9	50000	48000	60000	1.25
poly(MGE _{0.50})	22000	46.4	50000	54000	64000	1.19
poly(MGE _{0.55})	21000	55.5	50000	54000	65000	1.20
poly(MGE _{0.60})	21000	57.8	50000	55000	64000	1.16
poly(MGE _{0.65})	21000	63.3	50000	52000	62000	1.19
poly(MGE _{0.70})	21000	68.7	50000	54000	65000	1.20
poly(MGE _{0.75})	21000	74.4	50000	52000	64000	1.23
poly(MGE _{0.80})	22000	79.7	50000	59000	69000	1.17
poly(MGE _{0.85})	21000	85.0	50000	55000	65000	1.18
poly(MGE _{0.90})	21000	89.3	50000	53000	62000	1.17
poly(MGE _{0.95})	24000	93.9	50000	59000	69000	1.17
poly(MGE _{1.0})	22000	100	50000	61000	71000	1.16

^aMeasured by GPC in THF via light scattering.

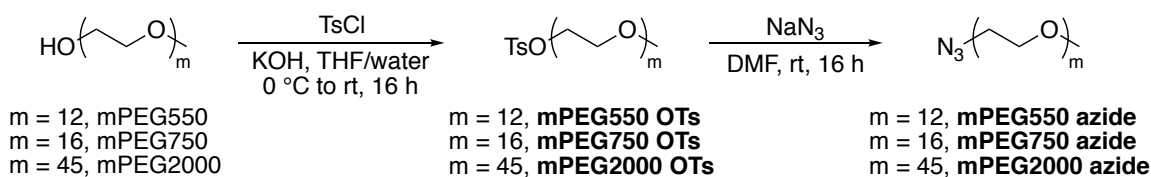
Scheme 15. PPM of poly(PGE) and poly(MGE) with mDEG azide, decyl azide, mPEG550 azide, mPEG750 azide, mPEG2000 azide, COOH azide, and aminium azide.

To further examine side chain effects on polymer properties, azides with longer hydrophilic segments, and others bearing ammonium or carboxylic acid groups, were

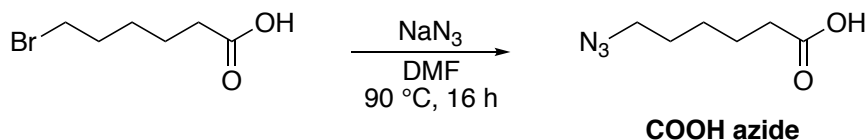
synthesized and PPMs of poly(PGE) and poly(MGE) were performed with these azides, as shown in

Scheme 15. The syntheses of more hydrophilic azides were modified from published procedures.^{229,230} 1-azido poly(ethylene glycol) monomethyl ether, 550 (**mPEG550 azide**), 1-azido poly(ethylene glycol) monomethyl ether, 750 (**mPEG750 azide**), and 1-azido poly(ethylene glycol) monomethyl ether, 2000 (**mPEG2000 azide**), were synthesized from the corresponding poly(ethylene glycol) monomethyl ethers and sodium azide as a liquid, viscous liquid, and solid, respectively (Scheme 16). 6-azidophexanoic acid (**COOH azide**) is used as a short chain negatively charged azide under physiological condition and was obtained from the reaction of 6-bromohexanoic acid and sodium azide as a clear liquid (Scheme 17).²³¹ For a short chain positively charged azide, 3-azido-*N,N,N*-trimethylpropan-1-aminium iodide (**aminium azide**) was chosen. The synthesis was carried out with 3-dimethylaminopropyl chloride hydrochloride and sodium azide followed by the addition of methyl iodide to acquire **aminium azide** as a pale-yellow solid (Scheme 18).^{232,233}

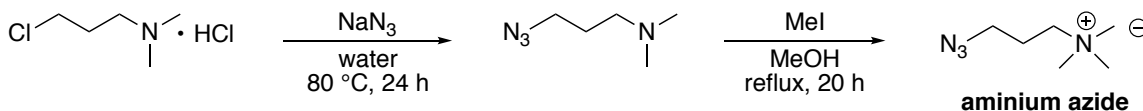
Scheme 16. Synthesis of **mPEG550 azide**, **mPEG750 azide**, and **mPEG2000 azide**.



Scheme 17. Synthesis of **COOH azide**.



Scheme 18. Synthesis of **aminium azide**.



PPM of poly(**PGE**) and poly(**MGE**) with various azides were carried out. Specifically, poly(**PGE**) ($M_n = 18000$, $\text{PDI} = 1.35$ or $M_n = 19000$, $\text{PDI} = 1.26$) or poly(**MGE**) ($M_n = 22000$, $\text{PDI} = 1.13$, $M_n = 21000$, $\text{PDI} = 1.20$), the desired amount of hydrophilic azide (**mDEG azide** or **mPEG550 azide** or **mPEG750 azide** or **mPEG2000 azide**), hydrophobic azide (**decyl azide**), charged azide (**COOH azide** and/or **aminium azide**), and 12 mol % sodium ascorbate were dissolved in DMF (all equivalents and mole percentages are with respect to acetylene units in poly(**PGE**) and poly(**MGE**)). Then, 5 mol % of $\text{CuSO}_4 \cdot 5\text{H}_2\text{O}$ in DMF was added via syringe. After the desired reaction time, the residual copper was removed by stirring the polymer solution with ion exchange resin beads for 16-24 hours and were purified via dialysis. A series of polymers poly(**PGE**_{0.a}-(**mPEG**#)-**Neg**_{0.d}-**Pos**_{0.c}) and poly(**MGE**_{0.a}-(**mPEG**#)-**Neg**_{0.d}-**Pos**_{0.c}) (a is the mole percent of hydrophilic azide, d is the mole percent of **COOH azide**, c is mole percent of **aminium azide**, if longer hydrophilic azide was used, # is the molecular weight of mPEG) were obtained.

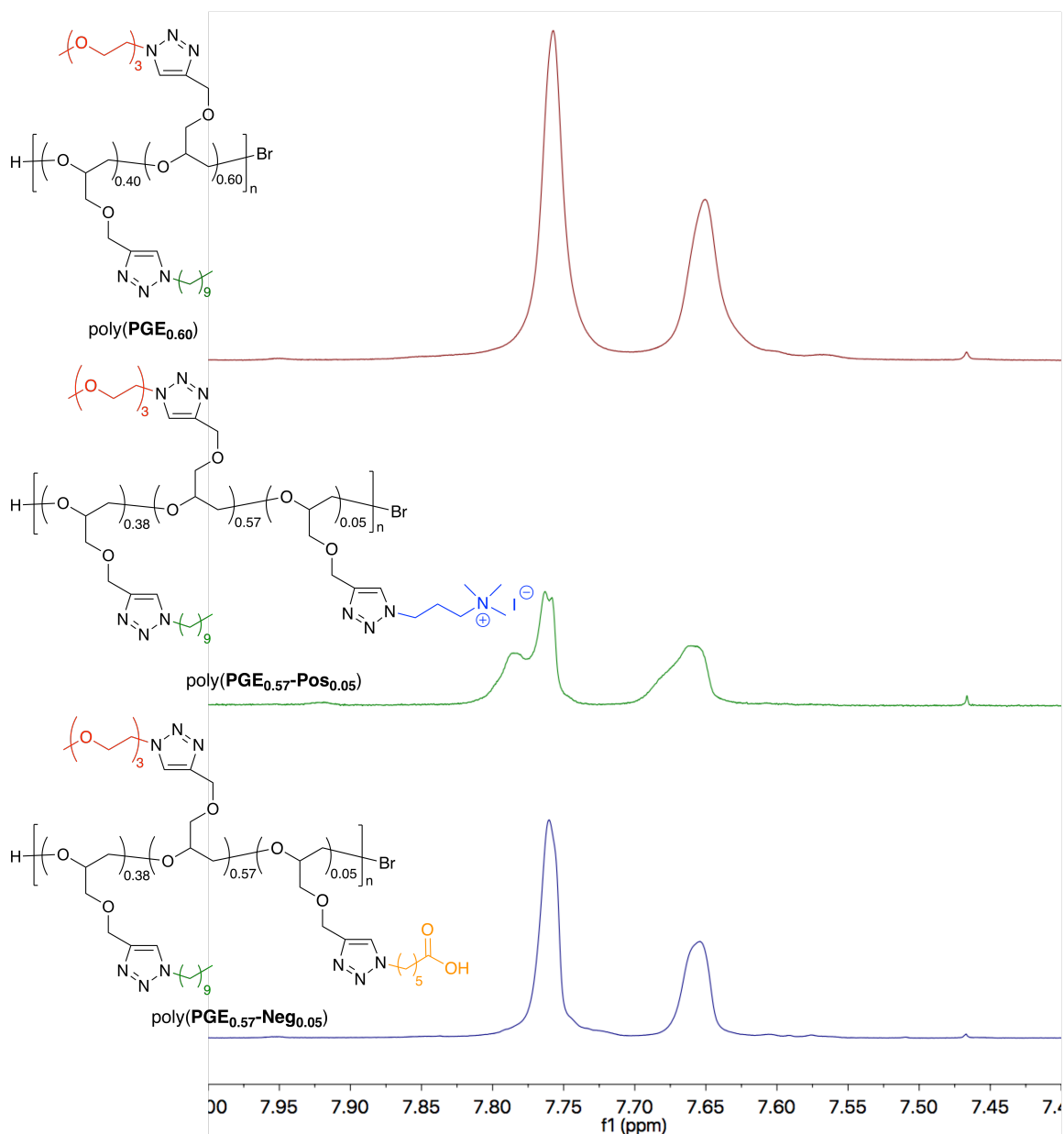


Figure 24. 500 MHz ^1H NMR spectra of poly(PGE_{0.60}) (red line), poly(PGE_{0.57}-Pos_{0.05}) (green line), and poly(PGE_{0.57}-Neg_{0.05}) (blue line) in CDCl_3 in aromatic region.

The ^1H NMR spectra of the aromatic region of poly(PGE_{0.60}), poly(PGE_{0.57}-Pos_{0.05}), and poly(PGE_{0.57}-Neg_{0.05}) are shown in Figure 24. Similar chemical shifts of the triazole protons at 7.66 and 7.76 ppm were observed for poly(PGE_{0.57}-Pos_{0.05}) and poly(PGE_{0.57}-Neg_{0.05}). However, peak broadening was seen for poly(PGE_{0.57}-Pos_{0.05}). The

new peak for the aminium methyl group on poly(**PGE_{0.57}-Pos_{0.05}**) appears at 3.23 ppm and the methylene protons on hexanoic acid group on poly(**PGE_{0.57}-Neg_{0.05}**) emerge at 1.60 and 2.22 ppm (Figure A106 and Figure A107, Appendix). Similarly, the protons on the triazole ring were seen at 7.59 ppm and 7.66 ppm for poly(**MGE_{0.75}**), poly(**MGE_{0.71}-Pos_{0.05}**), and poly(**MGE_{0.71}-Neg_{0.05}**) and the peak broadening was observed for poly(**MGE_{0.71}-Pos_{0.05}**) (Figure 25). It is worth noting that a shoulder peak appears at around 7.72 ppm for poly(**MGE_{0.71}-Neg_{0.05}**) and it is proposed to be the proton on the triazole ring bonded to hexanoic acid. This was confirmed by comparing the ¹H NMR spectrum of poly(**MGE_{0.71}-Neg_{0.05}**) and poly(**MGE_{0.68}-Neg_{0.10}**), shown in Figure 26, the integration the peak at 7.75 ppm in poly(**MGE_{0.68}-Neg_{0.10}**) was twice of the value in poly(**MGE_{0.71}-Neg_{0.05}**) (Figure A98 and Figure A105, Appendix). The new peak for the aminium methyl group on poly(**MGE_{0.71}-Pos_{0.05}**) appears at 2.45 ppm and the methylene protons on hexanoic acid group on poly(**PGE_{0.57}-Neg_{0.05}**) emerge at 2.27 ppm (Figure A108 and Figure A109, Appendix).

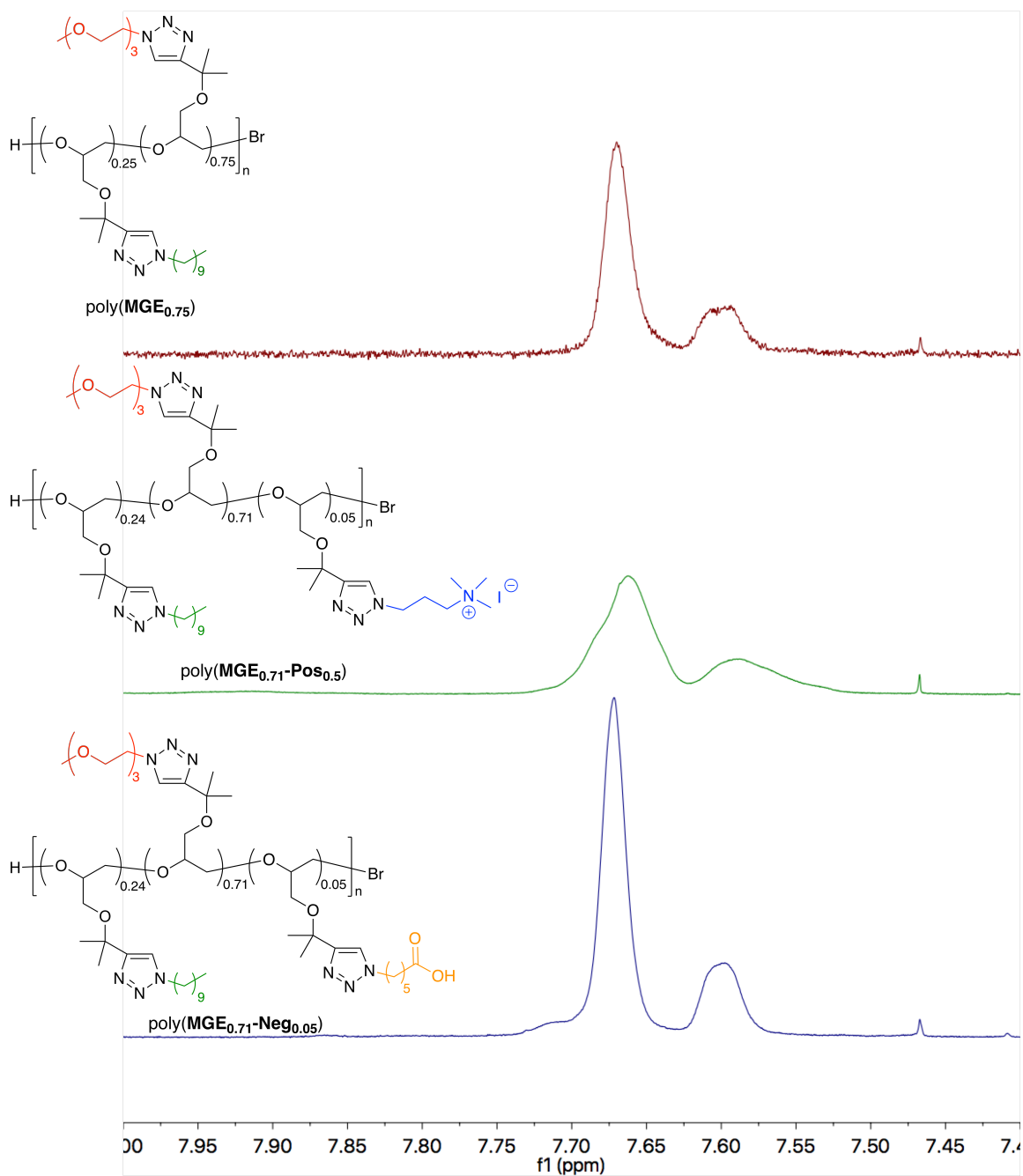


Figure 25. 500 MHz ¹H NMR spectra of poly(MGE_{0.75}) (red line), poly(MGE_{0.71}-Pos_{0.05}) (green line), and poly(MGE_{0.71}-Neg_{0.05}) (blue line) in CDCl₃ in aromatic region.

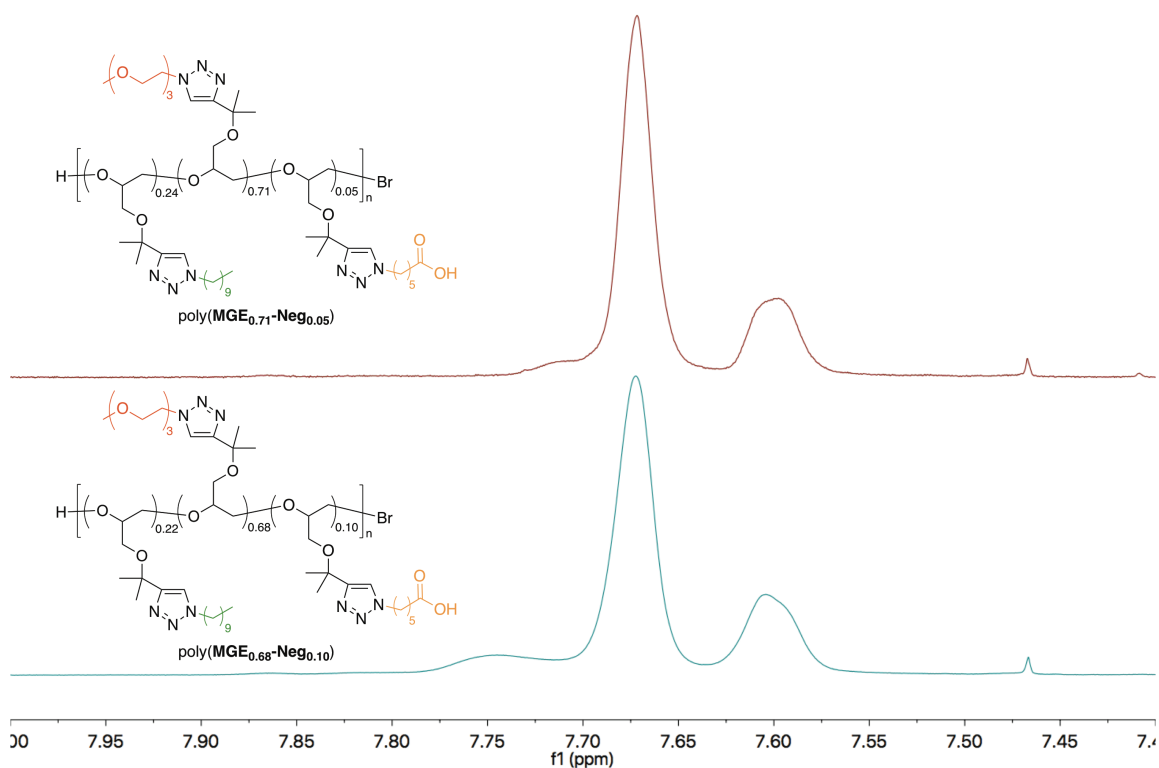


Figure 26. 500 MHz ^1H NMR spectra of $\text{poly}(\text{MGE}_{0.71}\text{-Neg}_{0.05})$ (red line) and $\text{poly}(\text{MGE}_{0.68}\text{-Neg}_{0.10})$ (green line) in CDCl_3 in aromatic region.

The physical appearance of polymers with charged side chains are different than the neutral polymers. For instance, positively charged polymer, $\text{poly}(\text{PGE}_{0.57}\text{-Pos}_{0.05})$, $\text{poly}(\text{PGE}_{0.57}\text{-mPEG550-Pos}_{0.05})$, $\text{poly}(\text{MGE}_{0.71}\text{-Pos}_{0.05})$, and $\text{poly}(\text{MGE}_{0.71}\text{-mPEG550-Pos}_{0.05})$, are red transparent viscous liquids due to oxidation of the iodide counterions associated with the aminium side chains. The color can be removed by ion exchange with chloride to generate off-white transparent viscous liquids. Furthermore, polymers with mPEG750 side chain, $\text{poly}(\text{PGE}_{0.57}\text{-mPEG750-Pos}_{0.05})$, $\text{poly}(\text{PGE}_{0.57}\text{-mPEG750-Neg}_{0.05})$, $\text{poly}(\text{MGE}_{0.71}\text{-mPEG750-Pos}_{0.05})$, and $\text{poly}(\text{MGE}_{0.71}\text{-mPEG750-Neg}_{0.05})$ were low-melting point solids. Polymers with mPEG2000 side chain, $\text{poly}(\text{PGE}_{0.57}\text{-mPEG2000-Pos}_{0.05})$, $\text{poly}(\text{PGE}_{0.57}\text{-mPEG2000-Neg}_{0.05})$, $\text{poly}(\text{MGE}_{0.71}\text{-mPEG2000-Pos}_{0.05})$, and $\text{poly}(\text{MGE}_{0.71}\text{-mPEG2000-Neg}_{0.05})$ were low-melting point solids.

Pos_{0.05}), and poly(**MGE_{0.71}-mPEG2000-Neg_{0.05}**) were obtained as solids. The charged side chains not only change the physical appearance of the polymers, but it also alters the lower critical solution temperature behavior. This will be further discussed in the following chapter.

2.5. Summary

Two alkyne-functionalized epoxides, **PGE** and **MGE**, were synthesized and characterized. The polymerization of **PGE** and **MGE** were carried out using *i*-Bu₃Al as catalyst and Oct₄NBr as initiator. Poly(**PGE**)s with molecular weight between 2,800 to 19,000 g/mol and poly(**MGE**)s with molecular weight between 3,900 to 31,000 g/mol were obtained with good to moderate PDI. PPM of poly(**PGE**) and poly(**MGE**) were performed with **mEDG azide** and **decyl azide** via CuAAC “click” reaction and a series of amphiphilic poly(**PGE_{0.X}**) and poly(**MGE_{0.X}**) were synthesized and characterized. Furthermore, charged side chains were placed via CuAAC with various hydrophilic azides (**mPEG550 azide**, **mPEG750 azide**, **mPEG2000 azide**) and charged azides (**COOH azide** and **aminium azide**). This modification further expanded the chemical properties of these non-degradable polymers.

poly(**MGE**_{0.55}), which are water insoluble at room temperature, dissolved when samples were cooled in an ice bath. To better quantify the LCST behavior of poly(**PGE**_{0.x}) and poly(**MGE**_{0.x}), cloud points were determined. First, aqueous solutions of poly(**PGE**_{0.x}) and poly(**MGE**_{0.x}) were prepared and filtered through 0.2 μm Whatman PTFE (poly(tetrafluoro-ethylene)) filter prior to analysis. Then the solutions were slowly heated in a temperature controlled bath until the transparent solution began to cloud. A representative picture of cloud point determination is shown in Figure 27. In the course of heating, the solution of poly(**MGE**_{0.65}), which was transparent below 32 °C (Figure 27a), rapidly became cloudy at 33 °C (Figure 27b).

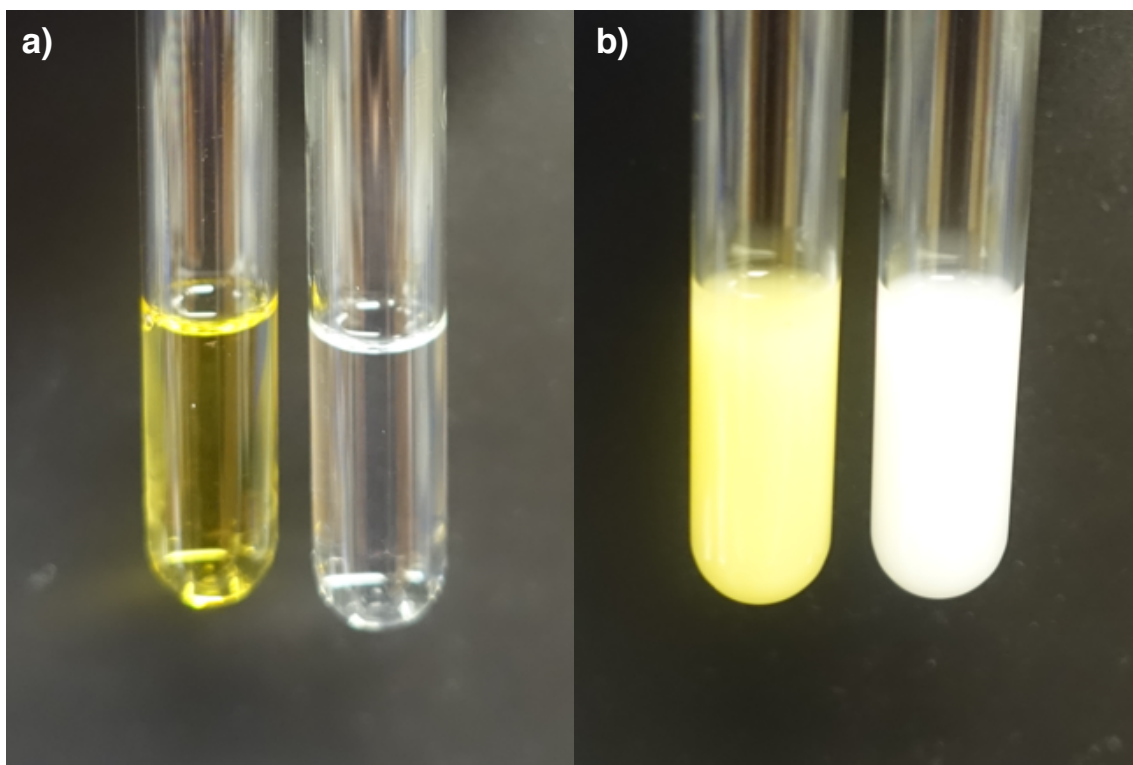


Figure 27. Photographs showing the lower critical solution temperature behavior of polymers p-MGE_{0.65} and *trans*-PhN=NPh@poly(MGE_{0.65}) in Milli-Q water. a) poly(MGE_{0.65}) (right) and *trans*-PhN=NPh@poly(MGE_{0.65}) (left) below LCST (taken at 25 °C) b) poly(MGE_{0.65}) (right) and *trans*-PhN=NPh@poly(MGE_{0.65}) (left) above LCST (taken at 33 °C).

To better LCST behavior for the large number of materials synthesized in this project, polymers were dissolved in Milli-Q water and solution turbidity was monitored via variable temperature UV-vis spectrometer (Figure 28). LCSTs were determined by dissolving each polymer in Milli-Q water (5 mg/mL except poly(PGE_{1.0}) and poly(MGE_{0.50}), for which 10 mg/mL was used), and then monitoring the solution absorbance at 450 nm as a function of temperature. Specifically, the first spectrum of the clear solution was recorded several degrees below the LCST. Then the temperature was increased by 1 °C increments and successive spectra were taken with 3 minutes

equilibration times between temperature jumps (except for poly(**MGE**_{0.50})). As the solution approaches the LCST, the solution becomes cloudy and the absorbance increases. The temperature was raised until the absorbance plateaued. The LCST is defined as the temperature at which the absorbance is half of the maximum value. Plots of the LCSTs as a function of the mole fraction of mDEG chains present in poly(**PGE**_{0.x}) and poly(**MGE**_{0.x}) are shown in Figure 29.

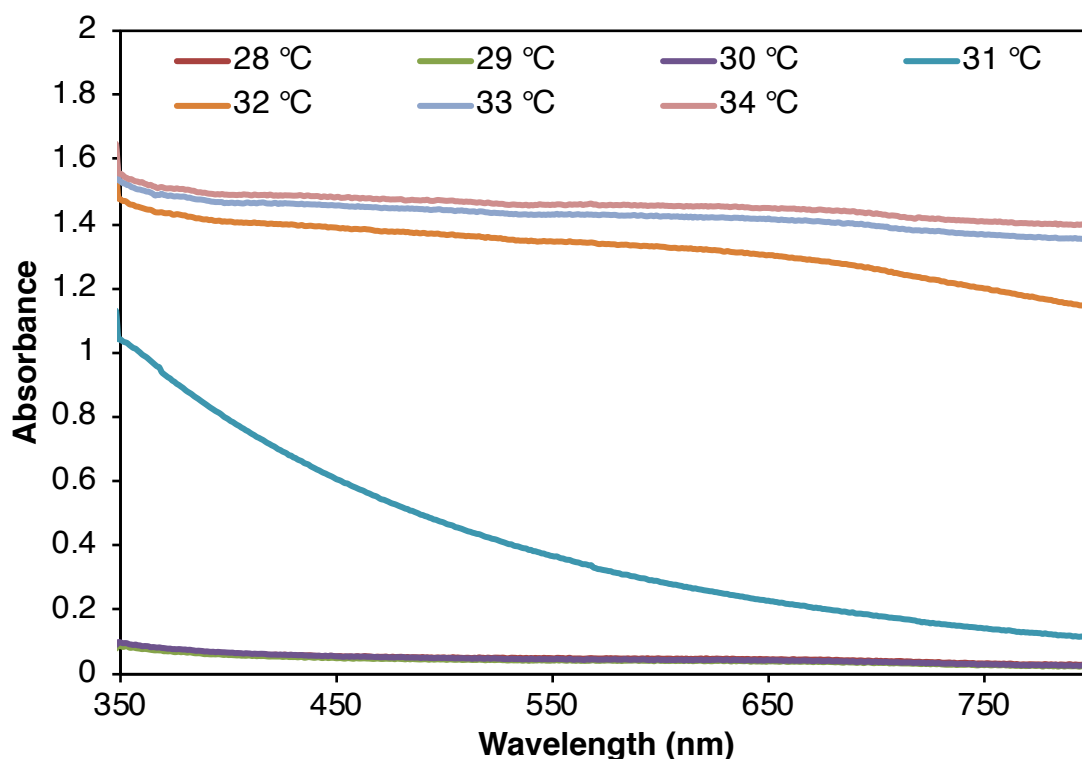


Figure 28. LCST determination via UV-vis spectrometer for poly(**MGE**_{0.70}) ($M_n = 54,000$, PDI = 1.21) in Milli-Q water (5 mg/mL) under various temperatures at 1 °C/3 min.

Similar to the previously reported click-modified glycolide analogs,⁴⁹ the LCSTs for poly(**PGE**_{0.x}) and poly(**MGE**_{0.x}) have an approximately linear relationship with mole fraction of mDEG side chains between 18.4 to 70.8 °C. The linear portions of the plots in

Figure 29 have similar slopes (0.5 for poly(**PGE**_{0,x}) and 0.7 for poly(**MGE**_{0,x})). Substitution at the propargyl C1 position significantly impacts the LCST with the dimethyl propargyl p-**MGE**_{0,x} polymers exhibiting LCSTs ~ 20 °C lower than poly(**PGE**_{0,x}) analogs. As shown in Figure 29, a solution of poly(**PGE**_{0.60}) has an LCST at 48.2 °C. Interestingly, solution of poly(**PGE**_{1.0}) gave an LCST near the boiling point of water of 96.8 °C. Near lower the freezing point of water, poly(**MGE**_{0.50}) gave an LCST at 3.6 °C, while poly(**MGE**_{1.0}) set the upper LCST limit for the poly(**MGE**_{0,x}) family at 55.5 °C. Combining the temperature ranges of poly(**PGE**_{0,x}) and poly(**MGE**_{0,x}), the LCSTs of these PEG-based polymers can extend to the full range of liquid phase water. It is worth noting that poly(**MGE**_{0.50}) has one of the lowest LCSTs measured in the literature (Table 5).

Table 5 compares previously reported polymers with low LCST values to poly(**MGE**_{0.50}).^{92,93,234–238} A low molecular weight oligomer of poly(propylene glycol) (**2**, $M_n = 1,025$), reported by Firman and Kahlweit in 1986, has the lowest LCST at 1.0 °C at 55 wt % concentration in water.²³⁴ In 2006, Laschewsky and co-workers published series of water soluble poly(acrylamide)s and poly(acrylate)s.²³⁵ Among these polymers, it was demonstrated that the LCST of poly(2-(2-ethoxyethoxy)ethyl acrylate) (**3**, $M_n = 17,500$, PDI = 1.66) is 9.0 °C in water. Satoh and co-workers synthesized a series of aliphatic glycidyl ethers and their homopolymers with LCSTs ranging from 10.3 °C (**4**, poly(ethoxy glycidyl ether) (poly(EtGE), $M_n = 5,290$, PDI = 1.04) to 91.6 °C (poly(2-methoxyethyl glycidyl ether) poly(MeEOGE), $M_n = 4,860$, PDI = 1.05) in 2017.²³⁶ In 2005, Mori, Endo and co-workers reported the synthesis of *N*-acryloyl-*L*-proline methyl ester (A-Pro-OMe) and poly(A-Pro-OMe) (**5**, $M_n = 5,500$, PDI = 1.15) with LCST at 15.0 °C.²³⁷ Kobayashi and co-workers presented the synthesis of a series of poly(vinyl ether)s with oxyethylene

pendant groups and the phase separation behavior in water.²³⁸ For example, poly(2-ethoxyethylvinylether) (**6**, $M_n = 22,000$, PDI = 1.13) exhibited a LCST at 20.0 °C. At 3.6 °C, the LCST for poly(**MGE**_{0.50}) lies between entries **2** and **3** in Table 5, but differs from those polymers by having a significantly higher M_n , and the LCST was measured at a much lower concentration than in entry **2**.

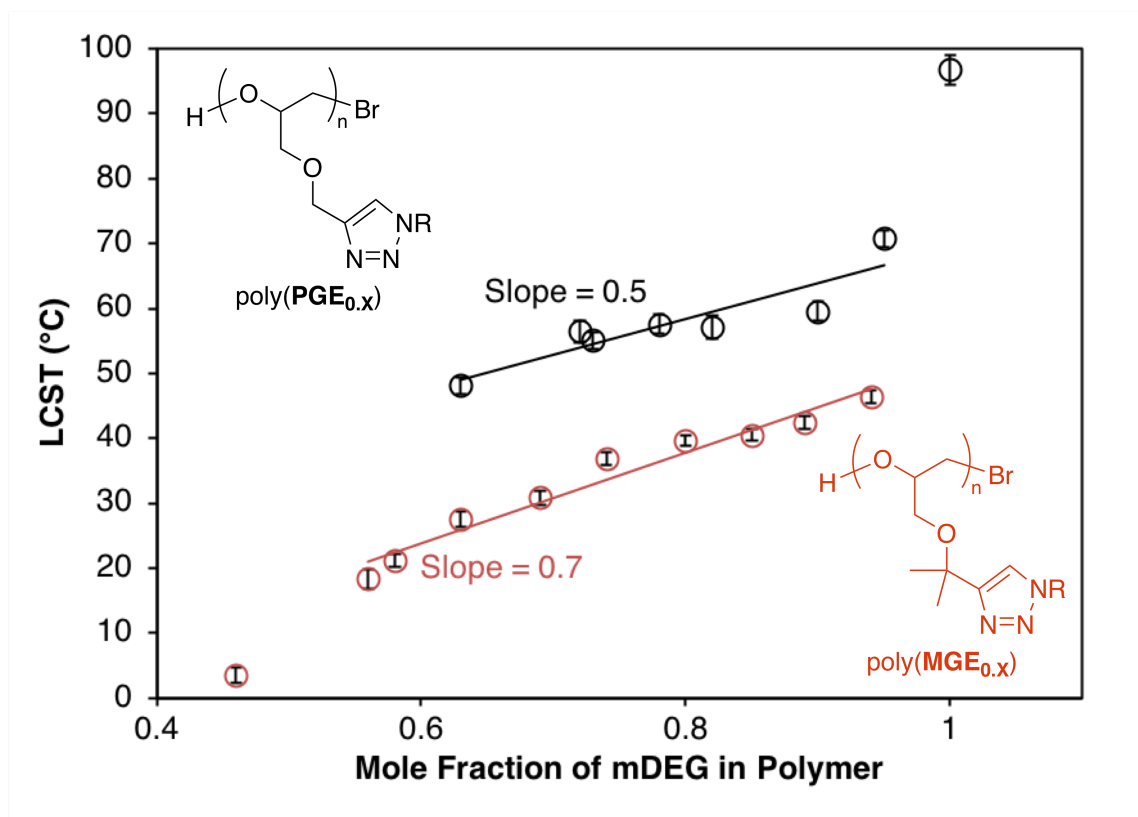
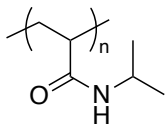
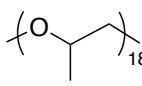
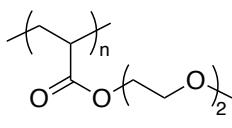
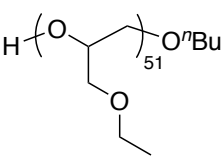
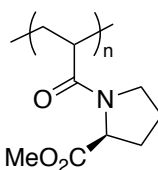
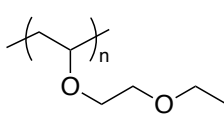
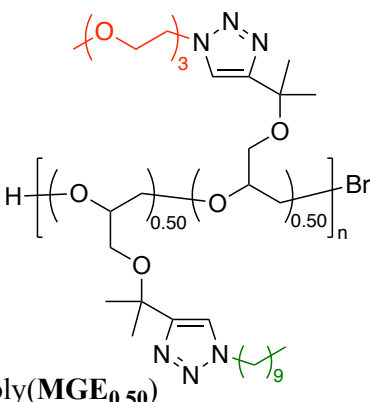


Figure 29. Plots of LCSTs vs. the mole fraction of mDEG chains in poly(**PGE**_{0.x}) and **poly(MGE**_{0.x}) obtained by UV-Vis spectrometer under various temperatures at 1 °C/3 min except **poly(MGE**_{0.50}) (at 1 °C/60 min).

Table 5. Selective polymers and their LCSTs.^{92,93,234–238}

Polymer Structure	M_n (g/mol)	PDI	LCST (°C)	Concentration (wt %)	Ref.
1 	290,000	3.50	31	-	92,93
2 	1,025	-	1	55.0	234
3 	17,500	1.66	9	-	235
4 	5,290	1.04	10	1	236
5 	5,500	1.15	15	0.1	237
6 	22,000	1.13	20	1.0	238
 <p>poly(MGE_{0.50})</p>	54,000	1.19	4	0.5	-

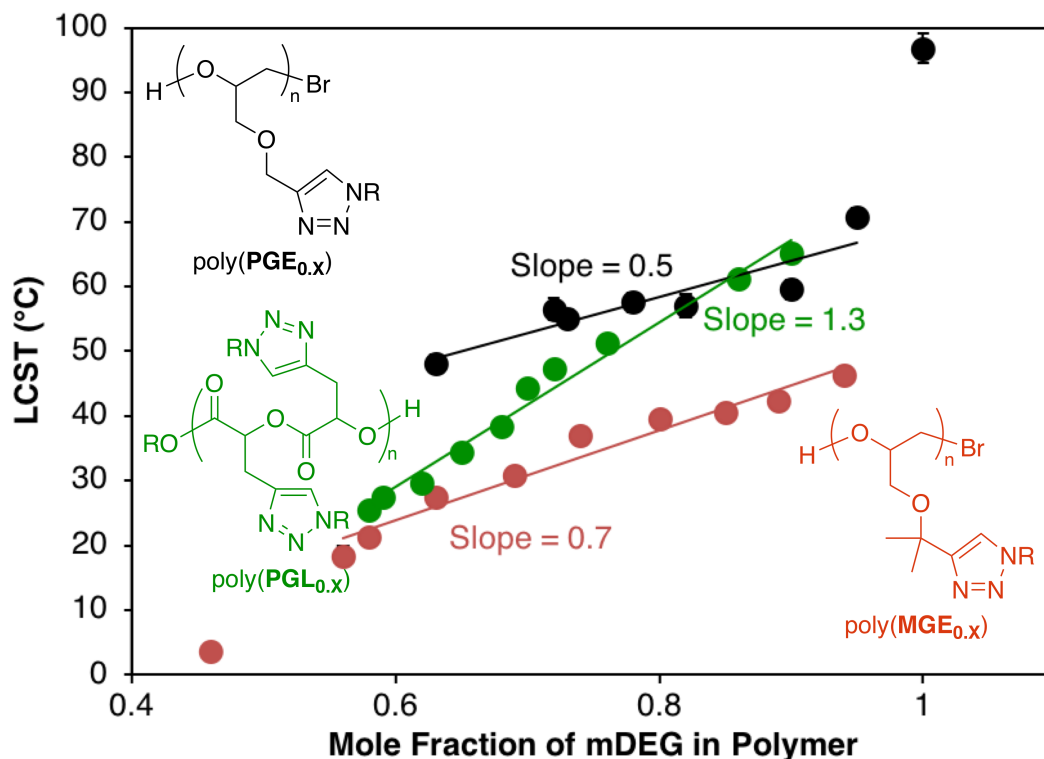


Figure 30. Plots of LCSTs vs. the mole fraction of mDEG chains in poly(PGE_{0.x}) and poly(MGE_{0.x}), and poly(PGL_{0.x}) obtained by UV-Vis spectrometer.

The comparison of degradable poly(PGL_{0.x}) and the non-degradable poly(PGE_{0.x}) and poly(MGE_{0.x}) is shown in Figure 30. The slope for p-PGL_{0.x} is 1.3, which is almost double the slope value for poly(PGE_{0.x}) and poly(MGE_{0.x}), 0.5 and 0.7, respectively. This result reveals that the backbone of the polymers influences the LCST behavior significantly. Not only can one use side chains to control the LCSTs of polymers, one can also use the backbone structure to adjust the LCSTs. This design allows a precise way to adjust the LCST in future applications. In addition, the result is in good agreement with our previous research on “click” modified poly(PGL_{0.x}).

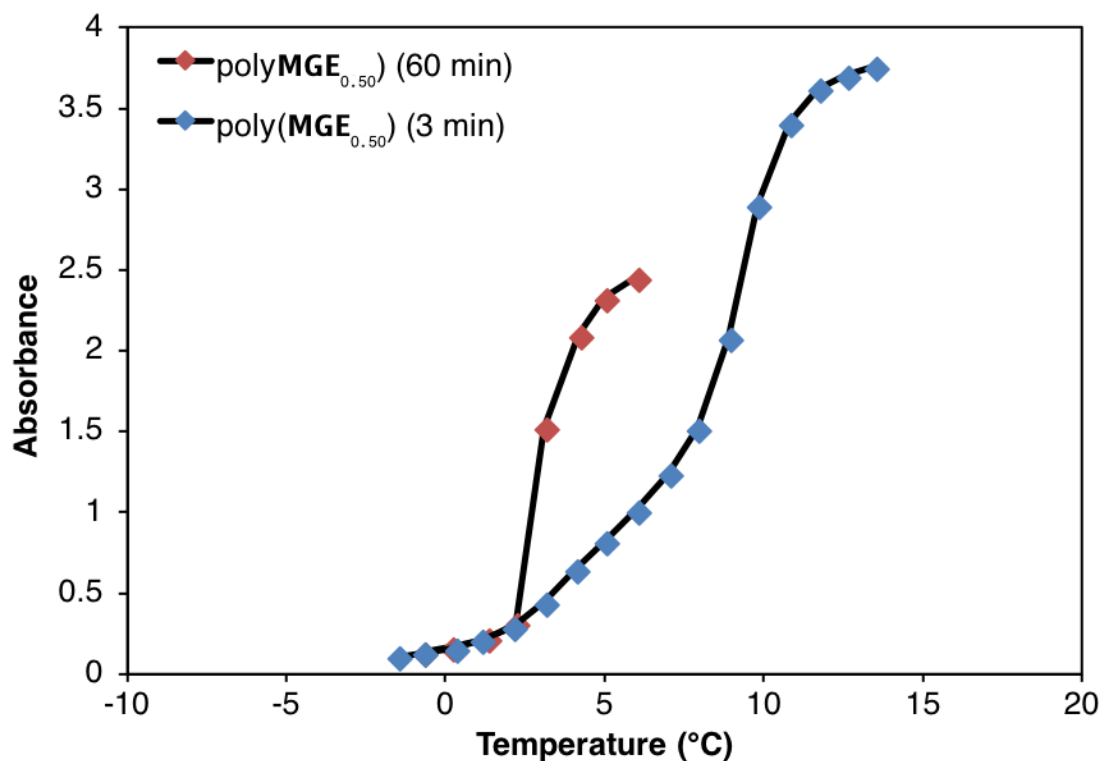


Figure 31. LCST determination via UV-vis spectrometer at 450 nm for poly(**MGE**_{0.50}) ($M_n = 54,000$, PDI = 1.19) in Milli-Q water (10 mg/mL) under various temperatures at 1 °C/3 min (blue diamond) and 1 °C/60 min (red diamond).

As shown in representative graph, Figure 31, the polymer exhibits the lowest LCST, poly(**MGE**_{0.50}) ($M_n = 54,000$, PDI = 1.19, 10 mg/mL), shows very broad change in absorbance at 1 °C/3 min heating rate over temperature range of 10 °C. On the contrary, the absorbance of poly(**MGE**_{0.70}) ($M_n = 54,000$, PDI = 1.21, 5 mg/mL) at 450 nm increases sharply during gel formation upon heating over temperature range of ~ 3 °C (Figure 32). When the heating rate was changed to 1 °C/60 min for poly(**MGE**_{0.50}), the absorbance increases sharply over temperature range of ~ 3 °C. For the less concentrated (5 mg/mL) sample of poly(**MGE**_{0.50}), it required more than 150 min to reach equilibrium.

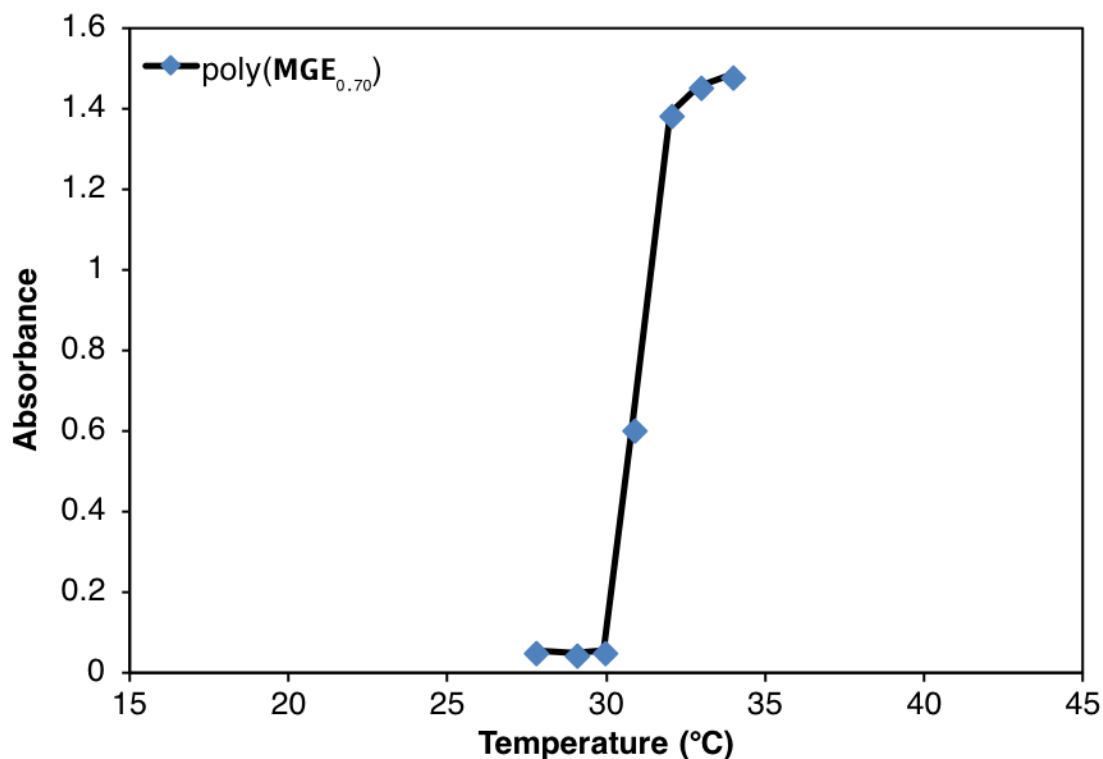


Figure 32. LCST determination via UV-vis spectrometer at 450 nm for poly(**MGE**_{0.70}) (M_n = 54,000, PDI = 1.21) in Milli-Q water (5 mg/mL) under various temperatures at 1 °C/3 min.

Variable temperature dynamic light scattering (DLS) can also be used to survey the LCST behavior by measuring the average hydrodynamic radius (R_h) as a function of temperature. The average hydrodynamic radius of poly(**MGE**_{0.70}) stays constant at ~7 nm before heating to its LCST. While heating to and above its LCST, the average hydrodynamic radius changed rapidly during gel formation (Figure 33). A similar roughly linear relationship between the LCST and the mole fraction of mDEG side chains in the polymers was observed in both UV-vis and DLS. Figure 34 shows the overlay of LCST vs. mole fraction of mDEG in polymer obtained from UV-Vis spectrometer and DLS. It is concluded that both methods gave comparable data.

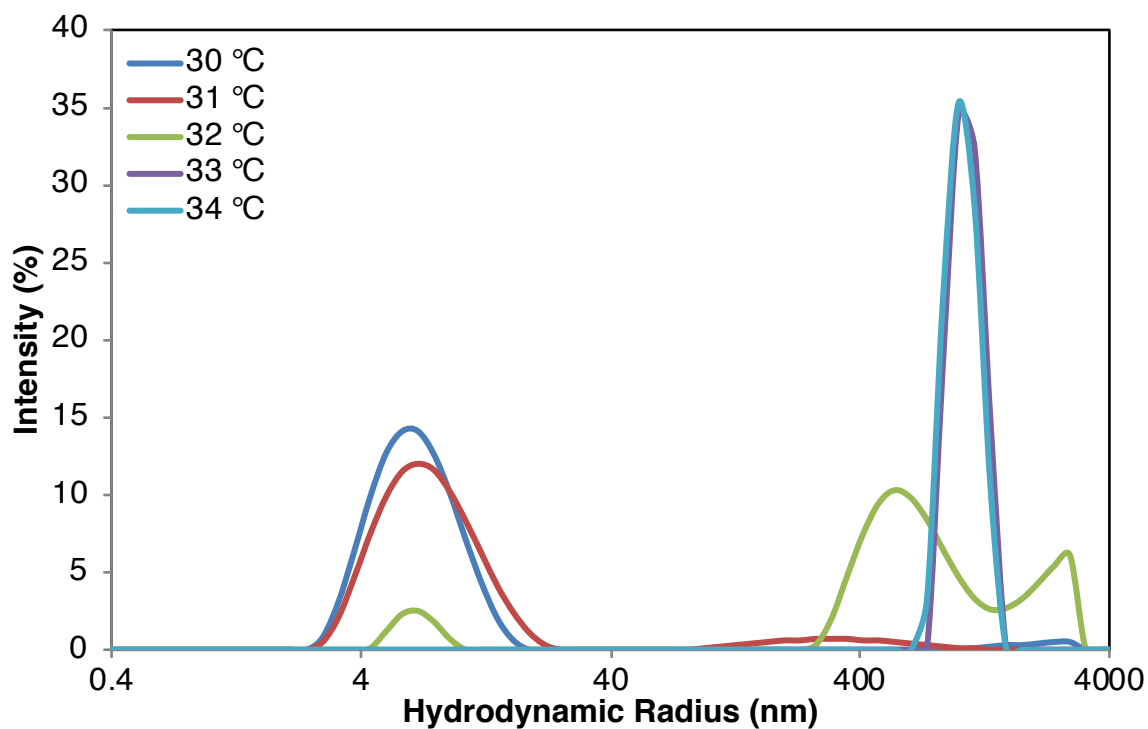


Figure 33. LCST determination via DLS for poly(MGE_{0.70}) ($M_n = 54,000$, PDI = 1.21) in Milli-Q water (5 mg/mL) under various temperatures at 1 °C/3 min.

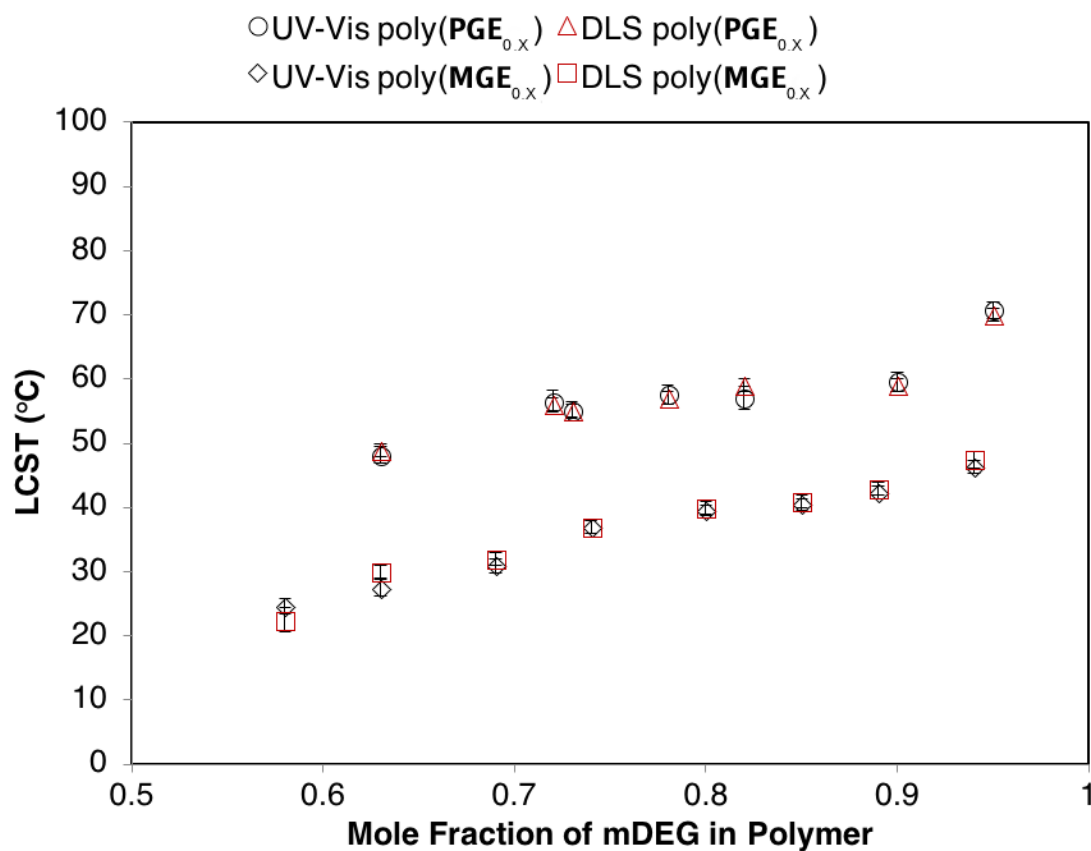


Figure 34. Plots of LCSTs vs. the mole fraction of mDEG chains in poly(**PGE**_{0.x}) by UV-Vis spectrometer (black circle) and by DLS (red triangle) and poly(**MGE**_{0.x}) by UV-Vis spectrometer (black diamond) and by DLS (red square).

As is the case for small molecules and salts, polymer solubilities are concentration and temperature dependent.⁸² Likewise, the LCSTs for most polymers that exhibit LCST behavior are concentration dependent. Nevertheless, examples where the LCST concentration dependence is small or undetected are documented.^{239,240} Generally, a polymer's LCST is concentration independent over wide concentration ranges but rises at low concentrations. The increase in LCST at low concentration can vary significantly with chemical composition as illustrated for selected examples from the literature (Table 6).^{239,241–244}

Table 6. Selective examples from literatures showing LCSTs at various concentrations.^{239,241–244}

Polymer Structure	M_n (g/mol)	Concentration (wt %)	LCST Range (°C)	LCST (°C)	Ref.
<p>7</p>	130,000	0.01-1.0	31.6-29.9	29.9	239
<p>8</p>	100,000	0.1-30.0	43.0-38.0	38.0	241
<p>9</p>	22,400	0.1-30.0	76.0-65.5	65.5	242
<p>R = Et (10), <i>n</i>-Pr (11), <i>n</i>-Bu (12)</p>	Et = 6,187 <i>n</i> -Pr = 4,711 <i>n</i> -Bu = 4,891	0.13-15.0	Et = 77.0-52.0 <i>n</i> -Pr = 73.0-41.0 <i>n</i> -Bu = 69.0-33.0	Et = 52.0 <i>n</i> -Pr = 41.0 <i>n</i> -Bu = 33.0	243, 244
<p>poly(MGE_{0.65})</p>	52,000	0.1-10.0	27.3-30.8	27.5	-

Freitag and co-workers synthesized and examined the LCSTs of poly-*N,N*-diethylacrylamide (polymer **7**, M_n = 130,000 g/mol) in 1994.²³⁹ The change in LCST at

various concentrations was minimal. The LCST was 29.9 °C at 1.0 wt % and rose to 31.6 °C at 0.01 wt %. Allcock and co-workers reported a series of alkyl ether based polyphosphazenes in 1996.²⁴¹ The LCSTs of these polyphosphazenes were investigated in the concentration range of 0.1-30 wt %. The LCSTs were concentration independent in the range of 2-30 wt %. For example, the LCST of polymer **8** ($M_n = 100,000$ g/mol) was 38.0 °C above 2 wt % and increased to 43.0 °C at 0.1 wt %. In 1999, Shon and co-workers published a series of polyphosphazenes with methoxy-PEGs and amino acid esters as side chains.²⁴² Majority of these polyphosphazenes exhibited LCSTs from 25.2 to 98.5 °C and the LCSTs were concentration independent between 3 to 30 wt %. For instance, polymer **9** ($M_n = 22,400$ g/mol) exhibited LCST at 65.5 °C above 3 wt % and the LCST rose sharply to 76.0 °C at 0.1 wt %. Bi and co-workers reported a series of polyphosphazenes containing lactate esters and 2-(2-methoxyethoxy)ethoxy side chains in 2010 and 2011.^{243,244} These polyphosphazenes exhibited LCSTs from 33 to 52 °C in water depending on the ester group (Et = 52 °C, **10**, $M_n = 6,187$ g/mol, *n*-Pr = 41 °C, **11**, $M_n = 4,711$ g/mol, *n*-Bu = 33 °C, **12**, $M_n = 4,891$ g/mol). The LCSTs were concentration independent in the range of 1.5-15 wt %. Below 1.5 wt %, the LCSTs increased sharply. For R = Et, the LCST at 0.13 wt % rose to 77 °C—an increase of 25 °C. The LCST for propyl and butyl analogs at 0.13 wt % rose by 32 and 36 °C, respectively.

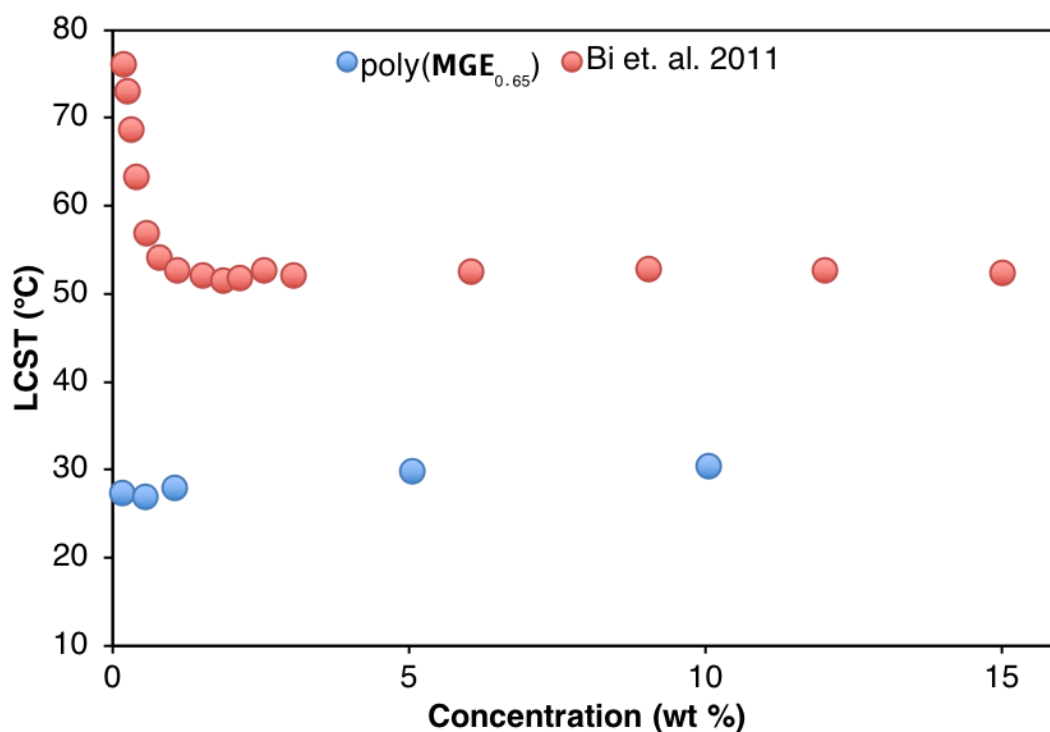


Figure 35. LCSTs as a function of concentration of poly(**MGE**_{0.65}) (blue circles) and polyphosphazene reported by Bi and co-workers (red circles).

The influence of polymer concentration on LCSTs for poly(**MGE**_{0.65}) ($M_n = 52,000$ g/mol, PDI = 1.19) was examined and is shown in Figure 35. Notably, the concentrations of poly(**MGE**_{0.65}) showed little impact on cloud points and only a ~ 3 °C difference was observed within the studied range, 0.1-10 wt %. The small variation of cloud points of poly(**MGE**_{0.65}) suggests a concentration independent LCST behavior in comparison with polyphosphazenes reported by Bi and co-workers even at low polymer concentration.

We have also found that addition of the charged side chains significantly altered the LCST behavior of the polymers. For example, the LCST for poly(**MGE**_{0.75}) is 36.9 °C; however, the LCST of poly(**MGE**_{0.71}-**Neg**_{0.05}) is 49.5 °C, with only 5% of the side chains were **COOH azide** incorporated. Moreover, the LCST for poly(**MGE**_{0.75}) was obtained at

5 mg/mL concentration but it requires 15 mg/mL in concentration to measure the LCST of poly(**MGE**_{0.71}-**Neg**_{0.05}). In addition, polymers containing 5% of **aminium azide** such as poly(**MGE**_{0.71}-**Pos**_{0.05}) showed no LCST behavior.

The interactions of salts with macromolecules in aqueous solution can influence their behaviors.^{245–254} In 1888, the ability of salts to precipitate proteins from an aqueous solution with a recurring trend was first systematically studied by Hofmeister.^{255,256} Now known as the Hofmeister series, the ionic sequence refers to the effectiveness of ions on a range of phenomena. In 2005, Bergbreiter, Cremer, and co-workers reported specific ion effects on the LCST behavior of PNIPAM.²⁵⁷ Herein, we have studied the effects of Na₂CO₃ and NaCl on the LCSTs of poly(**MGE**_{0.75}) and poly(**MGE**_{0.71}-**Neg**_{0.05}) at various concentrations, shown in Figure 36. In the Bergbreiter, Cremer, and co-workers' study, the changes in LCSTs of PNIPAM in Na₂CO₃ solution were the sharpest and the LCST was lowered to 21.0 °C with 0.33 M Na₂CO₃ in the solution.²⁵⁷ However, in our study, the LCST of poly(**MGE**_{0.71}-**Neg**_{0.05}) was first increased in 0.1 M Na₂CO₃ solution to 54.5 °C then was decreased to 27.1 °C when the concentration of Na₂CO₃ was increased to 0.4 M. On the contrary, the raise of the LCST of poly(**MGE**_{0.75}) in Na₂CO₃ solution was not observed. The LCST of poly(**MGE**_{0.75}) was lowered to 21.8 °C from 36.9 °C at 0.3 M Na₂CO₃ concentration. The effects of NaCl on the LCST behavior of poly(**MGE**_{0.71}-**Neg**_{0.05}) was also investigated and its LCST was reduced to 32.7 °C from 49.5 °C in 0.3 M NaCl solution. More studies should be conducted to further understand the effects of the Hofmeister series on the “click” derivatives of poly(**PGE**_{0.x}) and poly(**MGE**_{0.x}). This can provide another way to adjust LCSTs for future applications.

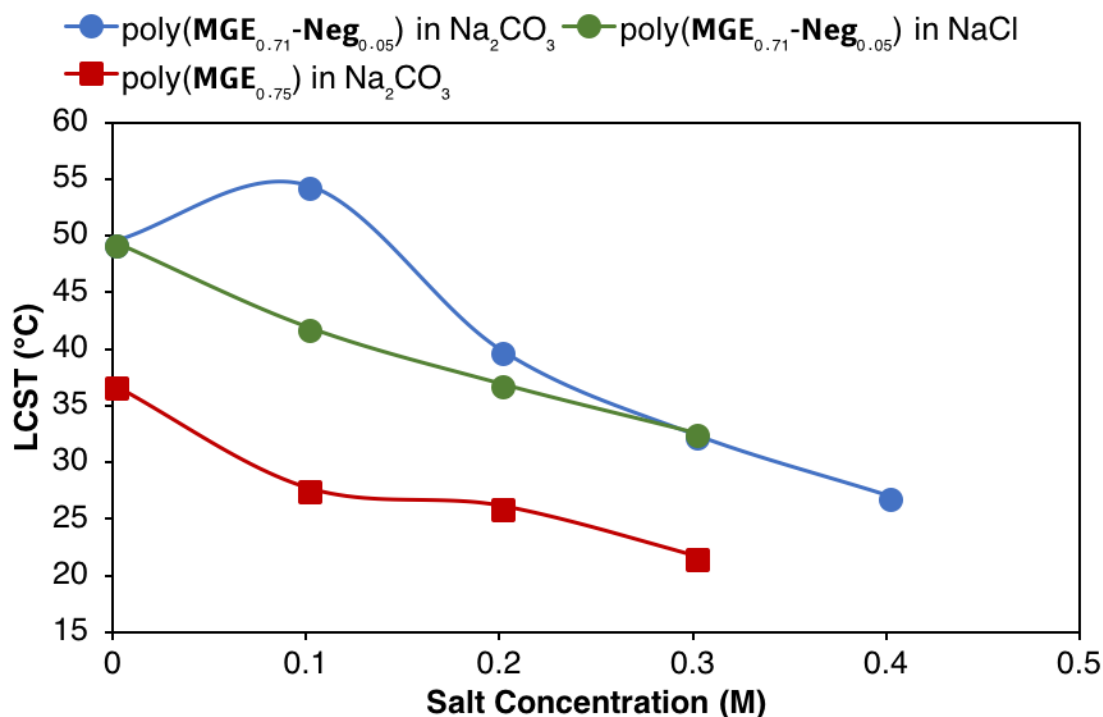


Figure 36. LCST values of poly(MGE_{0.75}) (red square) measured in sodium bicarbonate solutions at concentrations from 0 to 0.3 M, poly(MGE_{0.71}-Neg_{0.05}) (blue circle) measured in sodium bicarbonate solutions at concentrations from 0 to 0.4 M, and poly(MGE_{0.71}-Neg_{0.05}) (orange circle) measured in sodium chloride solutions at concentrations from 0 to 0.3 M.

3.2. Formations of Unimolecular Micelles

Micelles are dynamic aggregates of surfactant molecules above the critical micelle concentration (cmc). DLS is often used to determine the cmc. When traditional micelles reach the cmc, there is a dramatic change in the hydrodynamic radius. However, our previous work on “clickable” polyglycolides showed that hydrodynamic radius of the poly(propargyl glycolide)-*graft*-poly(ethylene glycol) monoethyl ether (poly(PGL_{1.0}))⁹⁵ polymers was unaffected by polymer concentration, which suggested the formation of unimolecular micelles.^{97,109,110,113,114,122} To perform the unimolecular micelle study on the amphiphilic poly(PGE_{0.x}) and poly(MGE_{0.x}), the polymer samples were dissolved in

Milli-Q water and filtered through 0.2 μm Whatman PTFE filter prior to analysis. All the analysis was done at a temperature below the LCST of the sample. Similar to poly(**PGL**_{0.x}) system, DLS data shows that the hydrodynamic radius of the particles at different concentrations was relatively similar, which indicates the formation of unimolecular micelles. As shown in Figure 37, the hydrodynamic radius of poly(**MGE**_{0.65}) ($M_n = 52,000$ g/mol, PDI = 1.19) is 7 ± 3 nm at 50 mg/mL and is 6 ± 2 nm at 10, 5, 1 mg/mL.

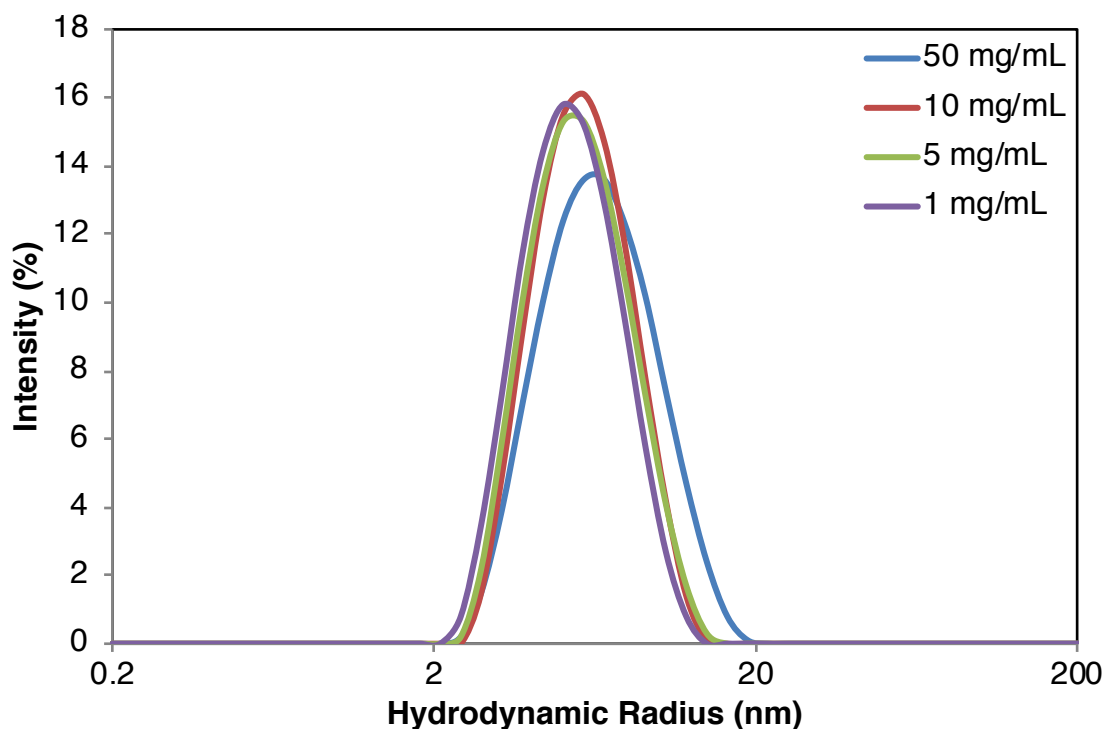


Figure 37. DLS results for poly(**MGE**_{0.65}) ($M_n = 52,000$ g/mol, PDI = 1.19, $R_H = 6 \pm 2$ nm) in Milli-Q water at different concentrations.

The formation of unimolecular micelles and the aggregation of polymer above its LCST can also be observed by TEM (Figure 38). Poly(**MGE**_{0.65}) was dissolved in Milli-Q water and filtered through 0.2 μm Whatman PTFE (poly(tetrafluoro-ethylene)) filter prior

to analysis. The solution was dropped on Formvar-coated copper grids below LCST for the preparation of TEM samples. One sample was kept below its LCST before removing the excess water and the other sample was heated on a hot plate above the LCST for 2 minutes before removing the excess water. Both samples were stained with 2% potassium phosphotungstate (PTA) solution to generate a dark background. As shown in Figure 38a, which was taken at 100,000x, the size of polymer particles is 20 ± 4 nm. This is slightly bigger than the hydrodynamic diameter of poly(MGE_{0.65}) measured by DLS (~ 13 nm). This is caused by the surface tension between the solution and the grid. After heating above its LCST (Figure 38b, taken at 40,000x), the size of the particles increased to 74 ± 45 nm.

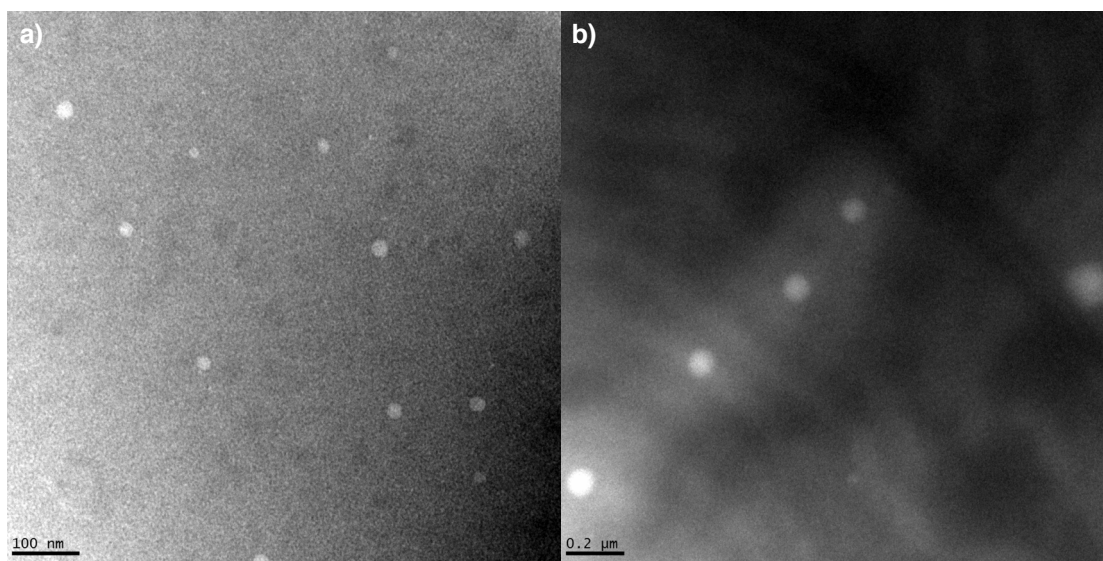


Figure 38. TEM images of polyMGE_{0.65} ($M_n = 52,000$ g/mol, PDI = 1.19) a) below (taken at 100,000x, scale bar = 100 nm, 20 ± 4 nm) and b) above (taken at 40,000x, scale bar = 200 nm, 74 ± 45 nm) its LCST.

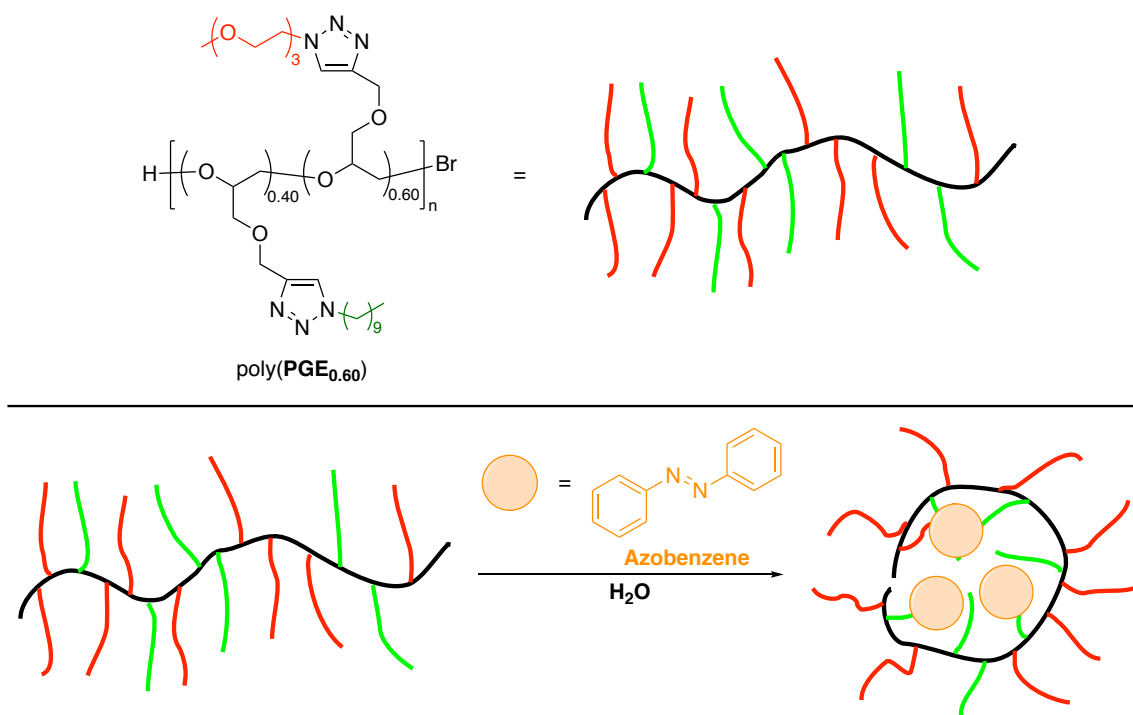
3.3. Summary

“Click” modified amphiphilic poly(**PGE_{0.x}**) and poly(**MGE_{0.x}**) showed water solubility and LCST behavior when X = 55 in poly(**PGE_{0.x}**) and X = 50 in poly(**MGE_{0.x}**). The LCST behavior was controlled through varying the ration between **mDEG azide** and **decyl azide**. In our study, both UV-Vis spectrometer and DLS gave consistent results for LCSTs. A close to linear relationship was obtained between 18.4 to 70.8 °C for both poly(**PGE_{0.x}**) and poly(**MGE_{0.x}**) with similar slopes but with nearly 20 °C differences. These results indicated the backbone and the pendant groups of the polymers both play an important role for tuning the LCSTs. It is worth highlighting that poly(**MGE_{0.50}**) with 3.6 °C for LCST and poly(**PGE_{1.0}**) with 96.8 °C for LCST. This allows us to manipulate the LCSTs of these polymers across the whole temperature span of liquid phase water. We also demonstrated that the LCSTs of poly(**PGE_{0.x}**) and poly(**MGE_{0.x}**) are concentration independent. Furthermore, it was found that the LCST of poly(**MGE_{0.71-Neg_{0.05}}**) is 49.5 °C, 12.6 °C higher than poly(**MGE_{0.75}**), with only 5% of side chains were acid derivatives. The effects of Na₂CO₃ and NaCl on poly(**MGE_{0.75}**) and poly(**MGE_{0.71-Neg_{0.05}}**) were also investigated and this provided another factor to alter the LCST behavior of polymers. Moreover, poly(**PGE_{0.x}**) and poly(**MGE_{0.x}**) formed unimolecular micelles, which can be characterized by DLS and TEM. The potential applications for unimolecular micelles will be further discussed in the following chapter.

Chapter 4. Unimicelles as Nanocarriers for Hydrophobic and Hydrophilic Guest Molecules

4.1. Encapsulation of Hydrophobic Guest Molecules

Scheme 20. Schematic representative of azobenzene encapsulation.



Polymers that form unimolecular micelles are promising as drug carriers because they can be prepared by controlled polymerization methods and are not subject to cmc. As a proof of concept, azobenzene (*trans*-PhN=NPh), which is a water insoluble, UV-active model for hydrophobic drugs, was chosen as a hydrophobic guest molecule to be encapsulated in the unimolecular micelles (Scheme 20). Azobenzene and poly(PGE_{0.60}) ($M_n = 44,000$ g/mol, PDI = 1.33), poly(MGE_{0.65}) ($M_n = 52,000$ g/mol, PDI = 1.19), and poly(MGE_{0.75}) ($M_n = 52,000$ g/mol, PDI = 1.22) were dissolved in Milli-Q water. The solution was stirred for 24 hours followed by filtered through 0.2 μm Whatman PTFE filter

to remove unencapsulated azobenzene. The resulting solution appeared yellow which indicates the encapsulation of azobenzene. Also, as shown in Figure 39, the characteristic absorbance at 425 nm in UV spectrum confirmed that azobenzene was encapsulated in the micelles. With increasing concentration of poly(**PGE**_{0.60}), an increase in absorbance was also observed. Furthermore, when the resulting solution was heated above the LCST of poly(**MGE**_{0.65}), turbidity of solution was observed (Figure 27b). After the mixture was cooled down below the LCST, the precipitates re-dissolved and the color of the solution returned to yellow again (Figure 27a).

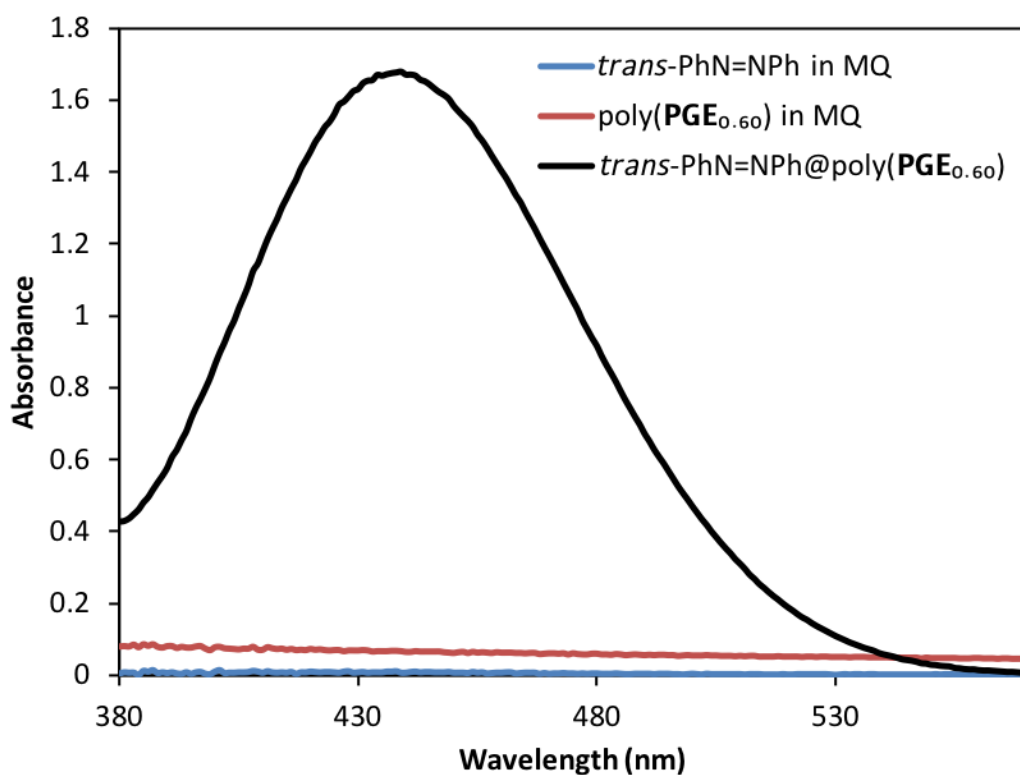


Figure 39. UV-vis spectra of *trans*-PhN=NPh, poly(**PGE**_{0.60}) ($M_n = 44,000$ g/mol, PDI = 1.33), and *trans*-PhN=NPh@poly(**PGE**_{0.60}) in Milli-Q water at room temperature.

The DLS results of poly(**MGE**_{0.65}) and poly(**MGE**_{0.75}) encapsulated azobenzene are shown in Figure 40 and Figure 41. Interestingly, when 10 mg/mL polymer concentration was used during the encapsulation process, the hydrodynamic radii of poly(**MGE**_{0.65}) encapsulated azobenzene (*trans*-PhN=NPh@ poly(**MGE**_{0.65})) were almost two times larger ($R_H = 12 \pm 8$ nm) than those of poly(**MGE**_{0.65}) ($R_H = 7 \pm 2$ nm) (Figure 40a). When 50 mg/mL polymer concentration was used, the hydrodynamic radii of *trans*-PhN=NPh@ poly(**MGE**_{0.65}) increased to 13 ± 6 nm and decreased to 9 ± 4 nm upon five-fold dilution (Figure 41a). A different trend was observed when poly(**MGE**_{0.75}) was used. The hydrodynamic radii of poly(**MGE**_{0.75}) and poly(**MGE**_{0.75}) encapsulated azobenzene (*trans*-PhN=NPh@poly(**MGE**_{0.75})) were practically identical, 6 ± 2 nm and 5 ± 2 nm, respectively (Figure 40b). The hydrodynamic radii of *trans*-PhN=NPh@ poly(**MGE**_{0.75}) increased only to 6 ± 3 nm when 50 mg/mL polymer concentration was used and decreased to 5 ± 2 nm upon five-fold dilution. Our hypothesis is that the polymer composition and its hydrophilicity are the potential reasons for the change in hydrodynamic radii, but more studies need to be conducted to explore this phenomenon further.

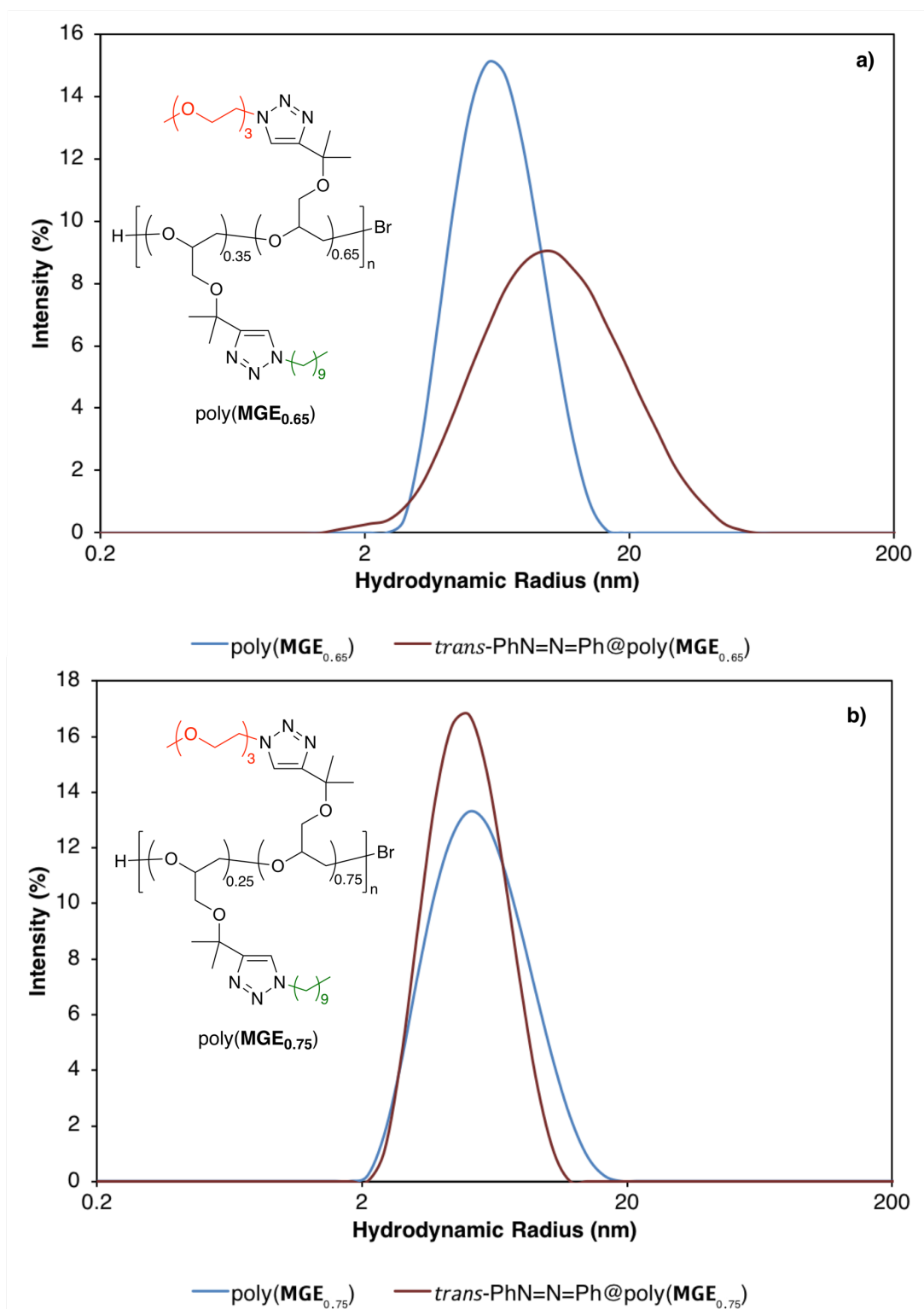


Figure 40. a) DLS results for poly(MGE_{0.65}) (blue curve, $M_n = 52,000$ g/mol, PDI = 1.19, $R_H = 7 \pm 2$ nm) and *trans*-PhN=N=Ph@poly(MGE_{0.65}) (red curve) in Milli-Q. b) DLS results for poly(MGE_{0.75}) (blue curve, $M_n = 52,000$ g/mol, PDI = 1.22, $R_H = 6 \pm 2$ nm) and *trans*-PhN=N=Ph@poly(MGE_{0.75}) (red curve) in Milli-Q

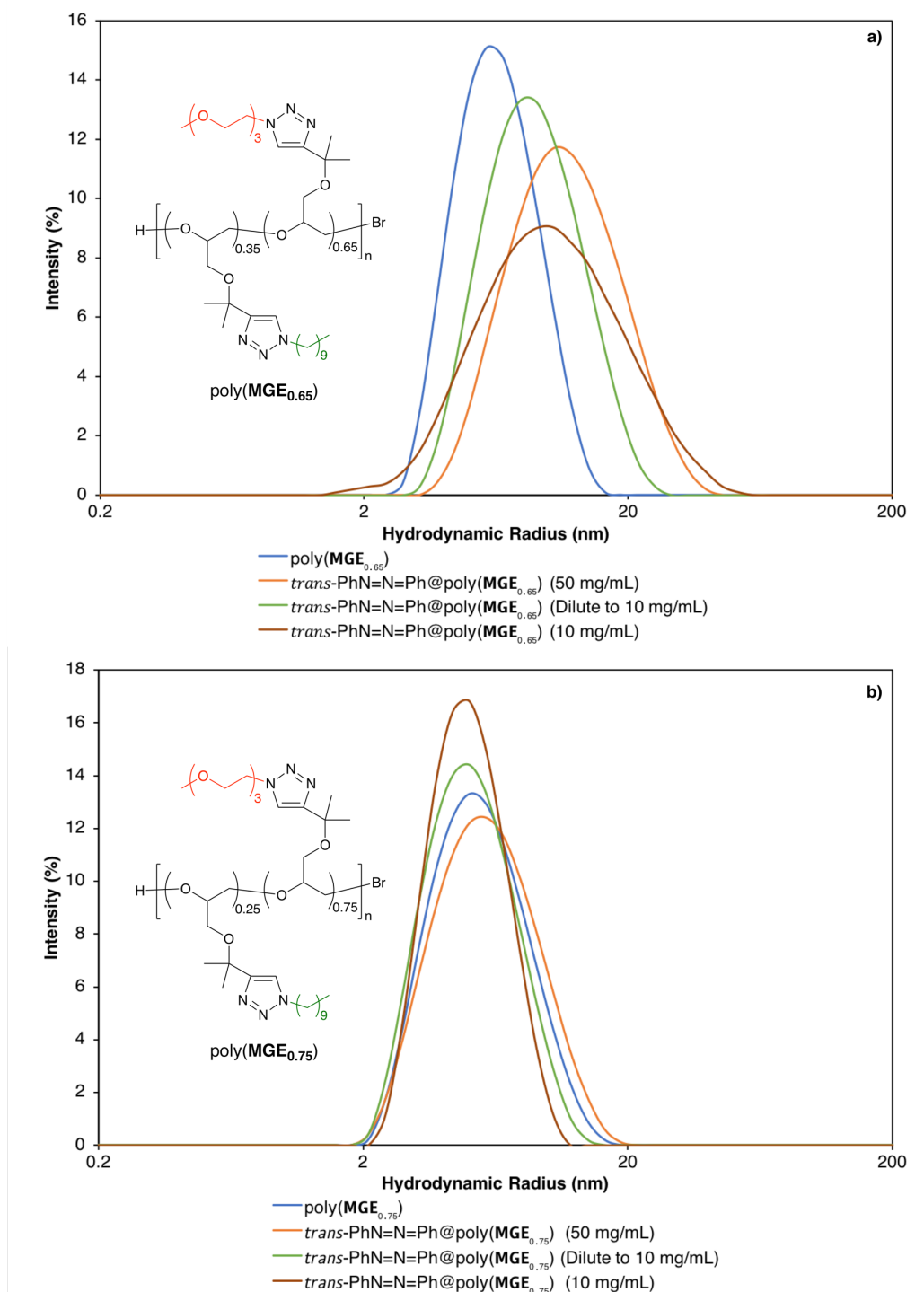


Figure 41. a) DLS results for poly(MGE_{0.65}) (blue curve, $M_n = 52,000$ g/mol, PDI = 1.19, $R_H = 7 \pm 2$ nm), *trans*-PhN=N=Ph@poly(MGE_{0.65}) (orange curve, 50 mg/mL; green curve, dilute to 10 mg/mL from 50 mg/mL; red curve, 10 mg/mL) in Milli-Q. b) DLS results for poly(MGE_{0.75}) (blue curve, $M_n = 52,000$ g/mol, PDI = 1.22, $R_H = 6 \pm 2$ nm) and *trans*-PhN=N=Ph@poly(MGE_{0.75}) (orange curve, 50 mg/mL; green curve, dilute to 10 mg/mL from 50 mg/mL; red curve, 10 mg/mL) in Milli-Q

4.2. Encapsulation of Hydrophilic Guest Biomacromolecules

Subtilisin Carlsberg (SC) was chosen as the hydrophilic guest biomacromolecule. Subtilisin is a non-specific protease and a serine protease originated from *Bacillus subtilis*.^{258–260} SC has been widely studied and used in enzyme-containing cleaning products.²⁶¹ Also, it is conveniently purchased from commercial sources. We have therefore chosen it as a model protein. To study the interaction between SC and polymers, DLS was utilized to monitor the particle sizes as the polymer solution was titrated in the SC solution. Poly(**MGE_{0.71}-mPEG2000-Pos_{0.05}**) (25 mg/mL) and SC (1 mg/mL) were dissolved in Milli-Q water to make the final polymer/SC mixture with a 2:1 molar ratio. As shown in Figure 42, the hydrodynamic radius of SC in Milli-Q water is 5 ± 2 nm (blue line) and poly(**MGE_{0.71}-mPEG2000-Pos_{0.05}**) is 9 ± 3 nm (orange line). When 5 μ L of poly(**MGE_{0.71}-mPEG2000-Pos_{0.05}**) was added, a new peak was observed and the hydrodynamic radii were 6 ± 3 nm and 55 ± 30 nm (green line). When 50 μ L of poly(**MGE_{0.71}-mPEG2000-Pos_{0.05}**) was added, the smaller size peak was shifted to 13 ± 12 nm with a shoulder and two larger size peaks at 198 ± 70 nm and 2603 ± 236 nm appeared (Figure 43). It is proposed that the large peaks are the results of the interaction between SC and poly(**MGE_{0.71}-mPEG2000-Pos_{0.05}**) forming large particles that are observable by DLS. When equal volumes of SC and poly(**MGE_{0.71}-mPEG2000-Pos_{0.05}**) were combined, a single peak appeared at 9 ± 4 nm (green line), similar to the hydrodynamic radius of poly(**MGE_{0.71}-mPEG2000-Pos_{0.05}**) (Figure 44). However, this is insufficient to prove that SC was encapsulated by poly(**MGE_{0.71}-mPEG2000-Pos_{0.05}**) due to the limitation in resolution of DLS. More studies are required to further investigate the interaction between SC and polymers.

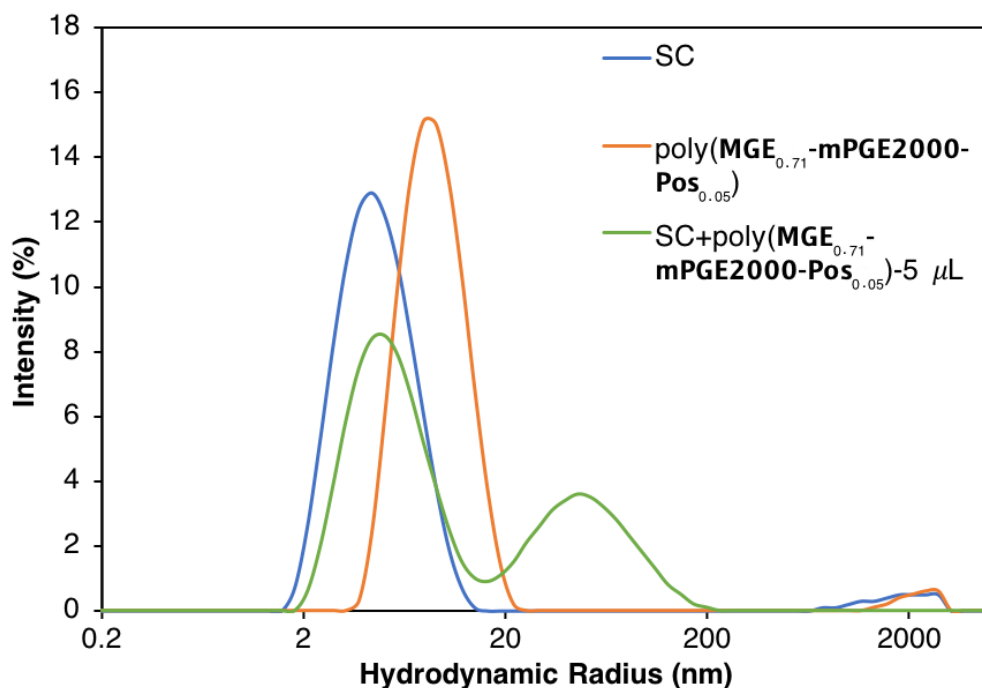


Figure 42. DLS results of SC (blue line), poly(MGE_{0.71}-mPEG2000-Pos_{0.05}) (orange line) and SC with 5 μ L of poly(MGE_{0.71}-mPEG2000-Pos_{0.05}) added (green line) in Milli-Q water.

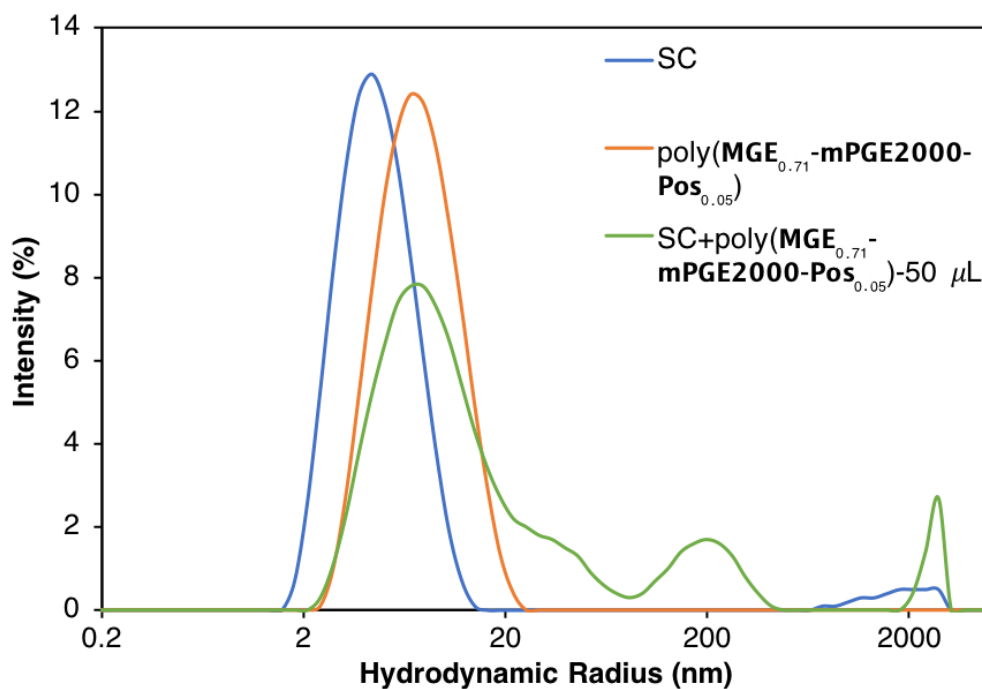


Figure 43. DLS results of SC (blue line), poly(MGE_{0.71}-mPEG2000-Pos_{0.05}) (orange line) and SC with 50 μ L of poly(MGE_{0.71}-mPEG2000-Pos_{0.05}) added (green line) in Milli-Q water.

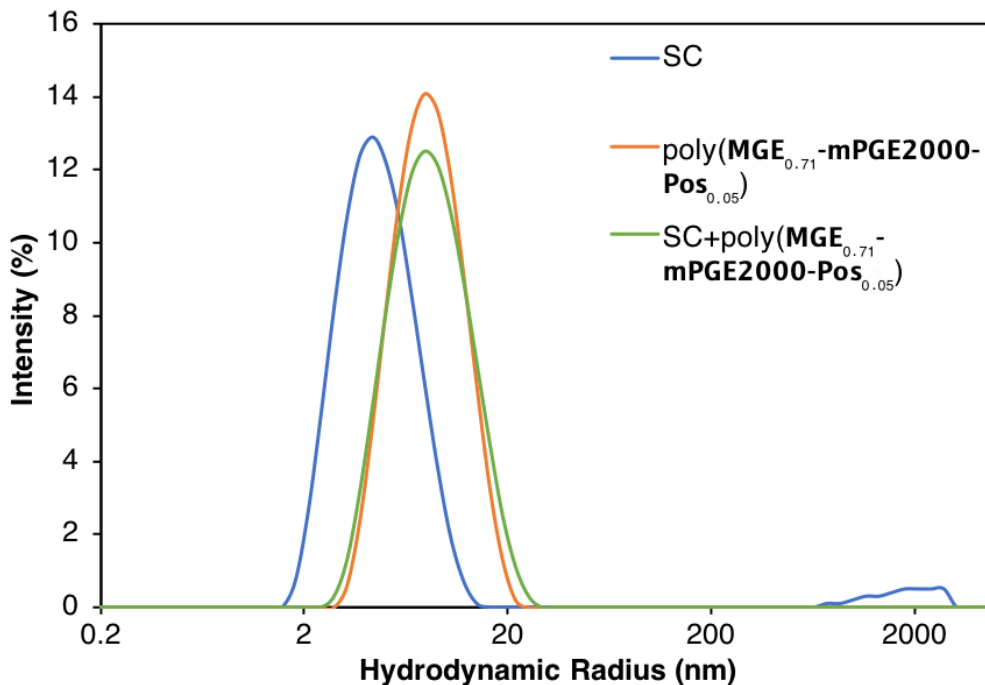
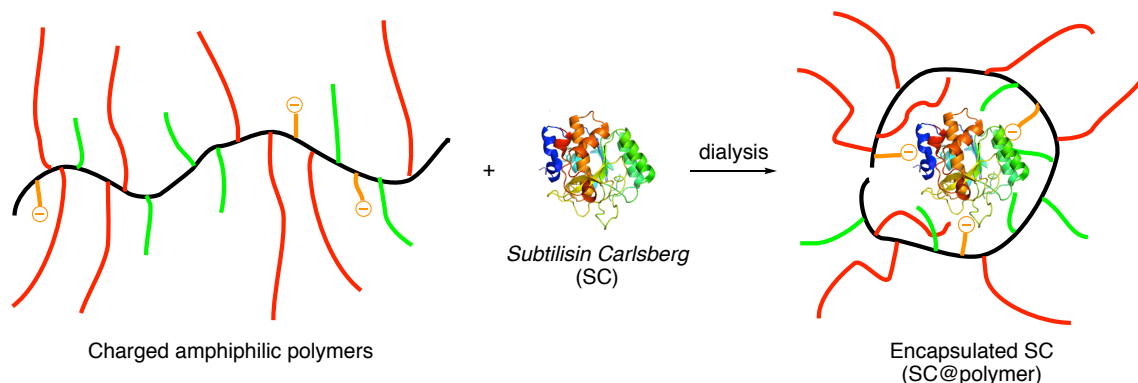


Figure 44. DLS results of SC (blue line), poly(MGE_{0.71}-mPEG2000-Pos_{0.05}) (orange line) and SC with poly(MGE_{0.71}-mPEG2000-Pos_{0.05}) added (green line) in Milli-Q water.

To investigate the polymers' ability to slow or stop the aggregation of proteins, SC was encapsulated by poly(MGE_{0.71}-mPEG2000-Pos_{0.05}) (SC@poly(MGE_{0.71}-mPEG2000-Pos_{0.05})) or poly(MGE_{0.71}-mPEG2000-Neg_{0.05}) (SC@poly(MGE_{0.71}-mPEG2000-Neg_{0.05})) in the following manner (Scheme 21). SC and poly(MGE_{0.71}-mPEG2000-Pos_{0.05}) or poly(MGE_{0.71}-mPEG2000-Neg_{0.05}) were dissolved in phosphate-buffered saline (PBS) solution (pH = 7.4), and the resulting solution was placed in a dialysis bag (MWCO = 6-8 kDa) with Milli-Q water for 24 h to replace the counterions at the protein surface with polymers. The solution was then dried under vacuum and re-dissolved in PBS. A set of control was prepared by dissolving only SC and poly(MGE_{0.71}-mPEG2000-Pos_{0.05}) or poly(MGE_{0.71}-mPEG2000-Neg_{0.05}) without the dialysis process.

It is worth noting that the hydrodynamic radius of SC in PBS is 3 ± 1 nm, which is smaller than in Milli-Q water.

Scheme 21. Schematic representation of Subtilisin Carlsberg (SC) encapsulation.



The solutions were left at room temperature for 48 h and the DLS of the solutions were taken at 0, 24, and 48 h. As shown in Figure 45 and Figure 46, the peak corresponding to the hydrodynamic radius of SC decreased over time as a new peak for aggregates at 26 ± 9 nm increased. If the aggregation process can be slowed or stopped by polymer, little to no aggregation should be observed overtime. However, as shown in Figure 45, the aggregation at 61 ± 47 nm was detected after 24 h for SC@poly(**MGE_{0.71}-mPEG2000-Pos_{0.05}**), similar as SC alone in solution. On the contrary, no aggregation was seen at 24 h for SC@poly(**MGE_{0.71}-mPEG2000-Neg_{0.05}**) and only small amount of aggregations at 602 ± 194 nm was observed after 72 h (Figure 46). It is concluded that polymers with COOH pendant groups exhibit a better ability to encapsulate SC and to slow down SC aggregation in solution. It is necessary to perform activity assay to evaluate the activity of SC before and after aggregations.

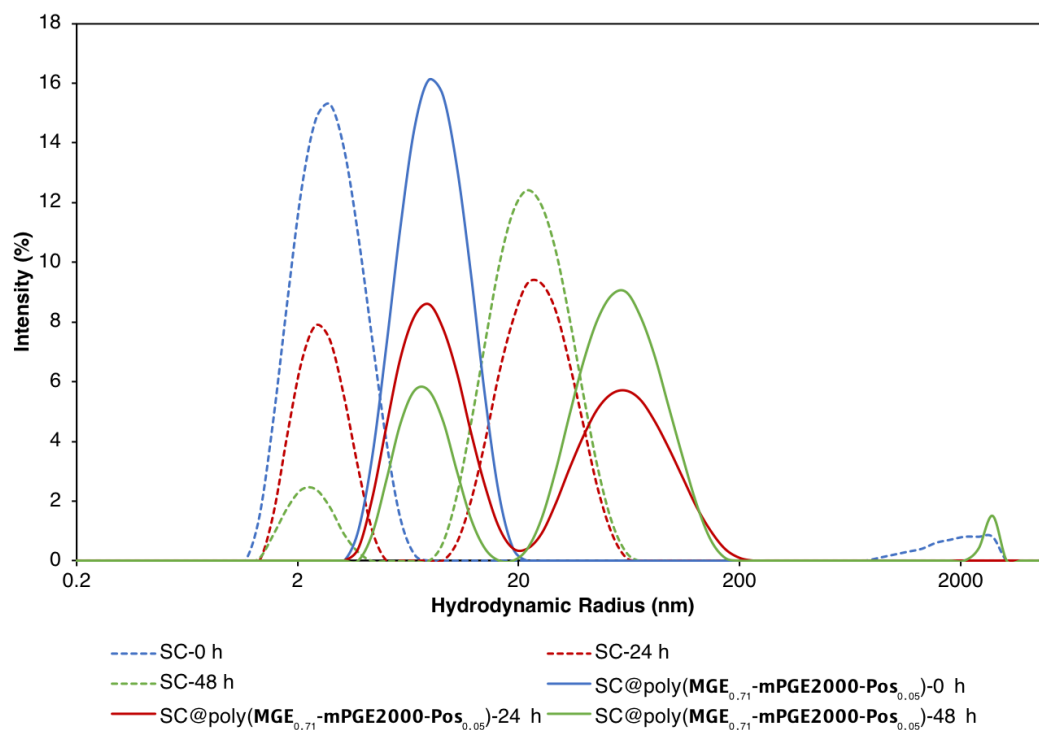


Figure 45. DLS results of SC (dotted line) and SC@poly(MGE_{0.71}-mPEG2000-Pos_{0.05}) (solid line) in Milli-Q water over 48 h.

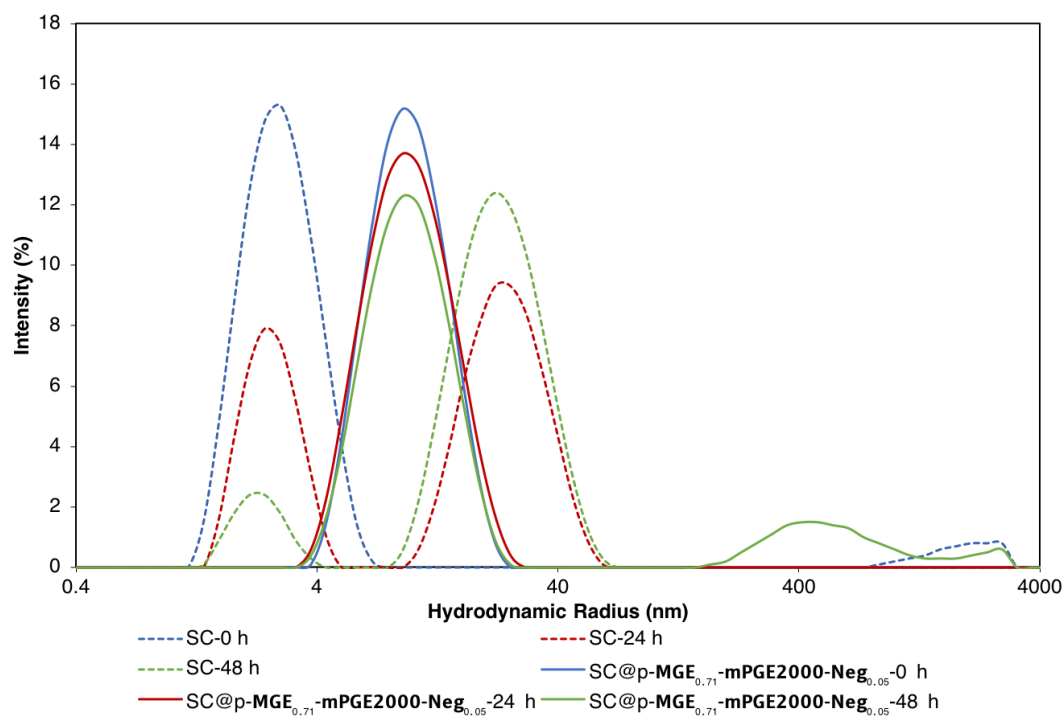


Figure 46. DLS results of SC (dotted line) and SC@poly(MGE_{0.71}-mPEG2000-Neg_{0.05}) (solid line) in Milli-Q water over 48 h.

The catalytic hydrolysis of *N*-succinyl-Ala-Ala-Pro-Phe-*p*-nitroanilide (Suc-AAPF-*p*NA, $\lambda_{\text{max}} = 315 \text{ nm}$, $\varepsilon = 14,000 \text{ M}^{-1} \text{ cm}^{-1}$) to amino acids and *p*-nitroaniline ($\lambda_{\text{max}} = 410 \text{ nm}$, $\varepsilon = 8,800 \text{ M}^{-1} \text{ cm}^{-1}$) by protease has been frequently employed as the activity assay for protease (Scheme 22).^{262–264} As shown in Figure 47, 5 μL of SC (0.04 mg/mL, Tris-HCl buffer, pH = 8.0) was added to 2 mL of Suc-AAPF-*p*NA (0.02 mM, Tris-HCl buffer, pH = 8.0) and the progression of the hydrolysis was monitored by UV-Vis spectrometer. Suc-AAPF-*p*NA was fully converted to *p*-nitroaniline in 35 min. For consistency, the conversion of Suc-AAPF-*p*NA was measured 5 min after aliquots of SC or SC@polymer were added.

It has been shown that the concentration of SC affects the rate of autolysis and denaturation.^{265–268} Therefore, a series of experiments were performed to investigate the effects of SC concentration at various temperatures on the activity. The half-life ($t_{1/2}$), which refers to the time required for the enzyme activity to reduce to half its original activity, of SC at 0.01, 0.4, and 1.0 mg/mL at room temperature, 40 °C, and 50 °C are listed in Table 7 (Figure A172Figure A175, Appendix). As expected, $t_{1/2}$ decreases as the temperature is increased. Additionally, higher SC concentrations results in longer $t_{1/2}$. We were puzzled by the fact that our results of the concentration effect were in contradicting with the results reported by Russell and co-workers.²⁶⁹ However, some studies have shown that SC aggregates remain active,^{265,267} which is consistent with what was observed in our studies.

Scheme 22. Catalytic hydrolysis of Suc-AAPF-*p*NA to *p*-nitroaniline by SC or SC@polymer.

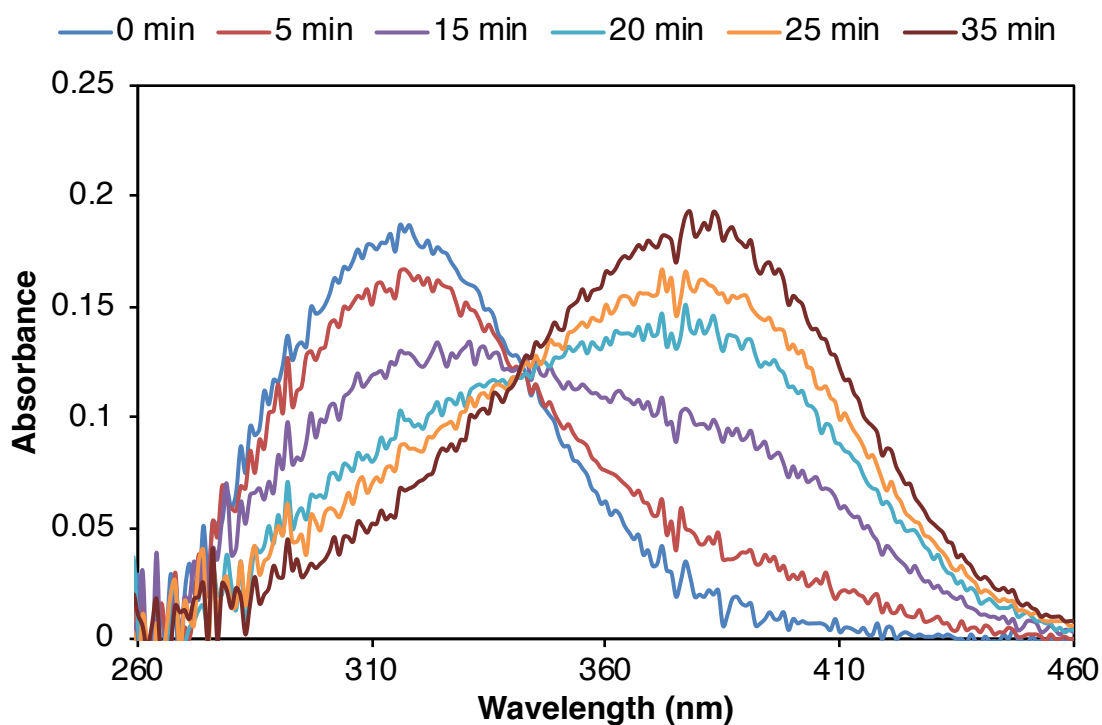
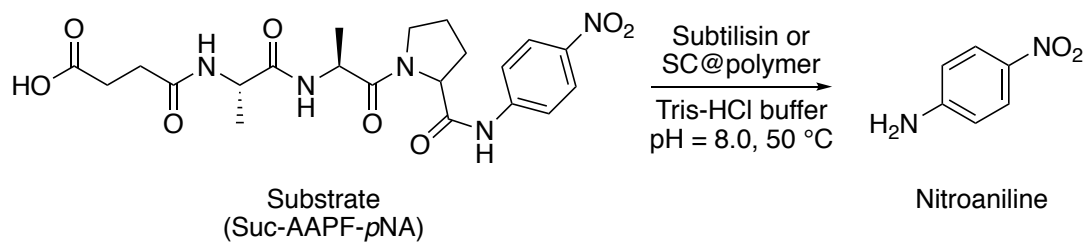


Figure 47. UV-Vis spectra of the catalytic conversion of Suc-AAPF-*p*NA to *p*-nitroaniline overtime.

Table 7. Effects of SC concentration and temperatures on SC stability.

SC Concentration (mg/mL)	Temperature (°C)	t _{1/2} (h)
0.04	25	94.1
	40	5.9
	50	1.6
0.1	25	244.5
	40	11.7
	50	2.0
1	25	390.4
	40	59.7
	50	14.8

To assess the ability of “click” modified poly(MGE)s to stabilize SC in solution, the activity of solutions of SC@polymer over 24 h was tested. As mentioned in previous section, polymers with COOH pendant groups display a better ability to slow down the aggregation of SC. Therefore, poly(MGE_{0.71}-Neg_{0.05}), poly(MGE_{0.71}-mPEG550-Neg_{0.05}), poly(MGE_{0.71}-mPEG750-Neg_{0.05}), and poly(MGE_{0.71}-mPEG2000-Neg_{0.05}) were first used in the study. The molar ratio of SC to polymer was kept at 1 to 2 and the solution were prepared by dissolving SC and polymer in Tris-HCl (pH = 8.0) buffer at room temperature. The dialysis process described above was eliminated for simplicity. The concentration of SC in SC@polymer solution was fixed at 0.1 mg/mL and solutions of SC@polymer were heated at 50 °C to accelerate the degradation of SC. Aliquots (10 μ L) of SC@polymer solutions were taken out at 0, 1, 2, 3, 4, and 24 h. Each aliquot was then added to a freshly prepared solution of Suc-AAPF-*p*NA in Tris-HCl buffer (2 mL, 0.02 mM, pH = 8.0). The UV-Vis spectrum was obtained after 5 min and the absorbance at 412 nm (ϵ = 8,480 M⁻¹ cm⁻¹) was used to calculate the concentration of *p*-nitroaniline. The control experiments were performed following the same procedure on solutions containing only SC.

Representative UV-Vis spectra of the activity study are presented in Figure 48. The blue solid line represents the absorbance for Suc-AAPF-*p*NA and the absorbance for *p*-nitroaniline is shown in yellow solid line. At 0 h, when SC@poly(MGE_{0.71}-mPEG750-Neg_{0.05}) solutions were freshly made, Suc-AAPF-*p*NA was fully converted to *p*-nitroaniline within 5 min. After SC and SC@poly(MGE_{0.71}-mPEG750-Neg_{0.05}) were heated at 50 °C for 1 h, the activity of SC decreased to 83% of its original activity (orange dotted line) and the activity of SC@poly(MGE_{0.71}-mPEG750-Neg_{0.05}) decreased to 87% of its original activity (purple solid line). The reduction of the activities after 1 h was similar but the differences became very noticeable after 2 h. The activity of SC decreased to 48% and the activity of SC@poly(MGE_{0.71}-mPEG750-Neg_{0.05}) remained at 72%. After 4 h, as shown in Figure 48, the activity of SC reduced to 33% (green dotted line) and the activity of SC@poly(MGE_{0.71}-mPEG750-Neg_{0.05}) only lowered to 52% (red solid line). Our results demonstrate that the activity of SC increases in the presence of polymers.

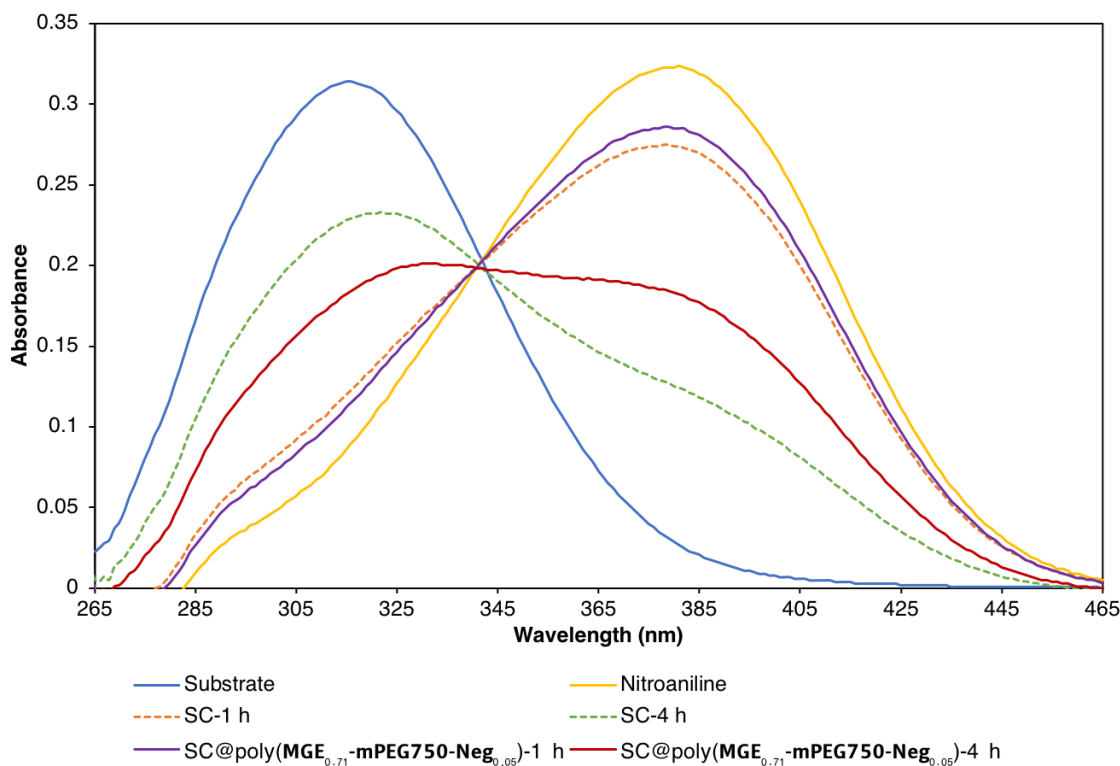


Figure 48. UV-Vis spectra of the conversion of Suc-AAPF-*p*NA (blue solid line) to *p*-nitroaniline (yellow solid line) by aliquots of SC (1 h, orange dotted line; 4 h green dotted line) or SC@poly(**MGE**_{0.71}-**mPEG750-Neg**_{0.05}) (1 h, purple solid line; 4 h, red solid line) taken at 1 or 4 h after heated at 50 °C.

$t_{1/2}$ values in the presence of various polymers are listed in Table 8. Poly(**MGE**_{0.71}-**Neg**_{0.05}) and poly(**MGE**_{0.71}-**mPEG750-Neg**_{0.05}) promoted the largest activity enhancements of SC and extended the $t_{1/2}$ to 9.8 h and 10.4 h, respectively. The neutral counterpart of poly(**MGE**_{0.71}-**Neg**_{0.05}) and poly(**MGE**_{0.71}-**mPEG750-Neg**_{0.05}), poly(**MGE**_{0.75}) and poly(**MGE**_{0.75}-**mPEG750**), also increased the $t_{1/2}$ to 7.0 h and 7.1 h. By adding 5% of COOH side chains, we were able to lengthen the $t_{1/2}$ by 3 h. Interestingly, polymers with mPEG750 outperformed polymers with mPEG550 and mPEG2000 as hydrophilic pendant groups. It is important to note that the studies were conducted without

the dialysis as encapsulation procedure; therefore, it will be necessary to carry out these experiments after dialysis to study the effects of dialysis procedure.

Table 8. Results of $t_{1/2}$ in the presence of various polymers.

SC or SC@polymer	$t_{1/2}$ (h)
SC	2.0
SC@poly(MGE _{0.75})	7.0
SC@poly(MGE _{0.75} -mPEG750)	7.1
SC@ poly(MGE _{0.71} -Neg _{0.05})	9.8
SC@poly(MGE _{0.71} -mPEG550-Neg _{0.05})	6.7
SC@poly(MGE _{0.71} -mPEG750-Neg _{0.05})	10.4
SC@poly(MGE _{0.71} -mPEG2000-Neg _{0.05})	8.2

The hydrodynamic radii of SC and SC@poly(MGE_{0.71}-mPEG750-Neg_{0.05}) at 50 °C were monitored by DLS over 4 h (Figure 49). Similar to SC in PBS, the hydrodynamic radius of SC in Tris-HCl buffer is 3 ± 1 nm (dotted lines). After 1 h of heating at 50 °C, only SC aggregates were detected, and the hydrodynamic radius of SC increased to 59 ± 18 nm. As shown in Figure 49, a broad peak was observed and the hydrodynamic radius of SC@poly(MGE_{0.71}-mPEG750-Neg_{0.05}) is 13 ± 11 nm (solid lines). Small amount of large aggregates, $R_H = 187 \pm 109$ nm, were seen after 1 h of heating at 50 °C. Combining with the activity studies, we propose that slower SC aggregation contributes to enhancing the SC activity. However, our study also shows that SC remains active upon aggregation. In order to establish a clearer correlation between protein aggregation and activity, proteins that lose their activity as they aggregate will be needed for future studies.

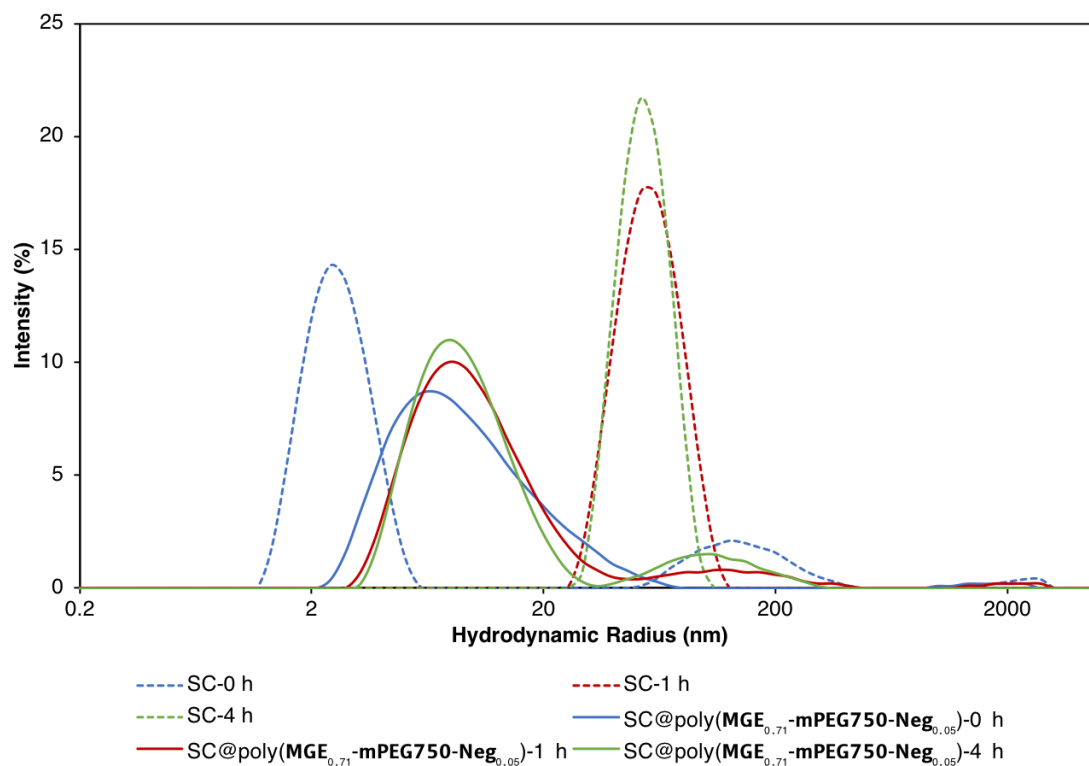
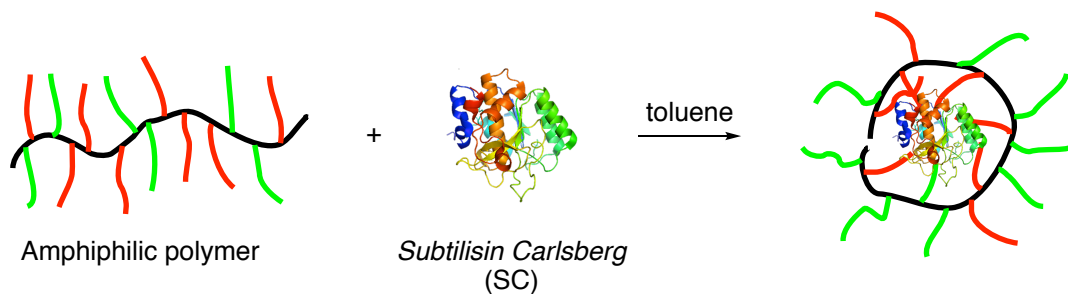


Figure 49. DLS results of SC (dotted line) and SC@poly(MGE_{0.71}-mPEG750-Neg_{0.05}) (solid line) in Tris-HCl buffer at 50 °C for 4 h.

Scheme 23. Schematic representation of SC encapsulation in toluene.



Aside from dissolving hydrophobic guest molecules in water, these amphiphilic polymers can also be utilized to solubilize hydrophilic guest molecules in organic media. As a proof of concept, poly(PGE_{0.60}) and poly(MGE_{0.65}) were used for SC encapsulation in organic media (Scheme 23). The encapsulation of SC was performed under two methods

which both led to similar results. The first method involved the addition of an aqueous solution of SC (1 mg/mL) and poly(**PGE**_{0.60}) or poly(**MGE**_{0.65}) (10 mg/mL), in which the molar ratio between SC and poly(**PGE**_{0.60}) or poly(**MGE**_{0.65}) was 1:2, to toluene. The resulting two-phase mixture was then vigorously evaporated in vacuo. The resulting solid was re-dissolved in toluene. In the second method, SC (1 mg/mL) and poly(**PGE**_{0.60}) or poly(**MGE**_{0.65}) (10 mg/mL) were dissolved in PBS, and the solution was lyophilized. The resulting solid was re-dissolved with toluene. The encapsulation of SC, SC@poly(**PGE**_{0.60}) or SC@poly(**MGE**_{0.65}), was confirmed by UV-Vis spectrometer. As shown in Figure 50, absorbance at 285 nm was detected for SC@poly(**MGE**_{0.65}), resulting from tyrosine, tryptophan, and phenylalanine. Control experiments were conducted following the same methods with SC in the absence of poly(**PGE**_{0.60}) or poly(**MGE**_{0.65}) and the resulting solid was insoluble in toluene. Therefore, no absorption was seen in the aromatic region of UV-vis spectrum.

The activity of SC@poly(**MGE**_{0.65}) was assayed by transesterification of benzyl alcohol and vinylbutyrate at 45 °C in toluene. GC-MS show approximately ~35% conversion after 16 h. Controls with lyophilized or as provided SC suspensions showed no activity in toluene. However, the generation of formaldehyde during the reaction would potentially compromise the activity of SC therefore a new approach should be taken to examine the enzymatic activity. These initial studies demonstrate that our “click” modified amphiphilic polymers enhance protein solubility as well as the activity in organic media.

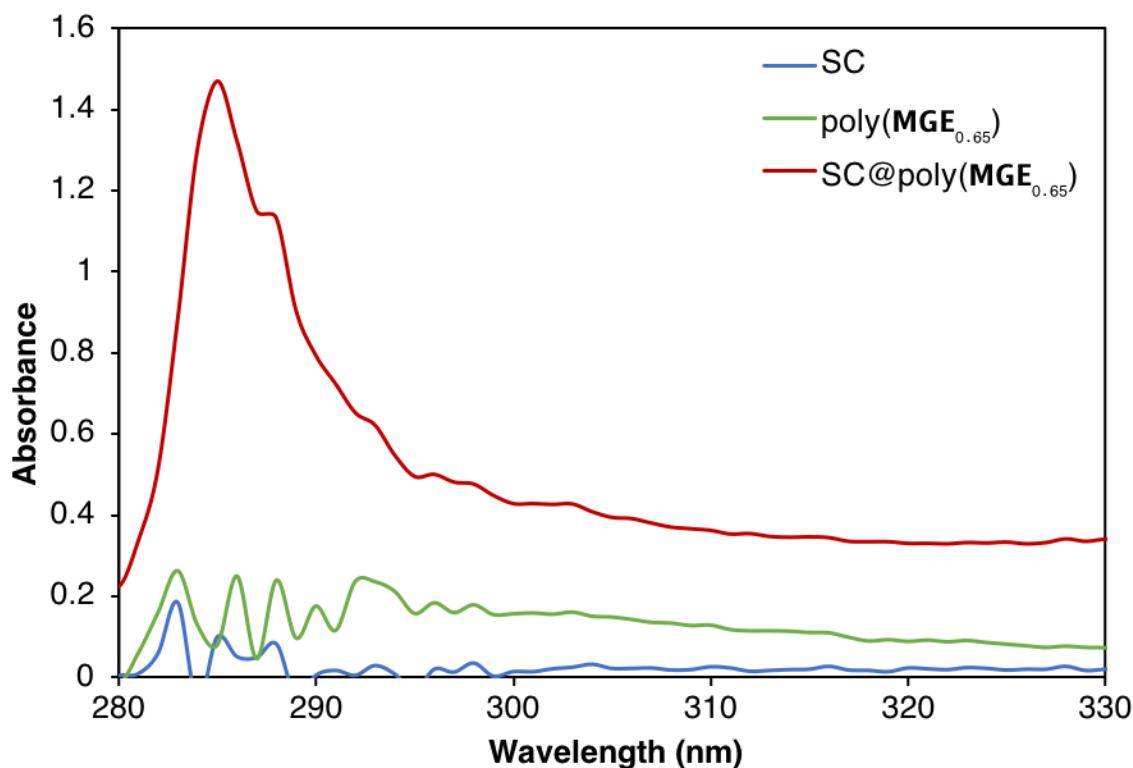


Figure 50. UV-Vis spectra of SC suspension in toluene (blue line), poly(**MGE**_{0.65}) in toluene (green line), and SC@ poly(**MGE**_{0.65}) in toluene (red line).

4.3. Summary

By employing the “click” modified amphiphilic polymers as unimicelles, we were able to solubilize a hydrophobic guest molecule, azobenzene, in water. Interestingly, when the solubilized azobenzene-loaded micelles were heated above the LCST of the polymer, the solution appeared cloudy and after it was cooled down below LCST, the precipitates re-dissolved and the color of the solution returned to yellow again. *Trans*-PhN=NPh@poly(**MGE**_{0.65}) showed different hydrodynamic radius compared to poly(**MGE**_{0.65}) but the same hydrodynamic radius was observed for poly(**MGE**_{0.75}) and *trans*-PhN=NPh@poly(**MGE**_{0.75}). It is proposed that the differences were caused by the

compositions and hydrophilicities of polymers, but further studies are required to investigate our hypothesis.

By exchanging surface ions on SC via dialysis in aqueous solutions, we encapsulated SC in poly(**MGE_{0.71}-mPEG2000-Pos_{0.05}**) and poly(**MGE_{0.71}-mPEG2000-Neg_{0.05}**). It was shown that only little aggregation of SC@poly(**MGE_{0.71}-mPEG2000-Neg_{0.05}**) was observed after 48 h. Furthermore, the activity of SC in the presence of polymers was assayed via the hydrolysis of Suc-AAPF-*p*NA and monitored by UV-Vis spectrometer. The half-life of SC was enhanced to about 10 h in the presence of poly(**MGE_{0.71}-Neg_{0.05}**) and poly(**MGE_{0.71}-mPEG750-Neg_{0.05}**), 5 times longer than in the absence of polymers. It is worth noting that poly(**MGE_{0.75}**) and poly(**MGE_{0.75}-mPEG750**) increased the $t_{1/2}$ of SC to ~7 h, 3 h shorter without the COOH pendant group. However, our studies indicated that SC aggregates remained active. In order to further investigate the correlation between reduced aggregation and enhanced activity of proteins, a different model should be selected. Preliminary studies also show that these amphiphilic polymers can not only solubilize SC but also stabilize SC in organic media.

Chapter 5. Experimental Section

5.1. Materials

(±)-Epichlorohydrin ($\geq 98\%$, Fluka), propargyl alcohol (99%, Sigma-Aldrich), 2-methyl-3-butyn-2-ol (98%, Aldrich), tetrabutylammonium hydrogensulfate (TBAHS, 97%, Aldrich), triethylene glycol monomethyl ether (95%, Sigma-Aldrich), polyethylene glycol monomethyl ether, 550 (Alfa Aesar), polyethylene glycol monomethyl ether, 750 (Acros), polyethylene glycol monomethyl ether, 2000 (Aldrich), *p*-toluenesulfonic chloride (Spectrum), 6-bromohexanoic acid (98+%, Alfa Aesar), 3-dimethylaminopropyl chloride hydrochloride (98%, Alfa Aesar), sodium *L*-ascorbate ($>98\%$, TCI), and sodium azide (Sigma-Aldrich) were used as received. Tetraoctylammonium bromide (Oct₄NBr, 98%, Sigma-Aldrich) and triisobutylaluminum (*i*-Bu₃Al, 1 mol/L in toluene, Sigma-Aldrich) were stored in glovebox under nitrogen atmosphere and were used without further purification. Ion exchange resin beads (Amberlite® IRC-748) were purchased from Alfa Aesar and soaked in *N,N*-dimethylformamide (DMF) prior to use. Toluene was dried by refluxing over sodium benzophenone and stored under nitrogen atmosphere. DMF, tetrahydrofuran (THF), dichloromethane (CH₂Cl₂), methanol, ethanol, diethyl ether, and ethyl acetate were used as received.

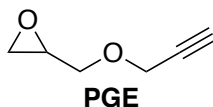
5.2. Characterization

The molecular weights of polymers were determined by gel permeation chromatography (GPC) at 35 °C using two PLgel 10 μ mixed-B columns in series (manufacturer stated linear molecular weight range of 500-10,000,000 g/mol) with THF as the eluent solvent at a flow rate of 1 mL/min. A Waters 2410 differential refractometer was

used as the detector. An Optilab rEX (Wyatt Technology Co.) and a DAWN EOS 18-angle light scattering detector (Wyatt Technology Co.) with a laser wavelength of 684 nm were used to calculate absolute molecular weights. Monodisperse polystyrene standards ($M_n = 2727, 3680, 12860, 24150, 32660, 45730, 95800, 184200, 401340$ g/mol) were used to calibrate the molecular weights. The concentration of polymer solutions used for GPC was 1-4 mg/mL and all samples were filtered through a 0.2 μm Whatman PTFE syringe filter. ^1H NMR (500 MHz) and ^{13}C NMR (125 MHz) spectra were acquired using either a Varian Inova-500 spectrometer or Agilent DirectDrive2 500 spectrometer. Chemical shifts for ^1H and ^{13}C spectra were recorded in parts per million relative to the residual ^1H and ^{13}C of CDCl_3 (δ 7.26, 77.0) and D_2O (δ 4.79). Elemental analyses were determined using a Perkin-Elmer 2400 CHNS/O analyzer. Mass spectral analyses were carried out on a Waters Xevo G2-S QToF UPLC/MS/MS. Dynamic light scattering (DLS) data were obtained using a Malvern Zetasizer Nano ZS. All samples were filtered through a 0.2 μm Whatman PTFE syringe filter and then equilibrated in the instrument for 2 minutes at each temperature before taking the data used to calculate the hydrodynamic radius (R_h). The particle size uniformity was determined by a monomodal curve fit, which assumes a single particle size with a gaussian distribution. TEM micrographs were collected at 40,000-100,000x magnifications on a JEOL-100CX11 transmission electron microscope. UV-vis spectra were recorded with an ATI UNICAM UV2 UV/Vis spectrometer or a Shimadzu UV-2600 UV-Vis spectrometer.

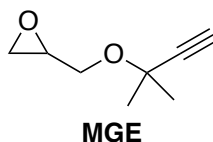
5.3. Procedures

Synthesis of propargyl glycidyl ether (PGE)²²²



In an Erlenmeyer flask, (±)-epichlorohydrin (98.53 g, 1.06 mol) and TBAHS (1.60 g, 4.71 mmol) were added to a 40% NaOH aqueous solution (60 mL) at 0 °C. Propargyl alcohol (14.85 g, 0.27 mol) was then added dropwise to the flask at 0 °C while stirring, and the mixture was allowed to reach room temperature. After 3 h, water was added to the reaction mixture to quench the reaction. The aqueous phase was extracted with diethyl ether (3×50 mL) and the organic phase was dried over Na₂SO₄. Diethyl ether was evaporated under reduced pressure. The product was purified by vacuum distillation (b.p. = 50 °C, 10 torr) to obtain a colorless liquid of propargyl glycidyl ether (**PGE**, 22.57 g, 0.20 mol, 76% yield). ¹H NMR (CDCl₃, 500 MHz): δ 2.44 (t, 1H, *J* = 2.5 Hz), 2.62 (dd, 1H, *J* = 5.0 and 2.7 Hz), 2.79 (t, 1H, *J* = 4.4 Hz), 3.12-3.17 (m, 1H), 3.46 (dd, 1H, *J* = 5.9 and 11.3 Hz), 3.81 (dd, 1H, *J* = 3.0 and 11.4 Hz), 4.19 (d, 1H, *J* = 2.4 Hz), 4.20 (d, 1H, *J* = 2.4 Hz). ¹³C NMR (CDCl₃, 125 MHz): δ 44.18, 50.40, 58.36, 70.25, 74.78, 79.18. Anal. Calcd. for C₆H₈O₂: C, 64.27; H, 7.19. Found: C, 64.48; H, 7.10.

Synthesis of 1,1'-dimethyl propargyl glycidyl ether (MGE)



In an Erlenmeyer flask, (±)-epichlorohydrin (98.04 g, 1.06 mol) and TBAHS (3.2 g, 9.42 mmol) were added to 25% NaOH aqueous solution (240 mL) at 0 °C. 2-Methyl-3-

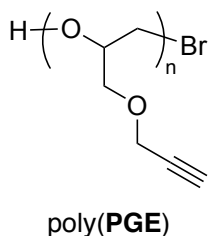
butyn-2-ol (44.56 g, 0.53 mol) was then added dropwise to the flask at 0 °C while stirring, and the mixture was allowed to reach room temperature.. After 24 h, water was added to the reaction mixture to quench the reaction. The aqueous phase was extracted with diethyl ether (3×100 mL) and the organic phase was dried over Na₂SO₄. Diethyl ether was evaporated under reduced pressure. The product was purified by vacuum distillation (b.p. = 60 °C, 10 torr) to obtain a colorless liquid of 1,1'-dimethyl propargyl glycidyl ether (**MGE**, 37.54 g, 0.27 mol, 50% yield). ¹H NMR (CDCl₃, 500 MHz): δ 1.45 (s, 3H), 1.46 (s, 3H), 2.42 (s, 1H), 2.62 (dd, 1H, *J* = 2.9 and 5.4 Hz), 2.79 (dd, 1H, *J* = 3.9 and 4.9 Hz), 3.11-3.15 (m, 1H), 3.55 (dd, 1H, *J* = 5.6 and 10.7 Hz), 3.75 (dd, 1H, *J* = 3.6 and 10.7 Hz). ¹³C NMR (CDCl₃, 125 MHz): δ 28.41, 28.66, 44.84, 50.86, 65.22, 70.37, 72.35, 85.52. HRMS-ESI (*m/z*): [*M* + *H*]⁺ calcd. for C₈H₁₃O₂, 141.0916; found, 141.0919.

General Procedure for Polymerization

All polymerizations were performed in a glovebox or using standard Schlenk techniques at 25 °C in an atmosphere of high-purity nitrogen. The Schlenk flasks were dried in an oven at 115 °C overnight and allowed to cool prior to use. Monomer(s), tetraoctylammonium bromide (Oct₄NBr, initiator), and triisobutylaluminum (*i*-Bu₃Al, catalyst) were transferred into Schlenk flasks in a glovebox under nitrogen atmosphere, and then the catalyst solution in toluene was transferred into the monomer and initiator mixture in toluene at -30 °C. After the reaction mixture reached room temperature, it was stirred until the reaction was completed or the desired reaction time was reached. A small amount of ethanol was then added to stop the polymerization. Then, the toluene solvent

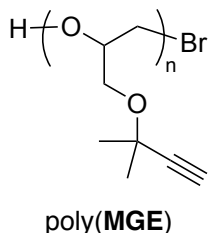
was removed *in vacuo*. Polymerization conversions were determined by ^1H NMR spectroscopy.

Synthesis of poly(propargyl glycidyl ether) (poly(PGE))



Under a nitrogen atmosphere, propargyl glycidyl ether (**PGE**, 1.12 g, 10 mmol) and Oct₄NBr (27.5 mg, 0.05 mmol) were dissolved in toluene (10 mL) and the solution was cooled to -30 °C. *i*-Bu₃Al (0.1 mL, 0.1 mmol) was added via syringe while stirring. The reaction mixture was slowly warmed up to room temperature and stirred for 2.5 h. A small amount of ethanol (1-2 mL) was added to quench the polymerization and toluene was removed under reduced pressure. Unreacted propargyl glycidyl ether was removed by washing with hexanes and then Oct₄NBr and *i*-Bu₃Al was removed by passing the crude product through silica plug with methanol/CH₂Cl₂ (1:19, v/v). The solvent was evaporated under reduced pressure to obtain clear viscous gel of poly(propargyl glycidyl ether) (poly(**PGE**), 1.02 g, 92% yield, $M_n = 19000$, PDI = 1.26). Polymerization conversions were calculated by comparing the ^1H NMR integrations of the monomer epoxide peaks at 2.66 ppm with those on the polymer backbone at 3.52-3.63 ppm. ^1H NMR (CDCl₃, 500 MHz): δ 2.46 (m, 1H), 3.41-3.81 (m, 5H), 4.16 (d, 2H, $J = 2.3$ Hz). ^{13}C NMR (CDCl₃, 125 MHz): δ 58.47, 69.54, 69.64, 69.70, 69.80, 69.84, 74.56, 74.62, 74.64, 78.41, 78.51, 78.60, 79.81, 79.82.

Synthesis of poly(1,1'-dimethyl propargyl glycidyl ether) (poly(**MGE**))

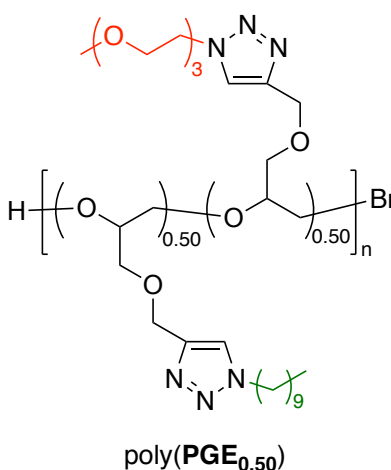


Under a nitrogen atmosphere, 1,1'-dimethyl propargyl glycidyl ether (**MGE**, 2.80 g, 20 mmol) and Oct₄NBr (55.0 mg, 0.05 mmol) were dissolved in toluene (20 mL) and the solution was cooled to -30 °C. *i*-Bu₃Al (0.2 mL, 0.2 mmol) was added via syringe. The reaction mixture was slowly warmed up to room temperature and stirred for 2.5 h. A small amount of ethanol (1-2 mL) was added to quench the reaction and toluene was removed under reduced pressure. Unreacted propargyl glycidyl ether was removed by washing with hexanes and then Oct₄NBr and *i*-Bu₃Al was removed by passing the crude product through silica plug with methanol/CH₂Cl₂ (1:19, v/v). The solvent was evaporated under reduced pressure to obtain clear viscous gel of poly(1,1'-dimethyl propargyl glycidyl ether) (poly(**MGE**), 2.38 g, 85% yield, $M_n = 21000$, PDI = 1.20). Polymerization conversions were determined by comparing the ¹H NMR integration of the residual epoxide peak at 2.64 ppm with those on polymer backbone at 3.56-3.63 ppm. ¹H NMR (CDCl₃, 500 MHz): δ 1.42 (s, 6H), 2.43 (s, 1H), 3.41-3.78 (m, 5H). ¹³C NMR (CDCl₃, 125 MHz): δ 28.63, 28.69, 28.75, 64.27, 64.30, 64.38, 64.44, 69.86, 69.88, 70.03, 70.06, 70.08, 70.12, 70.30, 70.33, 72.17, 72.19, 72.22, 72.25, 72.27, 78.54, 78.56, 78.68, 78.70, 78.73, 78.76, 78.85, 78.88, 86.06, 86.08.

General Procedure for “Click” Functionalization^{49,95}

The desired amount of acetylene-functionalized polymer, azide (1 equiv with respect to acetylene groups), and 12 mol % sodium ascorbate were dissolved in DMF. The resulting solution was transferred to a Schlenk flask and deoxygenated by three freeze-pump-thaw cycles. After the solution had warmed to room temperature, a 0.1 M solution of $\text{CuSO}_4 \cdot 5\text{H}_2\text{O}$ in deoxygenated DMF (5 mol % with respect to the acetylene groups) was added via syringe under nitrogen and the reaction mixture was stirred at room temperature for desired time. At the end of the reaction, the solids in the reaction mixture were removed by filtration. Ion exchange resin beads (Amberlite® IRC-748 ion exchange resin) were added to the solution and the solution was stirred for 12-24 hours to remove residual copper. The ion exchange resin beads were removed by filtration. The polymer was purified via dialysis (MWCO = 6-8 kDa) in acetone/water mixture (4:1 v/v) for 24 h and then dried under vacuum.

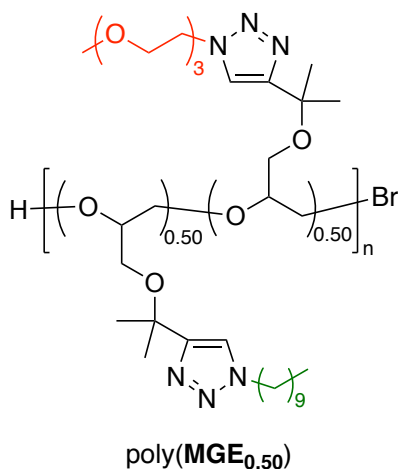
Synthesis of poly(PGE_{0.50})



Poly(PGE) (0.20 g, $M_n = 19000$, PDI = 1.26), **mDEG azide** (0.17 g, 0.9 mmol, 50 mol %), **decyl azide** (0.17 g, 0.9 mmol, 50 mol %), and sodium ascorbate (44.1 mg, 0.2

mmol, 12 mol %) were dissolved in DMF (6 mL). The resulting solution was transferred to a Schlenk flask and deoxygenated by three freeze-pump-thaw cycles. After the solution had warmed to room temperature, a 0.1 M solution of $\text{CuSO}_4 \cdot 5\text{H}_2\text{O}$ in deoxygenated DMF (0.9 mL, 5 mol %) was added via syringe under nitrogen and the reaction mixture was stirred at room temperature for 3.5 h. At the end of the reaction, the solids in the reaction mixture were removed by filtration. Ion exchange resin beads (Amberlite® IRC-748 ion exchange resin) were added to the filtrate and the solution was stirred for 18 h to remove residual copper. The ion exchange resin beads were removed by filtration. The polymer was purified via dialysis (MWCO = 6-8 kDa) in acetone/water mixture (4:1 v/v) for 24 h and the product was dried under vacuum to obtain poly(**PGE**_{0.50}) as a viscous gel (0.45 g, 84% yield). ¹H NMR (CDCl_3 , 500 MHz) δ 0.86 (t, 3H, J = 6.9 Hz), 1.24-1.30 (m, 12H), 1.64 (s, 2H), 1.87 (s, 2H), 3.35 (s, 3H), 3.39-3.71 (m, 14H), 3.84-3.86 (m, 2H), 4.29-4.32 (m, 2H), 4.44-4.54 (m, 2H), 4.54-4.68 (m, 3H), 7.66 (s, 1H), 7.76 (s, 1H). ¹³C NMR (CDCl_3 , 125 MHz) δ 14.10, 22.63, 26.51, 29.03, 29.24, 29.42, 29.48, 30.35, 31.83, 50.02, 50.22, 58.97, 64.66, 64.84, 69.38, 70.41, 70.44, 71.83, 122.77, 123.87, 144.70, 144.81.

Synthesis of poly(**MGE**_{0.50})



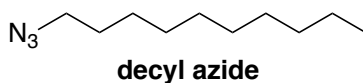
Poly(**MGE**) (0.20 g, $M_n = 22000$, PDI = 1.13), **mDEG azide** (0.13 g, 0.7 mmol, 50 mol %), **decyl azide** (0.13 g, 0.7 mmol, 50 mol %), and sodium ascorbate (35.6 mg, 0.2 mmol, 12 mol %) were dissolved in DMF (6 mL). The resulting solution was transferred to a Schlenk flask and deoxygenated by three freeze-pump-thaw cycles. After the solution had warmed to room temperature, a 0.1 M solution of $\text{CuSO}_4 \cdot 5\text{H}_2\text{O}$ in deoxygenated DMF (0.7 mL, 5 mol %) was added via syringe under nitrogen and the reaction mixture was stirred at room temperature for 3.5 h. At the end of the reaction, the solids in the reaction mixture were removed by filtration. Ion exchange resin beads (Amberlite® IRC-748 ion exchange resin) were added to the filtrate and the solution was stirred for 18 h to remove residual copper. The ion exchange resin beads were removed by filtration. The polymer was purified via dialysis (MWCO = 6-8 kDa) in acetone/water mixture (4:1 v/v) for 24 h and the product was dried under vacuum to obtain poly(**MGE**_{0.50}) as a viscous gel (0.39 g, 82% yield). ¹H NMR (CDCl_3 , 500 MHz) δ 0.86 (t, 3H, $J = 6.8$ Hz), 1.23-1.29 (m, 14H), 1.52 (s, 12H), 1.85-1.88 (m, 3H), 3.19-3.59 (m, 18H), 3.85-3.87 (m, 2H), 4.27-4.30 (m, 2H), 4.48-4.50 (m, 2H), 7.59 (s, 1H), 7.66 (s, 1H). ¹³C NMR (CDCl_3 , 125 MHz) δ 14.08, 22.61, 26.55, 26.71, 26.82, 26.89, 27.0, 27.01, 27.07, 27.27, 27.50, 29.03, 29.24, 29.41, 29.47, 30.40, 31.82, 49.94, 50.17, 58.95, 62.87, 63.03, 69.43, 69.61, 70.02, 70.41, 70.45, 71.83, 72.43, 72.64, 120.93, 122.00, 152.14, 152.39.

Safety Information for Synthesizing, Purifying, and Handling Organic Azides²⁷⁰

Organic azides are potentially explosive materials that can decomposed violently which may result in injury if proper precautions are not taken. Read material safety data sheet before conducting experiments. NEVER use chlorinated solvents as reaction solvent

or during workup. Chlorinated solvents, such as dichloromethane and chloroform, and sodium azide can generate explosive and unstable di- or tri- azomethane.

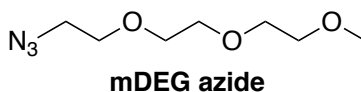
Synthesis of 1-azidodecane (decylazide)^{95,225,226}



WARNING! NEVER use chlorinated solvents as reaction solvent or during workup!

1-Bromodecane (10.00 g, 45.2 mmol) and sodium azide (14.70 g, 226.0 mmol) were dissolved in DMF (180 mL) and the solution was stirred and heated to 80 °C. After 24 h, the solution was cooled to room temperature and was added to a 600 mL beaker containing DI water (100 mL). The solution was extracted with diethyl ether (4×100 mL). The combined organic layers were washed with distilled water (3×100 mL), saturated aqueous NaCl solution (2×100 mL), and dried over MgSO₄. Diethyl ether was evaporated under reduced pressure and the product was purified via vacuum distillation (b.p. = 41.1 °C, 5 torr) to obtain 1-azidodecane as a clear liquid (7.18 g, 39.2 mmol, 87% yield). ¹H NMR (CDCl₃, 500 MHz) δ 0.88 (t, 3H, *J* = 6.9 Hz), 1.25-1.36 (m, 14H), 1.55-1.61 (m, 2H), 3.22-3.25 (t, 2H, *J* = 7.0 Hz). ¹³C NMR (CDCl₃, 125 MHz) δ 14.08, 22.66, 26.71, 28.82, 29.14, 29.27, 29.49, 31.86, 51.49.

Synthesis of 1-(2-azidoethoxy)-2-(2-methoxyethoxy)ethane (mDEG azide)⁹⁵



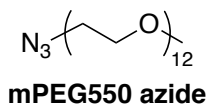
Triethylene glycol monomethyl ether (20.00 g, 0.12 mol) in THF (60 mL) was added dropwise to a solution of NaOH (14.60g, 0.37 mol) in a water/THF mixture (6:4 v/v,

200 mL) at 0 °C while stirring. The mixture was stirred at 0 °C for 30 minutes and then *p*-toluenesulfonic chloride (23.00 g, 0.12 mol) in THF (100 mL) was added dropwise. The mixture was stirred at 0 °C for 3 h and then at room temperature for 6 h. The mixture was then poured into a 600 mL beaker containing ice water (30 mL). The water layer was extracted with diethyl ether (3×100 mL). The combined organic layers were washed with saturated aqueous NaCl solution and dried over MgSO₄. Diethyl ether was evaporated under reduced pressure and the tosylate product was used without further purification (32.86 g, 0.10 mol, 85% yield).

WARNING! NEVER use chlorinated solvents as reaction solvent or during workup!

The mDEG tosylate (32.86 g, 0.10 mol) and sodium azide (13.43 g, 0.20 mol) were dissolved in DMF (200 mL) and the solution was heated to 60 °C. After 15 h, the solution was cooled to room temperature and was added to a 600 mL beaker containing water (100 mL). The solution was extracted with diethyl ether (4×100 mL). The combined organic layers were washed with saturated aqueous NaCl solution (2×100 mL) and dried over MgSO₄. Diethyl ether was evaporated, and the product was purified via vacuum distillation (b.p. = 141.7 °C, 5 torr) to obtain a clear liquid of 1-(2-azidoethoxy)-2-(2-methoxyethoxy)ethane (**mDEG azide**, 10.93g, 0.06 mol, 60% yield). ¹H NMR (CDCl₃, 500 MHz) δ 3.25-3.28 (m, 5H), 3.42-3.45 (m, 2H), 3.52-3.57 (m, 8H). ¹³C NMR (CDCl₃, 125 MHz) δ 50.36, 58.62, 58.64, 69.71, 70.26, 70.27, 70.33, 70.34, 70.36, 70.37, 71.61.

Synthesis of 1-azido poly(ethylene glycol) monomethyl ether, 550 (mPEG550 azide)^{229,230}



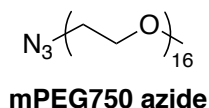
Polyethylene glycol monomethyl ether, 550 (mPEG550, 20.00 g, 36.4 mmol) and *p*-toluenesulfonic chloride (10.40 g, 54.5 mmol) were dissolved in THF (80 mL) and the mixture was cooled to 0 °C. A solution of KOH (13.4g, 0.24 mol) in water (15 mL) was added dropwise to the reaction mixture at 0 °C while stirring. The solution was stirred at 0 °C for 30 minutes then at room temperature for 16 h. A solid suspension was observed after 16 h. The reaction was quenched with CH₂Cl₂/water mixture (9:1 v/v) until all the solid was dissolved. The water layer was extracted with CH₂Cl₂ (3×100 mL). The combined organic layers were washed with saturated aqueous NaCl solution and stirred with Na₂SO₄ overnight. CH₂Cl₂ was evaporated under vacuum and the tosylate product was obtained as a colorless liquid and was used without further purification (22.37 g, 31.8 mmol, 87% yield).

WARNING! NEVER use chlorinated solvents as reaction solvent or during workup!

The tosyl mPEG550 (10.00 g, 14.2 mmol) and sodium azide (1.39 g, 21.3 mmol) were dissolved in DMF (100 mL) and the solution was stirred at room temperature overnight. DMF was evaporated under vacuum at 70 °C and the solid was redissolved in ethyl acetate. The solution was filtered through Celite and ethyl acetate was evaporated under reduced pressure to obtain 1-azido polyethylene glycol monomethyl ether, 550 as a clear liquid (**mPEG550 azide**, 7.76 g, 13.5 mmol, 95% yield). ¹H NMR (CDCl₃, 500 MHz) δ, 3.37-3.39 (m, 4H), 3.53-3.54 (m, 2H), 3.62-3.67 (m, 38H). ¹³C NMR (CDCl₃, 125 MHz)

δ 50.62, 59.00, 69.98, 70.45, 70.49, 70.53, 70.57, 70.60, 70.64, 71.86. IR (dry film, cm^{-1}):
2106 (N=N=N)

Synthesis of 1-azido poly(ethylene glycol) monomethyl ether, 750 (mPEG750 azide)^{229,230}



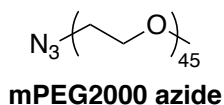
Polyethylene glycol monomethyl ether, 750 (mPEG750, 20.00 g, 26.7 mmol) and *p*-toluenesulfonic chloride (7.6 g, 40 mmol) were dissolved in THF (80 mL) and the mixture was cooled to 0 °C. A solution of KOH (9.8g, 0.18 mol) in water (11 mL) was added dropwise to the reaction mixture at 0 °C while stirring. The solution was stirred at 0 °C for 30 minutes then at room temperature for 16 h. A solid suspension was observed after 16 h. The reaction was quenched with CH_2Cl_2 /water mixture (9:1 v/v) until all the solid was dissolved. The water layer was extracted with CH_2Cl_2 (3×100 mL). The combined organic layers were washed with saturated aqueous NaCl solution and stirred with Na_2SO_4 overnight. CH_2Cl_2 was evaporated under vacuum and the tosylate product was obtained as a clear low melting point solid, which was used without further purification (21.20 g, 23.4 mmol, 88% yield).

WARNING! NEVER use chlorinated solvents as reaction solvent or during workup!

Tosyl mPEG750 (10.00 g, 11.1 mmol) and sodium azide (1.08 g, 16.6 mmol) were dissolved in DMF (100 mL) and the solution was stirred at room temperature overnight. DMF was evaporated under vacuum at 70 °C and the solid was redissolved in ethyl acetate. The solution was filtered through Celite and ethyl acetate was evaporated under reduced

pressure to obtain 1-azido polyethylene glycol monomethyl ether, 750 as a clear, low-melting point solid (**mPEG750 azide**, 7.16 g, 9.3 mmol, 84% yield). ^1H NMR (CDCl_3 , 500 MHz) δ , 3.33-3.35 (m, 4H), 3.49-3.51 (m, 2H), 3.58-3.64 (m, 50H). ^{13}C NMR (CDCl_3 , 125 MHz) δ 50.50, 58.88, 69.87, 70.34, 70.39, 70.43, 70.46, 70.49, 70.52, 71.75. IR (dry film, cm^{-1}): 2106 (N=N=N).

Synthesis of 1-azido poly(ethylene glycol) monomethyl ether, 2000 (mPEG2000 azide)^{229,230}



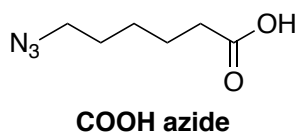
Polyethylene glycol monomethyl ether, 2000 (mPEG2000, 10.00 g, 5.0 mmol) and *p*-toluenesulfonic chloride (1.43 g, 7.5 mmol) were dissolved in THF (40 mL) at 50 °C and the mixture was cooled to room temperature. A solution of KOH (1.84 g, 32.8 mmol) in water (2 mL) was added dropwise to the reaction mixture while stirring and the solution was stirred at room temperature for 16 h. A solid suspension was observed after 16 h. The reaction was quenched with CH_2Cl_2 /water mixture (9:1 v/v) until all the solid was dissolved. The water layer was extracted with CH_2Cl_2 (3×100 mL). The combined organic layers were washed with saturated aqueous NaCl solution and stirred with Na_2SO_4 overnight. CH_2Cl_2 was evaporated under reduced pressure and the tosylate product was obtained as an off-white solid, which was used without further purification (9.43 g, 4.4 mmol, 88% yield).

WARNING! NEVER use chlorinated solvents as reaction solvent or during workup!

Tosyl mPEG2000 (8.73 g, 4.1 mmol) and sodium azide (0.40 g, 6.1 mmol) were dissolved in DMF (100 mL) and the solution was stirred at room temperature overnight.

DMF was evaporated under vacuum at 70 °C and the solid was redissolved in ethyl acetate. The solution was filtered through Celite and ethyl acetate was evaporated under reduced pressure to obtain 1-azido polyethylene glycol monomethyl ether, 2000 as a white solid (**mPEG2000 azide**, 7.83 g, 3.87 mmol, 95% yield). ¹H NMR (CDCl₃, 500 MHz) δ, 3.37 (s, 3H), 3.53 – 3.55 (m, 2H), 3.62-3.65 (m, 125H). ¹³C NMR (CDCl₃, 125 MHz) δ 50.63, 59.01, 70.47, 70.52, 70.56, 70.59, 70.62, 71.88. IR (dry film, cm⁻¹): 2105 (N=N=N).

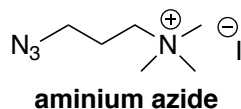
Synthesis of 6-azidohexanoic acid (COOH azide)²³¹



WARNING! NEVER use chlorinated solvents as reaction solvent or during workup!

6-Bromohexanoic acid (5.00 g, 25.6 mmol) and sodium azide (3.33 g, 51.2 mmol) were dissolved in DMF (20 mL). The solution was heated to 85 °C and was stirred for overnight. The solution was cooled to room temperature and was diluted with 0.1 M aqueous HCl solution (20 mL). The solution was extracted with ethyl acetate (3×50 mL). The combined organic layers were washed with 0.1 M aqueous HCl solution (5×20 mL) and dried over Na₂SO₄. Ethyl acetate was evaporated under reduced pressure to obtain 6-azidohexanoic acid as a clear liquid (1.57 g, 10.0 mmol, 39% yield). ¹H NMR (CDCl₃, 500 MHz) δ 1.39-1.47 (m, 2H), 1.60-1.68 (m, 4H), 2.37 (t, 2H, *J* = 7.4 Hz), 3.28 (t, 2H, *J* = 6.9 Hz). ¹³C NMR (CDCl₃, 125 MHz) δ 24.11, 26.11, 28.50, 33.81, 51.15, 179.93. IR (dry film, cm⁻¹): 2097 (N=N=N), 1708 (C=O).

Synthesis of 3-azido-*N,N,N*-trimethylpropan-1-aminium iodide (**aminium azide**)^{232,233}



WARNING! NEVER use chlorinated solvents as reaction solvent or during workup!

3-Dimethylaminopropyl chloride hydrochloride (10.01 g, 63.3 mmol) were dissolved in DI water (127 mL) and sodium azide (8.23 g, 126.6 mmol) was added. The solution was heated to 80 °C and was stirred for 24 h. The solution was cooled in ice bath, and KOH was added to adjust the pH to approximately 10. The solution was extracted with diethyl ether (3×50 mL). The combined organic layers were dried over MgSO₄. Diethyl ether was evaporated under reduced pressure to obtain 3-azido-*N,N*-dimethylpropan-1-amine as a pale-yellow liquid, which was used without further purification (7.11 g, 55.5 mmol, 88% yield).

To a solution of methyl iodide (1.00 g, 7.1 mmol) in methanol (5 mL), a solution of 3-azido-*N,N*-dimethylpropan-1-amine (1.11 g, 8.7 mmol) in methanol (5 mL) was added. The reaction mixture was refluxed for 20 h and then was cooled to room temperature. Methanol and the unreacted 3-azido-*N,N*-dimethylpropan-1-amine were evaporated under reduced pressure to obtain 3-azido-*N,N,N*-trimethylpropan-1-aminium iodide as pale-yellow solid (**aminium azide**, 1.60 g, 5.9 mmol, 84% yield). ¹H NMR (D₂O, 500 MHz) δ 2.03-2.17 (m, 2H), 3.14 (s, 9H), 3.40-3.47 (m, 2H), 3.50 (t, 2H, *J* = 6.4 Hz). ¹³C NMR (D₂O, 125 MHz) δ 22.25, 47.69, 47.71, 47.72, 52.95, 52.98, 53.01, 63.97, 64.00, 64.02

General Procedure for Azobenzene (*trans*PhN=NPh) Encapsulation

Two methods were used to encapsulate azobenzene, and the results obtained from both methods were identical. The first method was used as a direct comparison to previous work, where azobenzene and the “click” modified polymer were dissolved in acetone (<1 mL). The resulting solution was slowly added dropwise to stirred ice-cold Milli-Q water (5 mL) in a Schlenk flask.⁹⁵ The acetone was removed *in vacuo* and the solution was filtered to remove unencapsulated azobenzene. In the second azobenzene and the “click” modified polymer were dissolved in Milli-Q water. The solution was then stirred for 24 hours followed by filtration to remove unencapsulated azobenzene.

General Procedure for Subtilisin Carlsberg (SC) Encapsulation in Aqueous Media

SC and the “click” modified polymer, in which the molar ratio between SC and polymer was 1:2, were dissolved in phosphate-buffered saline (PBS) solution (pH = 7.4). The solution was then placed in dialysis bag (MWCO = 6-8 kDa) with Milli-Q water for 24 h to replace the counterions on protein surface with polymers. The solution was dried under vacuum and redissolved in Milli-Q water, PBS, or Tris-HCl.

General Procedure for Subtilisin Carlsberg (SC) Encapsulation in Organic Media

Two methods were used for the encapsulation of SC in organic media. The first method involved adding an aqueous solution of SC and the “click” modified polymer, in which the molar ratio between SC and polymer was 1:2, to toluene and the solvents in the vigorously mixed two-phase mixture were removed *in vacuo*. The resulting solid was redissolved in toluene. In the second method, SC and the “click” modified polymer were

dissolved in PBS, after which the solution was lyophilized. The resulting solid was redissolved in toluene.

General Procedure for *N*-succinyl-Ala-Ala-Pro-Phe-*p*-nitroanilide (Suc-AAPF-*p*NA)

Assay

Aliquots (10 μ L) of SC or SC@polymer solution were taken at designated time points. Each aliquot was immediately added to a freshly prepared solution of Suc-AAPF-*p*NA in Tris-HCl buffer (2 mL, 0.02 mM, pH = 8.0). The UV-Vis spectrum was obtained after 5 min and the absorbance at 412 nm ($\epsilon = 8,480 \text{ M}^{-1} \text{ cm}^{-1}$) was used to calculate the concentration of *p*-nitroaniline.

APPENDIX

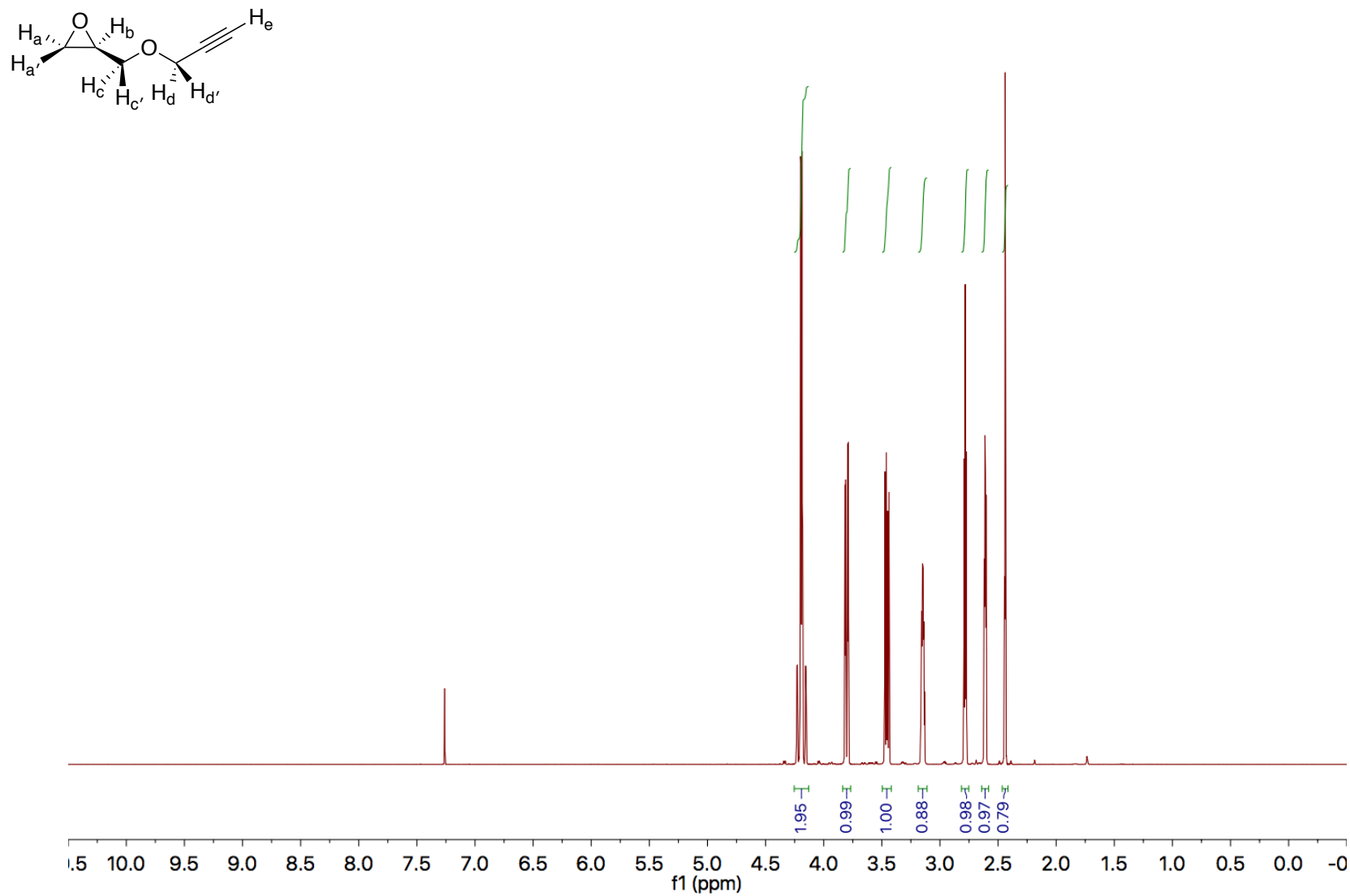


Figure A1. 500 MHz 1H NMR spectrum of **PGE** in $CDCl_3$.

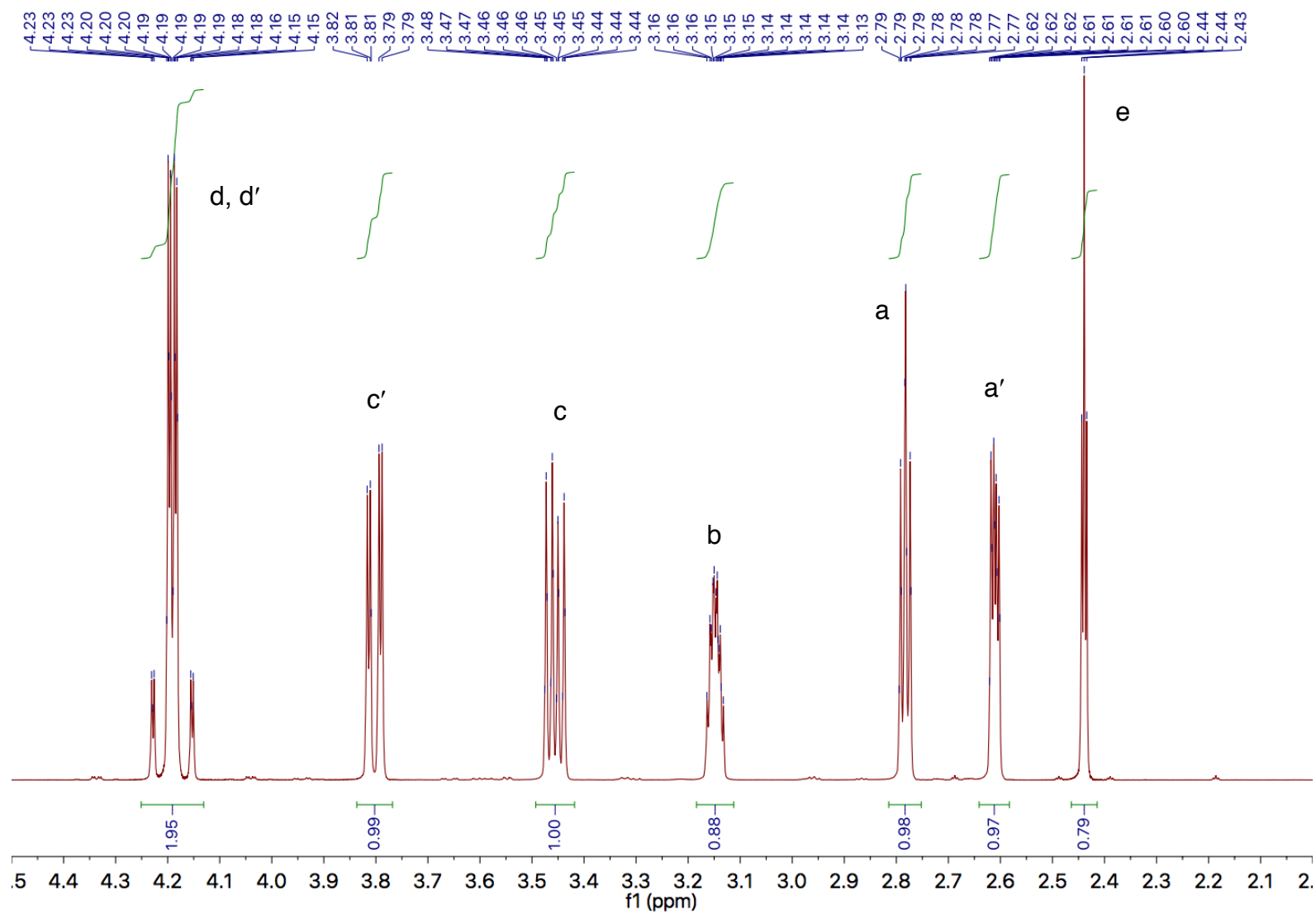


Figure A2. 500 MHz ^1H NMR spectrum of **PGE** in CDCl_3 between 2.0-4.5 ppm.

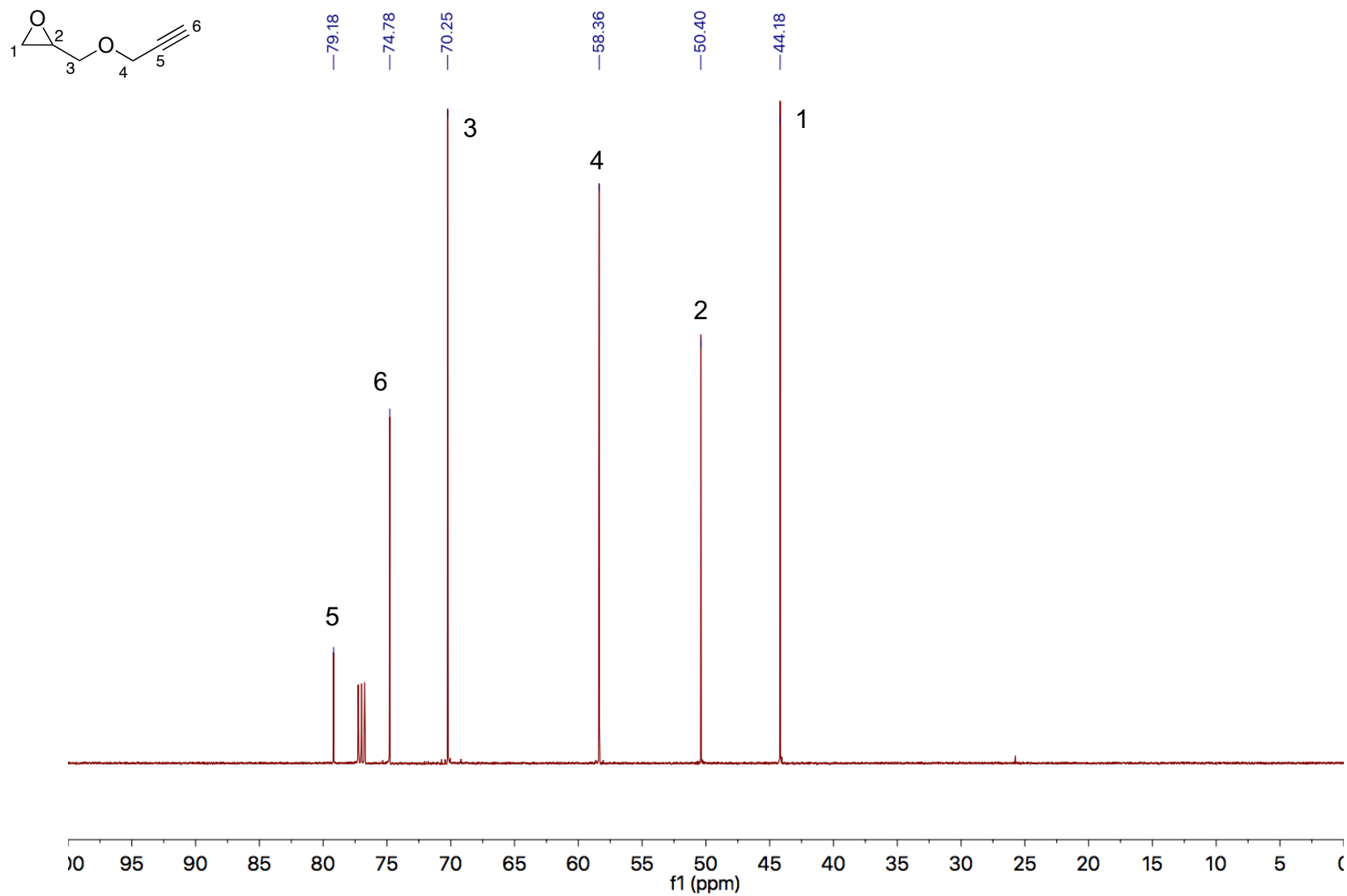


Figure A3. 125 MHz ¹³C NMR spectrum of **PGE** in CDCl₃.

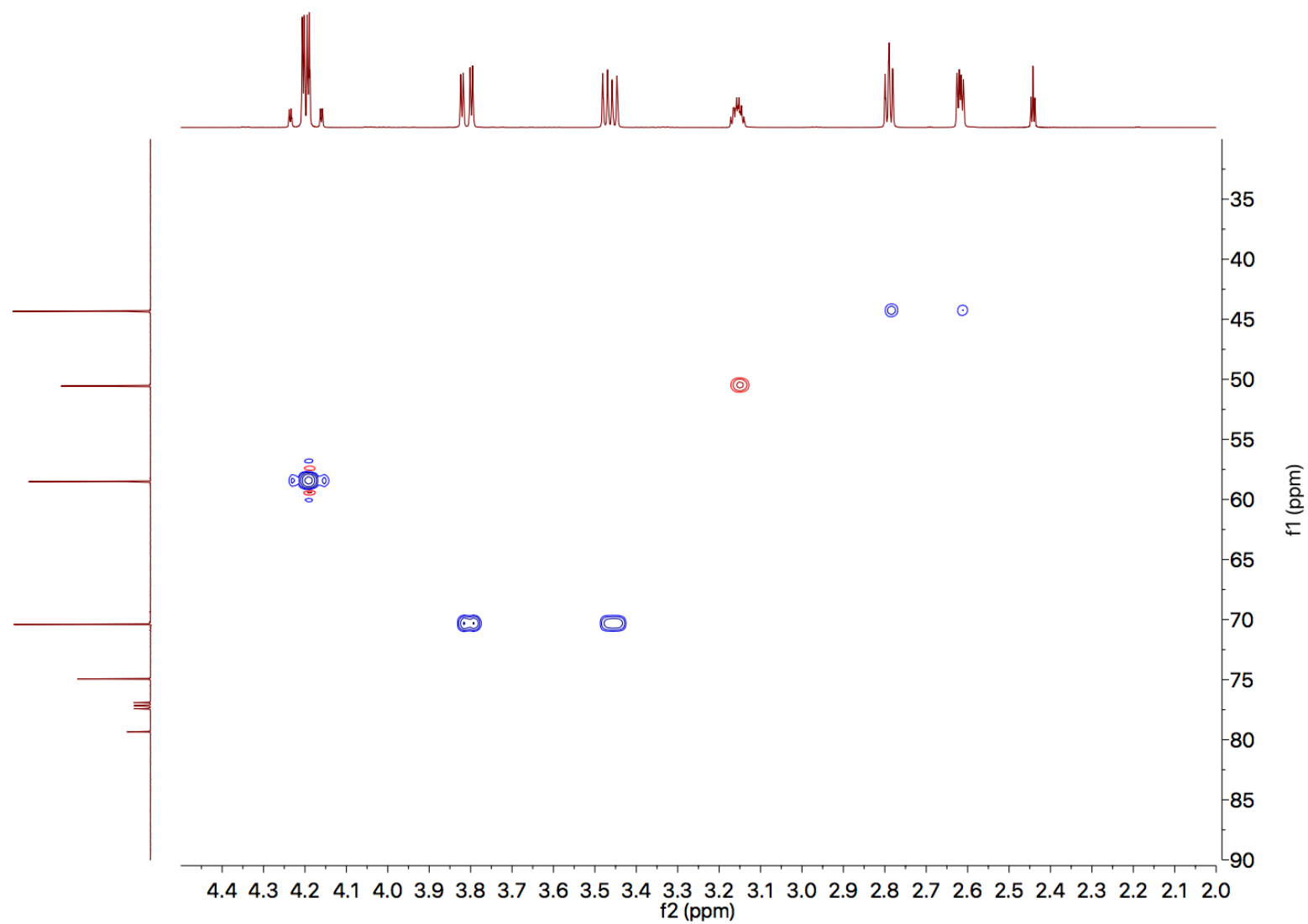


Figure A4. 2D HSQC NMR spectrum of **PGE** in CDCl₃.

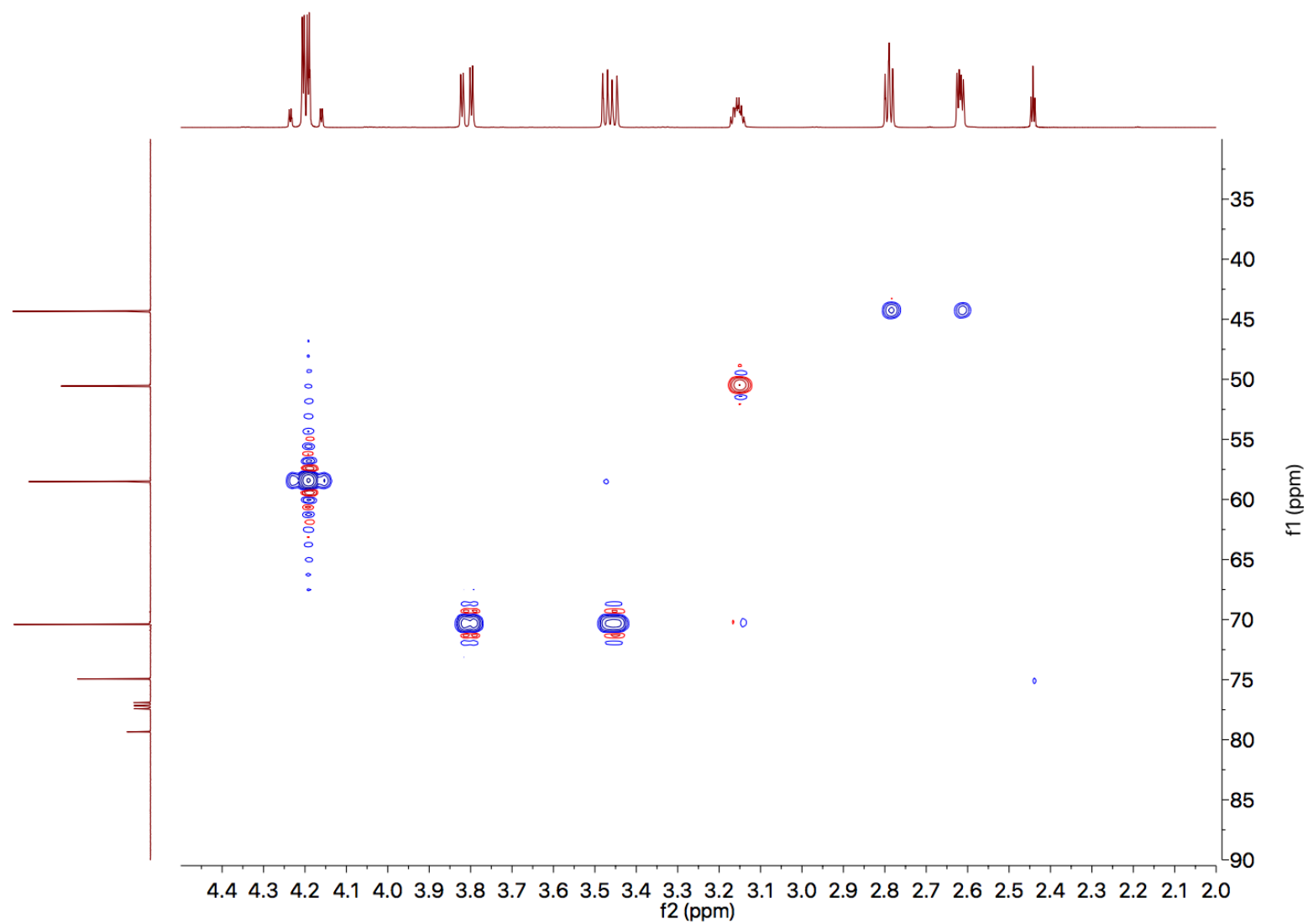


Figure A5. 2D HSQC NMR spectrum of **PGE** in CDCl_3 .

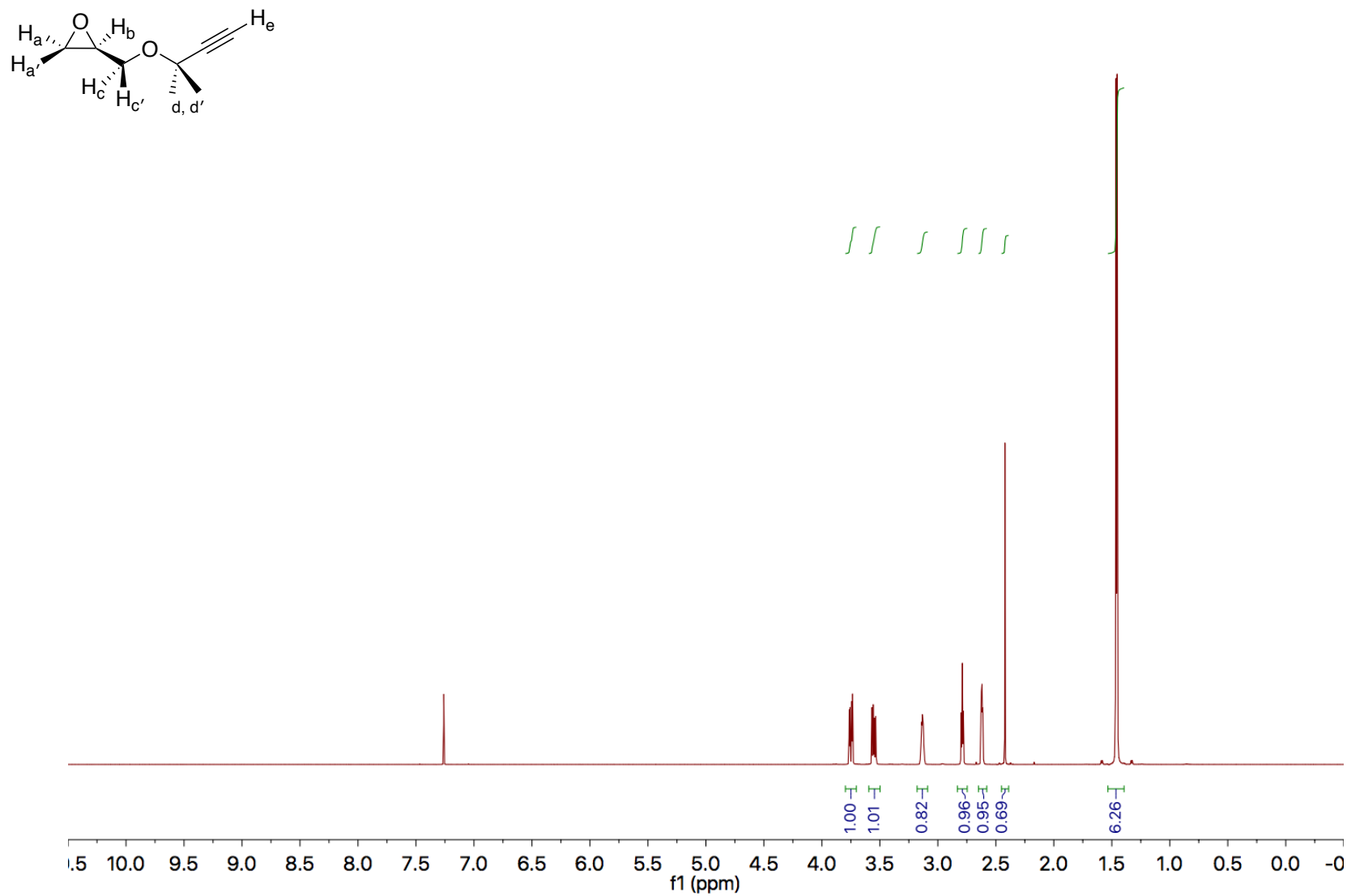


Figure A6. 500 MHz ¹H NMR spectrum of **MGE** in CDCl₃.

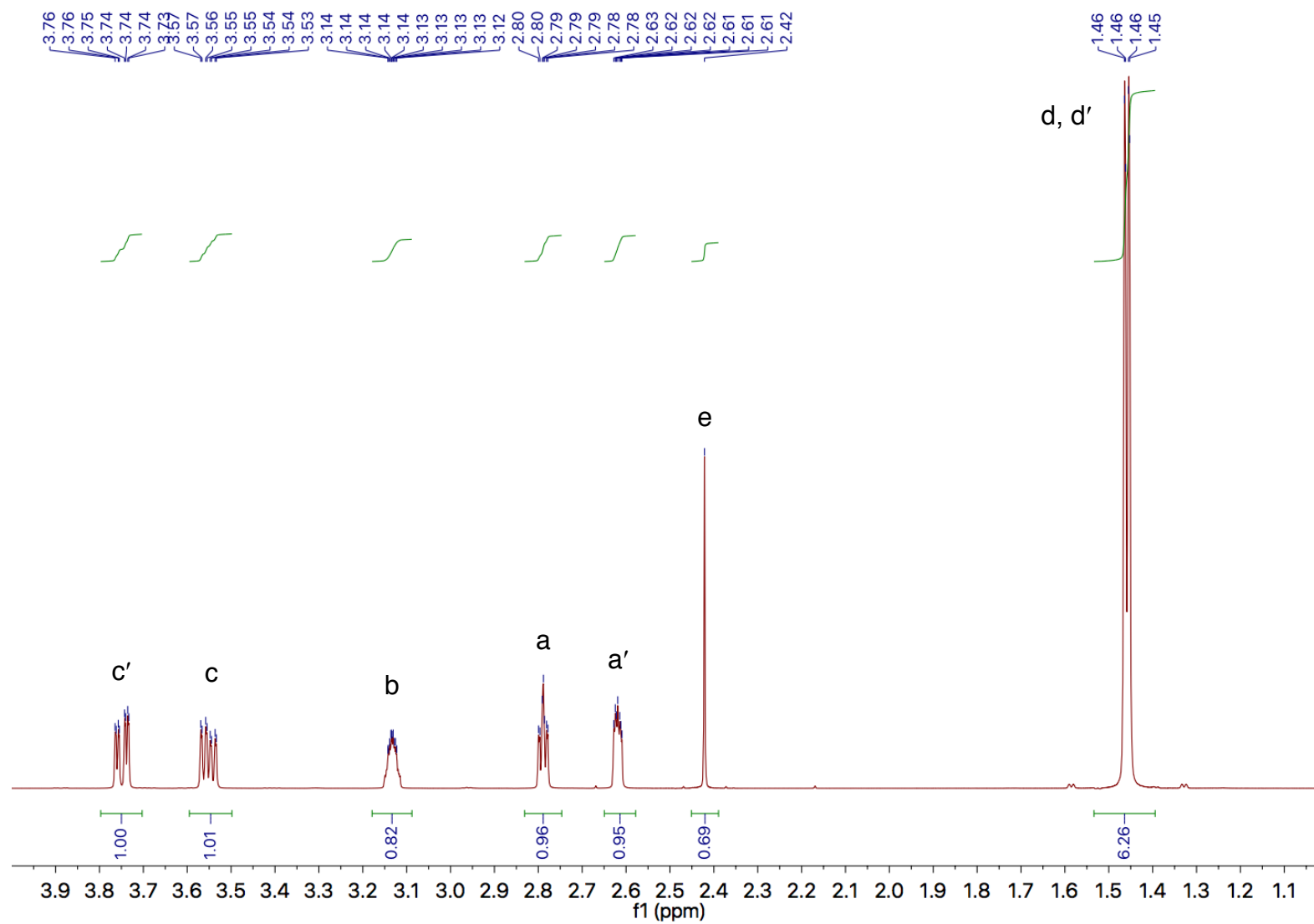


Figure A7. 500 MHz ^1H NMR spectrum of **MGE** in CDCl_3 between 1.0-4.0 ppm.

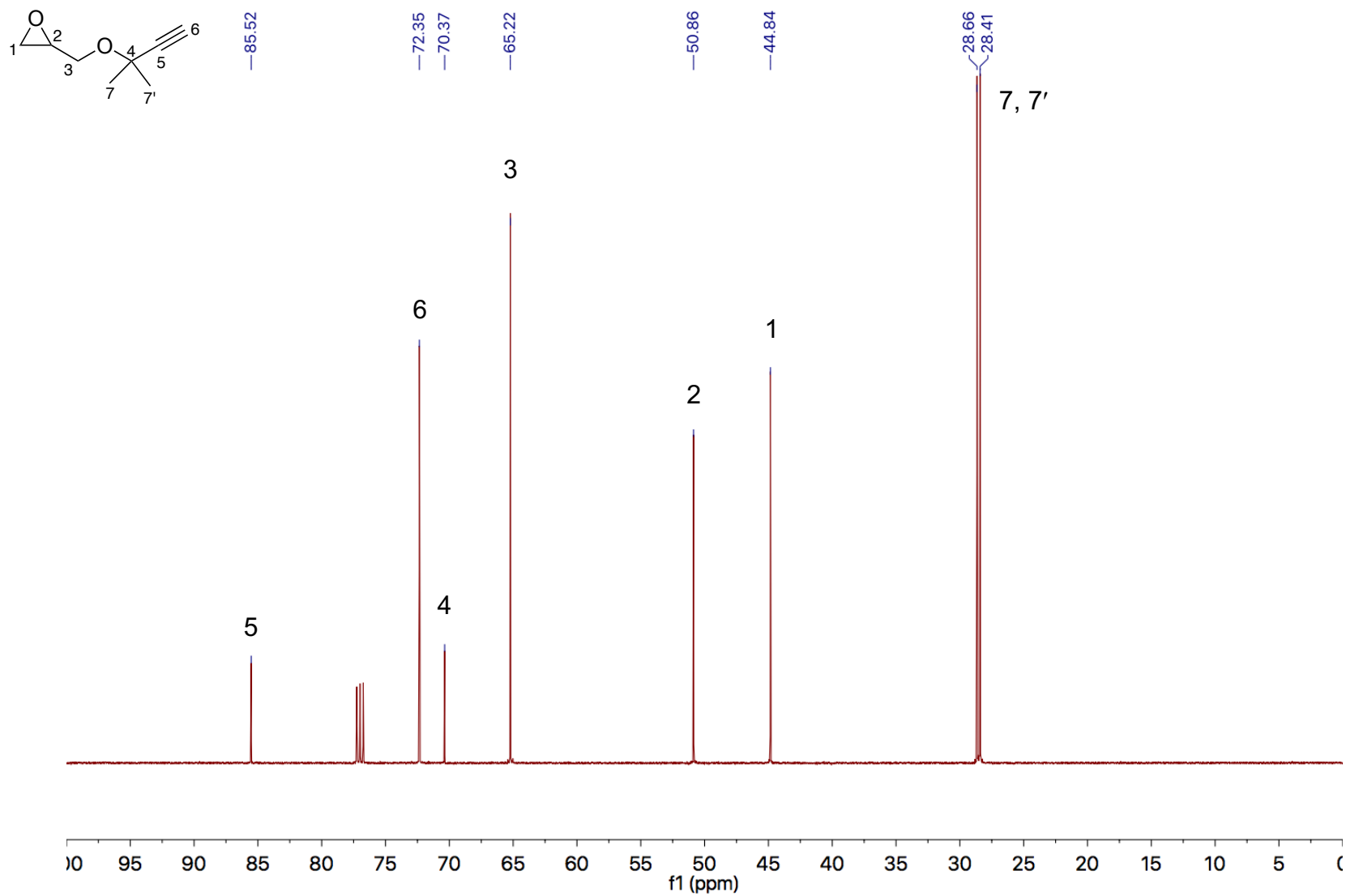


Figure A8. 125 MHz ¹³C NMR spectrum of **MGE** in CDCl₃.

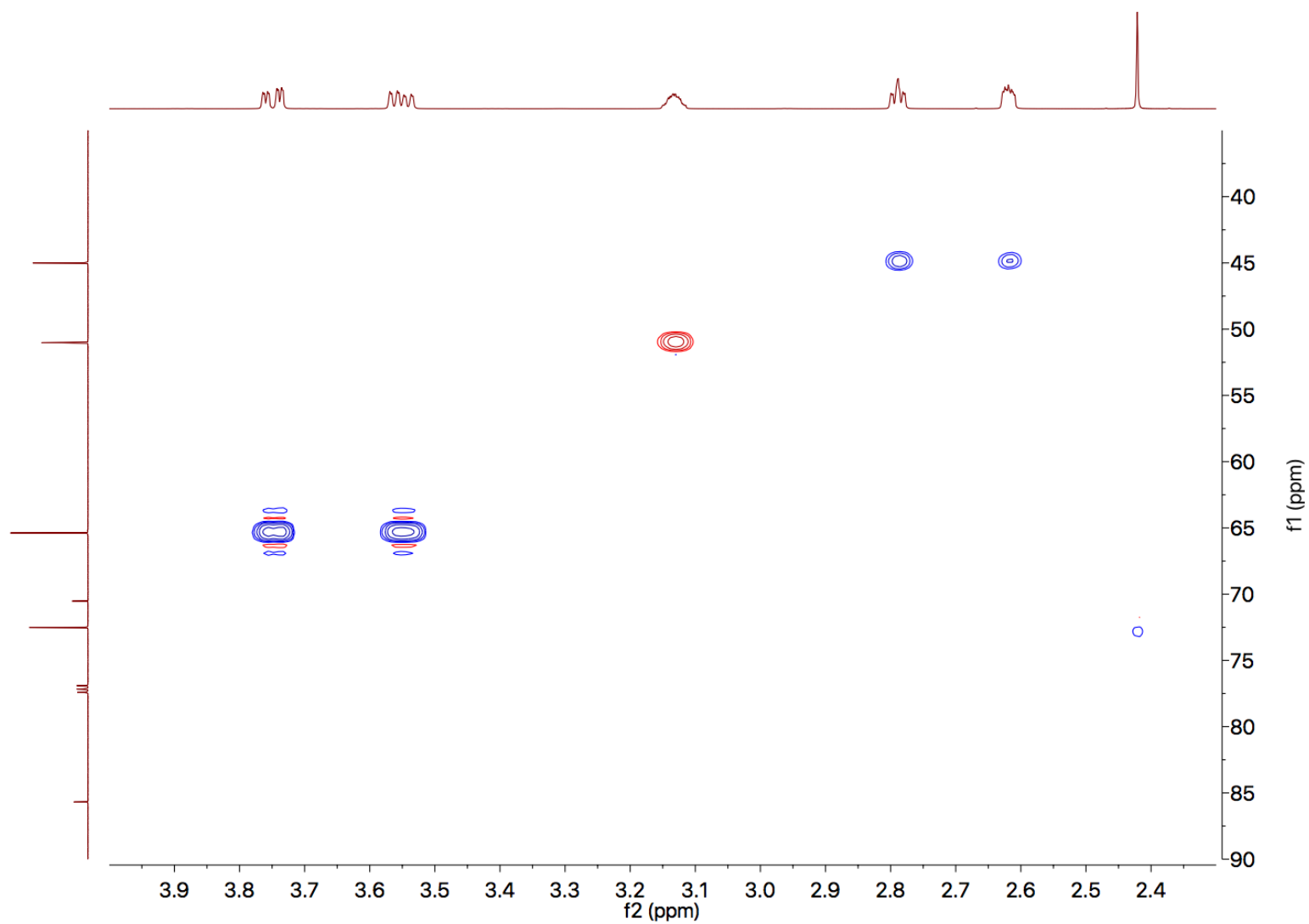


Figure A9. 2D HSQC NMR spectrum of **MGE** in CDCl_3 . Methyl region was omitted for clarity.

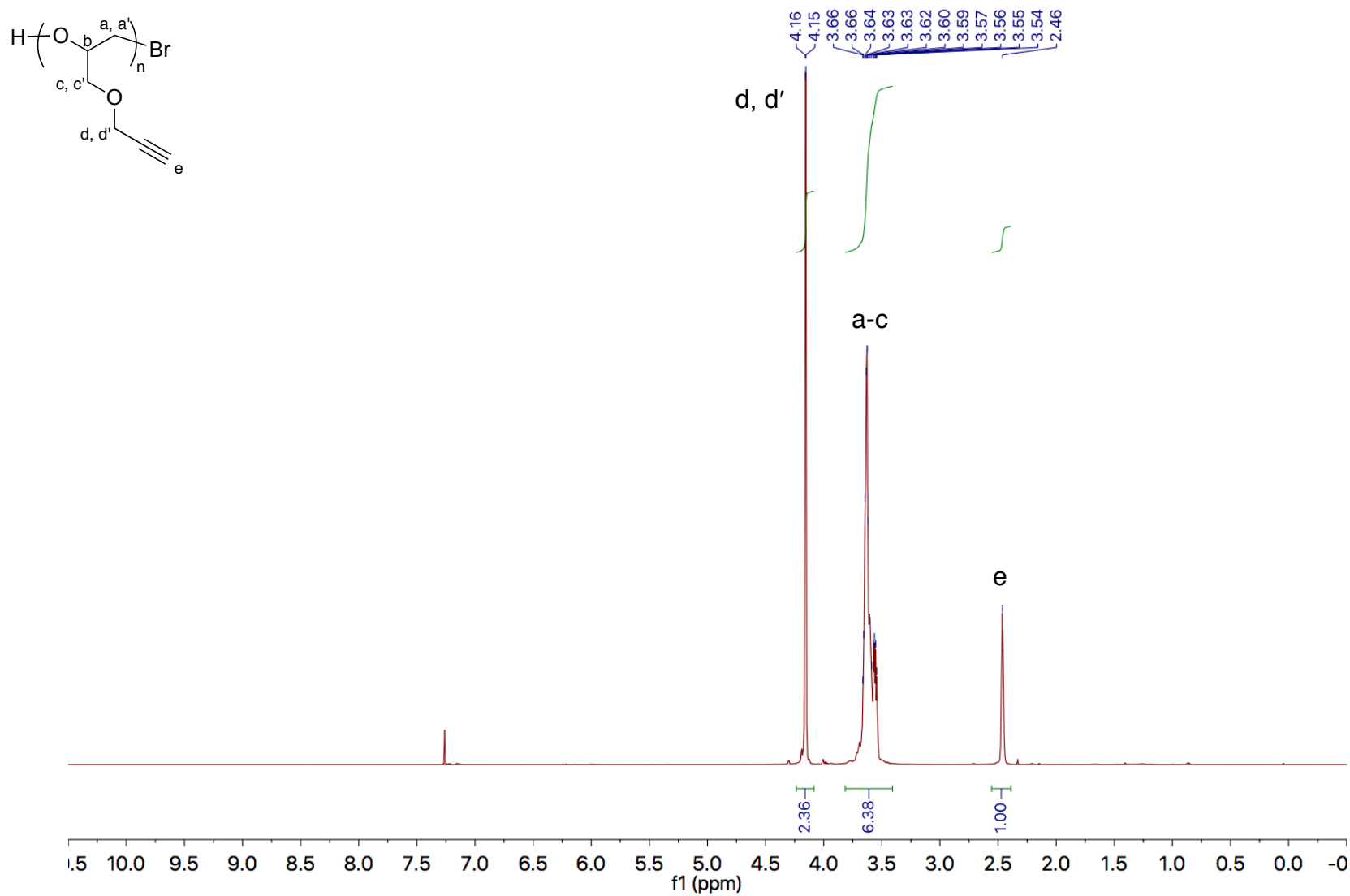


Figure A10. 500 MHz ¹H NMR spectrum of poly(PGE) in CDCl₃.

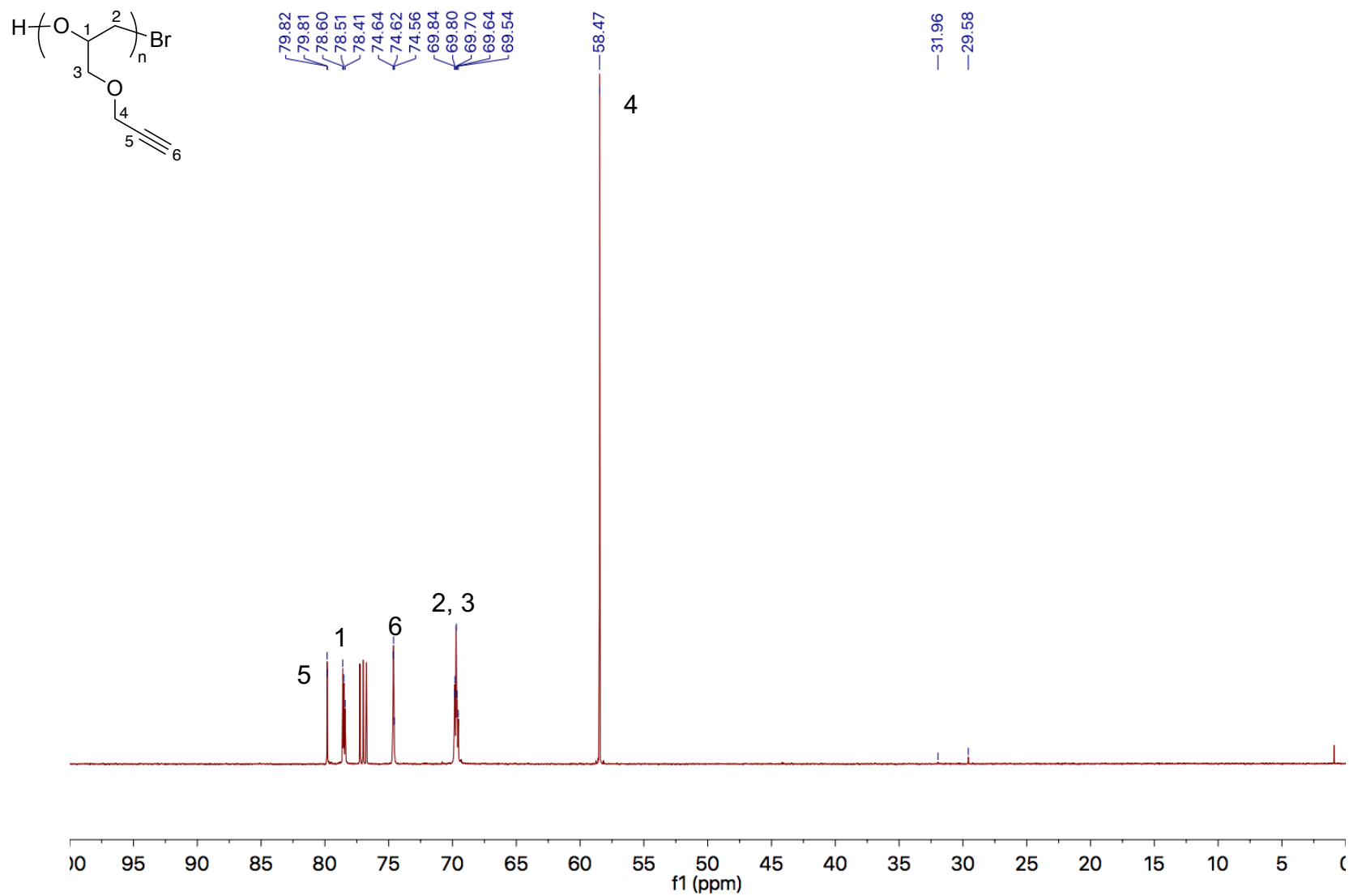


Figure A11. 125 MHz ^{13}C NMR spectrum of poly(PGE) in CDCl_3 .

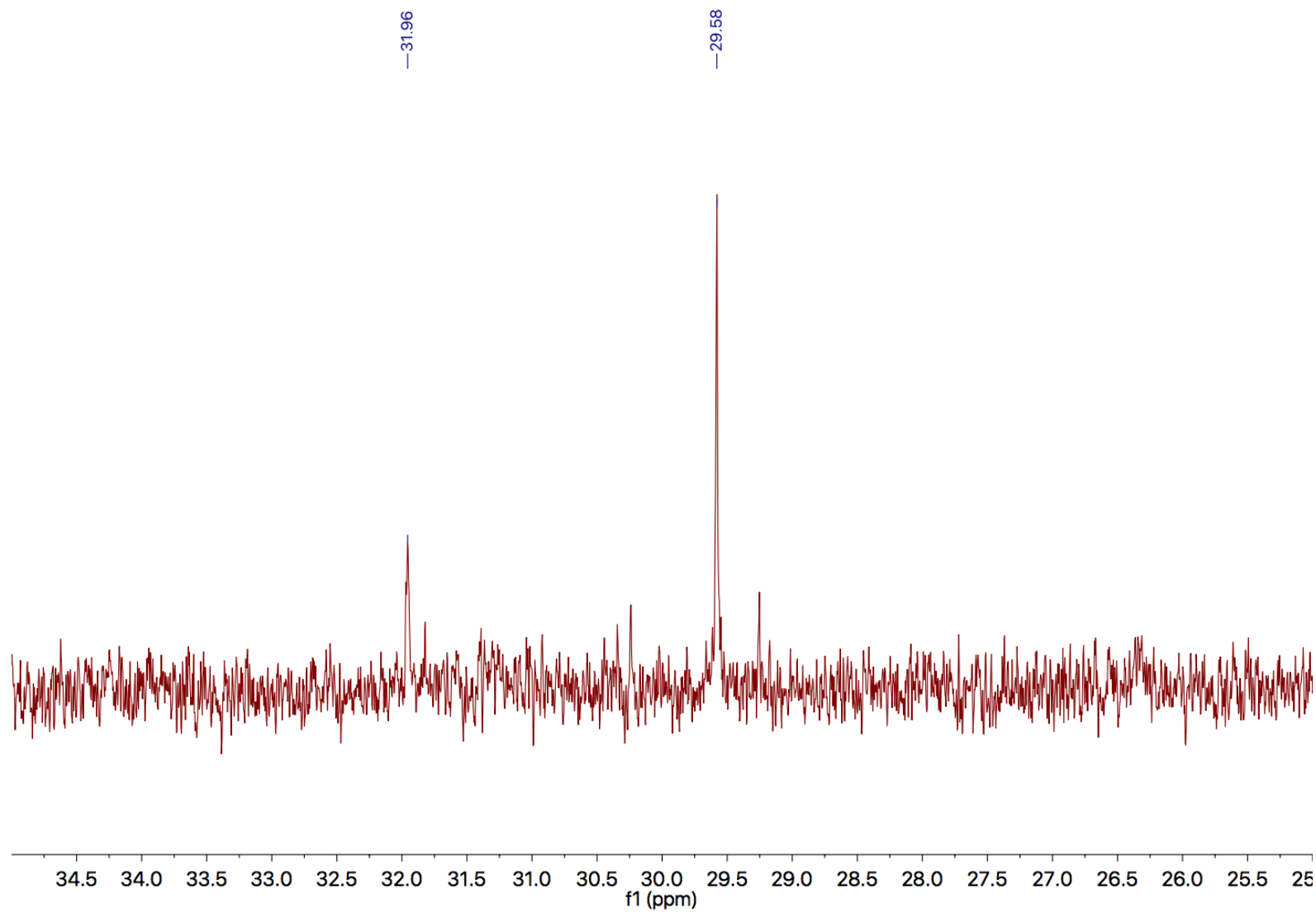


Figure A12. 125 MHz ^{13}C NMR spectrum of poly(PGE) in CDCl_3 between 25.0-35.0 ppm.

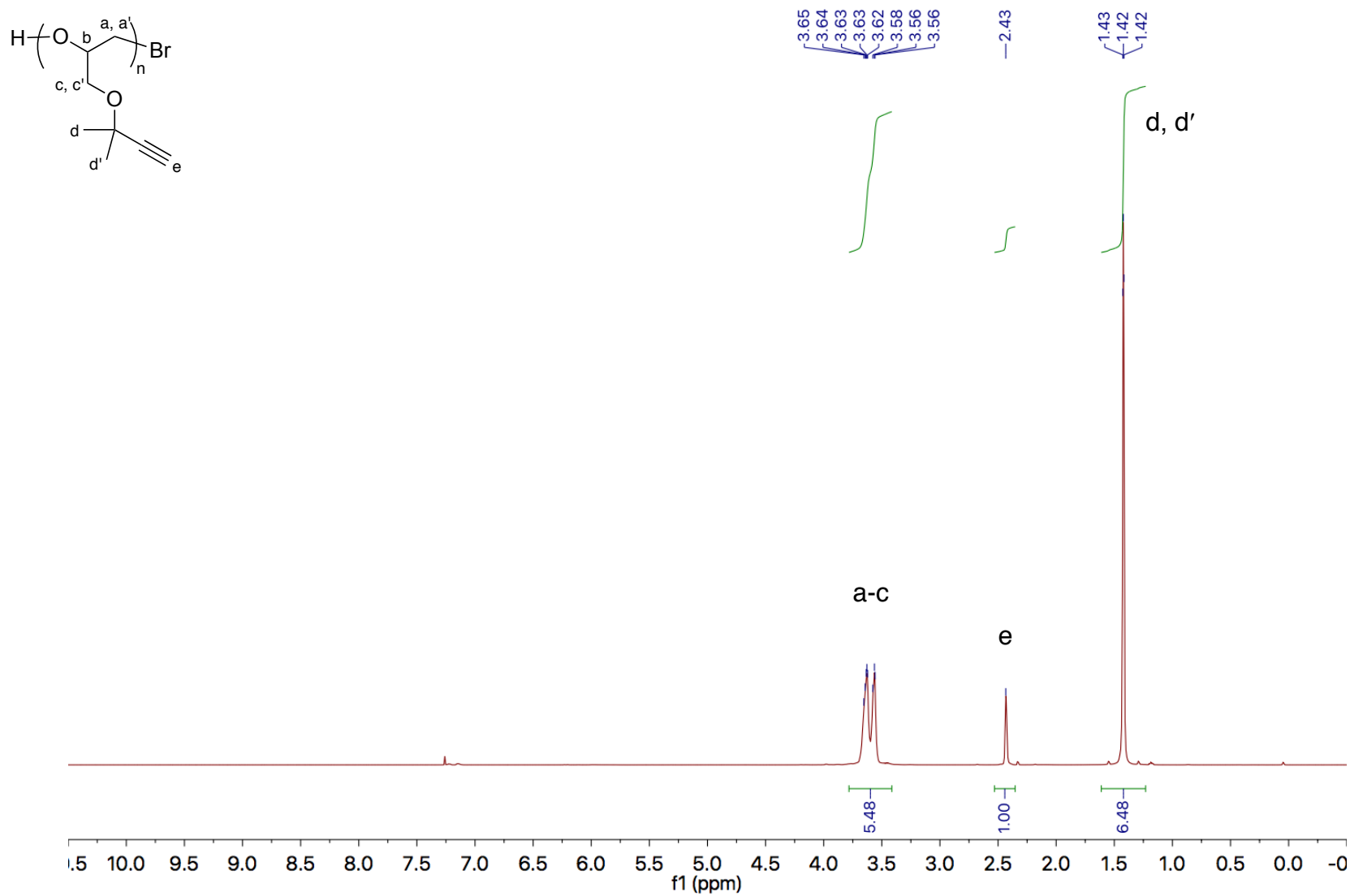


Figure A13. 500 MHz ^1H NMR spectrum of poly(MGE) in CDCl_3 .

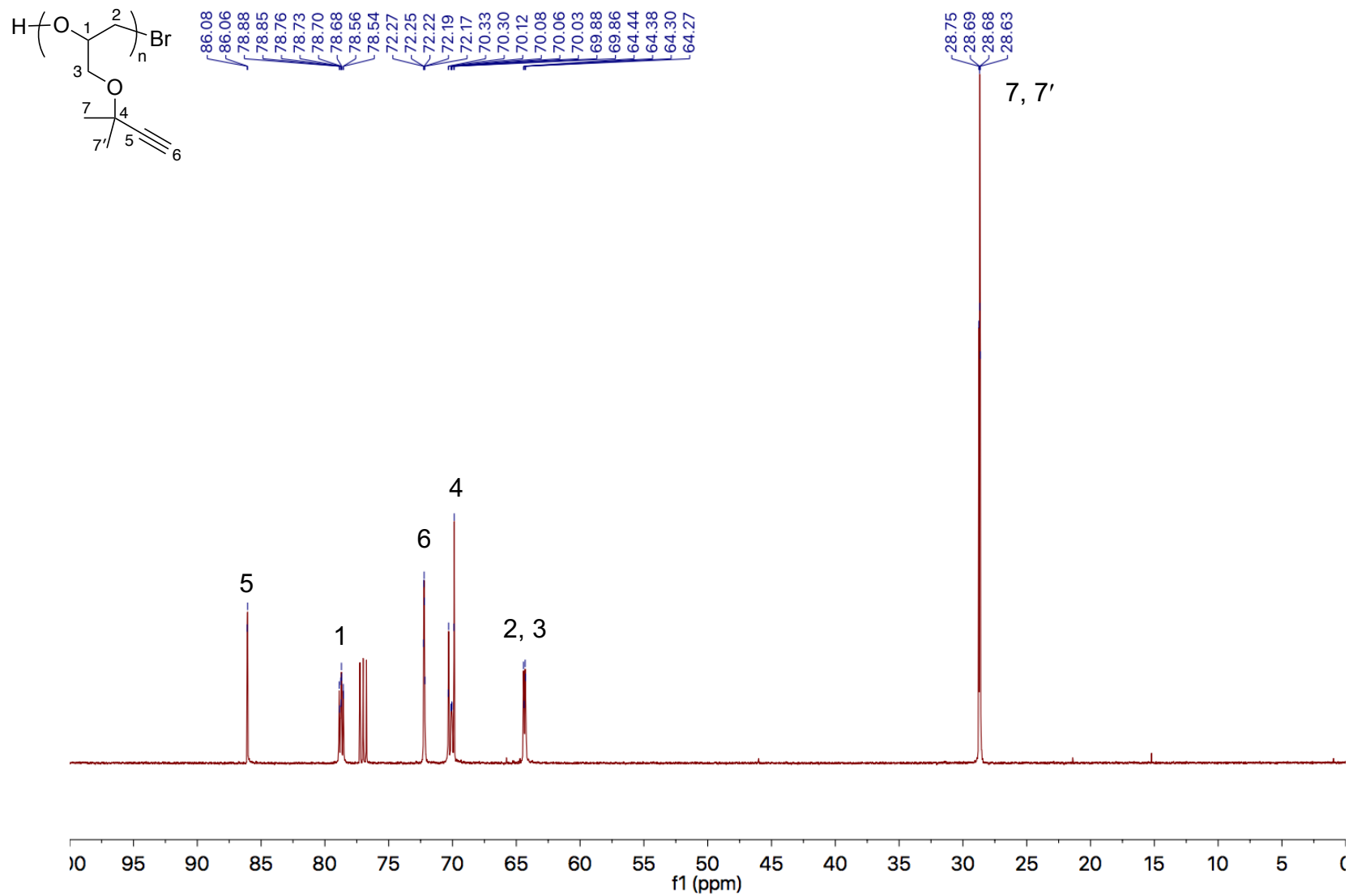


Figure A14. 125 MHz ^{13}C NMR spectrum of poly(MGE) in CDCl_3 .

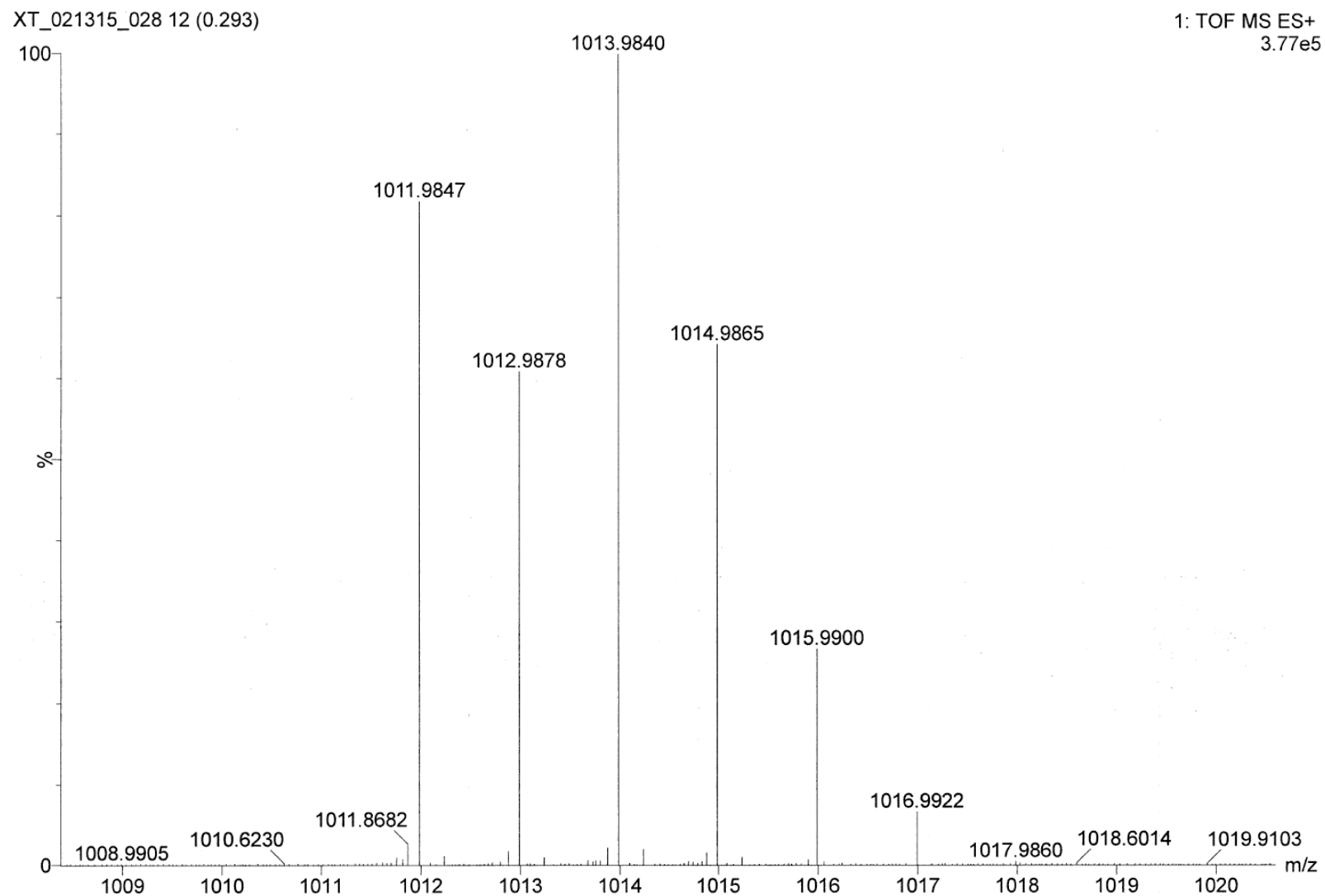


Figure A15. Mass spectrum of poly(PGE) ($M_n = 2800$, PDI = 1.14) via positive electrospray ionization.

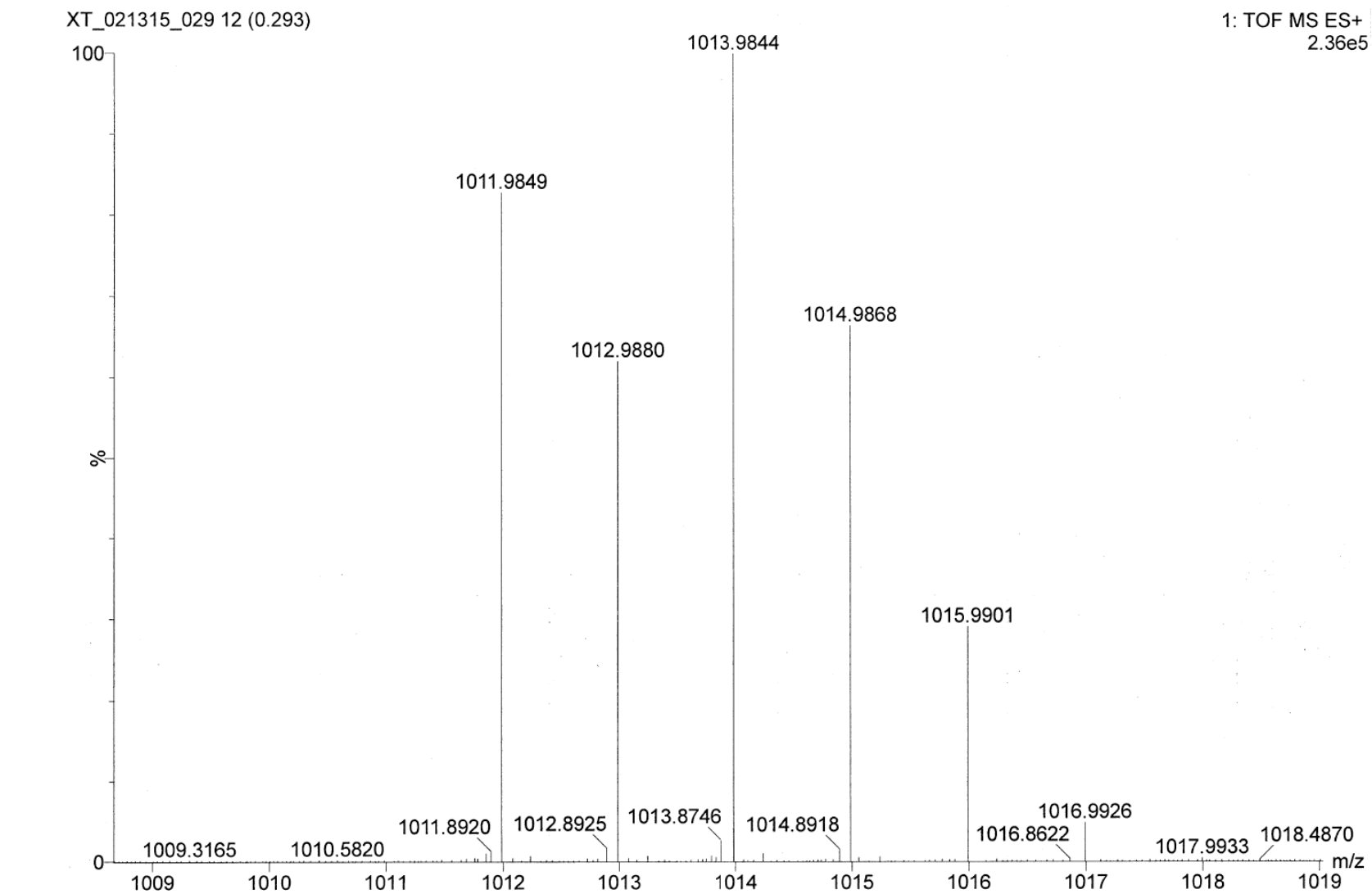


Figure A16. Mass spectrum of poly(MGE) ($M_n = 3900$, PDI = 1.16) via positive electrospray ionization.

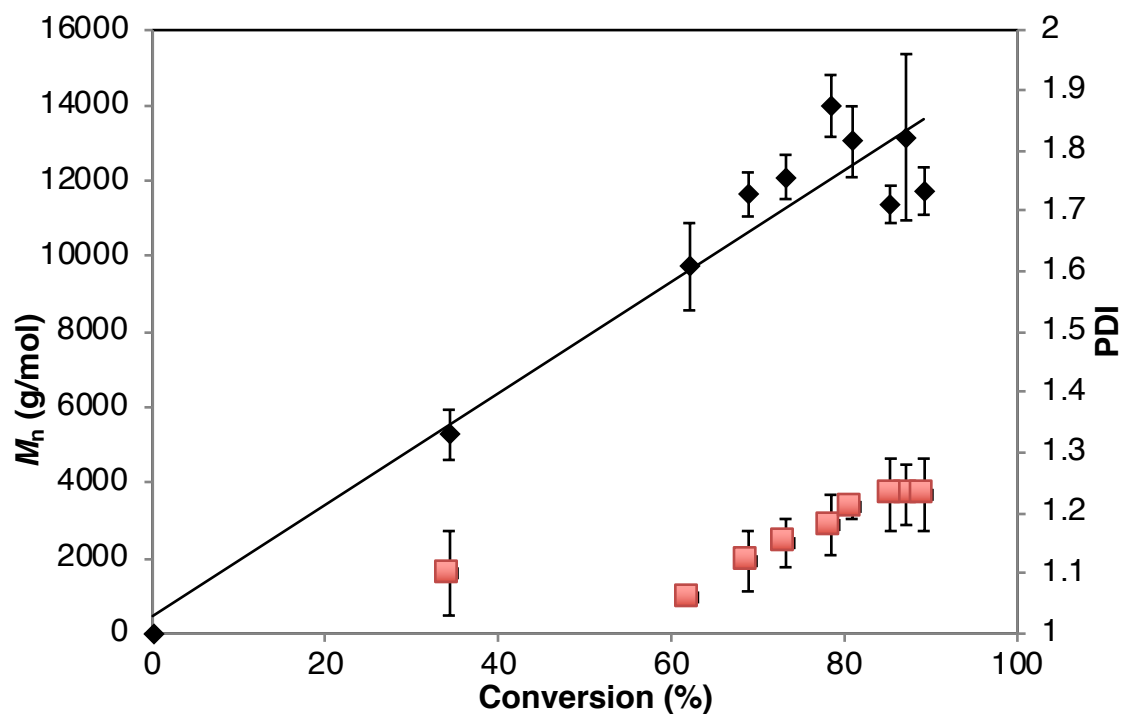


Figure A17. Variation of the number-average molar mass (black square) and PDI (red square) with **PGE** conversion ($[M]: [Al]: [I] = 200: 2: 1$).

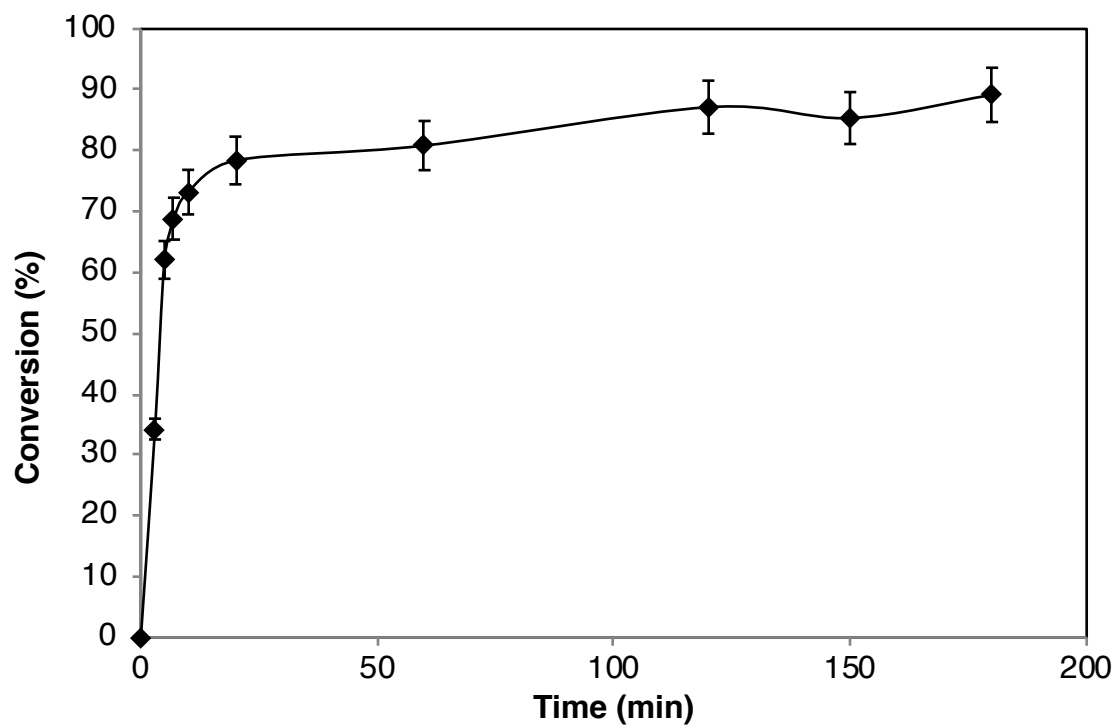


Figure A18. Conversion vs. time of the polymerization of **PGE** ($[M]: [Al]: [I] = 200: 2: 1$).

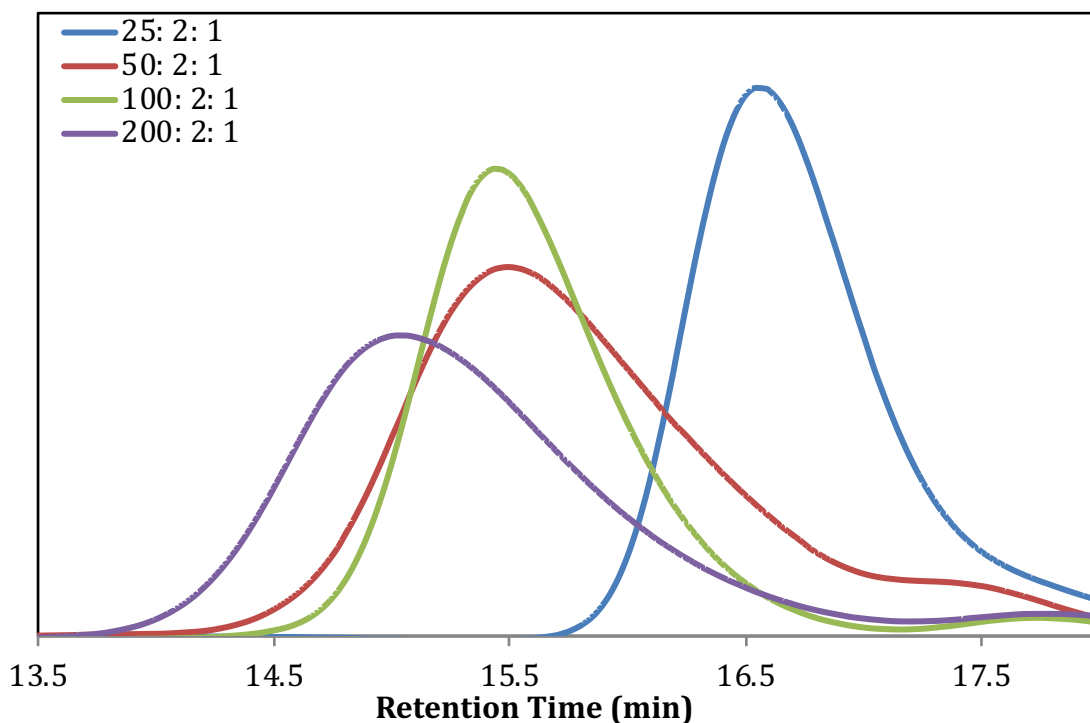


Figure A19. GPC traces of poly(PGE). The polymers were analyzed in THF at 35 °C, at 1 mL/min flow rate.

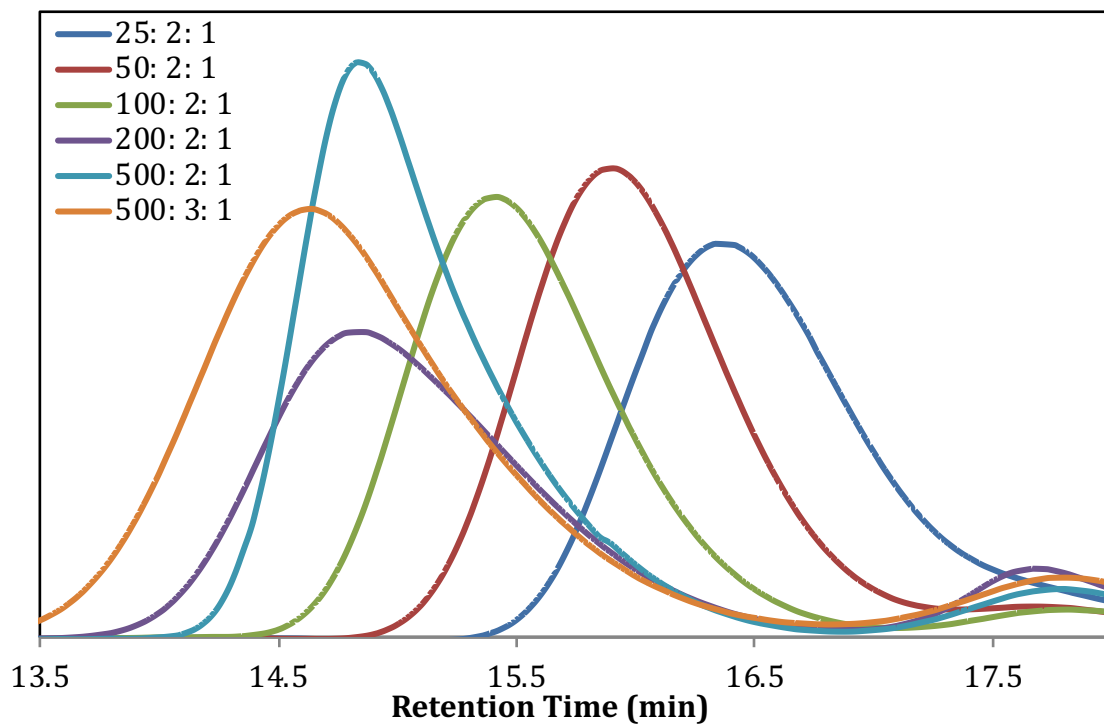


Figure A20. GPC traces of poly(MGE). The polymers were analyzed in THF at 35 °C, at 1 mL/min flow rate.

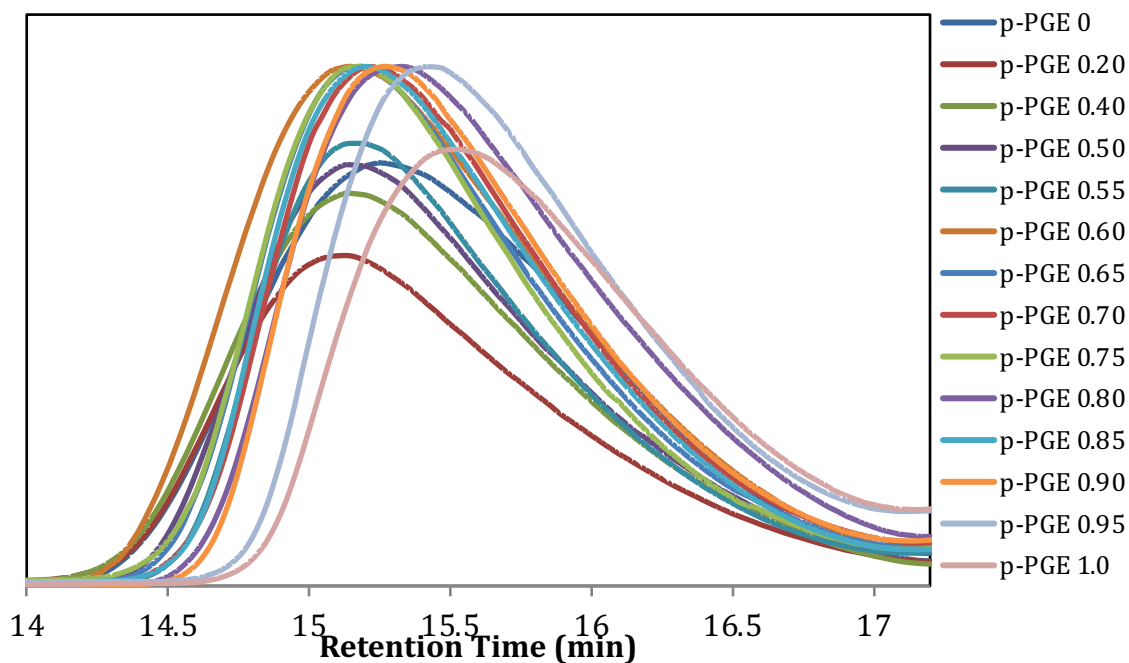


Figure A21. GPC traces of poly(PGE_{0.x}). The polymers were analyzed in THF at 35 °C, at 1 mL/min flow rate.

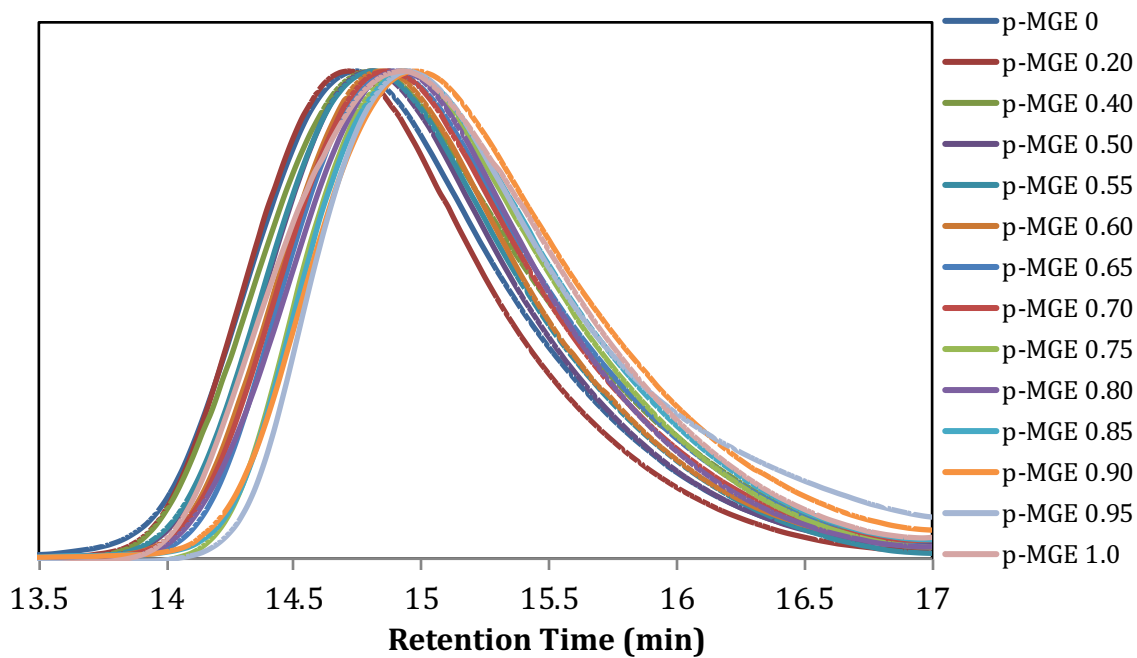


Figure A22. GPC traces of poly(MGE_{0.x}). The polymers were analyzed in THF at 35 °C, at 1 mL/min flow rate.

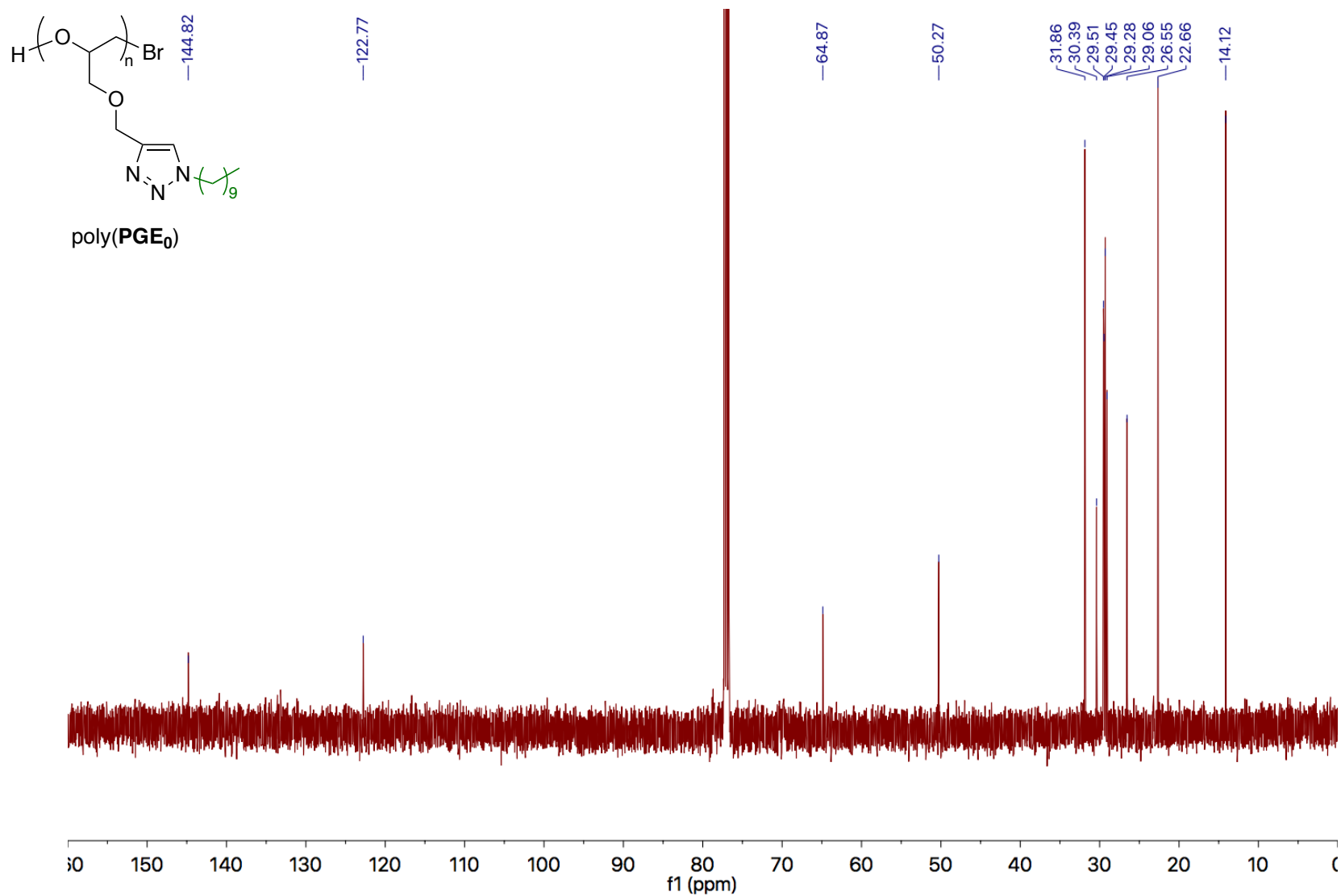


Figure A24. 125 MHz ^{13}C NMR spectrum of poly(PGE₀) in CDCl_3 .

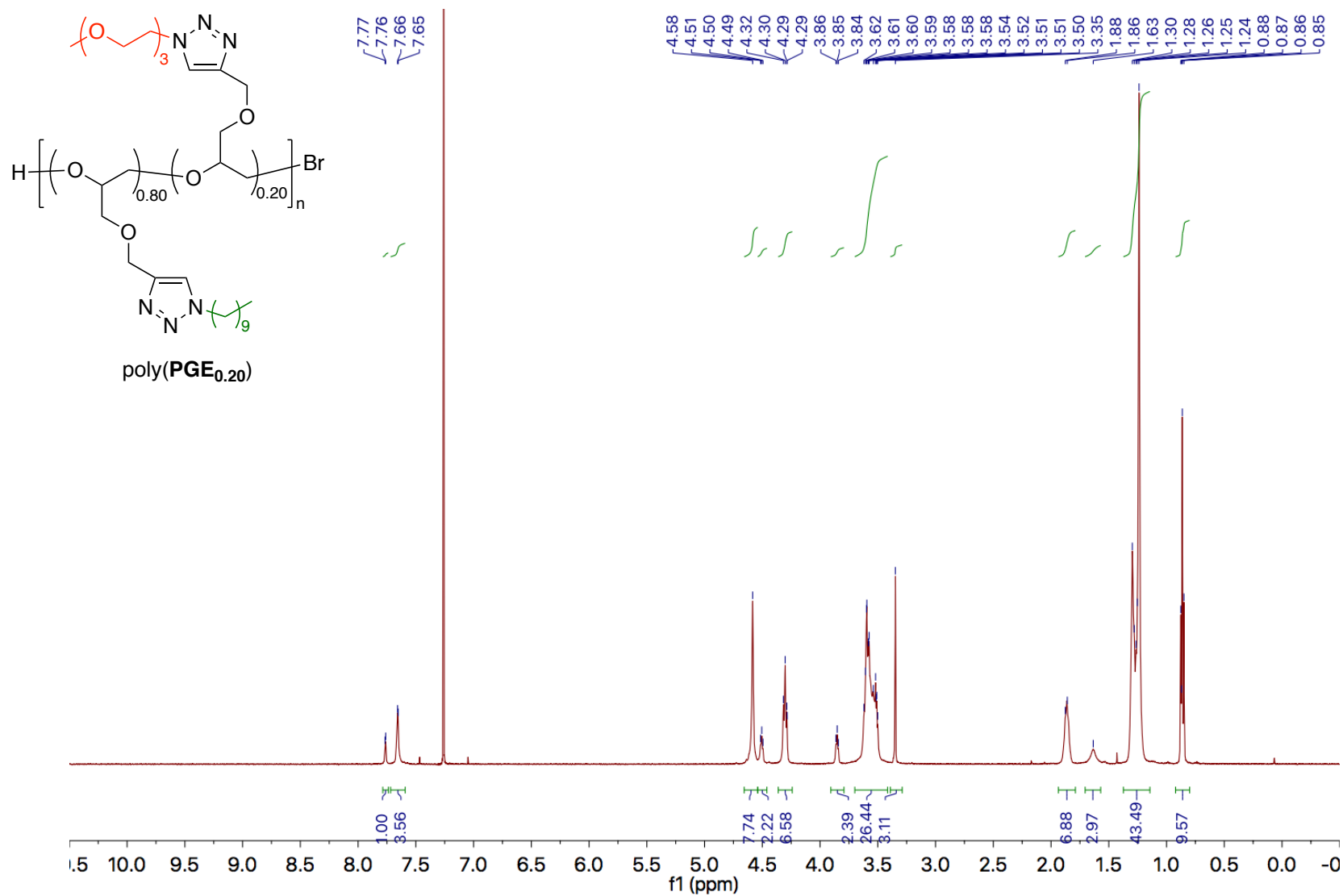


Figure A25. 500 MHz ¹H NMR spectrum of poly(PGE_{0.20}) in CDCl₃.

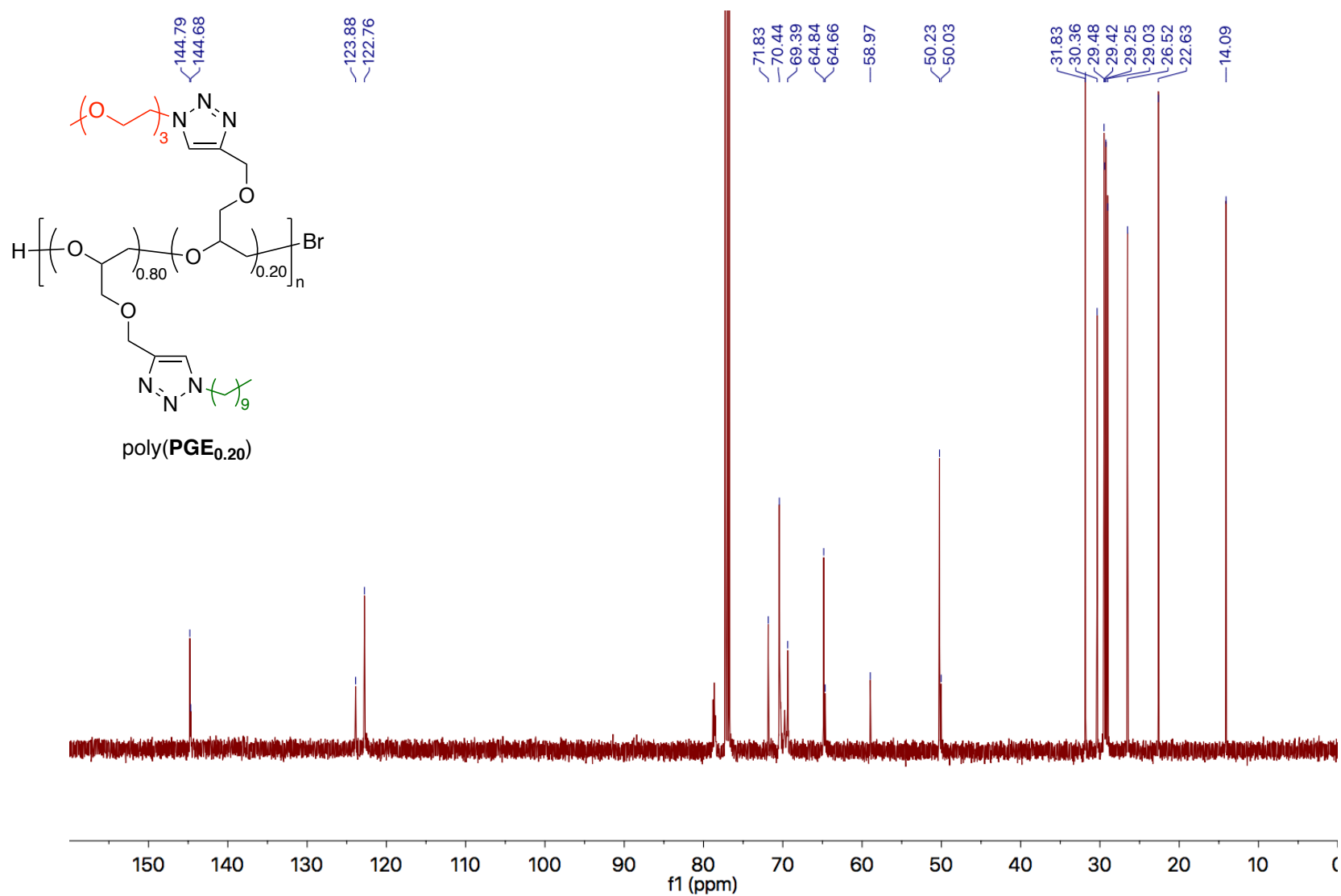


Figure A26. 125 MHz ¹³C NMR spectrum of poly(PGE_{0.20}) in CDCl₃.

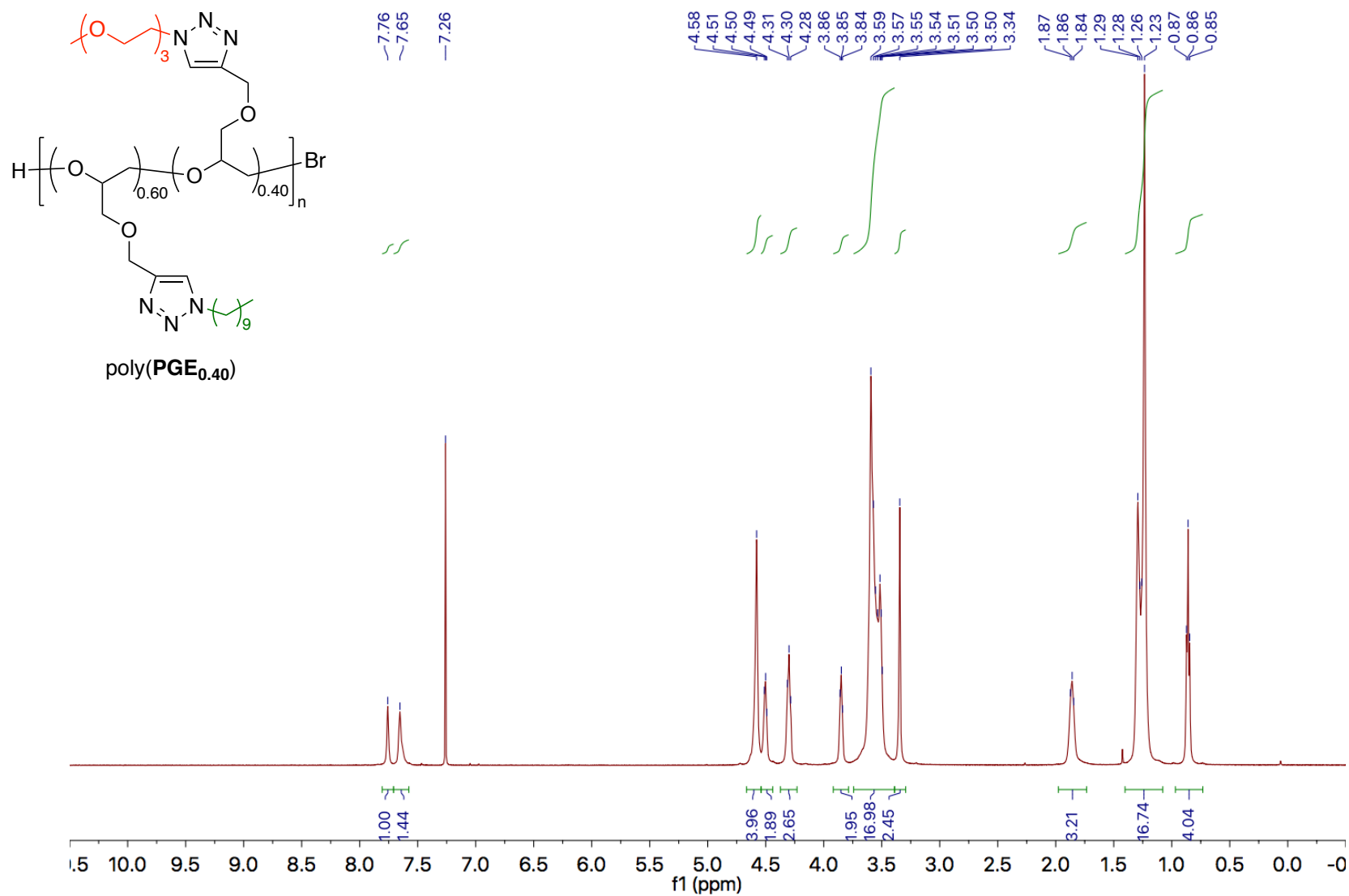


Figure A27. 500 MHz ¹H NMR spectrum of poly(PGE_{0.40}) in CDCl₃.

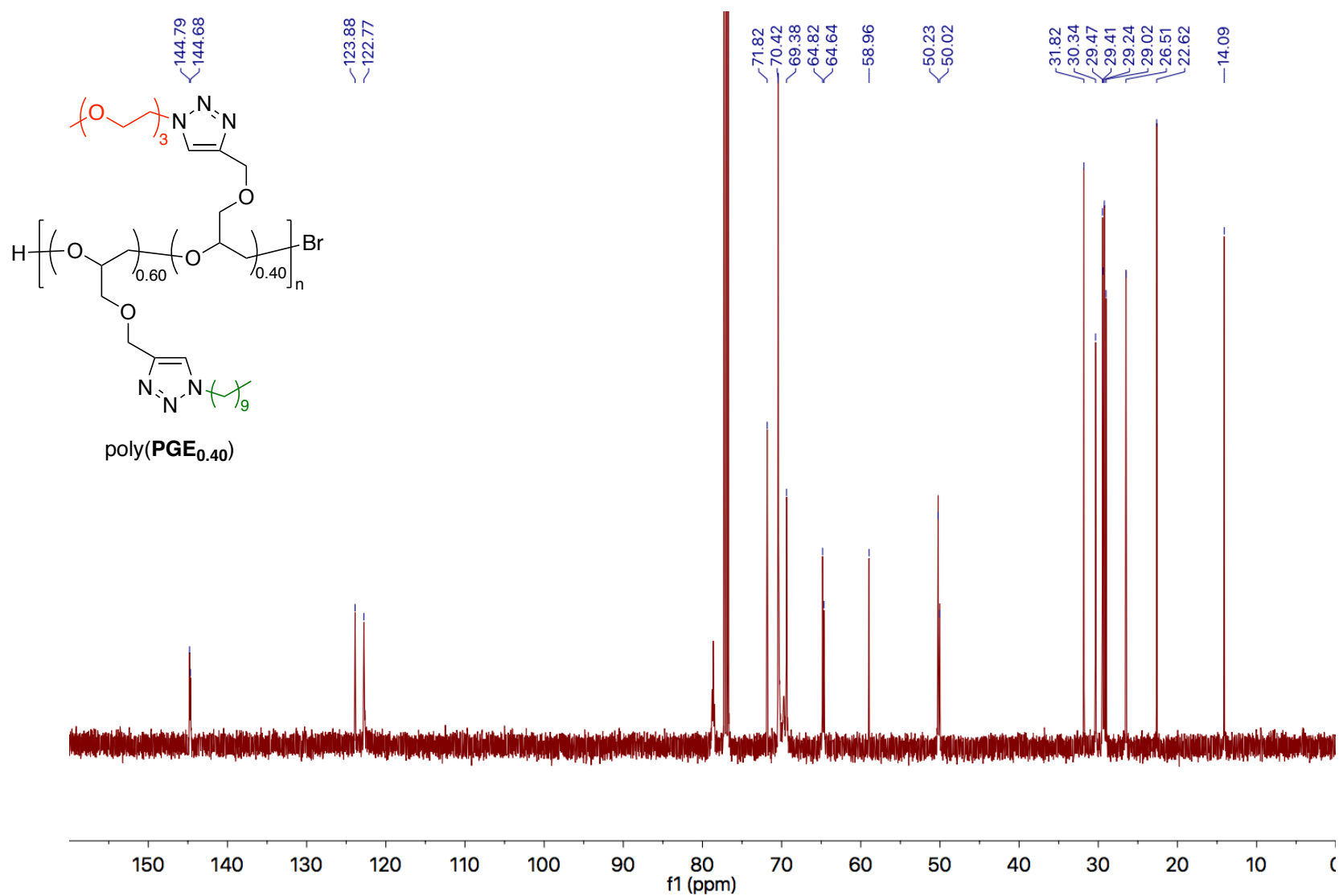


Figure A28. 125 MHz ¹³C NMR spectrum of poly(PGE_{0.40}) in CDCl₃.

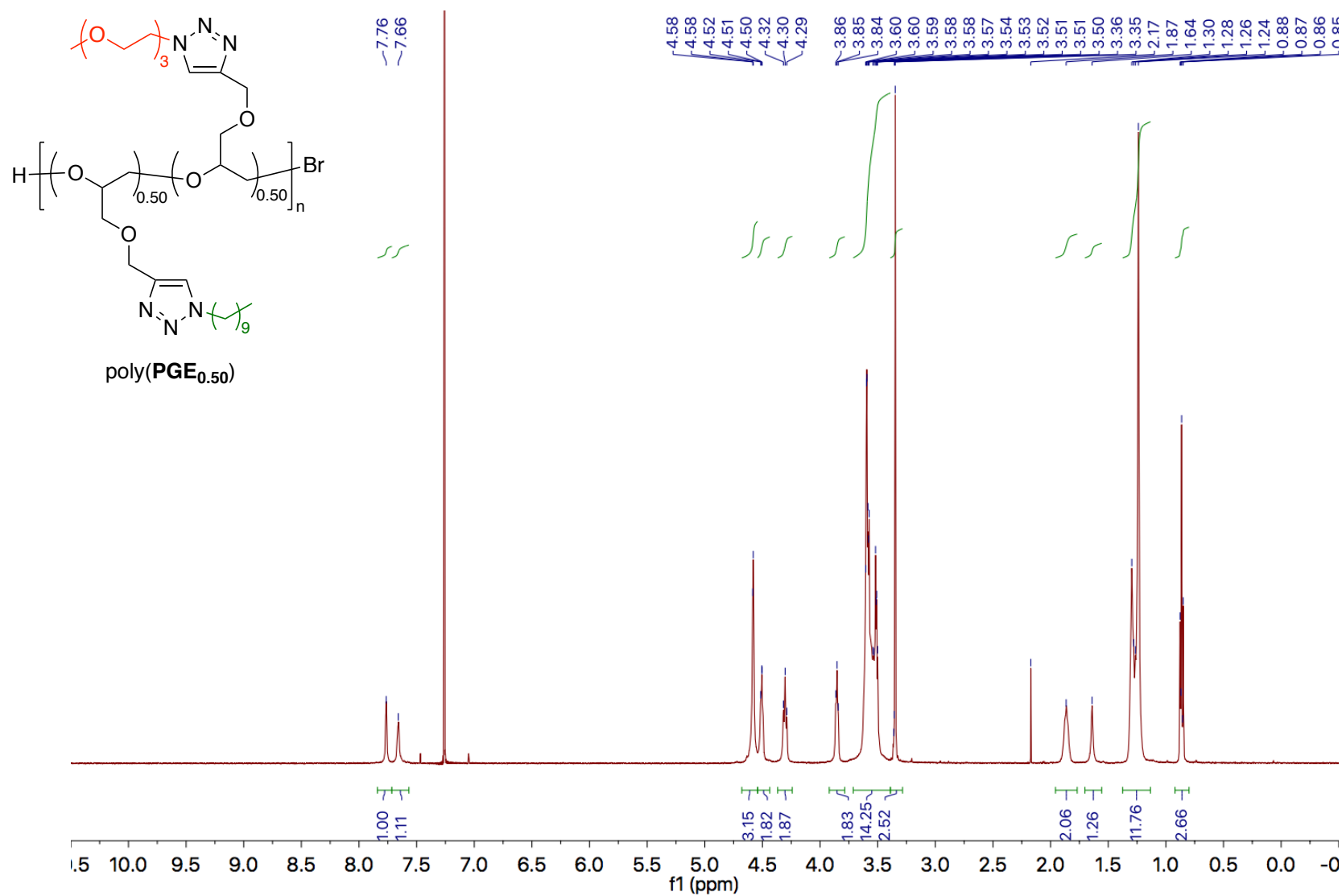


Figure A29. 500 MHz ¹H NMR spectrum of poly(PGE_{0.50}) in CDCl₃.

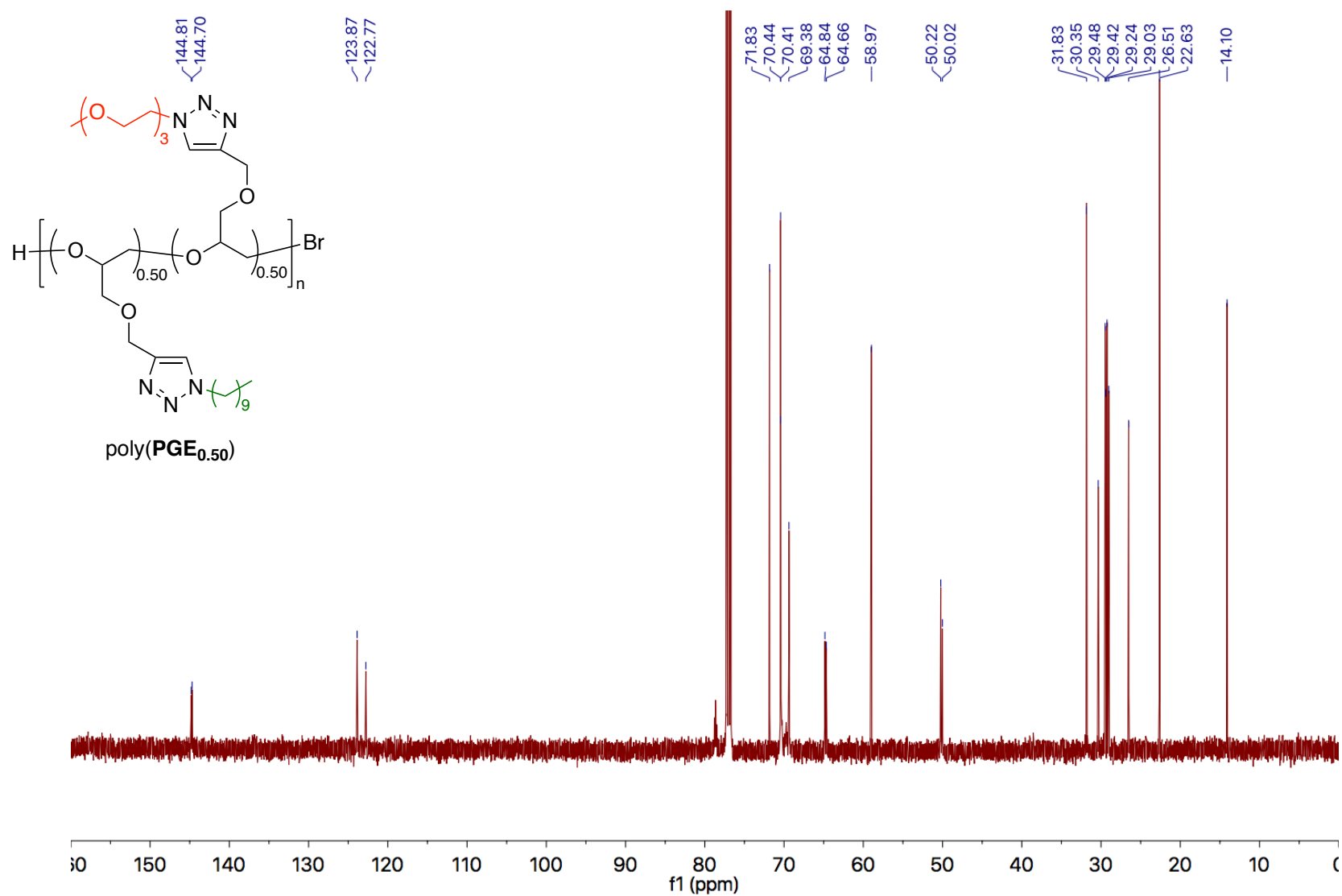


Figure A30. 125 MHz ¹³C NMR spectrum of poly(PGE_{0.50}) in CDCl₃.

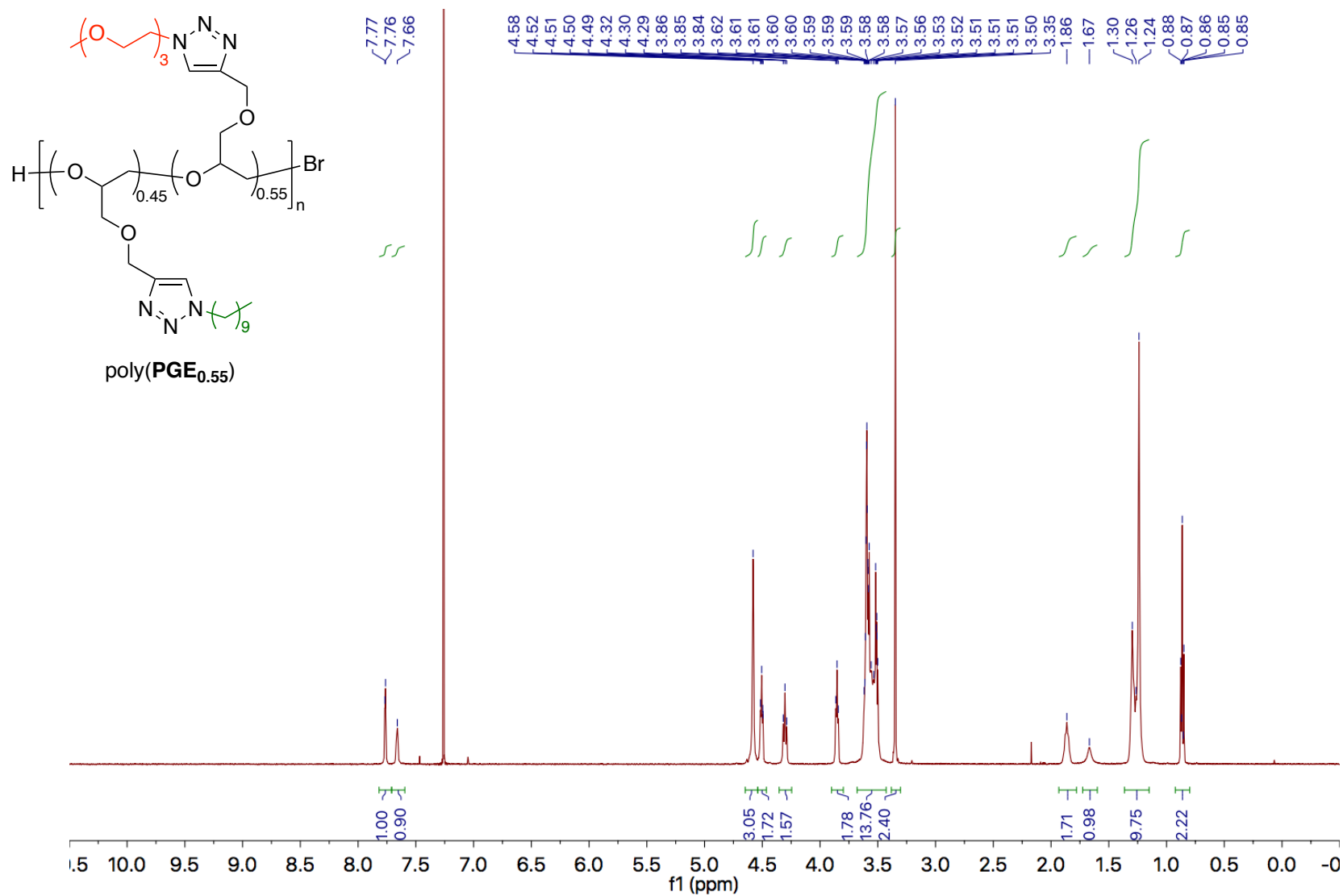


Figure A31. 500 MHz ¹H NMR spectrum of poly(PGE_{0.55}) in CDCl₃.

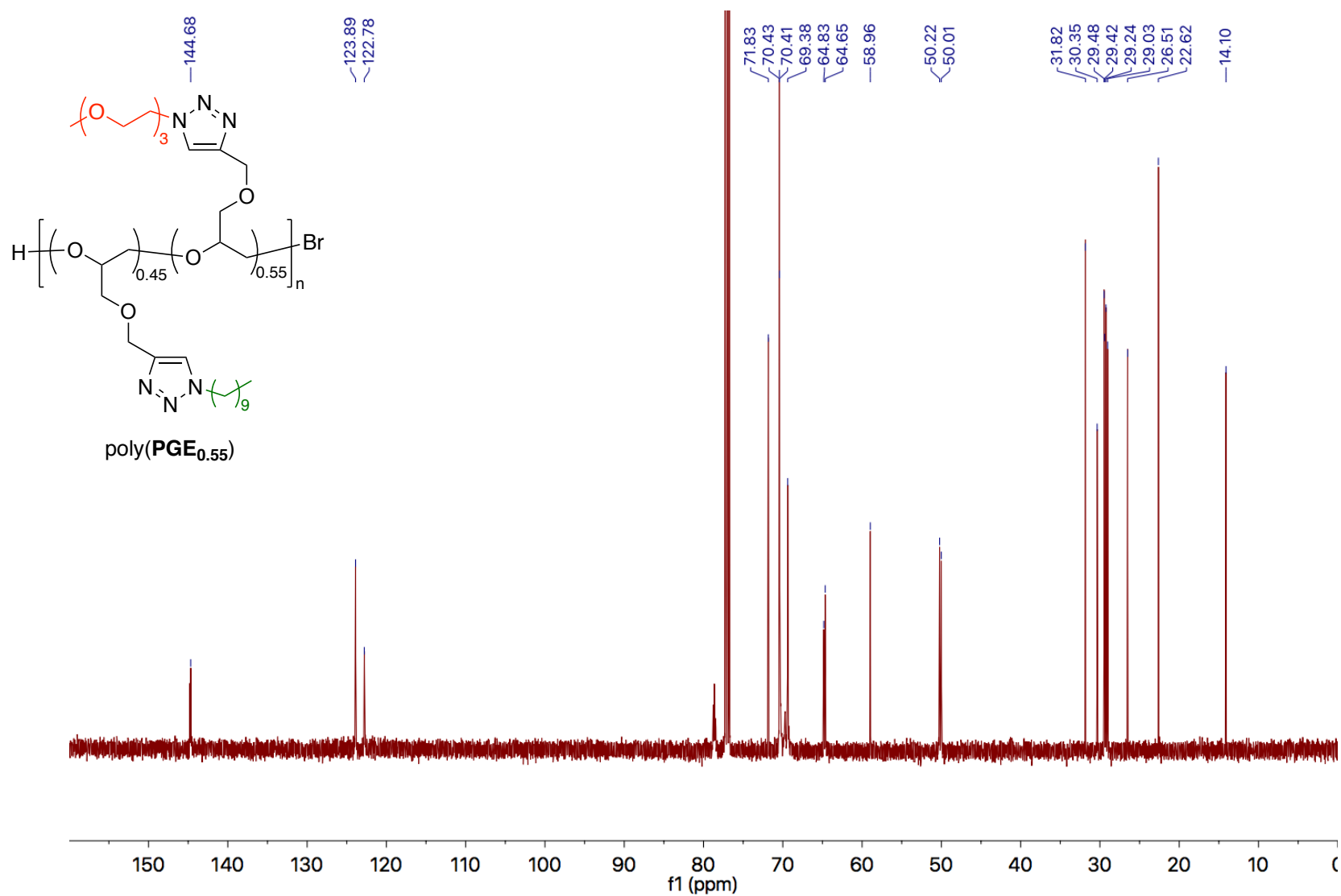


Figure A32. 125 MHz ¹³C NMR spectrum of poly(PGE_{0.55}) in CDCl₃.

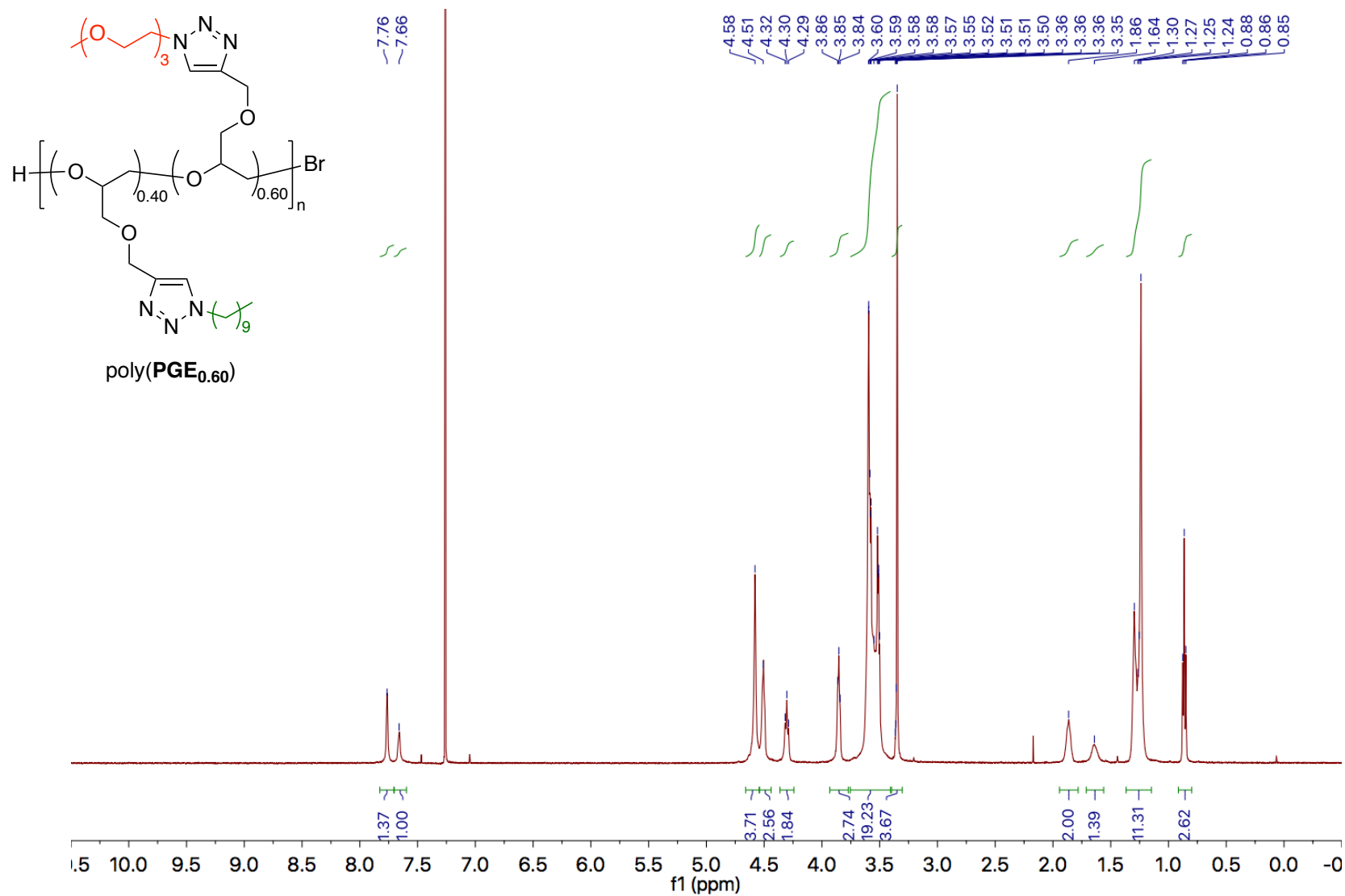


Figure A33. 500 MHz ¹H NMR spectrum of poly(PGE_{0.60}) in CDCl₃.

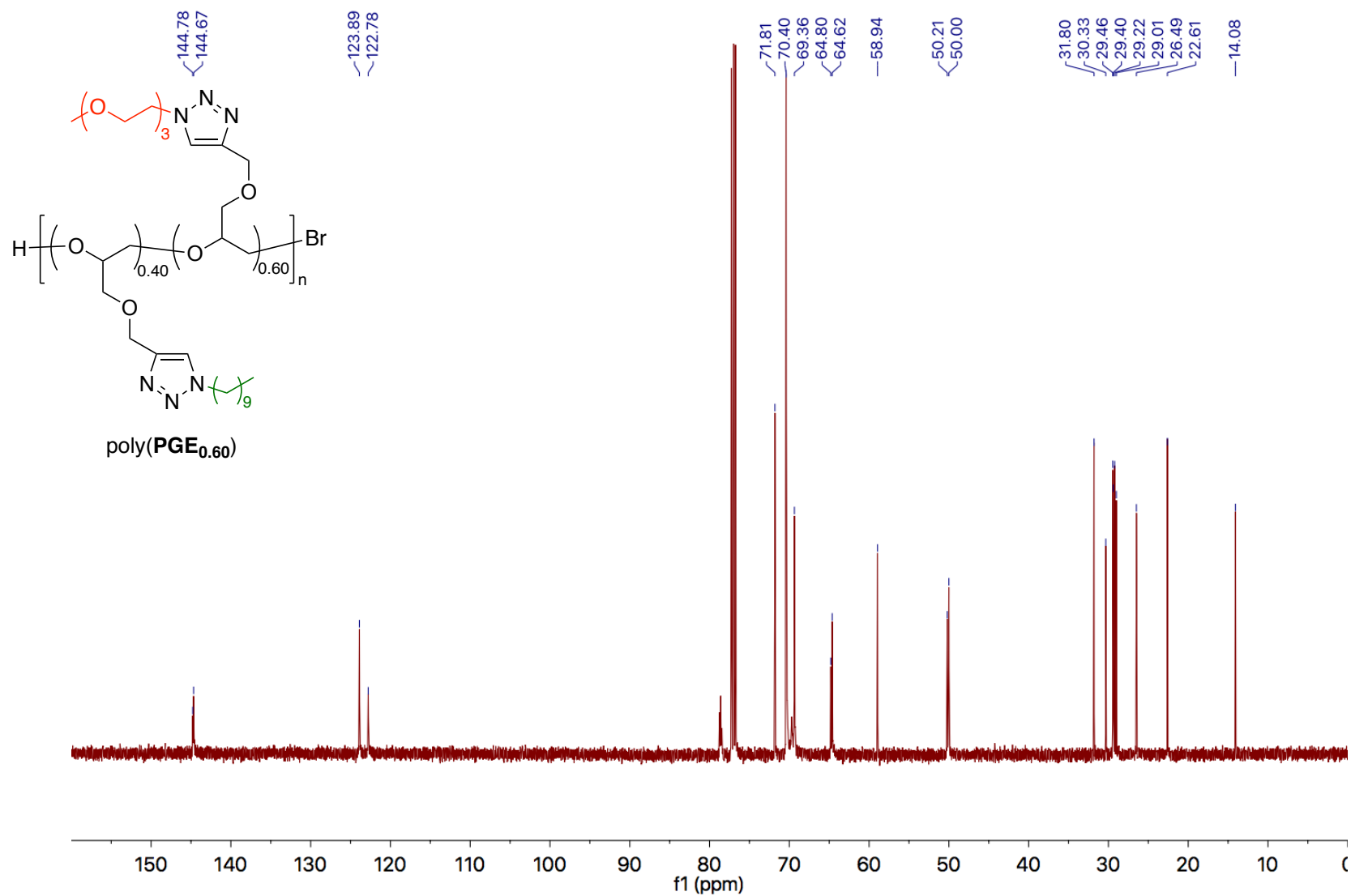


Figure A34. 125 MHz ^{13}C NMR spectrum of poly(PGE_{0.60}) in CDCl_3 .

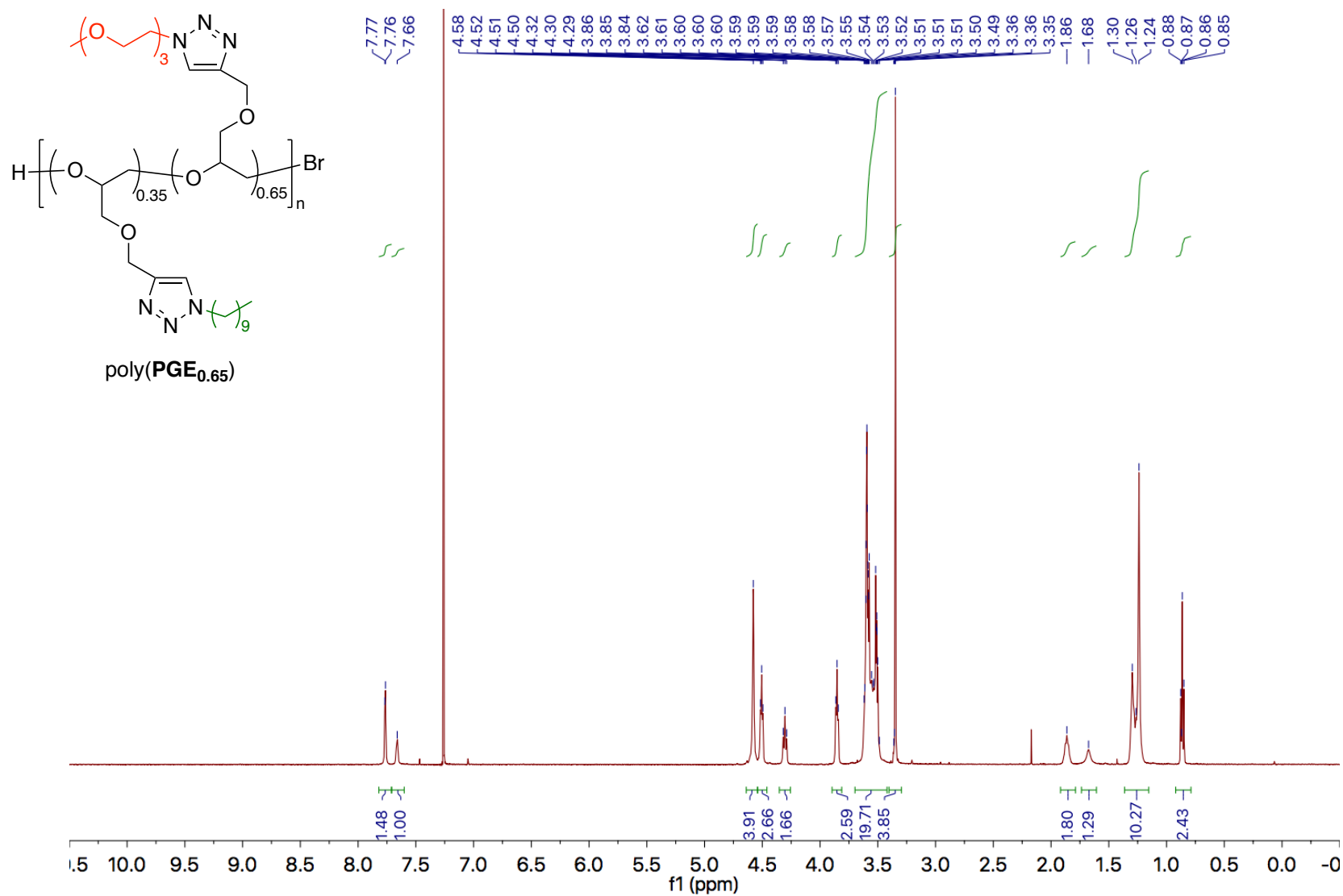


Figure A35. 500 MHz ¹H NMR spectrum of poly(PGE_{0.65}) in CDCl₃.

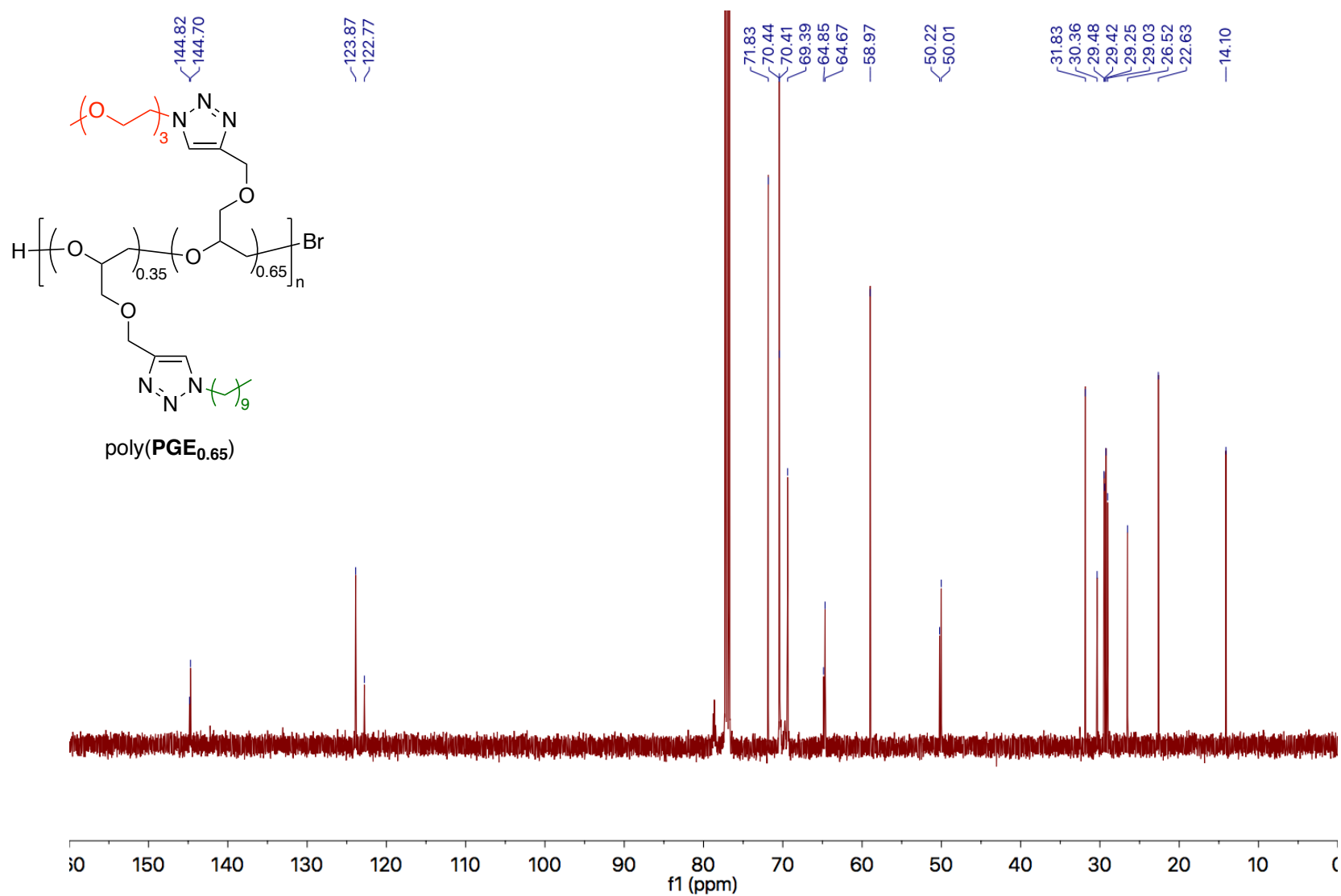


Figure A36. 125 MHz ¹³C NMR spectrum of poly(PGE_{0.65}) in CDCl₃.

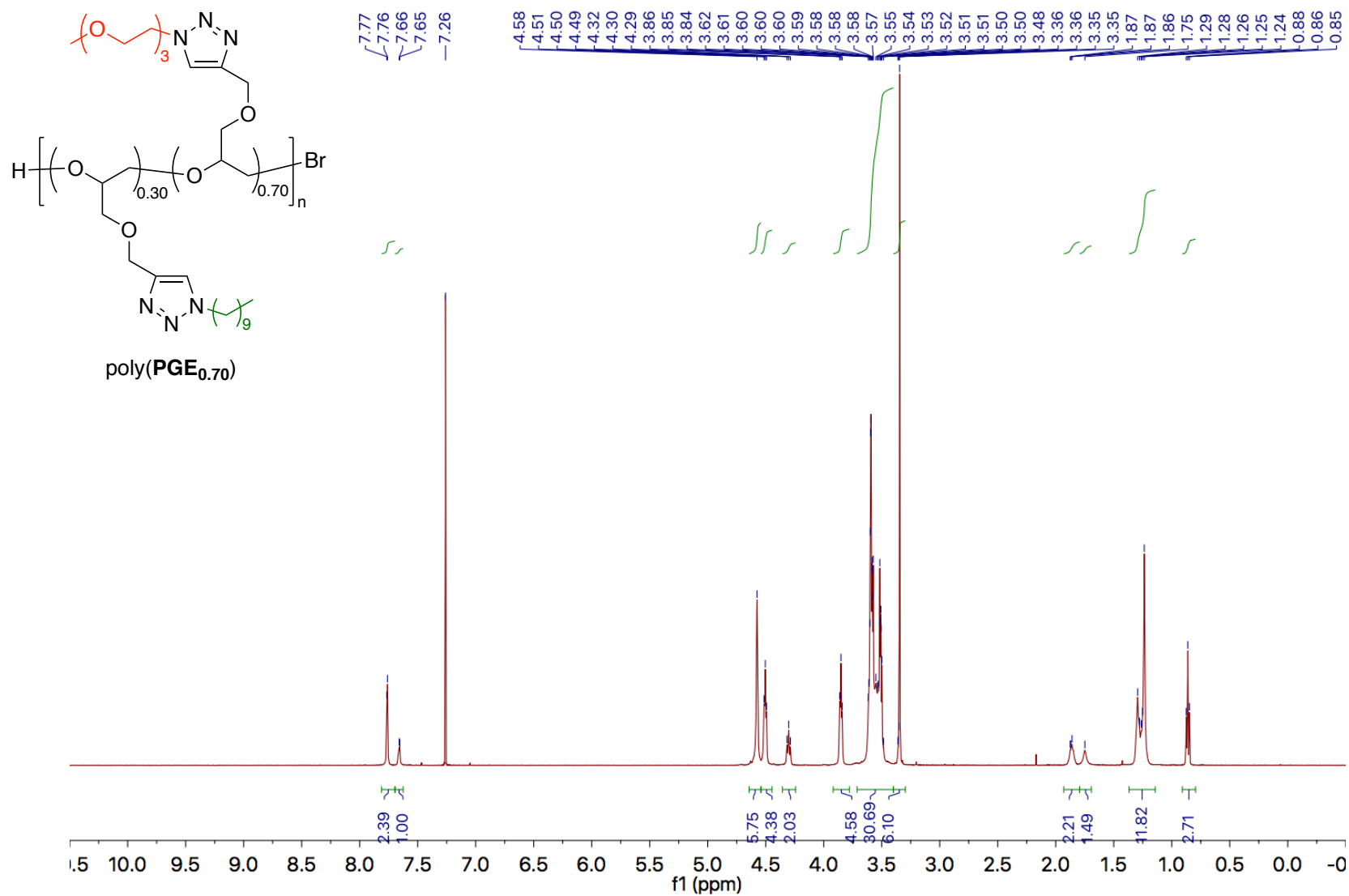


Figure A37. 500 MHz ^1H NMR spectrum of poly(PGE_{0.70}) in CDCl_3 .

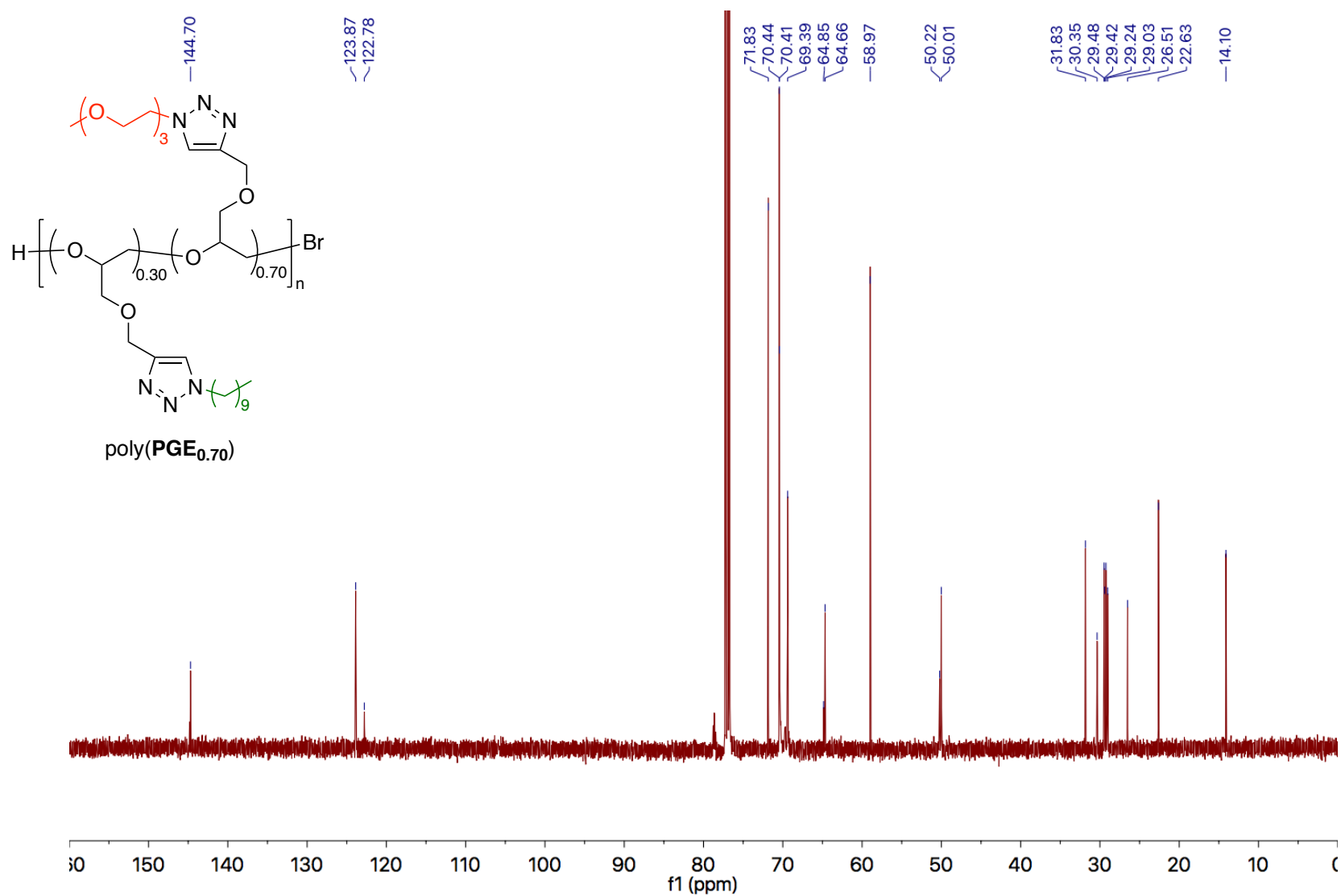


Figure A38. 125 MHz ¹³C NMR spectrum of poly(PGE_{0.70}) in CDCl₃.

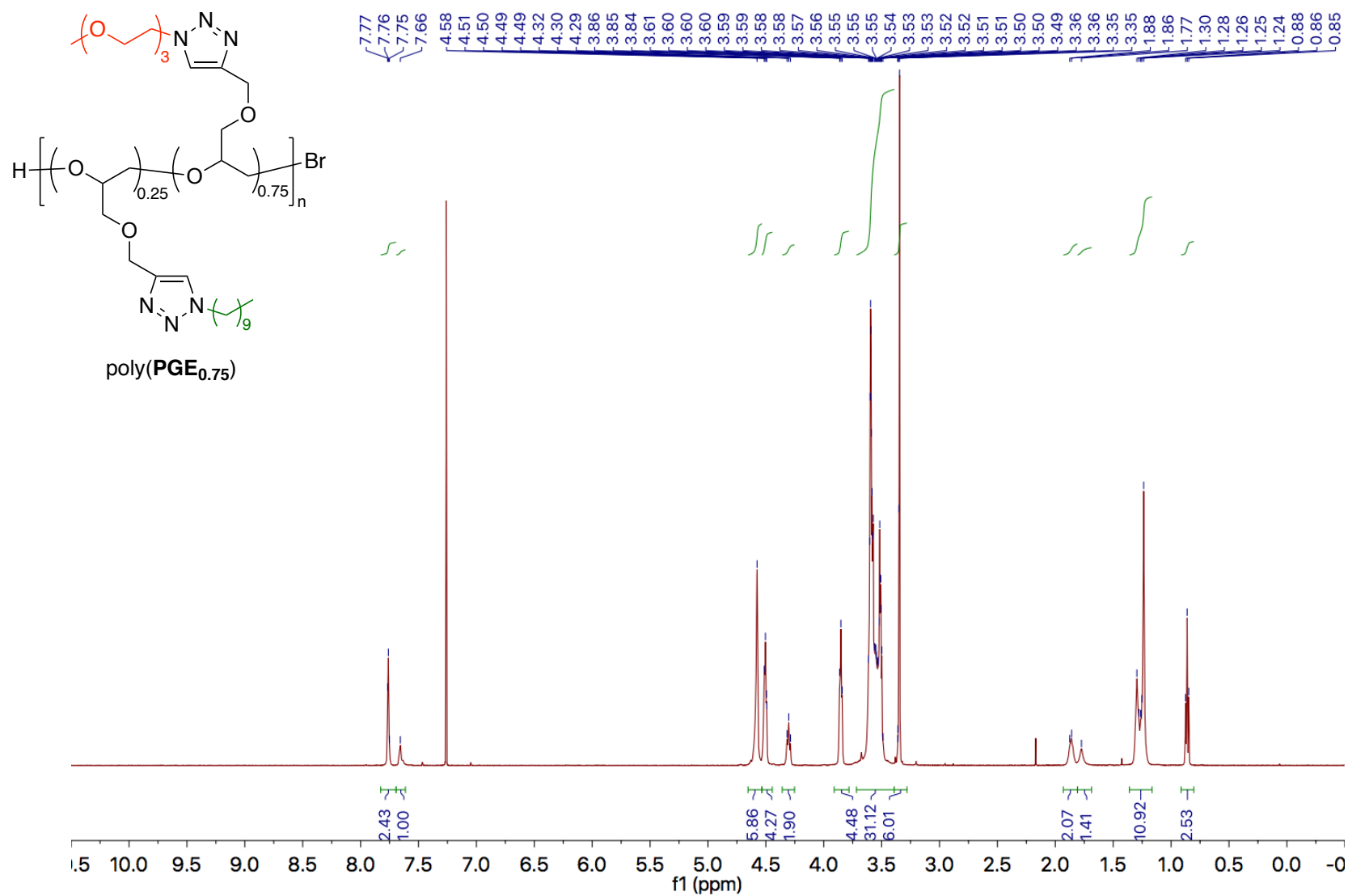


Figure A39. 500 MHz ¹H NMR spectrum of poly(PGE_{0.75}) in CDCl₃.

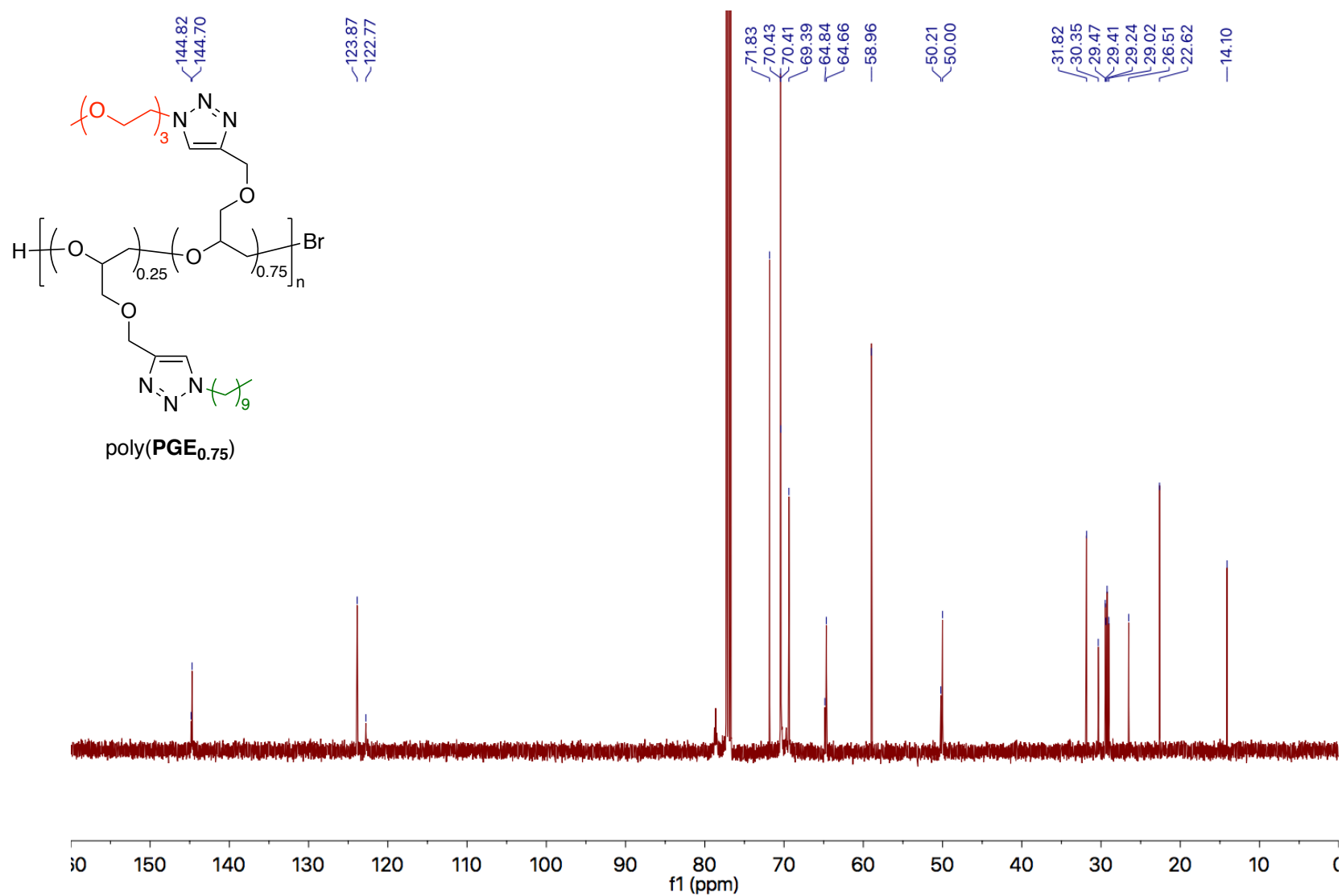


Figure A40. 125 MHz ¹³C NMR spectrum of poly(PGE_{0.75}) in CDCl₃.

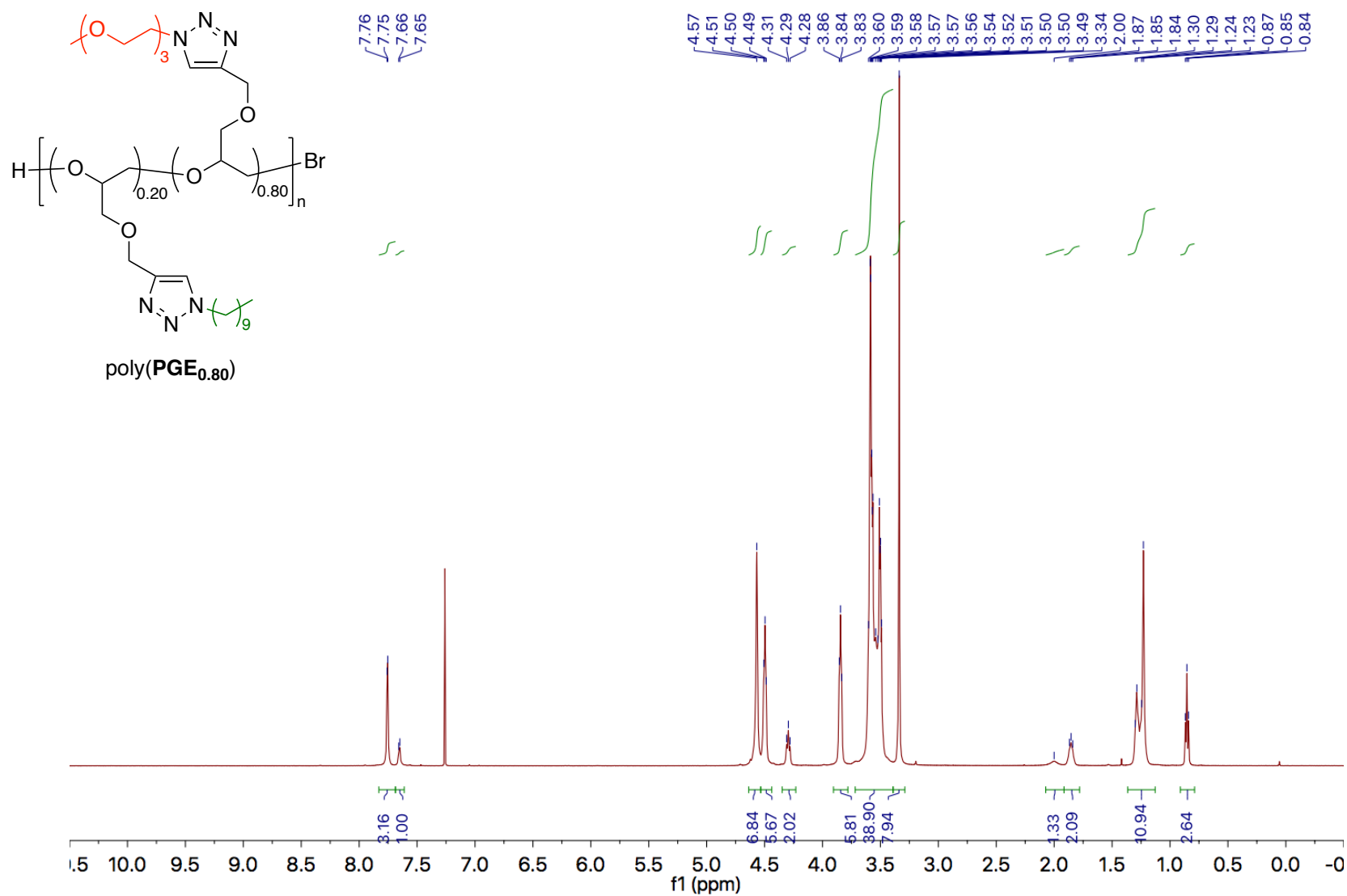


Figure A41. 500 MHz ^1H NMR spectrum of poly(PGE_{0.80}) in CDCl_3 .

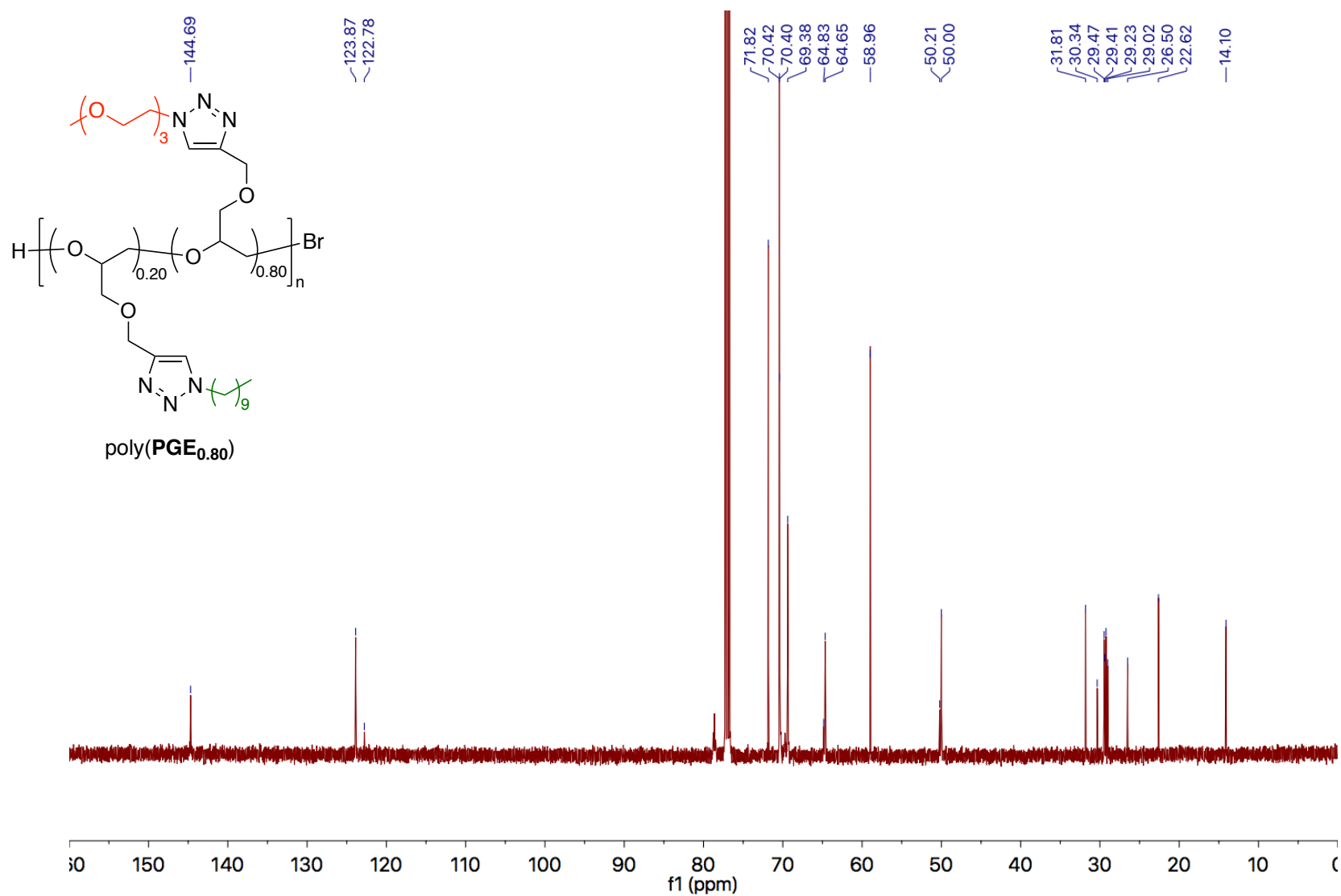


Figure A42. 125 MHz ¹³C NMR spectrum of poly(PGE_{0.80}) in CDCl₃.

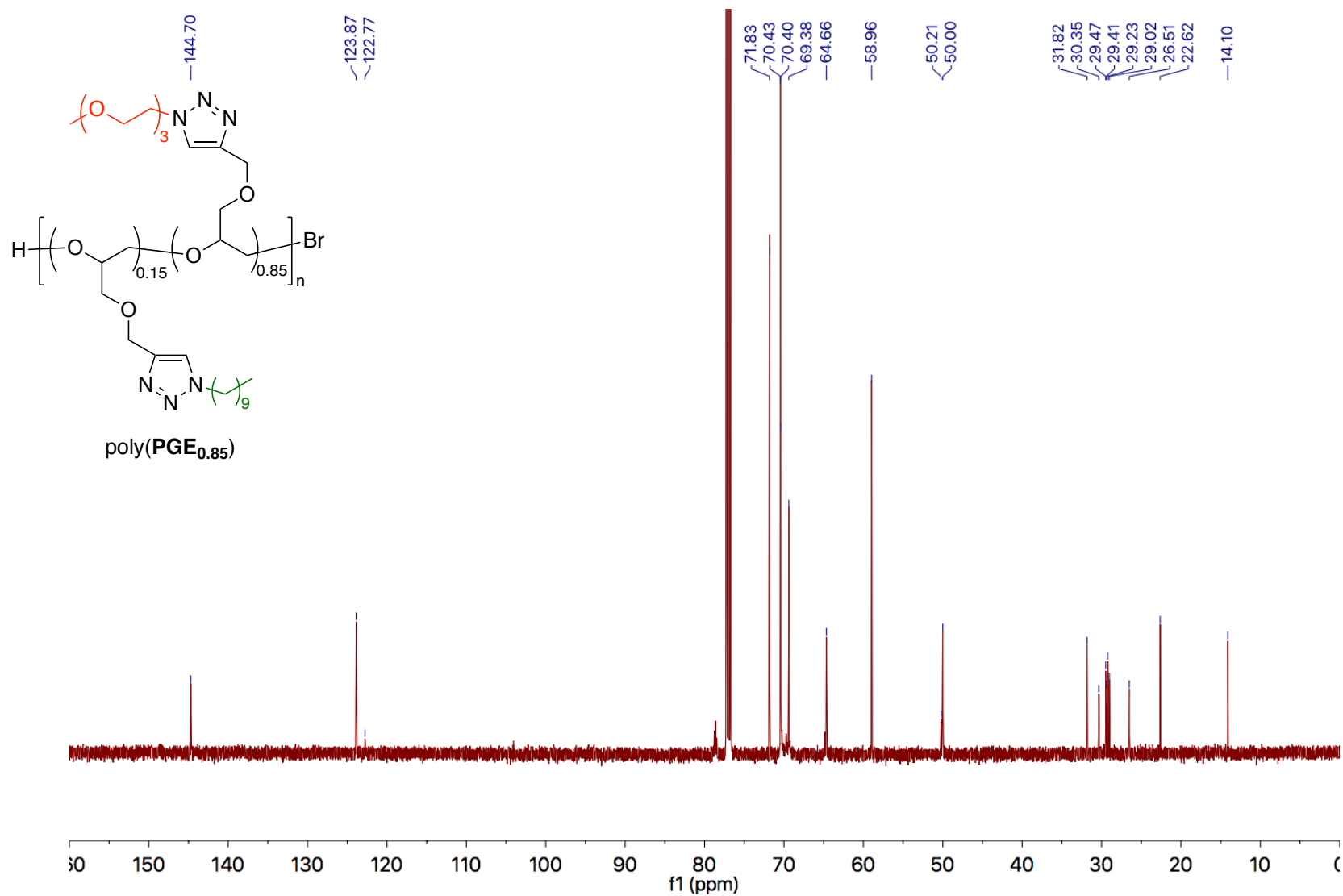


Figure A44. 125 MHz ¹³C NMR spectrum of poly(PGE_{0.85}) in CDCl₃.

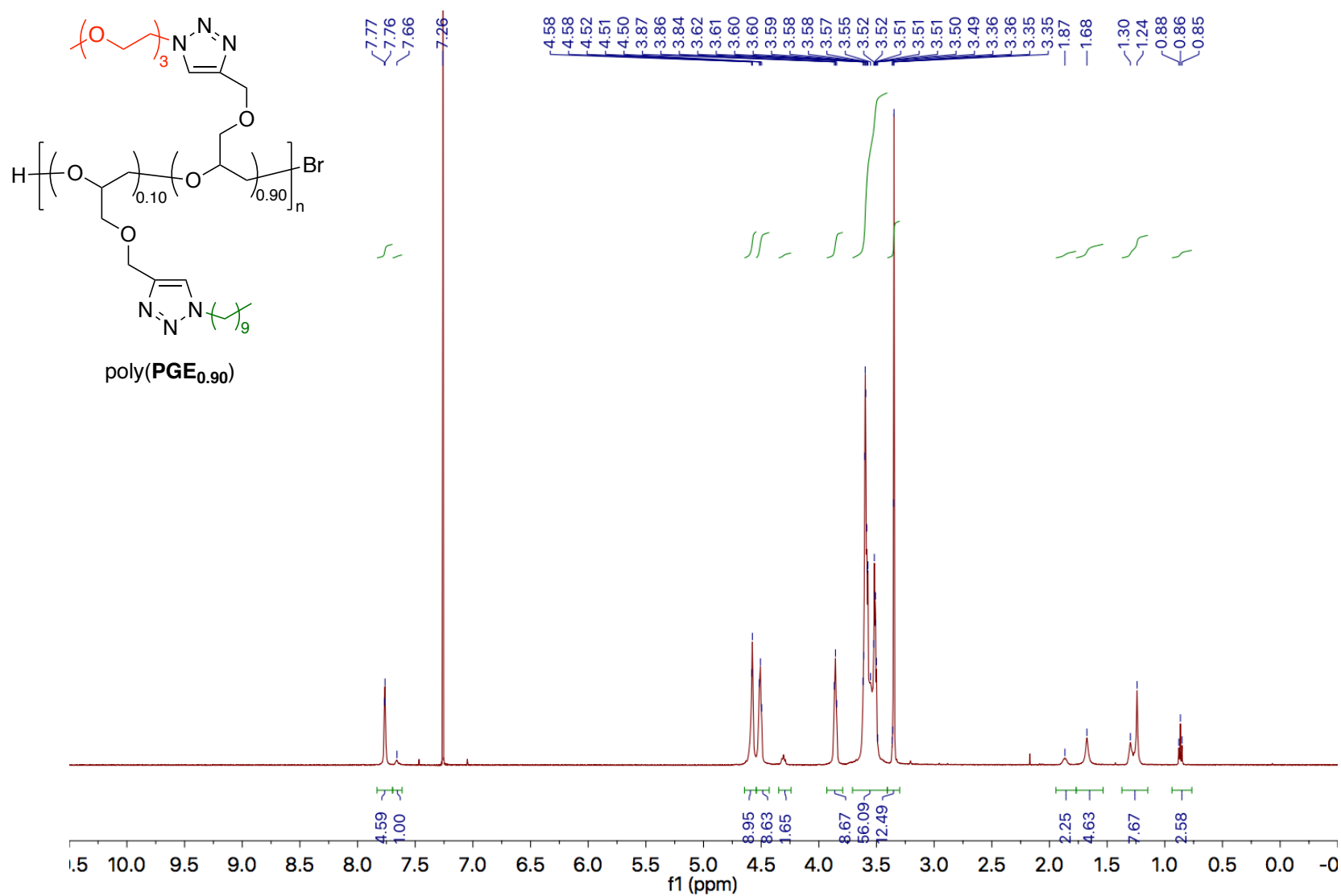


Figure A45. 500 MHz ¹H NMR spectrum of poly(PGE_{0.90}) in CDCl₃.

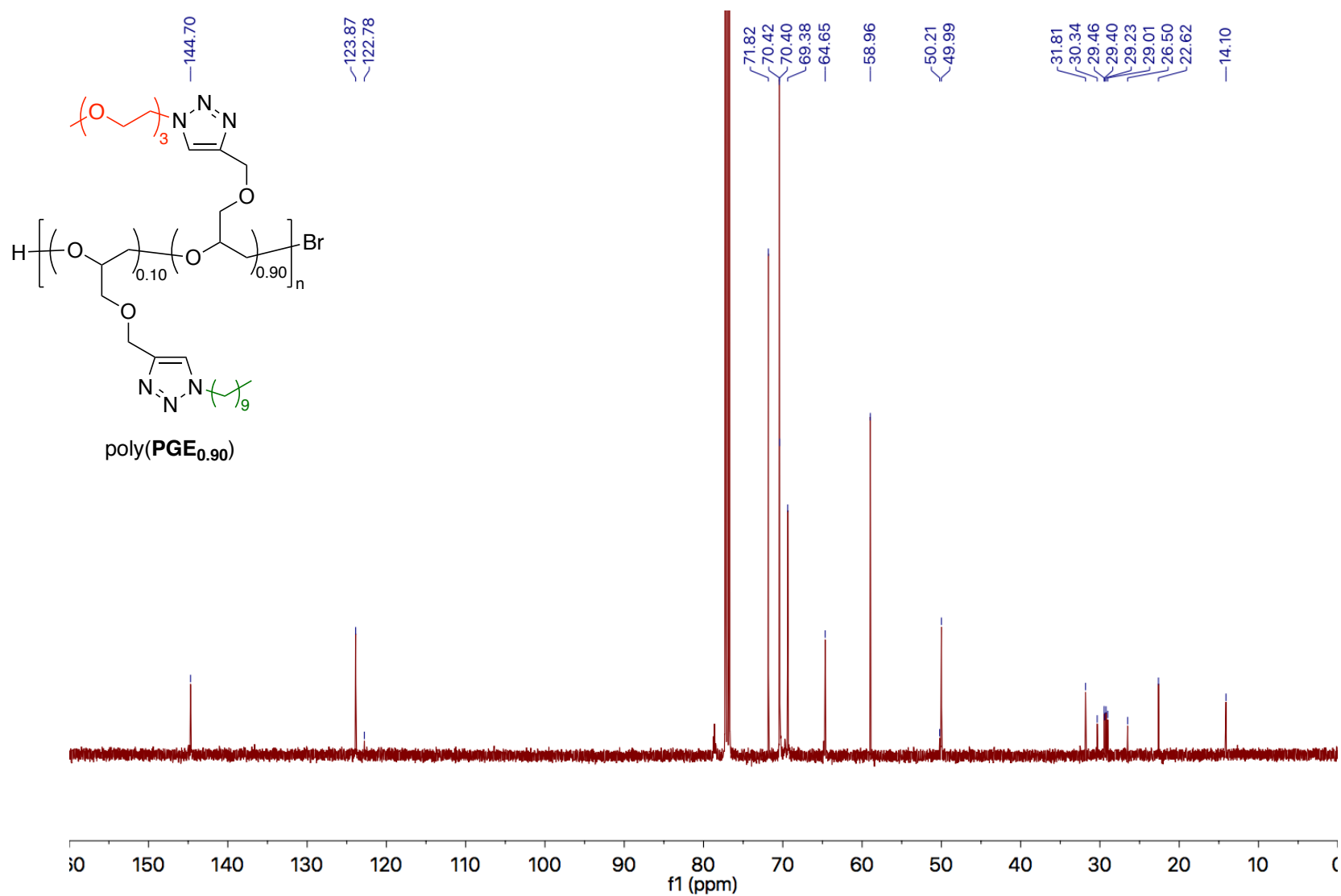


Figure A46. 125 MHz ¹³C NMR spectrum of poly(PGE_{0.90}) in CDCl₃

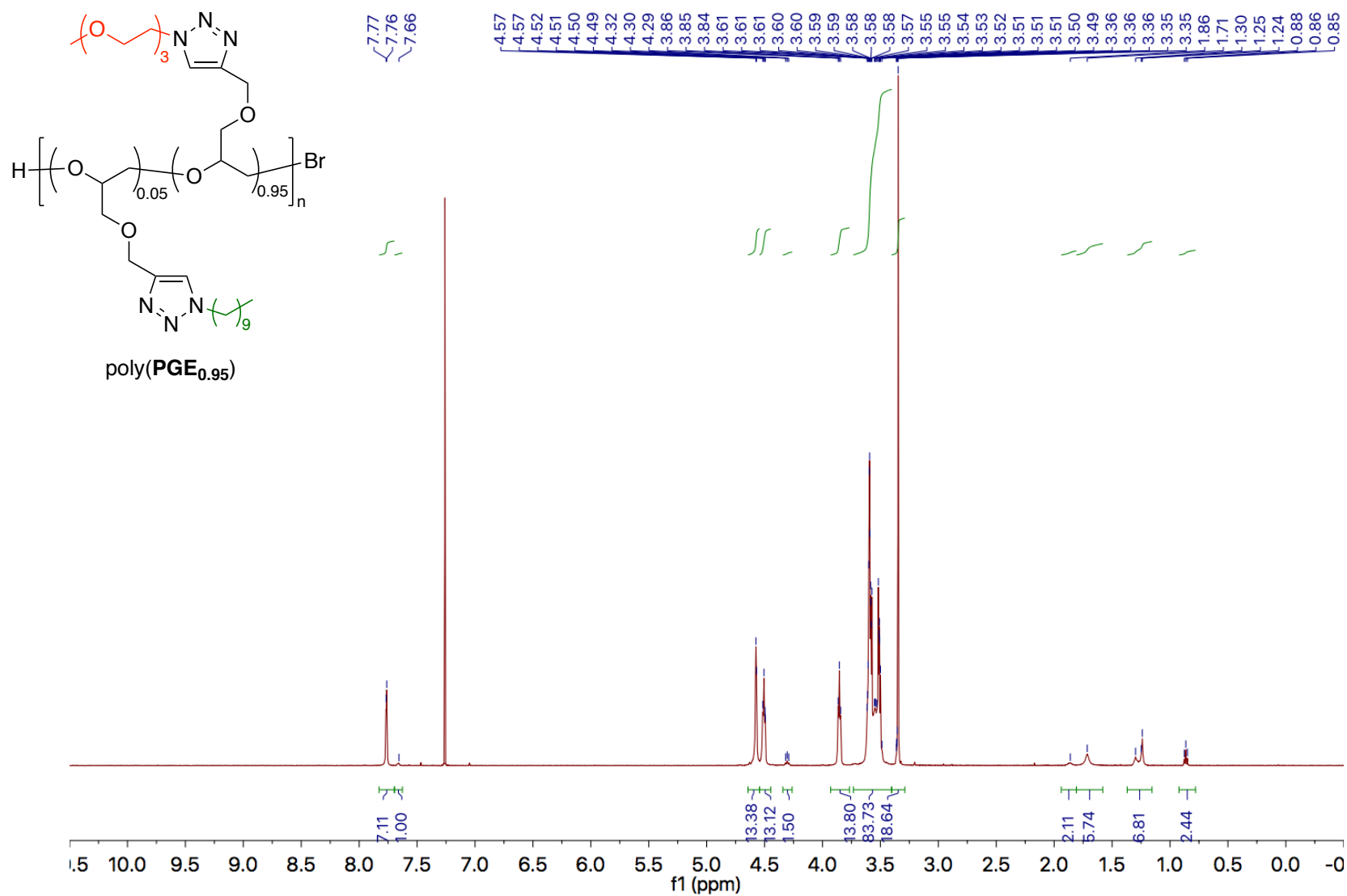


Figure A47. 500 MHz ^1H NMR spectrum of poly(PGE_{0.95}) in CDCl_3 .

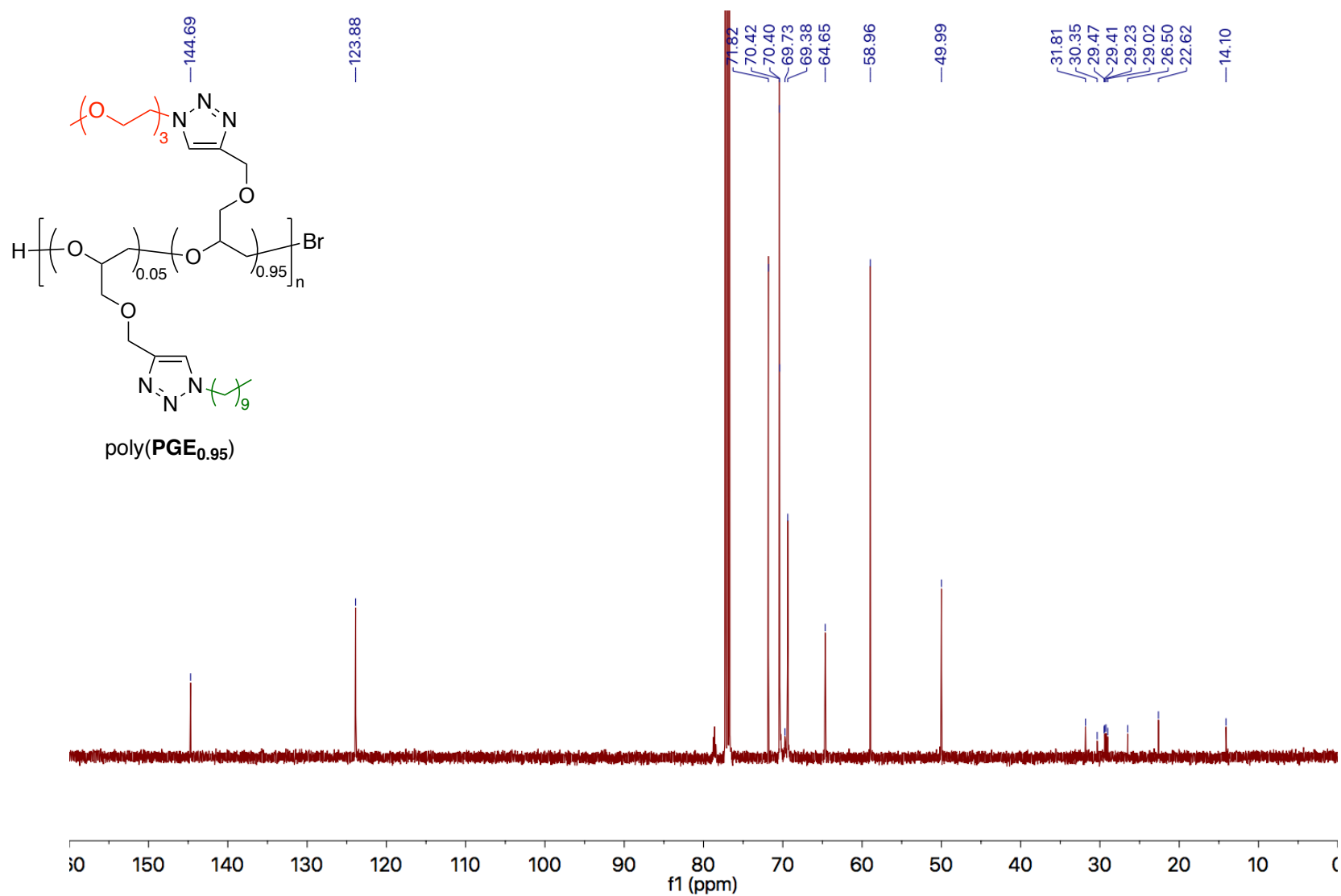


Figure A48. 125 MHz ¹³C NMR spectrum of poly(PGE_{0.95}) in CDCl₃.

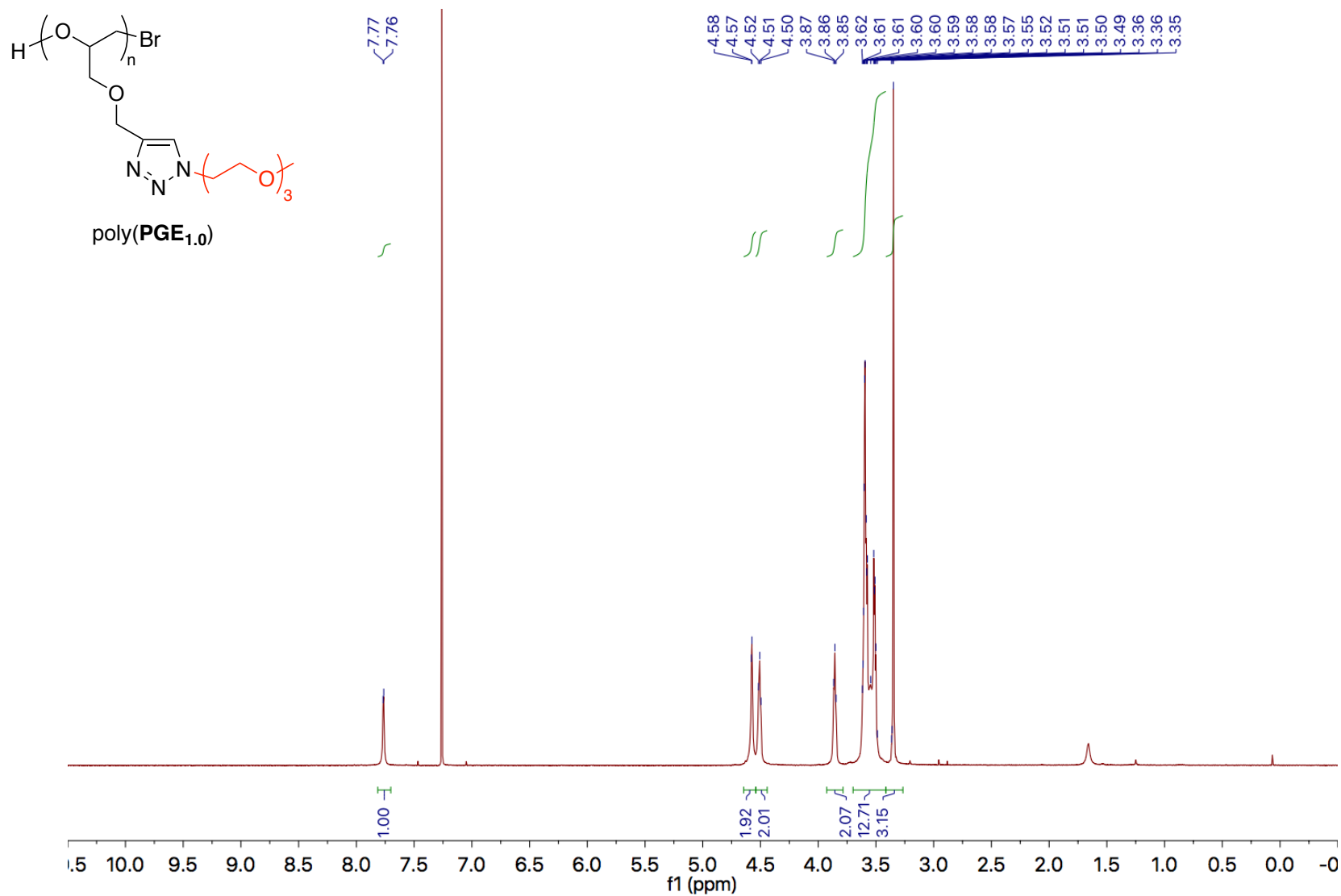


Figure A49. 500 MHz ¹H NMR spectrum of poly(PGE_{1.0}) in CDCl₃.

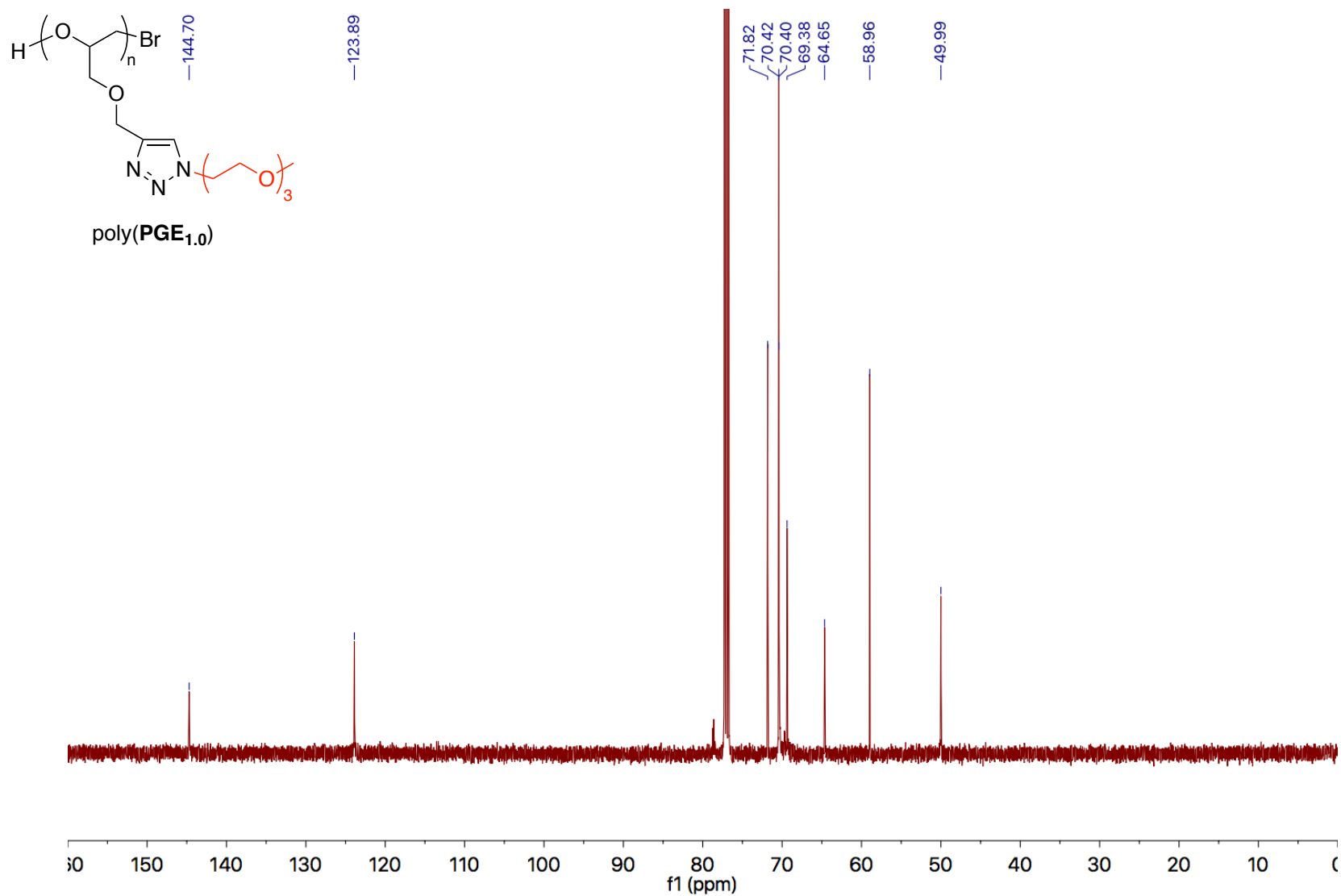


Figure A50. 125 MHz ¹³C NMR spectrum of poly(PGE_{1.0}) in CDCl₃.

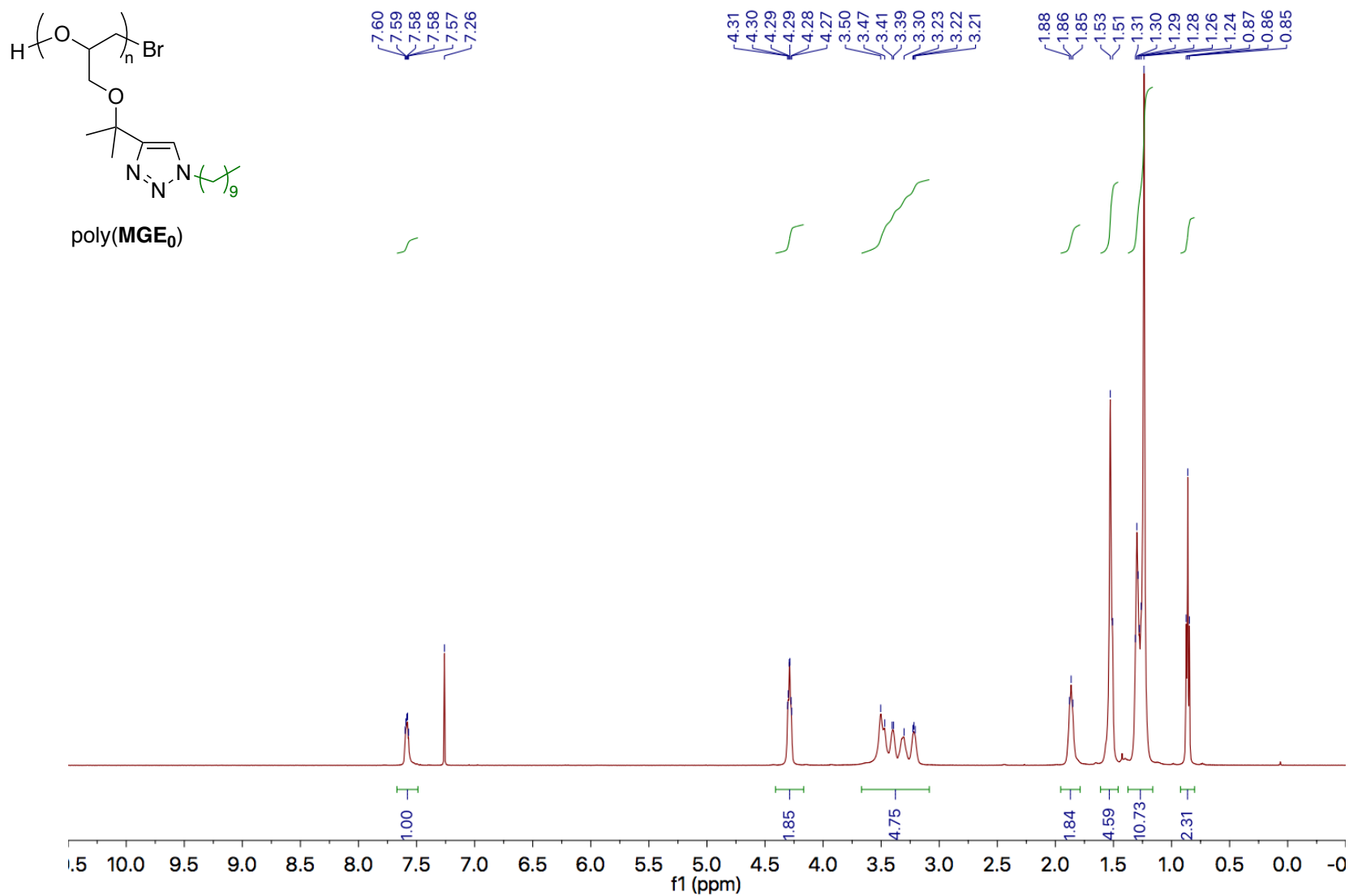


Figure A51. 500 MHz ¹H NMR spectrum of poly(MGE₀) in CDCl₃.

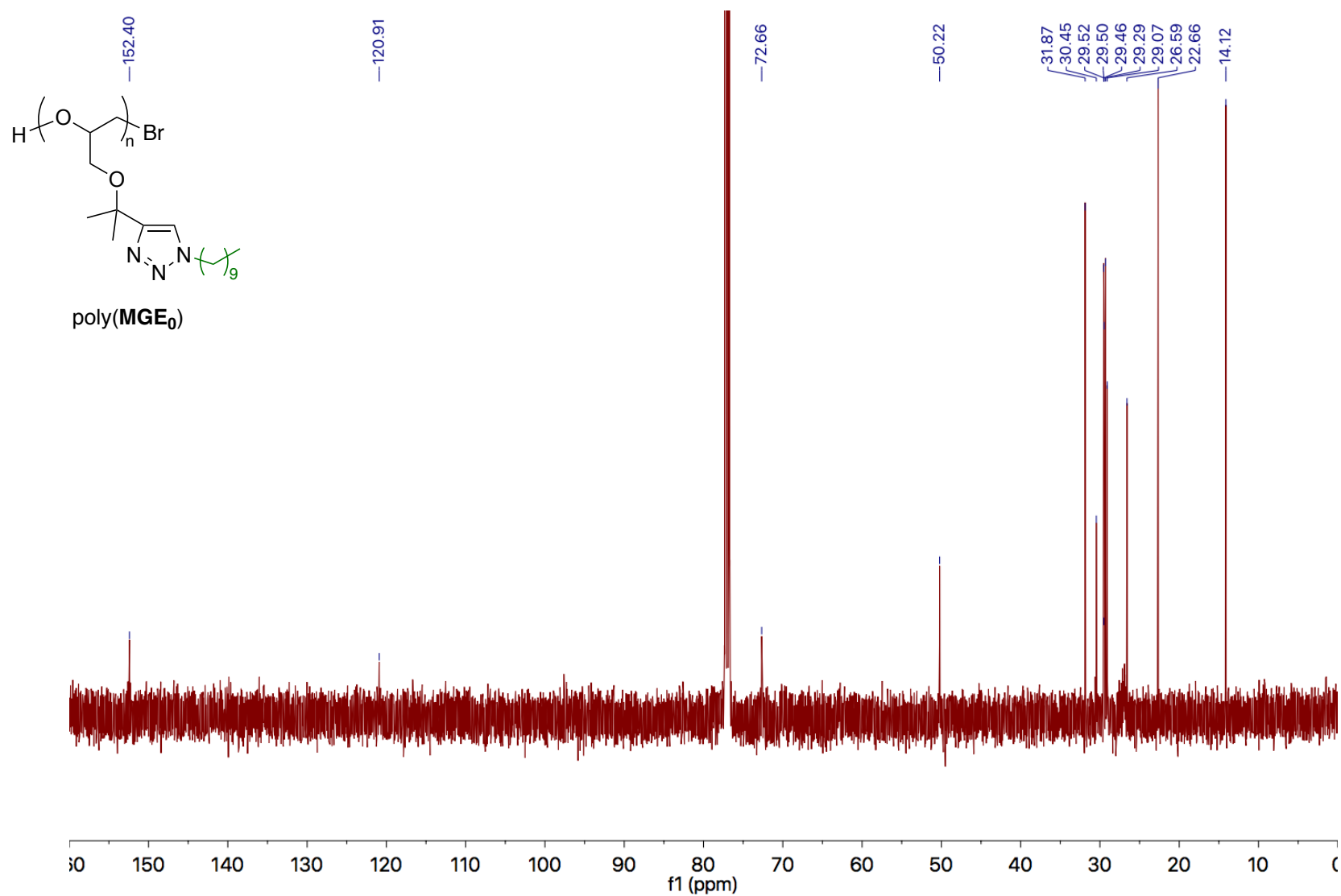


Figure A52. 125 MHz ¹³C NMR spectrum of poly(MGE₀) in CDCl₃.

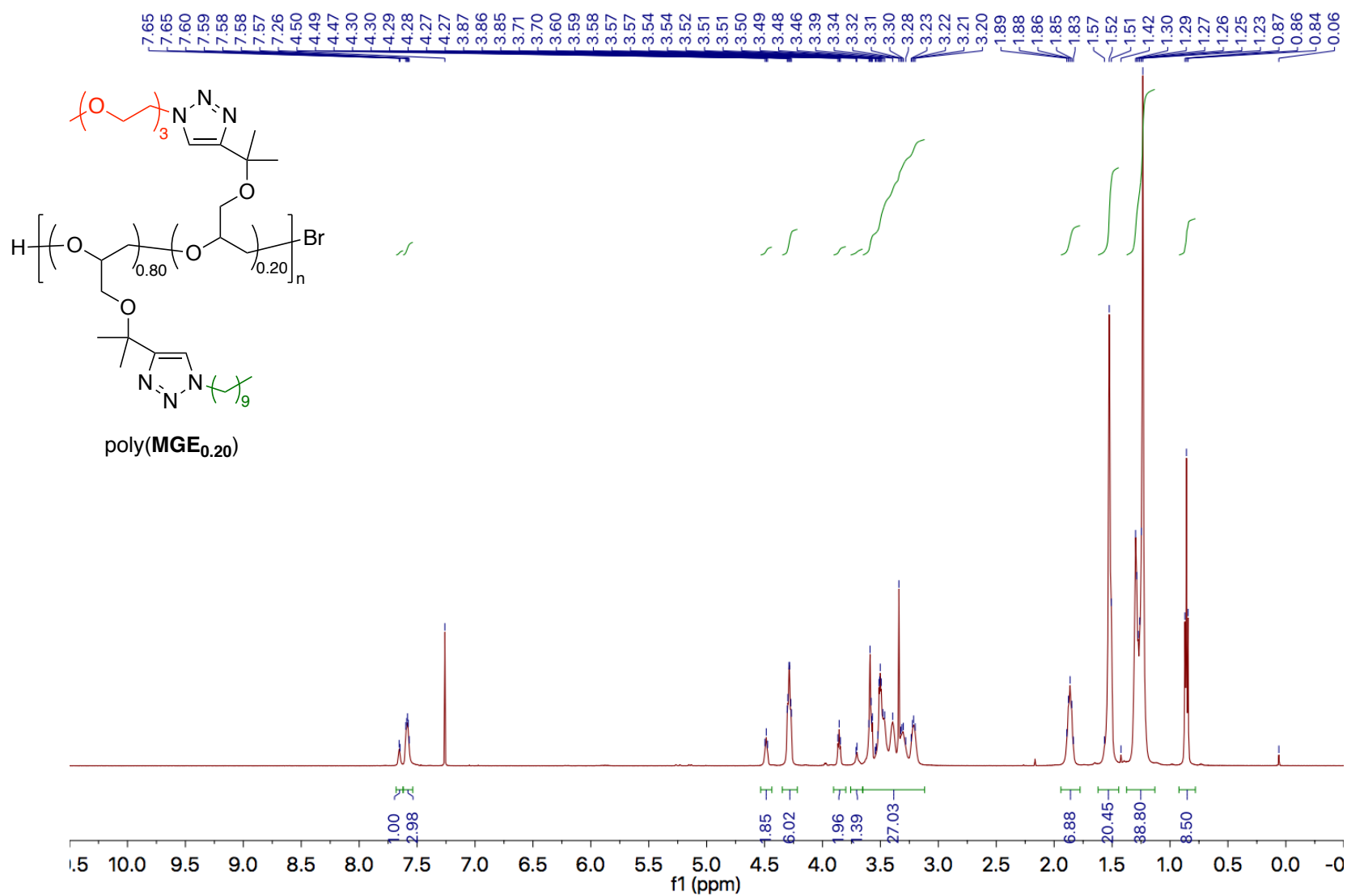


Figure A53. 500 MHz ¹H NMR spectrum of poly(MGE_{0.20}) in CDCl₃.

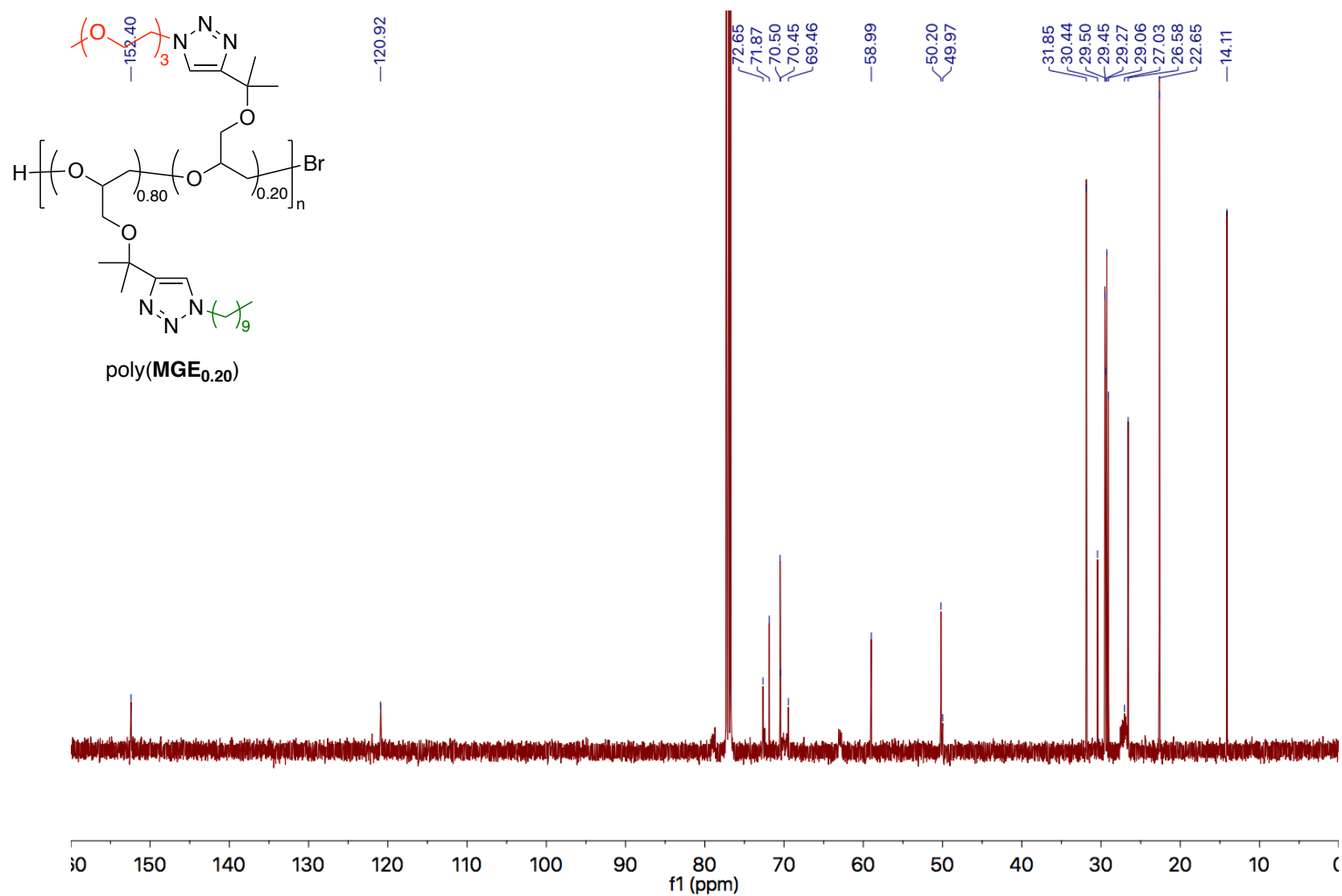


Figure A54. 125 MHz ¹³C NMR spectrum of poly(MGE_{0.20}) in CDCl₃.

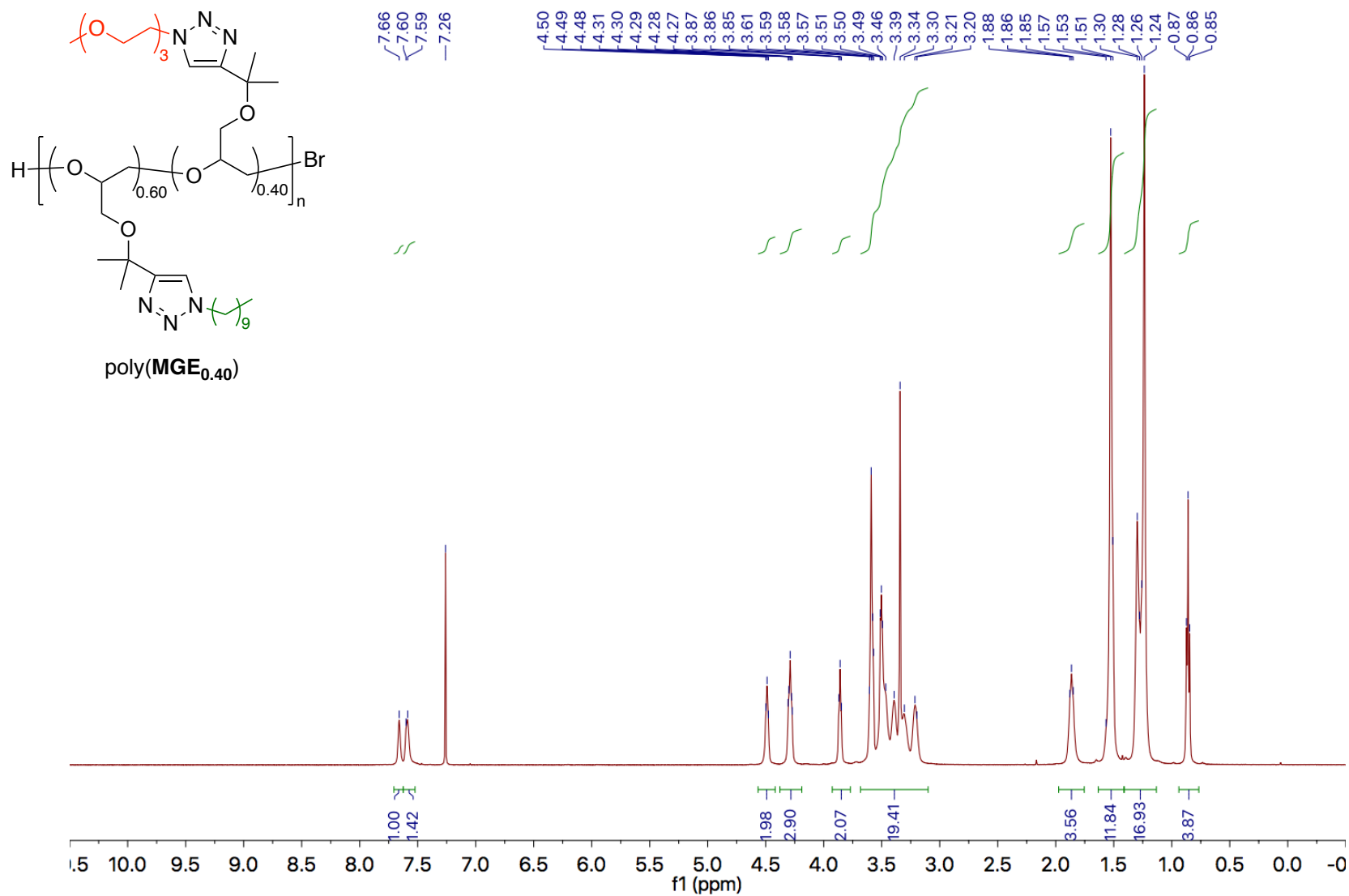


Figure A55. 500 MHz ¹H NMR spectrum of poly(MGE_{0.40}) in CDCl₃.

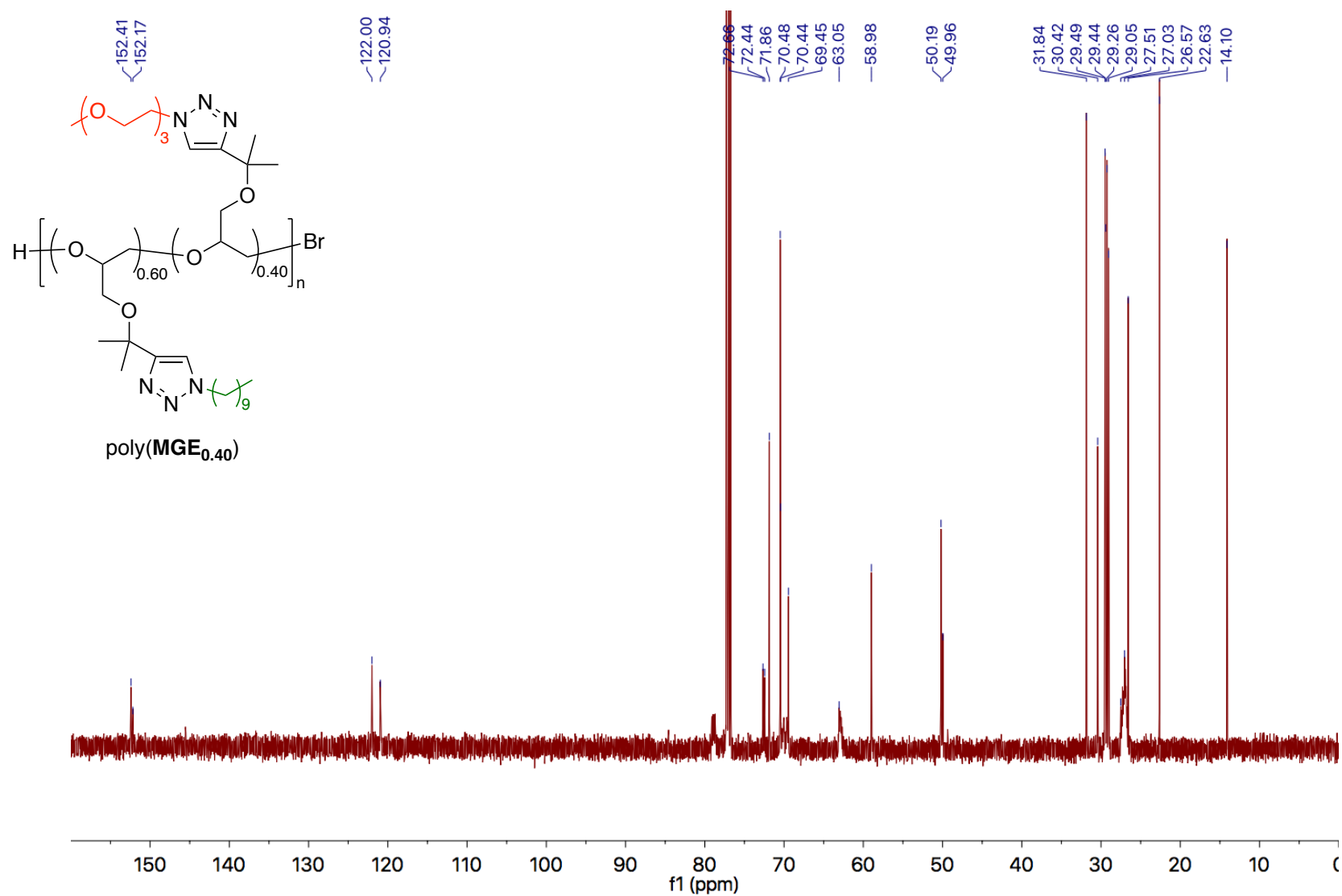


Figure A56. 125 MHz ^{13}C NMR spectrum of poly(MGE_{0.40}) in CDCl_3 .

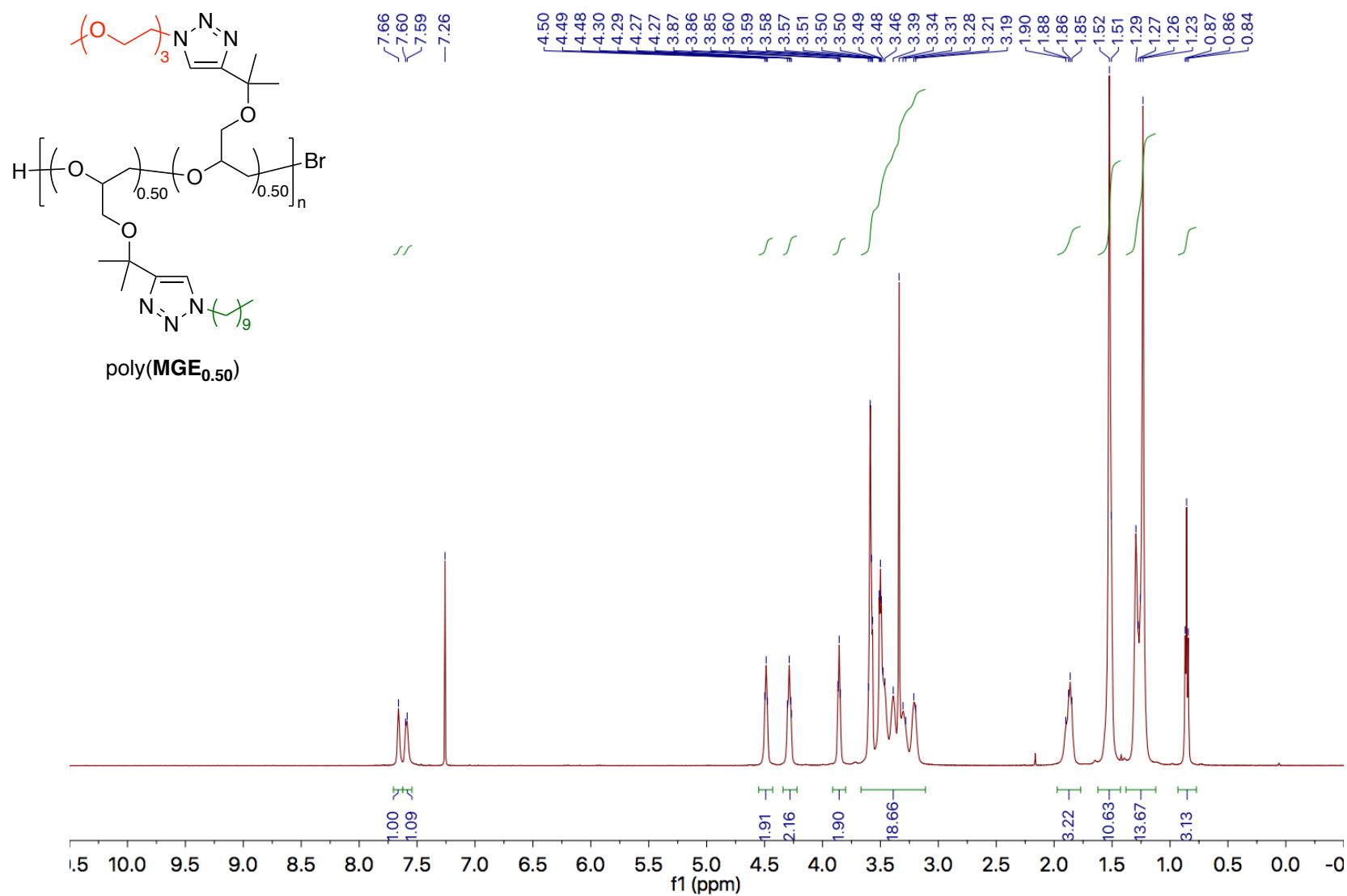


Figure A57. 500 MHz ¹H NMR spectrum of poly(MGE_{0.50}) in CDCl₃.

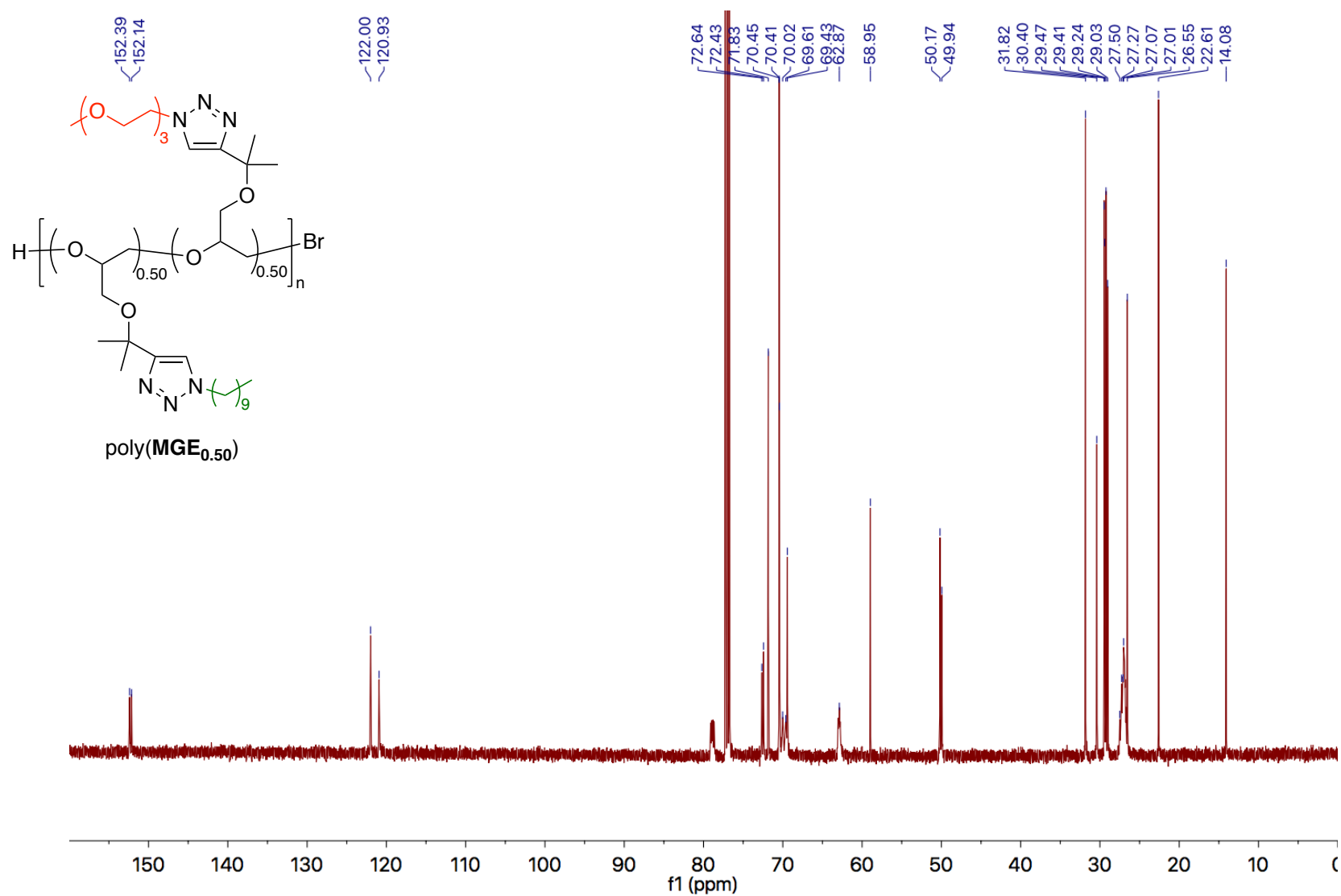


Figure A58. 125 MHz ^{13}C NMR spectrum of poly(MGE_{0.50}) in CDCl_3

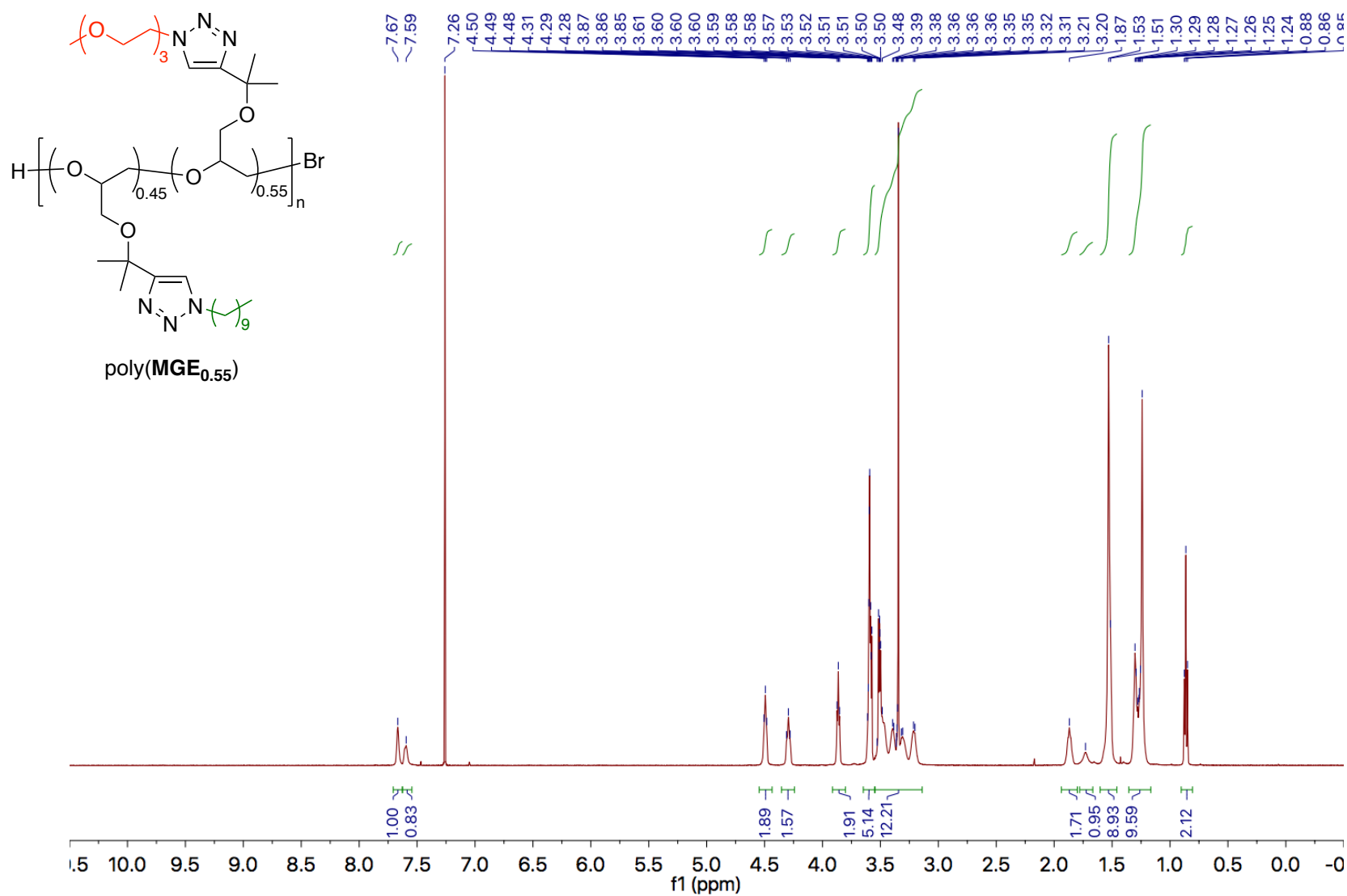


Figure A59. 500 MHz ¹H NMR spectrum of poly(MGE_{0.55}) in CDCl₃.

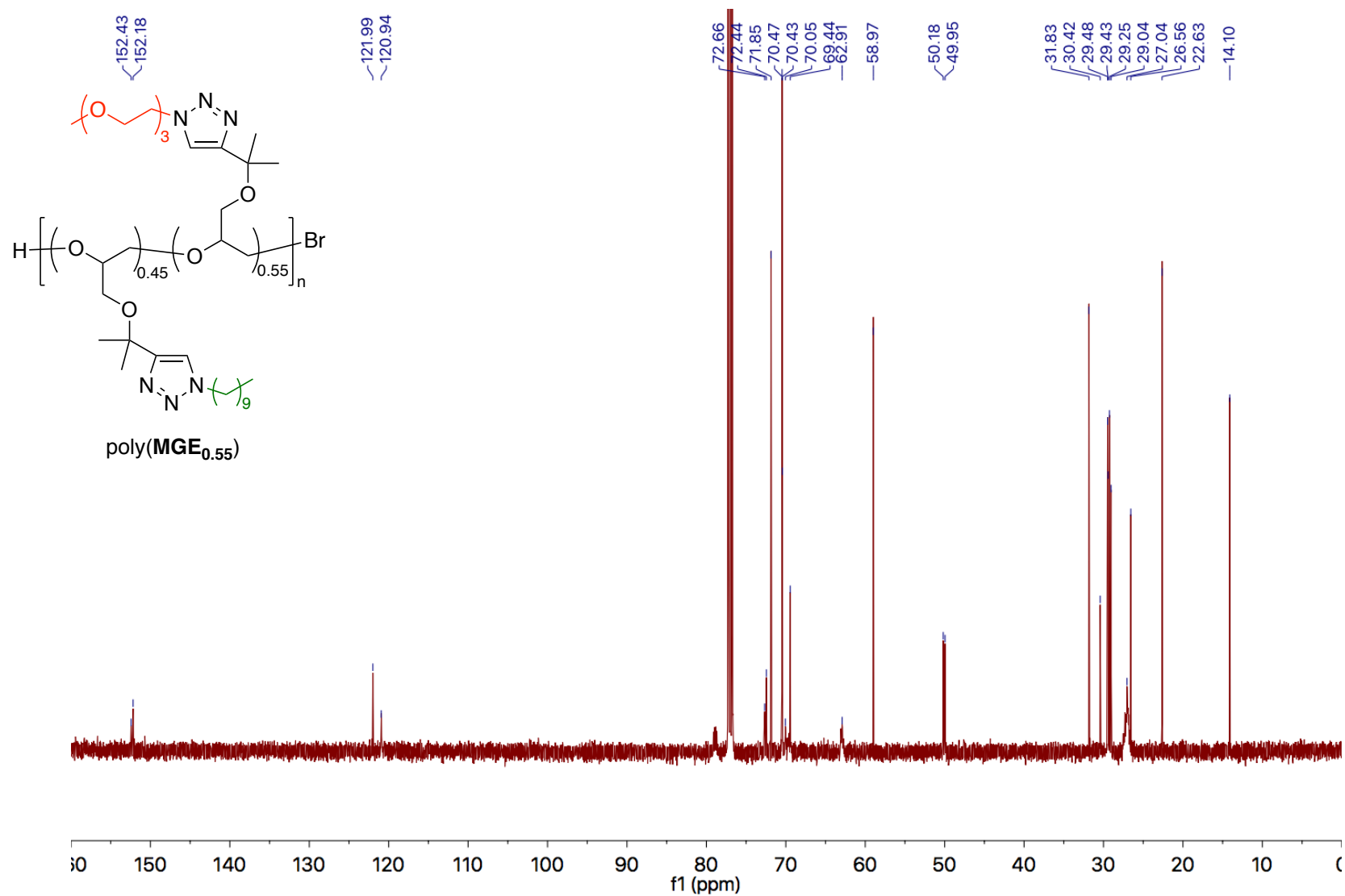


Figure A60. 125 MHz ^{13}C NMR spectrum of poly(MGE_{0.55}) in CDCl_3 .

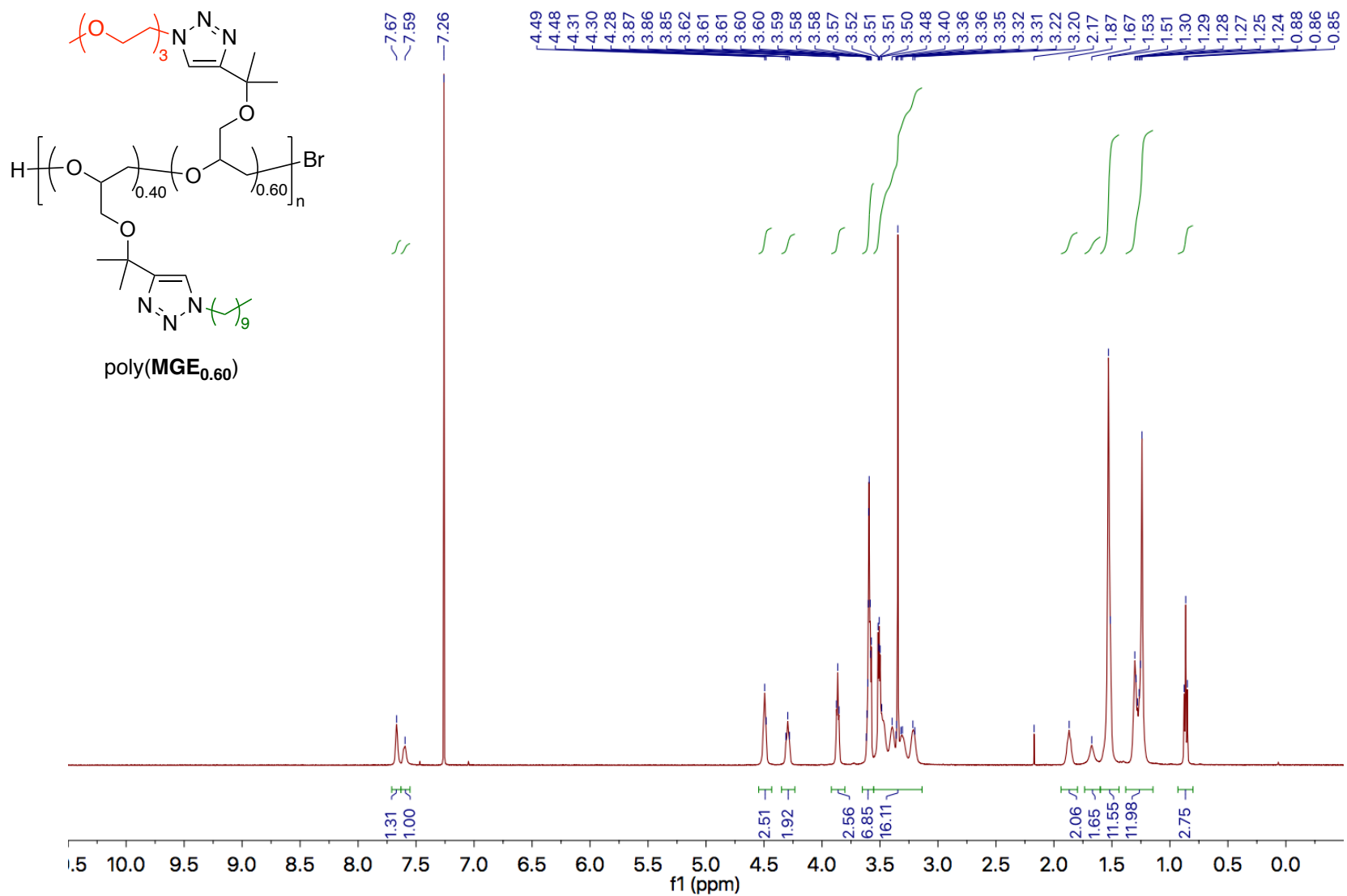


Figure A61. 500 MHz ¹H NMR spectrum of poly(MGE_{0.60}) in CDCl₃.

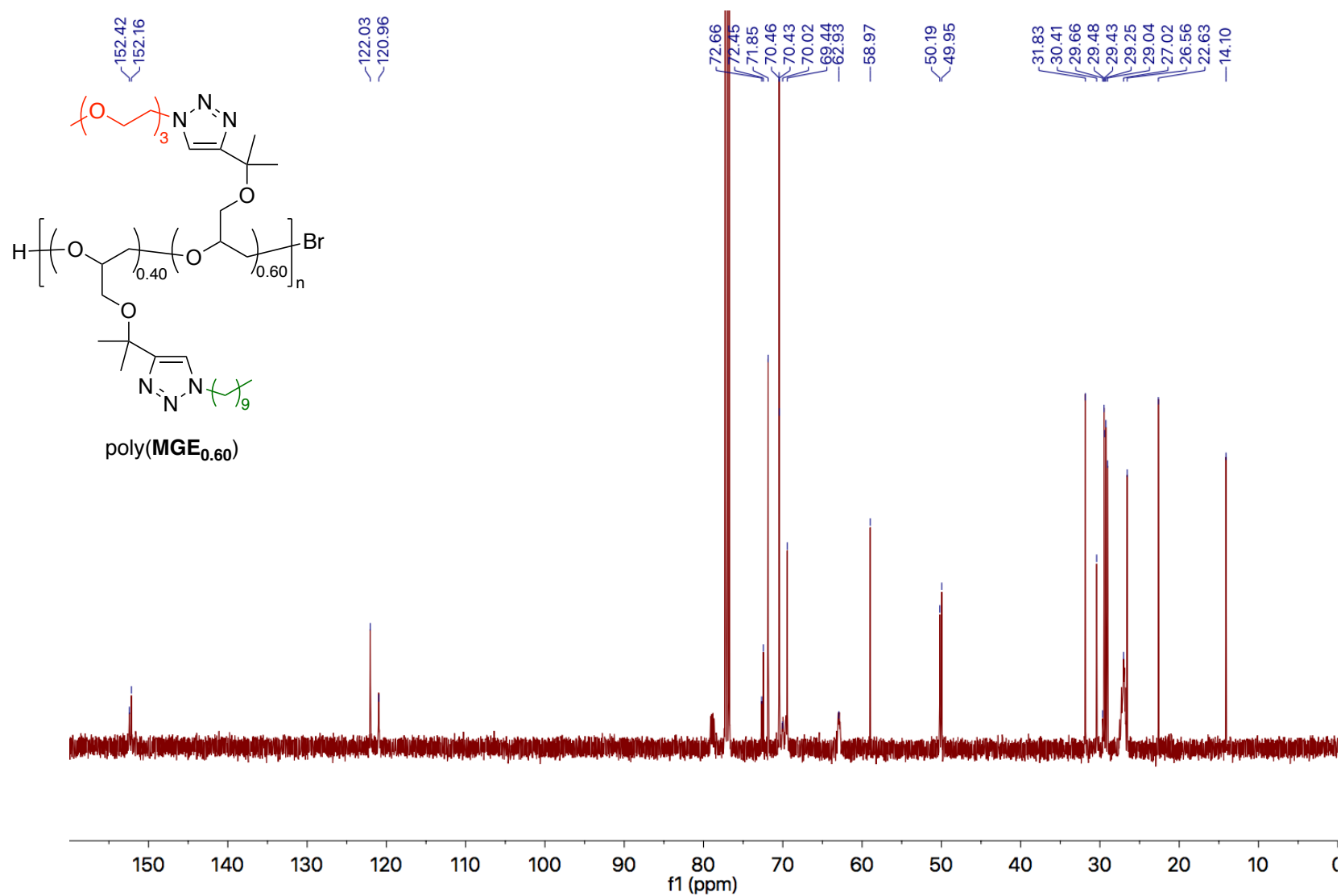


Figure A62. 125 MHz ^{13}C NMR spectrum of poly(MGE_{0.60}) in CDCl_3 .

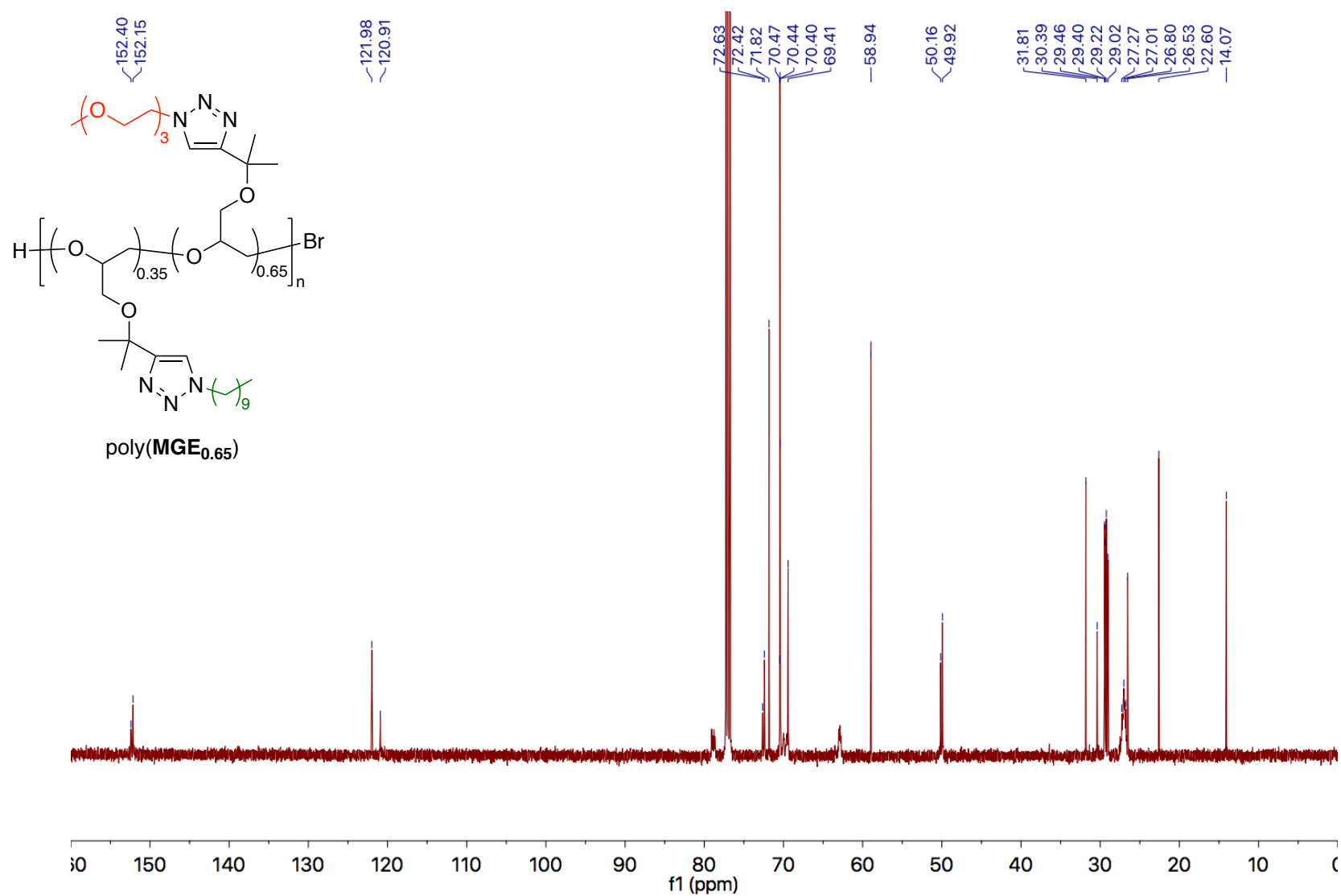


Figure A64. 125 MHz ¹³C NMR spectrum of poly(MGE_{0.65}) in CDCl₃.

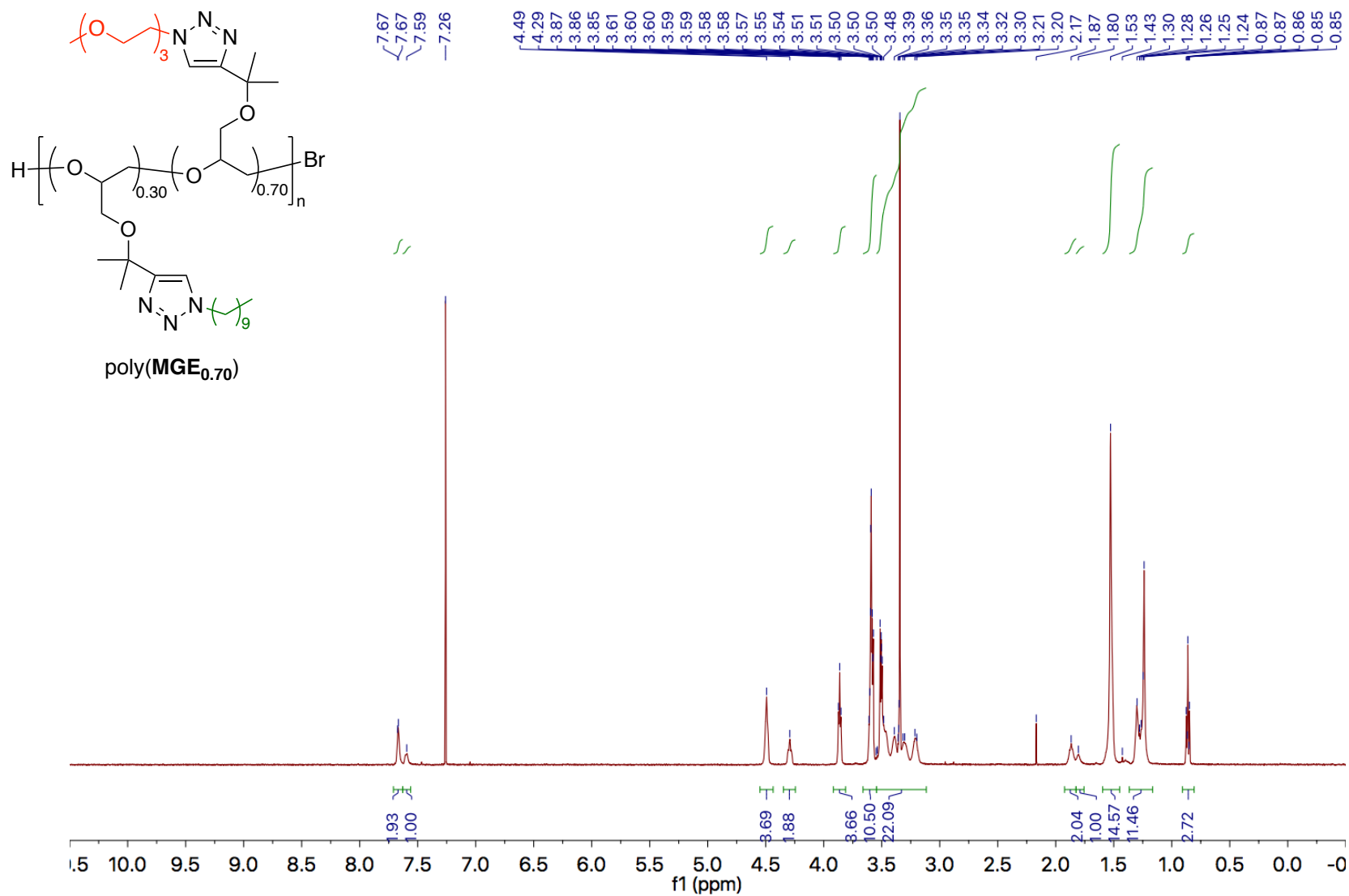


Figure A65. 500 MHz ¹H NMR spectrum of poly(MGE_{0.70}) in CDCl₃.

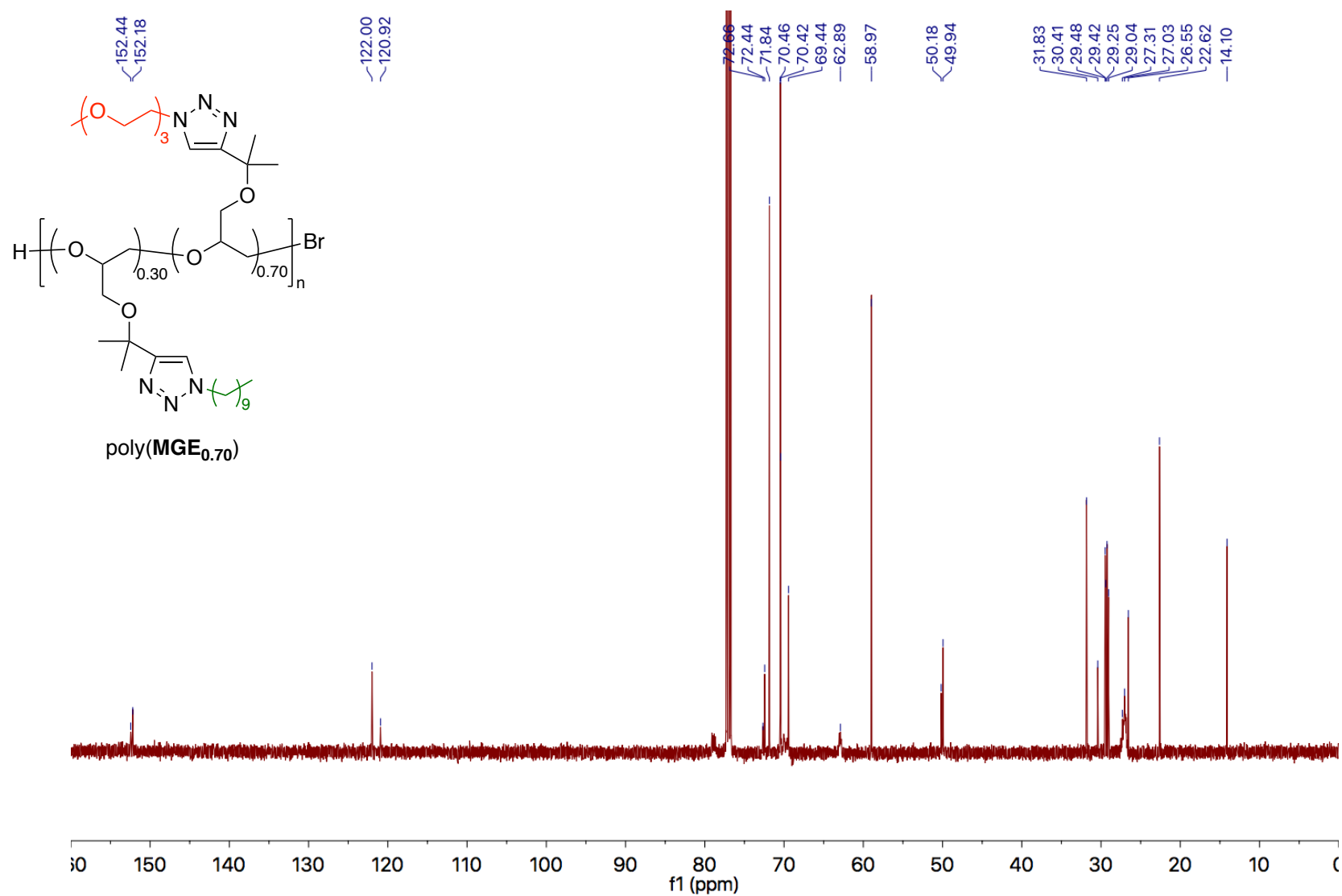


Figure A66. 125 MHz ¹³C NMR spectrum of poly(MGE_{0.70}) in CDCl₃.

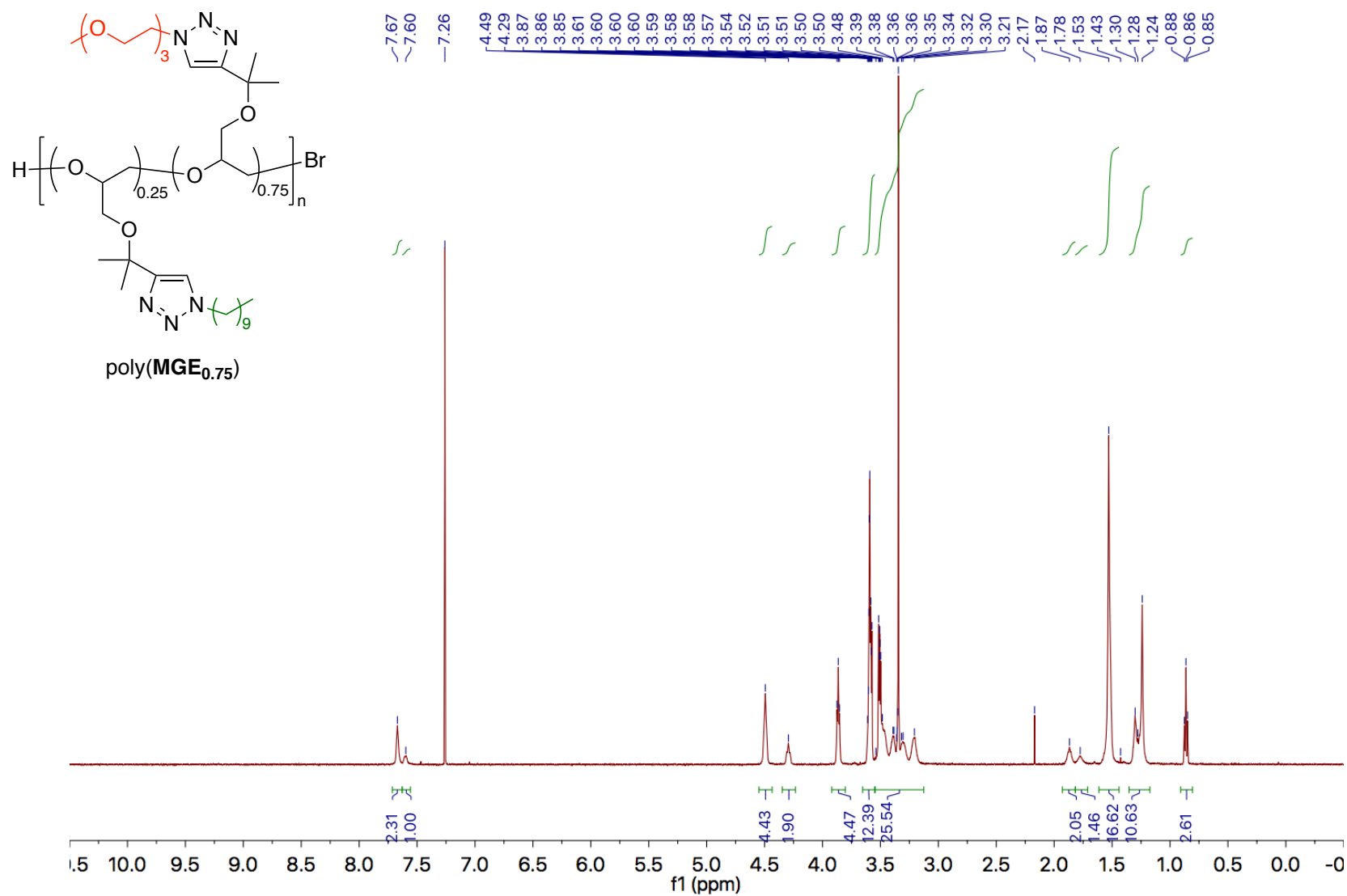


Figure A67. 500 MHz ¹H NMR spectrum of poly(MGE_{0.75}) in CDCl₃.

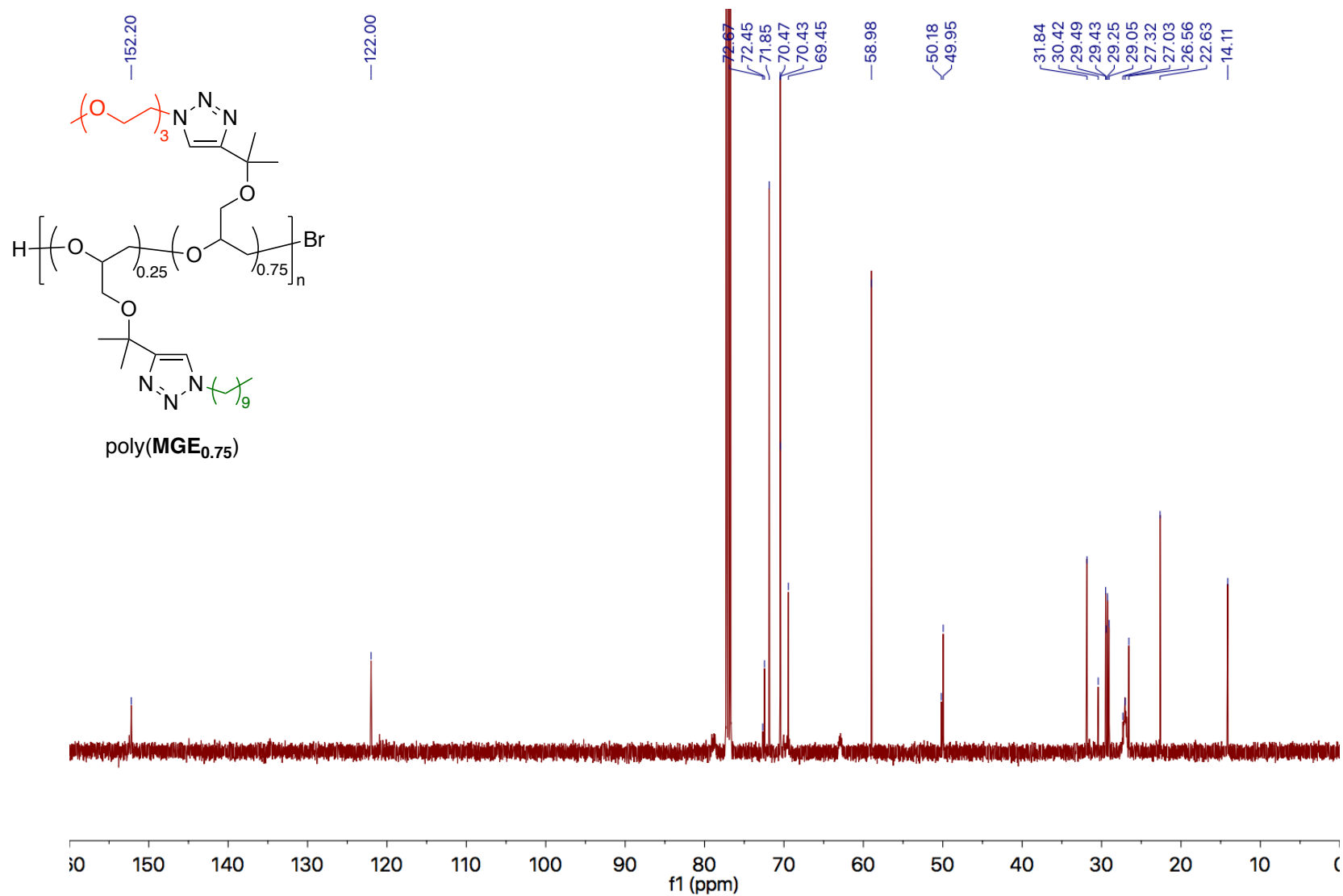


Figure A68. 125 MHz ¹³C NMR spectrum of poly(MGE_{0.75}) in CDCl₃.

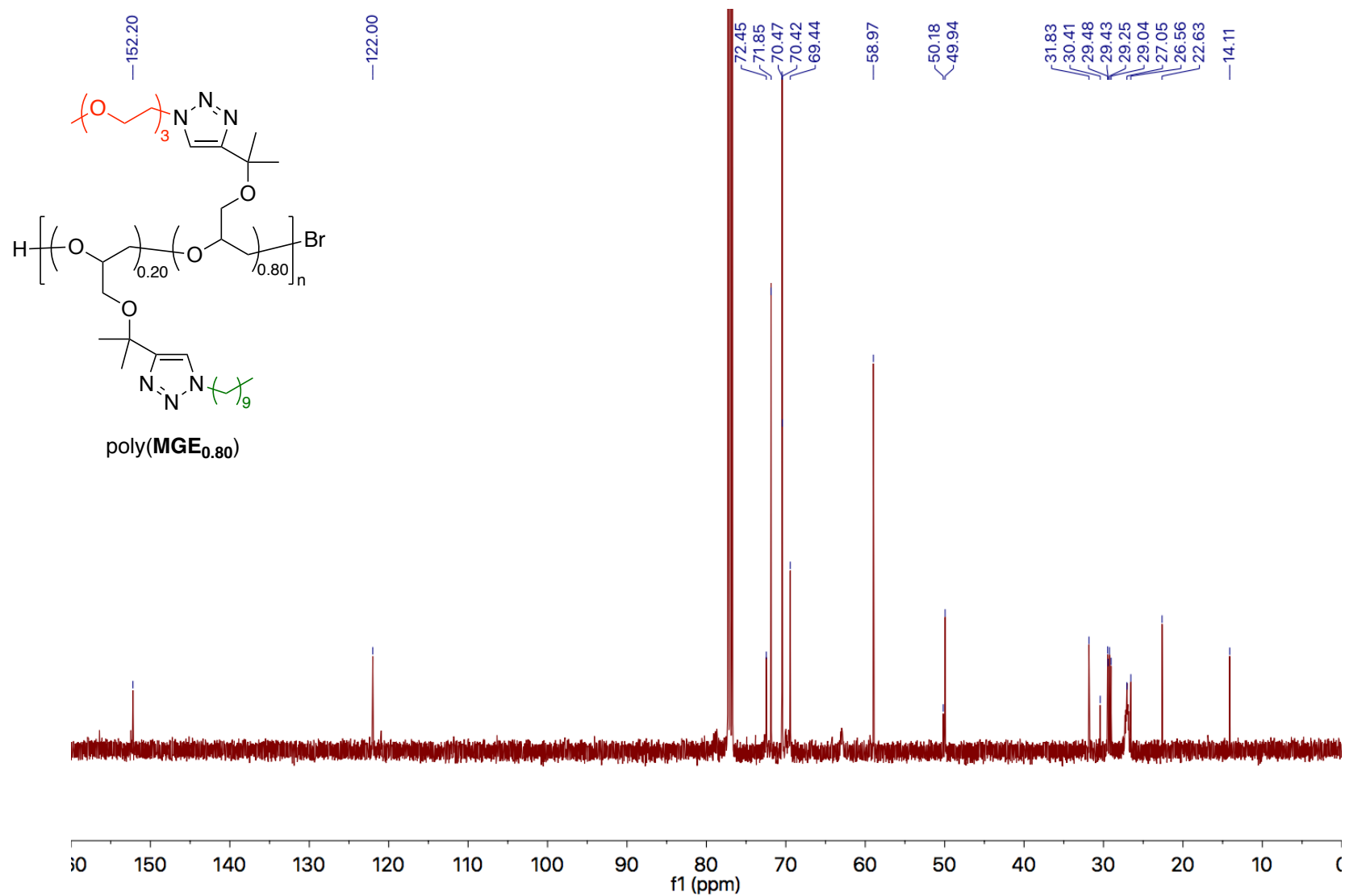


Figure A70. 125 MHz ^{13}C NMR spectrum of poly(MGE_{0.80}) in CDCl_3 .

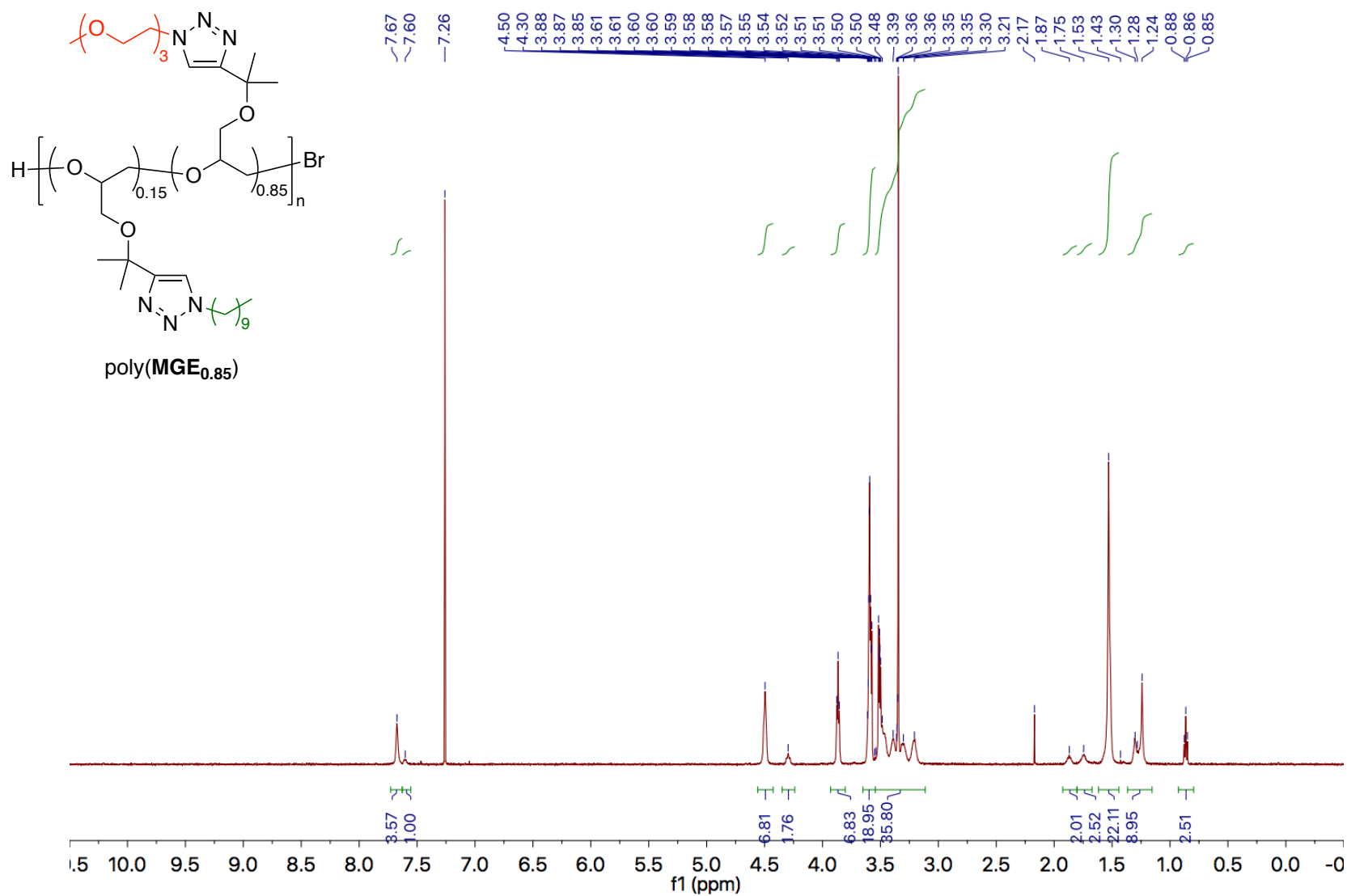


Figure A71. 500 MHz ¹H NMR spectrum of poly(MGE_{0.85}) in CDCl₃.

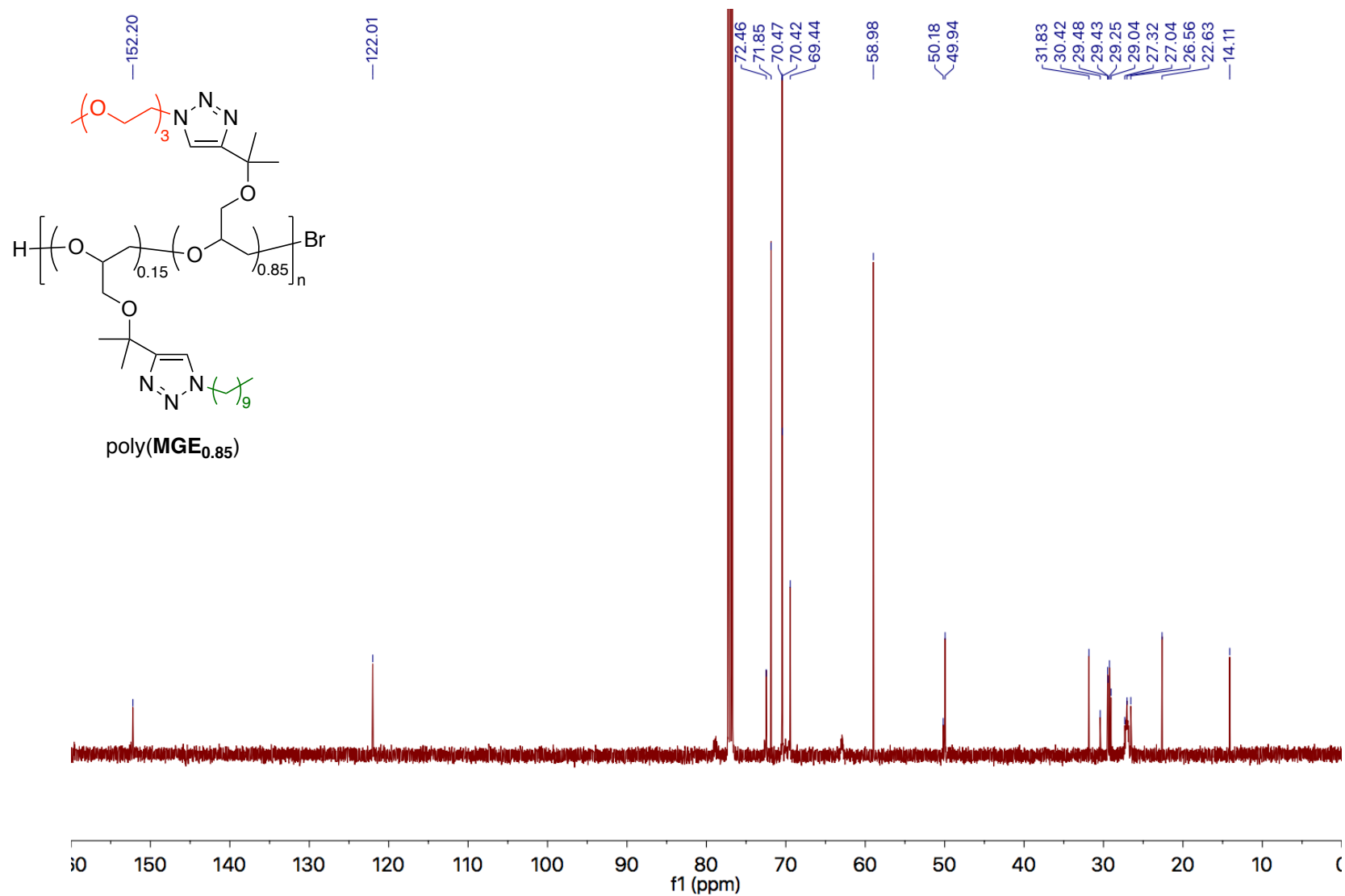


Figure A72. 125 MHz ^{13}C NMR spectrum of poly(MGE_{0.85}) in CDCl_3 .

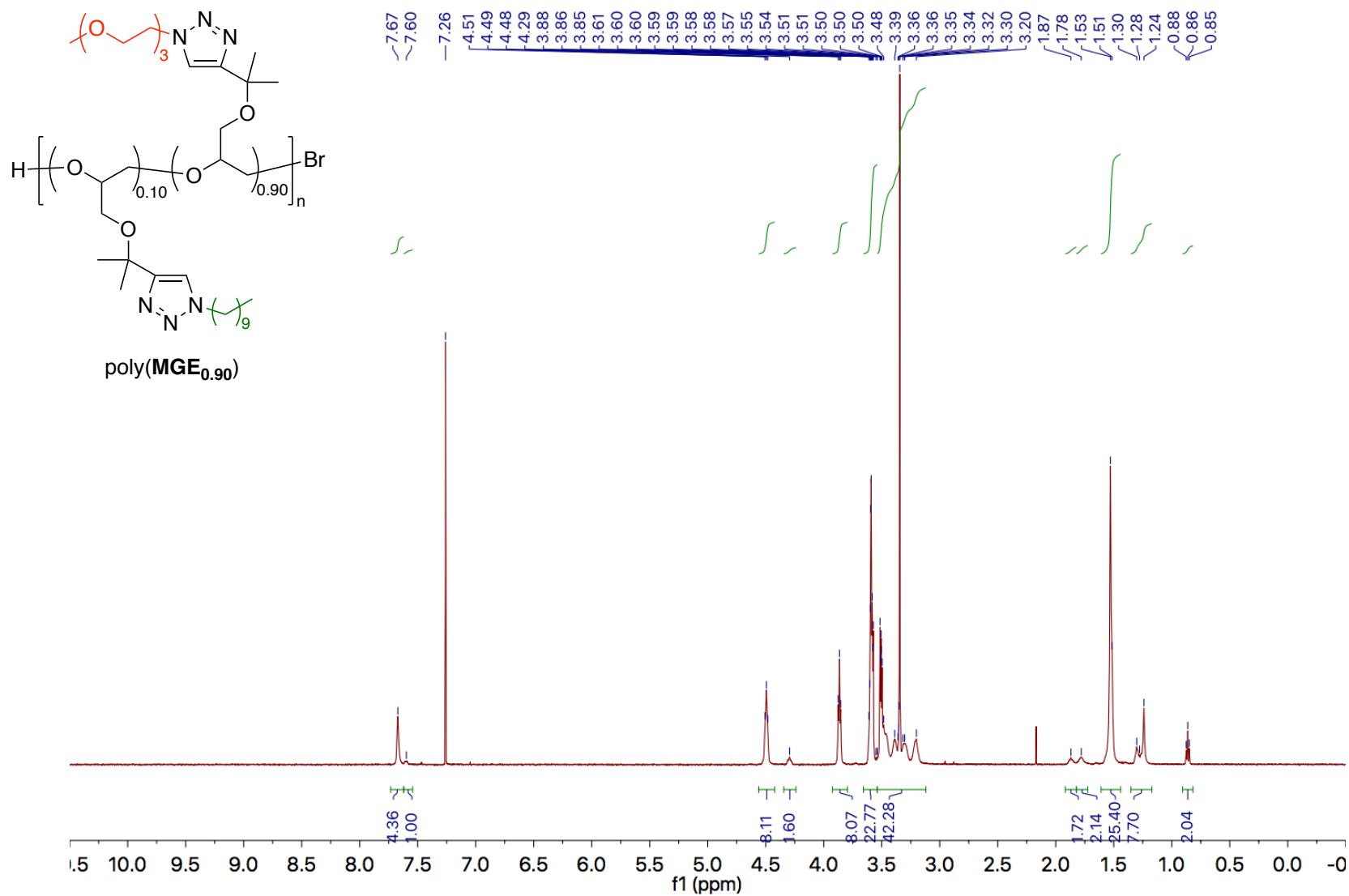


Figure A73. 500 MHz ¹H NMR spectrum of poly(MGE_{0.90}) in CDCl₃.

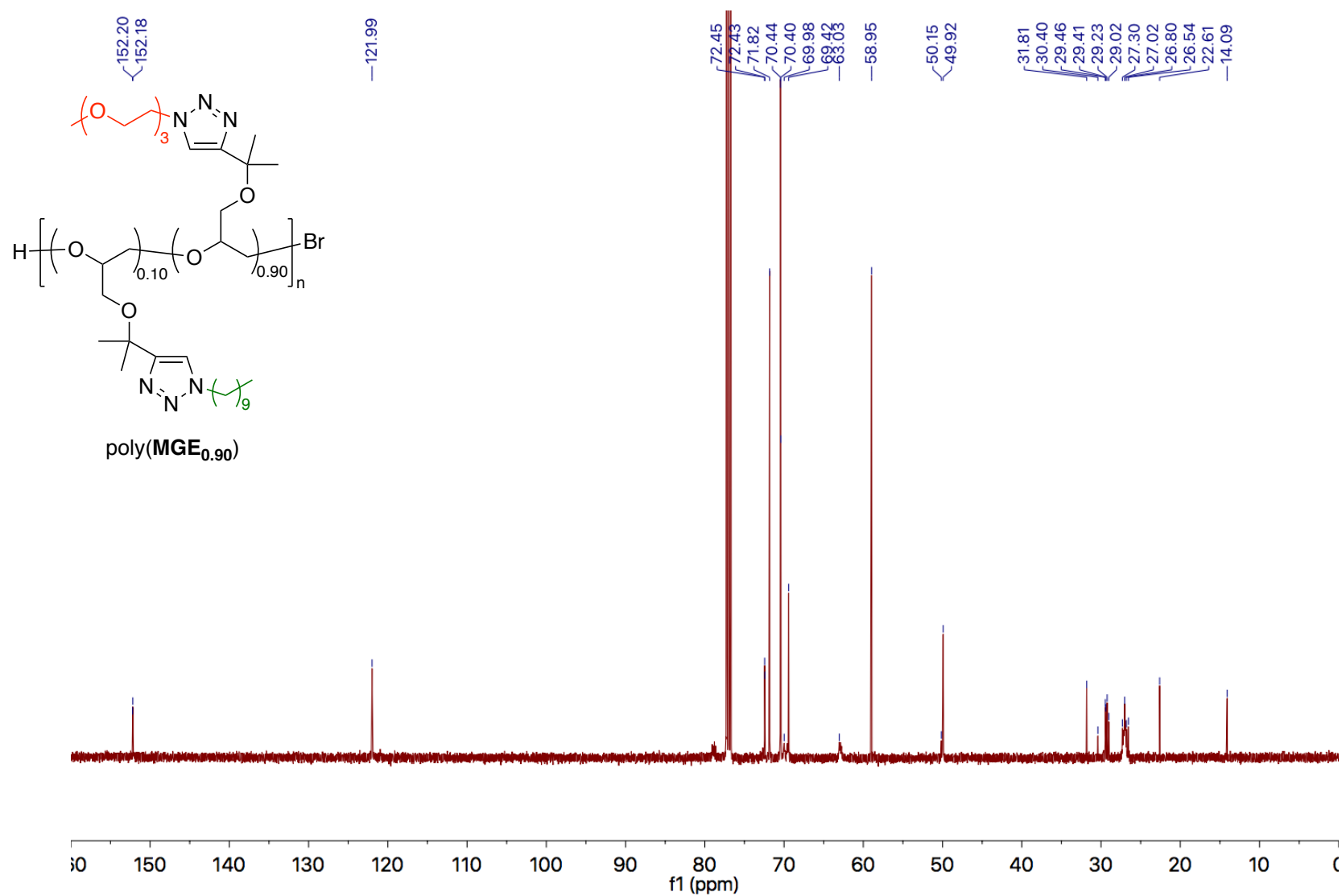


Figure A74. 125 MHz ¹³C NMR spectrum of poly(MGE_{0.90}) in CDCl₃.

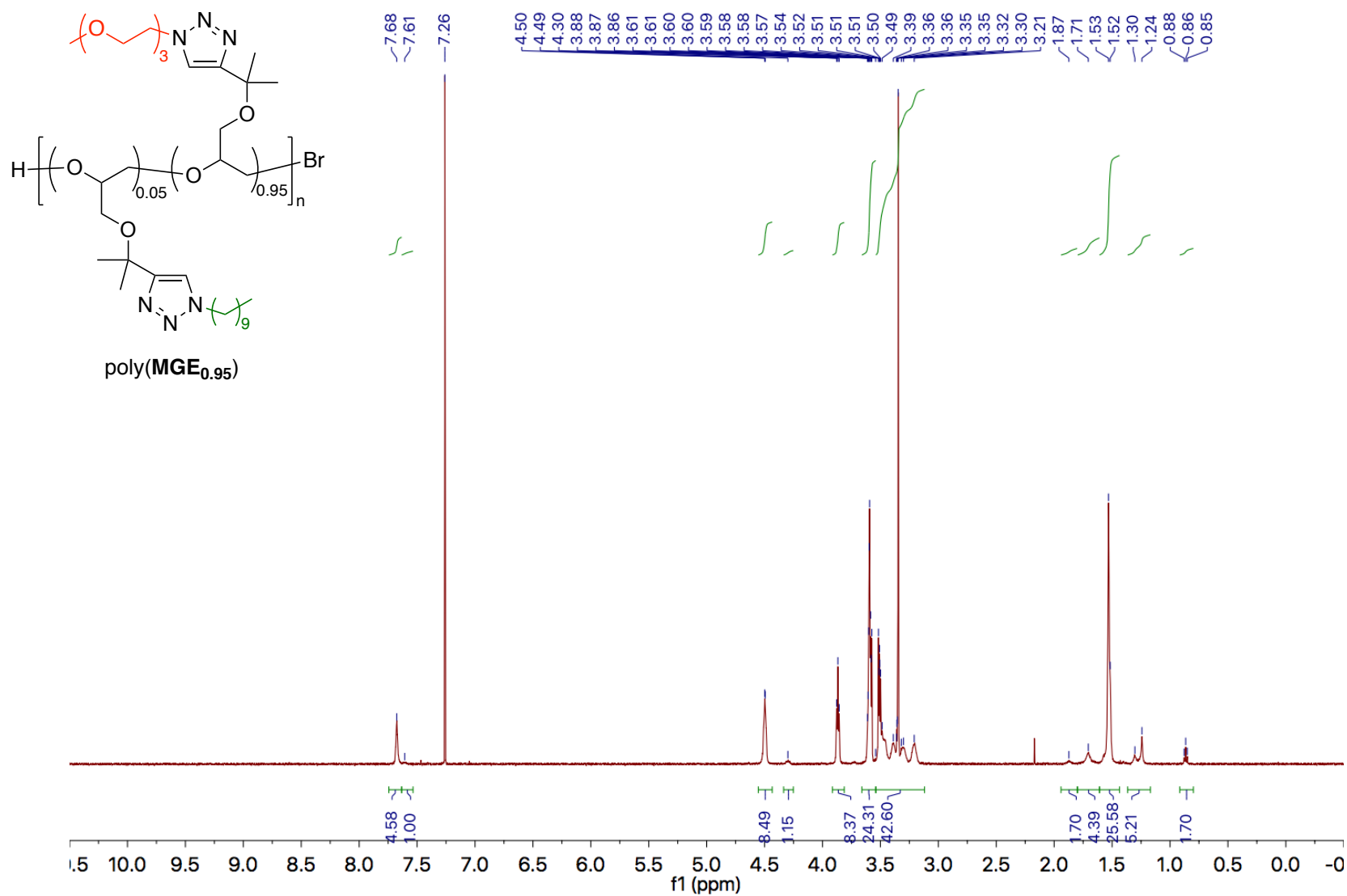


Figure A75. 500 MHz ¹H NMR spectrum of poly(MGE_{0.95}) in CDCl₃.

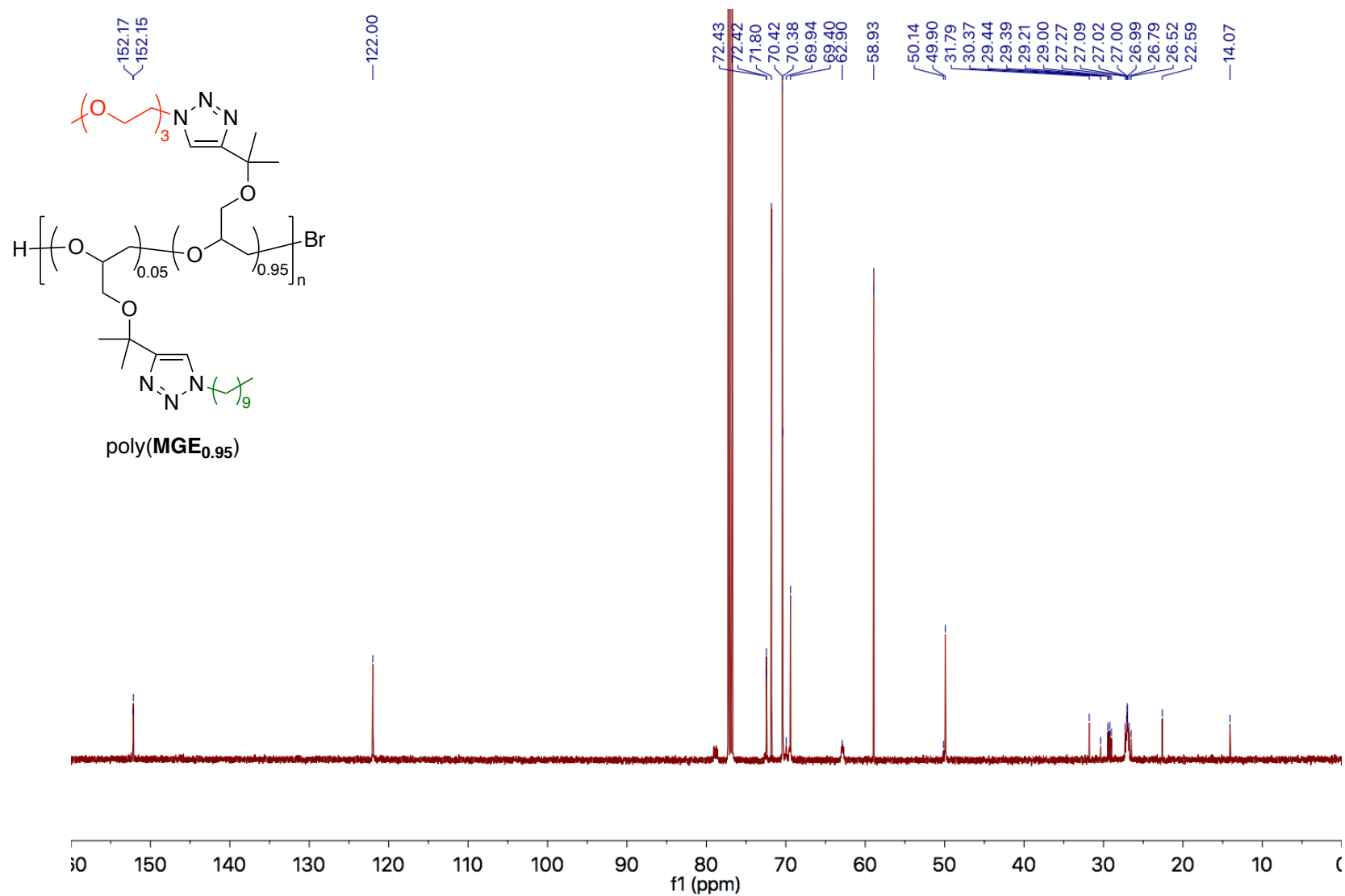


Figure A76. 125 MHz ¹³C NMR spectrum of poly(MGE_{0.95}) in CDCl₃.

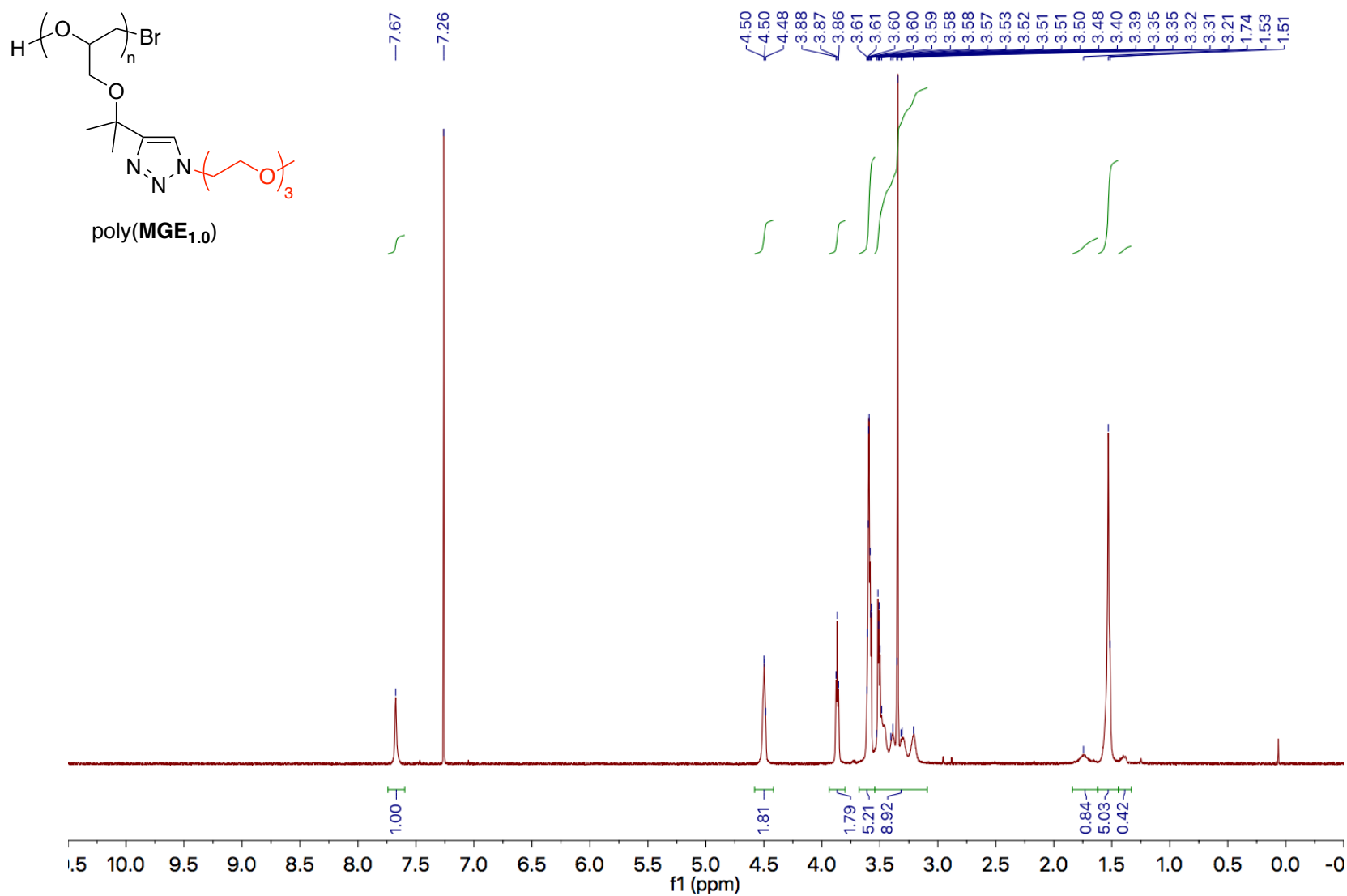


Figure A77. 500 MHz ¹H NMR spectrum of poly(MGE_{1.0}) in CDCl₃.

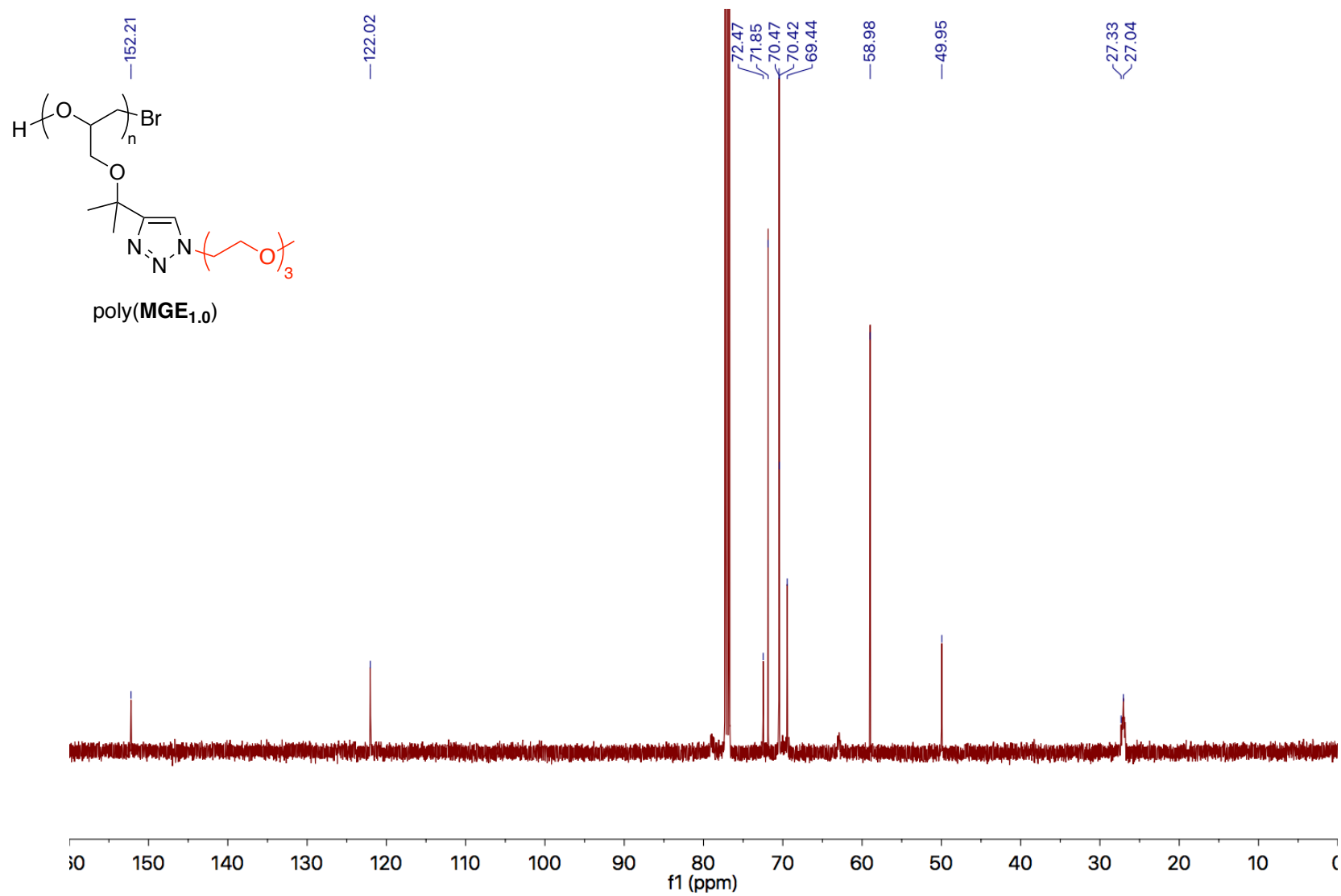


Figure A78. 125 MHz ^{13}C NMR spectrum of poly(**MGE**_{1.0}) in CDCl_3 .

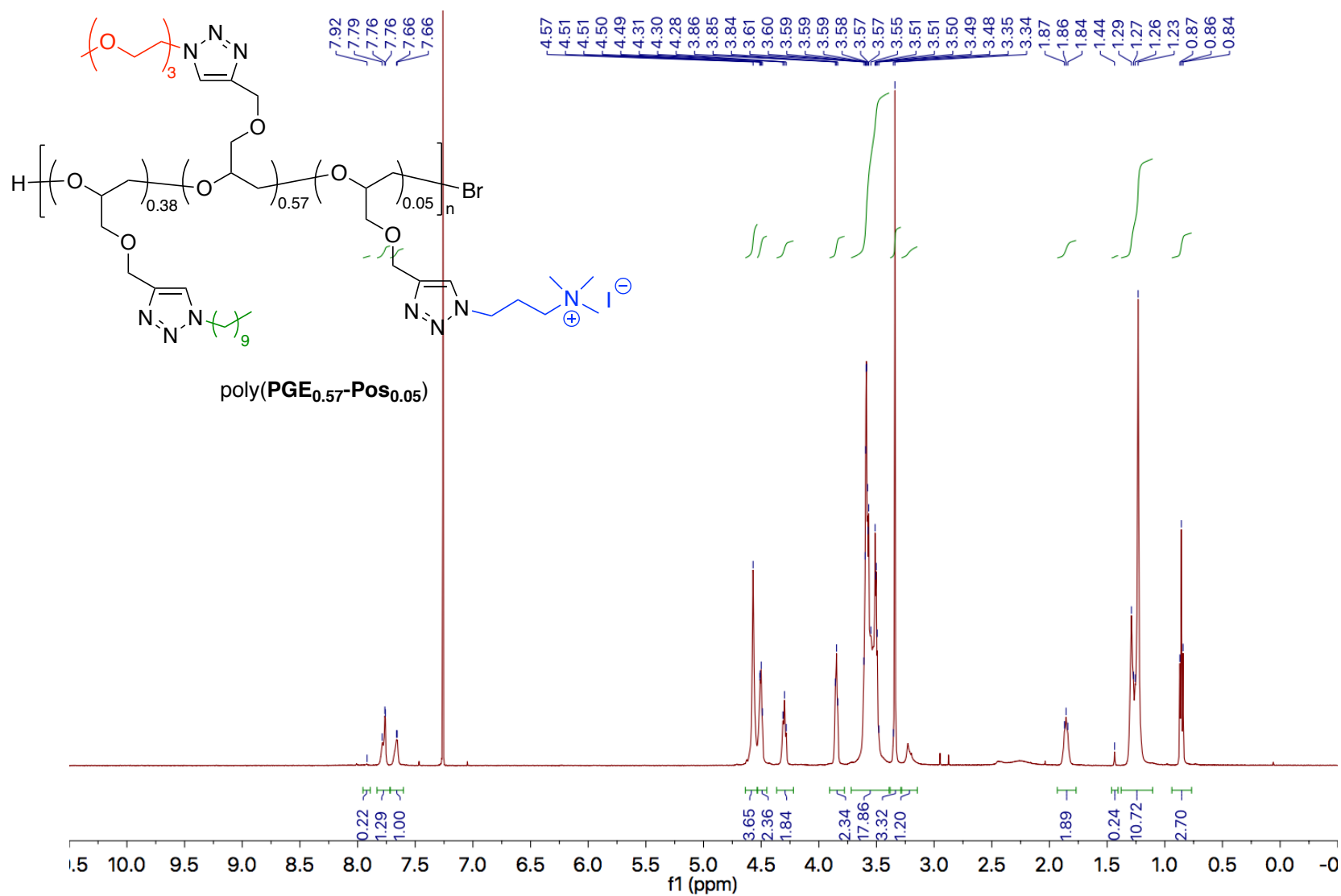


Figure A79. 500 MHz ^1H NMR spectrum of poly(PGE_{0.57}-Pos_{0.05}) in CDCl_3 .

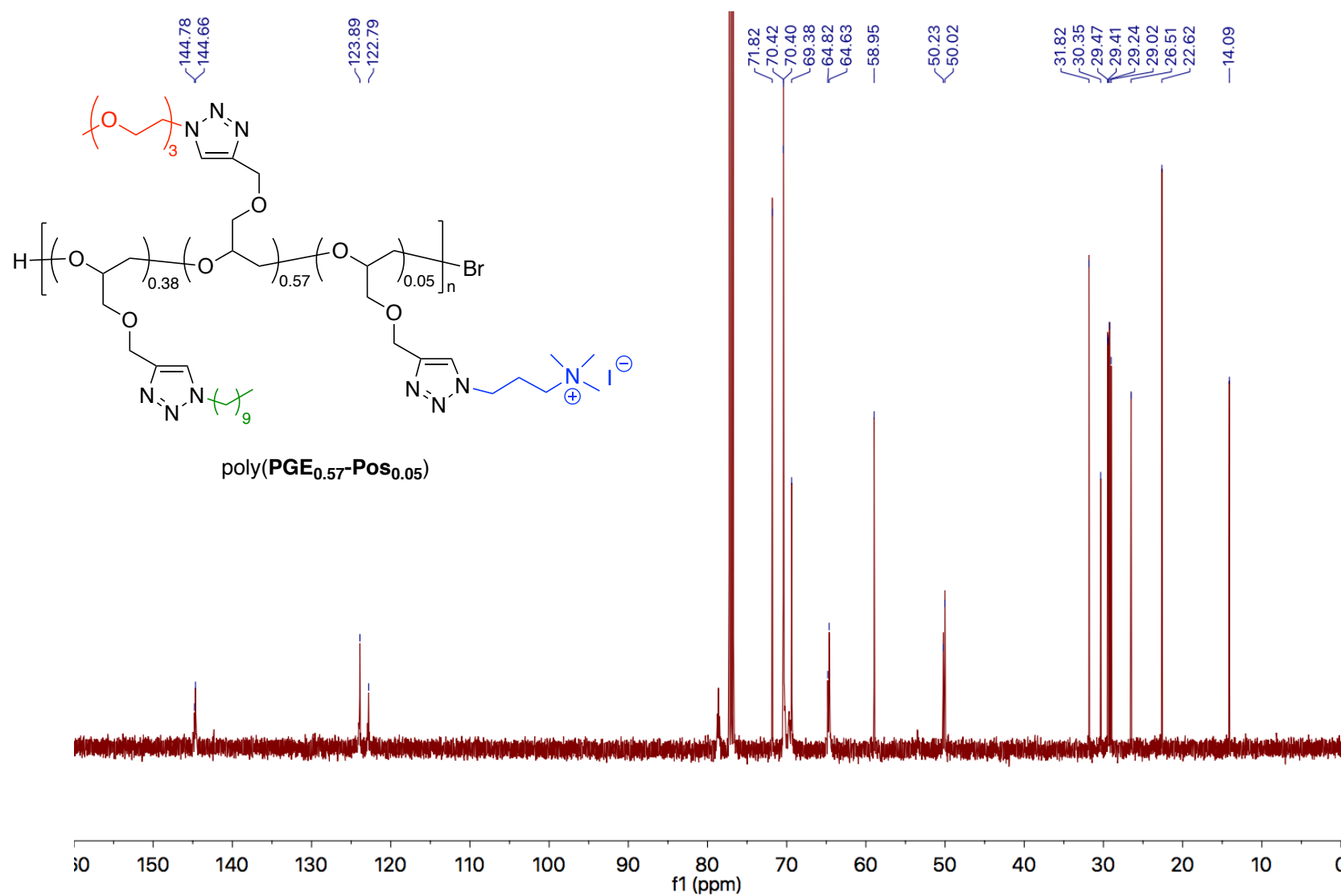


Figure A80. 125 MHz ^{13}C NMR spectrum of poly(PGE_{0.57}-Pos_{0.05}) in CDCl_3 .

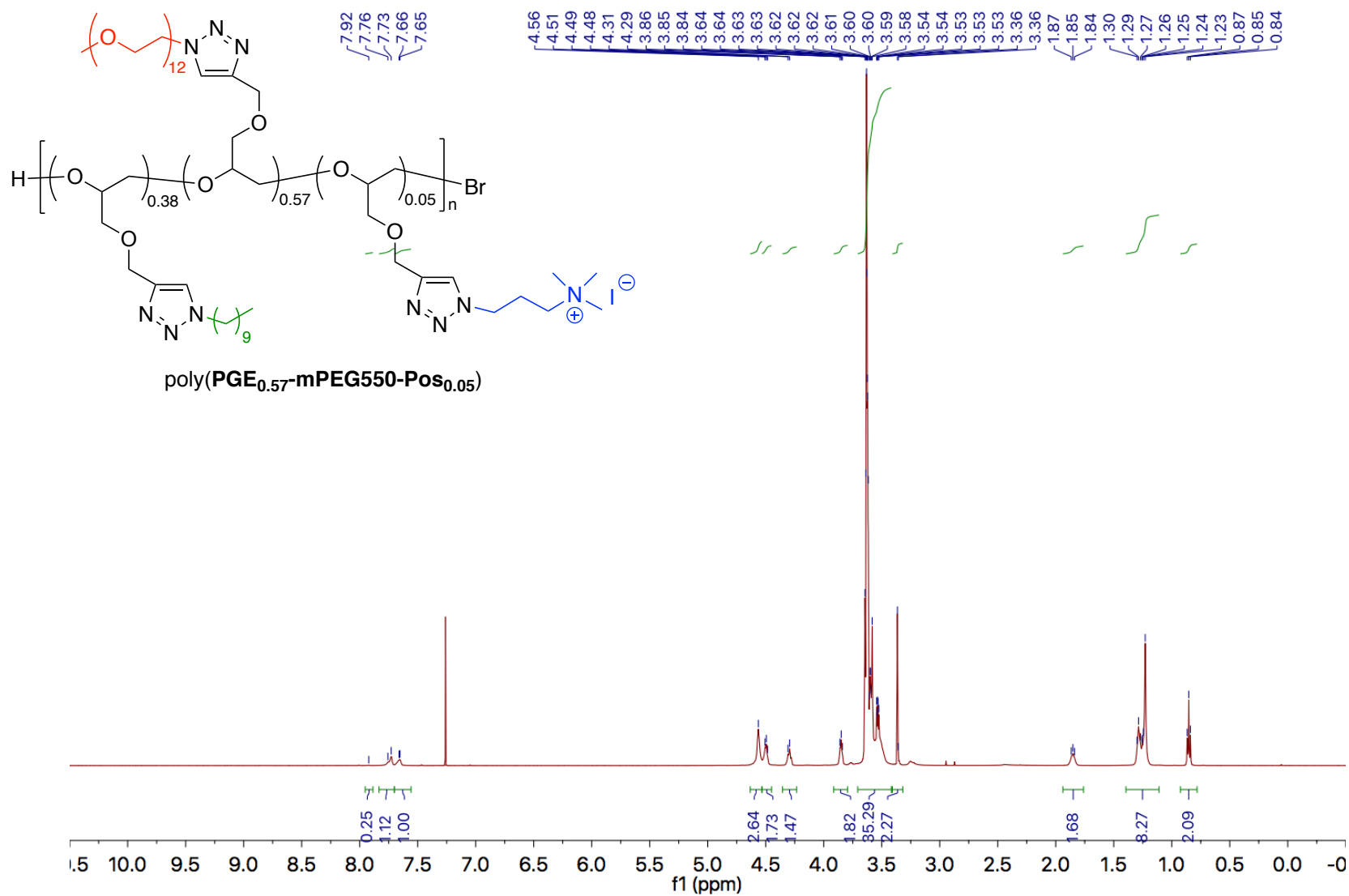


Figure A81. 500 MHz ¹H NMR spectrum of poly(PGE_{0.57}-mPEG550-Pos_{0.05}) in CDCl₃.

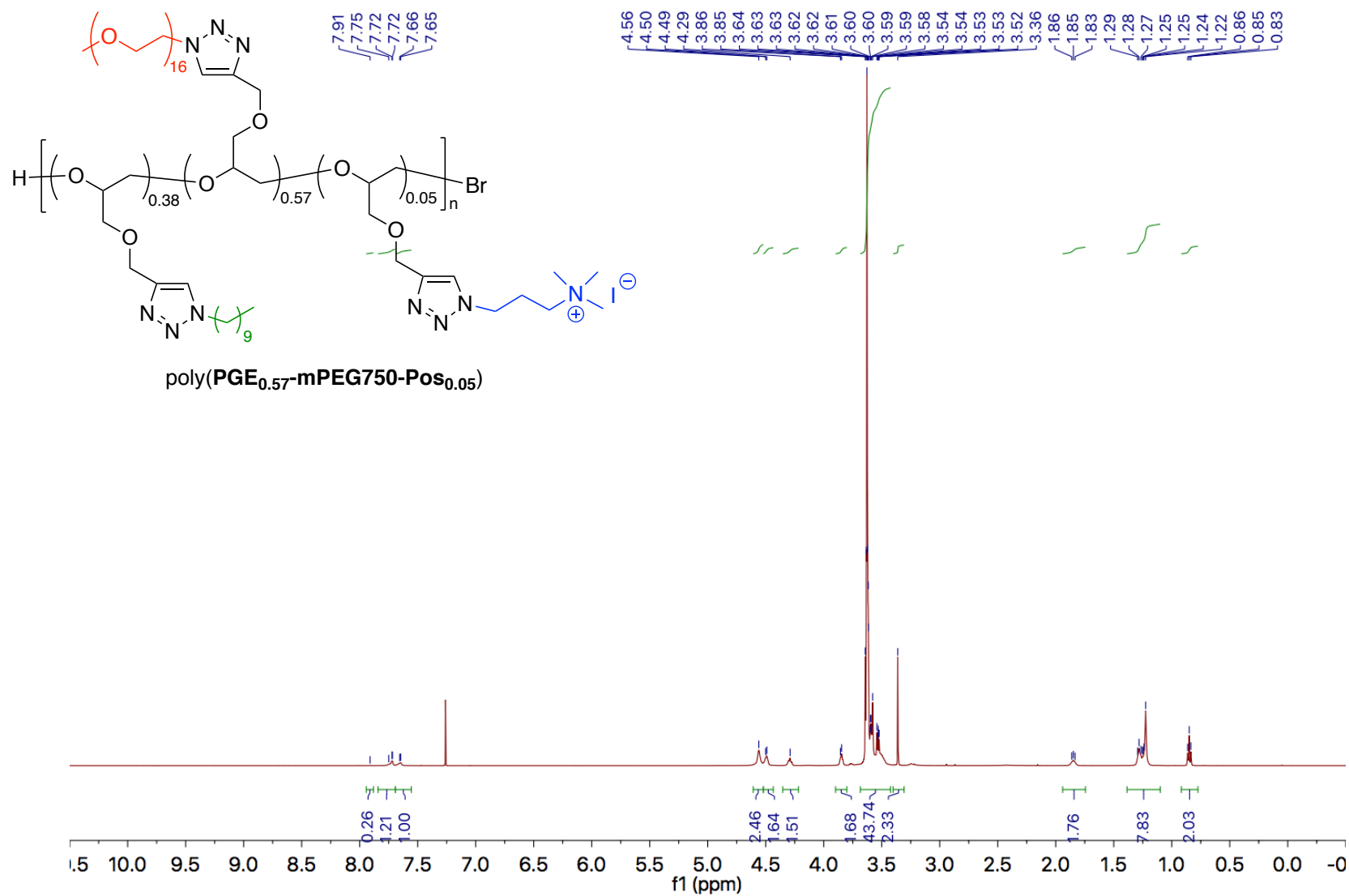


Figure A82. 500 MHz ¹H NMR spectrum of poly(PGE_{0.57}-mPEG750-Pos_{0.05}) in CDCl₃.

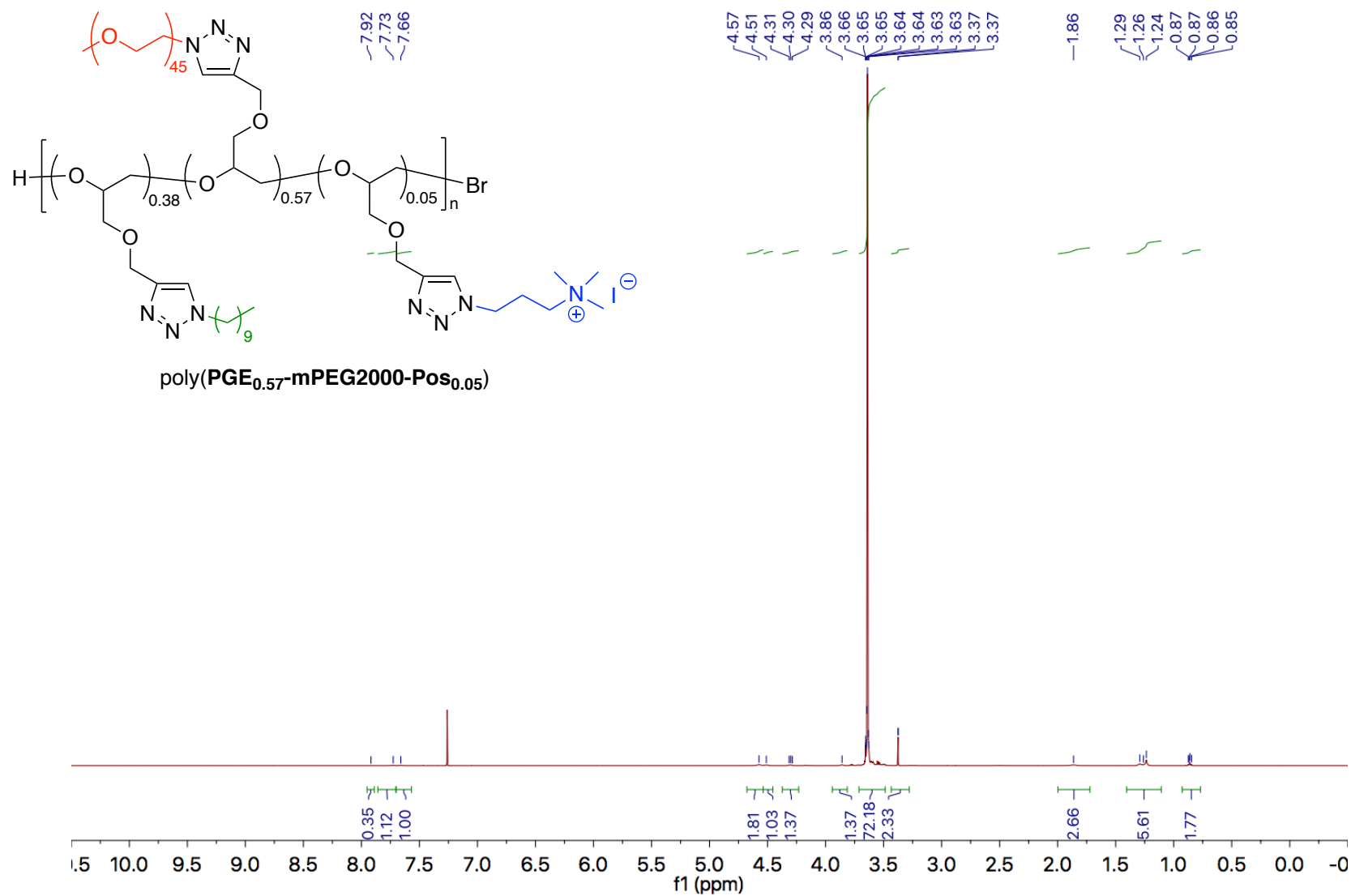


Figure A83. 500 MHz ¹H NMR spectrum of poly(PGE_{0.57}-mPEG2000-Pos_{0.05}) in CDCl₃.

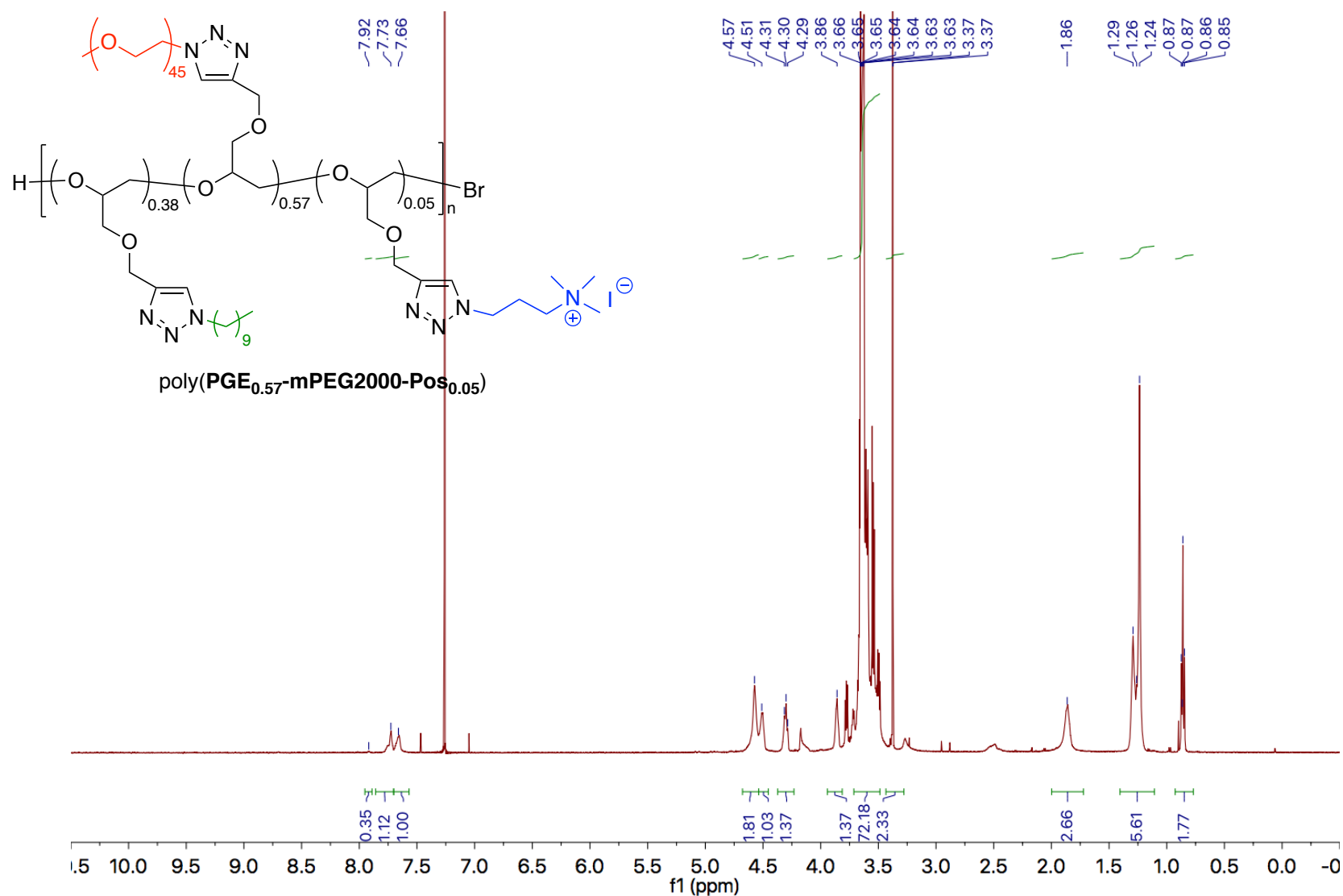


Figure A84. 500 MHz ^1H NMR spectrum of $\text{poly}(\text{PGE}_{0.57}\text{-mPEG2000-Pos}_{0.05})$ in CDCl_3 . Peak height was increased for clarity.

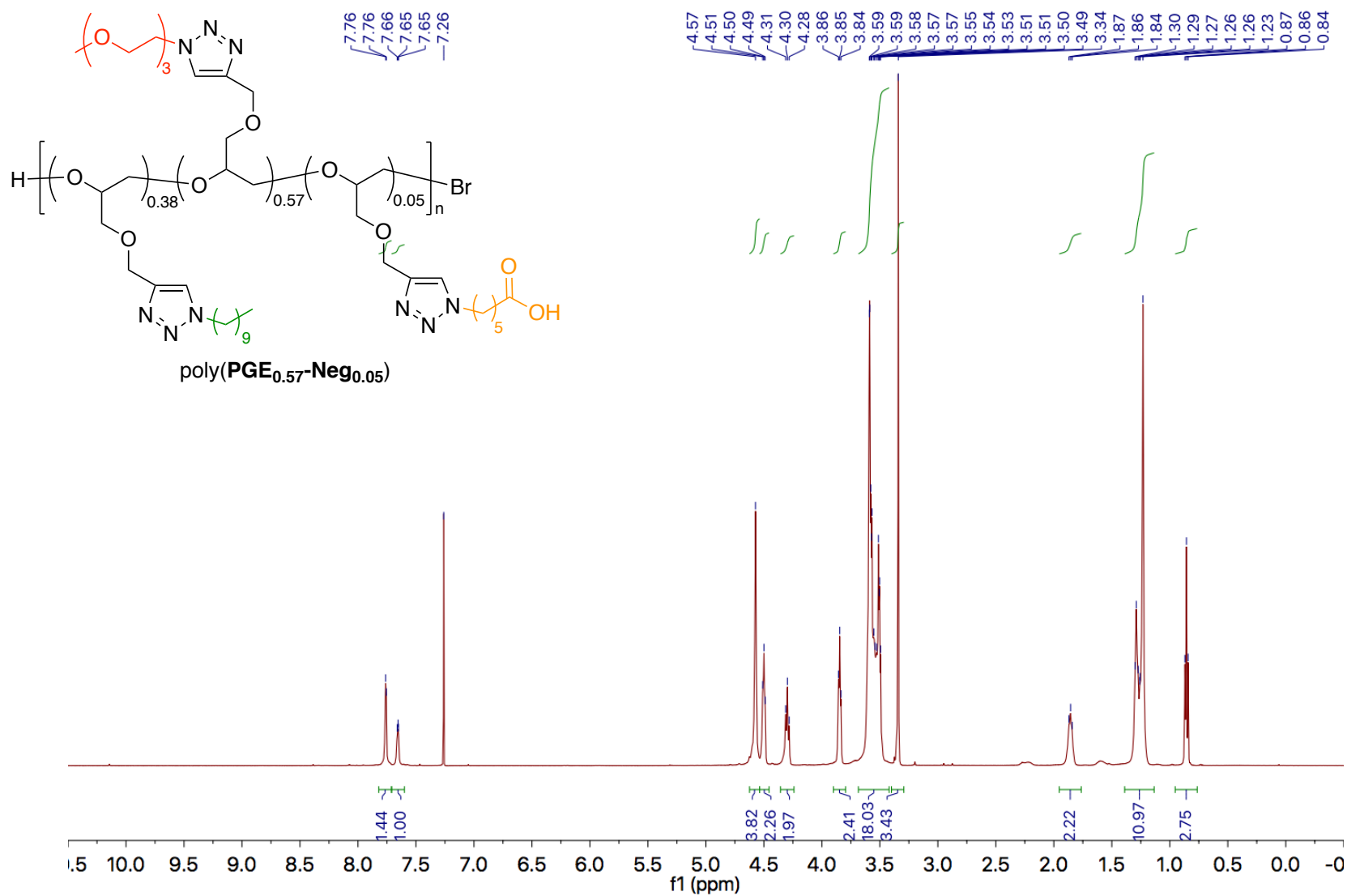


Figure A85. 500 MHz ¹H NMR spectrum of poly(PGE_{0.57}-Neg_{0.05}) in CDCl₃.

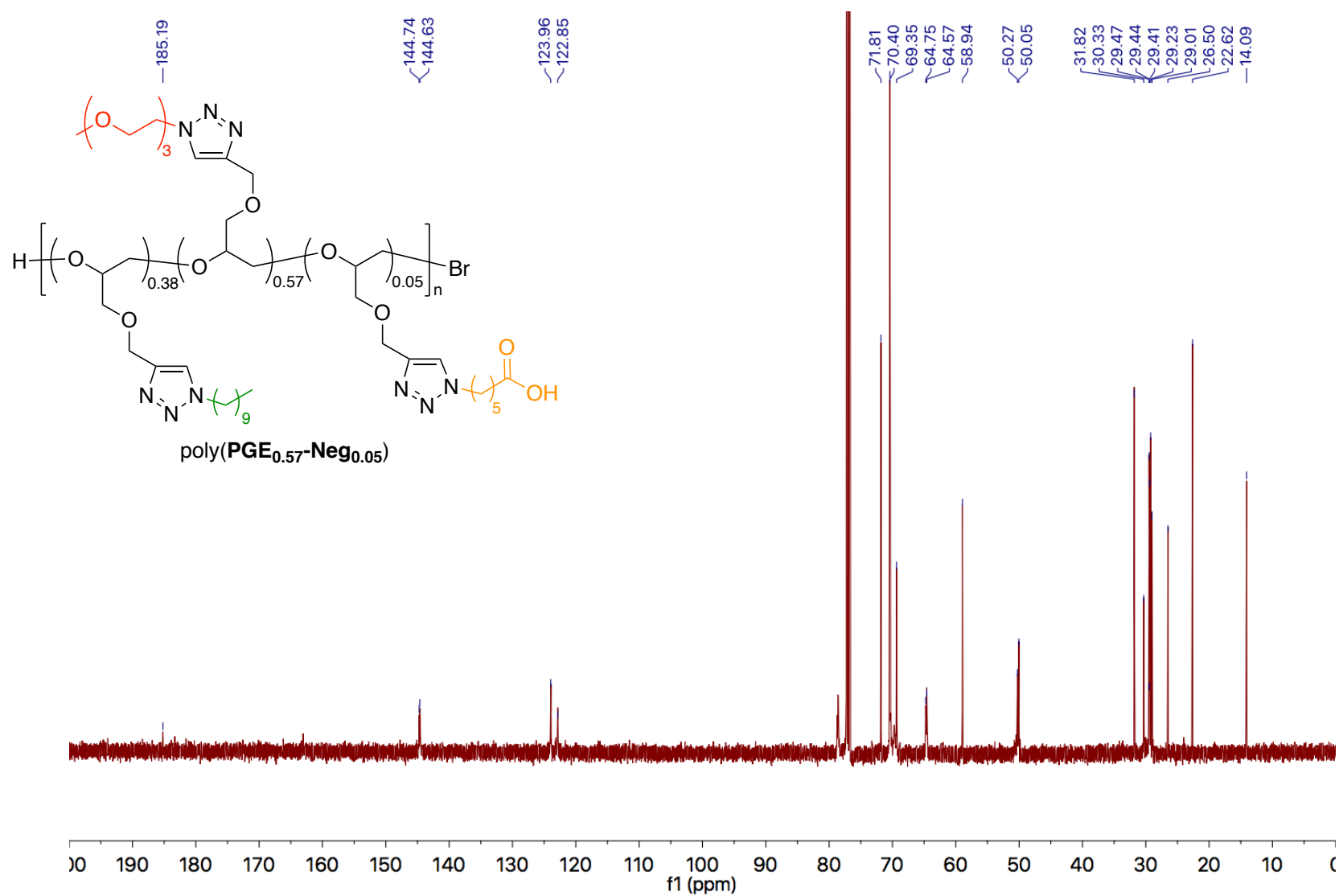


Figure A86. 125 MHz ^{13}C NMR spectrum of poly(PGE_{0.57}-Neg_{0.05}) in CDCl_3 .

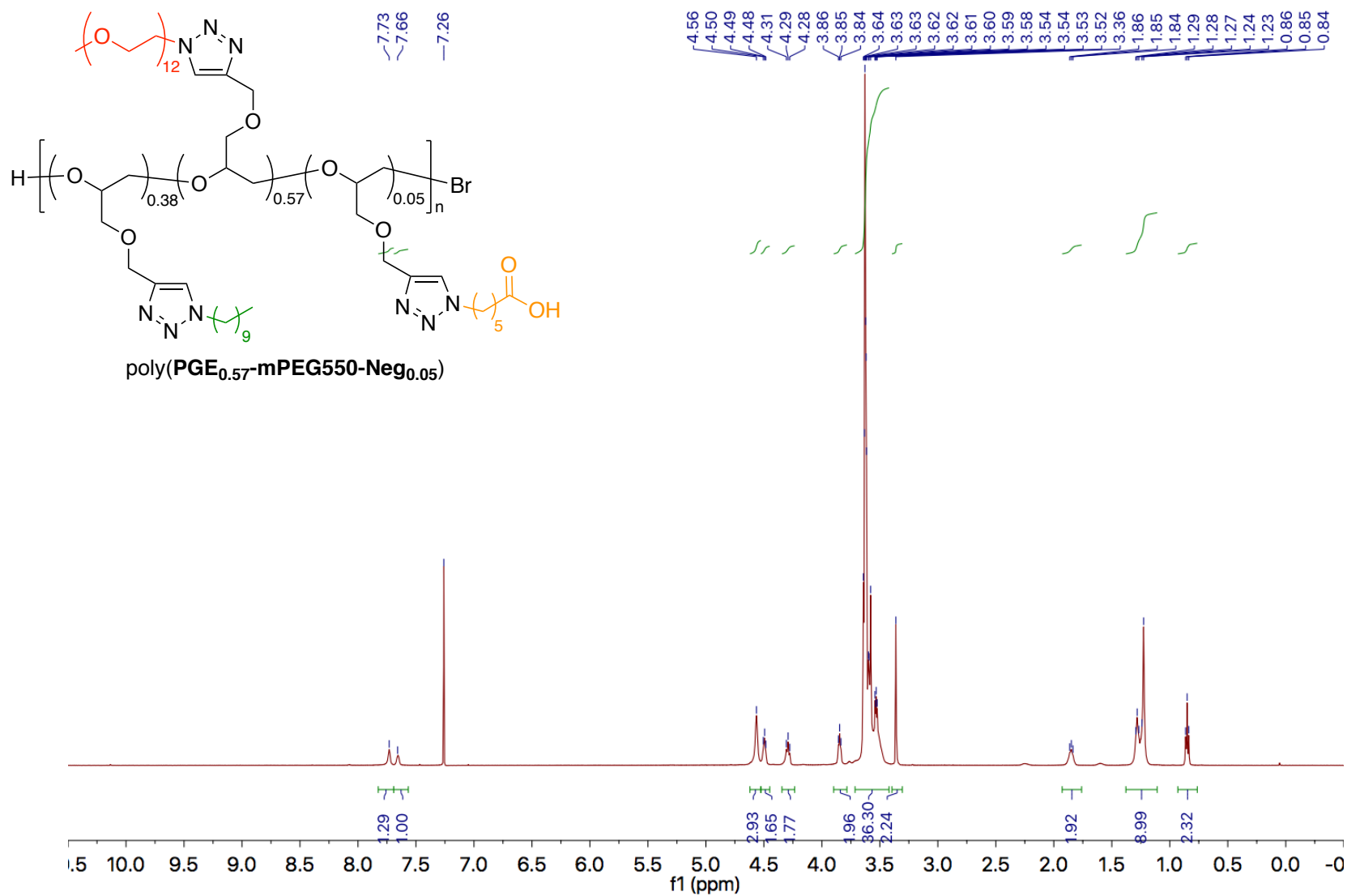


Figure A87. 500 MHz ^1H NMR spectrum of $\text{poly}(\text{PGE}_{0.57}\text{-mPEG550-Neg}_{0.05})$ in CDCl_3 .

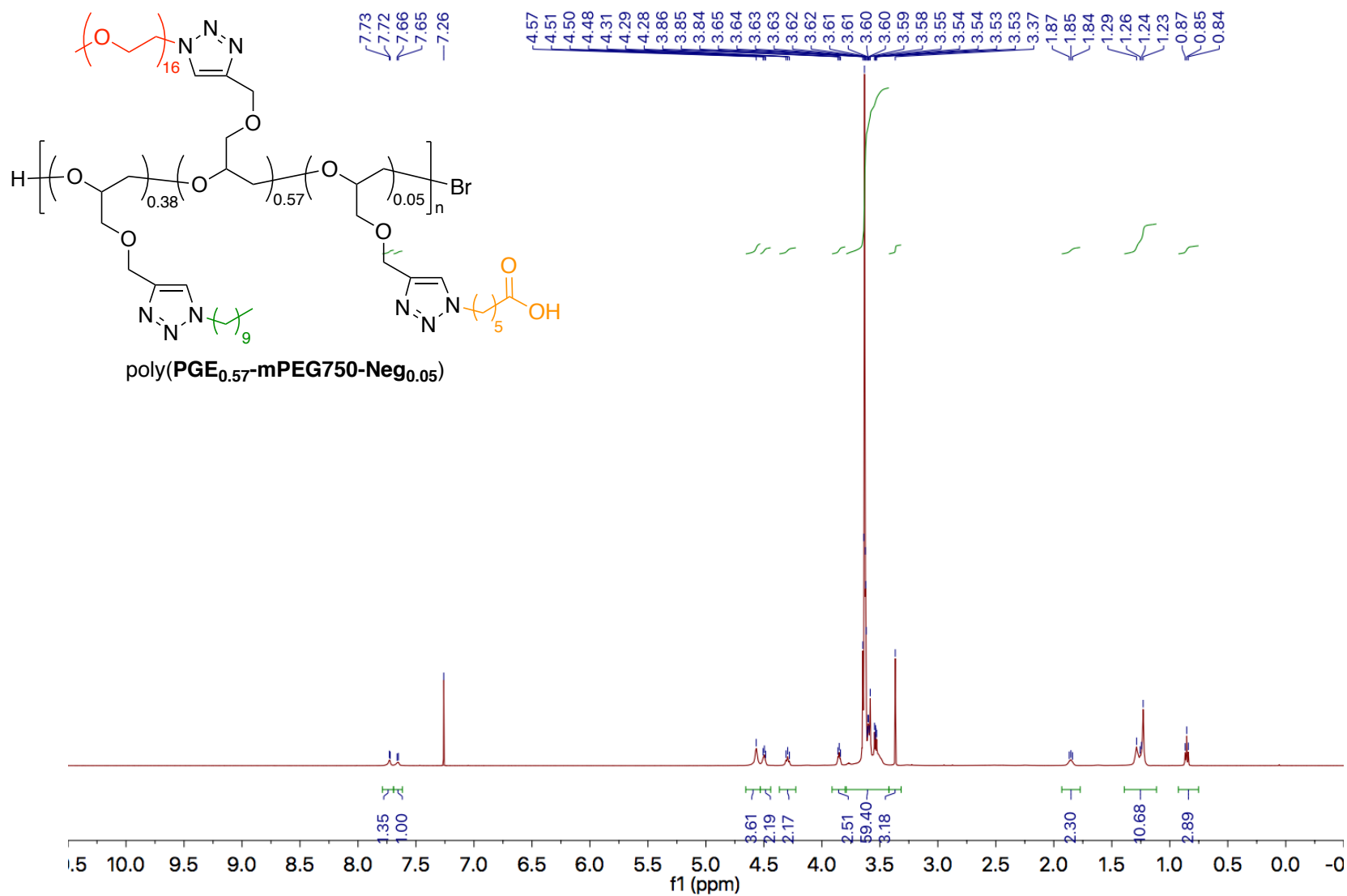


Figure A88. 500 MHz ^1H NMR spectrum of $\text{poly}(\text{PGE}_{0.57}\text{-mPEG750-Neg}_{0.05})$ in CDCl_3 .

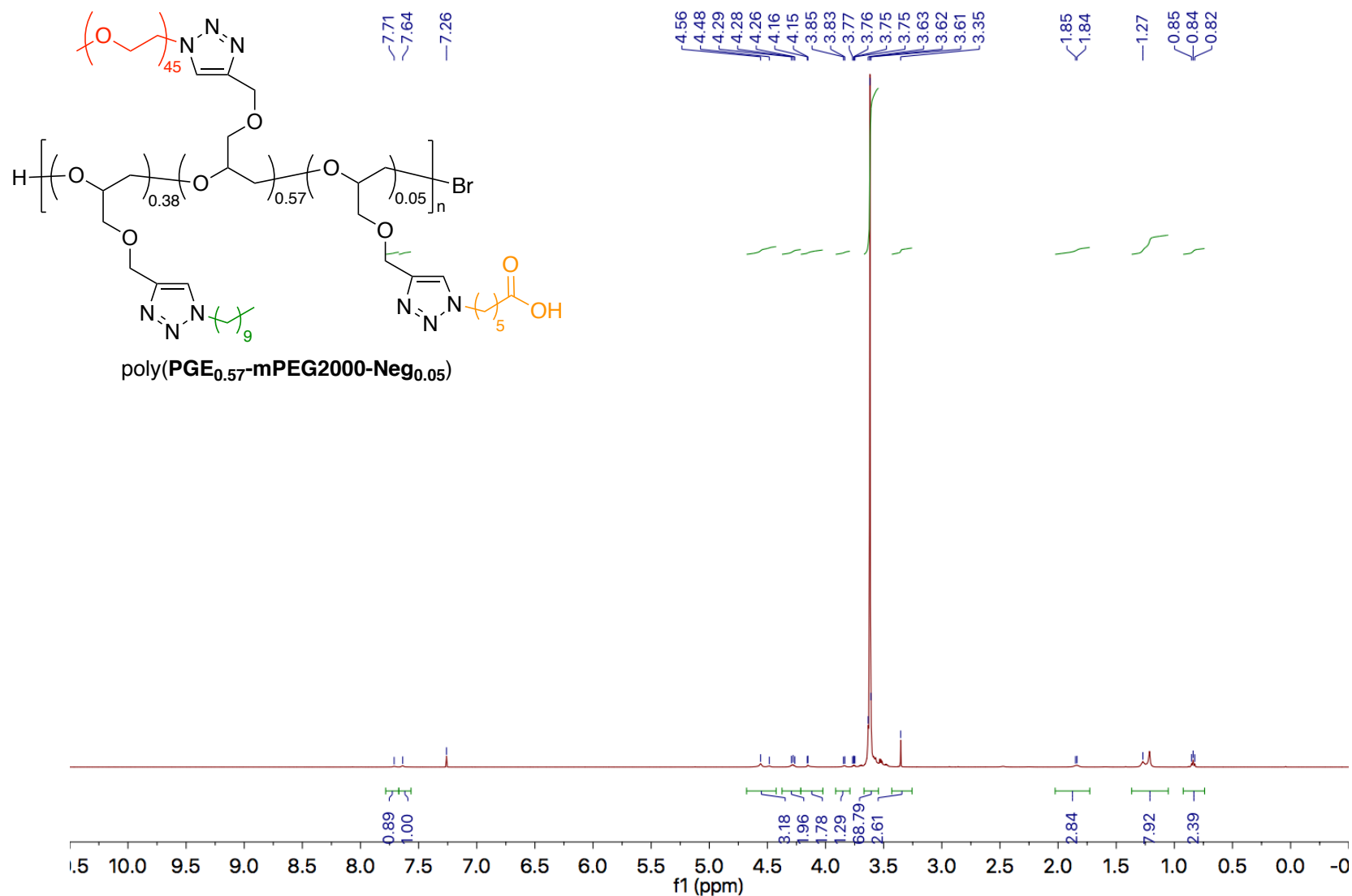


Figure A89. 500 MHz ¹H NMR spectrum of poly(PGE_{0.57}-mPEG2000-Neg_{0.05}) in CDCl₃.

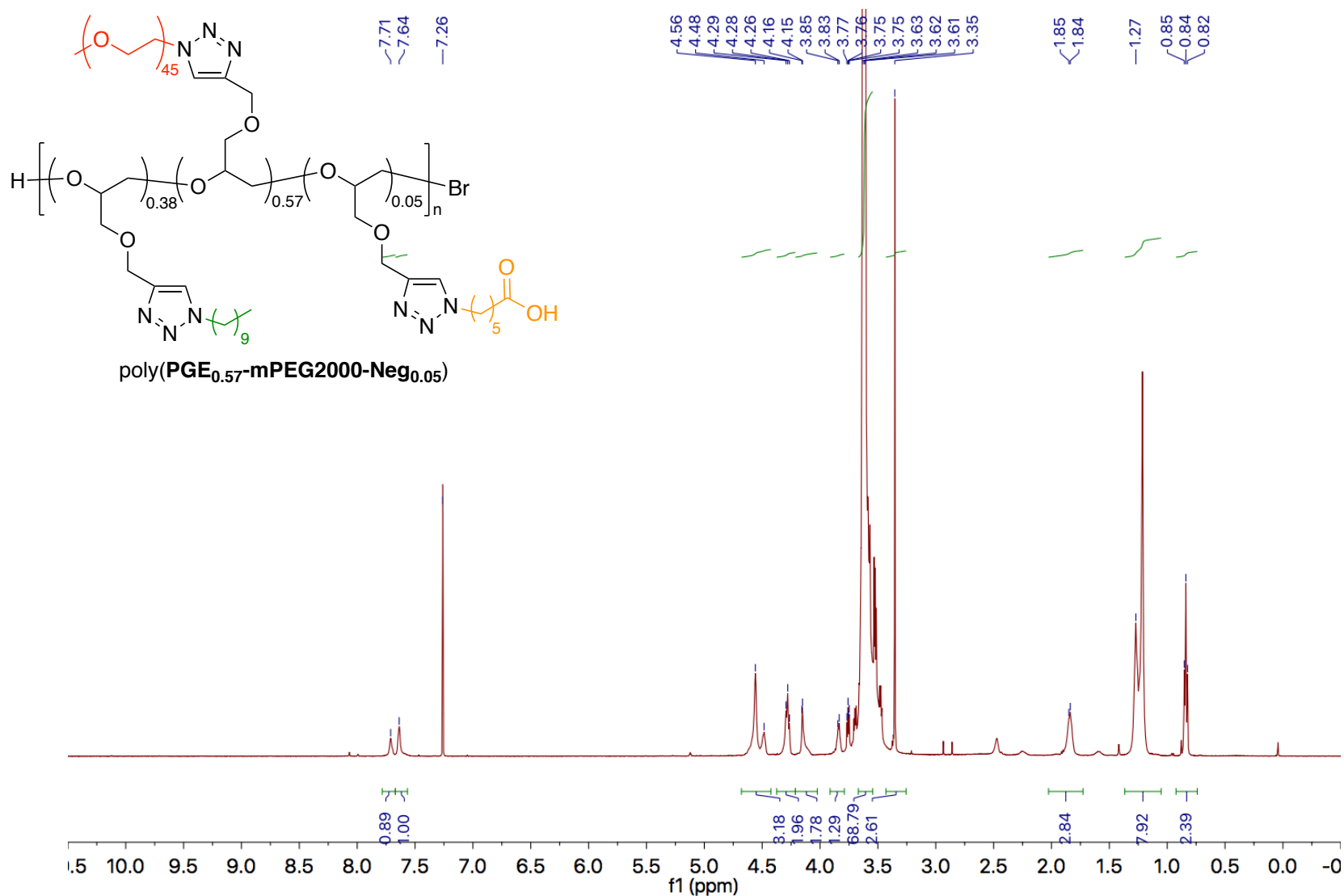


Figure A90. 500 MHz ¹H NMR spectrum of poly(PGE_{0.57}-mPEG2000-Neg_{0.05}) in CDCl₃. Peak height was increased for clarity.

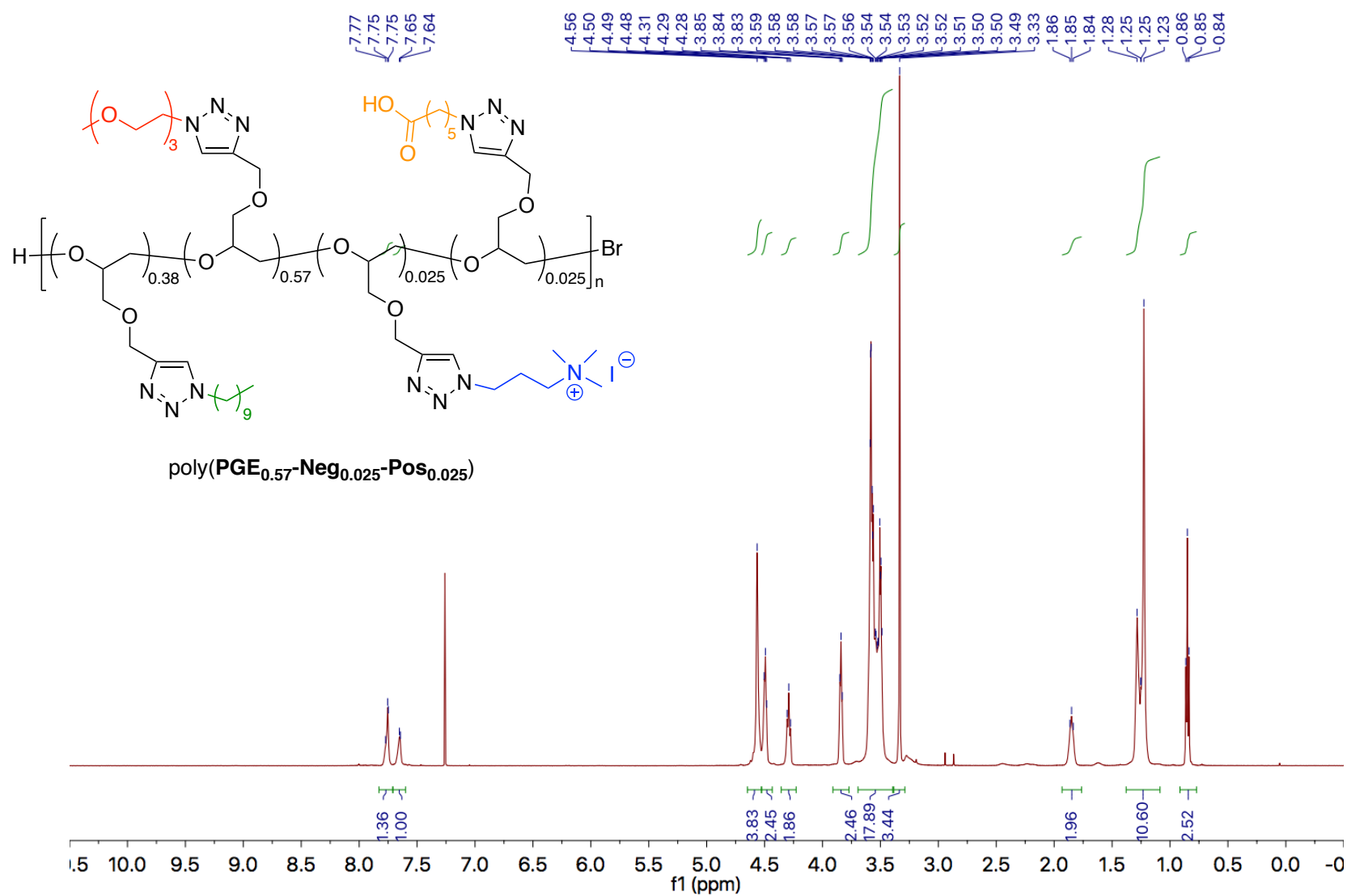


Figure A91. 500 MHz ^1H NMR spectrum of $\text{poly}(\text{PGE}_{0.57}\text{-Neg}_{0.025}\text{-Pos}_{0.025})$ in CDCl_3 .

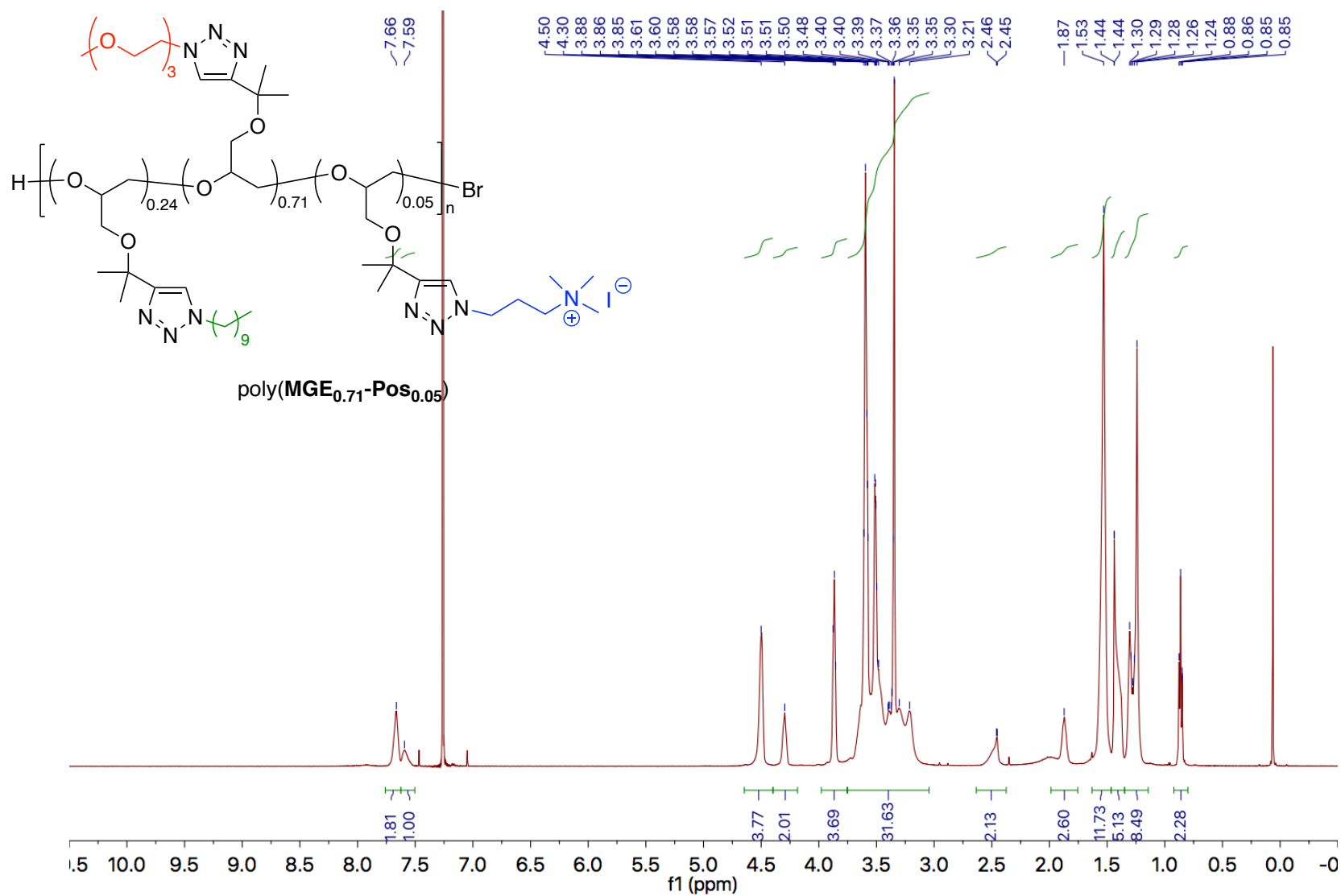


Figure A92. 500 MHz ^1H NMR spectrum of $\text{poly}(\text{MGE}_{0.71}\text{-Pos}_{0.05})$ in CDCl_3 .

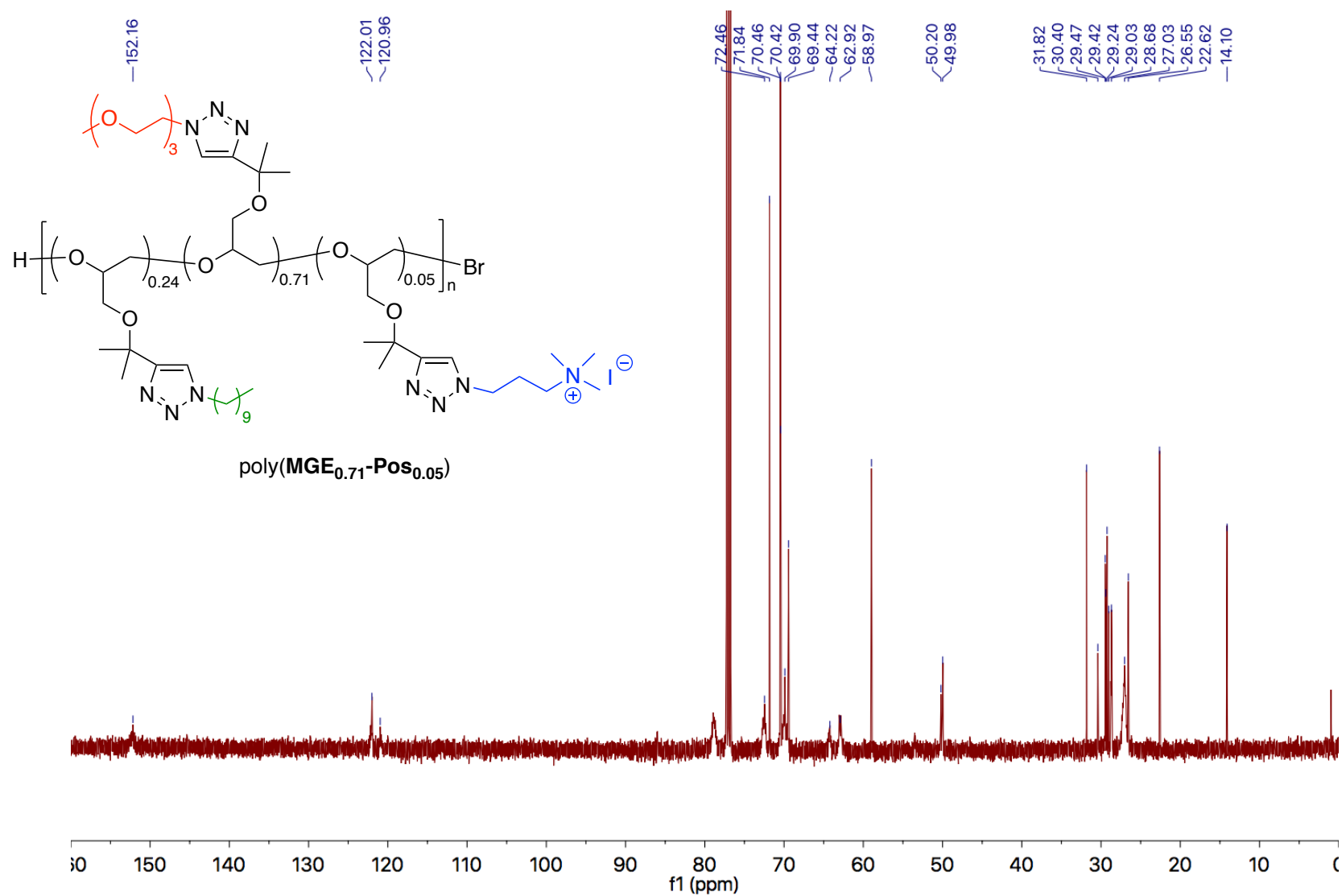


Figure A93. 125 MHz ¹³C NMR spectrum of poly(MGE_{0.71}-Pos_{0.05}) in CDCl₃.

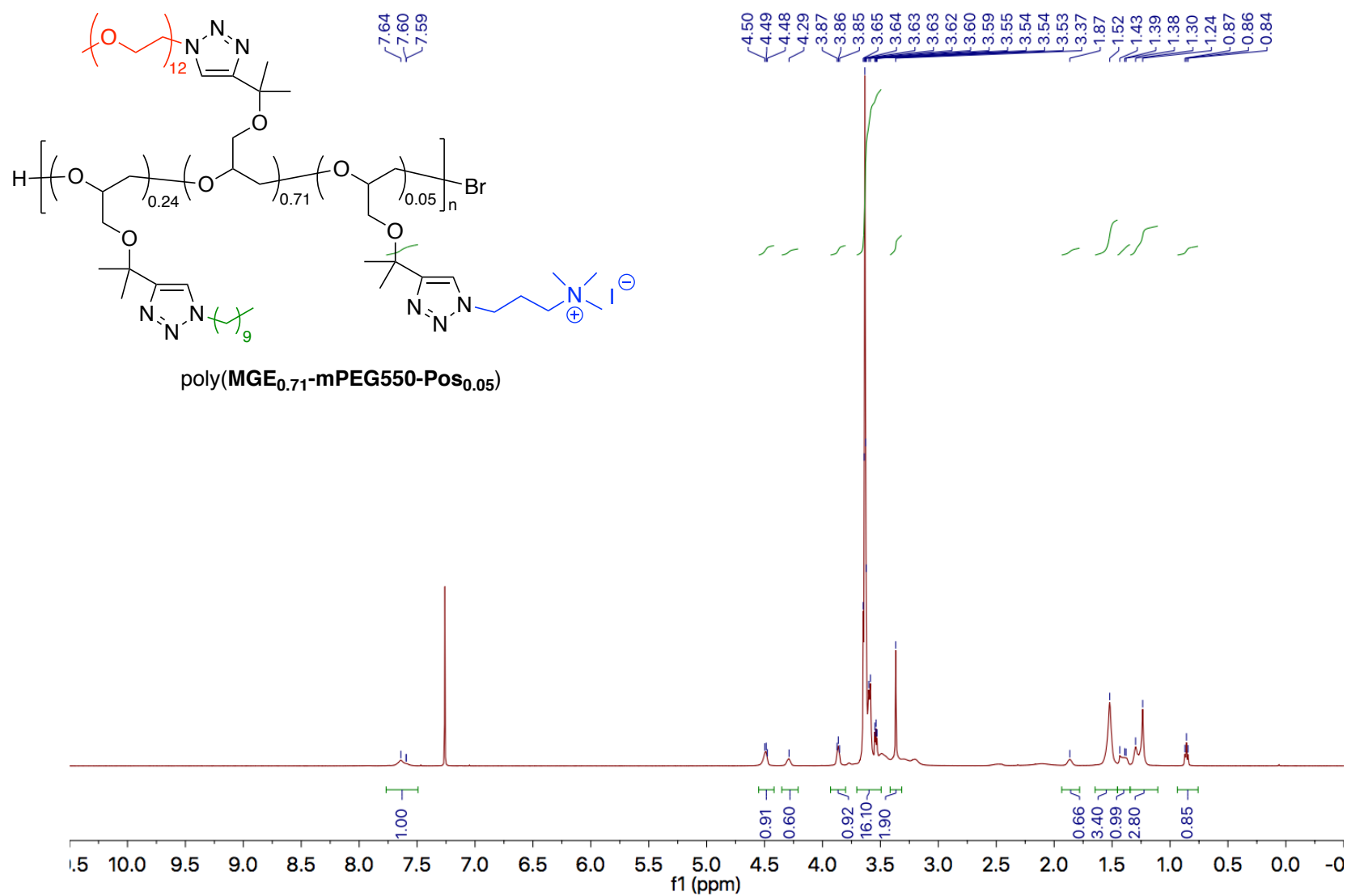


Figure A94. 500 MHz ^1H NMR spectrum of $\text{poly}(\text{MGE}_{0.71}\text{-mPEG550-Pos}_{0.05})$ in CDCl_3 .

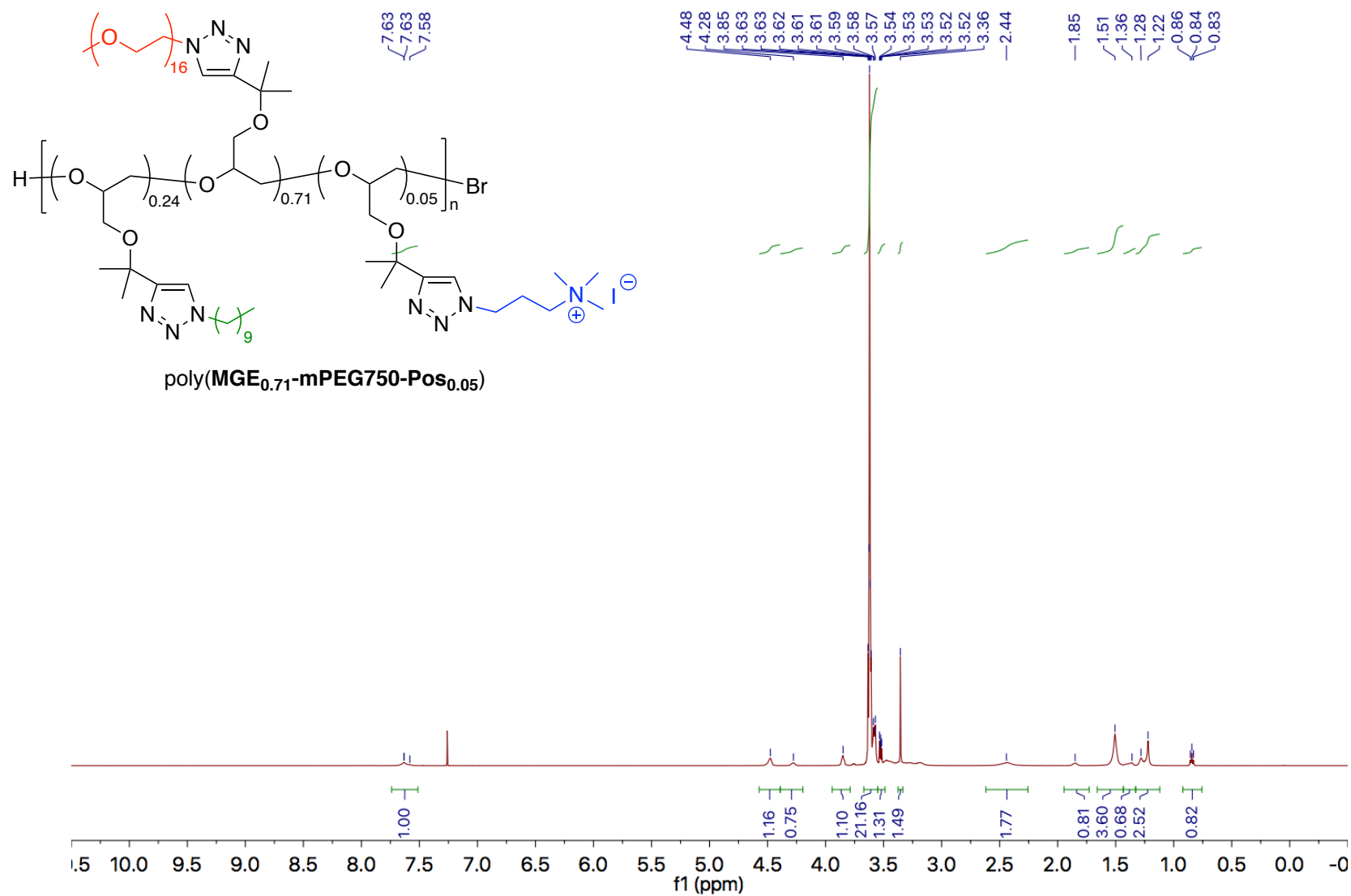


Figure A95. 500 MHz ^1H NMR spectrum of $\text{poly}(\text{MGE}_{0.71}\text{-mPEG750-Pos}_{0.05})$. in CDCl_3

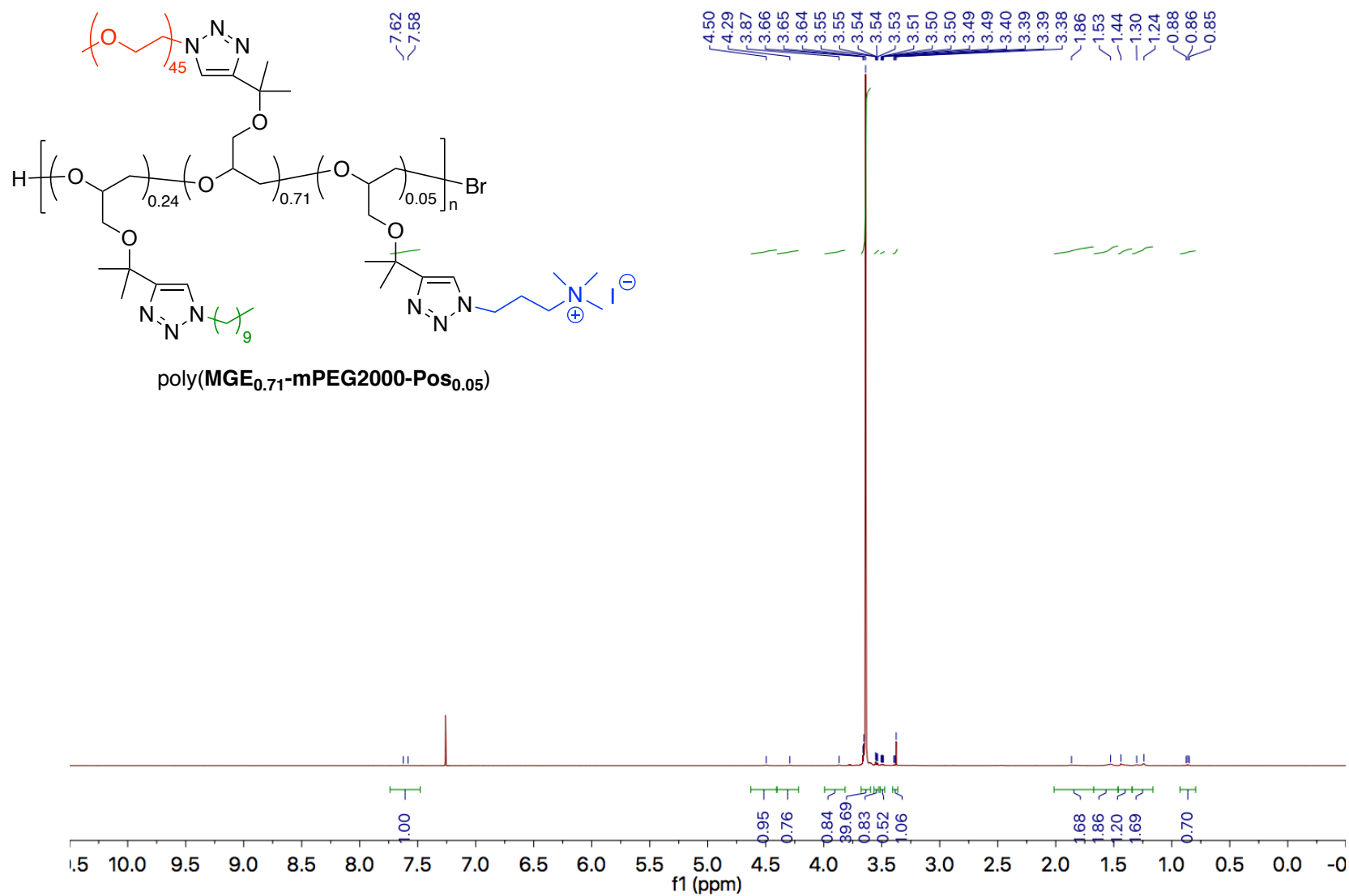


Figure A96. 500 MHz ¹H NMR spectrum of poly(MGE_{0.71}-mPEG2000-Pos_{0.05}) in CDCl₃.

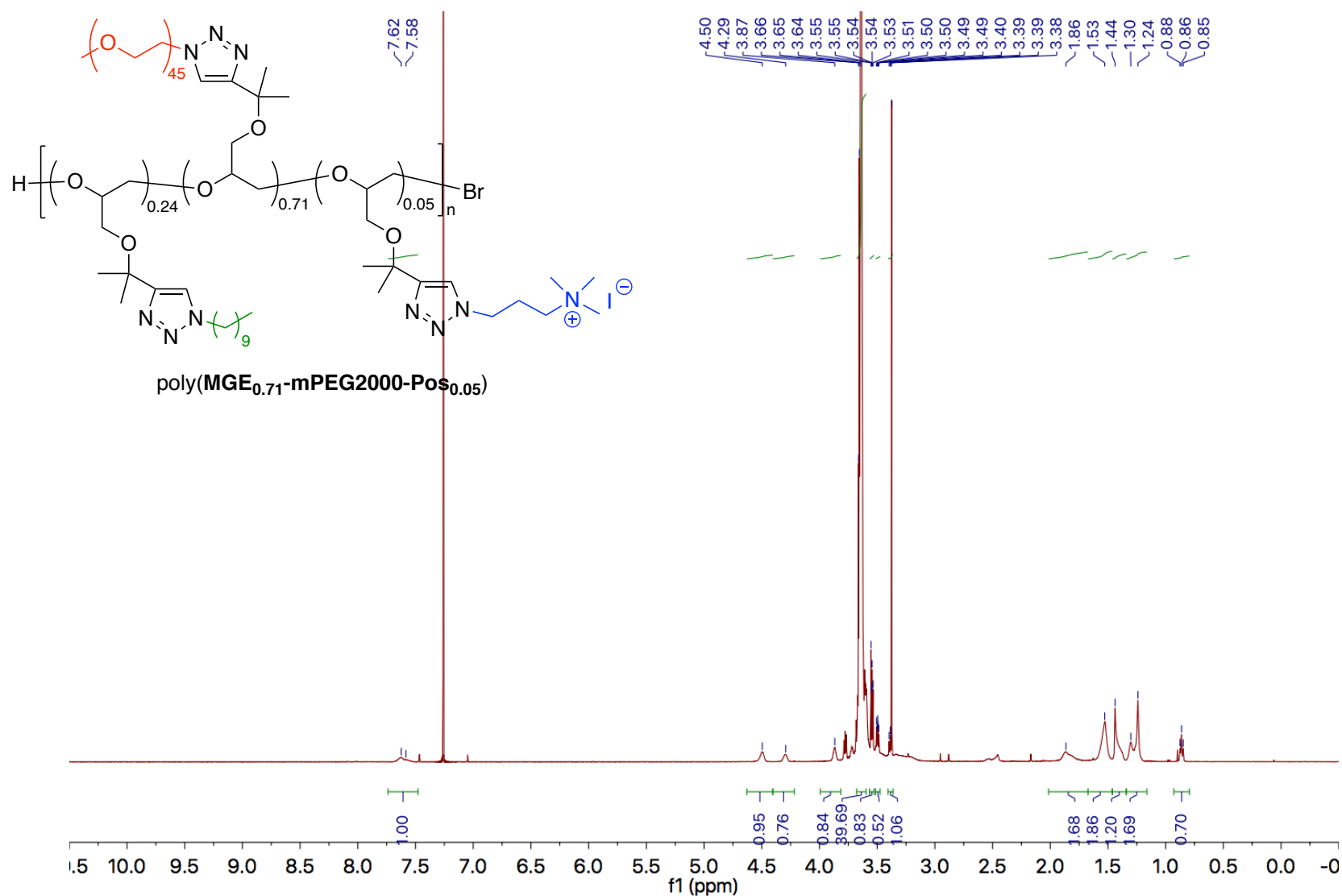


Figure A97. 500 MHz ¹H NMR spectrum of poly(MGE_{0.71}-mPEG2000-Pos_{0.05}) in CDCl₃. Peak height was increased for clarity.

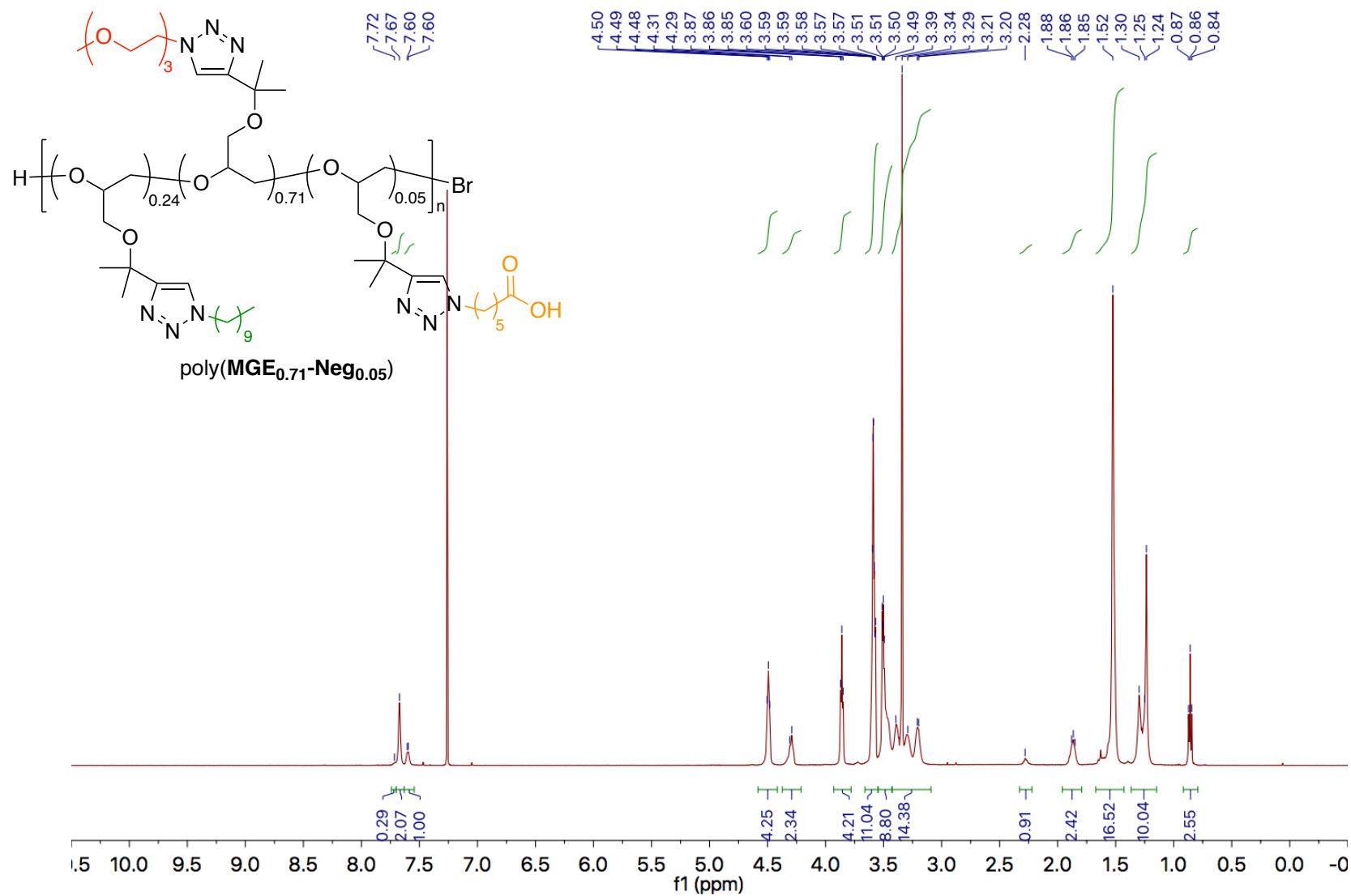


Figure A98. 500 MHz ¹H NMR spectrum of poly(MGE_{0.71}-Neg_{0.05}) in CDCl₃.

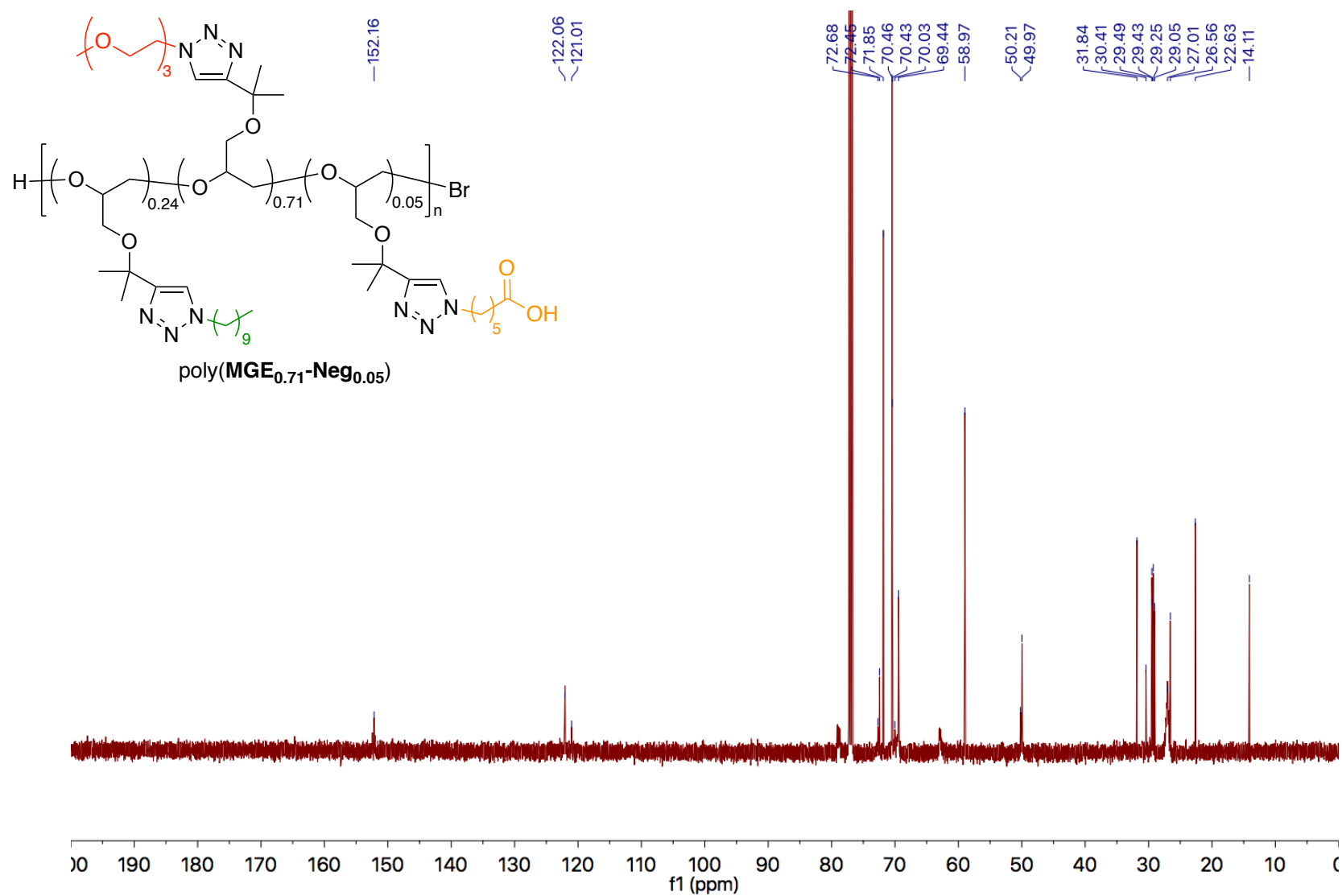


Figure A99. 125 MHz ^{13}C NMR spectrum of poly(MGE_{0.71}-Neg_{0.05}) in CDCl_3 .

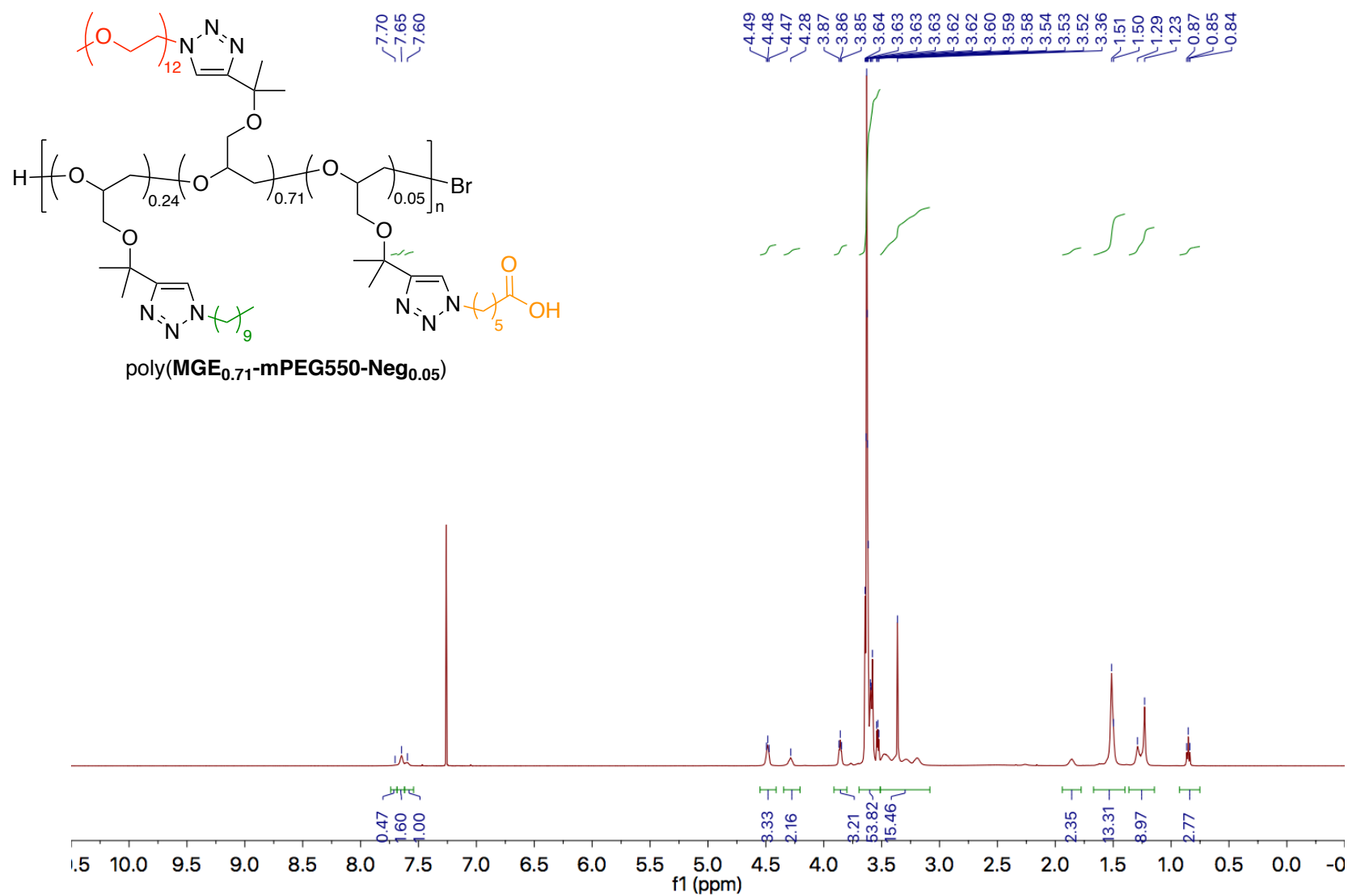


Figure A100. 500 MHz ¹H NMR spectrum of poly(MGE_{0.71}-mPEG550-Neg_{0.05}) in CDCl₃.

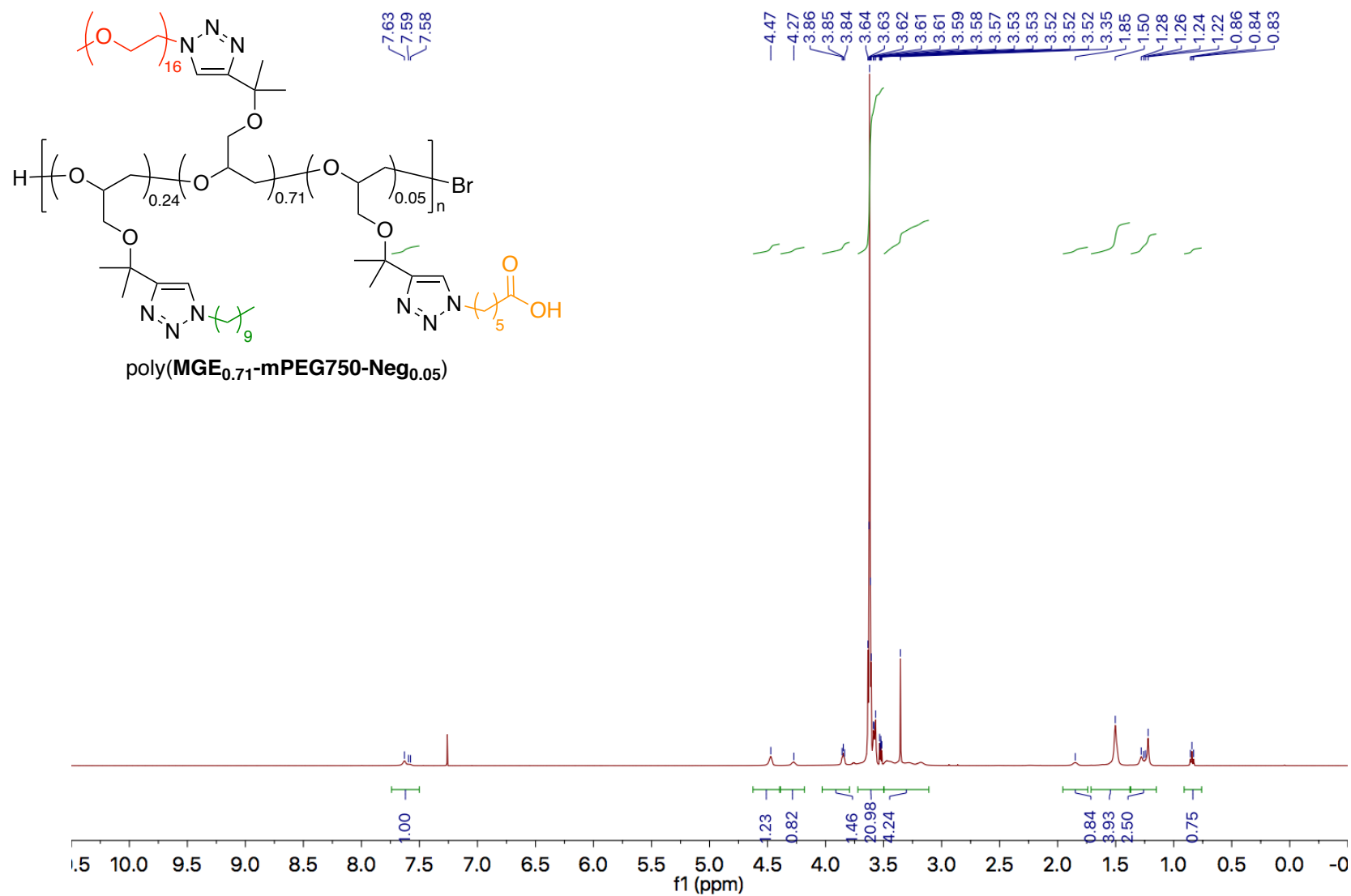


Figure A101. 500 MHz ¹H NMR spectrum of poly(MGE_{0.71}-mPEG750-Neg_{0.05}) in CDCl₃.

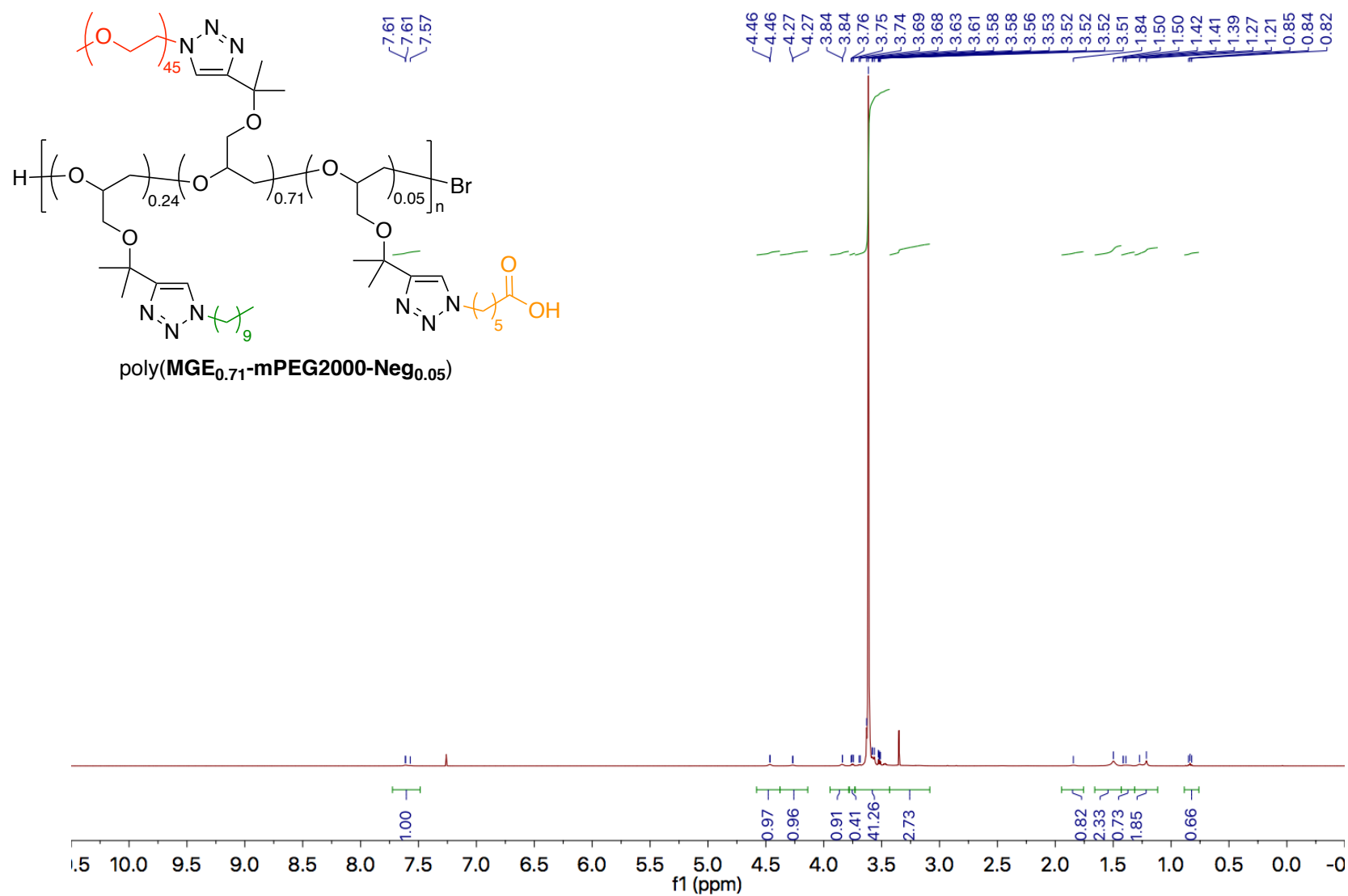


Figure A102. 500 MHz ¹H NMR spectrum of poly(MGE_{0.71}-mPEG2000-Neg_{0.05}) in CDCl₃.

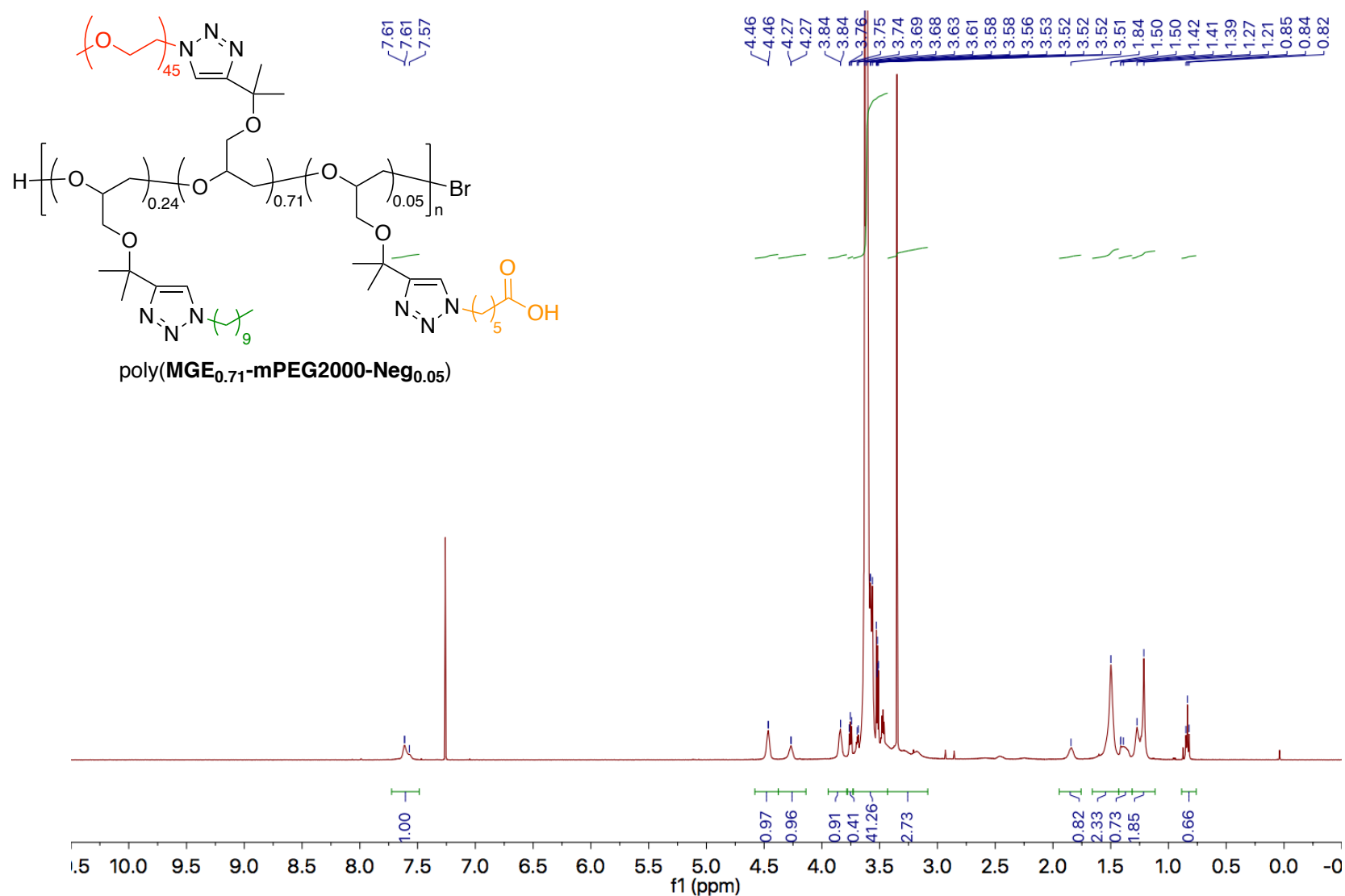


Figure A103. 500 MHz ^1H NMR spectrum of $\text{poly}(\text{MGE}_{0.71}\text{-mPEG2000-Neg}_{0.05})$ in CDCl_3 . Peak height was increased for clarity.

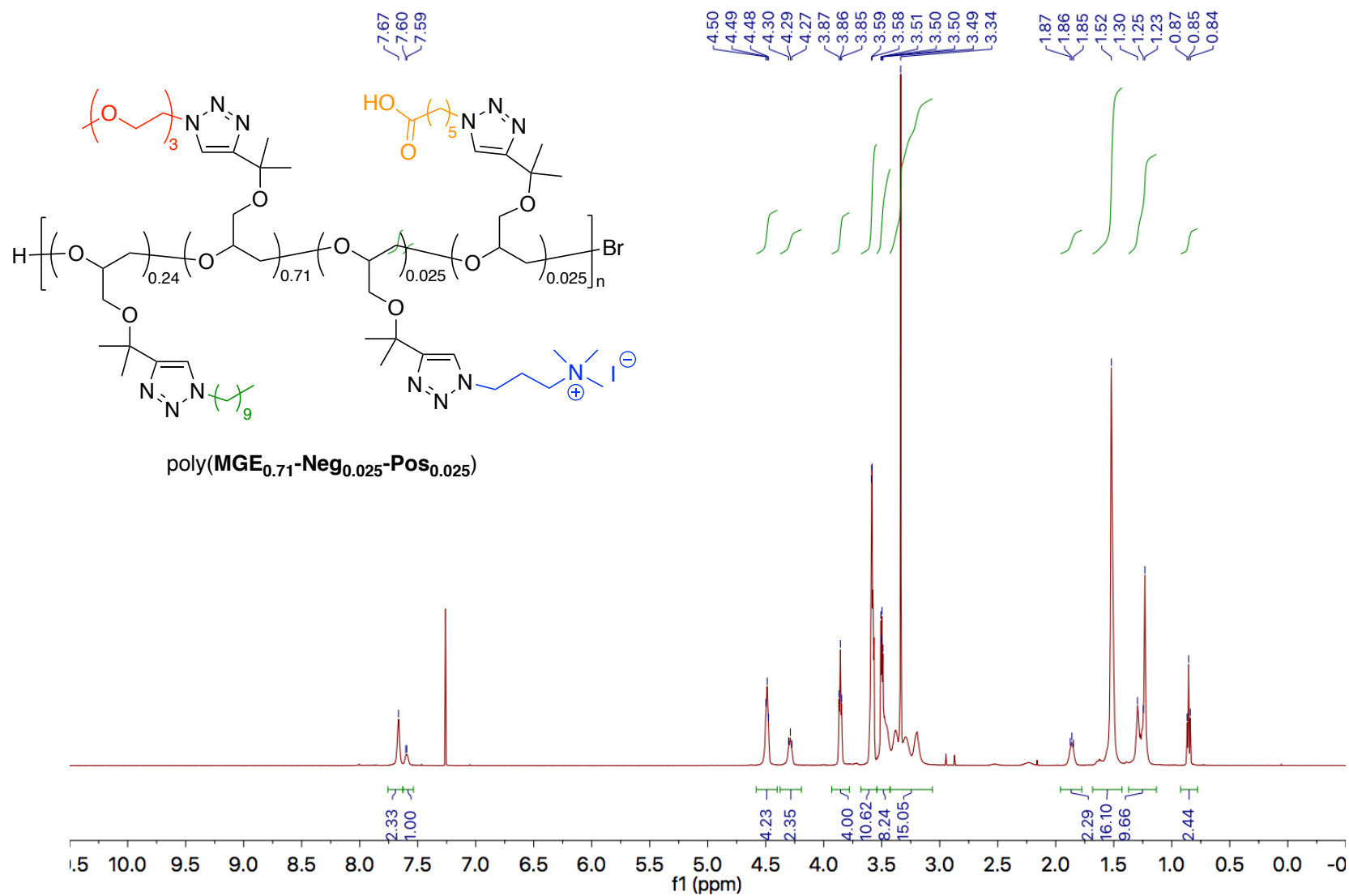


Figure A104. 500 MHz ^1H NMR spectrum of $\text{poly}(\text{MGE}_{0.71}\text{-Neg}_{0.025}\text{-Pos}_{0.025})$ in CDCl_3 .

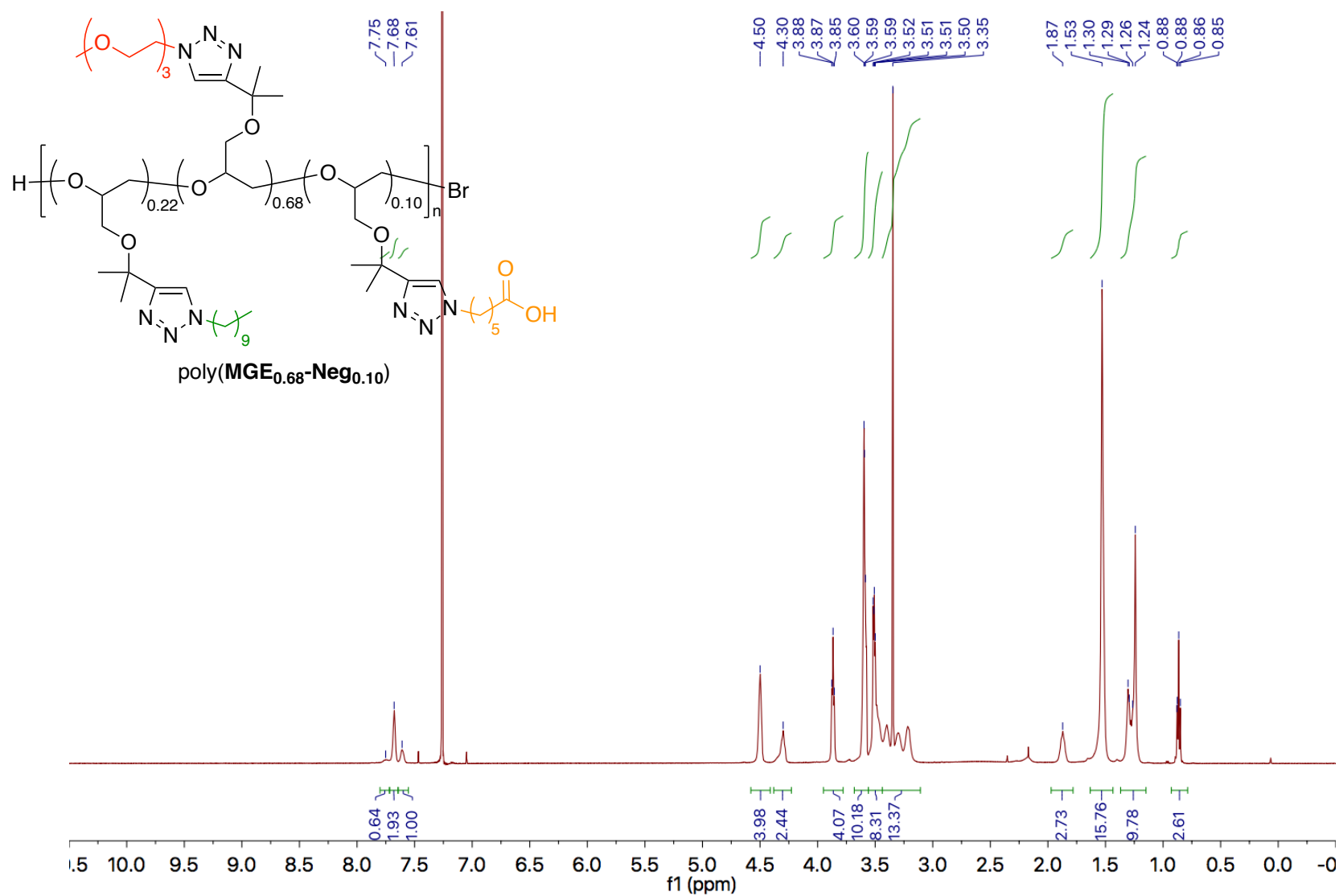


Figure A105. 500 MHz ^1H NMR spectrum of poly(MGE_{0.68}-Neg_{0.10}) in CDCl_3 .

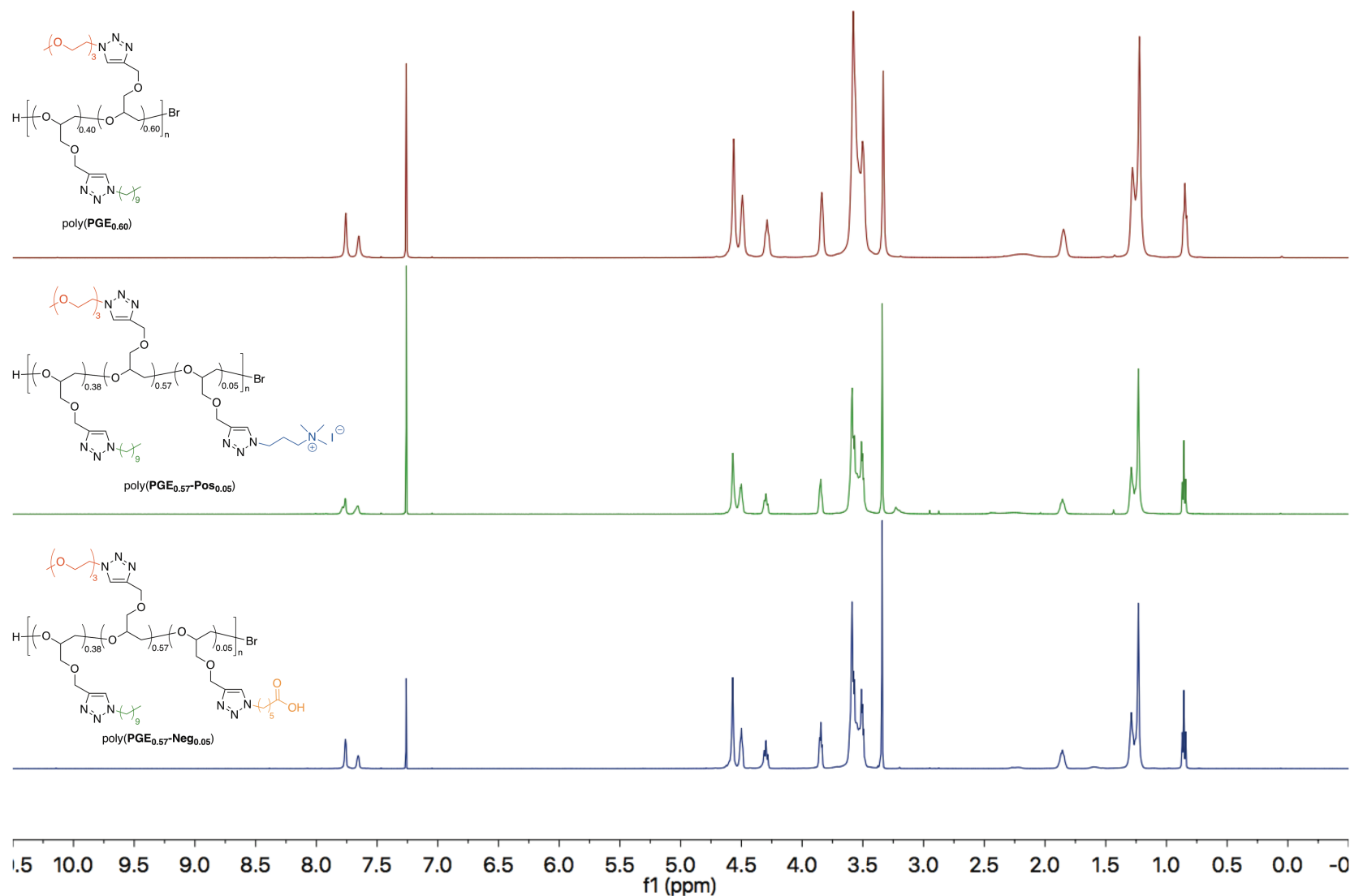


Figure A106. 500 MHz ¹H NMR spectra of poly(PGE_{0.60}) (red), poly(PGE_{0.57}-Pos_{0.05}) (green), and poly(PGE_{0.57}-Neg_{0.05}) (blue) in CDCl₃.

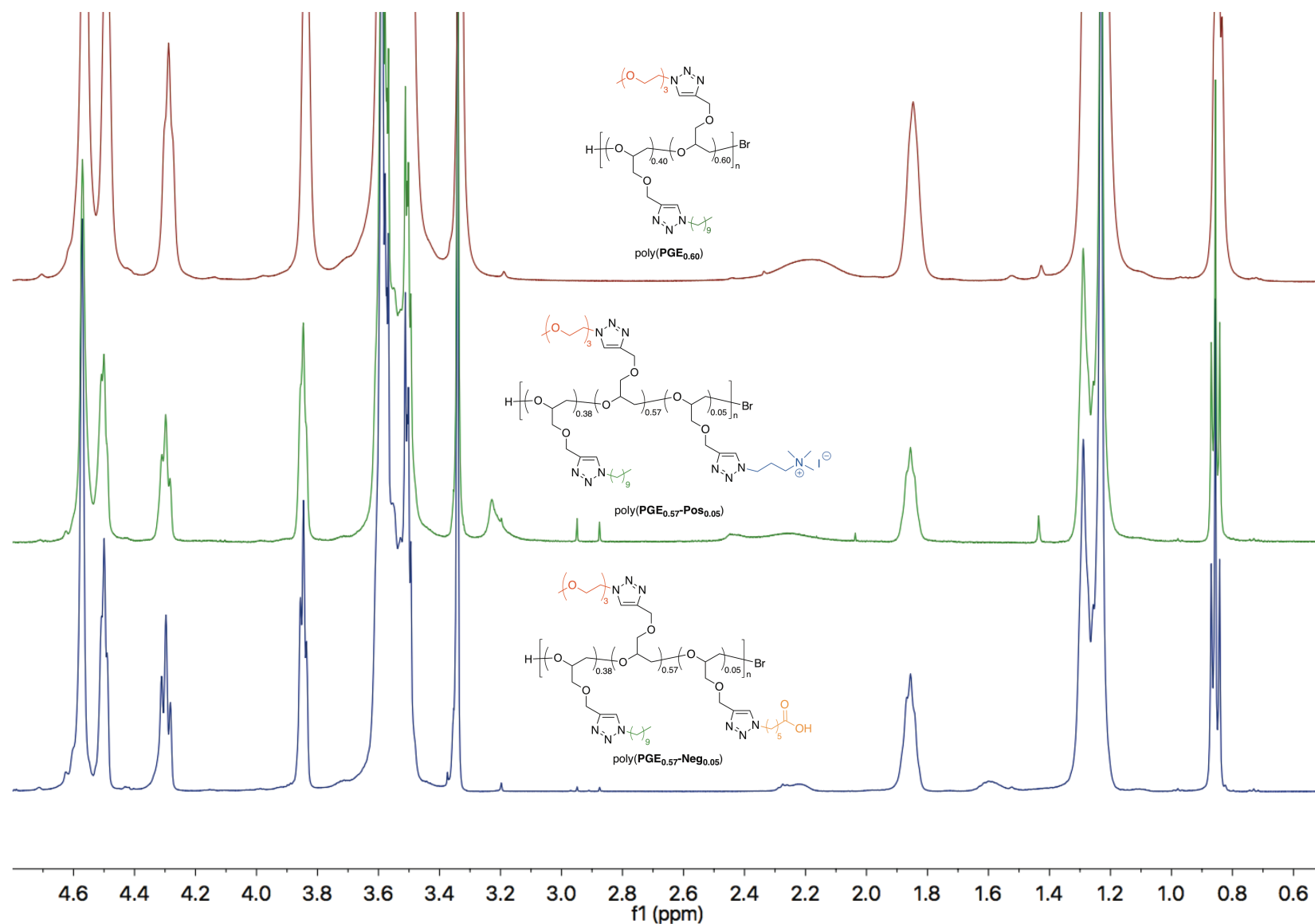


Figure A107. 500 MHz ¹H NMR spectra of poly(PGE_{0.60}) (red), poly(PGE_{0.57}-Pos_{0.05}) (green), and poly(PGE_{0.57}-Neg_{0.05}) (blue) in CDCl₃ in aliphatic region.

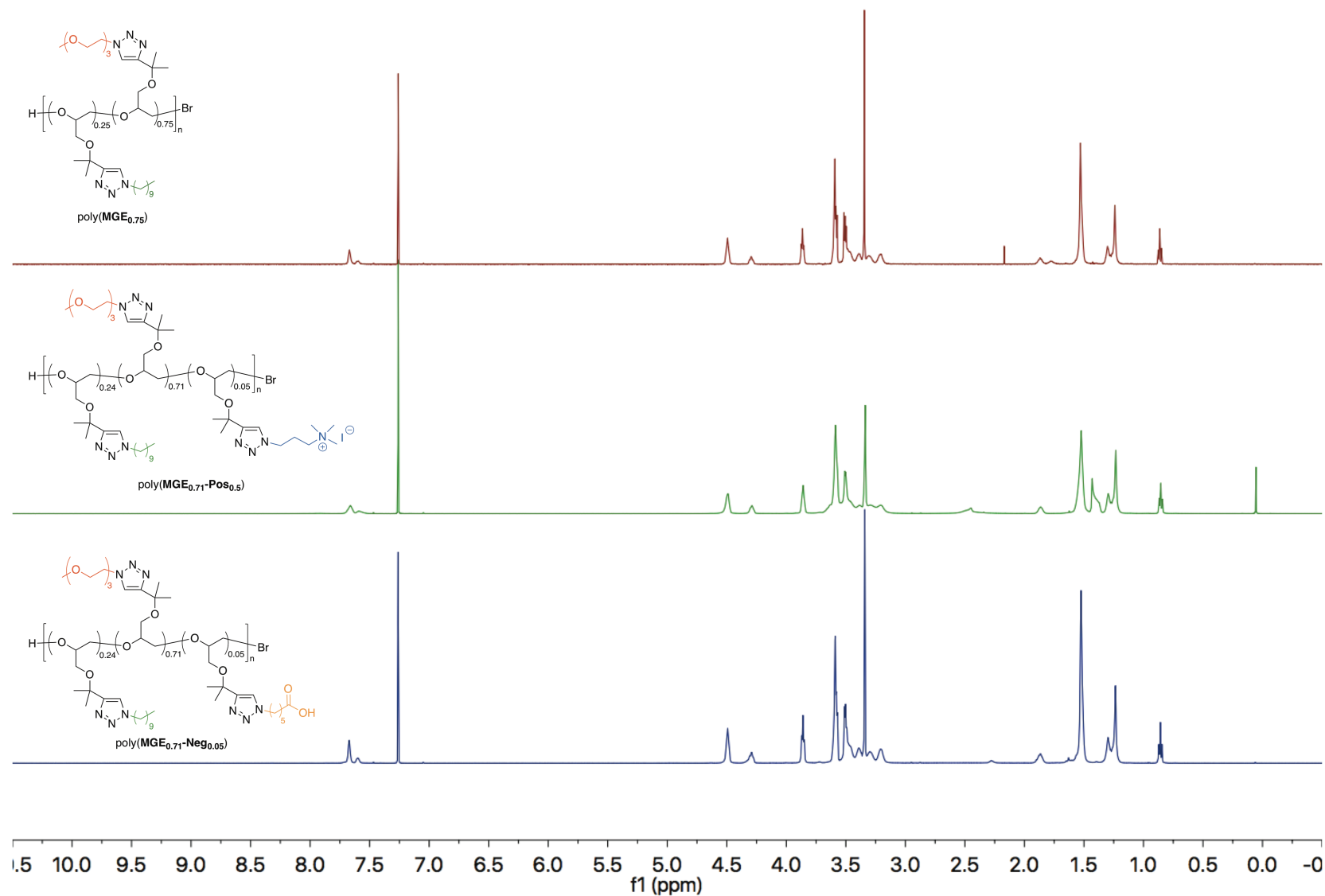


Figure A108. 500 MHz ^1H NMR spectra of poly(MGE_{0.75}) (red), poly(MGE_{0.71}-Pos_{0.05}) (green), and poly(MGE_{0.71}-Neg_{0.05}) (blue) in CDCl_3 .

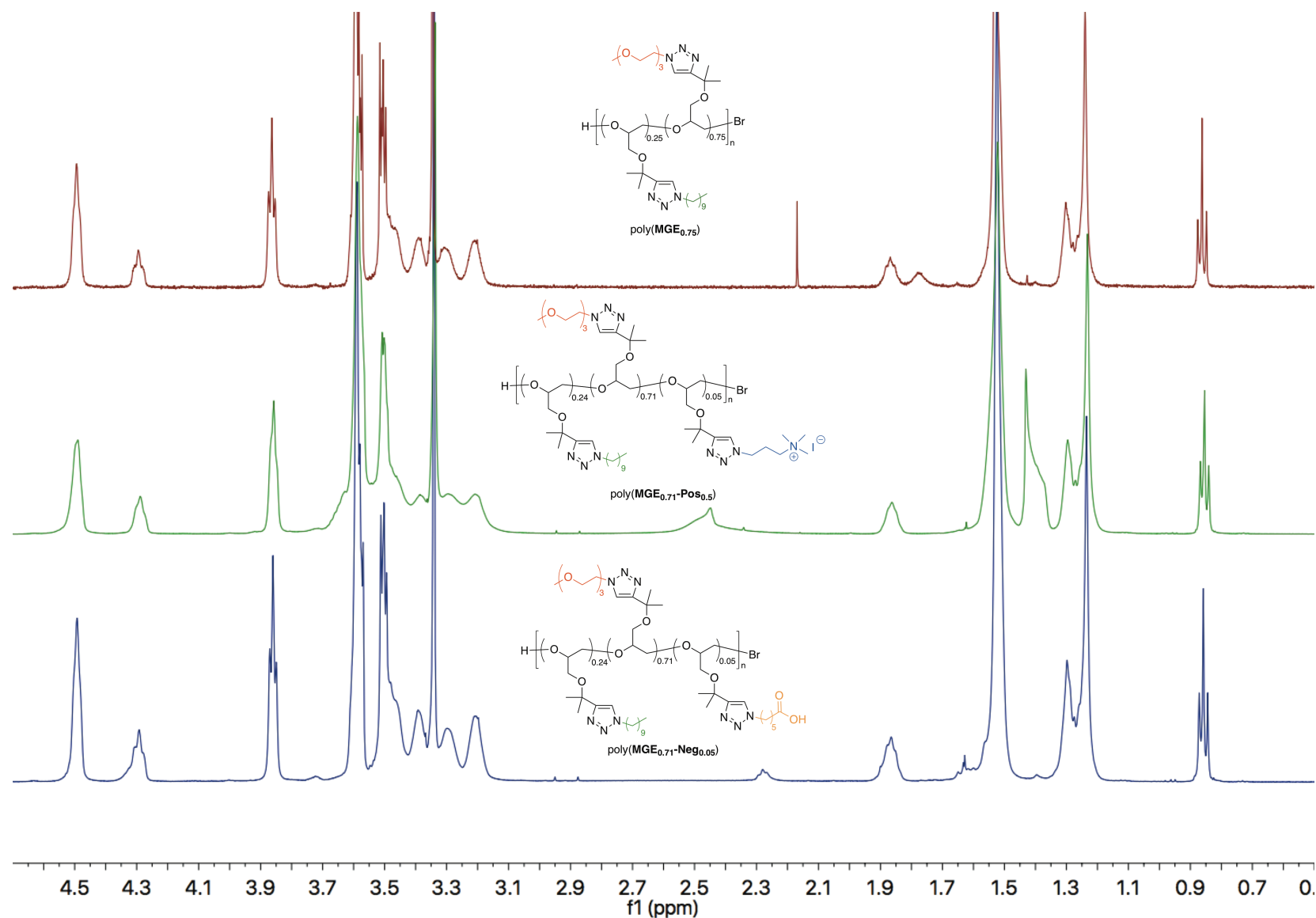


Figure A109. 500 MHz ^1H NMR spectra of poly(MGE_{0.75}) (red), poly(MGE_{0.71}-Pos_{0.05}) (green), and poly(MGE_{0.71}-Neg_{0.05}) (blue) in CDCl_3 in aliphatic region.

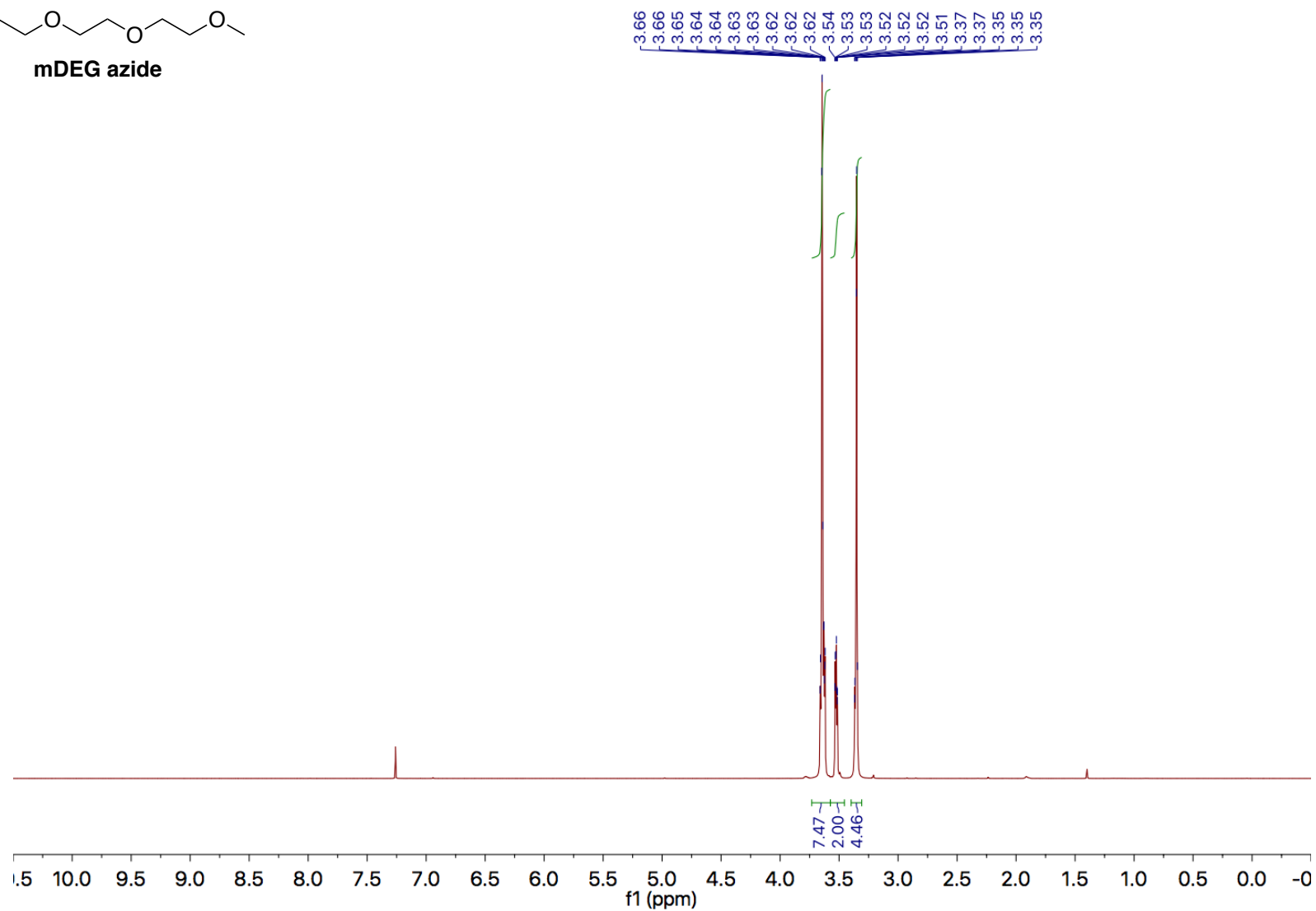
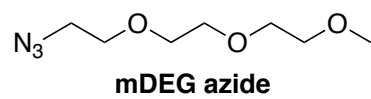


Figure A110. 500 MHz ^1H NMR spectrum of **mDEG azide** in CDCl_3 .

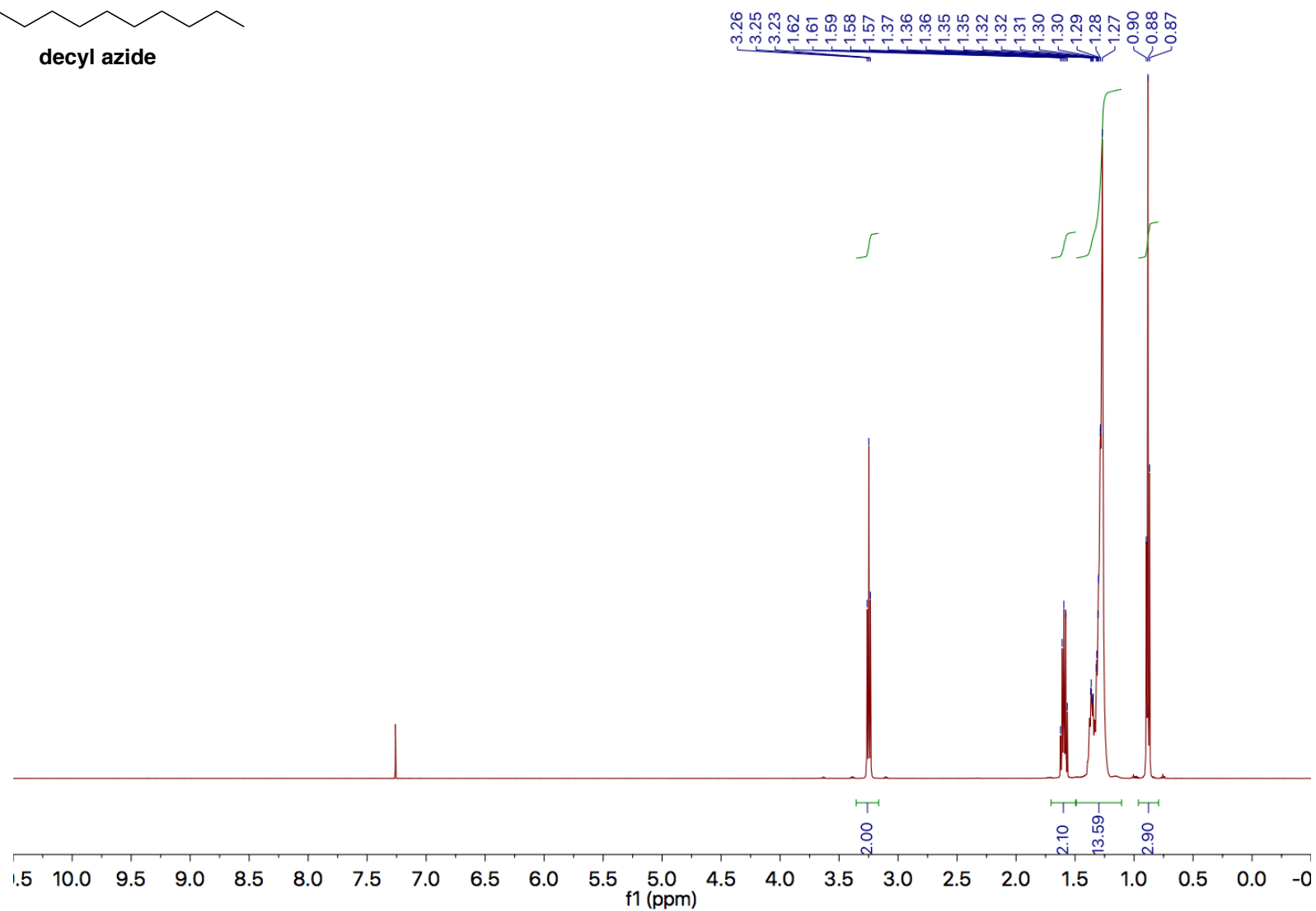
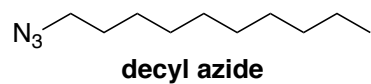
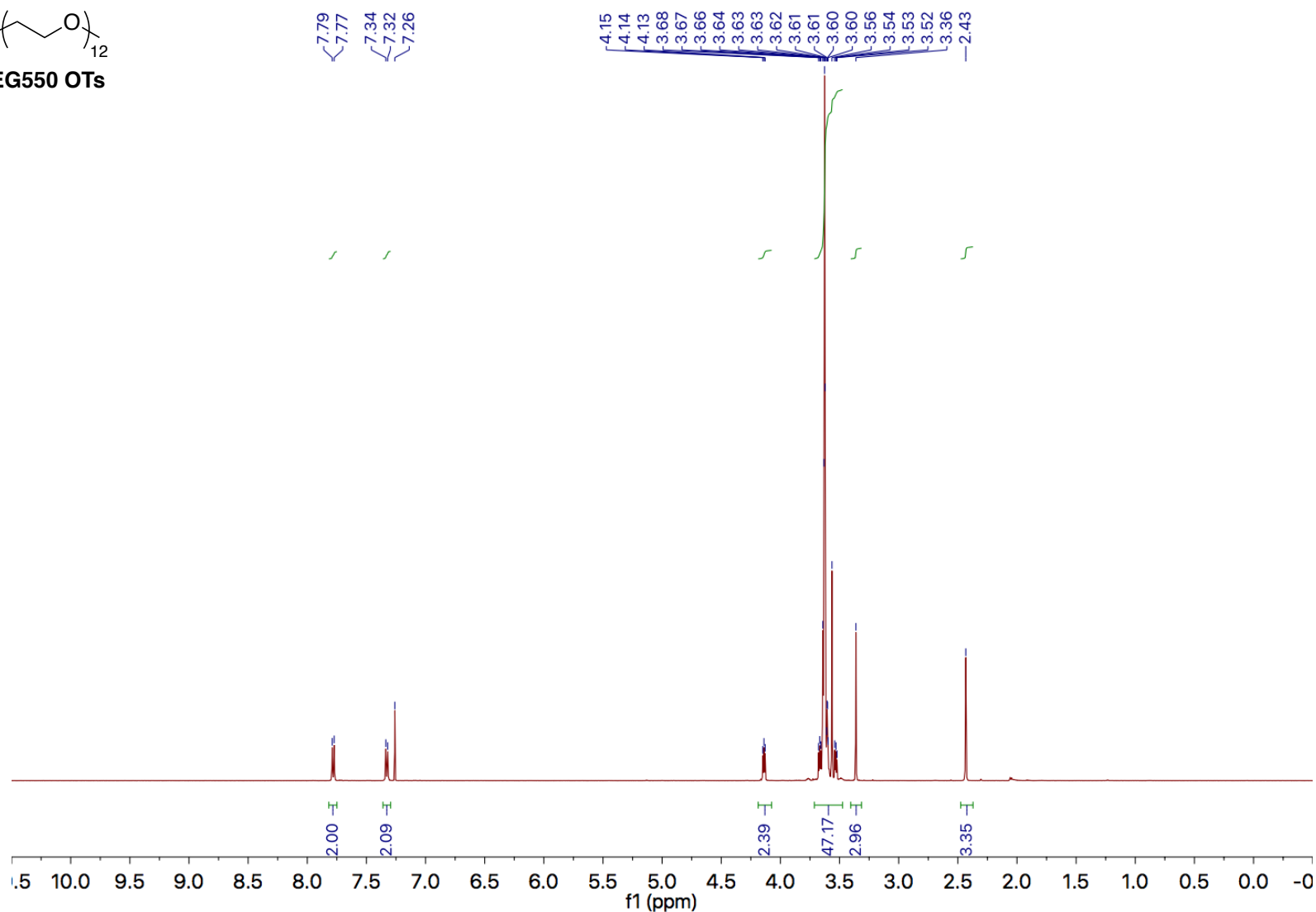


Figure A111. 500 MHz ^1H NMR spectrum of **decyl azide** in CDCl_3 .



226

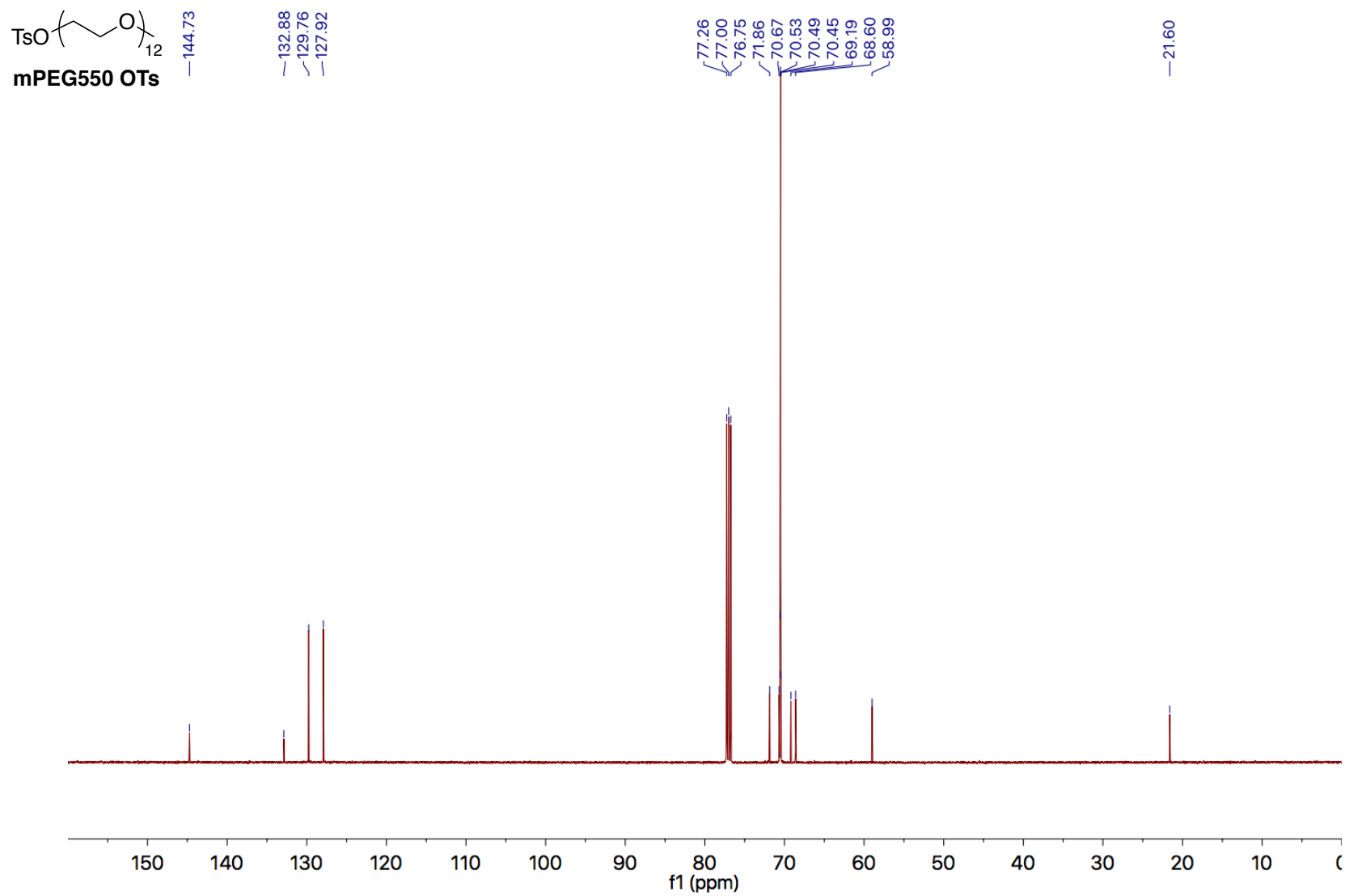


Figure A113. 125 MHz ^{13}C NMR spectrum of **mPEG550 OTs** in CDCl_3 .

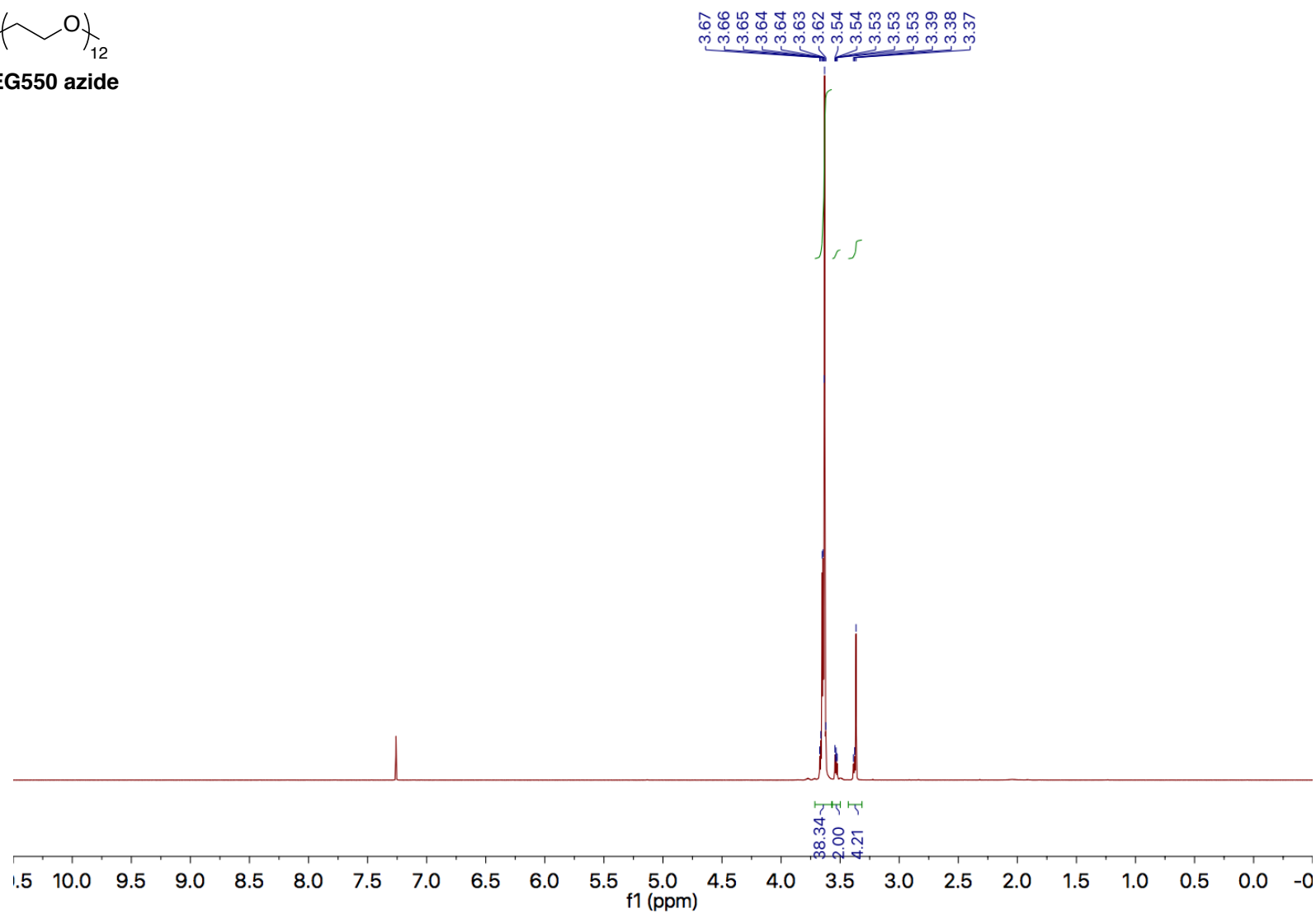
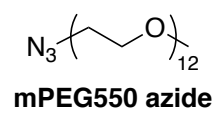


Figure A114. 500 MHz ¹H NMR spectrum of **mPEG550 azide** in CDCl₃.

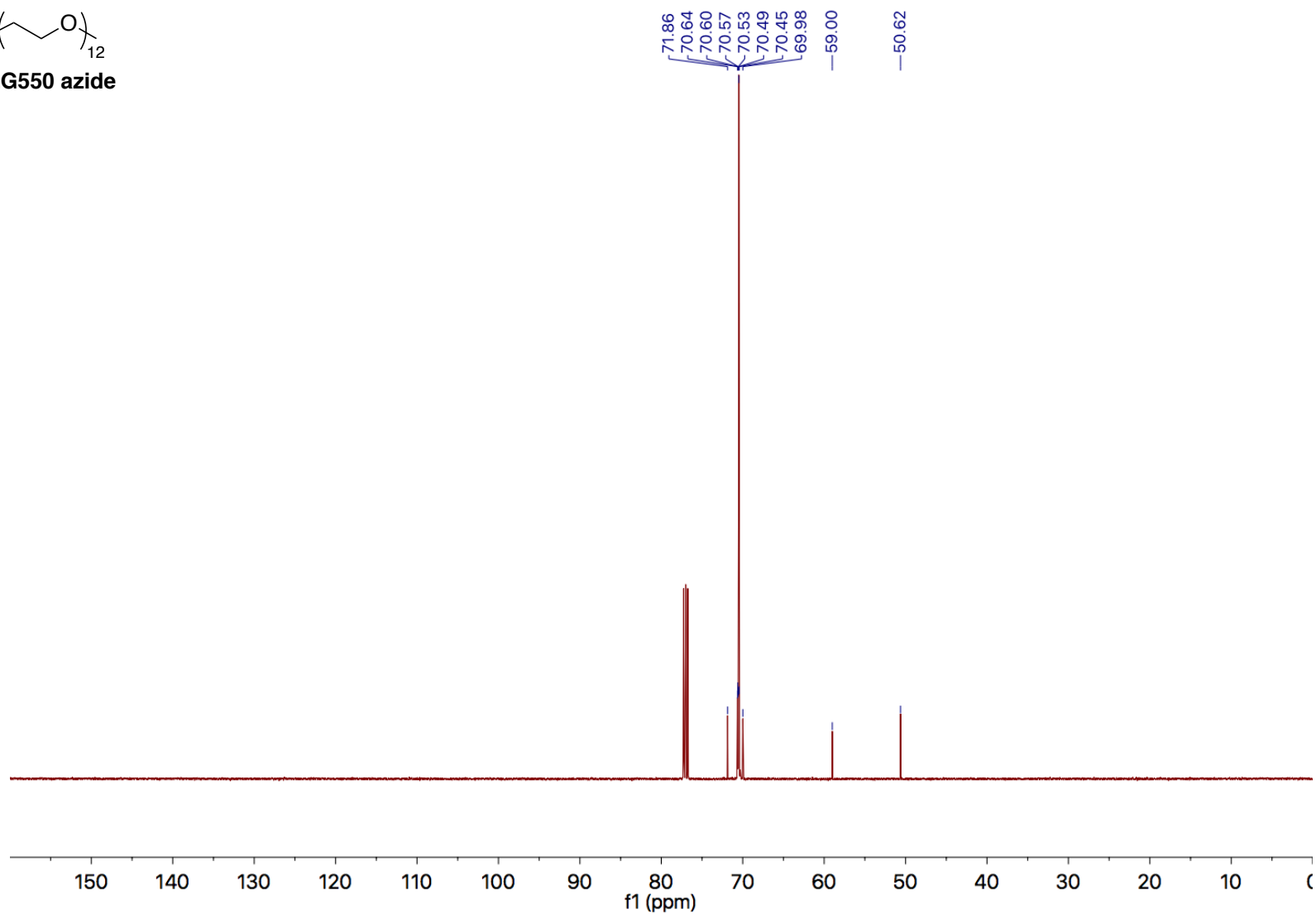
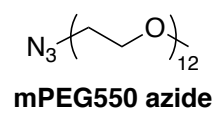


Figure A115. 125 MHz ^{13}C NMR spectrum of **mPEG550 azide** in CDCl_3 .

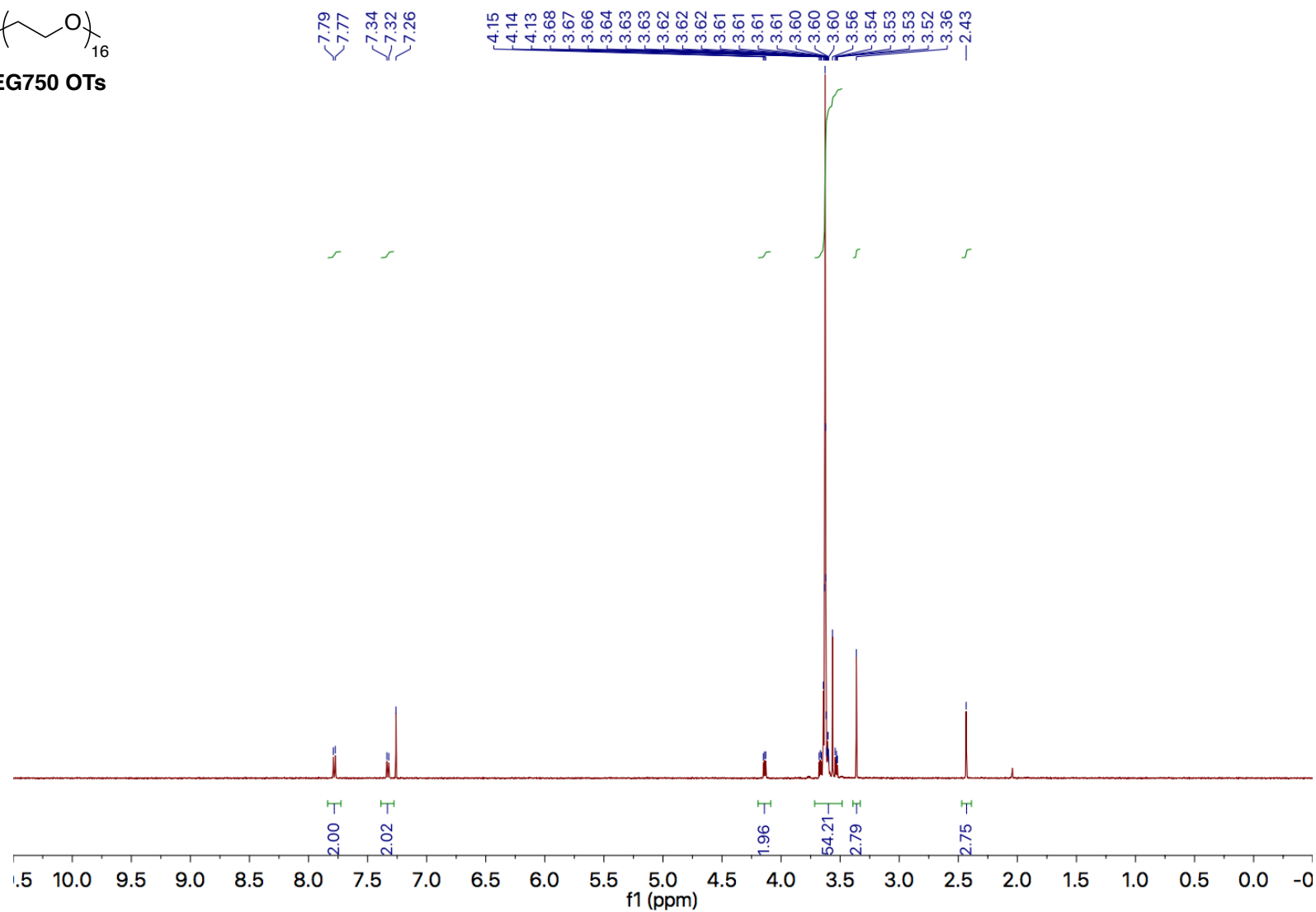
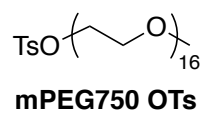
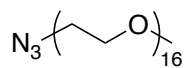


Figure A116. 500 MHz ^1H NMR spectrum of **mPEG750 OTs** in CDCl_3 .



mPEG750 azide

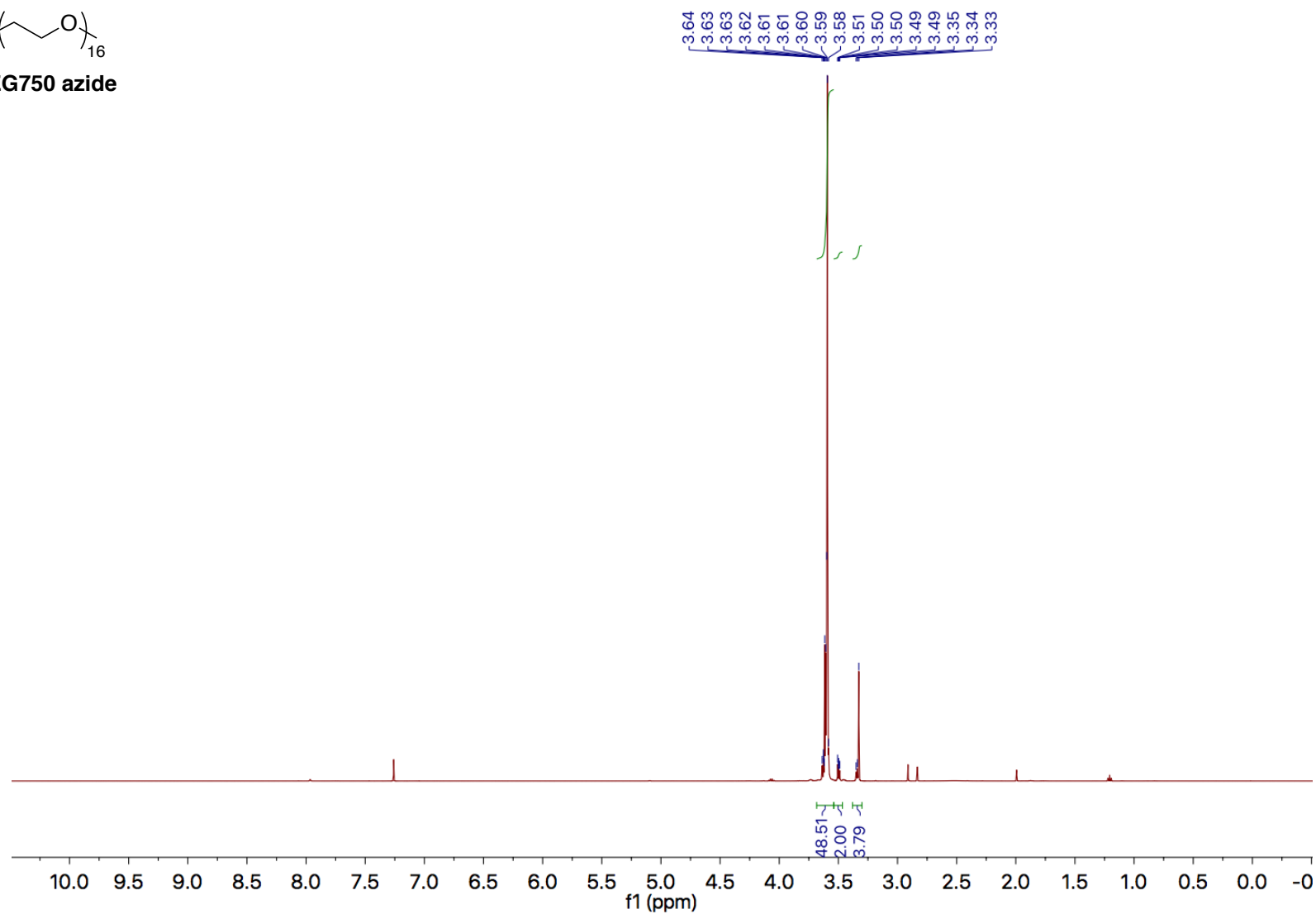


Figure A117. 500 MHz ¹H NMR spectrum of **mPEG750 azide** in CDCl₃.

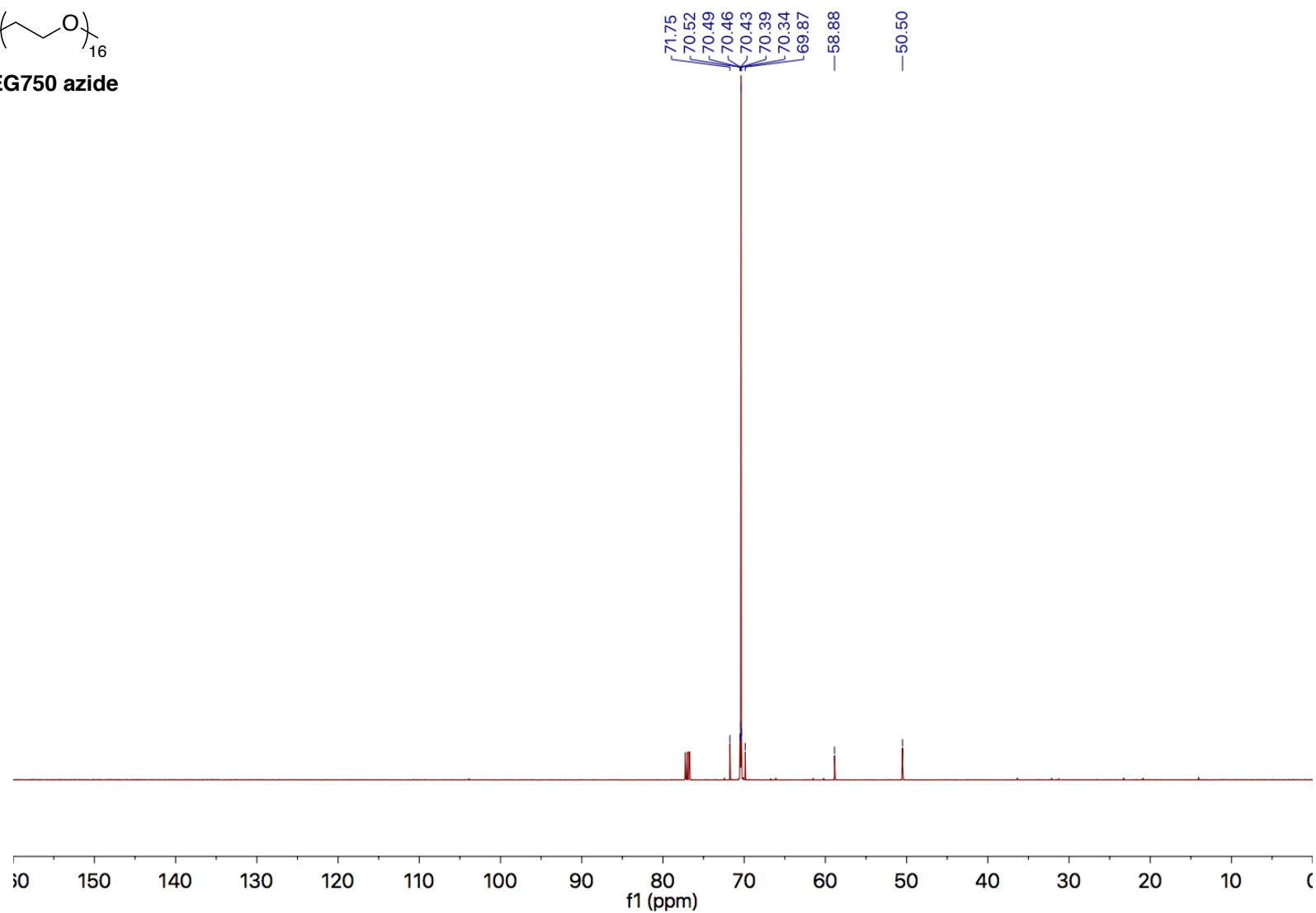
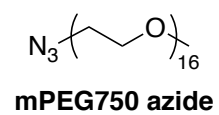
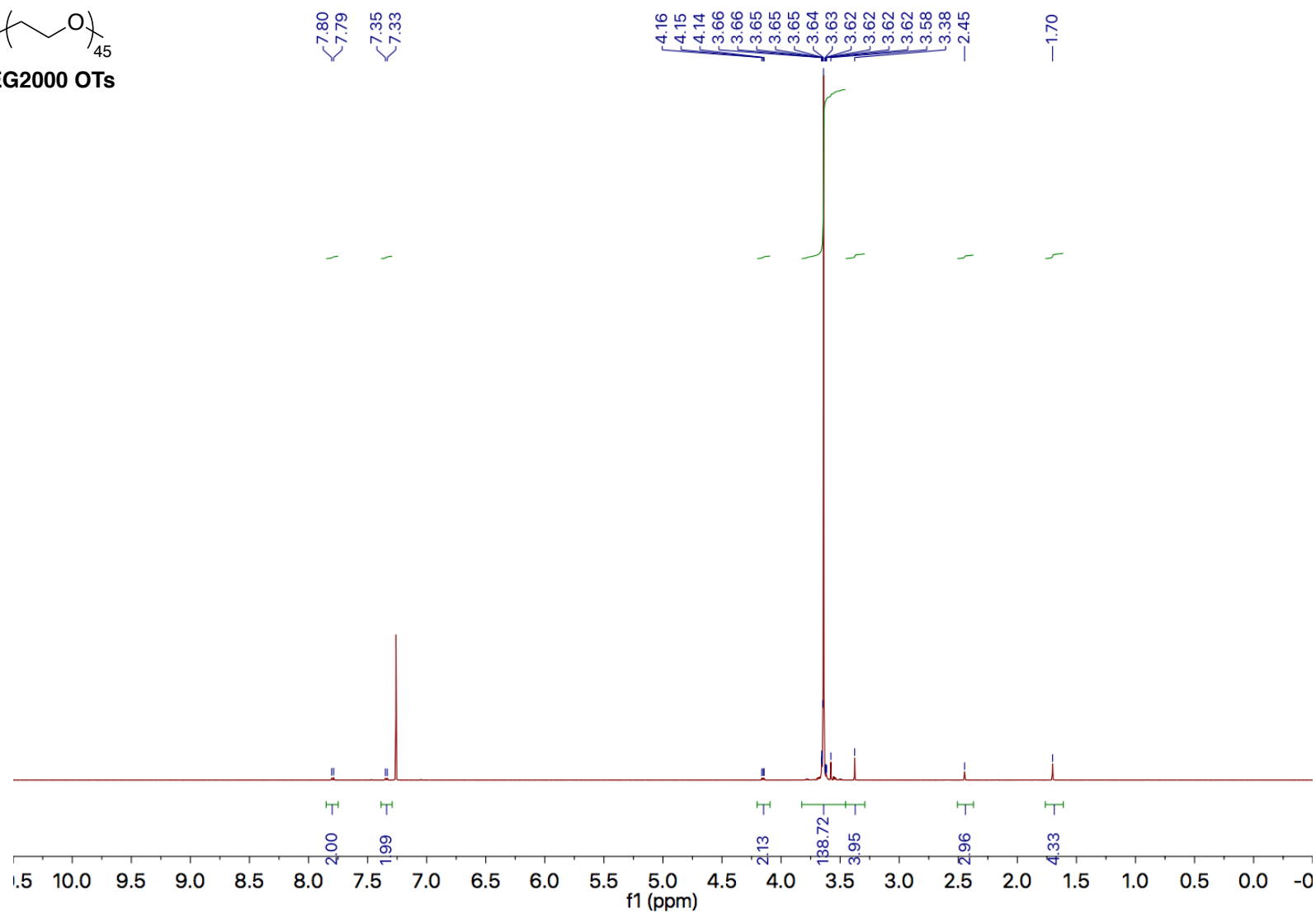
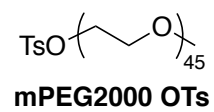


Figure A118. 125 MHz ^{13}C NMR spectrum of **mPEG750 azide** in CDCl_3 .



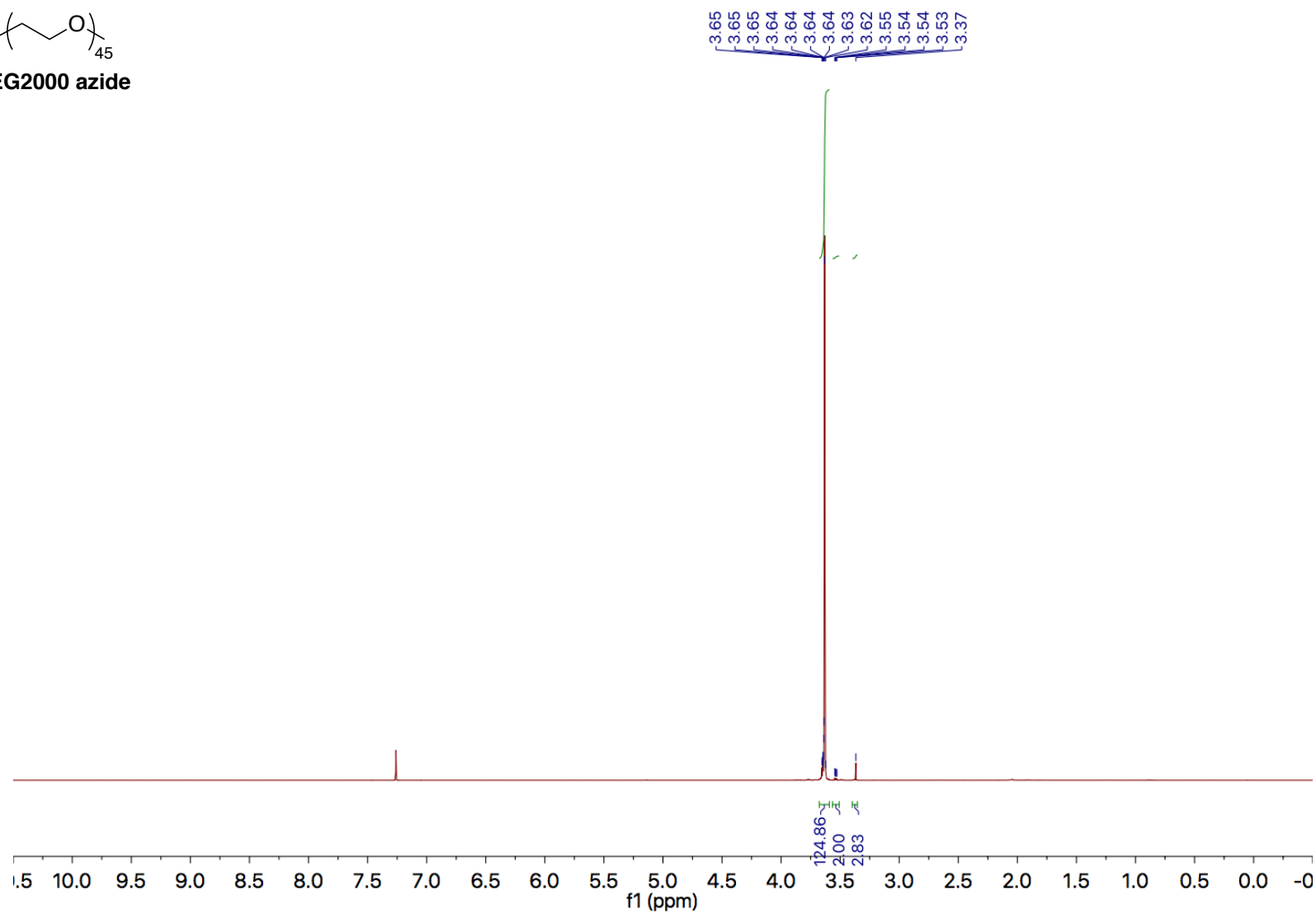
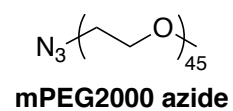


Figure A120. 500 MHz ^1H NMR spectrum of **mPEG2000 azide** in CDCl_3 .

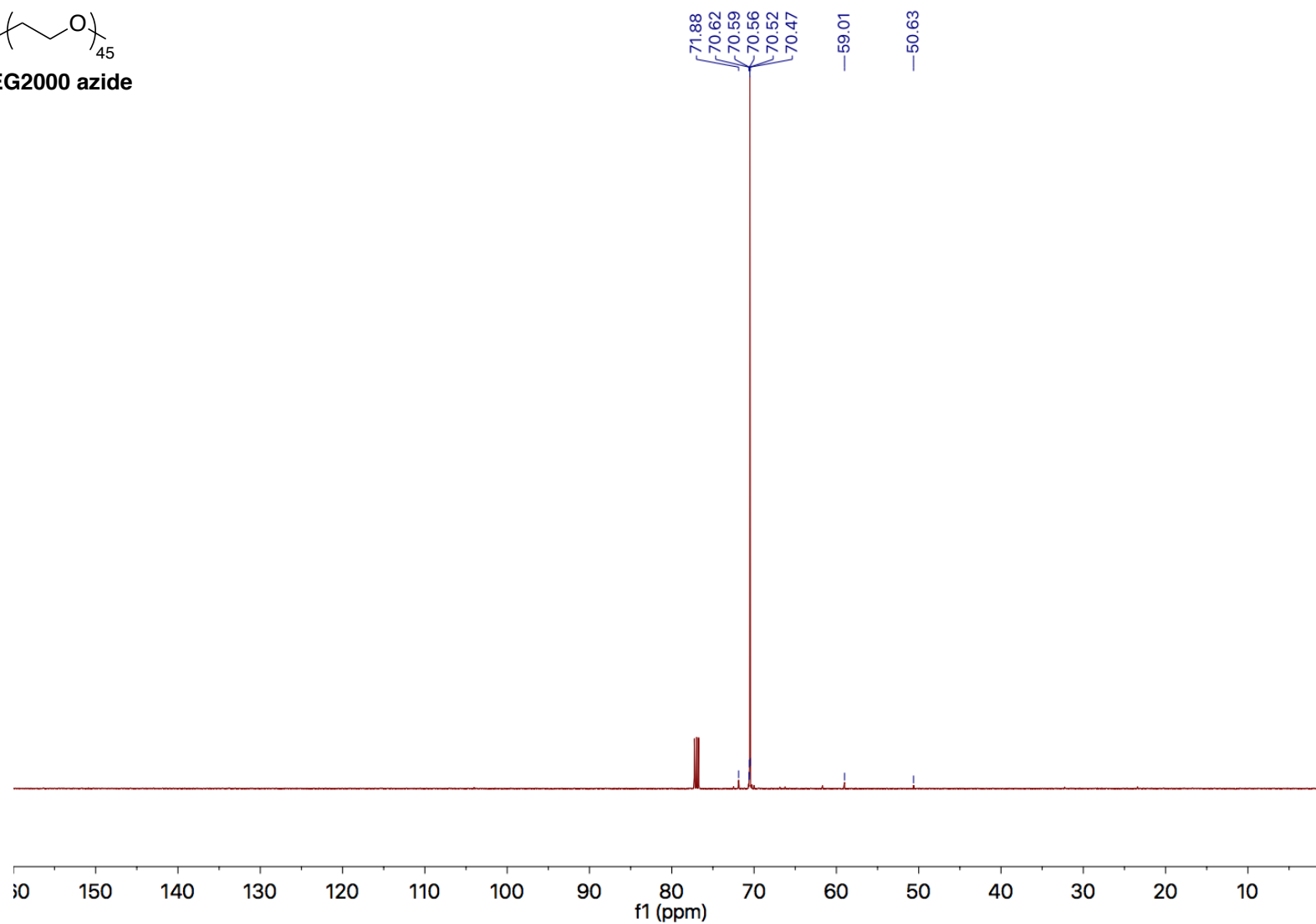
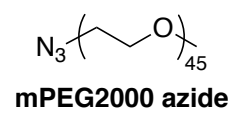


Figure A121. 125 MHz ^{13}C NMR spectrum of **mPEG2000 azide** in CDCl_3 .

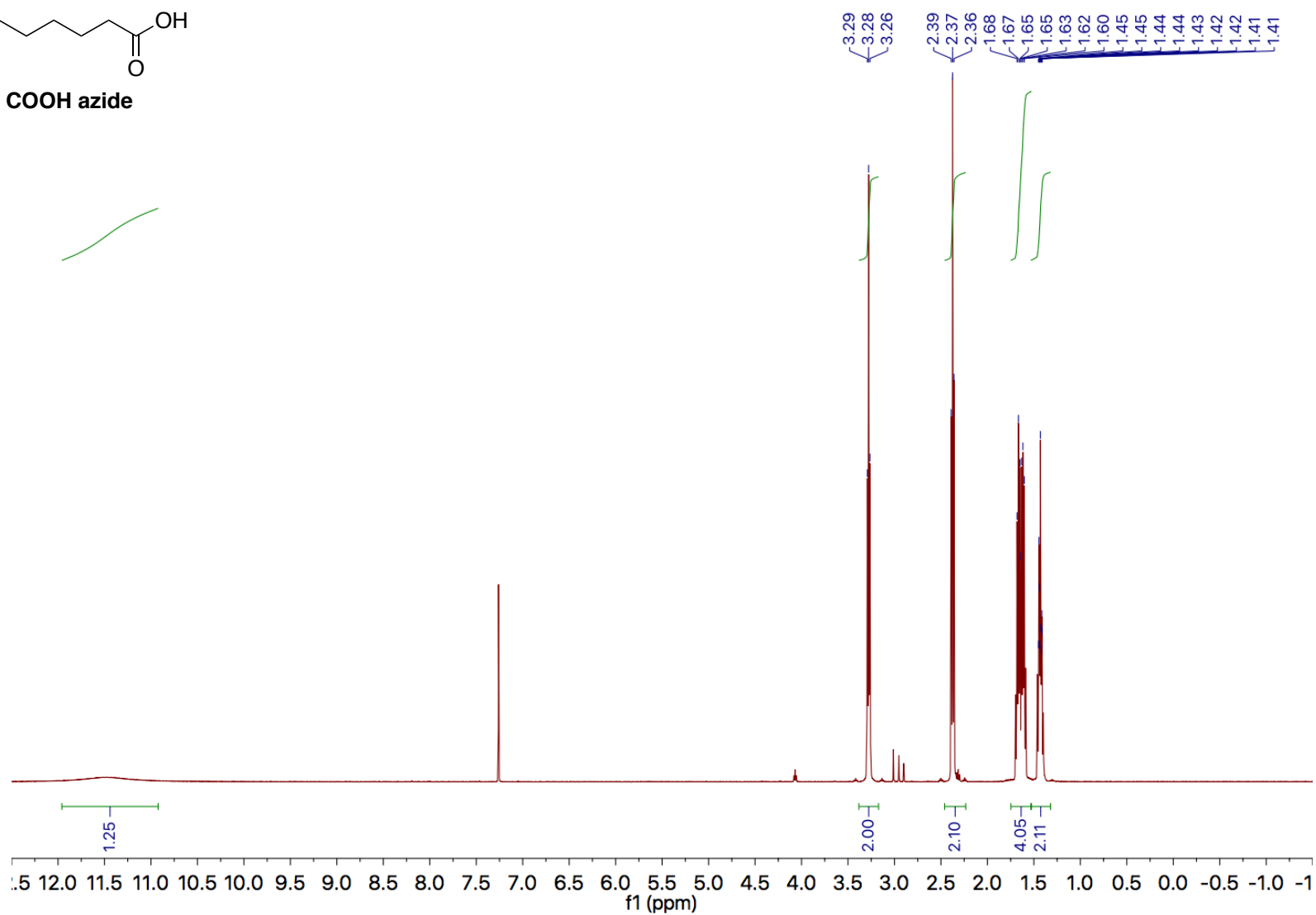
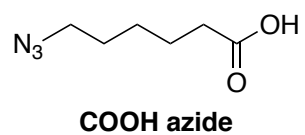


Figure A122. 500 MHz ^1H NMR spectrum of **COOH azide** in CDCl_3 .

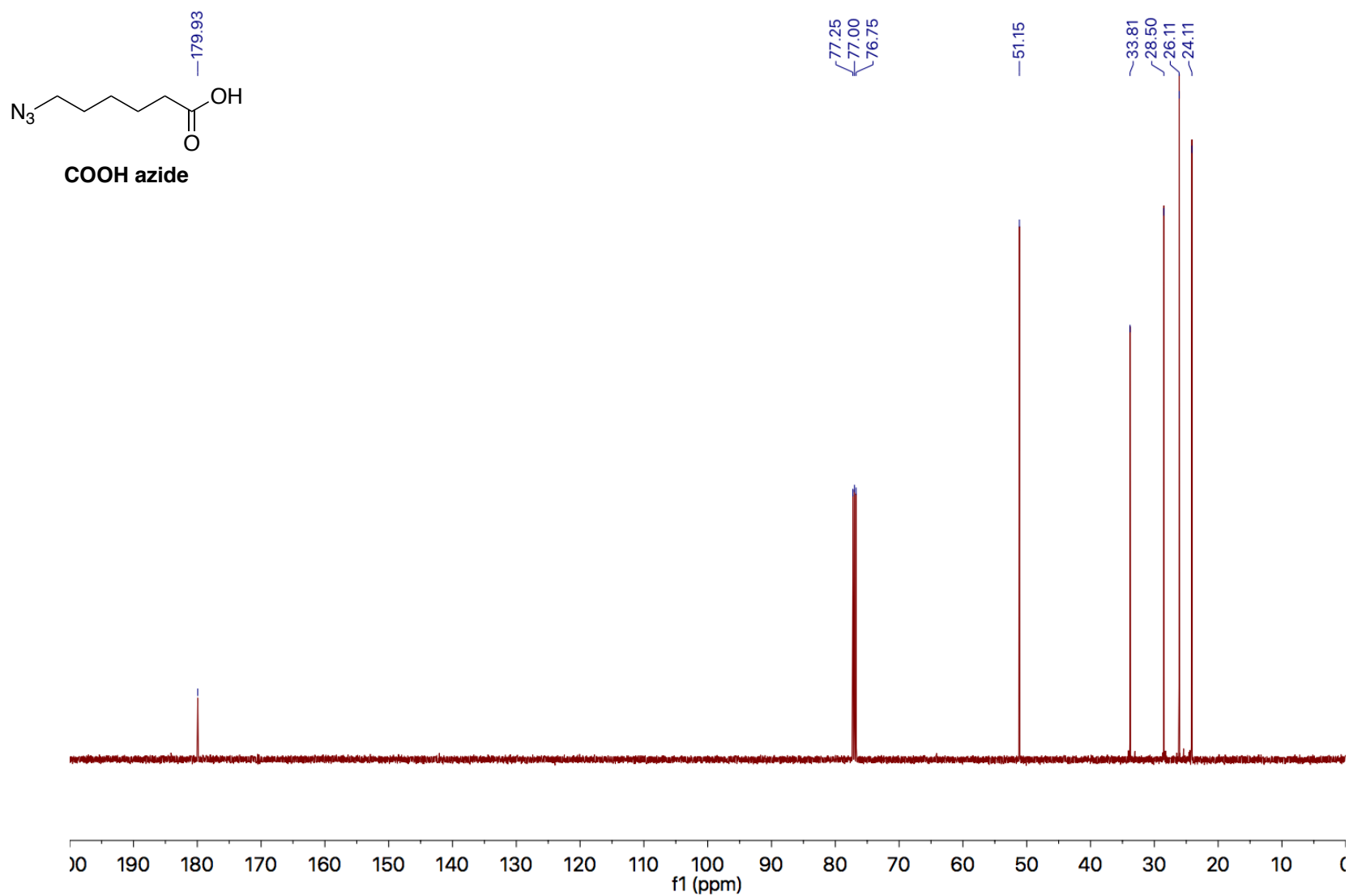


Figure A123. 125 MHz ^{13}C NMR spectrum of **COOH azide** in CDCl_3 .

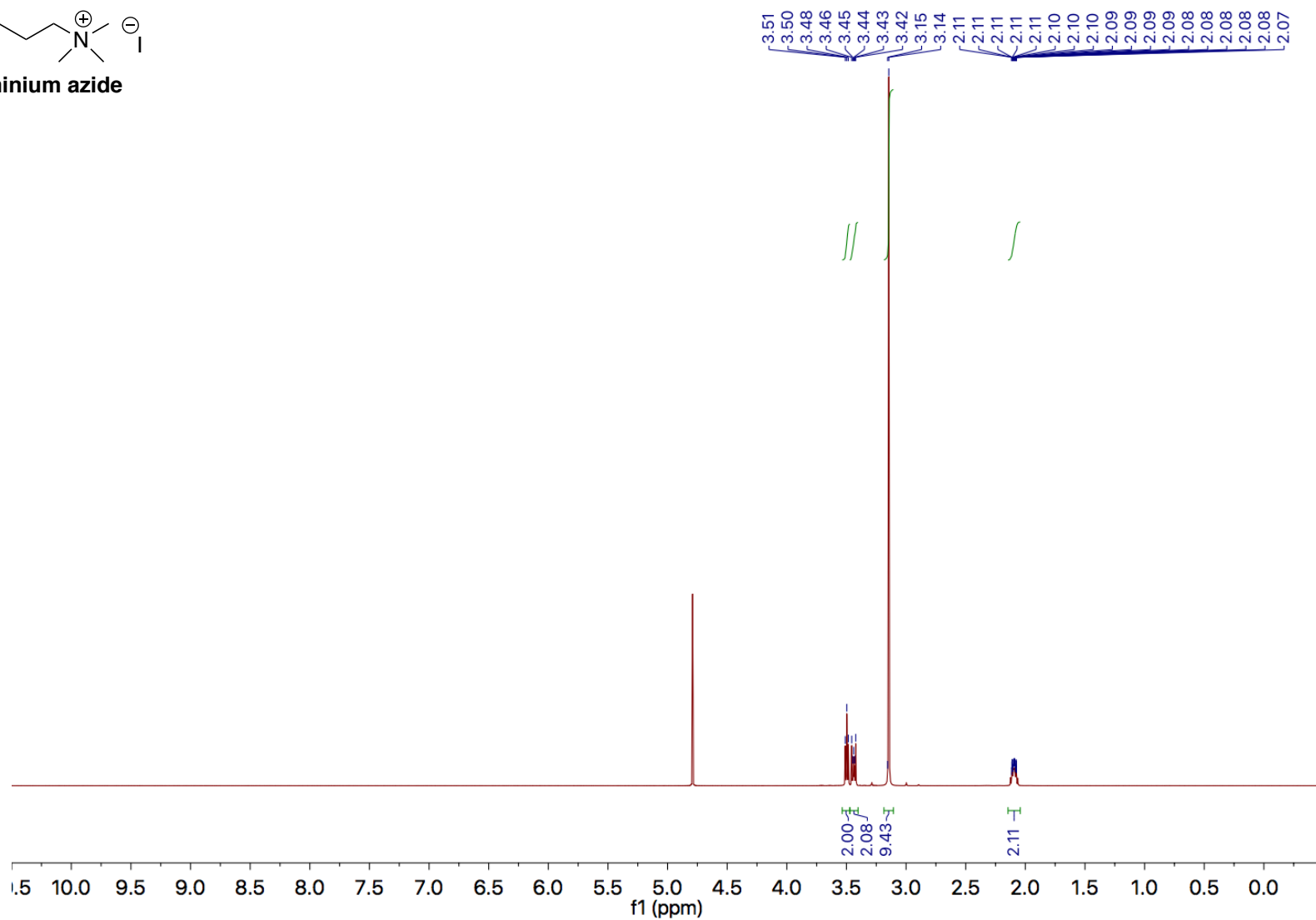
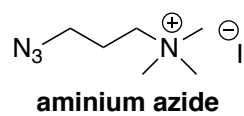


Figure A124. 500 MHz ^1H NMR spectrum of **aminium azide** in D_2O .

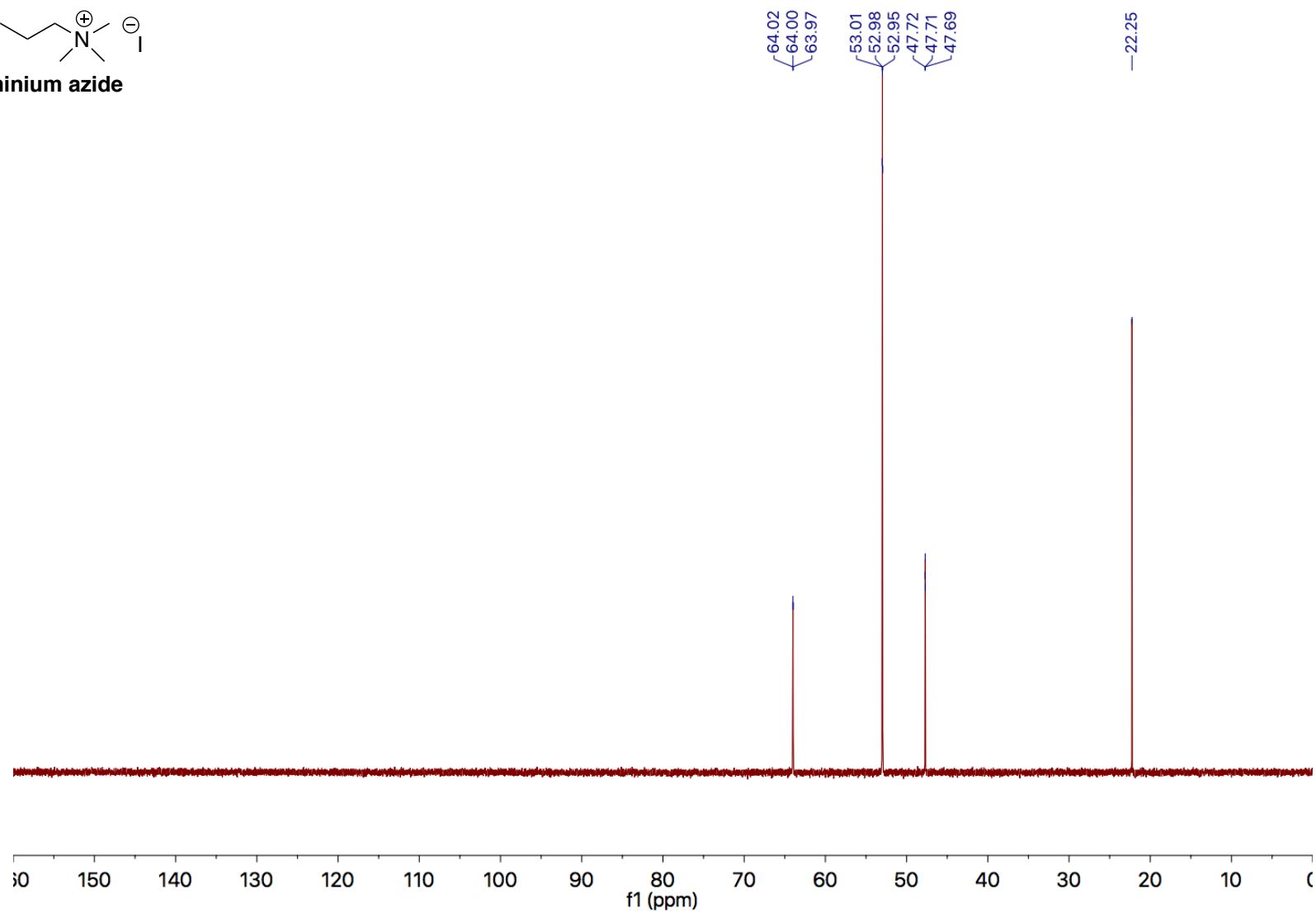
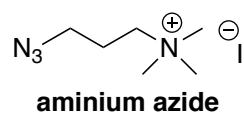


Figure A125. 125 MHz ^{13}C NMR spectrum of **aminium azide** in D_2O .

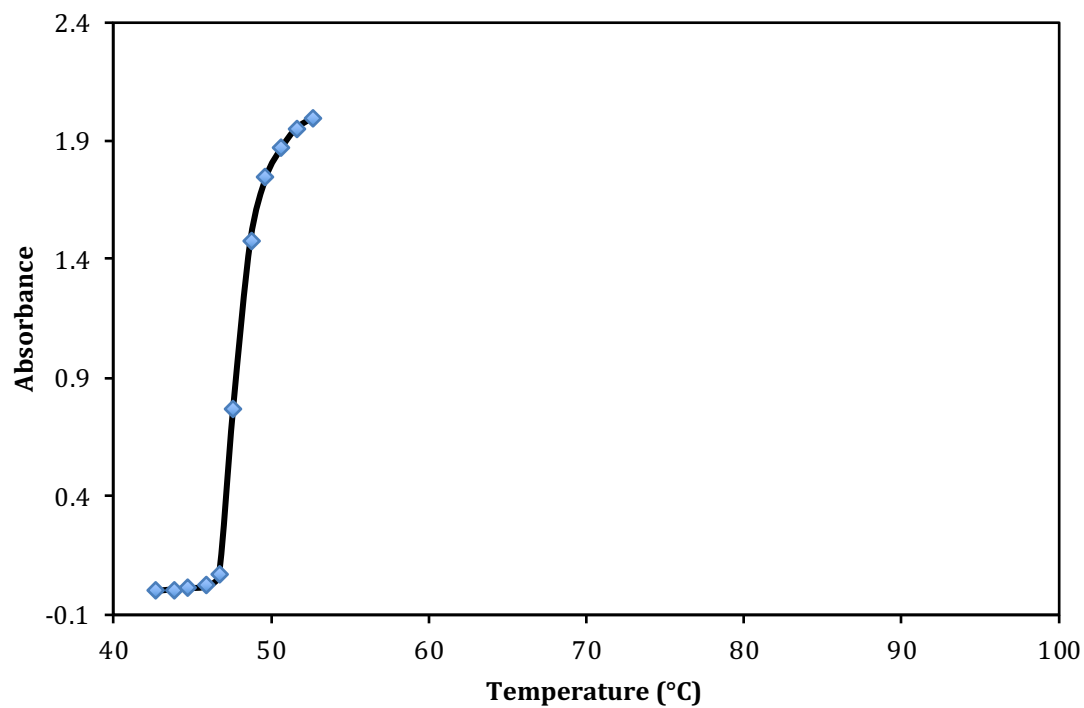


Figure A126. Study of LCST behavior of poly(PGE_{0.65}) via UV-vis.

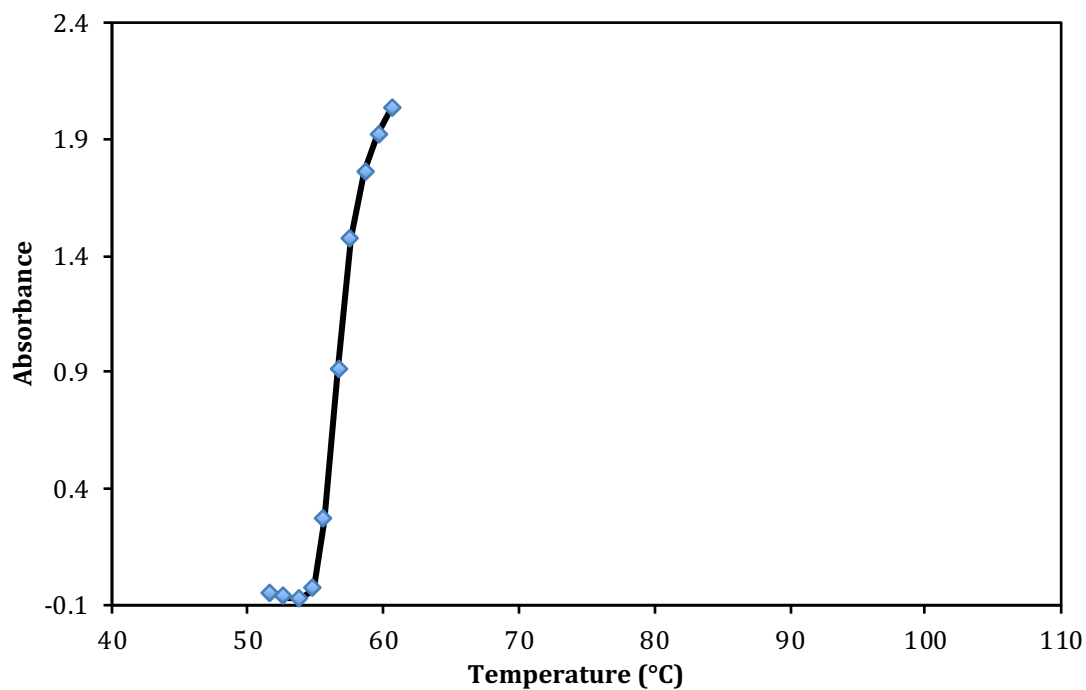


Figure A127. Study of LCST behavior of poly(PGE_{0.70}) via UV-vis.

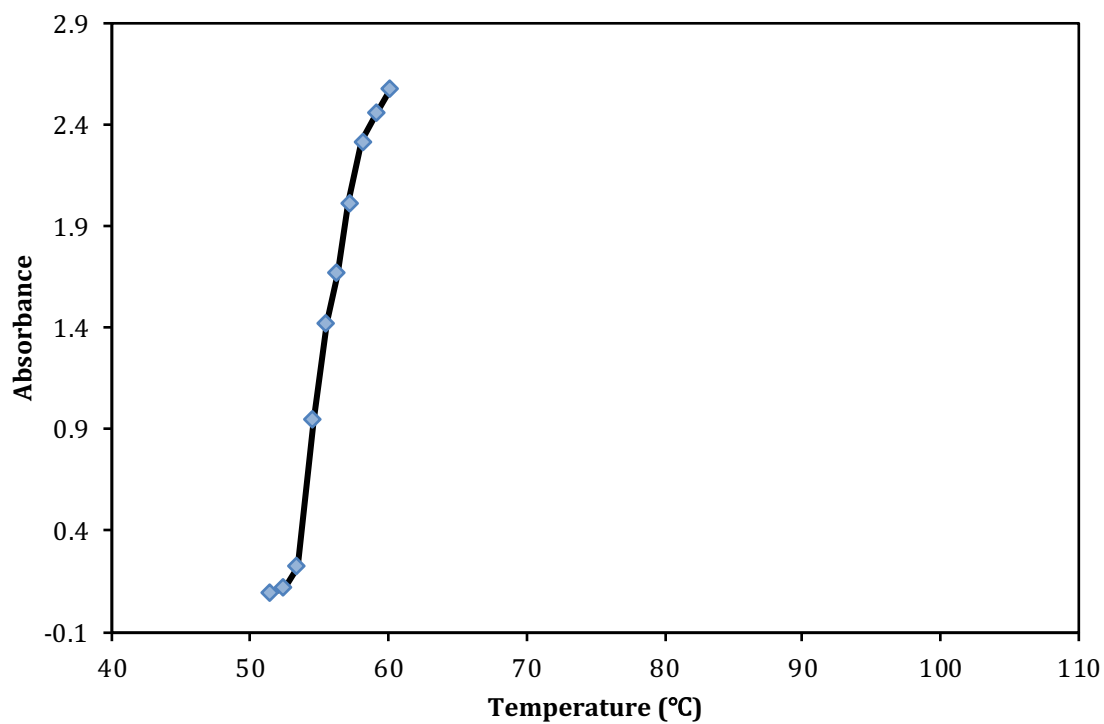


Figure A128. Study of LCST behavior of poly(PGE_{0.75}) via UV-vis.

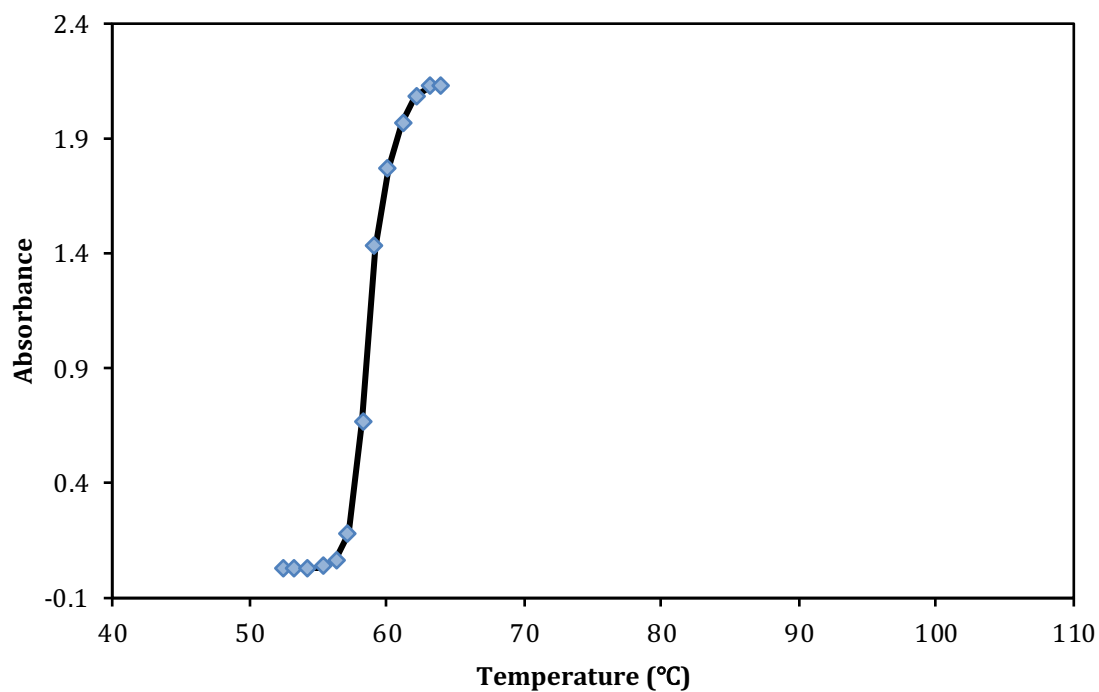


Figure A129. Study of LCST behavior of poly(PGE_{0.80}) via UV-vis.

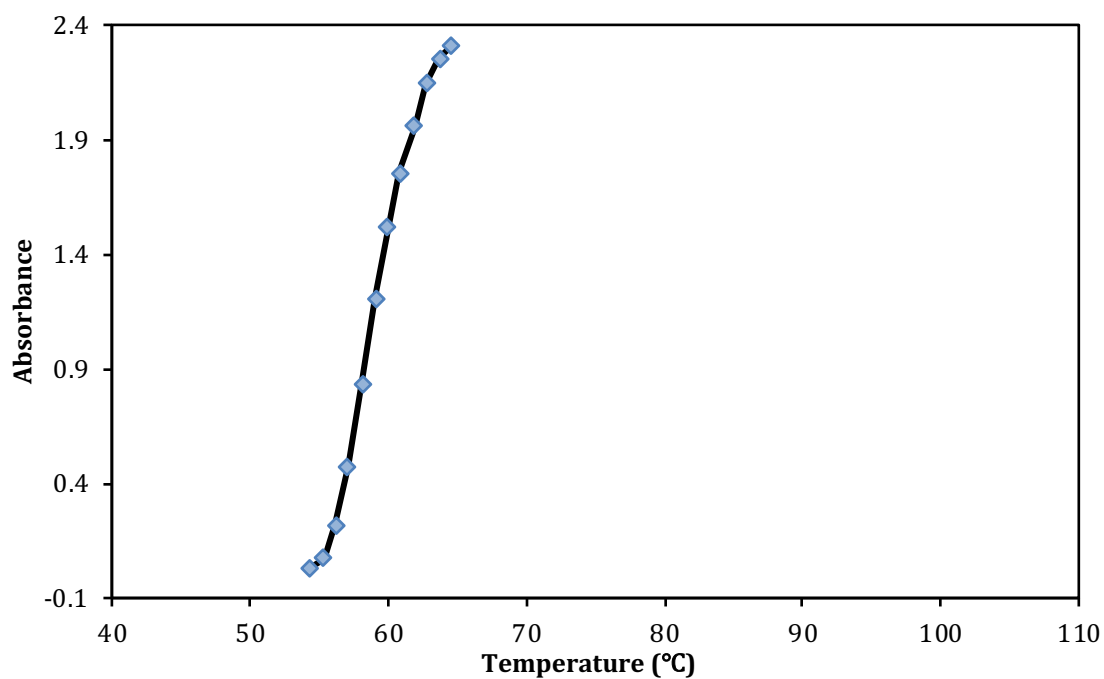


Figure A130. Study of LCST behavior of poly(PGE_{0.85}) via UV-vis.

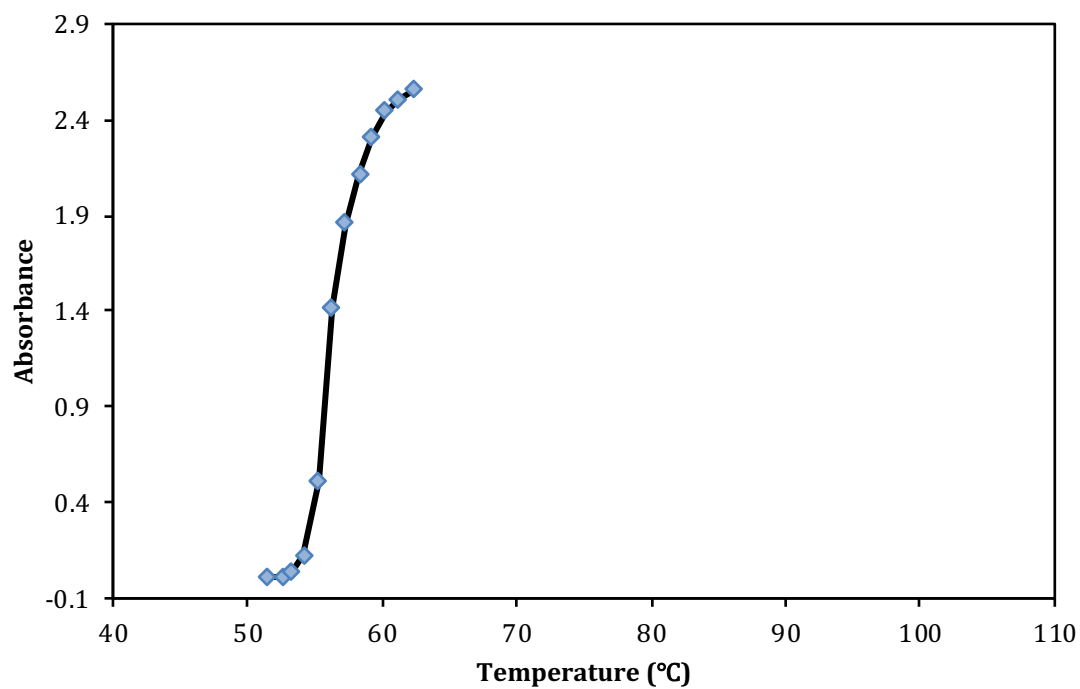


Figure A131. Study of LCST behavior of poly(PGE_{0.90}) via UV-vis.

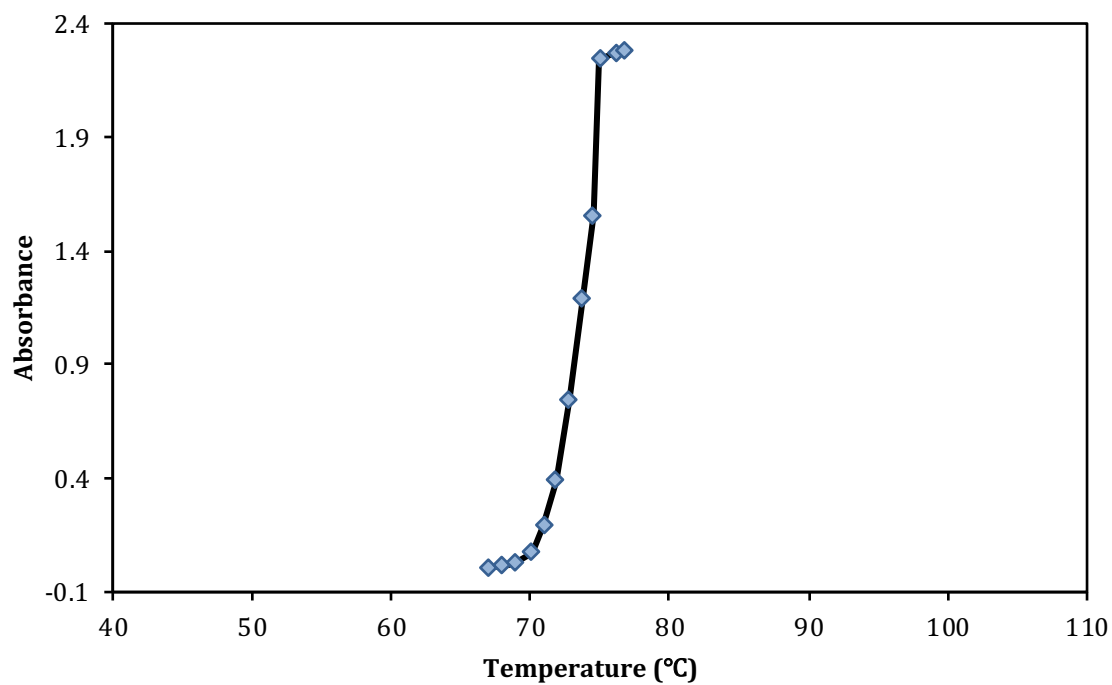


Figure A132. Study of LCST behavior of poly(PGE_{0.95}) via UV-vis.

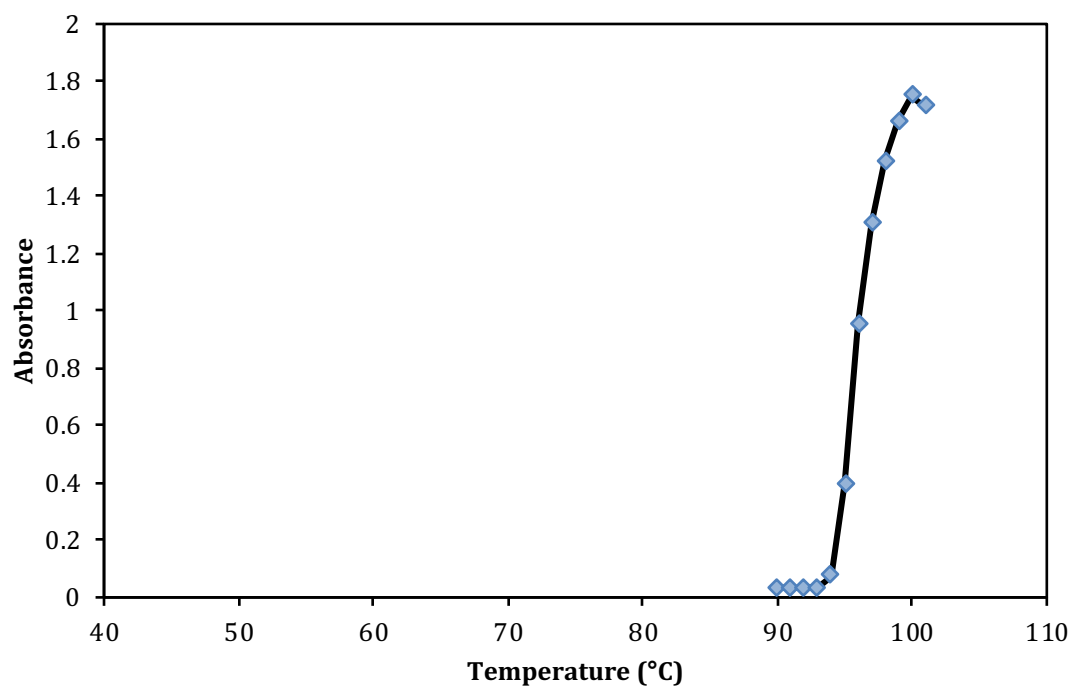


Figure A133. Study of LCST behavior of poly(PGE_{1.0}) via UV-vis.

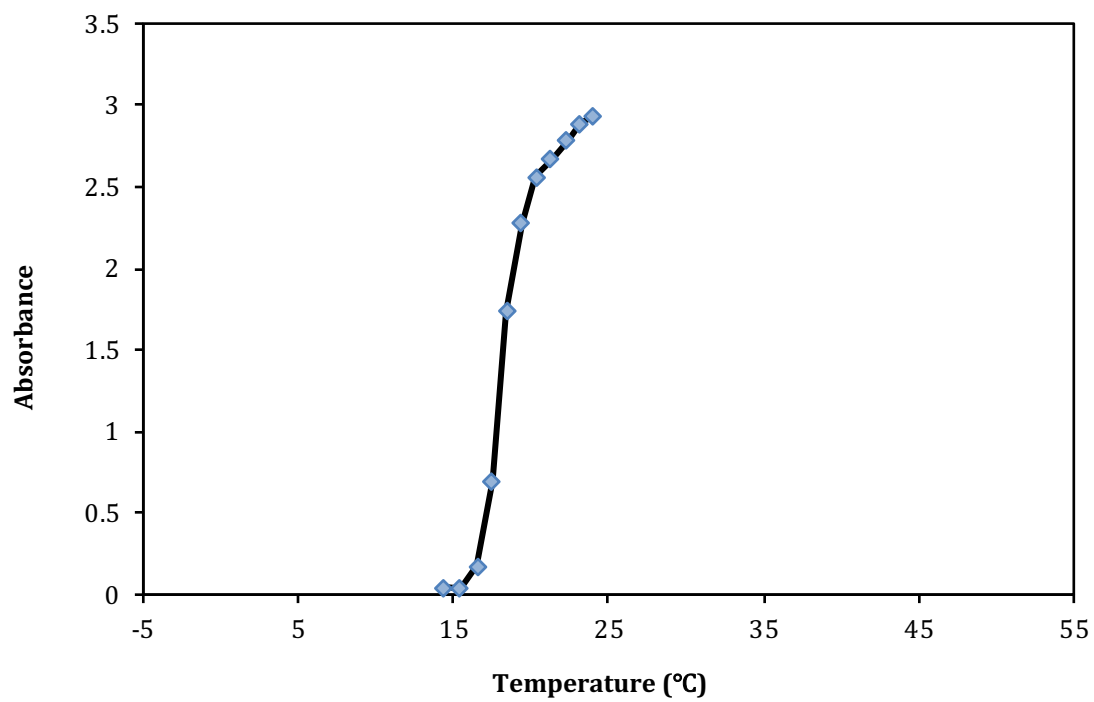


Figure A134. Study of LCST behavior of poly(MGE_{0.55}) via UV-vis.

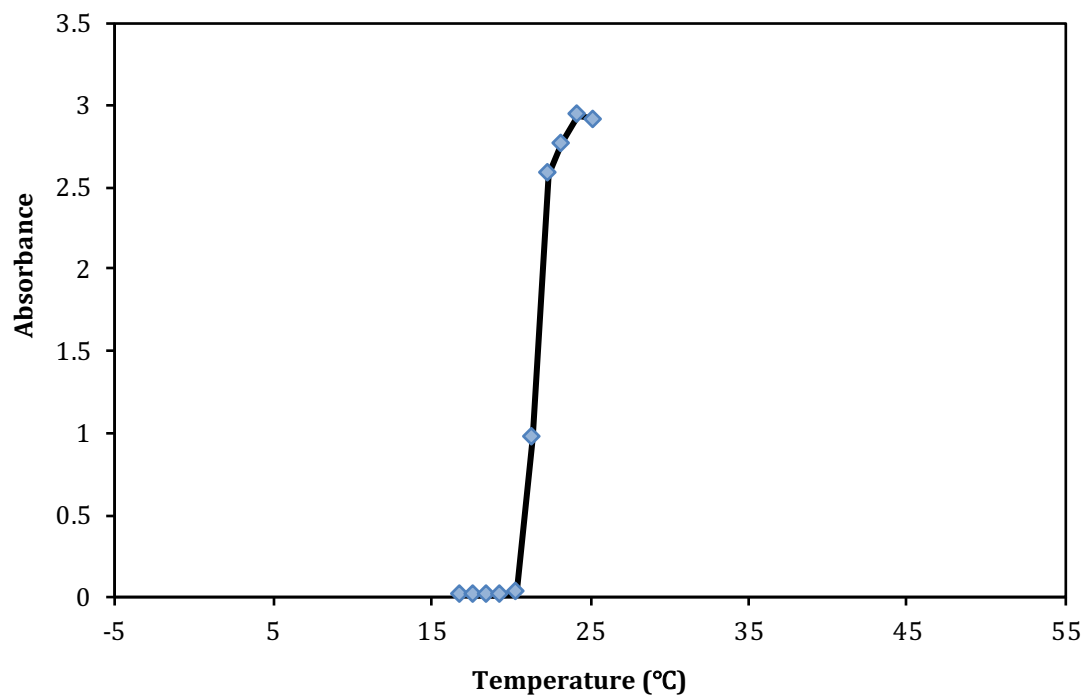


Figure A135. Study of LCST behavior of poly(MGE_{0.50}) via UV-vis.

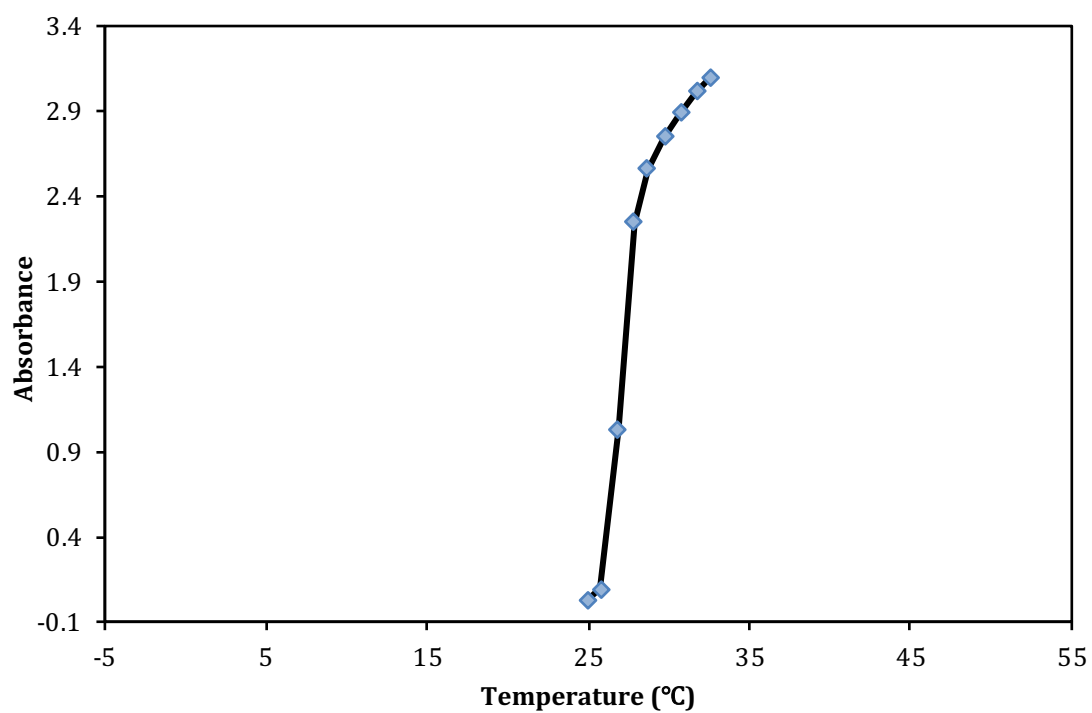


Figure A136. Study of LCST behavior of poly(MGE_{0.65}) via UV-vis.

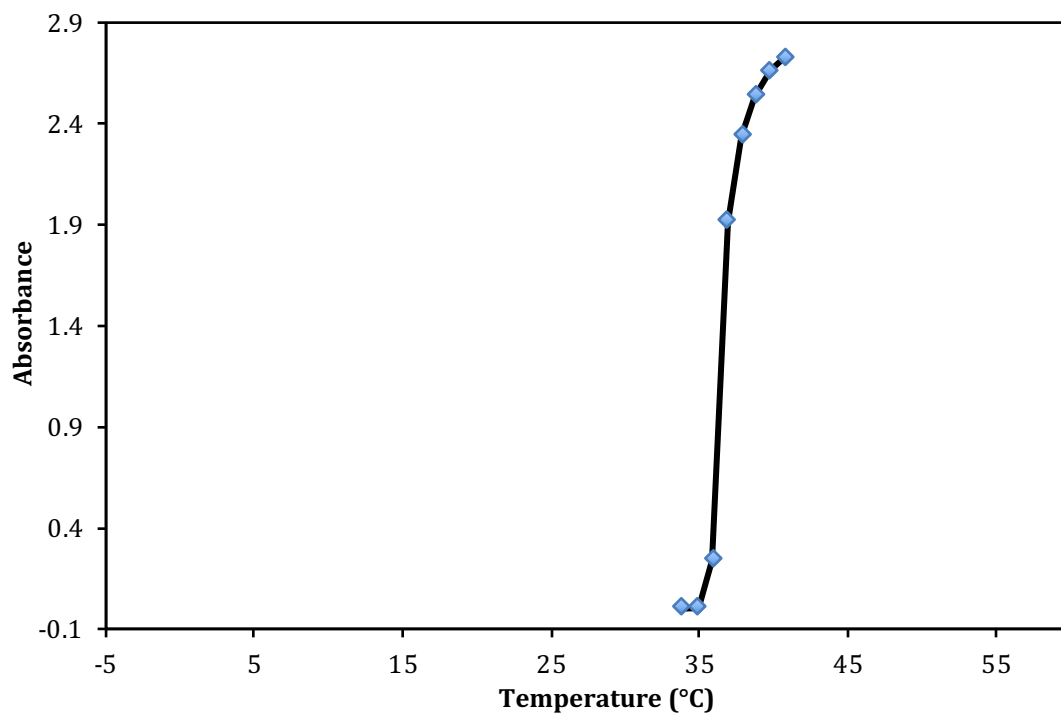


Figure A137. Study of LCST behavior of poly(MGE_{0.75}) via UV-vis.

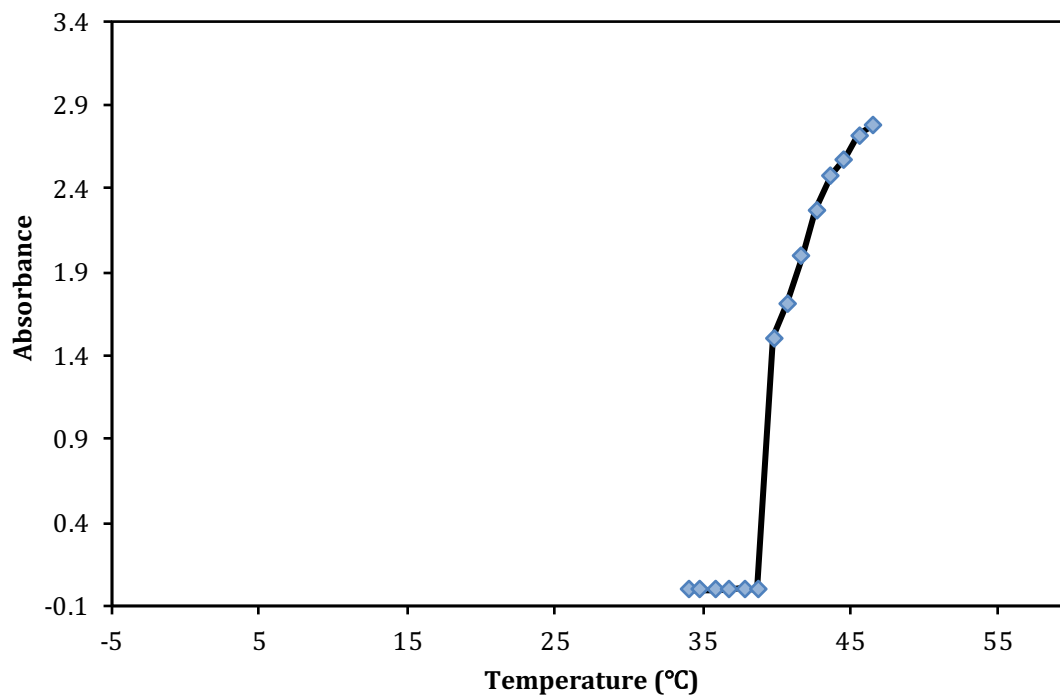


Figure A138. Study of LCST behavior of poly(MGE_{0.80}) via UV-vis.

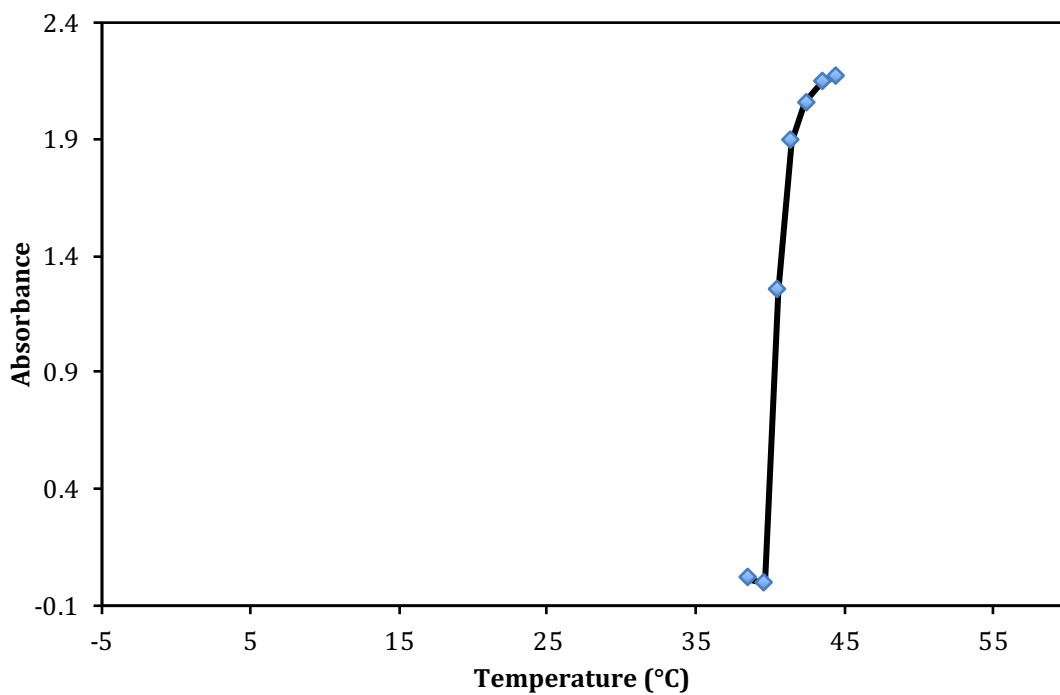


Figure A139. Study of LCST behavior of poly(MGE_{0.85}) via UV-vis.

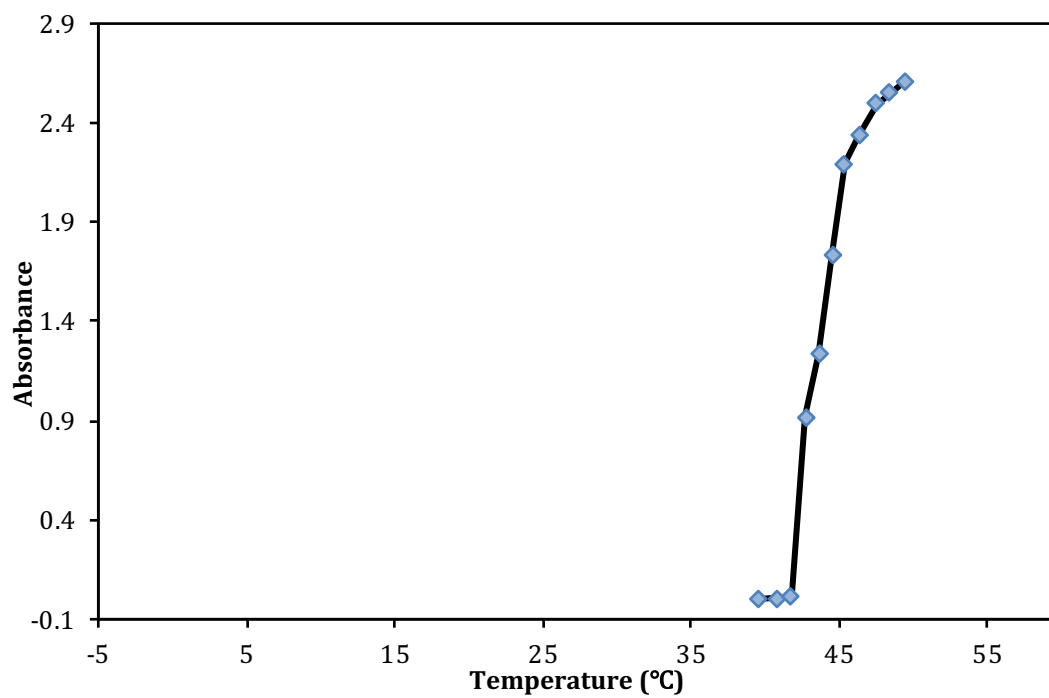


Figure A140. Study of LCST behavior of poly(MGE_{0.90}) via UV-vis.

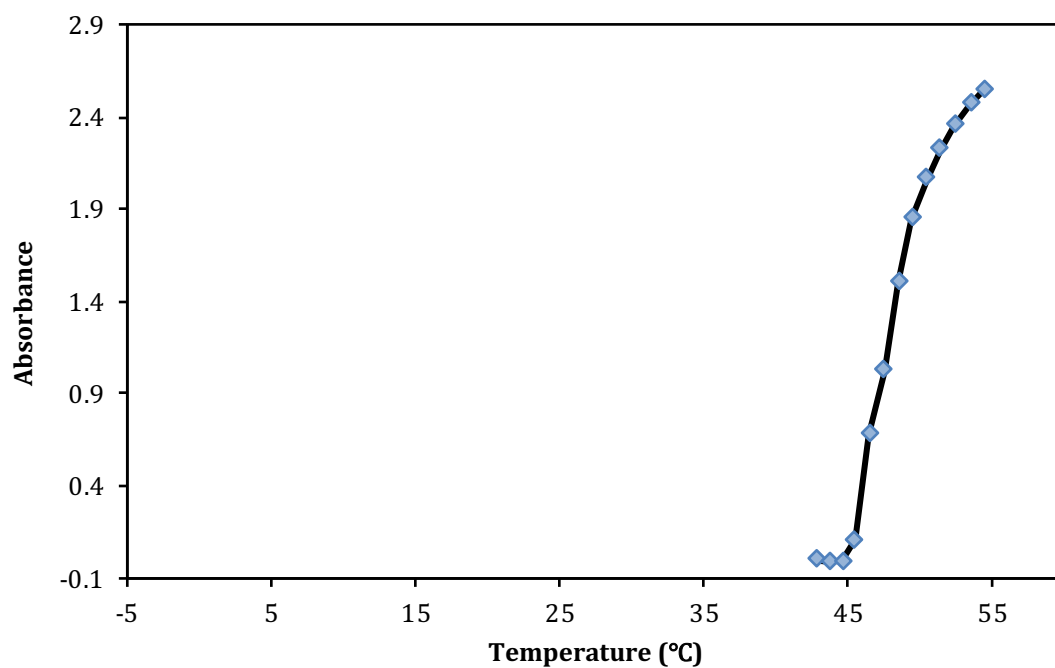


Figure A141. Study of LCST behavior of poly(MGE_{0.95}) via UV-vis.

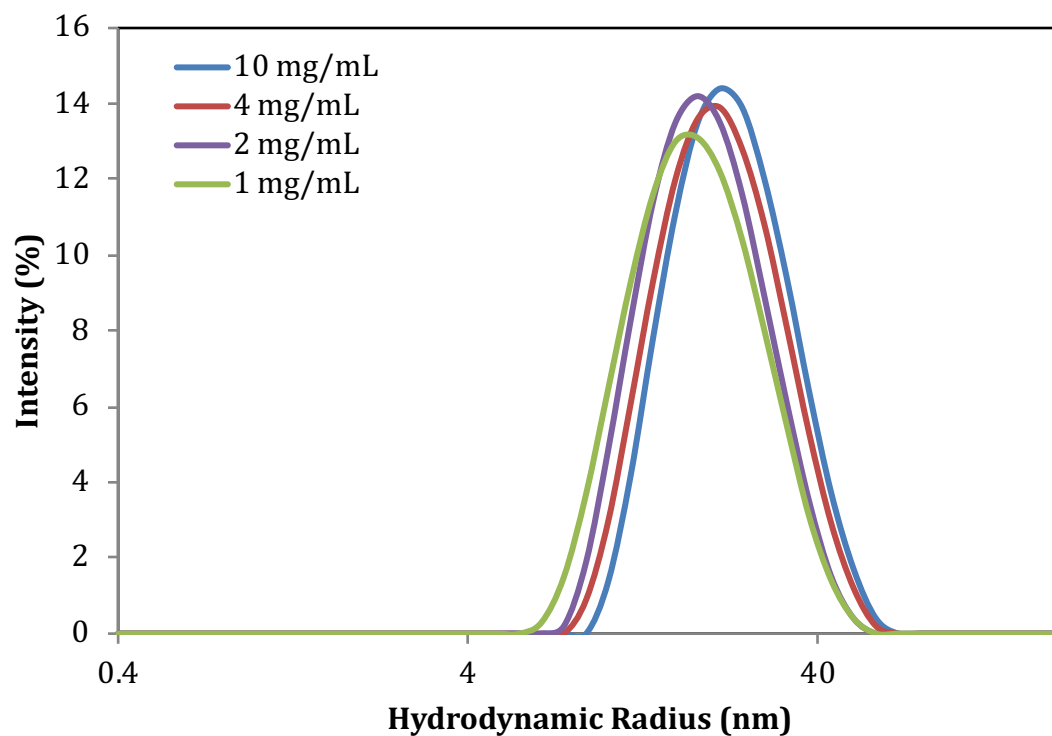


Figure A142. Hydrodynamic diameter of poly(PGE_{0.55}) determined by DLS.

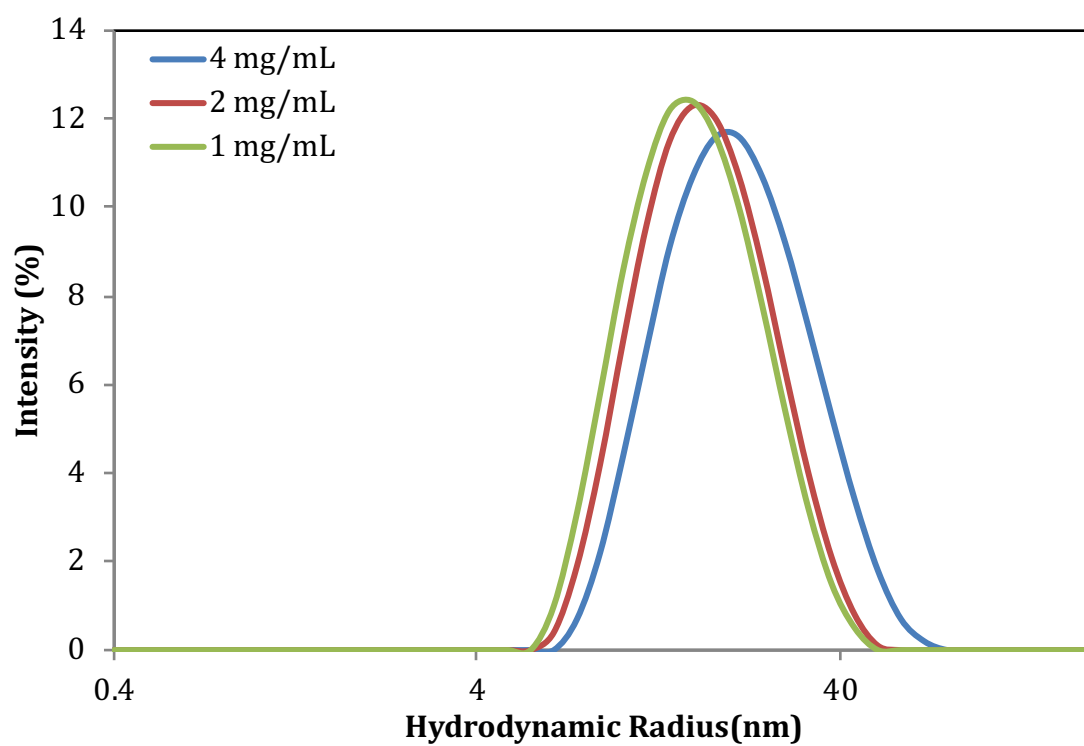


Figure A143. Hydrodynamic diameter of poly(MGE_{0.60}) determined by DLS.

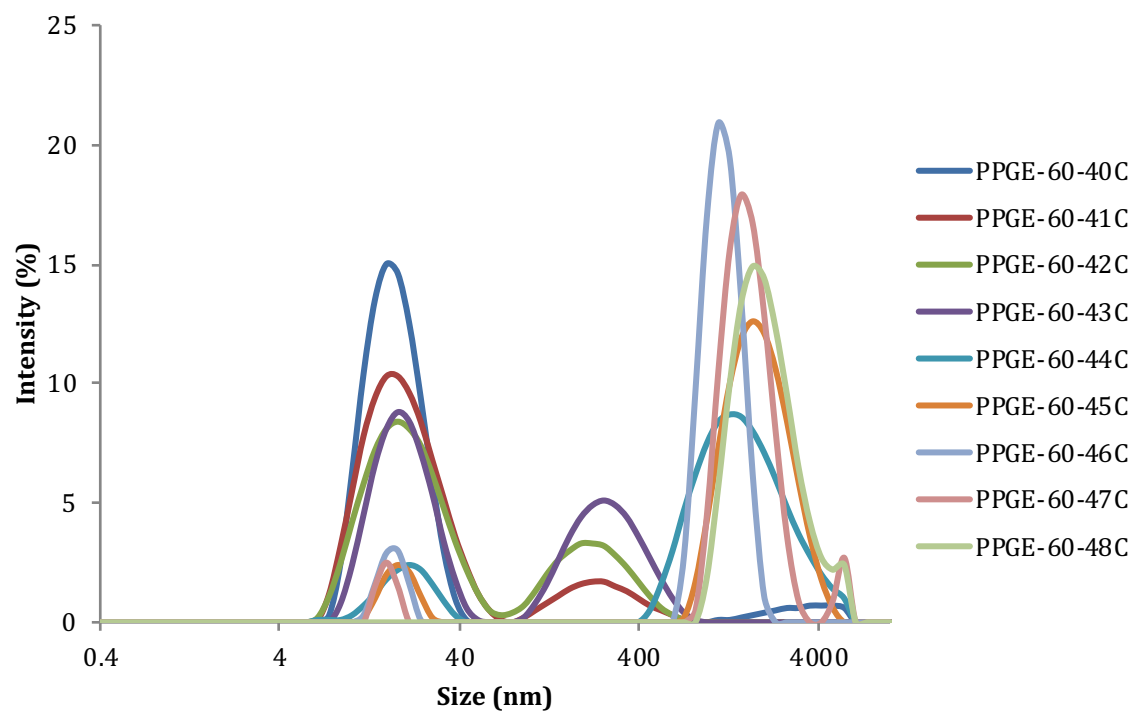


Figure A144. Study of LCST behavior of poly(PGE_{0.60}) via DLS.

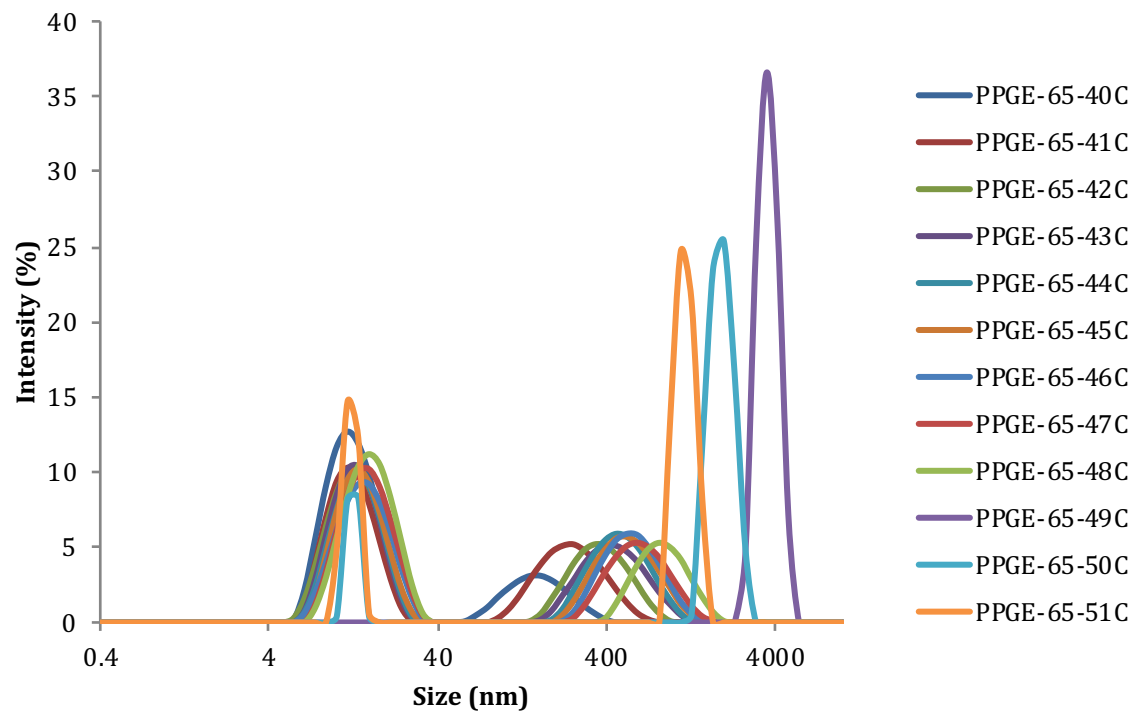


Figure A145. Study of LCST behavior of poly(PGE_{0.65}) via DLS.

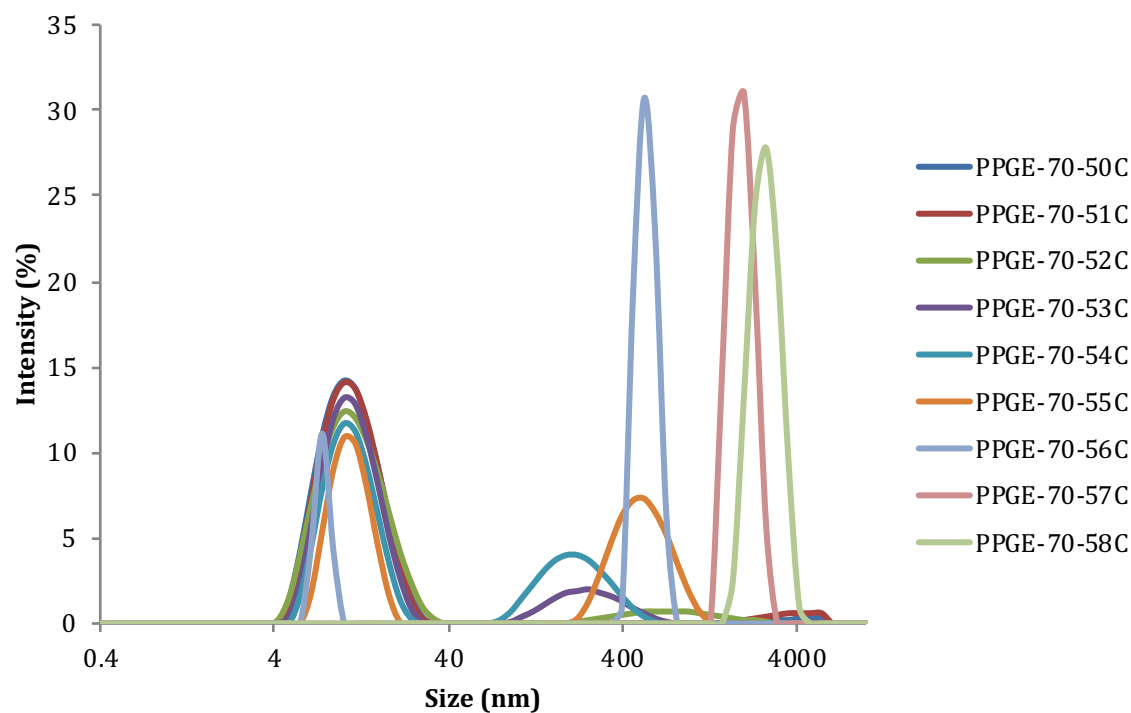


Figure A146. Study of LCST behavior of poly(PGE_{0.70}) via DLS.

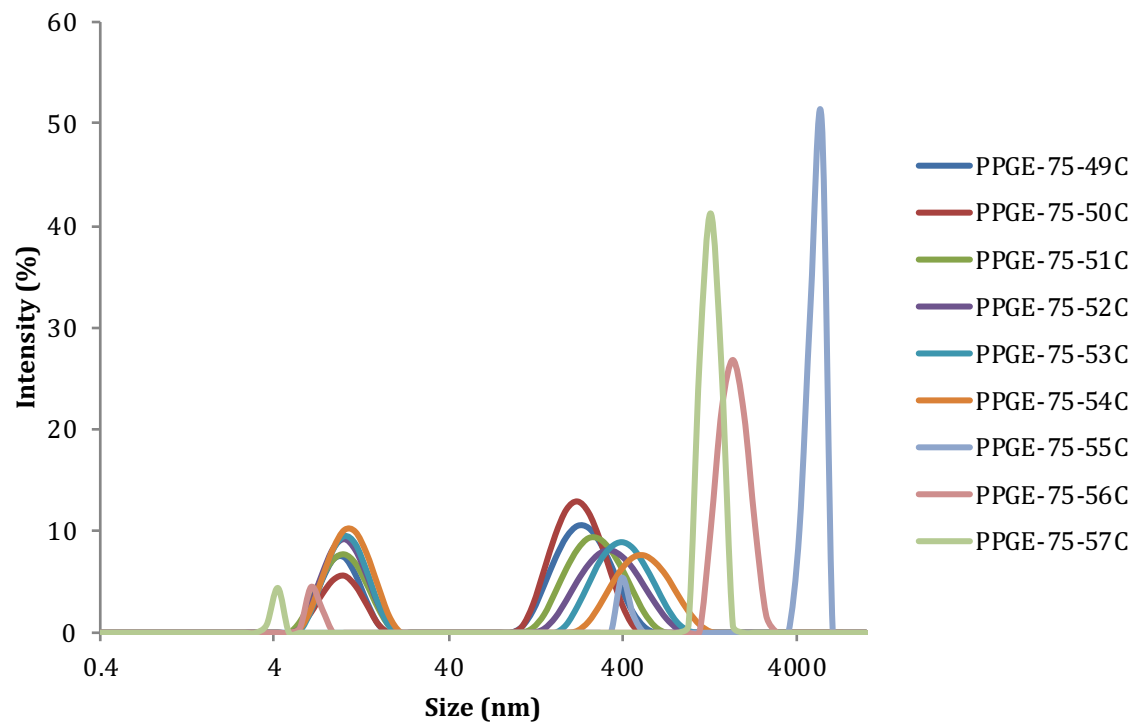


Figure A147. Study of LCST behavior of poly(PGE_{0.75}) via DLS.

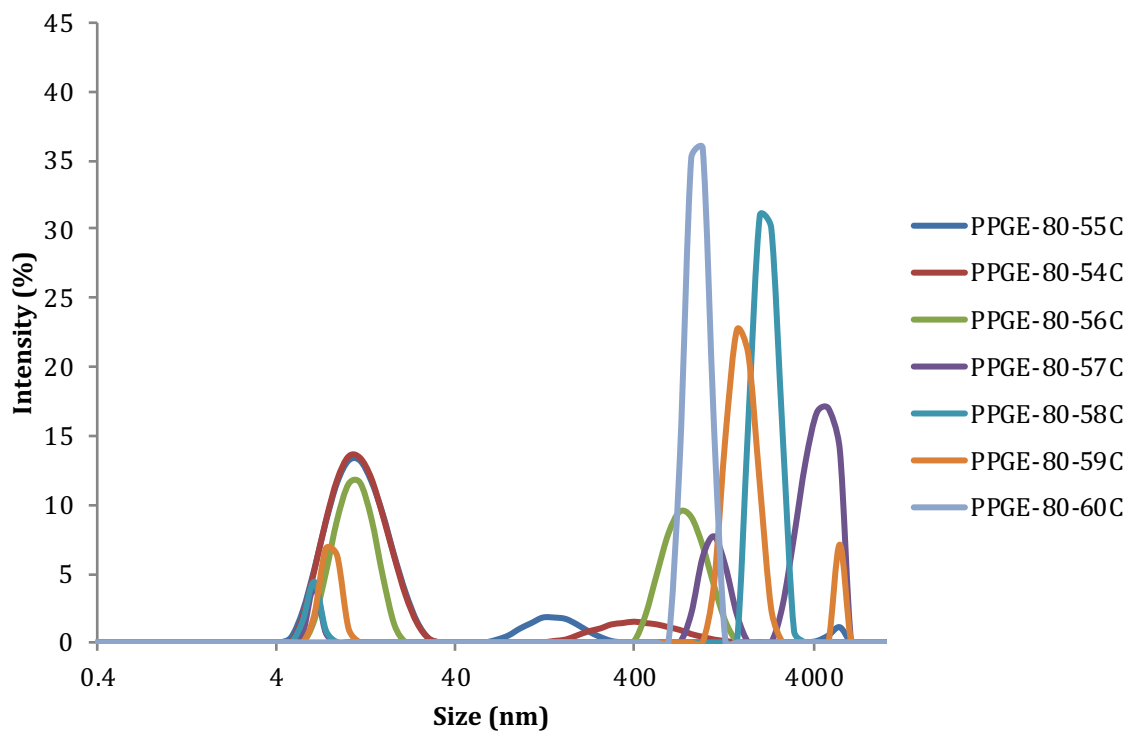


Figure A148. Study of LCST behavior of poly(PGE_{0.80}) via DLS.

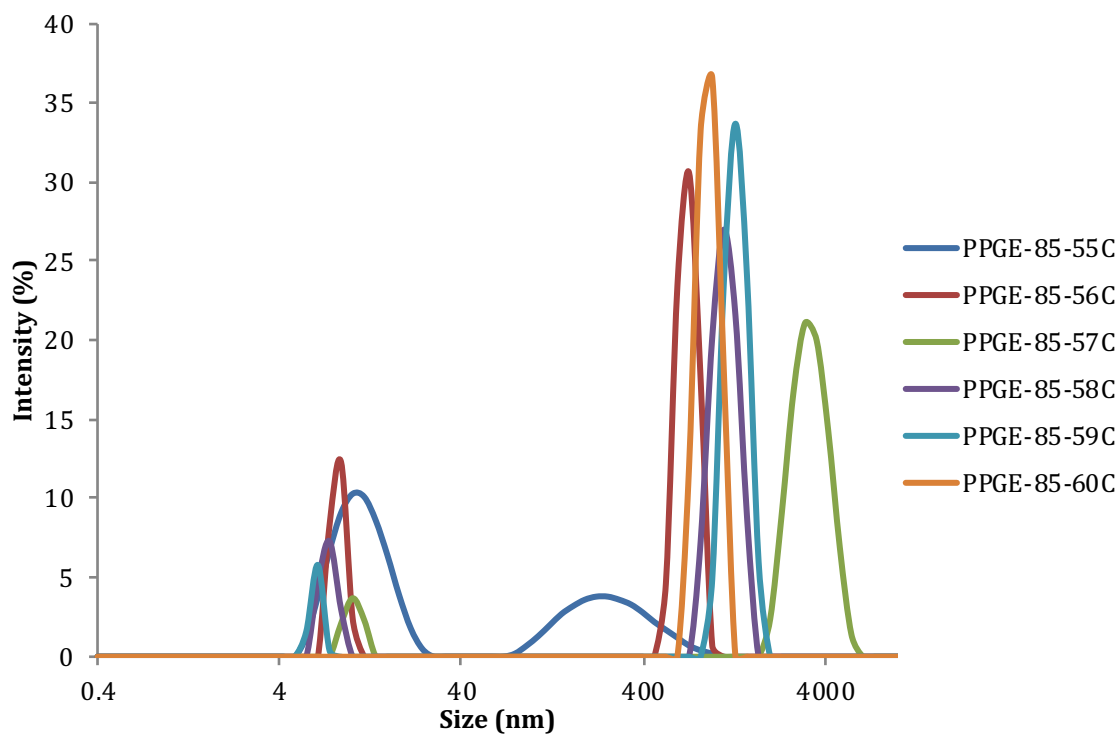


Figure A149. Study of LCST behavior of poly(PGE_{0.85}) via DLS.

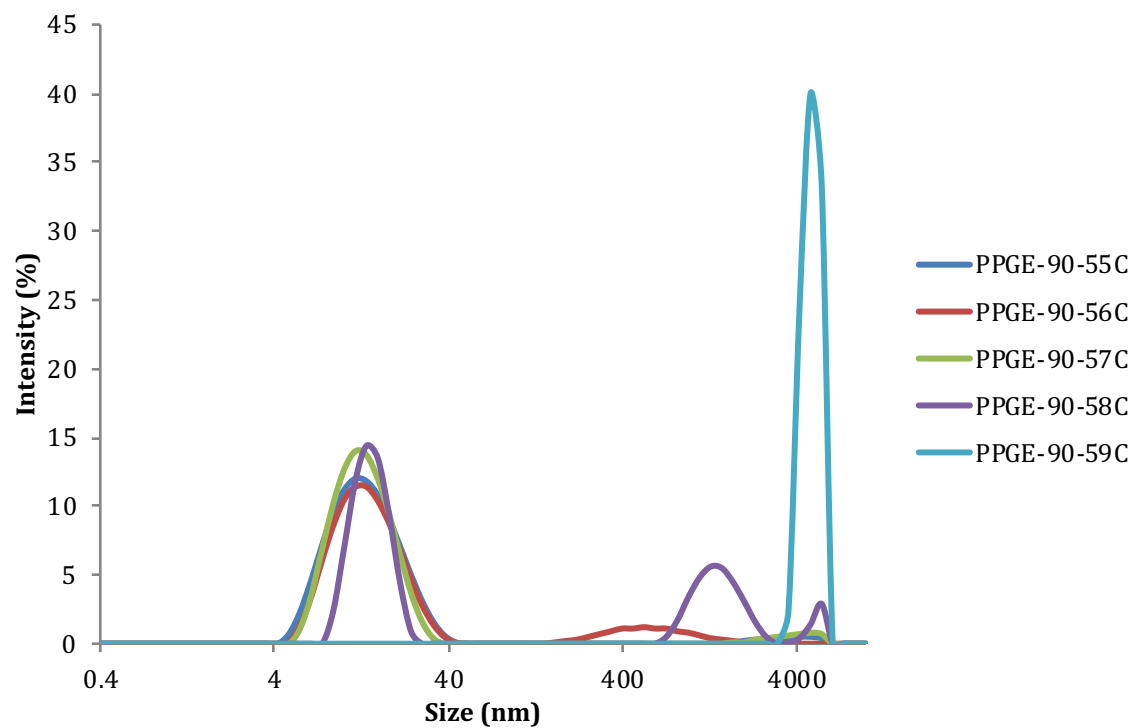


Figure A150. Study of LCST behavior of poly(PGE_{0.90}) via DLS.

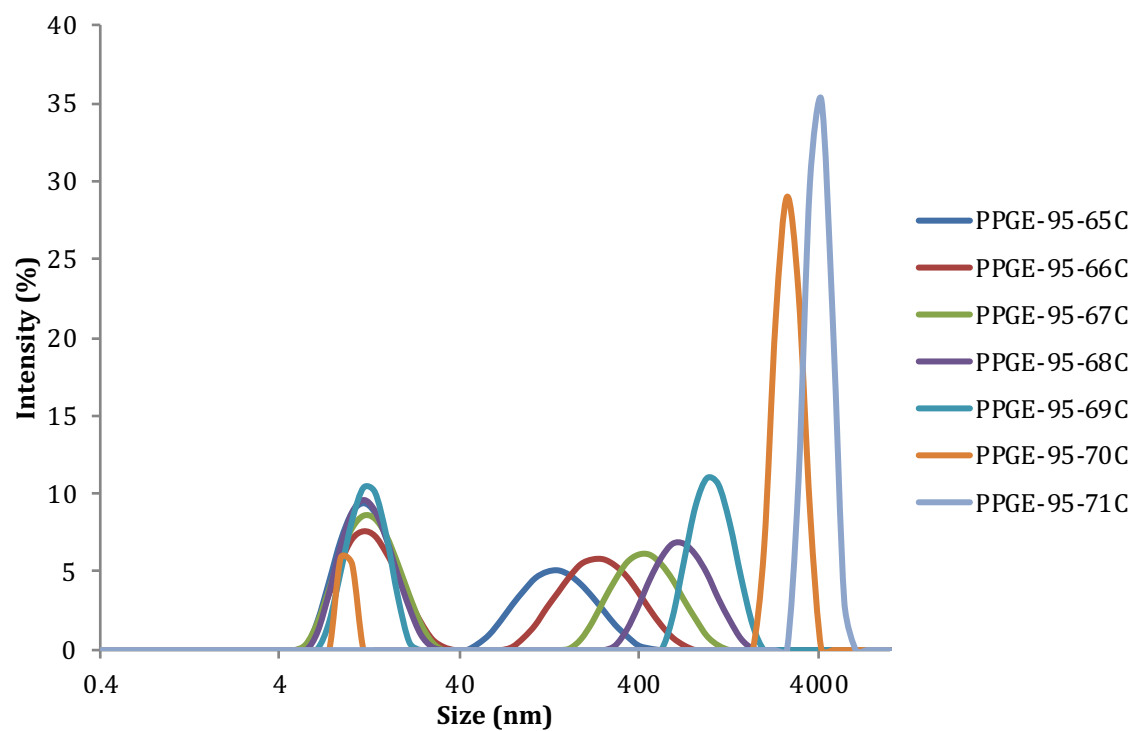


Figure A151. Study of LCST behavior of poly(PGE_{0.95}) via DLS.

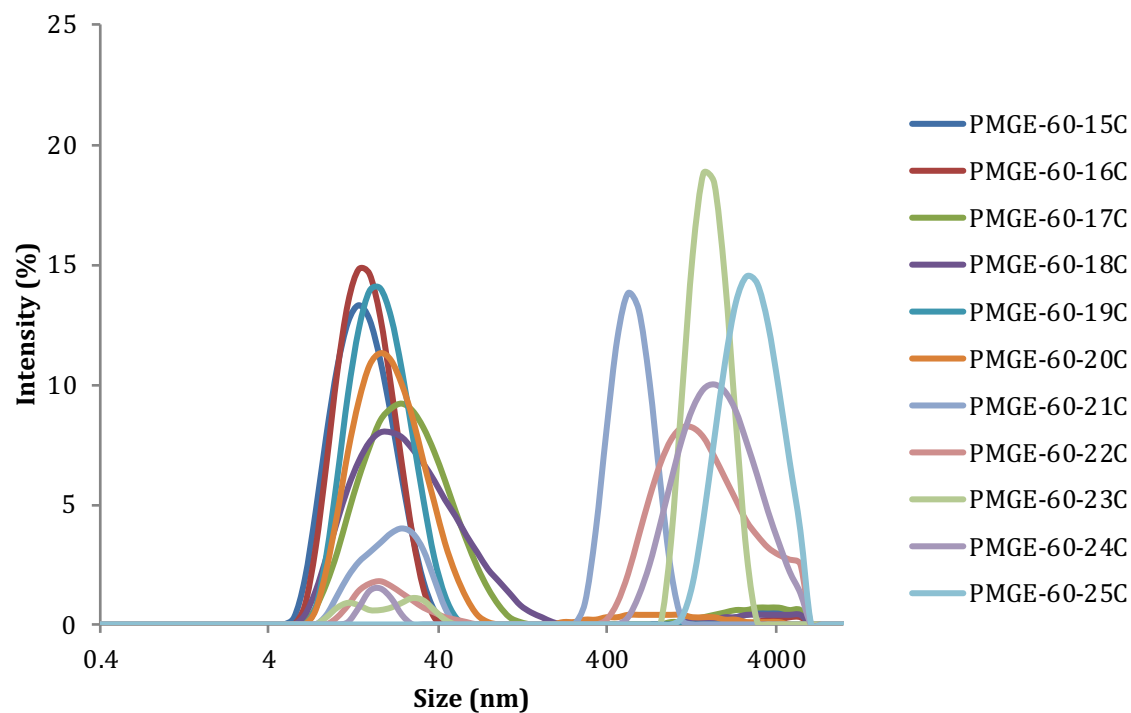


Figure A152. Study of LCST behavior of poly(MGE_{0.60}) via DLS.

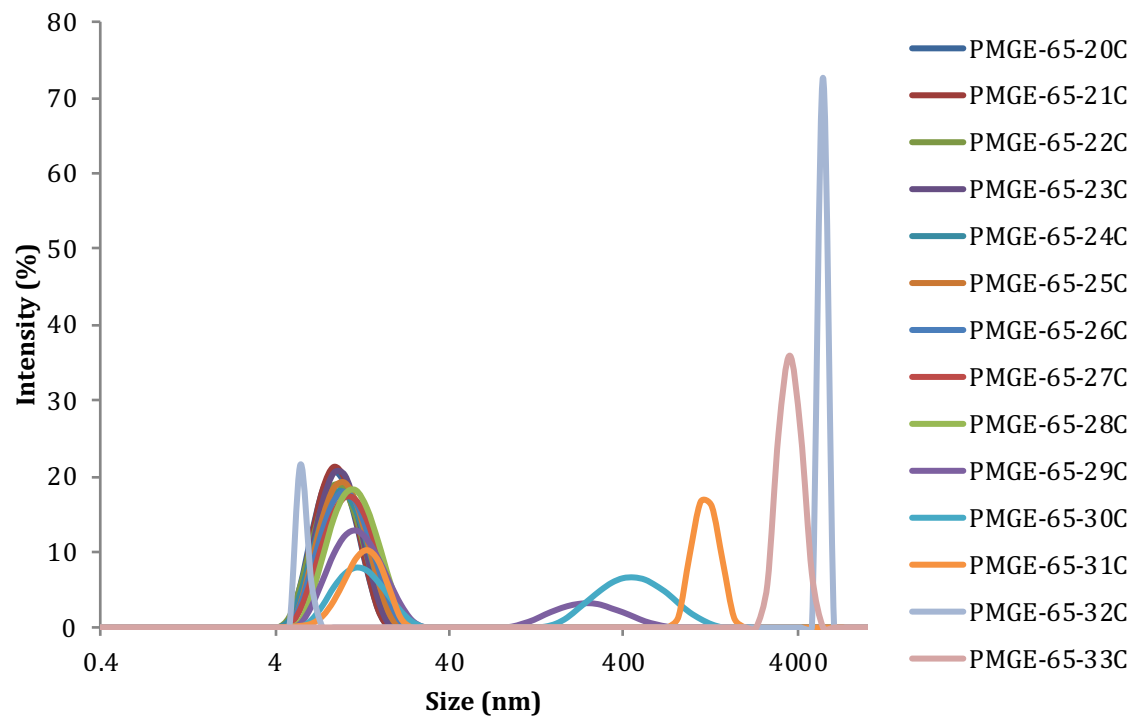


Figure A153. Study of LCST behavior of poly(MGE_{0.65}) via DLS.

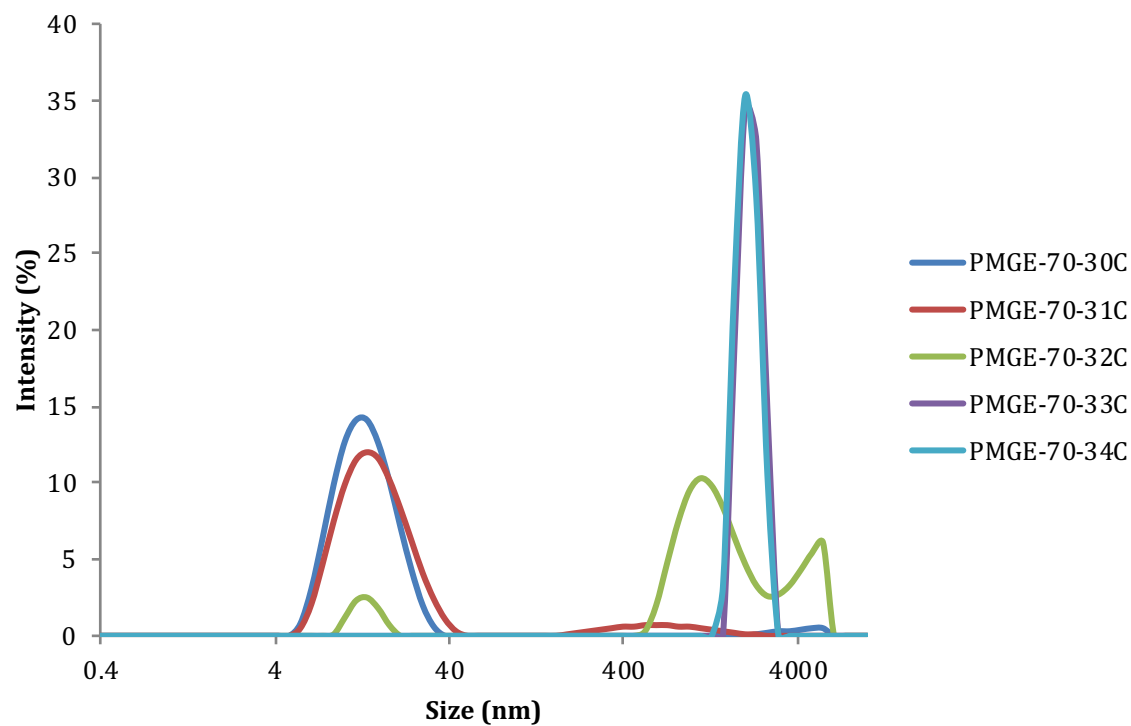


Figure A154. Study of LCST behavior of poly(MGE_{0.70}) via DLS.

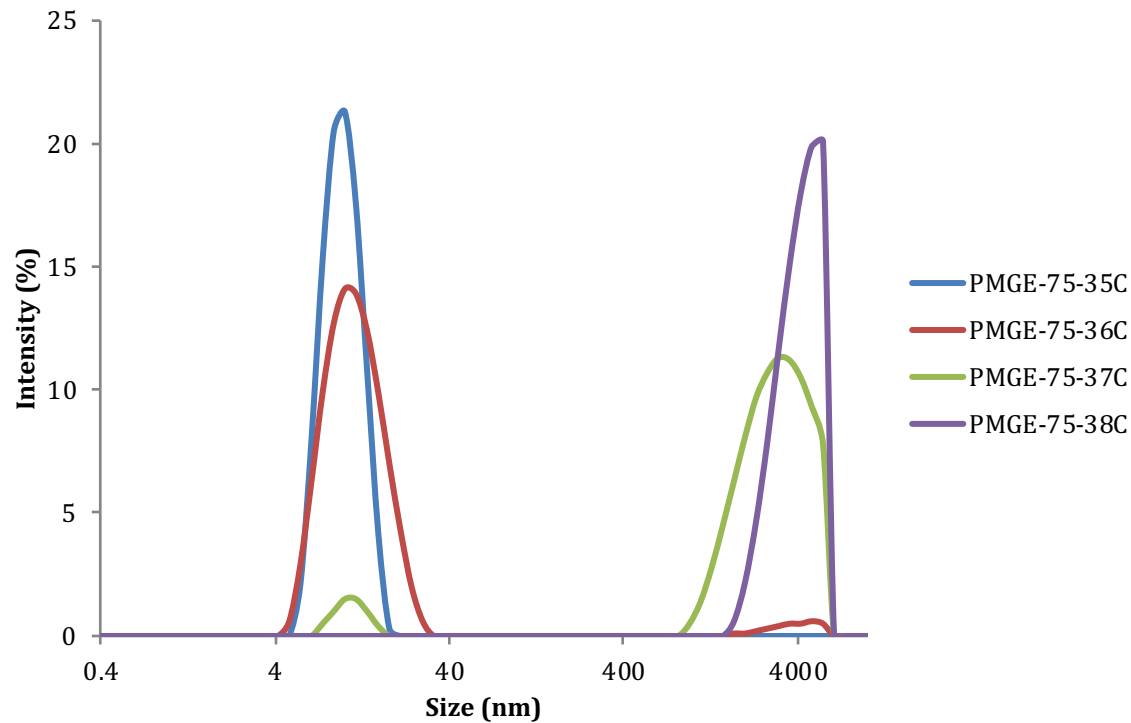


Figure A155. Study of LCST behavior of poly(MGE_{0.75}) via DLS.

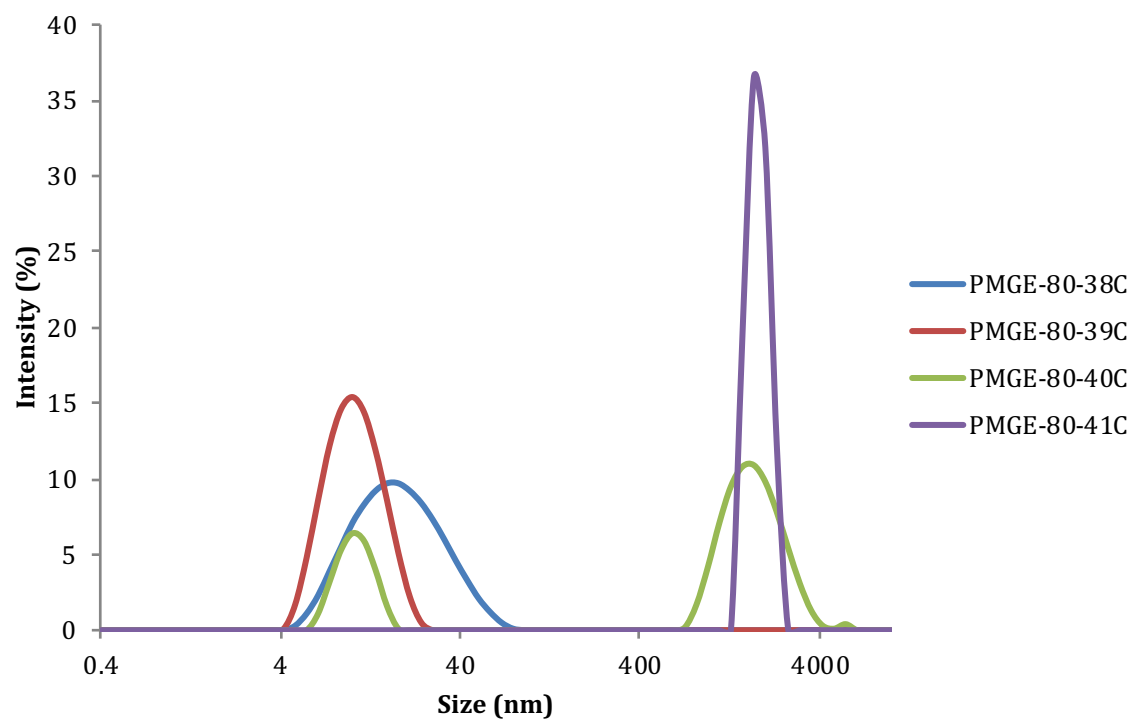


Figure A156. Study of LCST behavior of poly(MGE_{0.80}) via DLS.

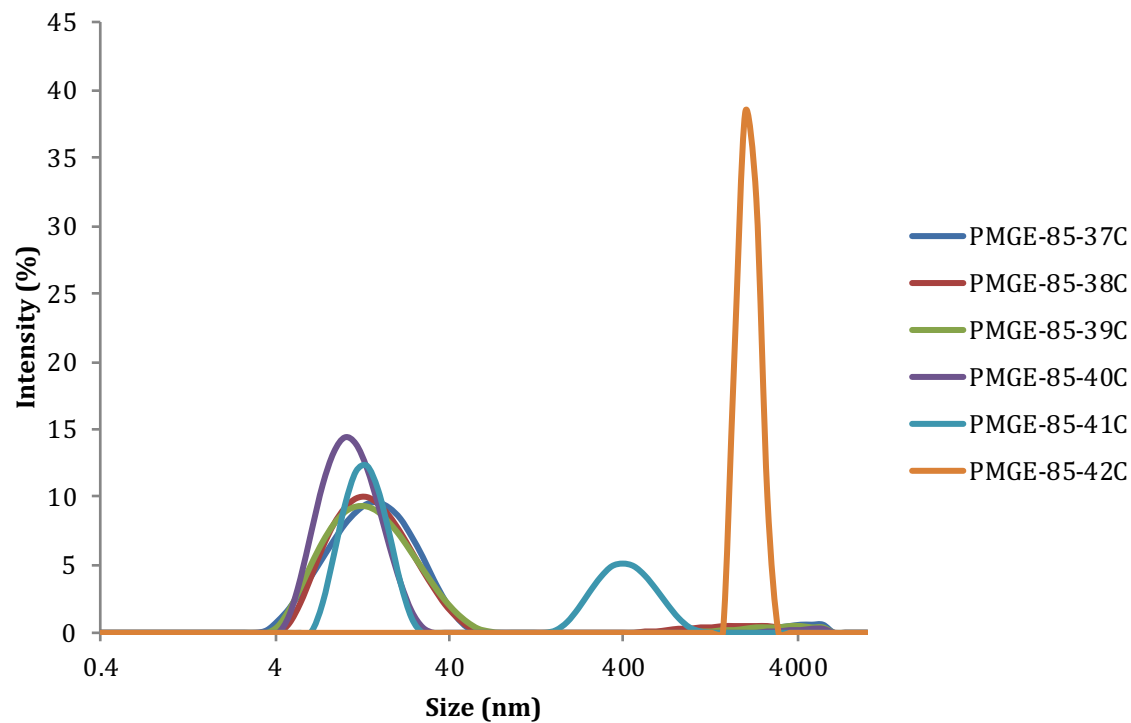


Figure A157. Study of LCST behavior of poly(MGE_{0.85}) via DLS.

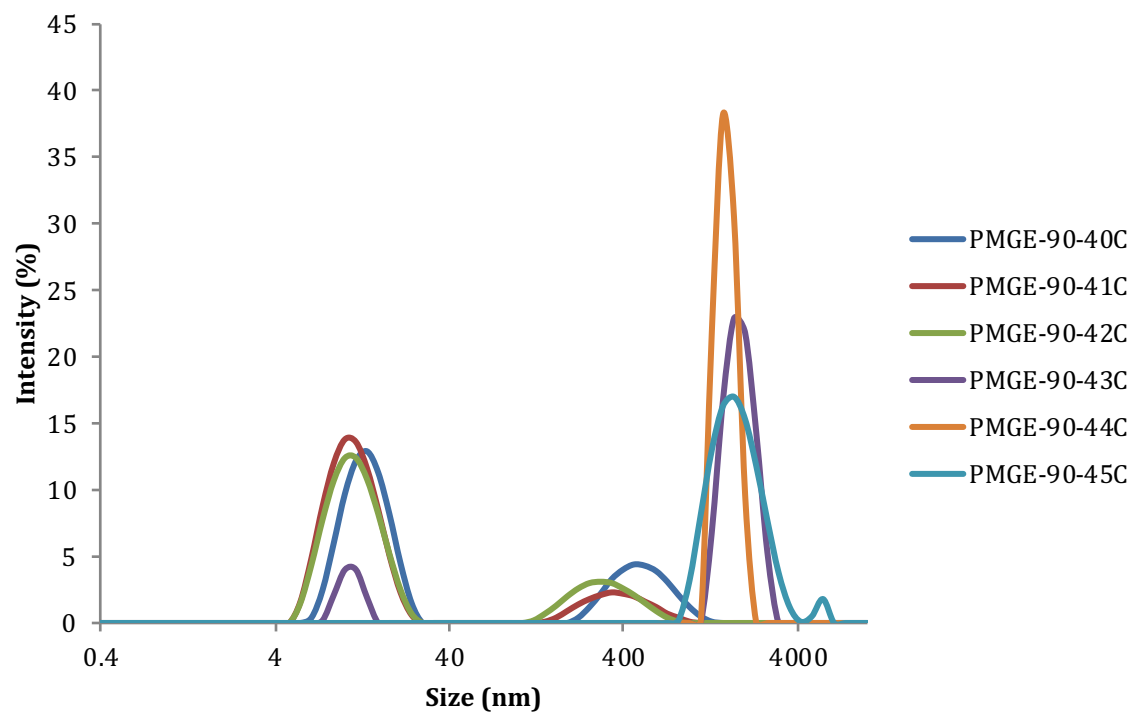


Figure A158. Study of LCST behavior of poly(MGE_{0.90}) via DLS.

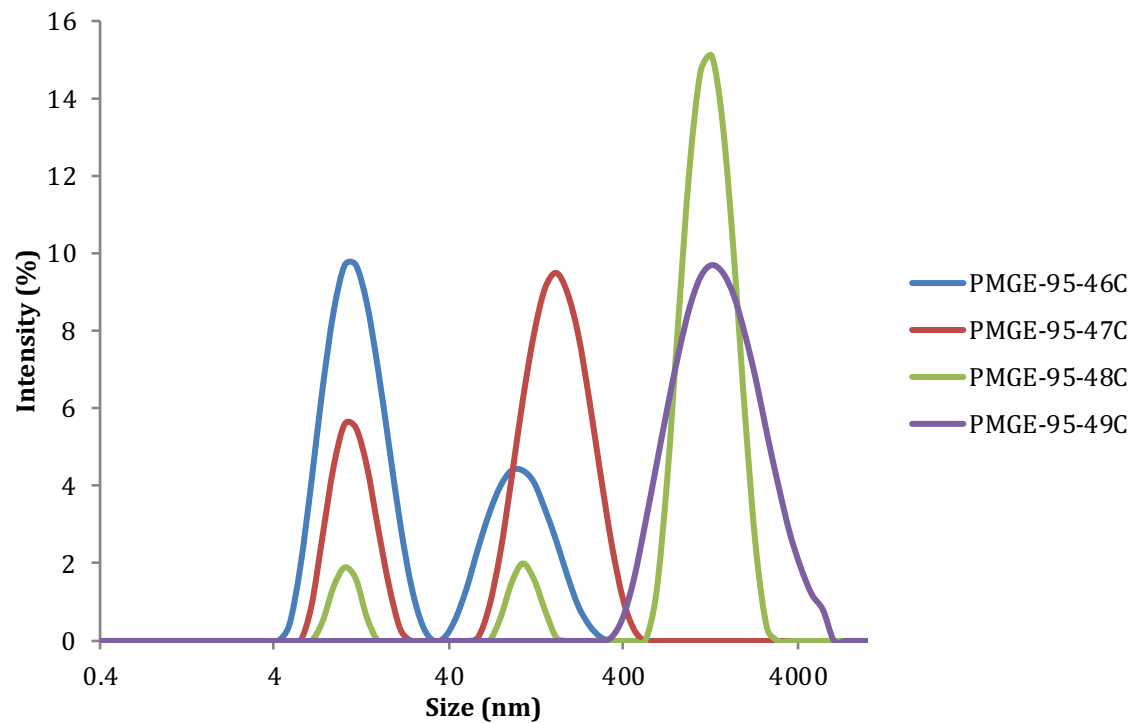


Figure A159. Study of LCST behavior of poly(MGE_{0.95}) via DLS.

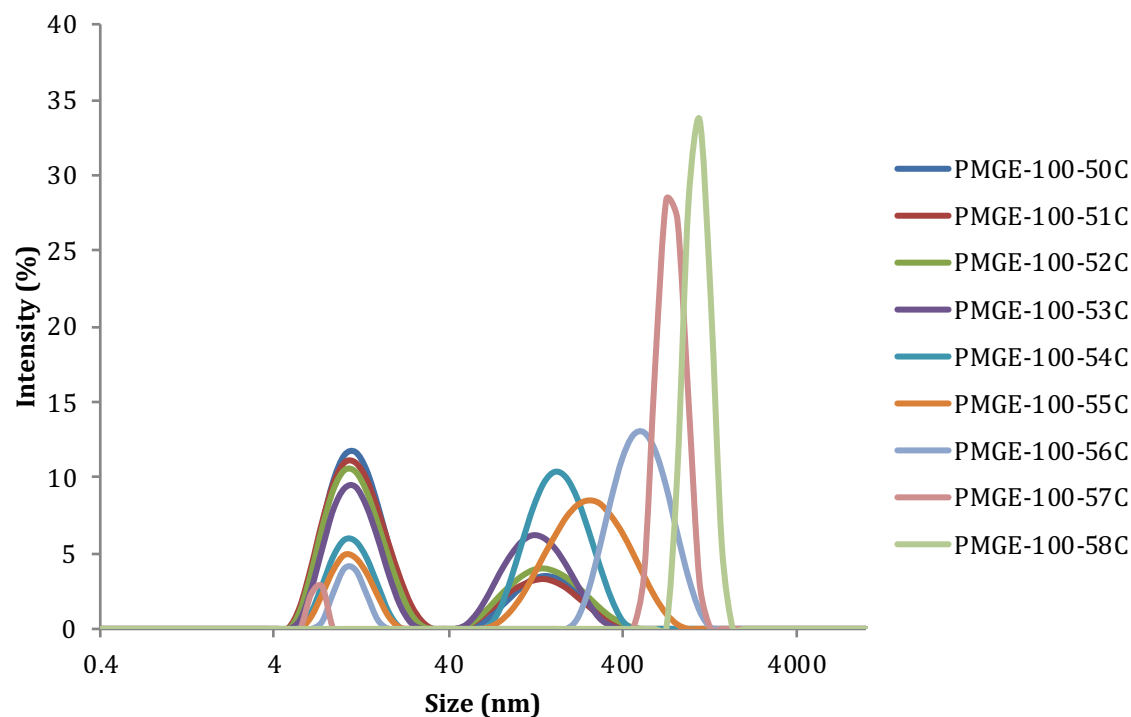


Figure A160. Study of LCST behavior of poly(MGE_{1.0}) via DLS.

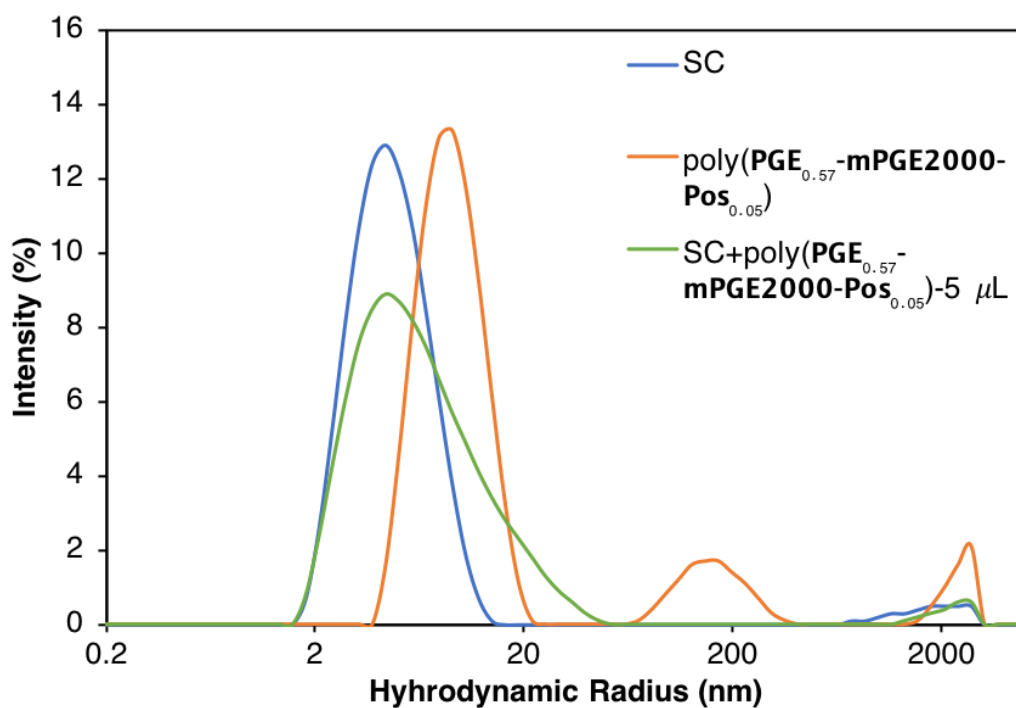


Figure A161. DLS results of SC (blue line), poly(PGE_{0.57}-mPEG2000-Pos_{0.05}) (orange line) and SC with 5 μ L of poly(PGE_{0.57}-mPEG2000-Pos_{0.05}) added (green line) in Milli-Q water.

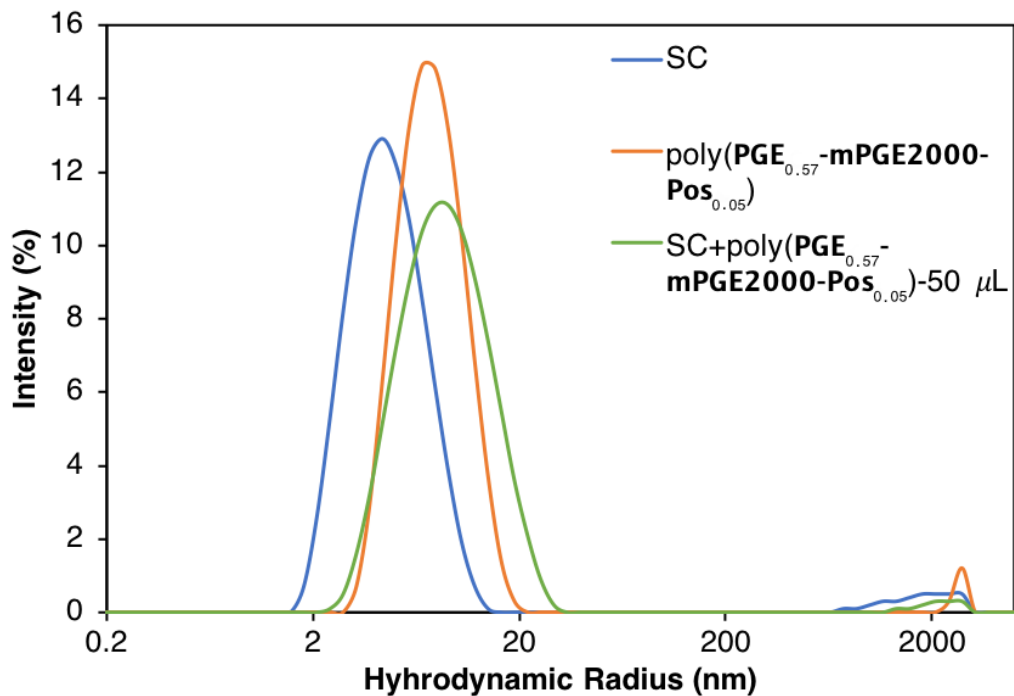


Figure A162. DLS results of SC (blue line), poly(PGE_{0.57}-mPEG2000-Pos_{0.05}) (orange line) and SC with 50 μ L of poly(PGE_{0.57}-mPEG2000-Pos_{0.05}) added (green line) in Milli-Q water.

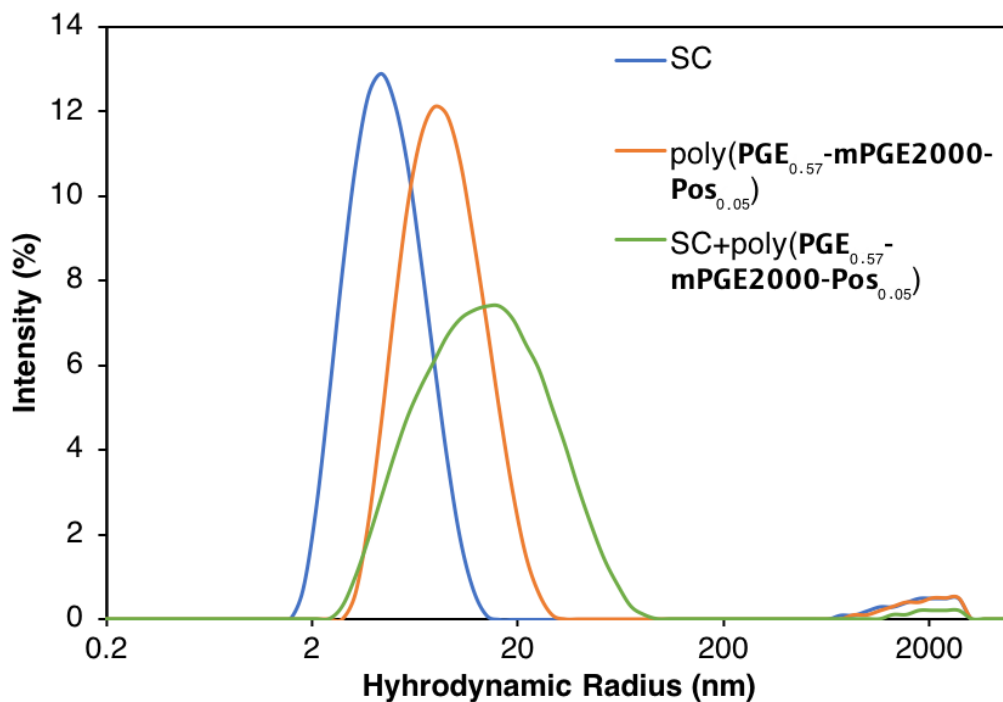


Figure A163. DLS results of SC (blue line), poly(PGE_{0.57}-mPEG2000-Pos_{0.05}) (orange line) and SC with poly(PGE_{0.57}-mPEG2000-Pos_{0.05}) added (green line) in Milli-Q water.

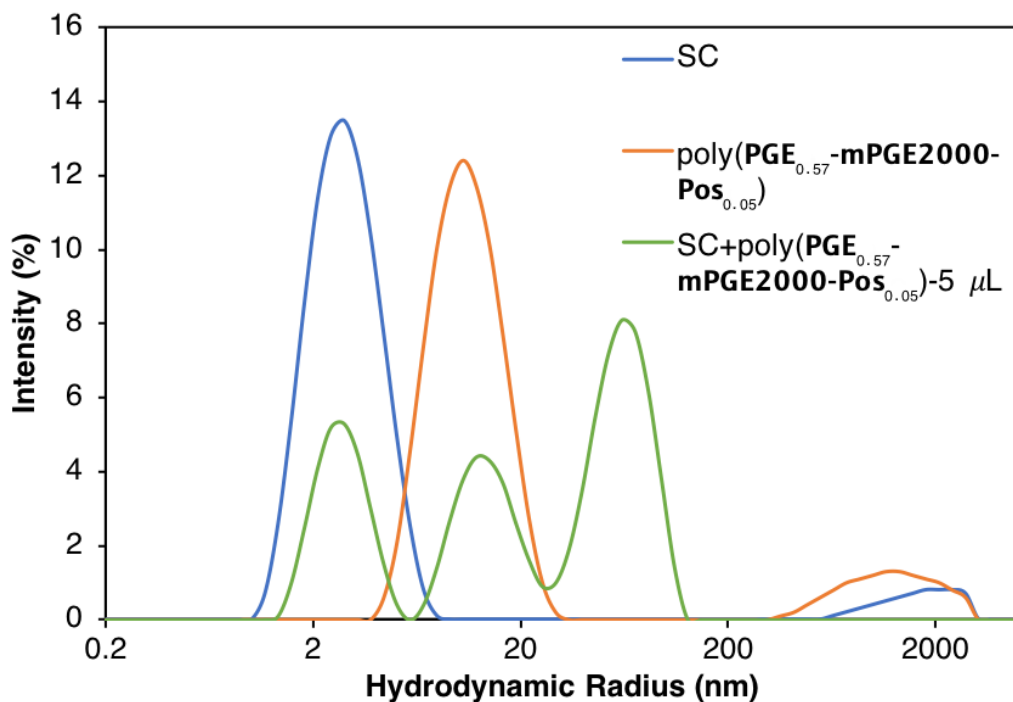


Figure A164. DLS results of SC (blue line), poly(PGE_{0.57}-mPEG2000-Pos_{0.05}) (orange line) and SC with 5 μ L of poly(PGE_{0.57}-mPEG2000-Pos_{0.05}) added (green line) in PBS.

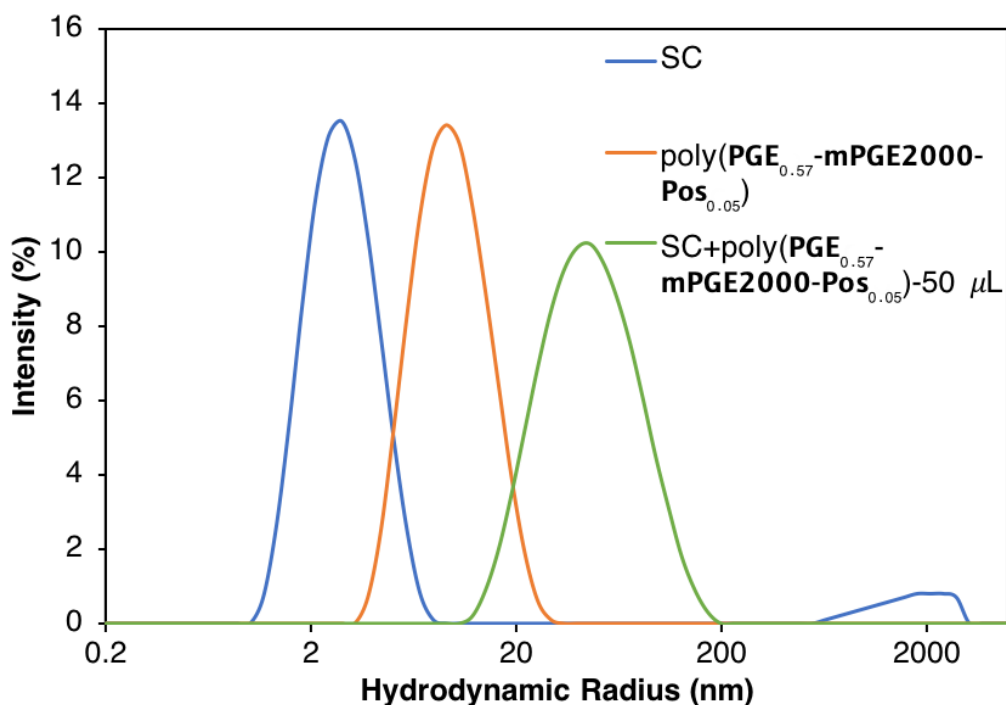


Figure A165. DLS results of SC (blue line), poly(PGE_{0.57}-mPEG2000-Pos_{0.05}) (orange line) and SC with 50 μ L of poly(PGE_{0.57}-mPEG2000-Pos_{0.05}) added (green line) in PBS.

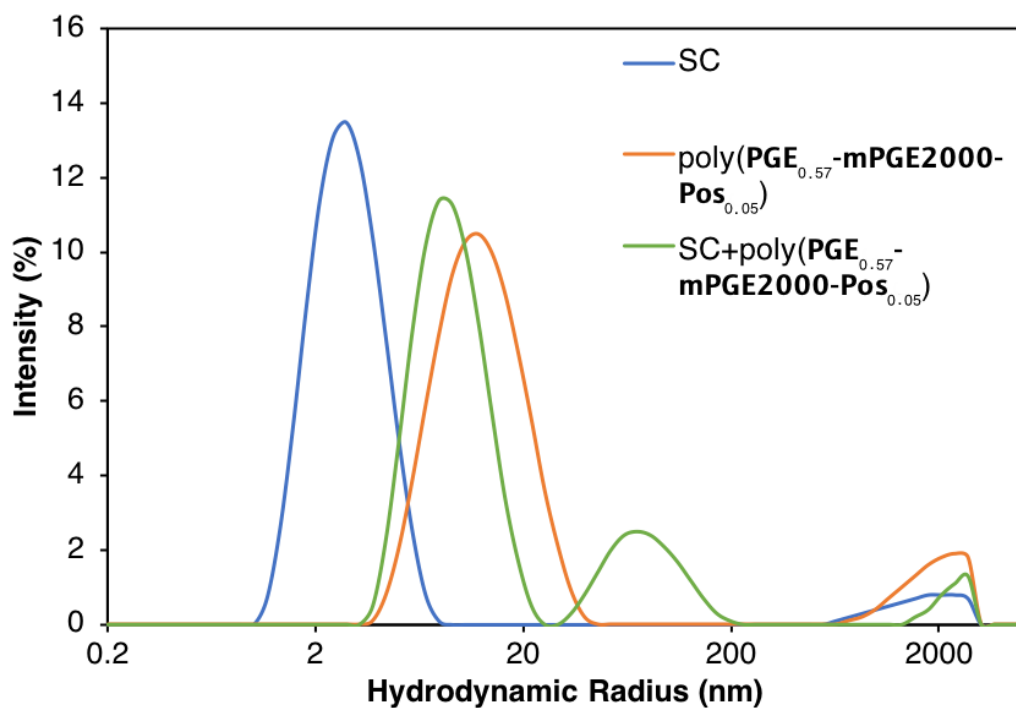


Figure A166. DLS results of SC (blue line), poly(PGE_{0.57}-mPEG2000-Pos_{0.05}) (orange line) and SC with poly(PGE_{0.57}-mPEG2000-Pos_{0.05}) added (green line) in PBS.

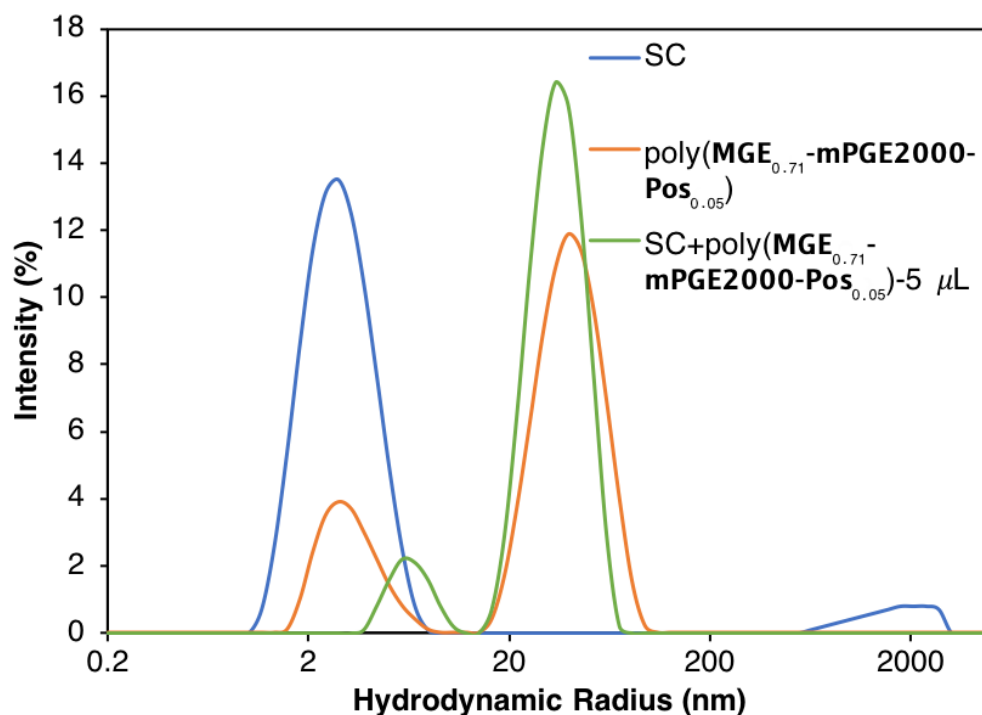


Figure A167. DLS results of SC (blue line), poly(MGE_{0.71}-mPEG2000-Pos_{0.05}) (orange line) and SC with 5 μ L of poly(MGE_{0.71}-mPEG2000-Pos_{0.05}) added (green line) in PBS.

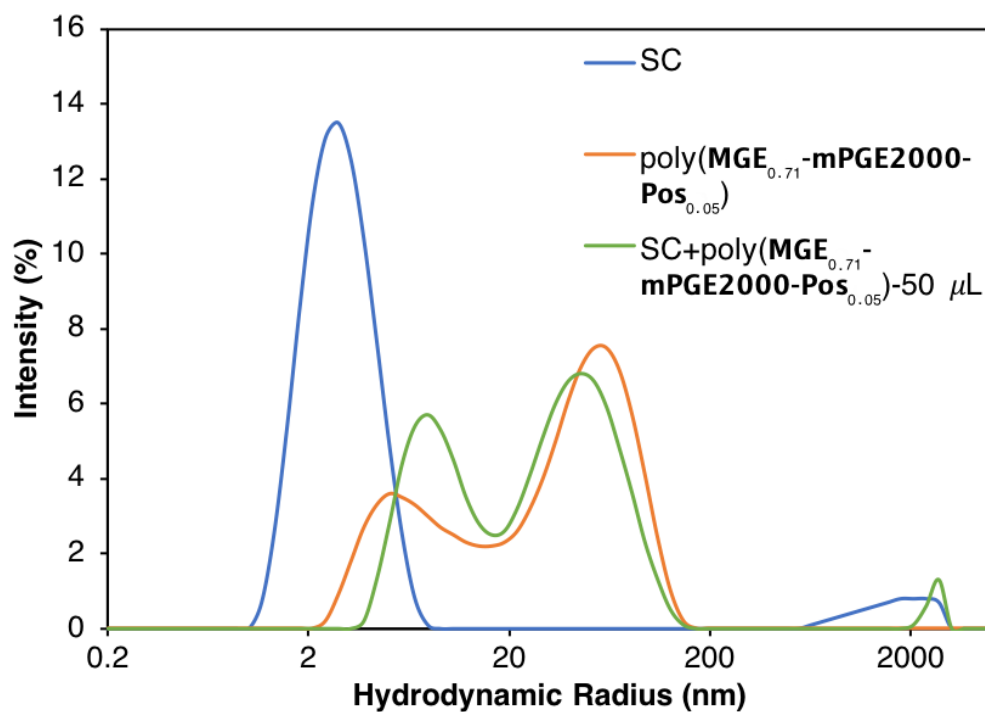


Figure A168. DLS results of SC (blue line), poly(MGE_{0.71}-mPEG2000-Pos_{0.05}) (orange line) and SC with 50 μL of poly(MGE_{0.71}-mPEG2000-Pos_{0.05}) added (green line) in PBS.

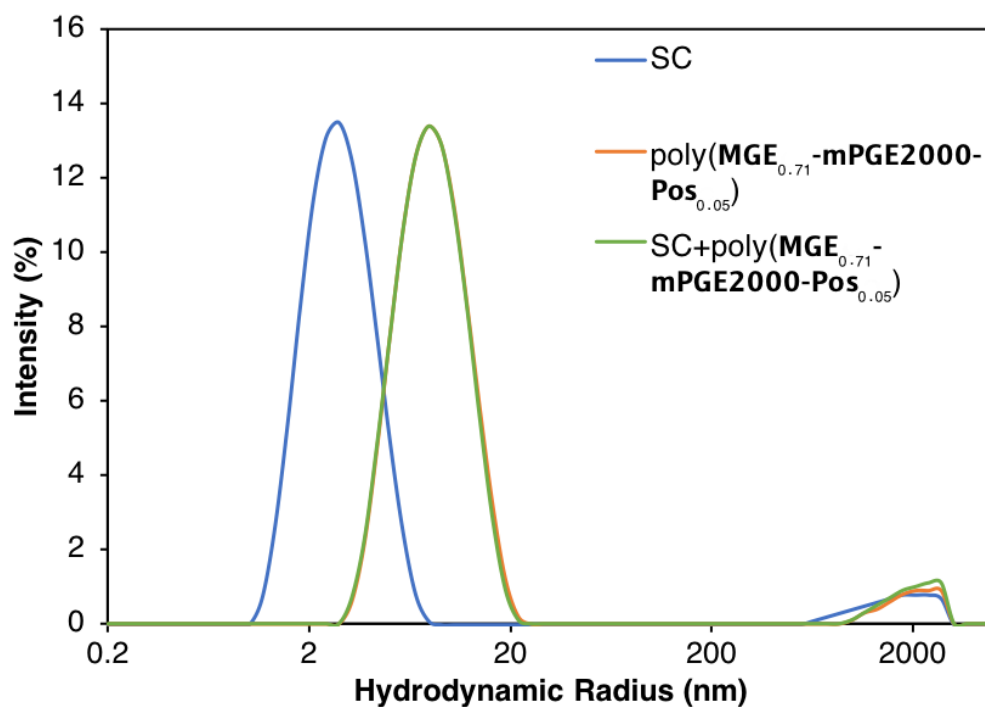


Figure A169. DLS results of SC (blue line), poly(MGE_{0.71}-mPEG2000-Pos_{0.05}) (orange line) and SC with poly(MGE_{0.71}-mPEG2000-Pos_{0.05}) added (green line) in PBS.

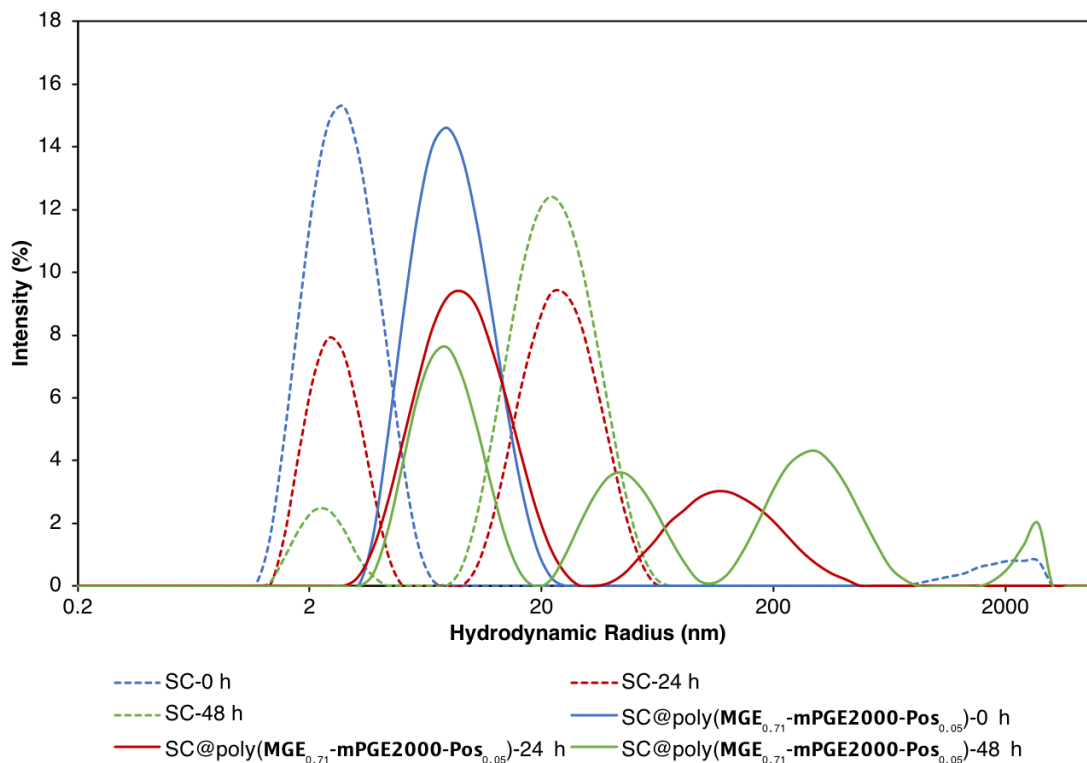


Figure A170. DLS results of control experiments for SC (dotted line) and SC@poly(MGE_{0.71}-mPGE2000-Pos_{0.05}) (solid line) in Milli-Q water over 48 h.

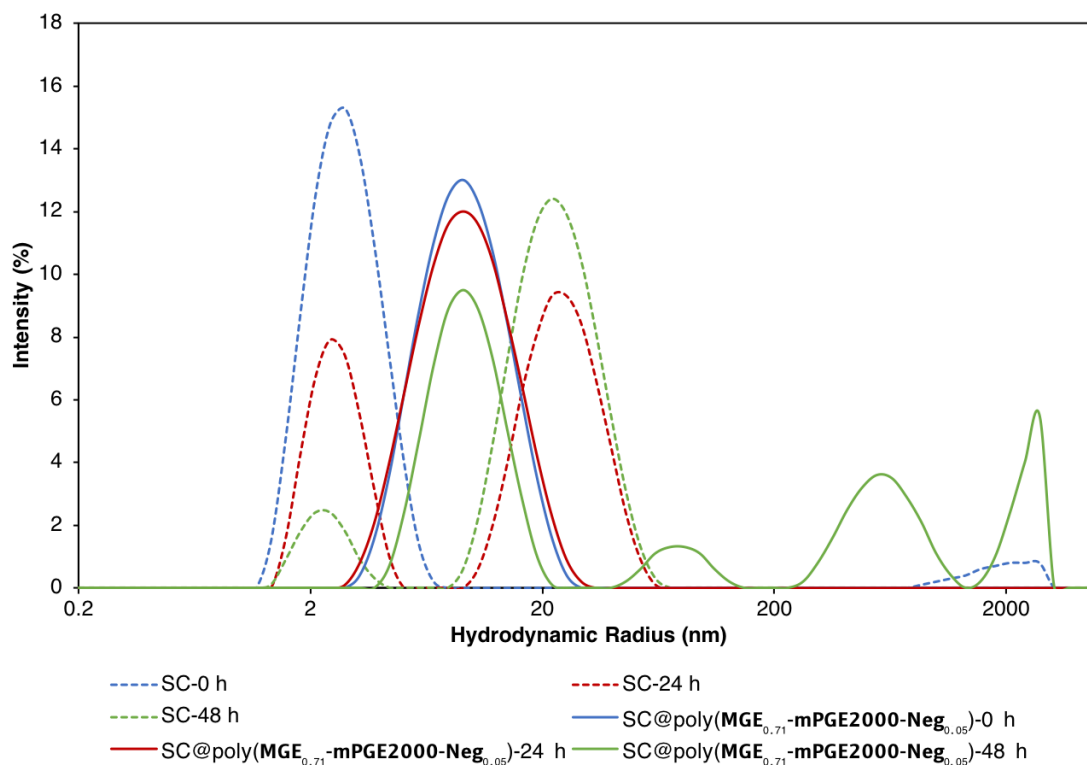


Figure A171. DLS results of control experiments for SC (dotted line) and SC@poly(MGE_{0.71}-mPGE2000-Neg_{0.05}) (solid line) in Milli-Q water over 48 h.

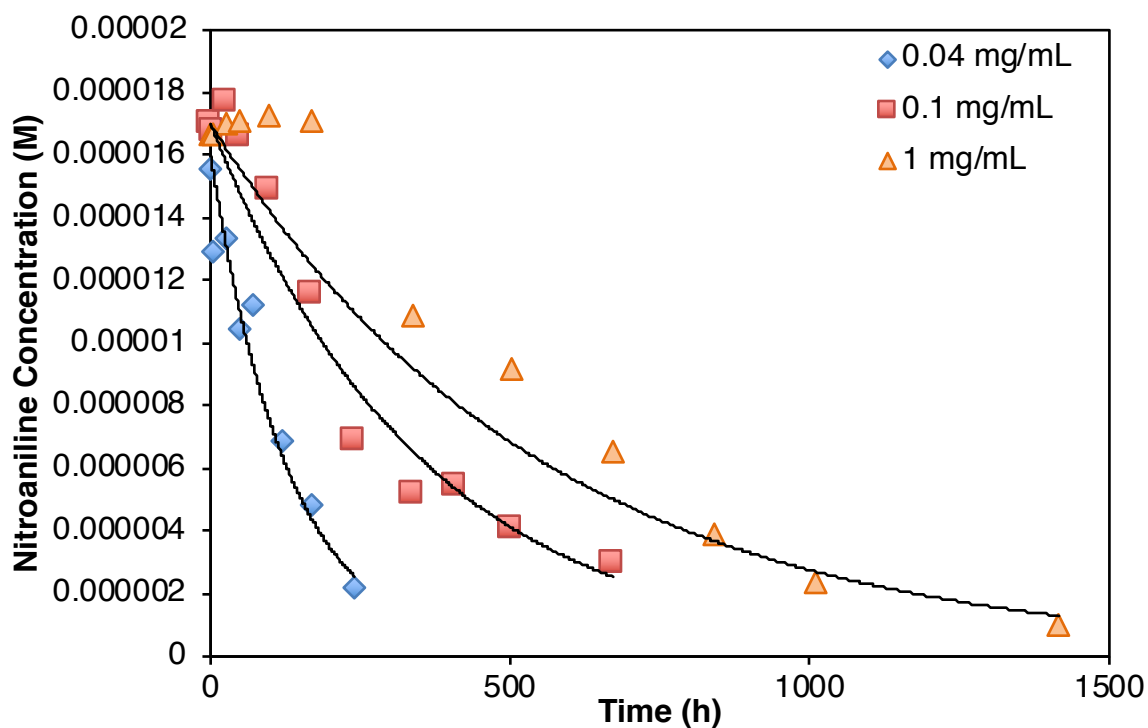


Figure A172. Concentrations of *p*-nitroaniline converted by SC (blue diamond, 0.04 mg/mL; red square, 0.1 mg/mL; orange triangle, 1.0 mg/mL) over time at room temperature.

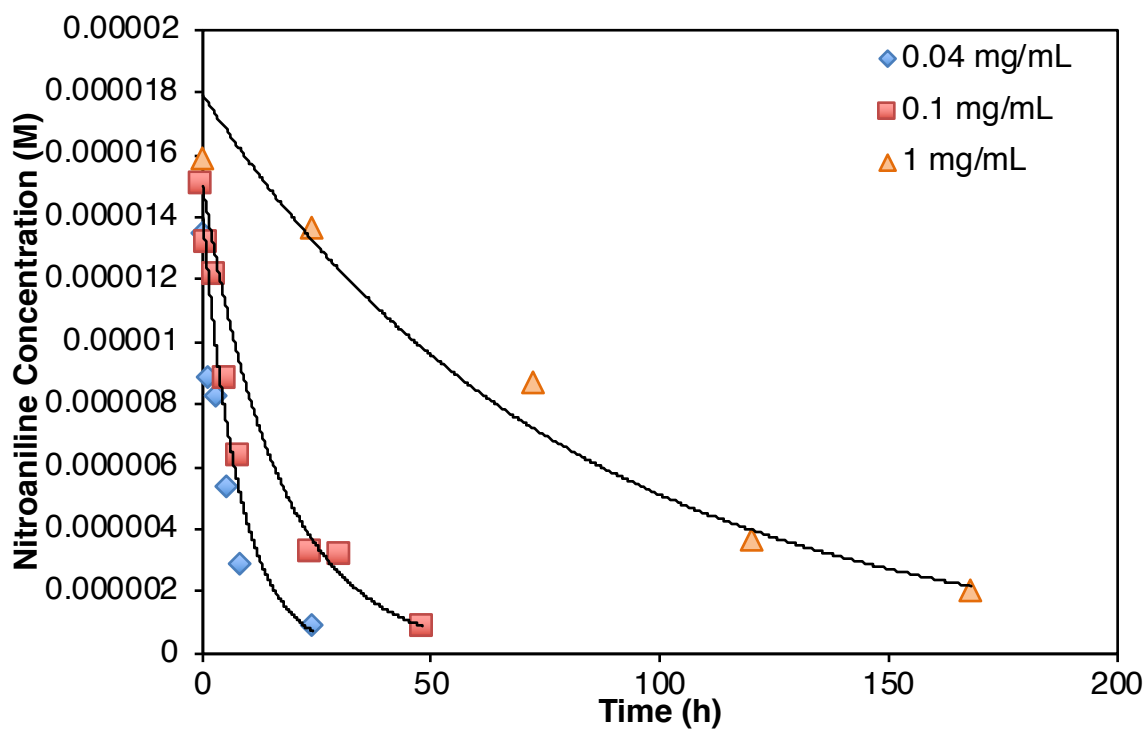


Figure A173. Concentrations of *p*-nitroaniline converted by SC (blue diamond, 0.04 mg/mL; red square, 0.1 mg/mL; orange triangle, 1.0 mg/mL) over time at 40 °C.

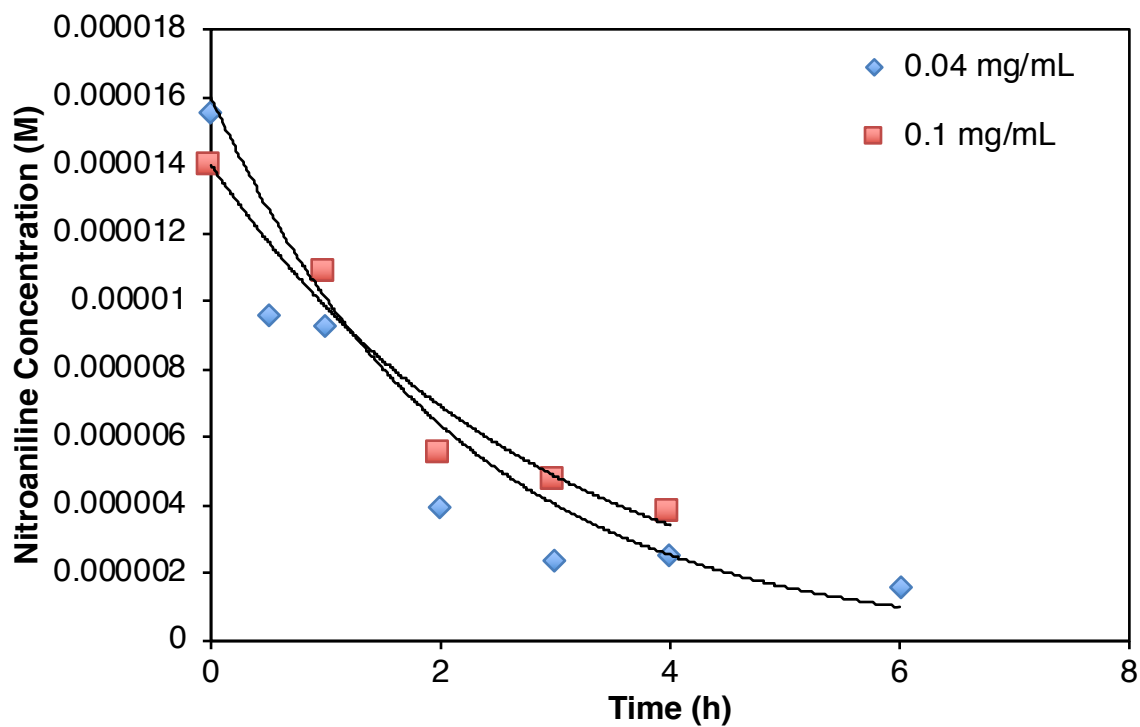


Figure A174. Concentrations of *p*-nitroaniline converted by SC (blue diamond, 0.04 mg/mL; red square, 0.1 mg/mL) over time at 50 °C.

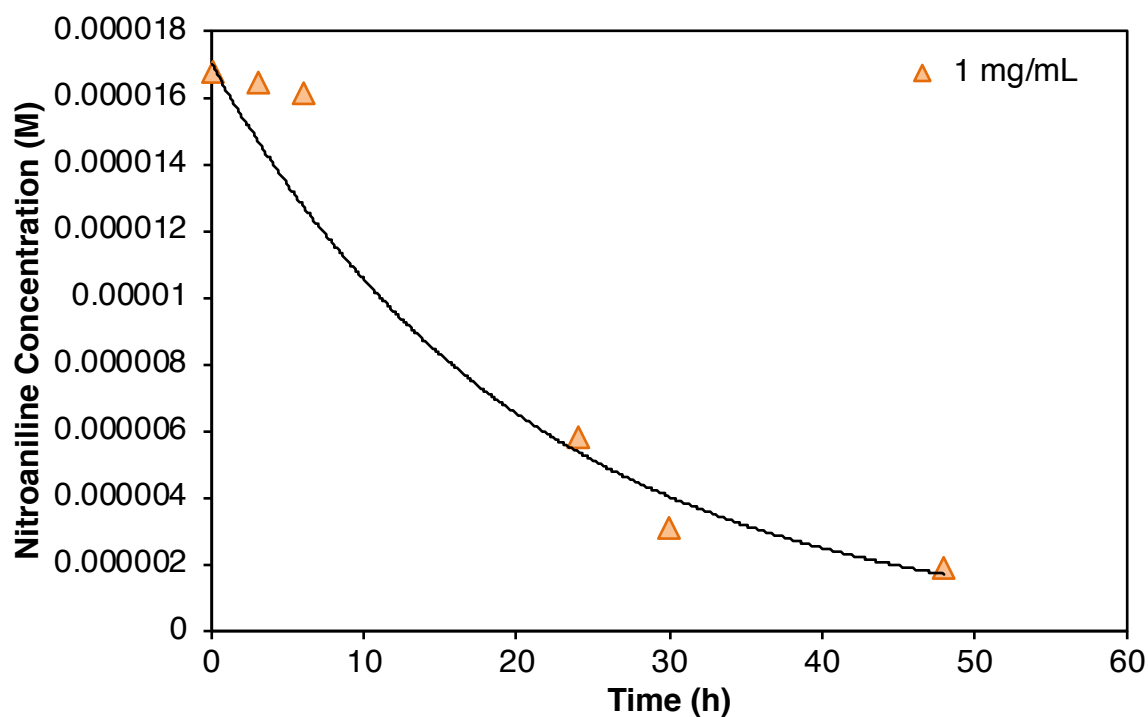


Figure A175. Concentrations of *p*-nitroaniline converted by SC (1 mg/mL) over time at 50 °C.

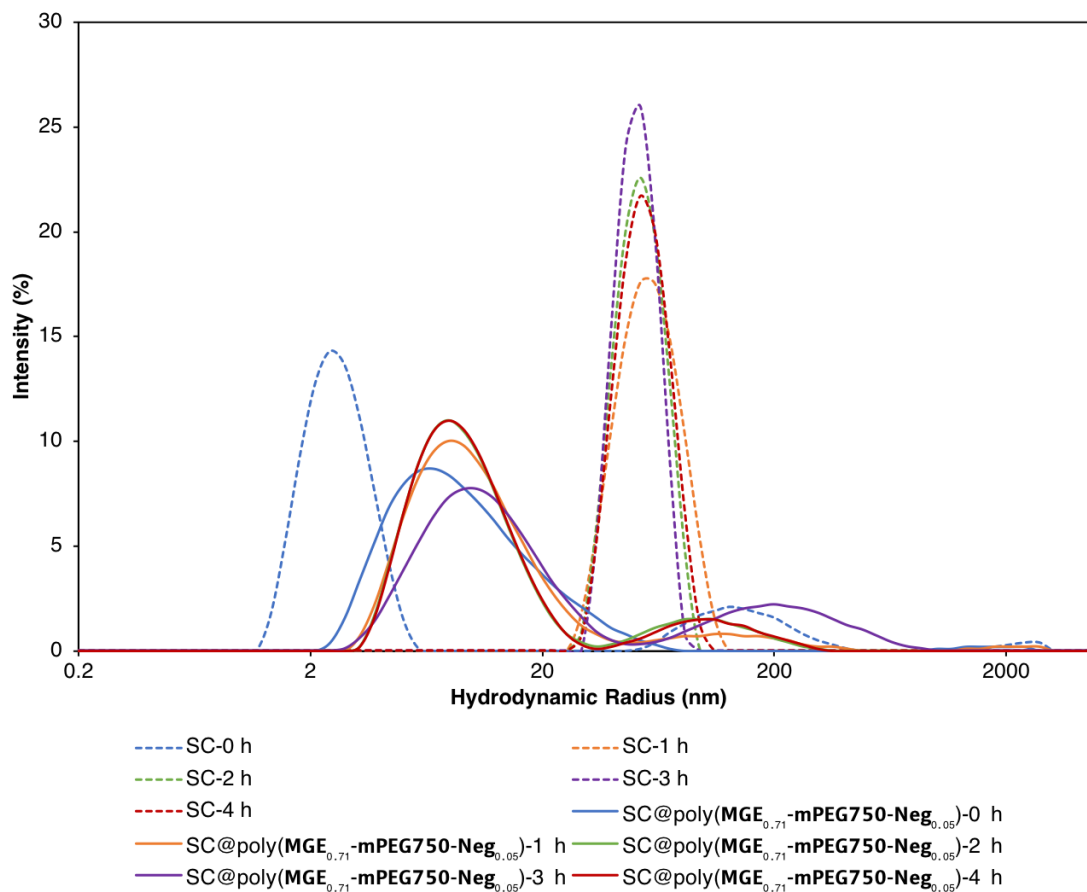


Figure A176. DLS results of SC (dotted line) and SC@poly(MGE_{0.71}-mPEG750-Neg_{0.05}) (solid line) in Tris-HCl buffer at 50 °C for 4 h.

REFERENCES

REFERENCES

1. Herzberger, J.; Niederer, K.; Pohlitz, H.; Seiwert, J.; Worm, M.; Wurm, F. R.; Frey, H. Polymerization of Ethylene Oxide, Propylene Oxide, and Other Alkylene Oxides: Synthesis, Novel Polymer Architectures, and Bioconjugation. *Chem. Rev.* **2016**, *116*, 2170–2243. DOI: 10.1021/acs.chemrev.5b00441.
2. Dingels, C.; Frey, H. From Biocompatible to Biodegradable: Poly(Ethylene Glycol)s with Predetermined Breaking Points. In *Hierarchical Macromolecular Structures: 60 Years after the Staudinger Nobel Prize II*; Percec, V., Ed.; Advances in Polymer Science; Springer International Publishing: Cham, 2013; Vol. 262, pp 167–190.
3. Mangold, C.; Wurm, F.; Frey, H. Functional PEG-Based Polymers with Reactive Groups via Anionic ROP of Tailor-Made Epoxides. *Polym. Chem.* **2012**, *3*, 1714–1721. DOI: 10.1039/c2py00489e.
4. Brocas, A.-L.; Mantzaridis, C.; Tunc, D.; Carlotti, S. Polyether Synthesis: From Activated or Metal-Free Anionic Ring-Opening Polymerization of Epoxides to Functionalization. *Prog. Polym. Sci.* **2013**, *38*, 845–873.
5. Odian, G. *Principles of Polymerization*, Fourth.; John Wiley & Sons, Inc., 2004.
6. Flory, P. J. Molecular Size Distribution in Ethylene Oxide Polymers. *J. Am. Chem. Soc.* **1940**, *62*, 1561–1565. DOI: 10.1021/ja01863a066.
7. Billouard, C.; Carlotti, S.; Desbois, P.; Deffieux, A. “Controlled” High-Speed Anionic Polymerization of Propylene Oxide Initiated by Alkali Metal Alkoxide/Trialkylaluminum Systems. *Macromolecules* **2004**, *37*, 4038–4043. DOI: 10.1021/ma035768t.
8. Carlotti, S.; Labbé, A.; Rejsek, V.; Doutaz, S.; Gervais, M.; Deffieux, A. Living/Controlled Anionic Polymerization and Copolymerization of Epichlorohydrin with Tetraoctylammonium Bromide–Triisobutylaluminum Initiating Systems. *Macromolecules* **2008**, *41*, 7058–7062. DOI: 10.1021/ma801422c.
9. Hatada, K.; Kitayama, T. Stereochemistry of Polymers. In *NMR Spectroscopy of Polymers*; Hatada, K., Kitayama, T., Eds.; Springer Berlin Heidelberg: Berlin, Heidelberg, 2004; pp 73–93.
10. Childers, M. I.; Longo, J. M.; Van Zee, N. J.; LaPointe, A. M.; Coates, G. W. Stereoselective Epoxide Polymerization and Copolymerization. *Chem. Rev.* **2014**, *114*, 8129–8152. DOI: 10.1021/cr400725x.
11. Peretti, K. L.; Ajiro, H.; Cohen, C. T.; Lobkovsky, E. B.; Coates, G. W. A Highly

- Active, Isospecific Cobalt Catalyst for Propylene Oxide Polymerization. *J. Am. Chem. Soc.* **2005**, *127*, 11566–11567. DOI: 10.1021/ja053451y.
12. Hirahata, W.; Thomas, R. M.; Lobkovsky, E. B.; Coates, G. W. Enantioselective Polymerization of Epoxides: A Highly Active and Selective Catalyst for the Preparation of Stereoregular Polyethers and Enantiopure Epoxides. *J. Am. Chem. Soc.* **2008**, *130*, 17658–17659. DOI: 10.1021/ja807709j.
 13. Thomas, R. M.; Widger, P. C. B.; Ahmed, S. M.; Jeske, R. C.; Hirahata, W.; Lobkovsky, E. B.; Coates, G. W. Enantioselective Epoxide Polymerization Using a Bimetallic Cobalt Catalyst. *J. Am. Chem. Soc.* **2010**, *132*, 16520–16525. DOI: 10.1021/ja1058422.
 14. Ahmed, S. M.; Poater, A.; Childers, M. I.; Widger, P. C. B.; LaPointe, A. M.; Lobkovsky, E. B.; Coates, G. W.; Cavallo, L. Enantioselective Polymerization of Epoxides Using Biaryl-Linked Bimetallic Cobalt Catalysts: A Mechanistic Study. *J. Am. Chem. Soc.* **2013**, *135*, 18901–18911. DOI: 10.1021/ja409521z.
 15. Morris, L. S.; Childers, M. I.; Coates, G. W. Bimetallic Chromium Catalysts with Chain Transfer Agents: A Route to Isotactic Poly(Propylene Oxide)s with Narrow Dispersities. *Angew. Chem. Int. Ed Engl.* **2018**, *130*, 5833–5836. DOI: 10.1002/ange.201801380.
 16. Gauthier, M. A.; Gibson, M. I.; Klok, H.-A. Synthesis of Functional Polymers by Post-Polymerization Modification. *Angew. Chemie Int. Ed.* **2009**, *48*, 48–58. DOI: 10.1002/anie.200801951.
 17. Günay, K. A.; Theato, P.; Klok, H.-A. History of Post-Polymerization Modification. In *Functional Polymers by Post-Polymerization Modification*; Theato, P., Klok, H.-A., Eds.; 1; Wiley-VCH Verlag GmbH & Co. KGaA, 2012; pp 1–44.
 18. Günay, K. A.; Theato, P.; Klok, H.-A. Standing on the Shoulders of Hermann Staudinger: Post-Polymerization Modification from Past to Present. *J. Polym. Sci. Part A Polym. Chem.* **2013**, *51*, 1–28. DOI: 10.1002/pola.26333.
 19. Liu, Y.; Pauloehrl, T.; Presolski, S. I.; Albertazzi, L.; Palmans, A. R. A.; Meijer, E. W. Modular Synthetic Platform for the Construction of Functional Single-Chain Polymeric Nanoparticles: From Aqueous Catalysis to Photosensitization. *J. Am. Chem. Soc.* **2015**, *137*, 13096–13105. DOI: 10.1021/jacs.5b08299.
 20. Zhu, Y.; Batchelor, R.; Lowe, A. B.; Roth, P. J. Design of Thermoresponsive Polymers with Aqueous LCST, UCST, or Both: Modification of a Reactive Poly(2-Vinyl-4,4-Dimethylazlactone) Scaffold. *Macromolecules* **2016**, *49*, 672–680. DOI: 10.1021/acs.macromol.5b02056.
 21. König, N. F.; Al Ouahabi, A.; Poyer, S.; Charles, L.; Lutz, J.-F. A Simple Post-Polymerization Modification Method for Controlling Side-Chain Information in

- Digital Polymers. *Angew. Chem. Int. Ed Engl.* **2017**, *56*, 7297–7301. DOI: 10.1002/anie.201702384.
22. Blasco, E.; Sims, M. B.; Goldmann, A. S.; Sumerlin, B. S.; Barner-Kowollik, C. 50th Anniversary Perspective: Polymer Functionalization. *Macromolecules* **2017**, *50*, 5215–5252. DOI: 10.1021/acs.macromol.7b00465.
 23. Roth, P. J. Composing Well-Defined Stimulus-Responsive Materials Through Postpolymerization Modification Reactions. *Macromol. Chem. Phys.* **2014**, *215*, 825–838. DOI: 10.1002/macp.201400073.
 24. Iha, R. K.; Wooley, K. L.; Nyström, A. M.; Burke, D. J.; Kade, M. J.; Hawker, C. J. Applications of Orthogonal “Click” Chemistries in the Synthesis of Functional Soft Materials. *Chem. Rev.* **2009**, *109*, 5620–5686. DOI: 10.1021/cr900138t.
 25. Mansfeld, U.; Pietsch, C.; Hoogenboom, R.; Remzi Becer, C.; Schubert, U. S. Clickable Initiators, Monomers and Polymers in Controlled Radical Polymerizations – a Prospective Combination in Polymer Science. *Polym. Chem.* **2010**, *1*, 1560–1598. DOI: 10.1039/C0PY00168F.
 26. Kempe, K.; Krieg, A.; Remzi Becer, C.; Schubert, U. S. “Clicking” on/with Polymers: A Rapidly Expanding Field for the Straightforward Preparation of Novel Macromolecular Architectures. *Chem. Soc. Rev.* **2011**, *41*, 176–191. DOI: 10.1039/C1CS15107J.
 27. Xi, W.; Scott, T. F.; Kloxin, C. J.; Bowman, C. N. Click Chemistry in Materials Science. *Adv. Funct. Mater.* **2014**, *24*, 2572–2590. DOI: 10.1002/adfm.201302847.
 28. Kolb, H. C.; Finn, M. G.; Sharpless, K. B. Click Chemistry: Diverse Chemical Function from a Few Good Reactions. *Angewandte Chemie - International Edition*. 2001, pp 2004–2021.
 29. Rostovtsev, V. V.; Green, L. G.; Fokin, V. V.; Sharpless, K. B. A Stepwise Huisgen Cycloaddition Process: Copper(I)-Catalyzed Regioselective “Ligation” of Azides and Terminal Alkynes. *Angew. Chemie Int. Ed.* **2002**, *41*, 2596–2599. DOI: 10.1002/1521-3773(20020715)41:14<2596::AID-ANIE2596>3.0.CO;2-4.
 30. Tornøe, C. W.; Christensen, C.; Meldal, M. Peptidotriazoles on Solid Phase: [1,2,3]-Triazoles by Regiospecific Copper(I)-Catalyzed 1,3-Dipolar Cycloadditions of Terminal Alkynes to Azides. *J. Org. Chem.* **2002**, *67*, 3057–3064. DOI: 10.1021/jo011148j.
 31. Meldal, M.; Tornøe, C. W. Cu-Catalyzed Azide–Alkyne Cycloaddition. *Chem. Rev.* **2008**, *108*, 2952–3015. DOI: 10.1021/cr0783479.
 32. Hoyle, C. E.; Lee, T. Y.; Roper, T. Thiol–Enes: Chemistry of the Past with Promise for the Future. *J. Polym. Sci. A Polym. Chem.* **2004**, *42*, 5301–5338. DOI: 10.1002/pola.20366.

33. Hoyle, C. E.; Lowe, A. B.; Bowman, C. N. Thiol-Click Chemistry: A Multifaceted Toolbox for Small Molecule and Polymer Synthesis. *Chem. Soc. Rev.* **2010**, *39*, 1355–1387. DOI: 10.1039/B901979K.
34. Hoyle, C. E.; Bowman, C. N. Thiol-Ene Click Chemistry. *Angew. Chem. Int. Ed Engl.* **2010**, *49*, 1540–1573. DOI: 10.1002/anie.200903924.
35. Kade, M. J.; Burke, D. J.; Hawker, C. J. The Power of Thiol-Ene Chemistry. *J. Polym. Sci. A Polym. Chem.* **2010**, *48*, 743–750. DOI: 10.1002/pola.23824.
36. Lowe, A. B. Thiol-Ene “Click” Reactions and Recent Applications in Polymer and Materials Synthesis. *Polym. Chem.* **2010**, *1*, 17–36. DOI: 10.1039/B9PY00216B.
37. Lowe, A. B. Thiol-Ene “Click” Reactions and Recent Applications in Polymer and Materials Synthesis: A First Update. *Polym. Chem.* **2014**, *5*, 4820–4870. DOI: 10.1039/C4PY00339J.
38. Nair, D. P.; Podgórski, M.; Chatani, S.; Gong, T.; Xi, W.; Fenoli, C. R.; Bowman, C. N. The Thiol-Michael Addition Click Reaction: A Powerful and Widely Used Tool in Materials Chemistry. *Chem. Mater.* **2014**, *26*, 724–744. DOI: 10.1021/cm402180t.
39. Hoogenboom, R. Thiol-Yne Chemistry: A Powerful Tool for Creating Highly Functional Materials. *Angew. Chem. Int. Ed Engl.* **2010**, *49*, 3415–3417. DOI: 10.1002/anie.201000401.
40. Lowe, A. B.; Hoyle, C. E.; Bowman, C. N. Thiol-Yne Click Chemistry: A Powerful and Versatile Methodology for Materials Synthesis. *J. Mater. Chem.* **2010**, *20*, 4745–4750. DOI: 10.1039/B917102A.
41. Lowe, A. B. Thiol-Yne ‘Click’/Coupling Chemistry and Recent Applications in Polymer and Materials Synthesis and Modification. *Polym.* **2014**, *55*, 5517–5549. DOI: 10.1016/j.polymer.2014.08.015.
42. Gevrek, T. N.; Arslan, M.; Sanyal, A. Design and Synthesis of Maleimide Group Containing Polymeric Materials via the Diels-Alder/Retro Diels-Alder Strategy. In *Functional Polymers by Post-Polymerization Modification*; Theato, P., Klok, H.-A., Eds.; Wiley-VCH Verlag GmbH & Co. KGaA, 2012; pp 119–151.
43. Yuksekdog, Y. N.; Gevrek, T. N.; Sanyal, A. Diels-Alder “Clickable” Polymer Brushes: A Versatile Catalyst-Free Conjugation Platform. *ACS Macro Lett.* **2017**, *6*, 415–420. DOI: 10.1021/acsmacrolett.7b00041.
44. Mather, B. D.; Viswanathan, K.; Miller, K. M.; Long, T. E. Michael Addition Reactions in Macromolecular Design for Emerging Technologies. *Prog. Polym. Sci.* **2006**, *31*, 487–531. DOI: 10.1016/j.progpolymsci.2006.03.001.
45. Golas, P. L.; Matyjaszewski, K. Marrying Click Chemistry with Polymerization:

- Expanding the Scope of Polymeric Materials. *Chem. Soc. Rev.* **2010**, 39, 1338–1354. DOI: 10.1039/B901978M.
46. Lutz, J.-F.; Sumerlin, B. S. The Role of Click Chemistry in Polymer Synthesis. In *Click Chemistry for Biotechnology and Materials Science*; Lahann, J., Ed.; John Wiley & Sons, Ltd, 2009; pp 69–88.
 47. Evans, R. A. The Rise of Azide–Alkyne 1,3-Dipolar ‘Click’ Cycloaddition and Its Application to Polymer Science and Surface Modification. *Aust. J. Chem.* **2007**, 60, 384–395. DOI: 10.1071/CH06457.
 48. Binder, W. H.; Sachsenhofer, R. ‘Click’ Chemistry in Polymer and Material Science: An Update. *Macromol. Rapid Commun.* **2008**, 29, 952–981. DOI: 10.1002/marc.200800089.
 49. Jiang, X.; Vogel, E. B.; Smith III, M. R.; Baker, G. L. “Clickable” Polyglycolides: Tunable Synthons for Thermoresponsive, Degradable Polymers. *Macromolecules* **2008**, 41, 1937–1944. DOI: 10.1021/ma7027962.
 50. Herzberger, J.; Leibig, D.; Langhanki, J.; Moers, C.; Opatz, T.; Frey, H. “Clickable PEG” via Anionic Copolymerization of Ethylene Oxide and Glycidyl Propargyl Ether. *Polym. Chem.* **2017**, 8, 1882–1887. DOI: 10.1039/C7PY00173H.
 51. Doran, S.; Yilmaz, G.; Yagci, Y. Tandem Photoinduced Cationic Polymerization and CuAAC for Macromolecular Synthesis. *Macromolecules* **2015**, 48, 7446–7452. DOI: 10.1021/acs.macromol.5b01857.
 52. Huisgen, R. 1,3-Dipolar Cycloaddition. *Proc. Chem. Soc.* **1961**, 0, 357–396. DOI: 10.1039/PS9610000357.
 53. Worrell, B. T.; Malik, J. A.; Fokin, V. V. Direct Evidence of a Dinuclear Copper Intermediate in Cu(I)-Catalyzed Azide-Alkyne Cycloadditions. *Science* **2013**, 340, 457–460. DOI: 10.1126/science.1229506.
 54. Cai, T.; Li, M.; Neoh, K.-G.; Kang, E.-T. Preparation of Stimuli Responsive Polycaprolactone Membranes of Controllable Porous Morphology via Combined Atom Transfer Radical Polymerization, Ring-Opening Polymerization and Thiol–Yne Click Chemistry. *J. Mater. Chem.* **2012**, 22, 16248–16258. DOI: 10.1039/C2JM33419D.
 55. Clodt, J. I.; Filiz, V.; Rangou, S.; Buhr, K.; Abetz, C.; Höche, D.; Hahn, J.; Jung, A.; Abetz, V. Double Stimuli-Responsive Isoporous Membranes via Post-Modification of PH-Sensitive Self-Assembled Diblock Copolymer Membranes. *Adv. Funct. Mater.* **2013**, 23, 731–738. DOI: 10.1002/adfm.201202015.
 56. Kumar, A.; Ujjwal, R. R.; Mittal, A.; Bansal, A.; Ojha, U. Polyacryloyl Hydrazide: An Efficient, Simple, and Cost Effective Precursor to a Range of Functional Materials through Hydrazide Based Click Reactions. *ACS Appl. Mater. Interfaces*

2014, 6, 1855–1865. DOI: 10.1021/am404837f.

57. Liu, X.; Hu, D.; Jiang, Z.; Zhuang, J.; Xu, Y.; Guo, X.; Thayumanavan, S. Multi-Stimuli-Responsive Amphiphilic Assemblies through Simple Postpolymerization Modifications. *Macromolecules* **2016**, 49, 6186–6192. DOI: 10.1021/acs.macromol.6b01397.
58. Qiu, Y.; Park, K. Environment-Sensitive Hydrogels for Drug Delivery. *Adv. Drug Deliv. Rev.* **2001**, 53, 321–339. DOI: 10.1016/S0169-409X(01)00203-4.
59. Schmaljohann, D. Thermo- and PH-Responsive Polymers in Drug Delivery. *Adv. Drug Deliv. Rev.* **2006**, 58, 1655–1670. DOI: 10.1016/j.addr.2006.09.020.
60. Wei, M.; Gao, Y.; Li, X.; Serpe, M. J. Stimuli-Responsive Polymers and Their Applications. *Polym. Chem.* **2016**, 8, 127–143. DOI: 10.1039/C6PY01585A.
61. Gulzar, A.; Gai, S.; Yang, P.; Li, C.; Ansari, M. B.; Lin, J. Stimuli Responsive Drug Delivery Application of Polymer and Silica in Biomedicine. *J. Mater. Chem. B Mater. Biol. Med.* **2015**, 3, 8599–8622. DOI: 10.1039/C5TB00757G.
62. Karimi, M.; Sahandi Zangabad, P.; Ghasemi, A.; Amiri, M.; Bahrami, M.; Malekzad, H.; Ghahramanzadeh Asl, H.; Mahdiah, Z.; Bozorgomid, M.; Ghasemi, A.; Rahmani Taji Boyuk, M. R.; Hamblin, M. R. Temperature-Responsive Smart Nanocarriers for Delivery Of Therapeutic Agents: Applications and Recent Advances. *ACS Appl. Mater. Interfaces* **2016**, 8, 21107–21133. DOI: 10.1021/acsami.6b00371.
63. Ganta, S.; Devalapally, H.; Shahiwala, A.; Amiji, M. A Review of Stimuli-Responsive Nanocarriers for Drug and Gene Delivery. *J. Control. Release* **2008**, 126, 187–204. DOI: 10.1016/j.jconrel.2007.12.017.
64. Matsumoto, A.; Ikeda, S.; Harada, A.; Kataoka, K. Glucose-Responsive Polymer Bearing a Novel Phenylborate Derivative as a Glucose-Sensing Moiety Operating at Physiological PH Conditions. *Biomacromolecules* **2003**, 4, 1410–1416. DOI: 10.1021/bm034139o.
65. Buenger, D.; Topuz, F.; Groll, J. Hydrogels in Sensing Applications. *Prog. Polym. Sci.* **2012**, 37, 1678–1719. DOI: 10.1016/j.progpolymsci.2012.09.001.
66. Islam, M. R.; Ahiabu, A.; Li, X.; Serpe, M. J. Poly (N-Isopropylacrylamide) Microgel-Based Optical Devices for Sensing and Biosensing. *Sensors* **2014**, 14, 8984–8995. DOI: 10.3390/s140508984.
67. Thomas, I. S. W.; Joly, G. D.; Swager, T. M. Chemical Sensors Based on Amplifying Fluorescent Conjugated Polymers. *Chem. Rev.* **2007**, 107, 1339–1386. DOI: 10.1021/cr0501339.
68. Mendes, P. M. Stimuli-Responsive Surfaces for Bio-Applications. *Chem. Soc. Rev.*

2008, 37, 2512–2529. DOI: 10.1039/b714635n.

69. Cole, M. A.; Voelcker, N. H.; Thissen, H.; Griesser, H. J. Stimuli-Responsive Interfaces and Systems for the Control of Protein-Surface and Cell-Surface Interactions. *Biomaterials* **2009**, 30, 1827–1850. DOI: 10.1016/j.biomaterials.2008.12.026.
70. Jiang, X.; Smith III, M. R.; Baker, G. L.; Smith, M. R.; Baker, G. L.; Smith III, M. R.; Baker, G. L. Water-Soluble Thermoresponsive Polylactides. *Macromolecules* **2008**, 41, 318–324. DOI: 10.1021/ma070775t.
71. Aseyev, V.; Tenhu, H.; Winnik, F. M. Non-Ionic Thermoresponsive Polymers in Water. In *Self Organized Nanostructures of Amphiphilic Block Copolymers II*; Müller, A. H. E., Borisov, O., Eds.; Advances in Polymer Science; Springer Berlin Heidelberg, 2010; pp 29–89.
72. Kohsaka, Y.; Matsumoto, Y.; Kitayama, T. α -(Aminomethyl)Acrylate: Polymerization and Spontaneous Post-Polymerization Modification of β -Amino Acid Ester for a PH/Temperature-Responsive Material. *Polym. Chem.* **2015**, 6, 5026–5029. DOI: 10.1039/C5PY00723B.
73. Tian, W.; Wei, X.-Y.; Liu, Y.-Y.; Fan, X.-D. A Branching Point Thermo and PH Dual-Responsive Hyperbranched Polymer Based on Poly(N-Vinylcaprolactam) and Poly(N,N-Diethyl Aminoethyl Methacrylate). *Polym. Chem.* **2013**, 4, 2850–2863. DOI: 10.1039/C3PY00218G.
74. Amato, D. N.; Strange, G. A.; Swanson, J. P.; Chavez, A. D.; Roy, S. E.; Varney, K. L.; Machado, C. A.; Amato, D. V.; Costanzo, P. J. Synthesis and Evaluation of Thermally-Responsive Coatings Based upon Diels–Alder Chemistry and Renewable Materials. *Polym. Chem.* **2013**, 5, 69–76. DOI: 10.1039/C3PY01024D.
75. Roy, D.; Brooks, W. L. A.; Sumerlin, B. S. New Directions in Thermoresponsive Polymers. *Chem. Soc. Rev.* **2013**, 42, 7214–7243. DOI: 10.1039/c3cs35499g.
76. Bose, A.; Jana, S.; Saha, A.; Mandal, T. K. Amphiphilic Polypeptide-Polyoxazoline Graft Copolymer Conjugate with Tunable Thermoresponsiveness: Synthesis and Self-Assembly into Various Micellar Structures in Aqueous and Nonaqueous Media. *Polym.* **2017**, 110, 12–24. DOI: 10.1016/j.polymer.2016.12.068.
77. Li, Y.-Y.; Hua, S.-H.; Xiao, W.; Wang, H.-Y.; Luo, X.-H.; Li, C.; Cheng, S.-X.; Zhang, X.-Z.; Zhuo, R.-X. Dual-Vectors of Anti-Cancer Drugs and Genes Based on PH-Sensitive Micelles Self-Assembled from Hybrid Polypeptide Copolymers. *J. Mater. Chem.* **2011**, 21, 3100–3106. DOI: 10.1039/C0JM03385E.
78. Yao, J.; Ruan, Y.; Zhai, T.; Guan, J.; Tang, G.; Li, H.; Dai, S. ABC Block Copolymer as “Smart” PH-Responsive Carrier for Intracellular Delivery of Hydrophobic Drugs. *Polym.* **2011**, 52, 3396–3404. DOI:

10.1016/j.polymer.2011.05.039.

79. Punnamaraju, S.; You, H.; Steckl, A. J. Triggered Release of Molecules across Droplet Interface Bilayer Lipid Membranes Using Photopolymerizable Lipids. *Langmuir* **2012**, *28*, 7657–7664. DOI: 10.1021/la3011663.
80. Dübner, M.; Spencer, N. D.; Padeste, C. Light-Responsive Polymer Surfaces via Postpolymerization Modification of Grafted Polymer-Brush Structures. *Langmuir* **2014**, *30*, 14971–14981. DOI: 10.1021/la503388j.
81. Zhao, Y. Light-Responsive Block Copolymer Micelles. *Macromolecules* **2012**, *45*, 3647–3657. DOI: 10.1021/ma300094t.
82. Shultz, A. R.; Flory, P. J. Phase Equilibria in Polymer—Solvent Systems^{1,2}. *J. Am. Chem. Soc.* **1952**, *74*, 4760–4767. DOI: 10.1021/ja01139a010.
83. Hoogenboom, R. 2 - Temperature-Responsive Polymers: Properties, Synthesis and Applications. In *Smart Polymers and their Applications*; Woodhead Publishing, 2014; pp 15–44.
84. Vanparijs, N.; Nuhn, L.; De Geest, B. G. Transiently Thermoresponsive Polymers and Their Applications in Biomedicine. *Chem. Soc. Rev.* **2017**, *46*, 1193–1239. DOI: 10.1039/c6cs00748a.
85. Knychala, P.; Timachova, K.; Banaszak, M.; Balsara, N. P. 50th Anniversary Perspective: Phase Behavior of Polymer Solutions and Blends. *Macromolecules* **2017**, *50*, 3051–3065. DOI: 10.1021/acs.macromol.6b02619.
86. Flory, P. J. Thermodynamics of High Polymer Solutions. *J. Chem. Phys.* **1942**, *10*, 660. DOI: 10.1063/1.1723621.
87. Flory, P. J. Thermodynamics of High Polymer Solutions. *J. Chem. Phys.* **1941**, *9*, 660. DOI: 10.1063/1.1750971.
88. Huggins, M. L. Solutions of Long Chain Compounds. *J. Chem. Phys.* **1941**, *9*, 440. DOI: 10.1063/1.1750930.
89. Huggins, M. L. THERMODYNAMIC PROPERTIES OF SOLUTIONS OF LONG-CHAIN COMPOUNDS. *Ann. N. Y. Acad. Sci.* **1942**, *43*, 1–32. DOI: 10.1111/j.1749-6632.1942.tb47940.x.
90. Freeman, P. I.; Rowlinson, J. S. Lower Critical Points in Polymer Solutions. *Polym.* **1960**, *1*, 20–26. DOI: 10.1016/0032-3861(60)90004-5.
91. Somcynsky, T. The Lower Critical Solution Temperature (LCST) of Non-Polar Polymer Solutions: An Introduction. *Polym. Eng. Sci.* **1982**, *22*, 58–63.
92. Heskins, M.; Guillet, J. E. Solution Properties of Poly(N-Isopropylacrylamide). *J.*

Macromol. Sci. Part A - Chem. **1968**, 2, 1441–1455. DOI: 10.1080/10601326808051910.

93. Halperin, A.; Kröger, M.; Winnik, F. M. Poly(N-Isopropylacrylamide) Phase Diagrams: Fifty Years of Research. *Angew. Chem. Int. Ed.* **2015**, 54, 15342–15367. DOI: 10.1002/anie.201506663.
94. Li, X.; Gao, Y.; Serpe, M. J. Responsive Polymer-Based Assemblies for Sensing Applications. *Macromol. Rapid Commun.* **2015**, 36, 1382–1392. DOI: 10.1002/marc.201500066.
95. Vogel, E. B. Synthesis, Characterization, and Applications of Functionalized Polyglycolides, Michigan State University, 2008, Vol. Doctor of.
96. Newkome, G. R.; Arai, S. Unimolecular Micelle - Synthesis of 4-Directional [9]4-Arborols. In *Abstracts of Papers of the American Chemical Society*; 1987; Vol. 193, p 65–ORGN.
97. Newkome, G. R.; Moorefield, C. N.; Baker, G. R.; Saunders, M. J.; Grossman, S. H. Unimolecular Micelles. *Angew. Chemie Int. Ed. English* **1991**, 30, 1178–1180. DOI: 10.1002/anie.199111781.
98. Newkome, G. R.; Moorefield, C. N.; Baker, G. R.; Johnson, A. L.; Behera, R. K. Alkane Cascade Polymers Possessing Micellar Topology: Micellanoic Acid Derivatives. *Angew. Chem. Int. Ed Engl.* **1991**, 30, 1176–1178. DOI: 10.1002/anie.199111761.
99. Bosman, A. W.; Janssen, H. M.; Meijer, E. W. About Dendrimers: Structure, Physical Properties, and Applications. *Chem. Rev.* **1999**, 99, 1665–1688. DOI: 10.1021/cr970069y.
100. Esfand, R.; Tomalia, D. A. Poly(Amidoamine) (PAMAM) Dendrimers: From Biomimicry to Drug Delivery and Biomedical Applications. *Drug Discov. Today* **2001**, 6, 427–436. DOI: [http://dx.doi.org/10.1016/S1359-6446\(01\)01757-3](http://dx.doi.org/10.1016/S1359-6446(01)01757-3).
101. Grayson, S. M.; Fréchet, J. M. Convergent Dendrons and Dendrimers: From Synthesis to Applications. *Chem. Rev.* **2001**, 101, 3819–3868. DOI: 10.1021/cr990116h.
102. Gao, C.; Yan, D. Hyperbranched Polymers: From Synthesis to Applications. *Prog. Polym. Sci.* **2004**, 29, 183–275. DOI: 10.1016/j.progpolymsci.2003.12.002.
103. Lee, C. C.; MacKay, J. A.; Fréchet, J. M. J.; Szoka, F. C. Designing Dendrimers for Biological Applications. *Nat. Biotechnol.* **2005**, 23, 1517–1526. DOI: 10.1038/nbt1171.
104. Wilms, D.; Stiriba, S.-E.; Frey, H. Hyperbranched Polyglycerols: From the Controlled Synthesis of Biocompatible Polyether Polyols to Multipurpose

Applications. *Acc. Chem. Res.* **2010**, *43*, 129–141. DOI: 10.1021/ar900158p.

105. Astruc, D.; Boisselier, E.; Ornelas, C. Dendrimers Designed for Functions: From Physical, Photophysical, and Supramolecular Properties to Applications in Sensing, Catalysis, Molecular Electronics, Photonics, and Nanomedicine. *Chem. Rev.* **2010**, *110*, 1857–1959. DOI: 10.1021/cr900327d.
106. Schömer, M.; Schüll, C.; Frey, H. Hyperbranched Aliphatic Polyether Polyols. *J. Polym. Sci. A Polym. Chem.* **2013**, *51*, 995–1019. DOI: 10.1002/pola.26496.
107. Vögtle, F.; Richardt, G.; Werner, N. *Dendrimer Chemistry*, 1. Aufl.; Wiley-VCH: Weinheim, 2009.
108. Mes, T.; van der Weegen, R.; Palmans, A. R. A.; Meijer, E. W. Single-Chain Polymeric Nanoparticles by Stepwise Folding. *Angew. Chem. Int. Ed Engl.* **2011**, *50*, 5085–5089. DOI: 10.1002/anie.201100104.
109. Ouchi, M.; Badi, N.; Lutz, J.-F.; Sawamoto, M. Single-Chain Technology Using Discrete Synthetic Macromolecules. *Nat. Chem.* **2011**, *3*, 917–924. DOI: 10.1038/nchem.1175.
110. Aiertza, M.; Odriozola, I.; Cabañero, G.; Grande, H.-J.; Loinaz, I. Single-Chain Polymer Nanoparticles. *Cell. Mol. Life Sci.* **2012**, *69*, 337–346. DOI: 10.1007/s00018-011-0852-x.
111. Altintas, O.; Barner-Kowollik, C. Single Chain Folding of Synthetic Polymers by Covalent and Non-Covalent Interactions: Current Status and Future Perspectives. *Macromol. Rapid Commun.* **2012**, *33*, 958–971. DOI: 10.1002/marc.201200049.
112. Sanchez-Sanchez, A.; Pérez-Baena, I.; Pomposo, J. A. Advances in Click Chemistry for Single-Chain Nanoparticle Construction. *Molecules* **2013**, *18*, 3339–3355. DOI: 10.3390/molecules18033339.
113. Lyon, C. K.; Prasher, A.; Hanlon, A. M.; Tuten, B. T.; Tooley, C. A.; Frank, P. G.; Berda, E. B. A Brief User's Guide to Single-Chain Nanoparticles. *Polym. Chem.* **2015**, *6*, 181–197. DOI: 10.1039/C4PY01217H.
114. Hanlon, A. M.; Lyon, C. K.; Berda, E. B. What Is Next in Single-Chain Nanoparticles? *Macromolecules* **2016**, *49*, 2–14. DOI: 10.1021/acs.macromol.5b01456.
115. Mavila, S.; Eivgi, O.; Berkovich, I.; Lemcoff, N. G. Intramolecular Cross-Linking Methodologies for the Synthesis of Polymer Nanoparticles. *Chem. Rev.* **2016**, *116*, 878–961. DOI: 10.1021/acs.chemrev.5b00290.
116. Mecerreyes, D.; Lee, V.; Hawker, C. J.; Hedrick, J. L.; Wursch, A.; Volksen, W.; Magbitang, T.; Huang, E.; Miller, R. D. A Novel Approach to Functionalized Nanoparticles: Self-Crosslinking of Macromolecules in Ultradilute Solution. *Adv.*

- Mater.* **2001**, *13*, 204–208. DOI: 10.1002/1521-4095(200102)13:3<204::AID-ADMA204>3.0.CO;2-9.
117. Wen, J.; Yuan, L.; Yang, Y.; Liu, L.; Zhao, H. Self-Assembly of Monotethered Single-Chain Nanoparticle Shape Amphiphiles. *ACS Macro Lett.* **2013**, *2*, 100–106. DOI: 10.1021/mz300636x.
 118. Tuten, B. T.; Chao, D.; Lyon, C. K.; Berda, E. B. Single-Chain Polymer Nanoparticles via Reversible Disulfide Bridges. *Polym. Chem.* **2012**, *3*, 3068–3071. DOI: 10.1039/C2PY20308A.
 119. Murray, B. S.; Fulton, D. A. Dynamic Covalent Single-Chain Polymer Nanoparticles. *Macromolecules* **2011**, *44*, 7242–7252. DOI: 10.1021/ma201331f.
 120. Buruaga, L.; Pomposo, J. A. Metal-Free Polymethyl Methacrylate (PMMA) Nanoparticles by Enamine “Click” Chemistry at Room Temperature. *Polymers* . 2011.
 121. Foster, E. J.; Berda, E. B.; Meijer, E. W. Metastable Supramolecular Polymer Nanoparticles via Intramolecular Collapse of Single Polymer Chains. *J. Am. Chem. Soc.* **2009**, *131*, 6964–6966. DOI: 10.1021/ja901687d.
 122. Terashima, T.; Sugita, T.; Fukae, K.; Sawamoto, M. Synthesis and Single-Chain Folding of Amphiphilic Random Copolymers in Water. *Macromolecules* **2014**, *47*, 589–600. DOI: 10.1021/ma402355v.
 123. Willenbacher, J.; Altintas, O.; Roesky, P. W.; Barner-Kowollik, C. Single-Chain Self-Folding of Synthetic Polymers Induced by Metal–Ligand Complexation. *Macromol. Rapid Commun.* **2013**, *35*, 45–51. DOI: 10.1002/marc.201300594.
 124. Gonzalez-Burgos, M.; Latorre-Sanchez, A.; Pomposo, J. A. Advances in Single Chain Technology. *Chem. Soc. Rev.* **2015**, *44*, 6122–6142. DOI: 10.1039/C5CS00209E.
 125. Chan, D.; Yu, A. C.; Appel, E. A. Single-Chain Polymeric Nanocarriers: A Platform for Determining Structure-Function Correlations in the Delivery of Molecular Cargo. *Biomacromolecules* **2017**, *18*, 1434–1439. DOI: 10.1021/acs.biomac.7b00249.
 126. Artar, M.; Souren, E. R. J.; Terashima, T.; Meijer, E. W.; Palmans, A. R. A. Single Chain Polymeric Nanoparticles as Selective Hydrophobic Reaction Spaces in Water. *ACS Macro Lett.* **2015**, *4*, 1099–1103. DOI: 10.1021/acsmacrolett.5b00652.
 127. Talapin, D. V.; Lee, J.-S.; Kovalenko, M. V.; Shevchenko, E. V. Prospects of Colloidal Nanocrystals for Electronic and Optoelectronic Applications. *Chem. Rev.* **2010**, *110*, 389–458. DOI: 10.1021/cr900137k.
 128. Lohse, S. E.; Murphy, C. J. Applications of Colloidal Inorganic Nanoparticles:

From Medicine to Energy. *J. Am. Chem. Soc.* **2012**, *134*, 15607–15620. DOI: 10.1021/ja307589n.

129. Mor, G. K.; Varghese, O. K.; Paulose, M.; Shankar, K.; Grimes, C. A. A Review on Highly Ordered, Vertically Oriented TiO₂ Nanotube Arrays: Fabrication, Material Properties, and Solar Energy Applications. *Sol. Energy Mater. Sol. Cells* **2006**, *90*, 2011–2075. DOI: 10.1016/j.solmat.2006.04.007.
130. Zhang, L.; Gu, F. X.; Chan, J. M.; Wang, A. Z.; Langer, R. S.; Farokhzad, O. C. Nanoparticles in Medicine: Therapeutic Applications and Developments. *Clin. Pharmacol. Ther.* **2008**, *83*, 761–769. DOI: 10.1038/sj.clpt.6100400.
131. Peer, D.; Karp, J. M.; Hong, S.; Farokhzad, O. C.; Margalit, R.; Langer, R. Nanocarriers as an Emerging Platform for Cancer Therapy. *Nat. Nanotechnol.* **2007**, *2*, 751–760.
132. Davis, M. E.; Chen, Z.; Shin, D. M. Nanoparticle Therapeutics: An Emerging Treatment Modality for Cancer. *Nat. Rev. Drug Discov.* **2008**, *7*, 771–782.
133. Torchilin, V. P. Micellar Nanocarriers: Pharmaceutical Perspectives. *Pharm. Res.* **2007**, *24*, 1–16. DOI: 10.1007/s11095-006-9132-0.
134. Sanvicens, N.; Marco, M. P. Multifunctional Nanoparticles--Properties and Prospects for Their Use in Human Medicine. *Trends Biotechnol.* **2008**, *26*, 425–433. DOI: 10.1016/j.tibtech.2008.04.005.
135. Torchilin, V. Multifunctional and Stimuli-Sensitive Pharmaceutical Nanocarriers. *Eur. J. Pharm. Biopharm.* **2009**, *71*, 431–444. DOI: 10.1016/j.ejpb.2008.09.026.
136. Petros, R. A.; DeSimone, J. M. Strategies in the Design of Nanoparticles for Therapeutic Applications. *Nat. Rev. Drug Discov.* **2010**, *9*, 615–627. DOI: 10.1038/nrd2591.
137. Torchilin, V. P. Multifunctional Nanocarriers. *Adv. Drug Deliv. Rev.* **2006**, *58*, 1532–1555. DOI: <http://dx.doi.org/10.1016/j.addr.2006.09.009>.
138. Shi, J.; Votruba, A. R.; Farokhzad, O. C.; Langer, R. Nanotechnology in Drug Delivery and Tissue Engineering: From Discovery to Applications. *Nano Lett.* **2010**, *10*, 3223–3230. DOI: 10.1021/nl102184c.
139. Kiparissides, C.; Kammona, O. Nanoscale Carriers for Targeted Delivery of Drugs and Therapeutic Biomolecules. *Can. J. Chem. Eng.* **2013**, *91*, 638–651. DOI: 10.1002/cjce.21685.
140. Farokhzad, O. C.; Langer, R. Impact of Nanotechnology on Drug Delivery. *ACS Nano* **2009**, *3*, 16–20. DOI: 10.1021/nn900002m.
141. Wang, A. Z.; Langer, R.; Farokhzad, O. C. Nanoparticle Delivery of Cancer

- Drugs. *Annu. Rev. Med.* **2012**, *63*, 185–198. DOI: 10.1146/annurev-med-040210-162544.
142. Danhier, F.; Feron, O.; Préat, V. To Exploit the Tumor Microenvironment: Passive and Active Tumor Targeting of Nanocarriers for Anti-Cancer Drug Delivery. *J. Control. Release* **2010**, *148*, 135–146. DOI: 10.1016/j.jconrel.2010.08.027.
 143. Shi, J.; Xiao, Z.; Kamaly, N.; Farokhzad, O. C. Self-Assembled Targeted Nanoparticles: Evolution of Technologies and Bench to Bedside Translation. *Acc. Chem. Res.* **2011**, *44*, 1123–1134. DOI: 10.1021/ar200054n.
 144. Nicolas, J.; Mura, S.; Brambilla, D.; Mackiewicz, N.; Couvreur, P. Design, Functionalization Strategies and Biomedical Applications of Targeted Biodegradable/Biocompatible Polymer-Based Nanocarriers for Drug Delivery. *Chem. Soc. Rev.* **2013**, *42*, 1147–1235. DOI: 10.1039/c2cs35265f.
 145. Bangham, A. D.; Horne, R. W. Negative Staining of Phospholipids and Their Structural Modification by Surface-Active Agents as Observed in the Electron Microscope. *J. Mol. Biol.* **1964**, *8*, 660–IN10. DOI: 10.1016/S0022-2836(64)80115-7.
 146. Bangham, A. D. Liposomes: The Babraham Connection. *Chem. Phys. Lipids* **1993**, *64*, 275–285. DOI: 10.1016/0009-3084(93)90071-A.
 147. Barenholz, Y. Liposome Application: Problems and Prospects. *Curr. Opin. Colloid Interface Sci.* **2001**, *6*, 66–77. DOI: [http://dx.doi.org/10.1016/S1359-0294\(00\)00090-X](http://dx.doi.org/10.1016/S1359-0294(00)00090-X).
 148. Woodle, M. C.; Papahadjopoulos, D. Liposome Preparation and Size Characterization. In *Methods in Enzymology*; Sidney Fleischer, B. F., Ed.; Academic Press, 1989; Vol. 171, pp 193–217.
 149. Sharma, A.; Sharma, U. S. Liposomes in Drug Delivery: Progress and Limitations. *Int. J. Pharm.* **1997**, *154*, 123–140. DOI: 10.1016/S0378-5173(97)00135-X.
 150. Tanner, P.; Baumann, P.; Enea, R.; Onaca, O.; Palivan, C.; Meier, W. Polymeric Vesicles: From Drug Carriers to Nanoreactors and Artificial Organelles. *Acc. Chem. Res.* **2011**, *44*, 1039–1049. DOI: 10.1021/ar200036k.
 151. Cabral, H.; Kataoka, K. Progress of Drug-Loaded Polymeric Micelles into Clinical Studies. *J. Control. Release* **2014**, *190*, 465–476. DOI: 10.1016/J.JCONREL.2014.06.042.
 152. Nishiyama, N.; Kataoka, K. Current State, Achievements, and Future Prospects of Polymeric Micelles as Nanocarriers for Drug and Gene Delivery. *Pharmacol. Ther.* **2006**, *112*, 630–648. DOI: 10.1016/j.pharmthera.2006.05.006.
 153. Xiong, X.-B.; Binkhathlan, Z.; Molavi, O.; Lavasanifar, A. Amphiphilic Block Co-

Polymers: Preparation and Application in Nanodrug and Gene Delivery. *Acta Biomater.* **2012**, *8*, 2017–2033. DOI: <http://dx.doi.org/10.1016/j.actbio.2012.03.006>.

154. Sutton, D.; Nasongkla, N.; Blanco, E.; Gao, J. Functionalized Micellar Systems for Cancer Targeted Drug Delivery. *Pharm. Res.* **2007**, *24*, 1029–1046. DOI: 10.1007/s11095-006-9223-y.
155. Haag, R. Supramolecular Drug-Delivery Systems Based on Polymeric Core–Shell Architectures. *Angew. Chemie Int. Ed.* **2004**, *43*, 278–282. DOI: 10.1002/anie.200301694.
156. Robb, M. J.; Connal, L. A.; Lee, B. F.; Lynd, N. A.; Hawker, C. J. Functional Block Copolymer Nanoparticles: Toward the next Generation of Delivery Vehicles. *Polym. Chem.* **2012**, *3*, 1618–1628. DOI: 10.1039/C2PY20131C.
157. Dechy-Cabaret, O.; Martin-Vaca, B.; Bourissou, D. Controlled Ring-Opening Polymerization of Lactide and Glycolide. *Chem. Rev.* **2004**, *104*, 6147–6176. DOI: 10.1021/cr040002s.
158. Vermonden, T.; Censi, R.; Hennink, W. E. Hydrogels for Protein Delivery. *Chem. Rev.* **2012**, *112*, 2853–2888. DOI: 10.1021/cr200157d.
159. Yasugi, K.; Nagasaki, Y.; Kato, M.; Kataoka, K. Preparation and Characterization of Polymer Micelles from Poly(Ethylene Glycol)-Poly(d,l-Lactide) Block Copolymers as Potential Drug Carrier. *J. Control. Release* **1999**, *62*, 89–100. DOI: [http://dx.doi.org/10.1016/S0168-3659\(99\)00028-0](http://dx.doi.org/10.1016/S0168-3659(99)00028-0).
160. Adams, M. L.; Lavasanifar, A.; Kwon, G. S. Amphiphilic Block Copolymers for Drug Delivery. *J. Pharm. Sci.* **2003**, *92*, 1343–1355. DOI: 10.1002/jps.10397.
161. Jackson, A. W.; Fulton, D. A. Making Polymeric Nanoparticles Stimuli-Responsive with Dynamic Covalent Bonds. *Polym. Chem.* **2013**, *4*, 31–45. DOI: 10.1039/C2PY20727C.
162. Xu, W.; Burke, J. F.; Pilla, S.; Chen, H.; Jaskula-Sztul, R.; Gong, S. Octreotide-Functionalized and Resveratrol-Loaded Unimolecular Micelles for Targeted Neuroendocrine Cancer Therapy. *Nanoscale* **2013**, *5*, 9924–9933. DOI: 10.1039/C3NR03102K.
163. Sapsford, K. E.; Algar, W. R.; Berti, L.; Gemmill, K. B.; Casey, B. J.; Oh, E.; Stewart, M. H.; Medintz, I. L. Functionalizing Nanoparticles with Biological Molecules: Developing Chemistries That Facilitate Nanotechnology. *Chem. Rev.* **2013**, *113*, 1904–2074. DOI: 10.1021/cr300143v.
164. Biju, V. Chemical Modifications and Bioconjugate Reactions of Nanomaterials for Sensing, Imaging, Drug Delivery and Therapy. *Chem. Soc. Rev.* **2014**, *43*, 744–764. DOI: 10.1039/c3cs60273g.

165. Ge, J.; Yang, C.; Zhu, J.; Lu, D.; Liu, Z. Nanobiocatalysis in Organic Media: Opportunities for Enzymes in Nanostructures. *Top. Catal.* **2012**, *55*, 1070–1080. DOI: 10.1007/s11244-012-9906-z.
166. Davis, F. F. The Origin of Pegnology. *Adv. Drug Deliv. Rev.* **2002**, *54*, 457–458. DOI: 10.1016/S0169-409X(02)00021-2.
167. Harris, J. M.; Chess, R. B. Effect of Pegylation on Pharmaceuticals. *Nat. Rev. Drug Discov.* **2003**, *2*, 214–221. DOI: 10.1038/nrd1033.
168. Duncan, R. The Dawning Era of Polymer Therapeutics. *Nat. Rev. Drug Discov.* **2003**, *2*, 347–360. DOI: 10.1038/nrd1088.
169. Roy, I.; Sharma, S.; Gupta, M. N. Smart Biocatalysts: Design and Applications. *Adv. Biochem. Eng. Biotechnol.* **2004**, *86*, 159–189. DOI: 10.1007/b12442APTER.
170. Ge, J.; Lu, D.; Liu, Z.; Liu, Z. Recent Advances in Nanostructured Biocatalysts. *Biochem. Eng. J.* **2009**, *44*, 53–59. DOI: 10.1016/j.bej.2009.01.002.
171. Matyjaszewski, K.; Tsarevsky, N. V. Macromolecular Engineering by Atom Transfer Radical Polymerization. *J. Am. Chem. Soc.* **2014**, *136*, 6513–6533. DOI: 10.1021/ja408069v.
172. Sheldon, R. A. Enzyme Immobilization: The Quest for Optimum Performance. *Adv. Synth. Catal.* **2007**, *349*, 1289–1307. DOI: 10.1002/adsc.200700082.
173. Rodrigues, R. C.; Berenguer-Murcia, Á.; Fernandez-Lafuente, R. Coupling Chemical Modification and Immobilization to Improve the Catalytic Performance of Enzymes. *Adv. Synth. Catal.* **2011**, *353*, 2216–2238. DOI: 10.1002/adsc.201100163.
174. Sheldon, R. A.; van Pelt, S. Enzyme Immobilisation in Biocatalysis: Why, What and How. *Chem. Soc. Rev.* **2013**, *42*, 6223–6235. DOI: 10.1039/c3cs60075k.
175. Cantone, S.; Ferrario, V.; Corici, L.; Ebert, C.; Fattor, D.; Spizzo, P.; Gardossi, L. Efficient Immobilisation of Industrial Biocatalysts: Criteria and Constraints for the Selection of Organic Polymeric Carriers and Immobilisation Methods. *Chem. Soc. Rev.* **2013**, *42*, 6262–6276. DOI: 10.1039/c3cs35464d.
176. Cipolatti, E. P.; Valério, A.; Henriques, R. O.; Moritz, D. E.; Ninow, J. L.; Freire, D. M. G.; Manoel, E. A.; Fernandez-Lafuente, R.; de Oliveira, D. Nanomaterials for Biocatalyst Immobilization – State of the Art and Future Trends. *RSC Adv.* **2016**, *6*, 104675–104692. DOI: 10.1039/C6RA22047A.
177. Murata, H.; Cummings, C. S.; Koepsel, R. R.; Russell, A. J. Polymer-Based Protein Engineering Can Rationally Tune Enzyme Activity, PH-Dependence, and Stability. *Biomacromolecules* **2013**, *14*, 1919–1926. DOI: 10.1021/bm4002816.

178. Cummings, C.; Murata, H.; Koepsel, R.; Russell, A. J. Dramatically Increased PH and Temperature Stability of Chymotrypsin Using Dual Block Polymer-Based Protein Engineering. *Biomacromolecules* **2014**, *15*, 763–771. DOI: 10.1021/bm401575k.
179. Dill, K. A.; MacCallum, J. L. The Protein-Folding Problem, 50 Years On. *Science* **2012**, *338*, 1042–1046. DOI: 10.1126/science.1219021.
180. Dobson, C. M. Protein Folding and Misfolding. *Nature* **2003**, *426*, 884–890. DOI: 10.1038/nature02261.
181. Hartl, F. U. Molecular Chaperones in Cellular Protein Folding. *Nature* **1996**, *381*, 571–579. DOI: 10.1038/381571a0.
182. Hartl, F. U.; Hayer-Hartl, M. Converging Concepts of Protein Folding in Vitro and in Vivo. *Nat. Struct. Mol. Biol.* **2009**, *16*, 574–581.
183. Gething, M. J.; Sambrook, J. Protein Folding in the Cell. *Nature* **1992**, *355*, 33–45. DOI: 10.1038/355033a0.
184. Dill, K. A. Dominant Forces in Protein Folding. *Biochemistry* **1990**, *29*, 7133–7155. DOI: 10.1021/bi00483a001.
185. Sela, M.; Jr, F. H. W.; Anfinsen, C. B. Reductive Cleavage of Disulfide Bridges in Ribonuclease. *Science* **1957**, *125*, 691–692. DOI: 10.2307/1754406.
186. Anfinsen, C. B.; Haber, E. Studies on the Reduction and Re-Formation of Protein Disulfide Bonds. *J. Biol. Chem.* **1961**, *236*, 1361–1363.
187. Kuriyan, J.; Konforti, B.; Wemmer, D. *The Molecules of Life: Physical and Chemical Principles*, 1st ed.; Garland Science, Taylor & Francis Group, LLC, 2012.
188. Anfinsen, C. B. Principles That Govern the Folding of Protein Chains. *Science* **1973**, *181*, 223–230. DOI: 10.1126/science.181.4096.223.
189. Nicholls, A.; Sharp, K. A.; Honig, B. Protein Folding and Association: Insights from the Interfacial and Thermodynamic Properties of Hydrocarbons. *Proteins* **1991**, *11*, 281–296. DOI: 10.1002/prot.340110407.
190. Lim, W. A.; Sauer, R. T. Alternative Packing Arrangements in the Hydrophobic Core of [Lambda]Repressor. *Nature* **1989**, *339*, 31–36. DOI: 10.1038/339031a0.
191. Matsumura, M.; Becktel, W. J.; Matthews, B. W. Hydrophobic Stabilization in T4 Lysozyme Determined Directly by Multiple Substitutions of Ile 3. *Nature* **1988**, *334*, 406–410.
192. Eriksson, A. E.; Baase, W. A.; Zhang, X. J.; Heinz, D. W.; Blaber, M.; Baldwin, E.

- P.; Matthews, B. W. Response of a Protein Structure to Cavity-Creating Mutations and Its Relation to the Hydrophobic Effect. *Science* **1992**, *255*, 178–183. DOI: 10.1126/science.1553543.
193. Kumar, S.; Nussinov, R. Salt Bridge Stability in Monomeric Proteins. *J. Mol. Biol.* **1999**, *293*, 1241–1255.
 194. Burley, S. K.; Petsko, G. A. Aromatic-Aromatic Interaction: A Mechanism of Protein Structure Stabilization. *Science* **1985**, *229*, 23–28. DOI: 10.1126/science.3892686.
 195. Scheinost, J. C.; Boldt, G. E.; Wentworth, P. Protein Misfolding and Disease. In *Chemical Biology*; John Wiley & Sons, Inc., 2012; pp 379–400.
 196. Hartl, F. U.; Bracher, A.; Hayer-Hartl, M. Molecular Chaperones in Protein Folding and Proteostasis. *Nature* **2011**, *475*, 324–332. DOI: 10.1038/nature10317.
 197. Walter, S.; Buchner, J. Molecular Chaperones—Cellular Machines for Protein Folding. *Angew. Chemie Int. Ed.* **2002**, *41*, 1098–1113. DOI: 10.1002/1521-3773(20020402)41:7<1098::AID-ANIE1098>3.0.CO;2-9.
 198. Hildenbrand, Z.; Bernal, R. Chaperonin-Mediated Folding of Viral Proteins. In *Viral Molecular Machines*; Rossmann, M. G., Rao, V. B., Eds.; Advances in Experimental Medicine and Biology; Springer US; Vol. 726, pp 307–324.
 199. Fink, A. L. Chaperone-Mediated Protein Folding. *Physiol. Rev.* **1999**, *79*, 425–449.
 200. Feder, M. E.; Hofmann, G. E. Heat-Shock Proteins, Molecular Chaperones, and the Stress Response: Evolutionary and Ecological Physiology. *Annu. Rev. Physiol.* **1999**, *61*, 243–282. DOI: 10.1146/annurev.physiol.61.1.243.
 201. Hartl, F. U.; Hayer-Hartl, M. Molecular Chaperones in the Cytosol: From Nascent Chain to Folded Protein. *Science* **2002**, *295*, 1852–1858. DOI: 10.1126/science.1068408.
 202. Bukau, B.; Horwich, A. L. The Hsp70 and Hsp60 Chaperone Machines. *Cell* **1998**, *92*, 351–366.
 203. Rozema, D.; Gellman, S. H. Artificial Chaperones: Protein Refolding via Sequential Use of Detergent and Cyclodextrin. *J. Am. Chem. Soc.* **1995**, *117*, 2373–2374. DOI: 10.1021/ja00113a036.
 204. Rozema, D.; Gellman, S. H. Artificial Chaperone-Assisted Refolding of Denatured-Reduced Lysozyme: Modulation of the Competition between Renaturation and Aggregation. *Biochemistry* **1996**, *35*, 15760–15771. DOI: 10.1021/bi961638j.

205. Rozema, D.; Gellman, S. H. Artificial Chaperone-Assisted Refolding of Carbonic Anhydrase B. *J. Biol. Chem.* **1996**, *271*, 3478–3487. DOI: 10.1074/jbc.271.7.3478.
206. Nomura, Y.; Ikeda, M.; Yamaguchi, N.; Aoyama, Y.; Akiyoshi, K. Protein Refolding Assisted by Self-Assembled Nanogels as Novel Artificial Molecular Chaperone. *FEBS Lett.* **2003**, *553*, 271–276. DOI: 10.1016/S0014-5793(03)01028-7.
207. Hirakura, T.; Nomura, Y.; Aoyama, Y.; Akiyoshi, K. Photoresponsive Nanogels Formed by the Self-Assembly of Spiropyran-Bearing Pullulan That Act as Artificial Molecular Chaperones. *Biomacromolecules* **2004**, *5*, 1804–1809. DOI: 10.1021/bm049860o.
208. Nomura, Y.; Sasaki, Y.; Takagi, M.; Narita, T.; Aoyama, Y.; Akiyoshi, K. Thermoresponsive Controlled Association of Protein with a Dynamic Nanogel of Hydrophobized Polysaccharide and Cyclodextrin: Heat Shock Protein-like Activity of Artificial Molecular Chaperone. *Biomacromolecules* **2005**, *6*, 447–452. DOI: 10.1021/bm049501t.
209. Sawada, S.-I.; Nomura, Y.; Aoyama, Y.; Akiyoshi, K. Heat Shock Protein-like Activity of a Nanogel Artificial Chaperone for Citrate Synthase. *J. Bioact. Compat. Polym.* **2006**, *21*, 487–501. DOI: 10.1177/0883911506070819.
210. Hirakura, T.; Yasugi, K.; Nemoto, T.; Sato, M.; Shimoboji, T.; Aso, Y.; Morimoto, N.; Akiyoshi, K. Hybrid Hyaluronan Hydrogel Encapsulating Nanogel as a Protein Nanocarrier: New System for Sustained Delivery of Protein with a Chaperone-like Function. *J. Control. Release* **2010**, *142*, 483–489. DOI: <http://dx.doi.org/10.1016/j.jconrel.2009.11.023>.
211. Sasaki, Y.; Nomura, Y.; Sawada, S.; Akiyoshi, K. Polysaccharide Nanogel-Cyclodextrin System as an Artificial Chaperone for in Vitro Protein Synthesis of Green Fluorescent Protein. *Polym J* **2010**, *42*, 823–828.
212. Takahashi, H.; Sawada, S.; Akiyoshi, K. Amphiphilic Polysaccharide Nanoballs: A New Building Block for Nanogel Biomedical Engineering and Artificial Chaperones. *ACS Nano* **2010**, *5*, 337–345. DOI: 10.1021/nn101447m.
213. Takeda, S.; Takahashi, H.; Sawada, S.; Sasaki, Y.; Akiyoshi, K. Amphiphilic Nanogel of Enzymatically Synthesized Glycogen as an Artificial Molecular Chaperone for Effective Protein Refolding. *RSC Adv.* **2013**, *3*, 25716–25718. DOI: 10.1039/C3RA44572K.
214. Liu, X.; Liu, Y.; Zhang, Z.; Huang, F.; Tao, Q.; Ma, R.; An, Y.; Shi, L. Temperature-Responsive Mixed-Shell Polymeric Micelles for the Refolding of Thermally Denatured Proteins. *Chem. A Eur. J.* **2013**, *19*, 7437–7442. DOI: 10.1002/chem.201300634.
215. Huang, F.; Wang, J.; Qu, A.; Shen, L.; Liu, J.; Liu, J.; Zhang, Z.; An, Y.; Shi, L.

Maintenance of Amyloid Beta Peptide Homeostasis by Artificial Chaperones Based on Mixed-Shell Polymeric Micelles. *Angew. Chemie-International Ed.* **2014**, *53*, 8985–8990. DOI: 10.1002/anie.201400735.

216. Wang, J.; Yin, T.; Huang, F.; Song, Y.; An, Y.; Zhang, Z.; Shi, L. Artificial Chaperones Based on Mixed Shell Polymeric Micelles: Insight into the Mechanism of the Interaction of the Chaperone with Substrate Proteins Using Förster Resonance Energy Transfer. *ACS Appl. Mater. Interfaces* **2015**, *7*, 10238–10249. DOI: 10.1021/acsami.5b00684.
217. Huang, F.; Shen, L.; Wang, J.; Qu, A.; Yang, H.; Zhang, Z.; An, Y.; Shi, L. Effect of the Surface Charge of Artificial Chaperones on the Refolding of Thermally Denatured Lysozymes. *ACS Appl. Mater. Interfaces* **2016**, *8*, 3669–3678. DOI: 10.1021/acsami.5b08843.
218. Wang, J.; Song, Y.; Sun, P.; An, Y.; Zhang, Z.; Shi, L. Reversible Interactions of Proteins with Mixed Shell Polymeric Micelles: Tuning the Surface Hydrophobic/Hydrophilic Balance toward Efficient Artificial Chaperones. *Langmuir* **2016**, *32*, 2737–2749. DOI: 10.1021/acs.langmuir.6b00356.
219. Ma, F.-H.; An, Y.; Wang, J.; Song, Y.; Liu, Y.; Shi, L. Synthetic Nanochaperones Facilitate Refolding of Denatured Proteins. *ACS Nano* **2017**, *11*, 10549–10557. DOI: 10.1021/acsnano.7b05947.
220. Jiang, X.; Vogel, E. B.; Smith III, M. R.; Baker, G. L. Amphiphilic PEG/Alkyl-Grafted Comb Polylactides. *J. Polym. Sci. Part A Polym. Chem.* **2007**, *45*, 5227–5236. DOI: 10.1002/pola.22268.
221. Brocas, A.-L.; Cendejas, G.; Caillol, S.; Deffieux, A.; Carlotti, S. Controlled Synthesis of Polyepichlorohydrin with Pendant Cyclic Carbonate Functions for Isocyanate-Free Polyurethane Networks. *J. Polym. Sci. Part A Polym. Chem.* **2011**, *49*, 2677–2684. DOI: 10.1002/pola.24699.
222. Baskaran, S.; Baig, M. H. A.; Banerjee, S.; Baskaran, C.; Bhanu, K.; Deshpande, S. P.; Trivedi, G. K. An Efficient and Stereoselective Synthesis of (2R,2'S)-1-O-(2'-Hydroxyhexadecyl)Glycerol and Its Oxo Analogs: Potential Antitumour Compounds from Shark Liver Oil. *Tetrahedron* **1996**, *52*, 6437–6452. DOI: 10.1016/0040-4020(96)00278-5.
223. Zimm, B. H. The Scattering of Light and the Radial Distribution Function of High Polymer Solutions. *J. Chem. Phys.* **1948**, *16*, 1093–1099. DOI: 10.1063/1.1746738.
224. Schärfl, W. *Light Scattering from Polymer Solutions and Nanoparticle Dispersions*, 1st ed.; Pasch, H., Alig, I., Janca, J., Kulicke, W.-M., Eds.; Springer Berlin Heidelberg: New York, 2007.
225. Lieber, E.; Chao, T. S.; Rao, C. N. R. Improved Method for the Synthesis of Alkyl

- Azides. *J. Org. Chem.* **1957**, *22*, 238–240. DOI: 10.1021/jo01354a003.
226. Díaz, L.; Bujons, J.; Casas, J.; Llebaria, A.; Delgado, A. Click Chemistry Approach to New N-Substituted Aminocyclitols as Potential Pharmacological Chaperones for Gaucher Disease. *J. Med. Chem.* **2010**, *53*, 5248–5255. DOI: 10.1021/jm100198t.
 227. Podzimek, S.; Vlcek, T.; Johann, C. Characterization of Branched Polymers by Size Exclusion Chromatography Coupled with Multiangle Light Scattering Detector. I. Size Exclusion Chromatography Elution Behavior of Branched Polymers. *J. Appl. Polym. Sci.* **2001**, *81*, 1588–1594. DOI: 10.1002/app.1589.
 228. Podzimek, S.; Vlcek, T. Characterization of Branched Polymers by SEC Coupled with a Multiangle Light Scattering Detector. II. Data Processing and Interpretation. *J. Appl. Polym. Sci.* **2001**, *82*, 454–460. DOI: 10.1002/app.1871.
 229. Chen, Y.; Baker, G. L. Synthesis and Properties of ABA Amphiphiles. *J. Org. Chem.* **1999**, *64*, 6870–6873. DOI: 10.1021/jo990620m.
 230. Müller, M. K.; Brunsveld, L. A Supramolecular Polymer as a Self-Assembling Polyvalent Scaffold. *Angew. Chemie Int. Ed.* **2009**, *48*, 2921–2924. DOI: 10.1002/anie.200900143.
 231. Joris, B.; Hu, C.; D., B. M. Visualizing the Chain-Flipping Mechanism in Fatty-Acid Biosynthesis. *Angew. Chemie Int. Ed.* **2014**, *53*, 14456–14461. DOI: 10.1002/anie.201408576.
 232. Xiao, C.; Cheng, Y.; Zhang, Y.; Ding, J.; He, C.; Zhuang, X.; Chen, X. Side Chain Impacts on PH- and Thermo-responsiveness of Tertiary Amine Functionalized Polypeptides. *J. Polym. Sci. Part A Polym. Chem.* **2013**, *52*, 671–679. DOI: 10.1002/pola.27048.
 233. Engler, A. C.; Shukla, A.; Puranam, S.; Buss, H. G.; Jreige, N.; Hammond, P. T. Effects of Side Group Functionality and Molecular Weight on the Activity of Synthetic Antimicrobial Polypeptides. *Biomacromolecules* **2011**, *12*, 1666–1674. DOI: 10.1021/bm2000583.
 234. Firman, P.; Kahlweit, M. Phase Behavior of the Ternary System H₂O - Oil - Polypropyleneglycol (PPG). *Colloid Polym. Sci. Colloid Polym. Sci.* **1986**, *264*, 936–942.
 235. Skrabania, K.; Kristen, J.; Laschewsky, A.; Akdemir, O.; Hoth, A.; Lutz, J.-F. Design, Synthesis, and Aqueous Aggregation Behavior of Nonionic Single and Multiple Thermoresponsive Polymers. *Langmuir* **2007**, *23*, 84–93. DOI: 10.1021/la061509w.
 236. Isono, T.; Miyachi, K.; Satoh, Y.; Sato, S.-I.; Kakuchi, T.; Satoh, T. Design and Synthesis of Thermoresponsive Aliphatic Polyethers with a Tunable Phase

- Transition Temperature. *Polym. Chem.* **2017**, *8*, 5698–5707. DOI: 10.1039/C7PY01238A.
237. Mori, H.; Iwaya, H.; Nagai, A.; Endo, T. Controlled Synthesis of Thermoresponsive Polymers Derived from L-Proline via RAFT Polymerization. *Chem. Commun.* **2005**, *0*, 4872–4874. DOI: 10.1039/B509212D.
 238. Aoshima, S.; Oda, H.; Kobayashi, E. Synthesis of Thermally-Induced Phase Separating Polymer with Well-Defined Polymer Structure by Living Cationic Polymerization. I. Synthesis of Poly(Vinyl Ether)s with Oxyethylene Units in the Pendant and Its Phase Separation Behavior in Aqueous Solution. *J. Polym. Sci. A Polym. Chem.* **1992**, *30*, 2407–2413. DOI: 10.1002/pola.1992.080301115.
 239. Freitag, R.; Baltes, T.; Eggert, M. A Comparison of Thermoreactive Water-Soluble Poly-N,N-Diethylacrylamide Prepared by Anionic and by Group Transfer Polymerization. *J. Polym. Sci. A Polym. Chem.* **1994**, *32*, 3019–3030. DOI: 10.1002/pola.1994.080321603.
 240. Ilavský, M.; Hrouz, J.; Havlíček, I. Phase Transition in Swollen Gels: 7. Effect of Charge Concentration on the Temperature Collapse of Poly(N,N-Diethylacrylamide) Networks in Water. *Polym.* **1985**, *26*, 1514–1518. DOI: 10.1016/0032-3861(85)90085-0.
 241. Allcock, H. R.; Dudley, G. K. Lower Critical Solubility Temperature Study of Alkyl Ether Based Polyphosphazenes. *Macromolecules* **1996**, *29*, 1313–1319.
 242. Song, S.-C.; Lee, S. B.; Jin, J.-I.; Sohn, Y. S. A New Class of Biodegradable Thermosensitive Polymers. I. Synthesis and Characterization of Poly(Organophosphazenes) with Methoxy-Poly(Ethylene Glycol) and Amino Acid Esters as Side Groups. *Macromolecules* **1999**, *32*, 2188–2193. DOI: 10.1021/ma981190p.
 243. Bi, Y. M.; Gong, X. Y.; Wang, W. Z.; Yu, L.; Hu, M. Q.; Shao, L. D. Synthesis and Characterization of New Biodegradable Thermosensitive Polyphosphazenes with Lactic Acid Ester and Methoxyethoxyethoxy Side Groups. *Chin. Chem. Lett.* **2010**, *21*, 237–241. DOI: 10.1016/j.ccllet.2009.10.003.
 244. Bi, Y.; Gong, X.; He, F.; Xu, L.; Chen, L.; Zeng, X.; Yu, L. Polyphosphazenes Containing Lactic Acid Ester and Methoxyethoxyethoxy Side Groups — Thermosensitive Properties and, in Vitro Degradation, and Biocompatibility. *Can. J. Chem.* **2011**, *89*, 1249–1256. DOI: 10.1139/v11-102.
 245. Von Hippel, P. H.; Schleich, T. Ion Effects on the Solution Structure of Biological Macromolecules. *Acc. Chem. Res.* **1969**, *2*, 257–265. DOI: 10.1021/ar50021a001.
 246. Baldwin, R. L. How Hofmeister Ion Interactions Affect Protein Stability. *Biophys. J.* **1996**, *71*, 2056–2063. DOI: 10.1016/S0006-3495(96)79404-3.

247. Cacace, M. G.; Landau, E. M.; Ramsden, J. J. The Hofmeister Series: Salt and Solvent Effects on Interfacial Phenomena. *Q. Rev. Biophys.* **1997**, *30*, 241–277.
248. Boström, M.; Williams, D. R. M.; Ninham, B. W. Specific Ion Effects: Why the Properties of Lysozyme in Salt Solutions Follow a Hofmeister Series. *Biophys. J.* **2003**, *85*, 686–694. DOI: 10.1016/S0006-3495(03)74512-3.
249. Kunz, W.; Lo Nostro, P.; Ninham, B. W. The Present State of Affairs with Hofmeister Effects. *Curr. Opin. Colloid Interface Sci.* **2004**, *9*, 1–18. DOI: 10.1016/j.cocis.2004.05.004.
250. Magnusson, J. P.; Khan, A.; Pasparakis, G.; Saeed, A. O.; Wang, W.; Alexander, C. Ion-Sensitive “Isothermal” Responsive Polymers Prepared in Water. *J. Am. Chem. Soc.* **2008**, *130*, 10852–10853. DOI: 10.1021/ja802609r.
251. Zhang, Y.; Cremer, P. S. Chemistry of Hofmeister Anions and Osmolytes. *Annu. Rev. Phys. Chem.* **2010**, *61*, 63–83. DOI: 10.1146/annurev.physchem.59.032607.093635.
252. Lo Nostro, P.; Ninham, B. W. Hofmeister Phenomena: An Update on Ion Specificity in Biology. *Chem. Rev.* **2012**, *112*, 2286–2322. DOI: 10.1021/cr200271j.
253. Salis, A.; Ninham, B. W. Models and Mechanisms of Hofmeister Effects in Electrolyte Solutions, and Colloid and Protein Systems Revisited. *Chem. Soc. Rev.* **2014**, *43*, 7358–7377. DOI: 10.1039/c4cs00144c.
254. Mazzini, V.; Craig, V. S. J. Specific-Ion Effects in Non-Aqueous Systems. *Curr. Opin. Colloid Interface Sci.* **2016**, *23*, 82–93. DOI: 10.1016/j.cocis.2016.06.009.
255. Hofmeister, F. Zur Lehre von Der Wirkung Der Salze. *Arch. für Exp. Pathol. und Pharmakologie* **1888**, *24*, 247–260. DOI: 10.1007/BF01918191.
256. Kunz, W.; Henle, J.; Ninham, B. W. ‘Zur Lehre von Der Wirkung Der Salze’ (about the Science of the Effect of Salts): Franz Hofmeister’s Historical Papers. *Curr. Opin. Colloid Interface Sci.* **2004**, *9*, 19–37. DOI: 10.1016/j.cocis.2004.05.005.
257. Zhang, Y.; Foryk, S.; Bergbreiter, D. E.; Cremer, P. S. Specific Ion Effects on the Water Solubility of Macromolecules: PNIPAM and the Hofmeister Series. *J. Am. Chem. Soc.* **2005**, *127*, 14505–14510. DOI: 10.1021/ja0546424.
258. Ottesen, M.; Svendsen, I. [11] The Subtilisins. In *Methods in Enzymology*; Academic Press, 1970; Vol. 19, pp 199–215.
259. Nedkov, P.; Oberthür, W.; Braunitzer, G. Determination of the Complete Amino-Acid Sequence of Subtilisin DY and Its Comparison with the Primary Structures of the Subtilisins BPN’, Carlsberg and Amylosacchariticus. *Biol. Chem. Hoppe*

- Seyler* **1985**, 366, 421–430. DOI: 10.1515/bchm3.1985.366.1.421.
260. Polgár, L. Chapter 3 Structure and Function of Serine Proteases. In *New Comprehensive Biochemistry*; Neuberger, A., Brocklehurst, K., Eds.; Elsevier, 1987; Vol. 16, pp 159–200.
 261. *Handbook of Detergents, Part A*, 1st ed.; Broze, G., Ed.; CRC Press: Boca Raton, 1999.
 262. Brode, P. F.; Erwin, C. R.; Rauch, D. S.; Barnett, B. L.; Armpriester, J. M.; Wang, E. S. F.; Rubingh, D. N. Subtilisin BPN⁺ Variants: Increased Hydrolytic Activity on Surface-Bound Substrates via Decreased Surface Activity. *Biochemistry* **1996**, 35, 3162–3169. DOI: 10.1021/bi951990h.
 263. Nakajima, K.; Powers, J. C.; Ashe, B. M.; Zimmerman, M. Mapping the Extended Substrate Binding Site of Cathepsin G and Human Leukocyte Elastase. Studies with Peptide Substrates Related to the Alpha 1-Protease Inhibitor Reactive Site. *J. Biol. Chem.* **1979**, 254, 4027–4032.
 264. Barrett, A. J. Cathepsin G. *Methods Enzym.* **1981**, 80 Pt C, 561–565.
 265. Bajorath, J.; Saenger, W.; Pal, G. P. Autolysis and Inhibition of Proteinase K, a Subtilisin-Related Serine Proteinase Isolated from the Fungus *Tritirachium Album* Limber. *Biochim. Biophys. Acta* **1988**, 954, 176–182.
 266. Shirai, M.; Aida, T. Autolysis of *Bacillus Colistinus*. *Agric. Biol. Chem.* **1980**, 44, 1513–1519. DOI: 10.1080/00021369.1980.10864176.
 267. Maroux, S.; Rivery, M.; Desnuelle, P. An Autolyzed and Still Active Form of Bovine Trypsin. *Biochim. Biophys. Acta* **1967**, 140, 377–380.
 268. Stoner, M. R.; Dale, D. A.; Gualfetti, P. J.; Becker, T.; Manning, M. C.; Carpenter, J. F.; Randolph, T. W. Protease Autolysis in Heavy-Duty Liquid Detergent Formulations: Effects of Thermodynamic Stabilizers and Protease Inhibitors. *Enzym. Microb. Technol.* **2004**, 34, 114–125. DOI: 10.1016/j.enzmictec.2003.09.008.
 269. Yang, Z.; Domach, M.; Auger, R.; Yang, F. X.; Russell, A. J. Polyethylene Glycol-Induced Stabilization of Subtilisin. *Enzym. Microb. Technol.* **1996**, 18, 82–89. DOI: 10.1016/0141-0229(95)00073-9.
 270. Bräse, S.; Gil, C.; Knepper, K.; Zimmermann, V. Organic Azides: An Exploding Diversity of a Unique Class of Compounds. *Angew. Chem. Int. Ed Engl.* **2005**, 44, 5188–5240. DOI: 10.1002/anie.200400657.